AFFDL-TR-71-20
SUPPLEMENT – 2

SURVIVABLE FLIGHT CONTROL SYSTEM
INTERIM REPORT NO. 1
STUDIES, ANALYSES AND APPROACH

SUPPLEMENT FOR CONTROL LAW DEVELOPMENT STUDIES

Robert L. Kisslinger
George J. Vetsch

FOREWORD

This report was prepared by McDonnell Aircraft Company, St. Louis, Missouri, 63166, under Air Force Contract F33615-69-C-1827, PZ05, "Development and Flight Test Demonstration of a Survivable Flight Control System." This contracted effort comprises a major portion of development under the Air Force Systems Command Program No. 680J, "Survivable Flight Control System (SFCS)." The work was administered under the direction of the Air Force Flight Dynamics Laboratory, Wright-Patterson Air Force Base, Ohio, 45433 by Major Robert C. Lorenzetti, Technical Manager.

The report covers work performed between July 1969 and May 1971.

Principal contributor to this supplement was George J. Vetsch under the direction of Robert L. Kisslinger, Senior Project Dynamics Engineer. The authors wish to acknowledge the contributions of B. B. Barnes, H. L. Jeffrie, and D. B. Schaefer of MCAIR, and the SFCES Project personnel of Sperry Rand Corp., Phoenix, Arizona to the information reported herein.

The manuscript was released by the authors in May 1971.

This technical report has been reviewed and is approved.

James W. Morris
Program Manager, Survivable Flight Control System
Flight Control Division
Air Force Flight Dynamics Laboratory

ABSTRACT

The Survivable Flight Control System (SFCS) Program is an advanced development program of which the principal objective is the development and flight test demonstration of an SFCS utilizing Fly-By-Wire and Integrated Actuator Package techniques. The studies and analyses conducted to date have sufficiently defined the system requirements to provide a definition of an approach to the implementation of the SFCS. The results of these studies and the definition of the approach are presented in the basic report. The details of the Control Criteria, and Hydraulic Power and Actuation studies are presented in report supplements 1 and 3, respectively. The results of the Control Law Development studies are presented in this supplement 2.

As a result of previous fly-by-wire technology development programs, certain guidelines and requirements were specified early in the SFCS design. Those specifications which are relevant to the control law development study are as follows:

- Model following closed-loop control system, utilizing a blend of pitch rate and normal acceleration feedback for the pitch axis, roll rate feedback for the roll axis, and a blend of yaw rate and lateral acceleration for the yaw axis.
- Selectable neutral speed stability with gear up
- Selectable fixed or adaptive gain operation
- Direct electrical link to control surface for emergency operation
- Center stick and sidestick fly-by-wire controllers
- Roll-to-Yaw crossfeed
- Structural mode compensation
- Failure detection and isolation
- Stall warning through increased stick force gradients
- Quadruplex electronics, sensors, secondary actuators and a duplex integrated actuator package in order to provide a two-fail operate capability.
- Mechanical back-up for Phase IIA (pitch and yaw axes only) and no mechanical back-up for Phases IIB and C.

Using the above guidelines, this study further defined the system concepts, requirements, and specific techniques to be utilized in the SFCS implementation. During the system synthesis, particular emphasis was placed on system stability, sensor location, gain schedules, appropriate filters, and component mechanization. Once the system math model was developed, both component and total system performance characteristics were investigated extensively. In addition to the comprehensive root locus and Bode analyses

and small perturbation simulations, a six-degree-of-freedom, fixed base, nonlinear, large amplitude, piloted simulation was conducted in order to evaluate the total system performance over the range of flight conditions and configurations available with the F-4 test aircraft.

The results of this study and simulation provided a basis for specifying the performance of the SFCS procured hardware. As a result of the design refinements which resulted from this work, the SFCS system will demonstrate superior stability and performance characteristics throughout the F-4 flight envelope.

TABLE OF CONTENTS

LIST OF ILLUSTRATIONS

LIST OF TABLES

LIST OF ABBREVIATIONS AND SYMBOLS

ABBREVIATIONS:

ADI - Attitude Director Indicator

B.L. (BL) - Buttline

CDC - Control Data Corporation

dB - decibels - a measure of gain = 20 $\log_{10}$ (Amplitude Ratio)

DFG - Discrete Function Generator

EBU - Electrical Back-up

FBW - Fly-by-Wire

FOM - Figure of Merit

F.S. (FS) - Fuselage Station

GD - Gear Down (landing gear extended)

GL - Gain Level

GU - Gear Up (landing gear retracted)

Hz - Hertz - (cycles per second)

LSI - Lear-Siegler, Incorporated

MBU - Mechanical Back-up

MCAUTO - McDonnell Douglas Automation Company

MIM - Mechanical Isolation Mechanism

NSS - Neutral Speed Stability (longitudinal SFCS function)

PA - Power Approach

Ph - Phugoid (longitudinal oscillatory mode)

PIO - Pilot induced oscillation

rms - root mean square

SAS - Stability Augmentation System

SFCS - Survivable Flight Control System

S.L. (SL) - Sea Level

SP - Short Period (longitudinal oscillatory mode)

SSAP - Survivable Stabilator Actuator Package

SSC - Side Stick Controller

SSD - Signal Selection Device

SW - Switching Logic

TF - Terrain Following

TOL - Take Off and Land (longitudinal SFCS function)

TOT - Take Off Trim (electrical bias - volts)

VCAL - Calibrated Airspeed

W.L. (WL) - Waterline

SYMBOLS:

SYMBOLS	DEFINITIONS	UNITS
A_β	Fuselage first torsion mode acceleration due to sideslip angle	$1/rad\text{-}sec^2$
A_p	Fuselage first torsion mode acceleration due to roll rate	$1/rad\text{-}sec$
A_r	Fuselage first torsion mode acceleration due to yaw rate	$1/rad\text{-}sec$
A_δ	Fuselage first torsion mode acceleration due to total lateral control surface deflection	$1/rad\text{-}sec^2$
$A_{\dot{\zeta}}$	Fuselage first torsion mode acceleration due to total lateral control surface deflection rate	$1/rad\text{-}sec$
A_{δ_R}	Fuselage first torsion mode acceleration due to rudder deflection	$1/rad\text{-}sec^2$
$A_{\dot{\delta}_R}$	Fuselage first torsion mode acceleration due to rudder deflection rate	$1/rad\text{-}sec$
A_{η_4}	Fuselage first torsion mode acceleration due to fuselage first torsion mode deflection	$1/sec^2$
$A_{\dot{\eta}_4}$	Fuselage first torsion mode acceleration due to fuselage first torsion mode rate	$1/sec$
A_{η_5}	Fuselage first torsion mode acceleration due to wing asymmetric bending mode deflection	$1/sec^2$
$A_{\dot{\eta}_5}$	Fuselage first torsion mode acceleration due to wing asymmetric bending mode rate	$1/sec$
A_{η_6}	Fuselage first torsion mode acceleration due to fuselage first lateral bending mode deflection	$1/sec^2$
$A_{\dot{\eta}_6}$	Fuselage first torsion mode acceleration due to fuselage first lateral bending mode rate	$1/sec$
$ax_{acc}, ay_{acc}, az_{acc}$	Acceleration components in body axis measured at accelerometer	g
$ax_{cg}, ay_{cg}, az_{cg}$	Acceleration components in body axis measured at center of gravity	g
$a_{y_{FO}}$	Output of lateral acceleration structural filter	volts

SYMBOLS	DEFINITIONS	UNITS
a_{y_p} , a_{z_p}	Acceleration components in body axis measured at pilot station	g
a_{y_s}	Acceleration sensed by lateral accelerometer	ft/sec^2
B_β	Wing asymmetric bending mode acceleration due to sideslip angle	1/rad-sec^2
B_p	Wing asymmetric bending mode acceleration due to roll rate	1/rad-sec
B_r	Wing asymmetric bending mode acceleration due to yaw rate	1/rad-sec
B_δ	Wing asymmetric bending mode acceleration due to total lateral control surface deflection	1/rad-sec^2
$B_{\dot{\delta}}$	Wing asymmetric bending mode acceleration due to total lateral control surface deflection rate	1/rad-sec
B_{δ_R}	Wing asymmetric bending mode acceleration due to rudder deflection	1/rad-sec^2
$B_{\dot{\delta}_R}$	Wing asymmetric bending mode acceleration due to rudder deflection rate	1/rad-sec
B_{η_4}	Wing asymmetric bending mode acceleration due to fuselage first torsion mode deflection	1/sec^2
$B_{\dot{\eta}_4}$	Wing asymmetric bending mode acceleration due to fuselage first torsion mode rate	1/sec
B_{η_5}	Wing asymmetric bending mode acceleration due to wing asymmetric bending mode deflection	1/sec^2
$B_{\dot{\eta}_5}$	Wing asymmetric bending mode acceleration due to wing asymmetric bending mode rate	1/sec
B_{η_6}	Wing asymmetric bending mode acceleration due to fuselage first lateral bending mode deflection	1/sec^2
$B_{\dot{\eta}_6}$	Wing asymmetric bending mode acceleration due to fuselage first lateral bending mode rate	1/sec
b	Wing span	ft

SYMBOLS	DEFINITIONS	UNITS
C_D	Drag coefficient	dimensionless
C_L	Lift coefficient	dimensionless
C_{l_p}	Roll moment stability derivative due to roll rate	dimensionless
C_{l_r}	Roll moment stability derivative due to yaw rate	dimensionless
C_{l_β}	Roll moment stability derivative due to sideslip angle	dimensionless
$C_{l_{\delta_A}}$	Roll moment stability derivative due to aileron deflection	dimensionless
$C_{l_{\delta_R}}$	Roll moment stability derivative due to rudder deflection	dimensionless
$C_{l_{\delta_{SP}}}$	Roll moment stability derivative due to spoiler deflection	dimensionless
C_M	Pitch moment coefficient	dimensionless
C_{m_q}	Pitch moment stability derivative due to pitch rate	dimensionless
$C_{m_{\dot{\alpha}}}$	Pitch moment stability derivative due to angle of attack rate	dimensionless
$C_{m_{\delta_s}}$	Pitch moment stability derivative due to stabilator deflection	dimensionless
C_{n_p}	Yaw moment stability derivative due to roll rate	dimensionless
C_{n_r}	Yaw moment stability derivative due to yaw rate	dimensionless
C_{n_β}	Yaw moment stability derivative due to sideslip angle	dimensionless
$C_{n_{\delta_a}}$	Yaw moment stability derivative due to aileron deflection	dimensionless
$C_{n_{\delta_R}}$	Yaw moment stability derivative due to rudder deflection	dimensionless

SYMBOLS	DEFINITIONS	UNITS
$C_{n_{\delta_{SP}}}$	Yaw moment stability derivative due to spoiler deflection	dimensionless
C_{ℓ_p}	Fuselage first lateral bending mode acceleration due to roll rate	1/rad-sec
C_{ℓ_r}	Fuselage first lateral bending mode acceleration due to yaw rate	1/rad-sec
C_{y_p}	Side force stability derivative due to roll rate	dimensionless
C_{y_r}	Side force stability derivative due to yaw rate	dimensionless
C_{y_β}	Side force stability derivative due to sideslip angle	dimensionless
$C_{y_{\delta_a}}$	Side force stability derivative due to aileron deflection	dimensionless
$C_{y_{\delta_R}}$	Side force stability derivative due to rudder deflection	dimensionless
$C_{y_{\delta_{SP}}}$	Side force stability derivative due to spoiler deflection	dimensionless
C_{ℓ_β}	Fuselage first lateral bending mode acceleration due to sideslip angle	1/rad-sec^2
C_{ℓ_δ}	Fuselage first lateral bending mode acceleration due to total lateral control surface deflection	1/rad-sec^2
$C_{\ell_{\dot{\delta}}}$	Fuselage first lateral bending mode acceleration due to total lateral control surface deflection rate	1/rad-sec
$C_{\ell_{\delta_R}}$	Fuselage first lateral bending mode acceleration due to rudder deflection	1/rad-sec^2
$C_{\ell_{\dot{\delta}_R}}$	Fuselage first lateral bending mode acceleration due to rudder deflection rate	1/rad-sec
C_{η_4}	Fuselage first lateral bending mode acceleration due to fuselage first torsion mode deflection	1/sec^2
$C_{\dot{\eta}_4}$	Fuselage first lateral bending mode acceleration due to fuselage first torsion mode rate	1/sec

SYMBOLS	DEFINITIONS	UNITS
C_{n_5}	Fuselage first lateral bending mode acceleration due to wing asymmetric bending mode deflection	$1/sec^2$
$C_{\dot{n}_5}$	Fuselage first lateral bending mode acceleration due to wing asymmetric bending mode rate	1/sec
C_{n_6}	Fuselage first lateral bending mode acceleration due to fuselage first lateral bending mode deflection	$1/sec^2$
$C_{\dot{n}_6}$	Fuselage first lateral bending mode acceleration due to fuselage first lateral bending mode rate	1/sec
C_i	Outputs of stall warning comparators, i=1,2,3	volts
C*	Longitudinal response criterion parameter	g
cg (CG)	Center of gravity	
cg (FS)	Fuselage station center of gravity location	in
cg (WL)	Water line center of gravity location	in
$\bar{c}$	Mean aerodynamic chord length	ft
D^*_1	Directional response criterion parameter	deg
F_{Lon}	Longitudinal stick force	lb
F_S	Lateral stick force above breakout	lb
F_α	Stabilator bending mode acceleration due to angle of attack	$1/sec^2$
$F_{\dot{\theta}}$	Stabilator bending mode acceleration due to pitch rate	1/sec
F_δ	Stabilator bending mode acceleration due to stabilator deflection	$1/sec^2$
$F_{\dot{\delta}}$	Stabilator bending mode acceleration due to stabilator rate	1/sec
$F_{\ddot{\delta}}$	Stabilator bending mode acceleration due to stabilator acceleration	dimensionless
F_{n_1}	Stabilator bending mode acceleration due to stabilator bending	$1/sec^2$

SYMBOLS	DEFINITIONS	UNITS
$F_{\dot{\eta}_1}$	Stabilator bending mode acceleration due to stabilator bending rate	1/sec
F_{η_2}	Stabilator bending mode acceleration due to first vertical bending	$1/sec^2$
$F_{\dot{\eta}_2}$	Stabilator bending mode acceleration due to first vertical bending rate	1/sec
F_{η_3}	Stabilator bending mode acceleration due to stabilator rotation mode	$1/sec^2$
$F_{\dot{\eta}_3}$	Stabilator bending mode acceleration due to stabilator rotation mode rate	1/sec
G_{α}	First vertical bending mode acceleration due to angle of attack	$1/sec^2$
$G_{\dot{\theta}}$	First vertical bending mode acceleration due to pitch rate	1/sec
G_{δ}	First vertical bending mode acceleration due to stabilator deflection	$1/sec^2$
$G_{\dot{\delta}}$	First vertical bending mode acceleration due to stabilator rate	1/sec
$G_{\ddot{\delta}}$	First vertical bending mode acceleration due to stabilator acceleration	dimension-less
G_{η_1}	First vertical bending mode acceleration due to stabilator bending	$1/sec^2$
$G_{\dot{\eta}_1}$	First vertical bending mode acceleration due to stabilator bending rate	1/sec
G_{η_2}	First vertical bending mode acceleration due to first vertical bending	$1/sec^2$
$G_{\dot{\eta}_2}$	First vertical bending mode acceleration due to first vertical bending mode rate	1/sec
G_{η_3}	First vertical bending mode acceleration due to stabilator rotation mode	$1/sec^2$
$G_{\dot{\eta}_3}$	First vertical bending mode acceleration due to stabilator rotation mode rate	1/sec
g	Acceleration due to gravity	ft/sec^2

SYMBOLS	DEFINITIONS	UNITS
H (h)	Altitude of the aircraft	ft
H_{α}	Stabilator rotation mode acceleration due to angle of attack	$1/sec^2$
$H_{\dot{\theta}}$	Stabilator rotation mode acceleration due to pitch rate	1/sec
H_{δ}	Stabilator rotation mode acceleration due to stabilator deflection	$1/sec^2$
$H_{\dot{\delta}}$	Stabilator rotation mode acceleration due to stabilator rate	1/sec
$H_{\ddot{\delta}}$	Stabilator rotation mode acceleration due to stabilator acceleration	dimension-less
H_{η_1}	Stabilator rotation mode acceleration due to stabilator bending	$1/sec^2$
$H_{\dot{\eta}_1}$	Stabilator rotation mode acceleration due to stabilator bending rate	1/sec
H_{η_2}	Stabilator rotation mode acceleration due to first vertical bending	$1/sec^2$
$H_{\dot{\eta}_2}$	Stabilator rotation mode acceleration due to first vertical bending rate	1/sec
H_{η_3}	Stabilator rotation mode acceleration due to stabilator rotation mode	$1/sec^2$
$H_{\dot{\eta}_3}$	Stabilator rotation mode acceleration due to stabilator rotation mode rate	1/sec
I_X	Moment of inertia about X axis	$slug\text{-}ft^2$
I_{XZ}	Cross product moment of inertia in XZ plane	$slug\text{-}ft^2$
I_Y	Moment of inertia about Y axis	$slug\text{-}ft^2$
I_Z	Moment of inertia about Z axis	$slug\text{-}ft^2$
K	Slope of the SSAP actuator velocity vs control valve position curve	in/sec/in
K_{BU}	Longitudinal electrical back-up gain	volts/volt

SYMBOLS	DEFINITIONS	UNITS
K_{CS}	Center stick longitudinal force transducer prefilter gain	volts/volt
K_E	Electrical equalization gain	volts/volt
K_F	Longitudinal forward loop variable gain	volts/volt
K_f	Attenuation factor due to rudder flexibility	dimension-less
K_i	SFCS electrical gains, i = 1 through 7	volts/volt
K_M	SSAP Secondary Actuator motor gain	rad/sec/ % Pulse Width
K_{MR}	Slope of the main actuator (Phase IIA, B) velocity vs control valve position curve	in/sec/ in
K_{ny}	Lateral acceleration output gain	volts/volt
K_{NZ}	Normal accelerometer output gain	volts/volt
K_{p_i}	Parameter identifier gains, i=0,1	volts/volt
K_q	Pitch rate gyro output gain	volts/volt
K_r	Yaw rate gyro output gain	volts/volt
K_{SG}	Longitudinal SFCS input gain used in implementation of stall warning	volts/volt
K_{S1}	Stall warning network time constant	sec
K_{SS}	Side stick longitudinal position transducer prefilter gain	volts/volt
K_{sw_p}	Lateral stall warning gain	volts/volt
K_{sw_q}	Longitudinal stall warning gain	volts/volt
K_V	Forward loop gain	volts/volt
K0, K1	Roll to yaw crossfeed gains	volts/volt
k	Ratio of "commanded roll performance" to "applicable roll performance requirement"	dimension-less
L/F	Normal load factor	g
L_p	Rolling acceleration due to roll rate	1/sec

SYMBOLS	DEFINITIONS	UNITS
L_r	Rolling acceleration due to yaw rate	1/sec
L_β	Rolling acceleration due to sideslip angle	$1/sec^2$
L_δ	Rolling acceleration due to total lateral control surface deflection	$1/sec^2$
L_{δ_R}	Rolling acceleration due to rudder deflection	$1/sec^2$
l_n	Distance between cg and normal accelerometer	ft
l_p	Distance from pilot's seat location to aircraft center of gravity	ft
M	Mach number	dimensionless
M_h	Pitch angular acceleration due to change of altitude	$1/sec^3$
M_q	Pitching angular acceleration due to pitch rate	1/sec
M_u	Pitching angular acceleration due to change of forward velocity	$1/sec^2$
M_α	Pitch angular acceleration due to angle of attack	$1/sec^2$
$M_{\dot{\alpha}}$	Pitching angular acceleration due to angle of attack rate	1/sec
M_δ	Pitching angular acceleration due to stabilator deflection	$1/sec^2$
M_{δ_c}	Computed stabilator effectiveness	$1/sec^2$
M_{δ_i}	Computed value of M_δ provided by each channel, i=1, 2, 3, 4	$1/sec^2$
$M_{\dot{\delta}}$	Pitching angular acceleration due to stabilator rate	1/sec
$M_{\dot{\delta}}'$	Pitch angular acceleration due to stabilator rate acceleration	dimensionless
M_{η_1}	Pitching angular acceleration due to the stabilator bending mode	$1/sec^2$

SYMBOLS	DEFINITIONS	UNITS
$M_{\dot{\eta}_1}$	Pitching angular acceleration due to rate of stabilator bending mode	1/sec
M_{η_2}	Pitching angular acceleration due to first vertical bending mode	$1/sec^2$
$M_{\dot{\eta}_2}$	Pitching angular acceleration due to first vertical bending mode rate	1/sec
M_{η_3}	Pitching angular acceleration due to stabilator rotation mode	$1/sec^2$
$M_{\dot{\eta}_3}$	Pitching angular acceleration due to stabilator rotation mode rate	1/sec
m	Mass of the aircraft	slugs
N_a	Number of secondary actuator motors operating - 2, 3, or 4	
N_p	Yawing acceleration due to roll rate	1/sec
N_r	Yawing acceleration due to yaw rate	1/sec
N_Z	Normal load factor	g's
N_{Z_A}	Normal acceleration at accelerometer	g's
N_{Z_i}	Normal acceleration at F.S. = i	g's
N_β	Yawing acceleration due to sideslip angle	$1/sec^2$
N_δ	Yawing acceleration due to total lateral control surface deflection	$1/sec^2$
N_{δ_R}	Yawing acceleration due to rudder deflection	$1/sec^2$
p	Roll rate, the angular velocity of airplane about X axis	rad/sec
p_{FI}	Input to lateral structural filter	volts
p_{FO}	Output of lateral structural filter	volts
p_G	Angular velocity sensed by roll rate gyro	rad/sec
p_N	Normalized roll rate	deg/sec
p_{ssMAX}	Max steady state roll rate	deg/sec

SYMBOLS	DEFINITIONS	UNITS
$\frac{p_{osc}}{p_{av}}$	A measure of the ratio of the oscillatory component of roll rate to the average component of roll rate	dimensionless
q	Pitch rate, the angular velocity of airplane about Y axis	rad/sec
$\bar{q}$	Dynamic pressure	lb/ft^2
r	Yaw rate, the angular velocity of airplane about Z axis	rad/sec
r_G	Angular velocity sensed by the yaw rate gyro	rad/sec
S	Wing area	ft^2
s	Laplace operator	sec
T	Thrust	lbs
$T_{1/2}$	Time for the bank angle to reach 1/2 amplitude	sec
T_2	Time for the bank angle to reach double amplitude	sec
u	Velocity component of the airplane in the X axis	ft/sec
V	Total velocity of the airplane	ft/sec
V_{CAL}	Calibrated airspeed	knots
V_E	Velocity component in earth axis in east direction	ft/sec
V_{GUST}	Velocity of wind gust	ft/sec
V_i	Stall warning voltage schedule break voltages i=0,1,2	volts
V_N	Velocity component in earth axis in north direction	ft/sec
v	Velocity component of the airplane in Y axis	ft/sec
X_α	Longitudinal linear acceleration due to angle of attack	1/sec
X_h	Longitudinal linear acceleration due to change of altitude	$1/sec^2$

SYMBOLS	DEFINITIONS	UNITS
X_o	Projection of the displacement of the lateral accelerometer from the cg onto the X axis in the equation of motion axis system	ft
X_u	Longitudinal linear acceleration due to change of velocity	$1/sec^2$
Y_p	Flight path angular velocity (lateral) due to roll rate	dimensionless
Y_r	Flight path angular velocity (lateral) due to yaw rate	dimensionless
Y_β	Flight path angular velocity (lateral) due to sideslip angle	1/sec
Y_δ	Flight path angular velocity (lateral) due to total lateral control surface deflection	1/sec
Y_{δ_R}	Flight path angular velocity (lateral) due to rudder deflection	1/sec
Y_ϕ	Flight path angular velocity (lateral) due to roll angle	1/sec
Z_h	Flight path angular velocity due to change of altitude	$1/sec^2$
Z_o	Projection of the position of the lateral accelerometer onto Z axis in the equation of motion axis system	ft
Z_q	Flight path angular velocity due to unit pitch rate	dimensionless
Z_u	Flight path angular velocity due to change of forward velocity	1/sec
Z_α	Flight path angular velocity due to unit angle of attack	1/sec
Z_δ	Flight path angular velocity due to stabilator deflection	1/sec
$Z_{\dot{\delta}}$	Flight path angular velocity due to stabilator rate	dimensionless
$Z_{\ddot{\delta}}$	Flight path angular velocity due to stabilator acceleration	sec

SYMBOLS	DEFINITIONS	UNITS
Z_{η_1}, Z_{η_2}, Z_{η_3}	Flight path angular velocity due to deflections of stabilator bending mode, first vertical bending mode, and stabilator rotation	1/sec
$Z_{\dot{\eta}_1}$, $Z_{\dot{\eta}_2}$, $Z_{\dot{\eta}_3}$	Flight path angular velocity due to deflection rates of stabilator bending mode, first vertical bending mode, and stabilator rotation mode, respectively	dimension-less
α	Angle of attack, positive when the reference axis is above the flight path	deg
α_{cp}	Cockpit indicated angle of attack	units
α_{L_i}	Angle of attack sensed by the left angle of attack probe from the first and second output potentiometers, i=1, 2	deg
α_p	Probe angle of attack	deg
α_{pG}	Roll rate gyro sensitive axis angle of attack	deg
α_{rG}	Yaw rate gyro sensitive axis angle of attack	deg
α_{R_i}	Angle of attack sensed by the right angle of attack probe from the first and second output potentiometers, i=1, 2	deg
α_w	Wing angle of attack	deg
α_{WL}	Water line angle of attack	rad
β	Sideslip angle	rad
γ	Flight path angle	rad
Δ	Incremental variation of a given quantity	dimension-less
$\Delta\beta_{MAX}$	Maximum sideslip excursion at the cg occurring within two seconds for a step aileron-control command	deg
δ	Control surface deflection	rad
δ_a	Aileron deflection	rad
δ_{CS}	Center stick longitudinal force transducer output	volts

SYMBOLS	DEFINITIONS	UNITS
δ_R	Rudder deflection	rad
δ_s	Stabilator deflection	rad
δ_{SP}	Spoiler deflection	rad
δ_{SSA}	Aft sidestick longitudinal position transducer output	volts
δ_{SSF}	Forward sidestick longitudinal position transducer output	volts
$\delta_{ST_{MECH}}$	Mechanical input to surface actuator	rad
δ_{TA}	Aft longitudinal SFCS trim wheel output	volts
δ_{TF}	Forward longitudinal SFCS trim wheel output	volts
δ_{VA}	Aft longitudinal vernier wheel output	volts
δ_{VF}	Forward longitudinal vernier wheel output	volts
ϵ	Parameter identifier error signal	volts
ζ	Damping ratio	dimensionless
ζ_d	Damping ratio of the Dutch Roll oscillation	dimensionless
ζ_D	Notch filter denominator damping ratio	dimensionless
ζ_N	Notch filter numerator damping ratio	dimensionless
η_1	Generalized coordinate of stabilator bending mode. Displacement at fuselage station j positive down	dimensionless
η_2	Generalized coordinate of first vertical bending mode. Displacement at fuselage station j positive down	dimensionless
η_3	Generalized coordinate of stabilator rotation mode. Displacement of fuselage station j positive down	dimensionless
η_4	Normal coordinate for fuselage first torsion mode	dimensionless
η_5	Normal coordinate for wing first asymmetric bending mode	dimensionless

SYMBOLS	DEFINITIONS	UNITS
η_6	Normal coordinate for fuselage first lateral bending mode	dimension-less
θ	Pitch angle	rad
$\dot{\theta}_i$	Pitch rate sensed by the red channel and blue channel pitch rate gyros, i=1, 2	volts/deg/sec
$\dot{\theta}_{mj}$	Pitch rate measured at pitch rate gyro fuselage station (j = 383, 179, 313), positive nose up	rad/sec
ρ	Air density	slug/ft^3
τ_D	Time to double amplitude	sec
τ_M	SSAP secondary actuator motor time constant	sec
τ_R	First-order roll mode time constant, positive for stable modes	sec
ϕ	Bank angle	rad
ϕ_G	Roll angle about the longitudinal principal axis	rad
$(\phi_1)_i$	Measured normal acceleration due to stabilator bending mode at fuselage station i	feet
$(\phi_2)_i$	Measured normal acceleration due to first vertical bending mode at fuselage station i	feet
$(\phi_3)_i$	Measured normal acceleration due to stabilator rotation mode at fuselage station i	feet
Ψ	Yaw angle	rad
Ψ_β	Phase angle expressed as a lag for a cosine representation of the dutch roll oscillation in sideslip	deg
ω	Frequency	rad/sec
ω_d	Notch filter denominator frequency	rad/sec
ω_N	Notch filter numerator frequency	rad/sec
ω_n	Undamped natural frequency	rad/sec
ω_1	Center stick longitudinal force transducer prefilter break frequency	rad/sec

SYMBOLS	DEFINITIONS	UNITS
ω_2	Sidestick longitudinal position transducer prefilter break frequency	rad/sec
ω_3	Normal accelerometer output filter break frequency	rad/sec
ω_{ϕ_M}	Frequency at which phase margin is computed (Gain 0 dB, crossover frequency)	rad/sec
$(\partial\phi_1/\partial x)_j$	Slope of the stabilator bending mode shape at fuselage station j	dimension-less
$(\partial\phi_2/\partial x)_j$	Slope of the first vertical bending mode shape at fuselage station j	dimension-less
$(\partial\phi_3/\partial x)_j$	Slope of the stabilator rotation mode shape at fuselage station j	dimension-less
$\partial h_t/\partial\eta_6$	Lateral bending mode shape for η_6, positive right	ft
$\partial\phi_T/\partial\eta_i$	Roll slope per η_i, i=4, 5, 6, positive right wing down	rad
$\partial\Psi_T/\partial\eta_6$	Yaw slope per η_6, positive nose right	rad
% cg	Location of the center of gravity expressed as a percent of the mean aerodynamic chord	dimension-less
1.2/5	Denotes flight condition Mach 1.2, 5000 feet altitude, typical of notation for flight condition identification	Mach number/ Altitude (1000 feet)
$(\cdot)$	First derivative of a variable with respect to time	
$(\cdot\cdot)$	Second derivative of a variable with respect to time	

SECTION I

INTRODUCTION

The Survivable Flight Control System (SFCS) Program is a flight control advanced development program being conducted primarily by MCAIR under contract to the Air Force Flight Dynamics Laboratory. The principal objective of this program is the development and flight test demonstration on an F-4 aircraft of a Survivable Flight Control System utilizing fly-by-wire and power-by-wire techniques.

Recent combat experience has shown that relatively minor damage, in the form of small arms fire, can result in aircraft loss due to loss of control. This is brought about by either hits in the hydraulic distribution system which drain the fluid, or hits which sever or jam the non-redundant mechanical flight control linkages. The power-by-wire concept of integrating electric motor driven hydraulic pumps with the surface actuator reduces system vulnerability through elimination of dependence on long exposed runs of hydraulic plumbing. The fly-by-wire concept of redundant and physically dispersed electrical control channels improves survivability by eliminating the single-failure points of the conventional mechanical control linkages.

The SFCS Program is being performed in two phases. Phase I, which included flight test evaluation of a Simplex integrated actuator package, has been completed and is documented in Reference 1. The Phase II program and objectives are illustrated by Figure 1, and include the development and flight test evaluation of a flight control system employing fly-by-wire and power-by-wire concepts.

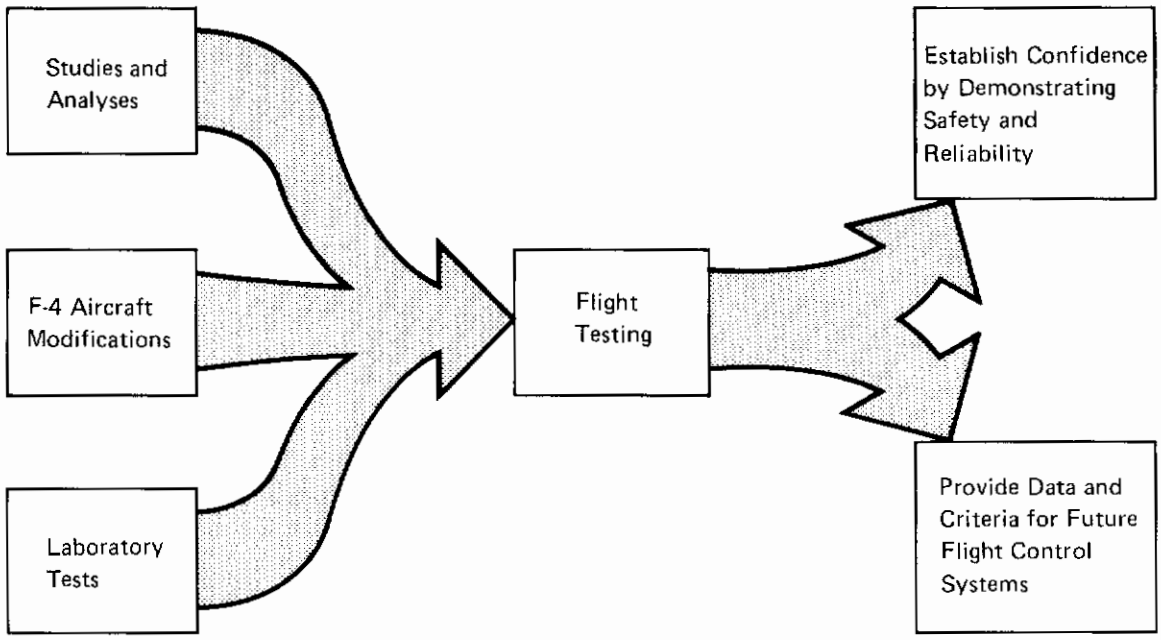

FIGURE 1

PHASE II - PROGRAM AND OBJECTIVES

F-4 WITH SURVIVABLE FLIGHT CONTROL SYSTEM

Fly-by-wire (FBW) is a primary flight control system which uses an electrical signaling path to provide the desired aircraft response to pilot commands, without a mechanical connection between the cockpit controller and the control surface actuator. It can incorporate aircraft motion sensors such that aircraft motion, rather than control surface position, is the controlled variable. To be accepted by the aerospace industry as more than a research tool, the reliability of the FBW system must meet or exceed the reliability of the mechanical system it is replacing, while showing advantages in other areas. The benefits foreseen for an FBW system include:

- o Enhanced survivability
- o Superior aiming, tracking, and weapon delivery
- o Reduced pilot workload
- o Flight control design and installation savings
- o Decreased cost of ownership
- o More airframe design freedom

Power-by-wire (PBW) is the transmission of power from the aircraft engines to the flight control surface actuators by electrical rather than hydraulic means. Hydraulic power is generated by electric motor driven hydraulic pump(s) integral to the actuators. Power-by-wire equipment has been called "integrated actuator packages" in this country, and simply "packaged actuators" in England.

The redundancy and dispersion of a fly-by-wire system and the get-home-and land capability provided by an actuator with an emergency-only electric motor driven pump could be combined to provide a measurable improvement in flight control survivability. An F-4 Simplex Actuator Package with this emergency-only PBW capability was successfully flight tested in Phase I of the SFCS Program, with results reported in Reference 1. However, a survivable flight control system requires use of power-by-wire integrated actuator packages which are capable of full-time operation independent of the aircraft central hydraulic systems and their exposed plumbing. The Survivable Stabilator Actuator Package (SSAP) to be flight tested in Phase IIC of the SFCS Program will be a duplex PBW actuator capable of full-time operation throughout the F-4 flight envelope. The SSAP will be controlled by the fly-by-wire system installed and flight tested in Phases IIA and IIB of the program.

The location of the fly-by-wire system components, the SSAP, and the other SFCS equipment in the F-4 test aircraft is shown in Figure 2.

The results of the SFCS studies and analyses to date, and the definition of the SFCS approach are presented in the basic report. The details of the Control Law Development Studies are presented in this supplement. The details of the Control Criteria and Hydraulic Power and Actuation Studies are presented in report supplements 1 and 3, respectively.

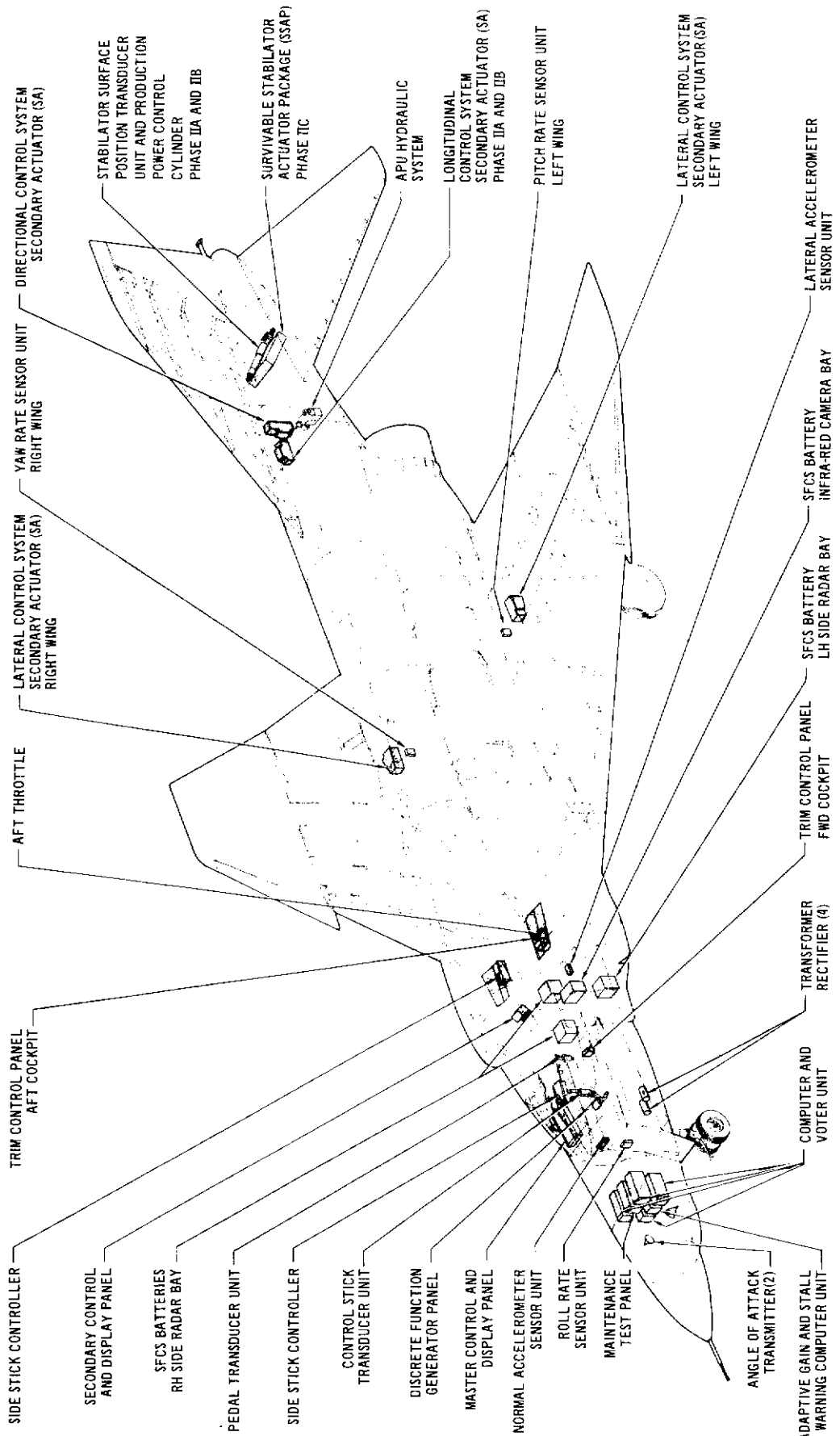

FIGURE 2
SFCS EQUIPMENT LOCATION

SECTION II

SUMMARY

The SFCS will utilize fly-by-wire control of all primary flight control surfaces. Applied pilot inputs will command aircraft motion rather than surface position. Improved control response characteristics are expected throughout the flight envelope. Improved stability characteristics also are expected through the use of feedback control, proper placement of aircraft motion sensors, and the application of structural mode filters to attenuate aircraft resonant frequencies.

An adaptive gain changer is planned to be implemented in the SFCS to provide automatic gain changing in the pitch and yaw axes as a function of stabilator effectiveness. The gains in the roll to yaw interconnect are also programmed as a function of stabilator effectiveness to obtain improved turn coordination and aiming accuracy at all flight conditions. The automatically selected gain values were chosen to partially compensate for the normal changes in surface effectiveness which occur as a function of flight condition. The total gain variation was restricted to obtain adequate attenuation at airframe resonant frequencies. Provisions for manual selection of each of the variable gains are also included.

The longitudinal and lateral-directional control laws were initially implemented to comply with the requirements of MIL-F-8785B (ASG) and the C* criterion. A handling qualities criteria development program was conducted concurrently with the control law development effort and is reported in Supplement I to TR-71-20. The control law mechanization was subsequently evaluated against the proposed handling quality criteria. The results of this evaluation, which show compliance in all essential parameters, are included herein.

A six-degree-of-freedom man-in-the-loop simulation program was conducted to evaluate the control law implementation. This simulation included the capability to maneuver the aircraft throughout the F-4E flight envelope including stall and post stall conditions. As a result of this simulation, eight design modifications were identified and evaluated. These modifications were subsequently implemented into the SFCS design.

The longitudinal and lateral-directional control law development studies, manned simulation results, and conclusions relative to these studies and simulations are presented in the following sections.

SECTION III

LONGITUDINAL CONTROL LAW DEVELOPMENT

1. SYSTEM DESCRIPTION

The functional block diagram of the SFCS longitudinal control system is presented in Figures 3 and 4. The block diagram depicts the longitudinal SFCS as configured for the Phase IIA portion of the flight test program.

a. Normal Mode

The longitudinal control system is a fly-by-wire system in which aircraft motion is the controlled parameter. This is accomplished by utilizing normal acceleration and pitch rate feedbacks which are subtracted from the center stick force transducer commands and the side stick position transducer commands to obtain an error signal. The error signal is used as a position command for the stabilator actuator.

The Normal mode of operation provides neutral speed stability (NSS) for all nonterminal flight phases. Since the speed stability is neutral, no steady state pilot applied stick force or trim input is required in order to compensate for the change in stabilator position required to trim the airplane due to changes in airspeed and/or altitude. An interconnect with the nose gear position switches removes the function which provides the neutral speed stability when the landing gear are lowered. The pilot may also override the neutral speed stability function using the mode select switch.

The neutral speed stability characteristic is obtained by generating an integration in the forward path of the control system. The integration maintains zero steady-state error between force command and the blended pitch rate and normal acceleration feedback. The airplane is kept in trim since any uncommanded pitch rate and acceleration is automatically reduced to zero by the action of the integrator. For nonterminal flight conditions, only occasional trim inputs initiated by the pilot are required to offset any electrical biases which may be present. Since the integration function is removed when the landing gear are extended, nominal trimming action by the pilot will be required during terminal flight phases.

The secondary actuator is used to provide the integration function. This is accomplished by incorporating washout circuits in the secondary actuator ram position and main actuator ram position feedback signals, which transform the position feedbacks into velocity feedbacks for low frequency inputs ($\omega < 1$ rad/sec).

b. Electric Back-Up Mode

The control system includes an electric back-up mode which consists of a simple forward path connecting the longitudinal force input pre-filter to the secondary actuator. In order to minimize transients, selection of electric back-up mode by the pilot causes the

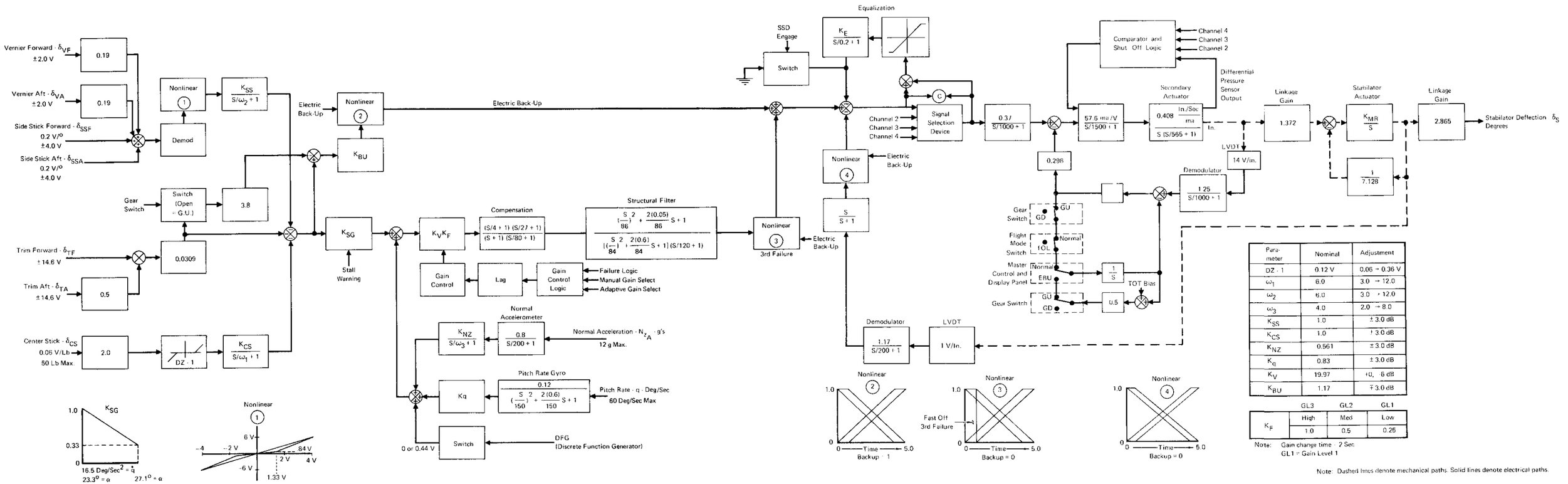

Parameter	Nominal	Adjustment
DZ · 1	0.12 V	0.06 → 0.36 V
ω_1	6.0	3.0 → 12.0
ω_2	6.0	3.0 → 12.0
ω_3	4.0	2.0 → 8.0
K_{SS}	1.0	± 3.0 dB
K_{CS}	1.0	± 3.0 dB
K_{NZ}	0.561	± 3.0 dB
K_q	0.83	± 3.0 dB
K_V	19.97	+0, -6 dB
K_{BU}	1.17	∓ 3.0 dB

K_F	GL3	GL2	GL1
	High	Med	Low
	1.0	0.5	0.25

Note: Gain change time - 2 Sec
GL1 = Gain Level 1

Note: Dashed lines denote mechanical paths. Solid lines denote electrical paths.

FIGURE 3
LONGITUDINAL SFCS (PHASE IIA, B) FUNCTIONAL BLOCK DIAGRAM

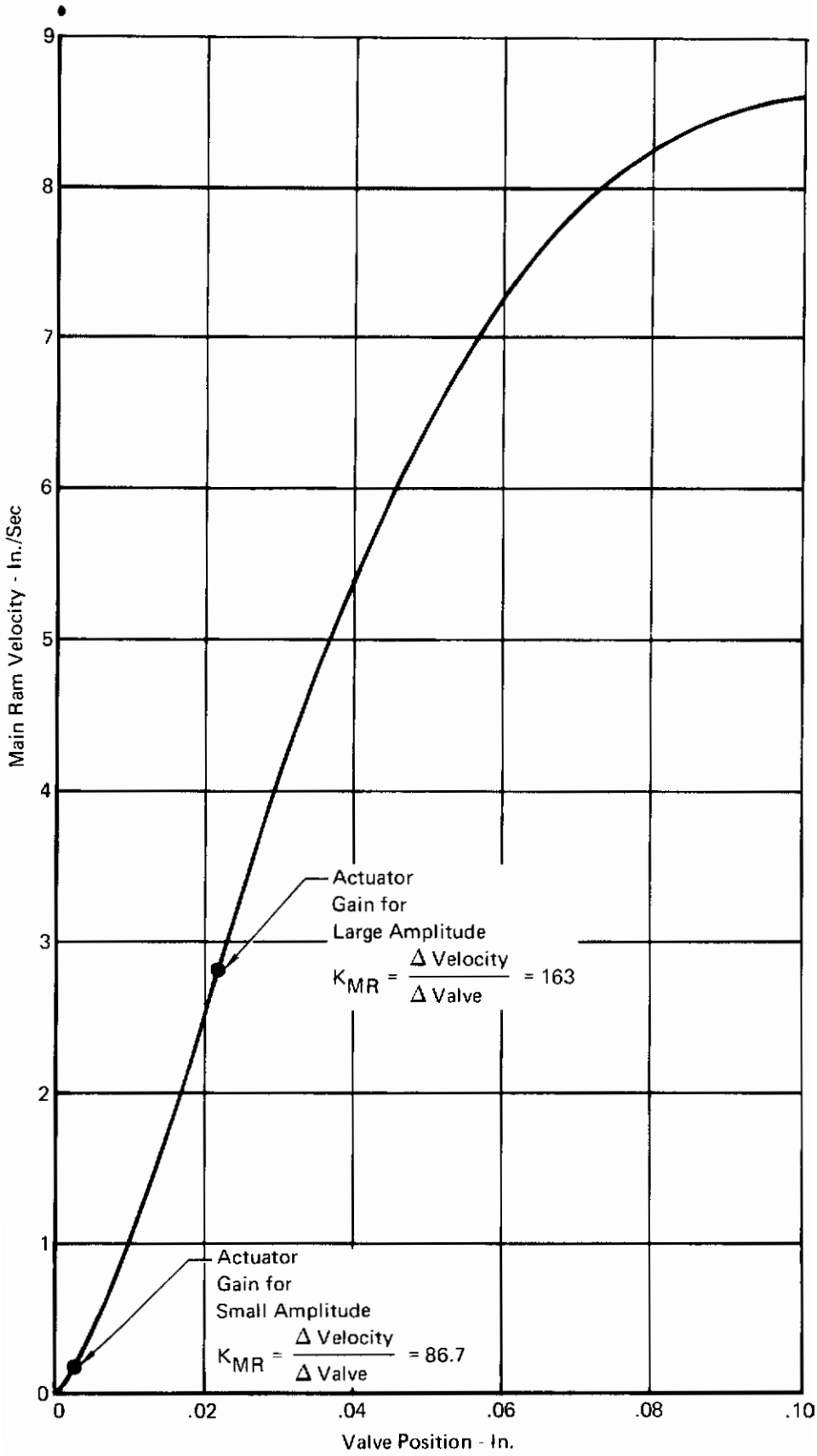

FIGURE 4
STABILATOR ACTUATOR VELOCITY (PHASE IIA, B)

direct electric path to be faded in (Nonlinear 2) as the normal SFCS forward path is faded open (Nonlinear 3). The actuator main ram electrical feedback path is also simultaneously faded open (Nonlinear 4).

c. Adaptive Gain Changing

Pilot selection of adaptive gain changing or fixed gain operation is available. The adaptive gain changer provides 3 gain states in the longitudinal axis which change the forward loop gain, K_F, over a range of 4 to 1 as the aircraft stabilator effectiveness parameter, M_δ, varies due to flight condition and aircraft configuration changes as shown in Table I. By selecting fixed gain operation, the pilot may manually select either K_F=.25, .5 or 1. The system is configured to provide stable operation over the entire flight envelope for the lowest gain value of K_F=.25.

TABLE I
ADAPTIVE GAIN VALUES

M_{δ_c}	K_F
$M_{\delta_c} < 10$	$K_F = 1$ (HI)
$10 \leq M_{\delta_c} \leq 20$	$K_F = 0.5$ (MID)
$M_{\delta_c} > 20$	$K_F = 0.25$ (LO)

Adaptive gain operation may be selected only if the manual gain select switch is first placed in the low gain position. Repositioning of the manual gain select switch after selection of adaptive gain operation causes disengagement of the adaptive gain changer and reversion to fixed gain operation.

A functional block diagram of the gain changer (Parameter Identifier) is provided in Figure 5. The function of the gain changer is as follows:

- The voltage controlled oscillator develops an interrogator signal consisting of a 4Hz sine wave with a nominal duty cycle of 1.5 seconds on and 15 seconds off. The amplitude of the signal is controlled by a feedback of computed pitch acceleration to provide a relatively constant value of actual aircraft pitch acceleration within limits set for computational ability and pilot detection level.

- The interrogation signal is fed to the pitch servo amplifiers to produce an aircraft pitch rate, $\dot{\theta}$. The measured $\dot{\theta}$ output of one of the pitch rate gyros is passed through a bandpass filter which provides a value of pitch acceleration, $\ddot{\theta}$, at 4Hz.

- The interrogation signal is also fed to a model of the pitch actuator which computes the value of stabilator deflection, δ, which will be seen if all but the 4Hz components are filtered out.

- The 4Hz δ signal is multiplied by the computed value of stabilator effectiveness, M_{δ_c}, so that an error signal $\varepsilon = \ddot{\theta} - M_{\delta}\delta$ may

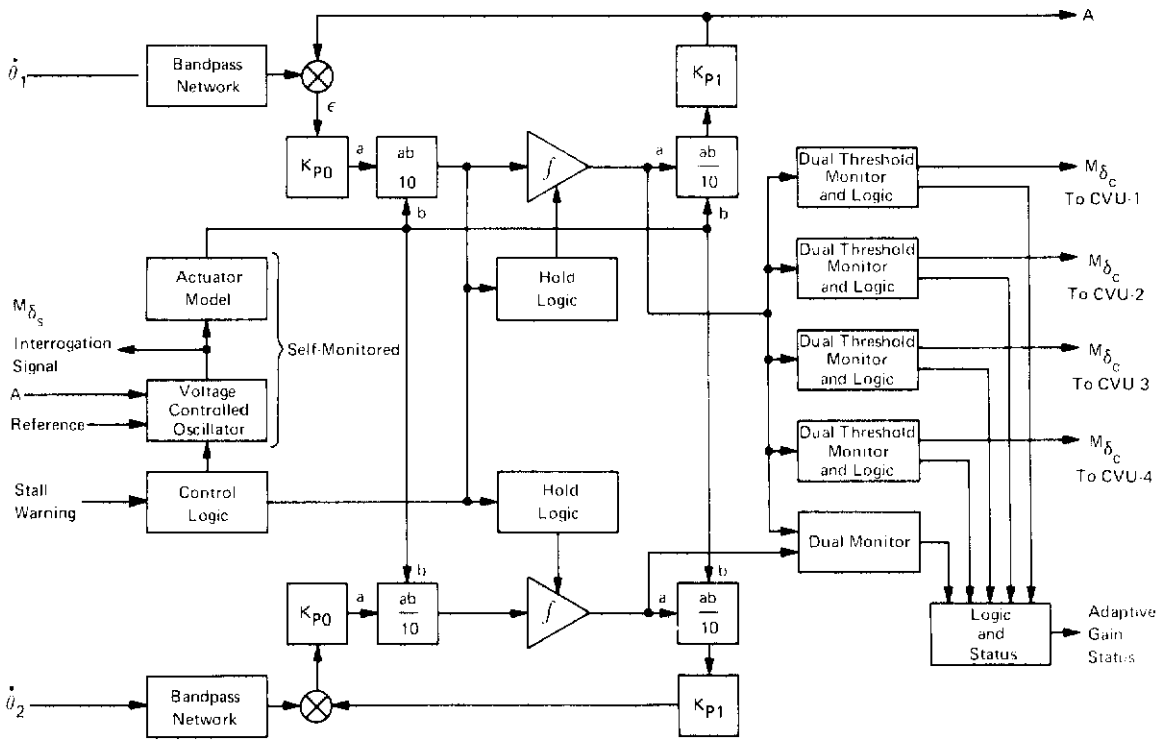

FIGURE 5
ADAPTIVE GAIN CHANGER FUNCTIONAL BLOCK DIAGRAM

be computed. This error signal is also multiplied by the 4Hz δ signal to provide the proper sign for use in the computation of M_{δ_c}.

- The δ x ε signal is used as the input to an integrator which provides as its output the value of M_δ which will satisfy the equation $\ddot{\theta} = M_\delta \delta$. This equation is a good approximation at the 4Hz frequency.

- Level detectors determine the range of values of M_δ in which the aircraft is being operated and provide output signals to set the pitch forward loop, yaw rate, and roll to yaw crossfeed gains. Under normal circumstances the use of a clean δ signal provides a good correlation function and allows rapid, accurate computation of M_{δ_c}. Thus a rather wide variation in M_δ can be accommodated within the 1.5 sec computation time, even in the presence of severe gusts or pilot input commands. In the event that M_δ is changing very rapidly over a large range, such as in a powered dive, the δ x ε signal will hold the control logic on until the product is below a preset value of error. An activity monitor detects the output of the actuator model and shuts off the computer if a full period (16.5 sec) of activity is encountered.

d. Stall Warning System

A functional block diagram of the stall warning system is presented in Figure 6. The stall warning system provides stick force cues to the pilot when the region of impending accelerated stall is entered. The warning becomes increasingly more pronounced with progression into the stall region. This is accomplished by decreasing the electrical gradient through which the stick force transducer and the Side Stick Controller (SSC) outputs are passed prior to the point at which they are summed with the sensor feedback signals. Thus, the pilot applied maneuvering force for either center stick or SSC must be increased in order to maintain a given maneuver if the maneuver causes entry into the stall region. The warning signal is initiated at 23.3° angle of attack and linearily increases to a maximum at 27.1° angle of attack, at which point, the stick force electrical gradient, K_{cs}, (Figure 3) is correspondingly decreased to one-third its nominal value. Cancelled pitch rate is used to generated a stall anticipatory signal. This signal, which is proportional to pitch angular acceleration, activates the stall warning system at 16.5 deg/sec^2 and provides full warning output at 24 deg/sec^2 for zero angle of attack. The angle of attack signals and cancelled pitch rate signals are summed through appropriate gains so that any combination of angle of attack and positive pitch acceleration which satisfy the equation, $\alpha + 1.41\ddot{\theta} \geq 23.3$, will activate the stall warning system. In order that negative pitch accelerations will not cause deactivations of the stall warning when $\alpha \geq 23.3$, only positive pitch accelerations are used. Appropriate filtering is applied to the summed acceleration and angle of attack signals to prevent momentary variations in signal caused by air turbulence from actuating the stall warning system.

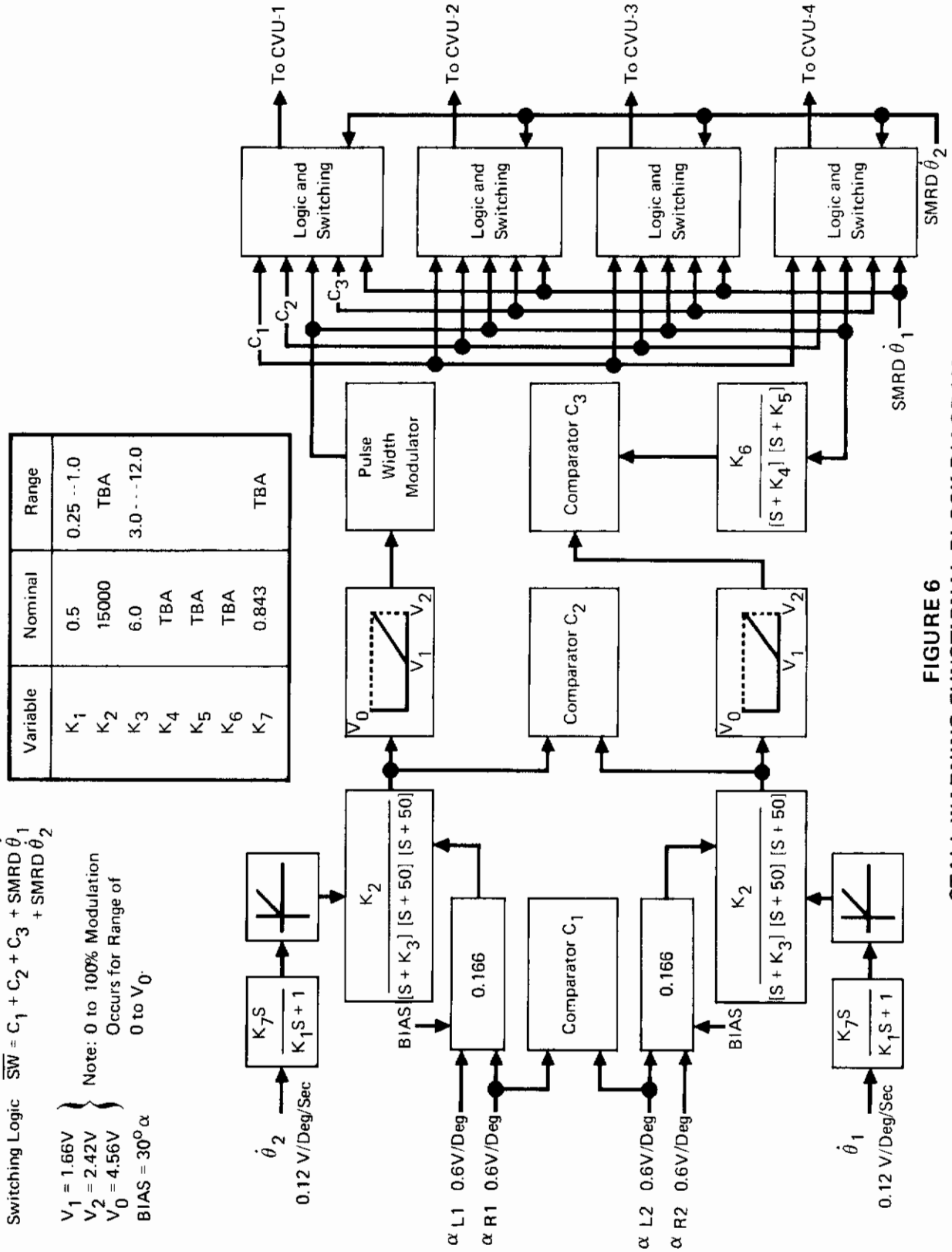

Variable	Nominal	Range
K_1	0.5	0.25 - - 1.0
K_2	15000	TBA
K_3	6.0	3.0 - - 12.0
K_4	TBA	
K_5	TBA	
K_6	TBA	TBA
K_7	0.843	

FIGURE 6
STALL WARNING FUNCTIONAL BLOCK DIAGRAM

2. SYSTEM SYNTHESIS

a. Guidelines and Assumptions

Early in the SFCS longitudinal control law development effort a design approach was formulated and certain guidelines and assumptions were delineated to provide a logical starting point for the system design. Listed below are those guidelines and assumptions for the SFCS control laws:

- o Selectable neutral speed stability must be provided.
- o Pilot selection of fixed or adaptive gains must be provided.
- o The system will use blended normal acceleration and pitch rate feedback.
- o A filter would probably be incorporated to attenuate the aircraft structural modes.
- o The system should be designed to accommodate the Phase IIC stabilator actuator (SSAP) with a minimum of modification to the electronics and control laws.
- o Switching of sensor feedback signals should be avoided if possible and switching internal to the control and feedback paths should be minimized.
- o The system should provide safe and acceptable performance throughout the flight envelope with a single fixed gain.
- o All requirements of the Statement of Work should be met to the maximum extent possible.
- o The capability to trim the aircraft into constant altitude turns is desirable.
- o All components should be math modeled to represent the actual component properties as closely as practicable.

Figure 7 presents a summary of the stability and response guidelines used in the design and evaluation of the longitudinal SFCS.

(1) Handling Qualities Criteria Time History Response Guidelines

Since the SFCS control performance criteria study was still in work during the formative stages of the longitudinal design, the decision was made to utilize the C* criteria of Reference 1 as a guideline and then to evaluate the SFCS responses relative to the new criteria when they became available. The response envelopes given in Figure 7 are the MCAIR revised C* criteria described in Supplement 1 of this report. All responses were evaluated relative to the revised criteria throughout this supplement. Additionally, the Level 1 requirements of MIL-F-8785B(ASG) for short period frequency, damping ratio, and stick force per g were used as guidelines.

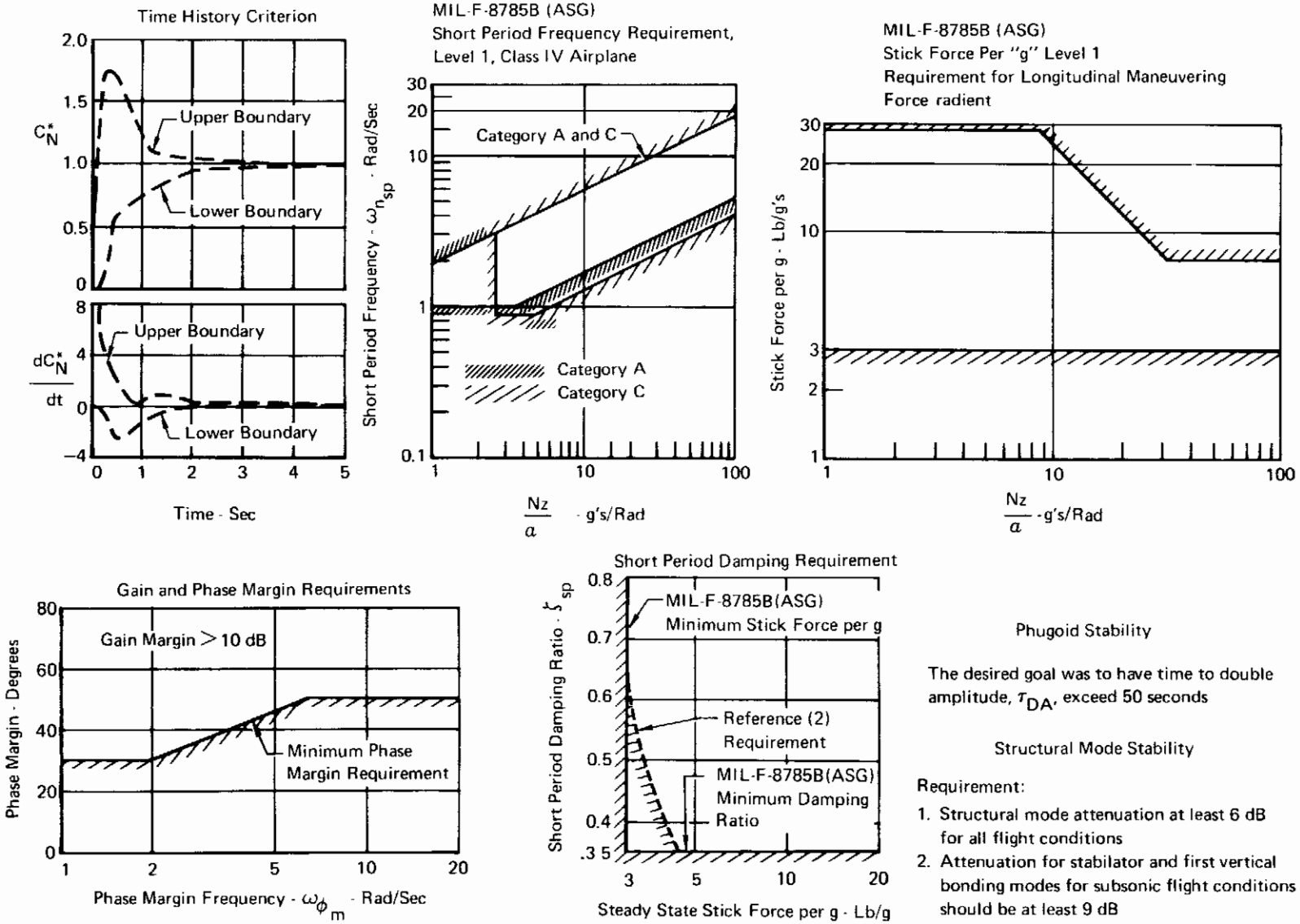

Phugoid Stability

The desired goal was to have time to double amplitude, τ_{DA}, exceed 50 seconds

Structural Mode Stability

Requirement:

1. Structural mode attenuation at least 6 dB for all flight conditions
2. Attenuation for stabilator and first vertical bonding modes for subsonic flight conditions should be at least 9 dB

FIGURE 7
LONGITUDINAL SFCS DESIGN REQUIREMENTS

Reference 2 presents in a combined plot the MIL-F-8785B (ASG) short period damping ratio requirement (Paragraph 3.2.2.1.2) and dynamic stick force per g requirement (Paragraph 3.2.2.3.1). The solid lines of Figure 7 represent the boundaries for short period damping ratio and steady state stick force per g established by MIL-F-8785B (ASG). The dashed line of Figure 7 represents the relationship between short period damping and steady-state stick force per g as presented in Reference 2 by inclusion of the MIL-F-8785B (ASG) requirements for dynamic stick force per g . This criterion was also imposed as a design guideline.

(2) Stability Guidelines

Stability guidelines for the SFCS design were established for the three frequency ranges which contain the aircraft and control system oscillatory modes: namely, the aircraft phugoid mode, $\omega < .3$ radians/second; the aircraft short period and control system modes, $.3 < \omega < 50$ radians/second; and the aircraft structural modes, $50 < \omega < 200$ radians/second.

The desirability of stable phugoid at all flight conditions is recognized; however, the phugoid mode stability guideline did not prohibit phugoid mode instability. The requirement was that any phugoid instability have a time to double amplitude of at least 50 seconds when computed using small perturbation aircraft equations of motion. Phugoid instabilities are barely noticeable when the time to double amplitude is 50 seconds or greater.

The guidelines for the aircraft short period and control system modes were that the system should exhibit at least 10 db gain margin at all flight conditions and that phase margins of at least 50 degrees at high $\bar{q}$ flight conditions and 30 degrees at low $\bar{q}$ flight conditions should be maintained. The phase margin guideline was later refined to coordinate the phase margin requirement with the frequency at which the system would oscillate if an instability were induced by increased phase lags. Figure 7 presents this criterion in graphic form. As can be seen from Figure 7, a phase margin of 50° is required for frequencies equal to or greater than 6.28 radians per second (1 Hz). A phase margin of 30° is allowed for frequencies below 2 rad/sec (.32 Hz). The direct dependence of the phase margin requirement with flight condition is eliminated; however, it should be noted that the frequencies associated with high $\bar{q}$ flight conditions will, in general, be higher than those associated with the low $\bar{q}$ flight conditions. Thus the original requirement for 50° phase margin at high $\bar{q}$ and 30° phase margin at low $\bar{q}$ is, in general, maintained. Nonlinearities in components such as the actuator have a diminishing effect at lower frequencies.

The structural mode stability guideline was that all structural mode amplitudes should be attenuated by a minimum of 6 dB. The normal gain and phase margin requirements specify a minimum attenuation at the point where the phase angle reaches -180° or any odd multiple thereof, and a minimum phase margin when the gain reaches 0 dB. A requirement for gain margin would, therefore, allow any amount of structural mode peaking so long as the gain margin requirement is met when phase is -180°.

The guideline used in the SFCS design is more stringent and requires that structural modes be attenuated by at least 6 dB regardless of phase angle. F-4 experience indicates that structural mode stability during subsonic flight is of more significance than during supersonic flight. Occurrence of F-4 structural mode resonance has been confined to subsonic flight and to the modes between 70 and 100 radians per second. This knowledge of the F-4 experience led to the additional requirements that a minimum of 9 dB attenuation would be maintained for those structural modes between 70 and 100 rad/sec at subsonic flight conditions.

b. Feedback Configuration

Both pitch rate and normal acceleration feedbacks were assumed to be required at the outset of the control law development studies. Normal acceleration feedback is needed in order to reduce the steady state stick force per g variation with aircraft velocity. This is readily apparent by inspection of the stick force per g curves of Figure 8. This figure shows the variation in force per g with aircraft velocity for pitch rate feedback only and for normal acceleration to pitch rate feedback ratios of 4.5:1, 6:1, and 9:1. The configurations using pitch rate feedback alone exhibit stick force per g characteristics which vary from 47.2 to 4.7 lb/g. The extremely large stick force per g values at low aircraft velocities are of course totally unsatisfactory.

The addition of normal acceleration feedback eliminates the wide variation in stick force per g . The higher normal acceleration to pitch rate feedback ratios provides the least variation in force per g gradient. However, the lowest ratio, 4.5:1, easily meets the stick force per g requirements of MIL-F-8785B (ASG).

Normal acceleration feedback, while greatly enhancing the stick force per g properties, has a tendency to reduce system stability margins at some flight conditions. Figure 9 provides an example of the deterioration in phase margin which occurs during high speed, low altitude flight as the normal acceleration to pitch rate ratio is increased from 4.5:1 to 9:1. A penalty of 28% reduction in phase margin would be experienced if a blend ratio of 9:1 were chosen instead of 4.5:1 ratio. For this reason, a ratio of 4.5:1 was selected for the SFCS.

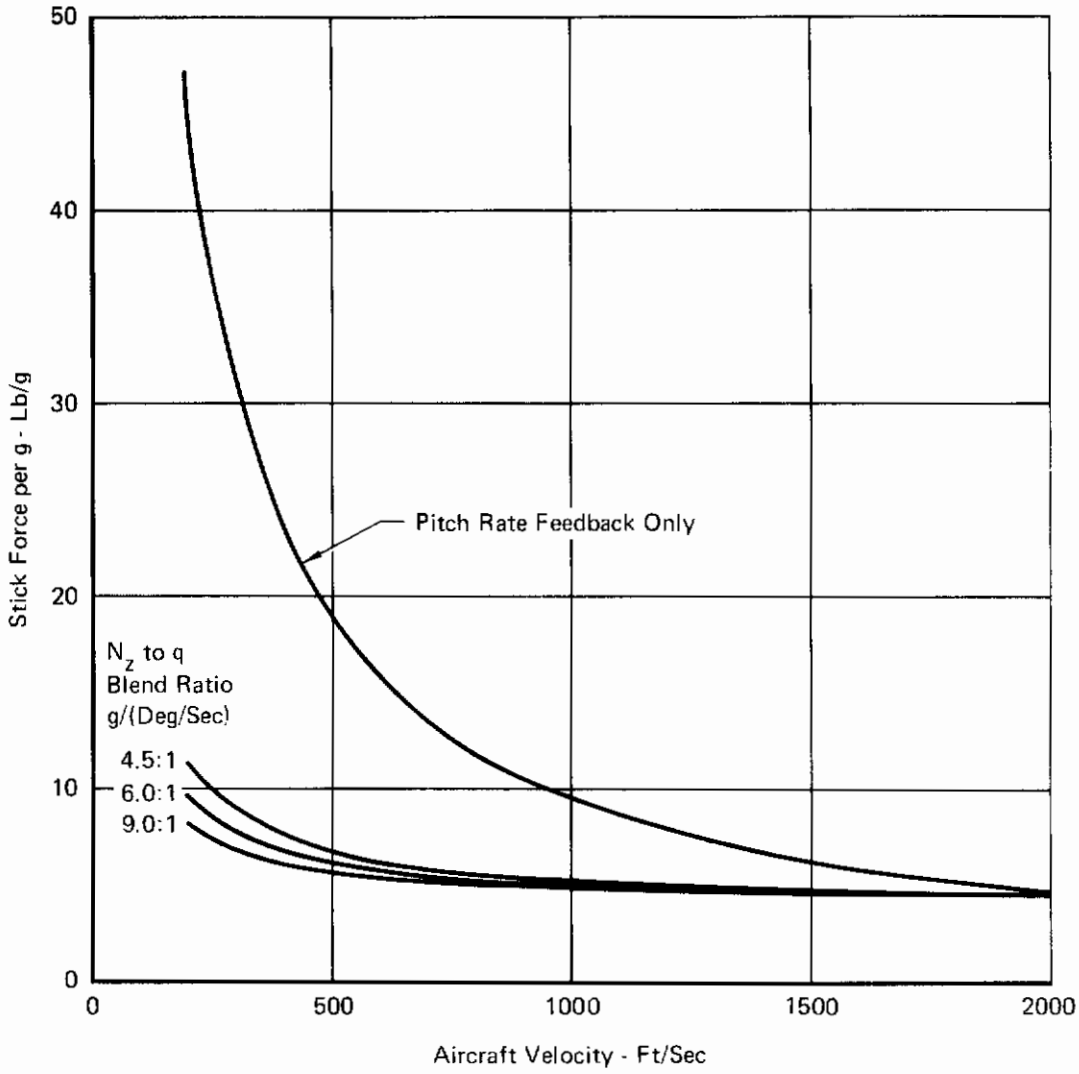

FIGURE 8
STICK FORCE PER g FOR VARIOUS N_z TO q FEEDBACK BLEND RATIOS

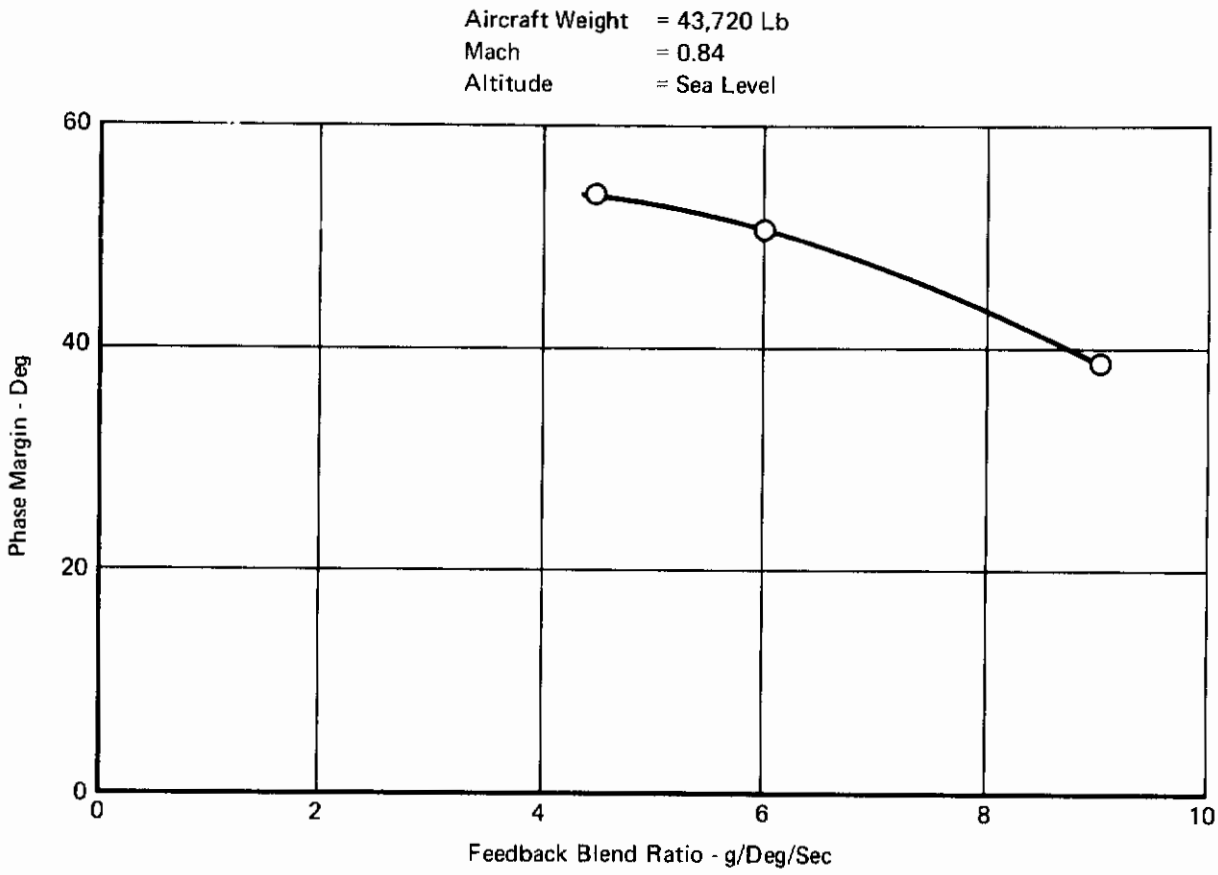

FIGURE 9
PHASE MARGINS FOR VARIATIONS OF THE FEEDBACK BLEND RATIO

The normal accelerometer output is passed through a first order lag filter prior to the point where it is summed with the pitch rate gyro signal. The lag was originally incorporated primarily to reduce structural mode pickup from the accelerometer. Studies showed that this network also has a significant contribution to improvement in the SFCS response characteristics when the break frequency, ω_3, is properly placed. C* time history response plots and stability margins for two flight conditions with the fixed, low gain selected are shown in Figures 10 through 12 for 4 values of ω_3 ranging from 1 to 8 rad/second. The fixed, low forward loop gain values were used for this evaluation in lieu of the other selectable or adaptive gains in order to isolate the effectiveness of the lag alone in shaping the C* response. The higher system bandwidth provided by the selectable gain values will, of course, improve the speed of response at all low $\bar{q}$ flight conditions. For this reason, no particular significance should be attached to whether a particular value of ω_3 causes the response to fall entirely within the envelope. The relative improvement which can be achieved by using the proper value for ω_3 is the significant factor. As shown in Figure 10, the responses for ω_3=2 and 4 exhibit the best characteristics of the 4 lags shown for the Mach.5

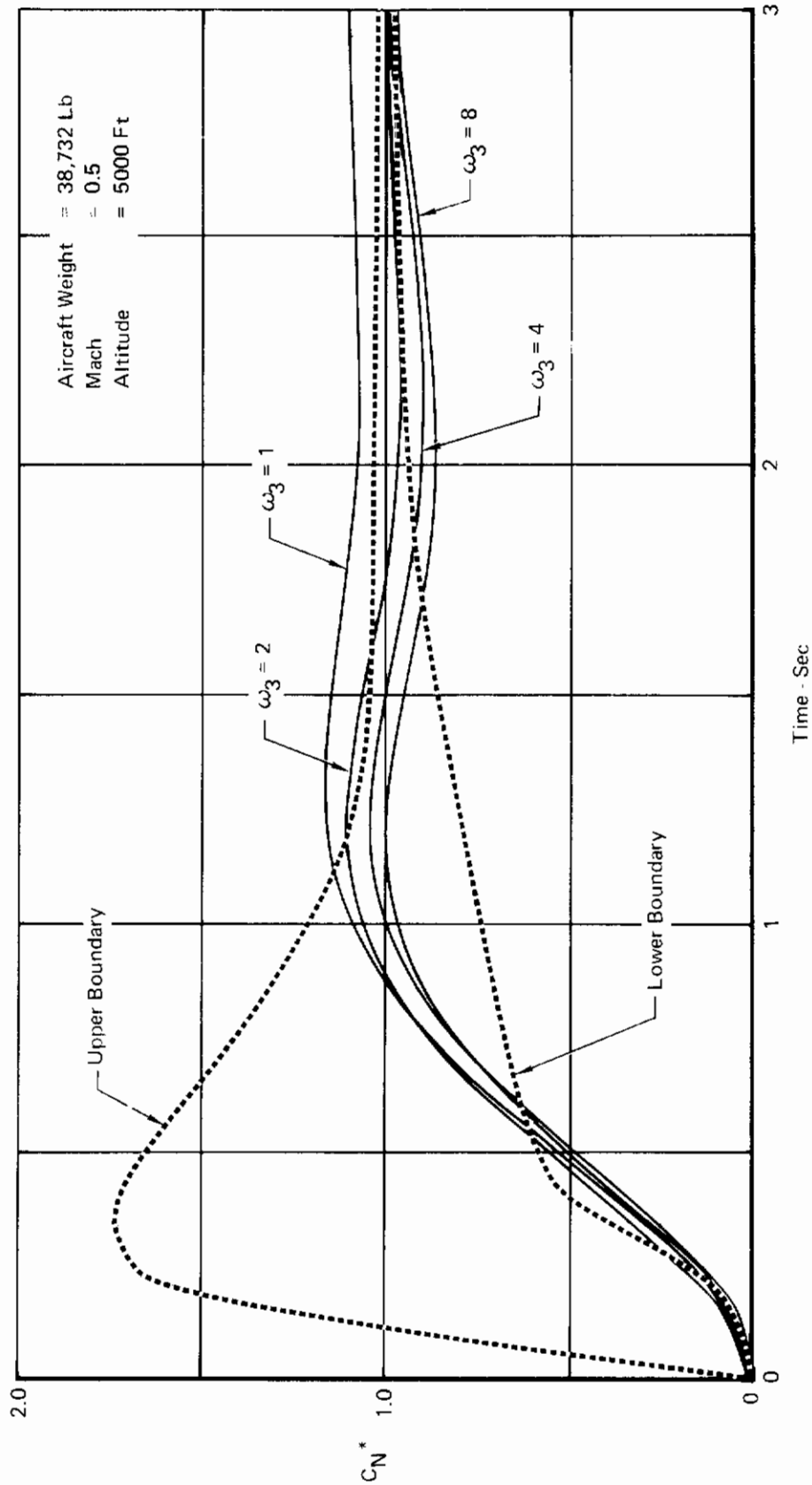

FIGURE 10
EFFECT OF N_Z LAG ON C* RESPONSE
NSS, $K_F = 0.25$

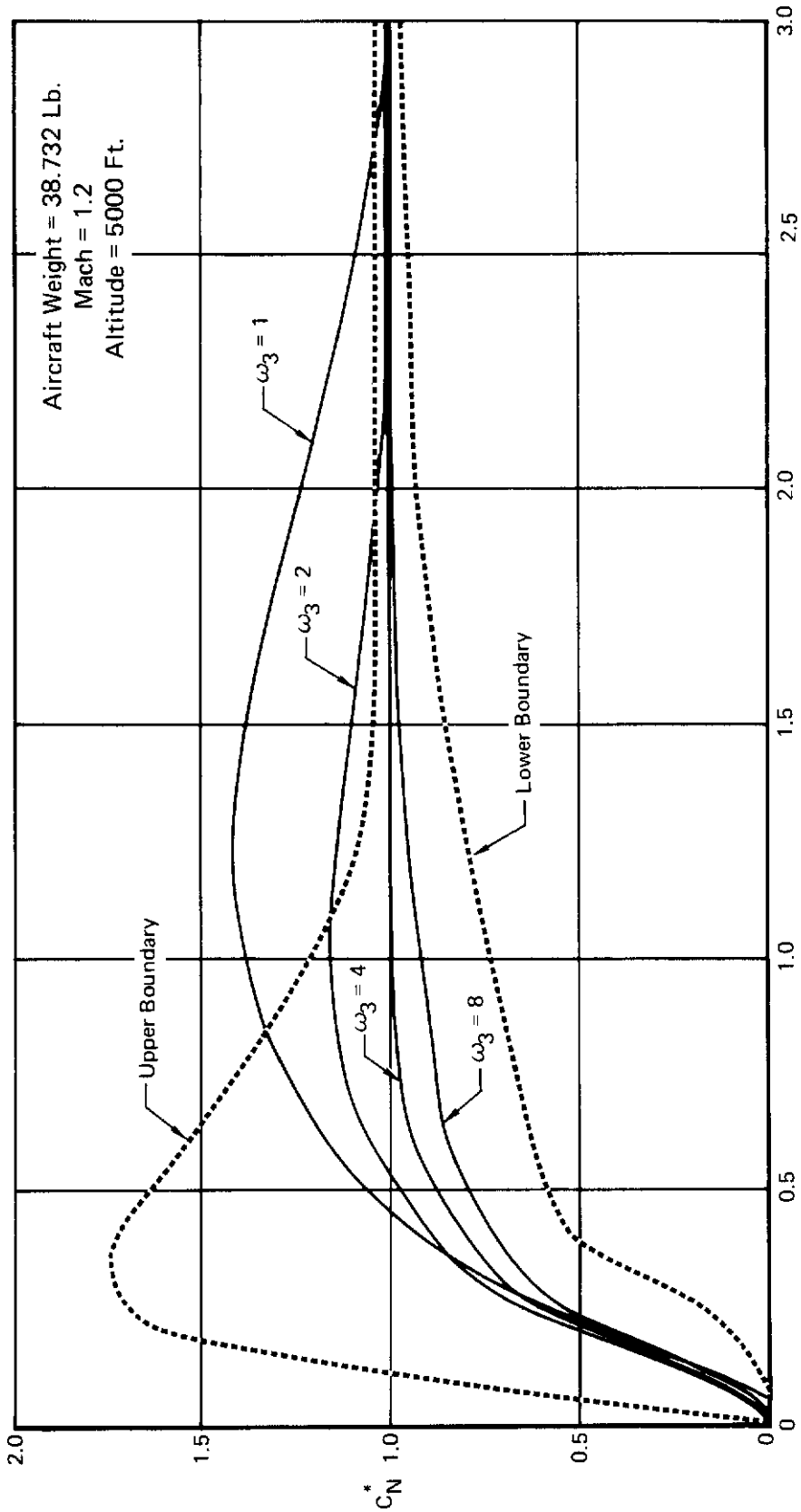

FIGURE 11
EFFECT OF N_Z LAG ON C* RESPONSE
NSS, $K_F = 0.25$

Aircraft Weight = 38,732 Lb
Mach = 0.5 Normal Mode
Altitude = 5,000 Ft K_F = 0.25

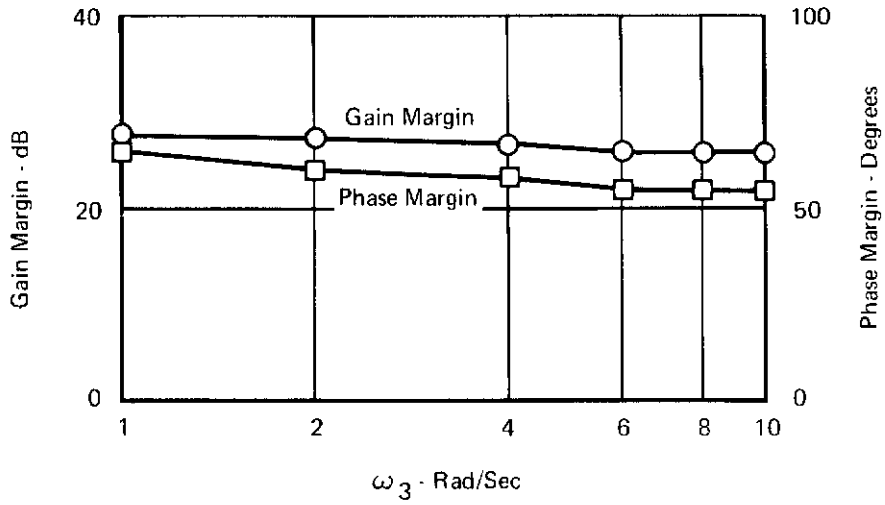

Aircraft Weight = 38,732 Lb
Mach = 1.2 Normal Mode
Altitude = 5,000 Ft K_F = 0.25

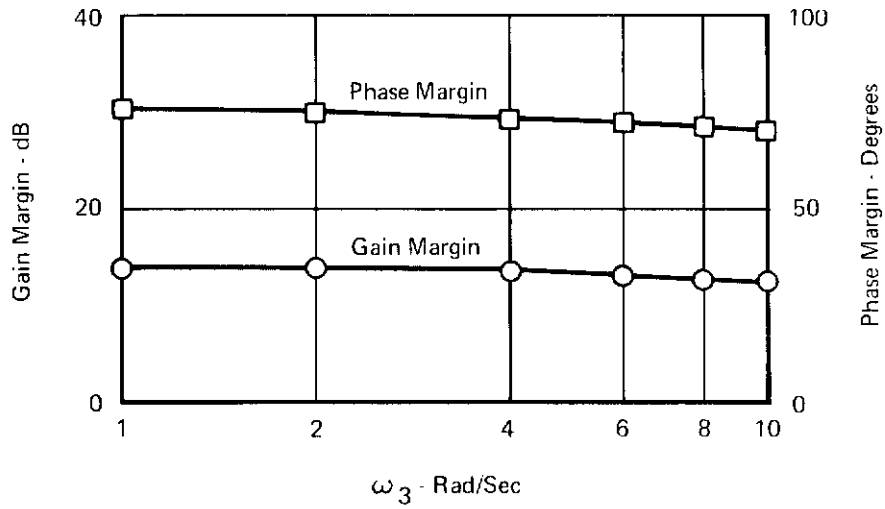

FIGURE 12
STABILITY MARGINS FOR VARIOUS
NORMAL ACCELEROMETER LAG VALUES

5000 ft. altitude flight condition. With ω_3=1, an undesirably long time constant overshoot resembling a steady state offset exists. At the other extreme, ω_3=8, there exists a similar undershoot characteristic. Examination of the comparable responses for Mach 1.2 5,000 ft. altitude shown in Figure 11 reveals that ω_3=1 and 2 produce undesirable ballooning overshoot in the C* response. For ω_3=4 and 8 the system has good response properties; however, ω_3=4 appears to be the better of the two. Since values of ω_3 less than 4 produce unacceptable responses for Mach 1.2, 5,000 ft. altitude, and values of ω_3 greater than 4 are unacceptable for Mach = .5, 5,000 ft. altitude, the normal accelerometer lag filter break frequency was set at 4 rad/sec.

The C* time histories referenced above were taken from the data of Appendix III, which also includes time histories for seven other aircraft parameters for each value of ω_3.

c. Forward Loop Configuration

The premise upon which the SFCS and most high-gain control systems are designed is that desirable response characteristics can be achieved by maintaining the closed loop bandwidth at a high value and passing the input command through an electrical model whose output response shape represents the desired aircraft response. In this way, the aircraft gain variations, which occur due to flight condition change, weight change, etc., do not significantly degrade aircraft response characteristics. Stability considerations usually force a somewhat compromised application of this basic principle. For example, the bandwidth is directly proportional to gain. The maximum gain which can be allowed is, in turn, a direct function of the amplitude of the aircraft structural modes and the structural filtering phase lag which can be tolerated.

The SFCS design goal was to design a high gain adaptive control system which can also effectively and safely control the aircraft at all flight conditions with one fixed gain value.

The problem was approached by first defining and documenting the performance of the fixed gain system, while incorporating the structural filtering required for satisfactory margins for operation with the higher adaptive gains.

In order to provide the wide closed loop bandwidth desired for satisfactory response characteristics, it is necessary to maintain the open loop bandwidth as wide as possible. The aircraft gain varies with flight condition, so the system bandwidth varies with flight condition for fixed gain operation. A design goal of 10-12 rad/sec open loop bandwidth at the highest M_δ flight conditions was selected as being attainable. Thus, the open loop gain should

have a 0 dB crossover frequency of 10-12 rad/sec. Bode design criteria indicate that the slope of the gain curve at the 0 dB crossover frequency should be 6 dB per octave (Reference 3). In order to maintain the 6 dB per octave slope and fulfill the 10 dB gain margin requirement, the frequency at which the open loop phase angle crosses the -180° point must be removed by 1 1/2 octaves from the 0 dB crossover frequency. This establishes that the -180° phase angle crossover frequency must occur in the range of 30-36 rad/sec.

The feedback configuration was established in Paragraph 2b above. Frequency responses of the airframe and feedback portion of the control system were computed for several flight conditions. From these data, it was found that for frequencies of 30 rad/sec. and above, the phase lag from the airframe and feedback of the system is essentially independent of flight condition. For example, at 35 rad/sec., the phase lag is $-102° \pm 2°$ for all flight conditions examined. There is significant phase variation with flight condition for frequencies below 30 rad/sec; the phase is as high as -90° at 10 rad/sec for many flight conditions. Therefore, in order to maintain 50° phase margin at 10 rad/sec (0 dB gain crossover frequency), the forward loop phase cannot exceed: $-180° + 50-(-90) = -40°$. Similarly, the forward loop phase cannot exceed $-180°-(-102°) = -78°$ at 35 rad/sec (the -180° phase crossover frequency). The structural filter and actuator contribute approximately -100° at 35 rad/sec. Therefore, phase compensation is necessary.

A frequency response of the compensation filter chosen is presented in Figure 13. As can be seen from this figure, the compensation filter provides phase lead for frequencies above 10 rad/sec. The frequency response for the total SFCS forward loop is presented in Figure 14. The maximum phase lag requirements outlined above are seen to be met. Open loop frequency responses were computed and time history responses were generated for selected flight conditions to verify the design procedure. These data are presented in Appendix II.

d. Structural Filter

A second order notch and first order lag filter for structural mode attenuation were included in the longitudinal SFCS forward loop from the outset of the longitudinal control law development studies. The design for these components was not finalized until an aeroelastic math model of the aircraft was analyzed and other system components functionally designed.

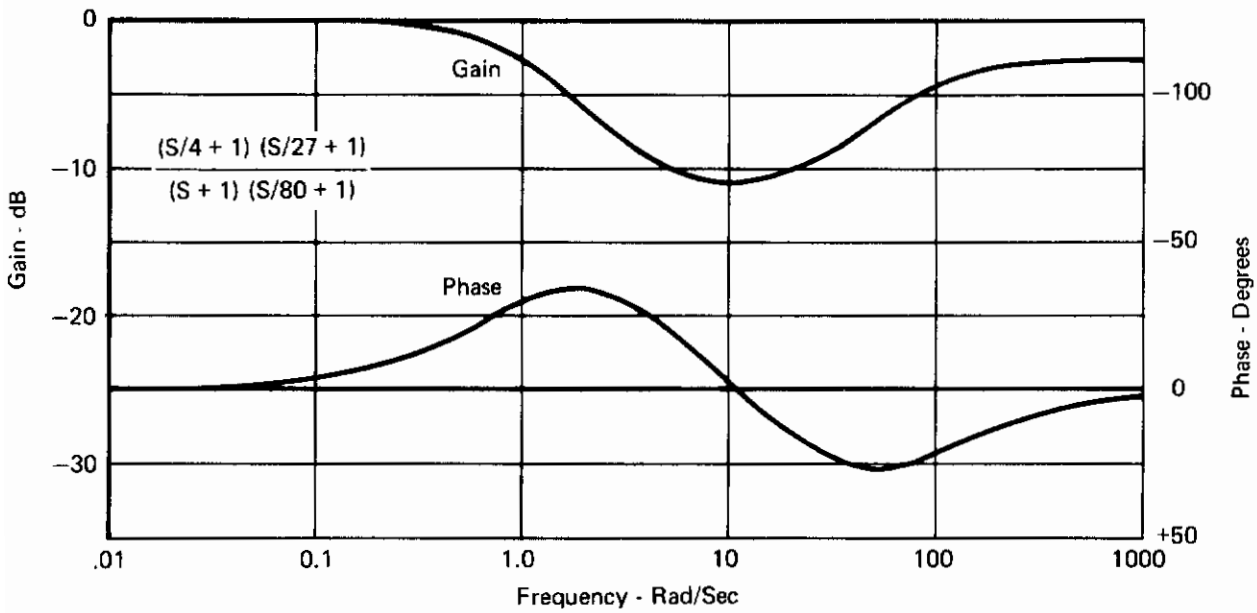

FIGURE 13
FORWARD LOOP COMPENSATION FREQUENCY RESPONSE

Open loop frequency responses of the longitudinal SFCS were computed with the original structural filter deleted. Figure 15 presents a composite plot of these frequency responses for eleven flight conditions. Although individual responses for each flight condition are not readily distinguishable on this plot, the frequencies at which structural mode peaks occur and the amplitudes of the peaks are easily seen. For the flight conditions considered, it may be seen from the figure that the major attenuation effort must be concentrated in the frequency range of the first two structural modes. For this reason the second order notch was redesigned so that its resonant frequency is 86 rad/sec. This frequency plus increased notch depth in the redesigned second order notch was sufficient to provide the desired attenuation of the first two structural modes at all flight conditions. The third structural mode, occurring in a frequency range of 120 to 140 rad/sec, with its maximum peak of zero dB occurring at 120 rad/sec,was attenuated further by redesigning the first order lag so that its break frequency is 120 rad/sec. Figure 16 presents the frequency response of the redesigned structural filter. Open loop frequency responses with the new structural filter were computed. These data are presented in Appendix III for eleven flight conditions and two aircraft weights.

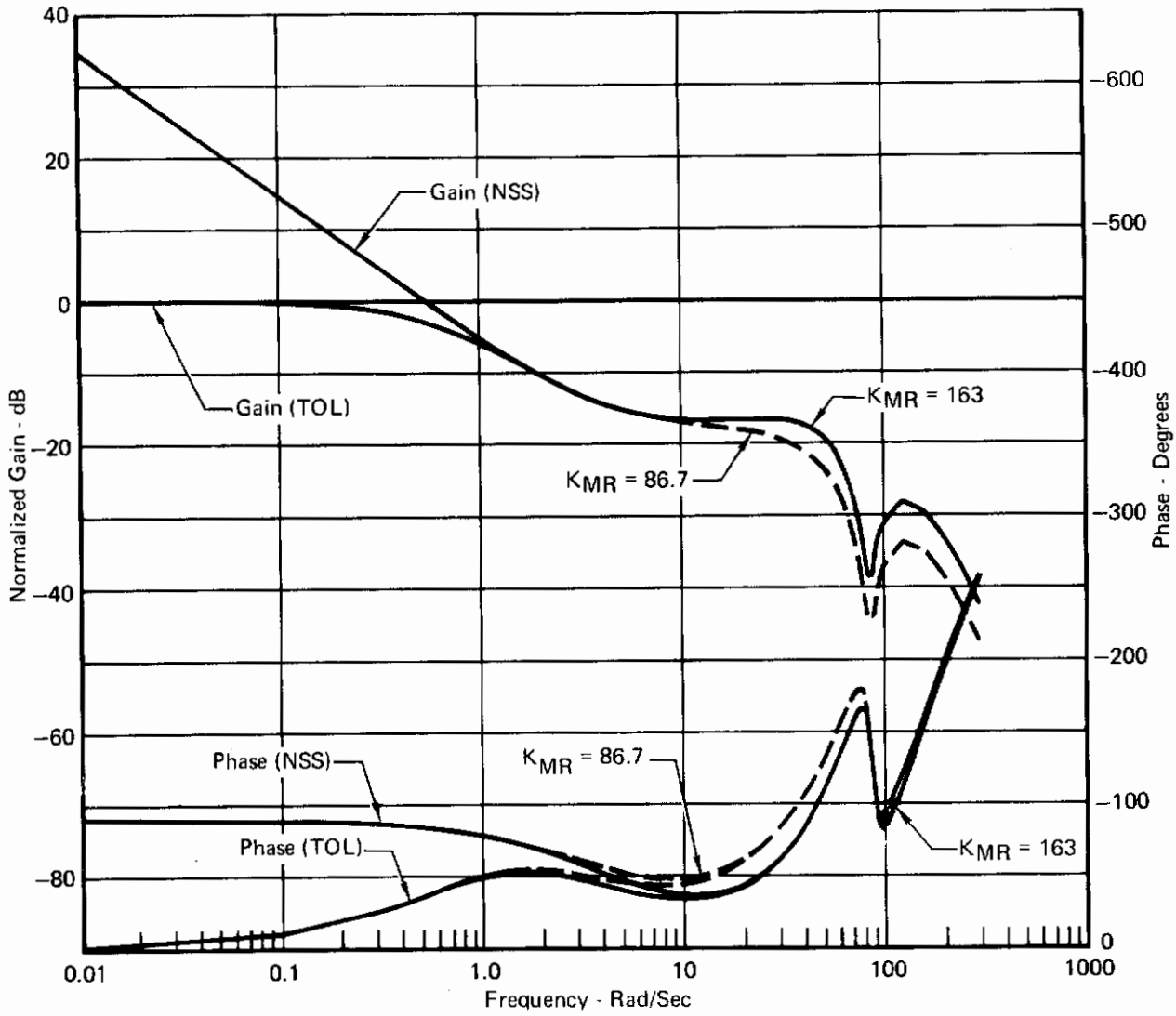

FIGURE 14
FORWARD LOOP FREQUENCY RESPONSE (PHASE IIA, B)

e. Sensor Placement

The number of candidate locations for the normal accelerometers and pitch rate gyros were few in number due to the limited space available in the test aircraft. It is desirable to locate the normal accelerometer forward of the aircraft c.g. in order to capitalize on the stabilizing characteristics of the pitch angular acceleration which accompanies forward located accelerometers. Based upon this consideration and the space available, candidate locations at Fuselage Station 24 and 77 were chosen. Of these two locations, Fuselage Station 77 provides the lower structural mode contamination on the normal accelerometer output as explained in

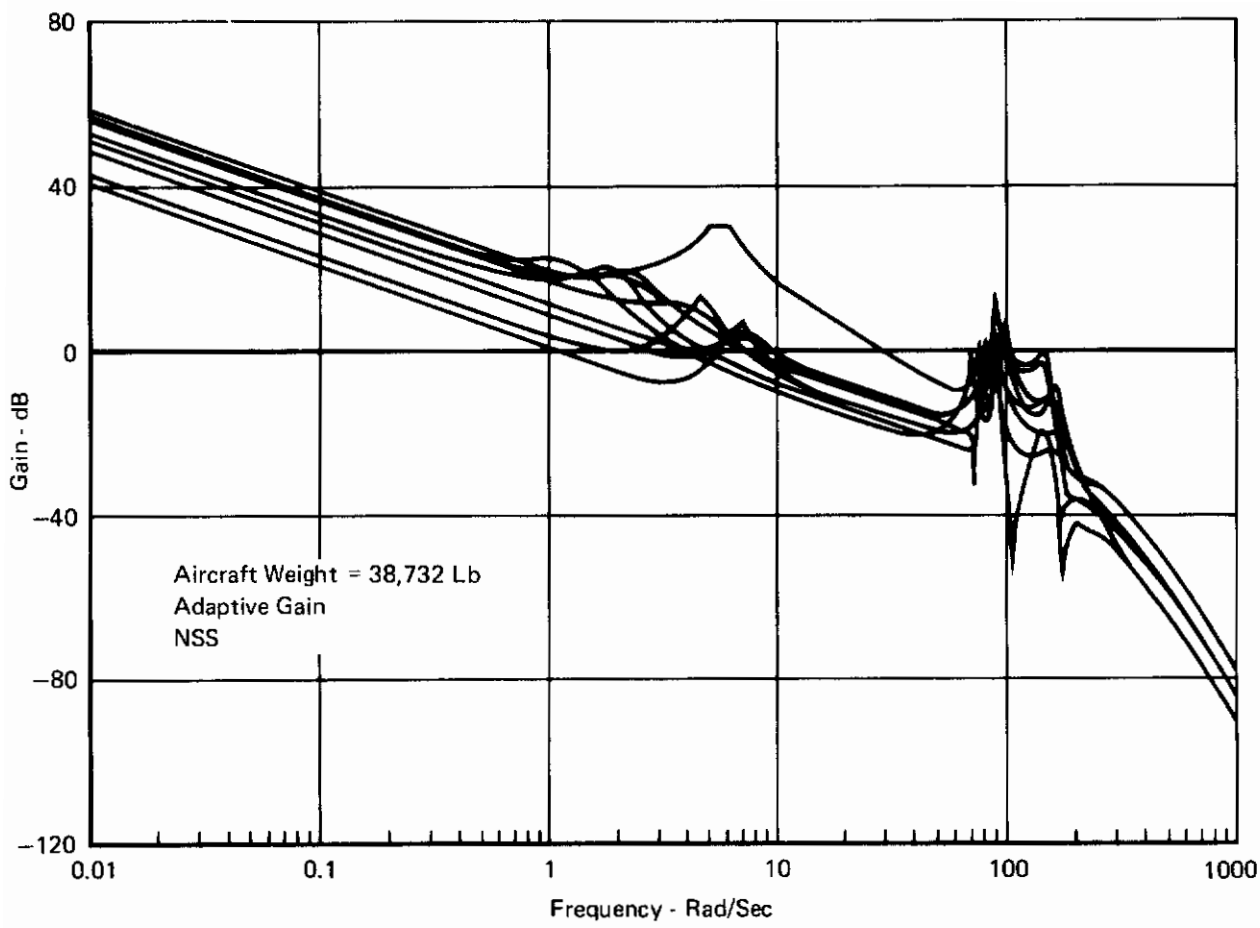

FIGURE 15
OPEN LOOP FREQUENCY RESPONSES WITHOUT STRUCTURAL NOTCH FILTER (PHASE II A, B)

Appendix III. Also, the space available at F.S.77 allows installation very near the aircraft center line, which reduces the roll rate cross-coupling. For these reasons the normal accelerometer is located at F.S.77.

Three possible locations for the pitch rate gyro were investigated: F.S.383, 313 and 179. These locations represent the production pitch rate gyro location (F.S.383) and the first two available spaces forward of F.S.383. As shown in Appendix III, the structural mode amplitudes sensed by the pitch rate gyro are lower at F.S.383 than at the other locations; therefore F.S.383 was chosen as the location for this sensor.

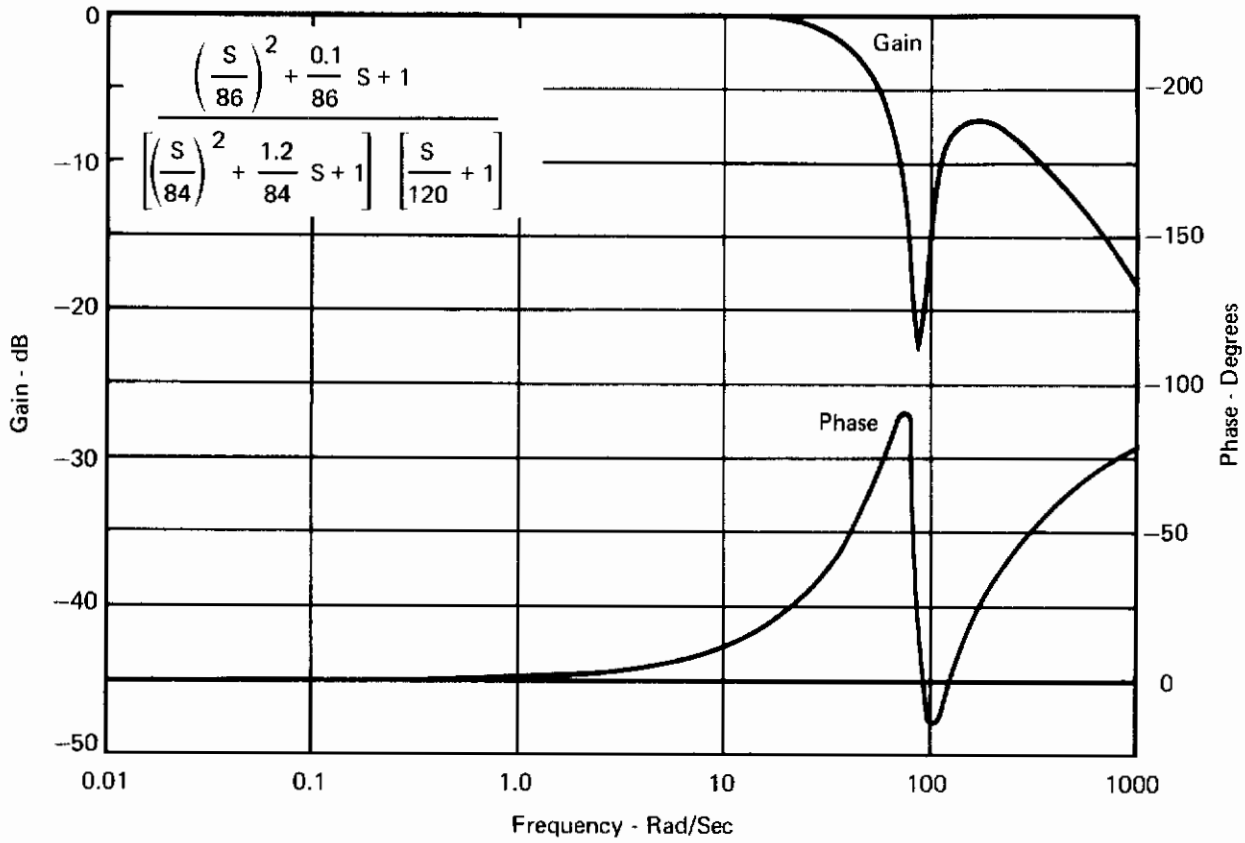

FIGURE 16
STRUCTURAL FILTER FREQUENCY RESPONSE

f. Sensor Switching

The six degree of freedom digital program used for the manned simulation program was utilized to conduct a brief study of the effect of landing gear reaction on the sensor outputs and the resultant effect on the aircraft controllability during landings. A worst case hard landing was simulated with the aircraft in the power approach configuration. The aircraft was trimmed for flight at Mach .225, at 15 feet altitude on an initial 3-degree glide slope and allowed to contact the ground without flaring. The throttles were retarded to idle thrust upon main gear impact. Runs were made for landings with mechanical back-up, electrical back-up, and Normal mode of the SFCS. Figure 17 presents pitch rate, pitch attitude, and altitude time histories for these three runs. As can be seen from these plots, the landings with electrical back-up and mechanical back-up are identical. The response for the landing with the SFCS has a slightly lower pitch rate,indicating a desirable retardation as the aircraft rotated onto the nose gear. There is no indication that the effect of the landing gear reaction upon the SFCS sensor outputs will cause an undesirable condition to exist. It was therefore concluded that there is no need to remove the sensor outputs after touchdown.

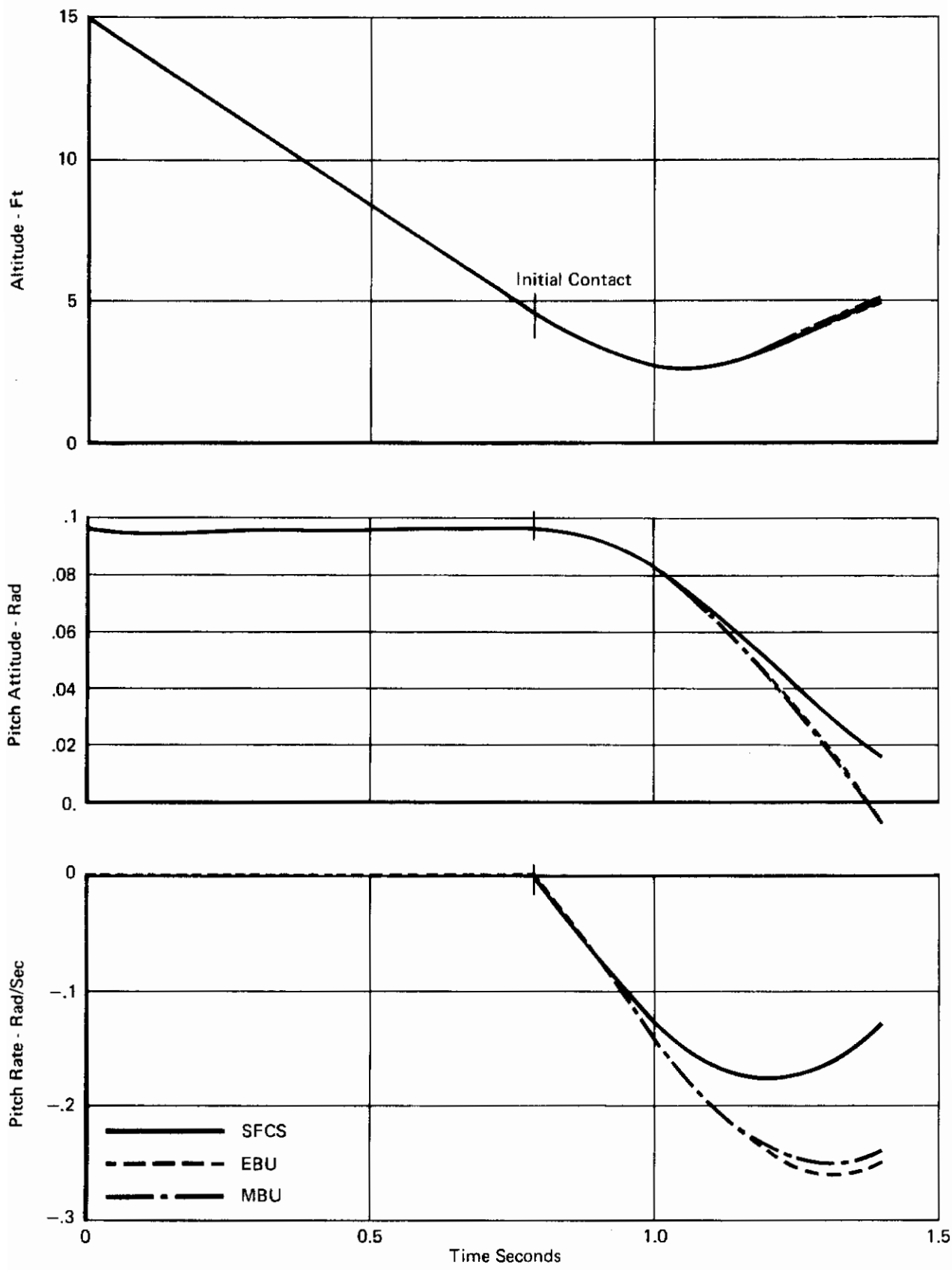

FIGURE 17
SIMULATED APPROACH AND LANDING (PHASE IIA, B)

g. Gain Switch Points

Three gain states are available for longitudinal SFCS adaptive gain operation. The states are K_F=.25(LO), K_F=.5(MID), and K_F=1.0(HI). The LO gain state is used for high M_δ flight conditions, M_δ > 20; the MID gain is used at midrange M_δ flight conditions, 10 < M_δ < 20; and the HI gain is used for low M_δ flight conditions, M_δ < 10. A threshold of ΔM_δ = 1 is used at the switch points in order to inhibit extraneous gain switching for momentary minor changes in the computed M_δ value. The switch points at M_δ = 10 and M_δ = 20 were chosen based upon stability and time history response considerations.

Time history responses were obtained at fifteen flight conditions and two aircraft weights for each of the three gain states. When the C* and dC*/dt responses were compared with the response criteria, it was found that switch points at M_δ = 10 and M_δ = 20 are satisfactory. Time history responses for each flight condition are documented in Appendix II for the adaptive gain values. The open loop frequency responses included in Appendix II were used to verify that satisfactory stability margins are maintained.

3. CONTROL SYSTEM PERFORMANCE EVALUATION

a. System Stability

(1) Aircraft Short Period and Control System Oscillatory Modes

Stability margins for the aircraft short period and control system oscillatory modes were determined by the Bode frequency response method. Open loop frequency response plots were obtained for fifteen flight conditions and are presented in Appendix II. Two aircraft weights were used for each flight condition documented. Table II shows the gain and phase margin exhibited by the system at each flight condition for adaptive gain operation.

The lowest gain margin value presented in Table II is 13.2 dB which is well within the gain margin guideline of 10 dB. The phase margin data of Table II are shown in comparison to the phase margin guideline in Figure 18. As can be seen, all points are within the guideline.

Table III contains stability margin data for the fixed gain (K_F=.25, LO) condition. For each flight condition the gain margin is increased by operation in the fixed, low gain rather than adaptive gain by 6 to 12 dB depending, of course, upon whether the proper adaptive gain value is 2 or 4 times the fixed low gain value. The phase margins, on the other hand,

TABLE II
STABILITY MARGINS (PHASE IIA,B)
(Adaptive Gain)

Mach	Altitude (Ft)	Weight (Lb)	Function (NSS/TOL)	K_F	Phase Margin (Deg)	Phase Margin Freq	Gain Margin (dB)	Gain Margin Freq
0.206	SL	32,500	TOL	1.0	47.7	2.3	28.1	36.3
0.214	SL	43,720	TOL	1.0	45.8	2.1	29.5	36.2
0.318	SL	32,500	TOL	1.0	54.2	4.0	20.8	36.4
0.318	SL	43,720	TOL	1.0	49.7	3.3	23.1	36.3
0.5	5,000	38,732	NSS	1.0	57.0	7.1	14.9	36.1
0.5	5,000	43,720	NSS	1.0	55.1	6.5	15.4	36.0
0.5	25,000	38,732	NSS	1.0	45.5	4.0	21.7	35.8
0.5	25,000	43,720	NSS	1.0	41.8	3.6	22.3	35.8
0.84	SL	38,732	NSS	0.25	64.1	6.1	17.4	36.4
0.84	SL	43,720	NSS	0.25	53.5	5.2	18.1	36.3
0.9	15,000	38,732	NSS	0.5	60.0	7.7	14.5	36.3
0.9	15,000	43,720	NSS	0.5	56.4	6.8	15.1	36.2
0.9	35,000	38,732	NSS	1.0	53.9	6.8	15.2	35.9
0.9	35,000	43,720	NSS	1.0	52.0	6.2	15.9	35.9
0.9	45,000	38,732	NSS	1.0	47.7	4.9	19.2	35.8
0.9	45,000	43,720	NSS	1.0	45.0	4.4	19.8	35.8
1.1	SL	38,732	NSS	0.25	75.5	9.7	13.2	37.0
1.1	SL	43,720	NSS	0.25	71.3	8.4	13.9	36.9
1.2	5,000	38,732	NSS	0.25	74.2	10.4	13.3	36.9
1.2	5,000	43,720	NSS	0.25	71.8	9.1	13.9	36.8
1.5	15,000	38,732	NSS	0.25	71.8	9.4	15.5	35.7
1.5	15,000	43,720	NSS	0.25	67.1	8.3	16.2	35.7
1.5	35,000	38,732	NSS	0.5	60.0	9.5	14.3	36.1
1.5	35,000	43,720	NSS	0.5	59.1	8.6	15.0	36.0
1.5	45,000	38,732	NSS	0.5	57.8	7.1	18.1	35.9
1.5	45,000	43,720	NSS	0.5	56.1	6.5	18.7	35.9
1.8	55,000	38,732	NSS	1.0	53.7	8.0	15.2	35.8
1.8	55,000	43,720	NSS	1.0	52.8	7.4	14.9	35.7
2.15	36,000	38,732	NSS	0.25	64.6	8.5	19.5	35.9
2.15	36,000	43,720	NSS	0.5	55.9	9.8	14.2	35.8

TABLE III
STABILITY MARGINS (PHASE IIA, B)
(Fixed Gain)

Mach	Altitude (Ft)	Weight (Lb)	Function (NSS/TOL)	K_F	Phase Margin (Deg)	Phase Margin Freq	Gain Margin (dB)	Gain Margin Freq
0.206	SL	32,500	TOL	0.25	52.9	1.0	40.1	36.3
0.214	SL	43,720	TOL	0.25	51.2	0.9	41.5	36.2
0.318	SL	32,500	TOL	0.25	51.1	1.8	32.8	36.4
0.318	SL	43,720	TOL	0.25	43.6	1.4	35.1	36.3
0.5	5,000	38,732	NSS	0.25	56.7	3.1	26.9	36.1
0.5	5,000	43,720	NSS	0.25	46.7	2.7	27.9	36.0
0.5	25,000	38,732	NSS	0.25	38.6	1.88	33.7	35.8
0.5	25,000	43,720	NSS	0.25	26.6	1.63	34.3	35.8
0.84	SL	38,732	NSS	0.25	64.1	6.1	17.4	36.4
0.84	SL	43,720	NSS	0.25	53.5	5.2	18.1	36.3
0.9	15,000	38,732	NSS	0.25	64.3	5.1	20.5	36.3
0.9	15,000	43,720	NSS	0.25	52.9	4.4	21.1	36.2
0.9	35,000	38,732	NSS	0.25	51.0	3.3	27.2	35.9
0.9	35,000	43,720	NSS	0.25	39.8	2.8	27.9	35.9
0.9	45,000	38,732	NSS	0.25	48.2	2.6	31.2	35.8
0.9	45,000	43,720	NSS	0.25	32.4	2.2	31.2	35.8
1.1	SL	38,732	NSS	0.25	75.5	9.7	13.2	37.0
1.1	SL	43,720	NSS	0.25	71.3	8.4	13.9	36.9
1.2	5,000	38,732	NSS	0.25	74.2	10.4	13.3	36.9
1.2	5,000	43,720	NSS	0.25	71.8	9.1	13.9	36.8
1.5	15,000	38,732	NSS	0.25	71.8	9.4	15.5	35.7
1.5	15,000	43,720	NSS	0.25	67.1	8.3	16.2	35.7
1.5	35,000	38,732	NSS	0.25	70.5	7.1	20.3	36.1
1.5	35,000	43,720	NSS	0.25	67.5	6.4	21.0	36.0
1.5	45,000	38,732	NSS	0.25	68.3	5.7	24.1	35.9
1.5	45,000	43,720	NSS	0.25	61.8	5.1	24.7	35.9
1.8	55,000	38,732	NSS	0.25	64.1	4.9	27.2	35.8
1.8	55,000	43,720	NSS	0.25	58.2	4.5	26.9	35.7
2.15	36,000	38,732	NSS	0.25	64.6	8.5	19.5	35.9
2.15	36,000	43,720	NSS	0.25	63.0	7.6	20.2	35.8

are increased at some flight conditions and decreased at others. All points except one are within the phase margin guideline as shown in Figure 19. Violation of the guideline for fixed, low gain operation at the one flight condition (Mach=.5, Alt=25,000 ft. Wt.=43,720 lb) is not considered serious since the frequency (.26 Hz) at which it occurs is low. The significance is also diminished by the fact that at the same flight condition, with aircraft weight at 38,732 lbs. the system meets the guideline. The takeoff gross weight for the SFCS aircraft is 43,720 lbs. and it is doubtful that actual flight at Mach .5, 25,000 feet altitude will ever occur with the 43,720 lbs. gross weight configuration.

Analyses were performed to determine compatibility of the SSAP with the SFCES control laws. A functional block diagram depicting the mechanization of the SSAP is presented in Figures 20, 21 and 22. A nonlinear math model for the electro-mechanical secondary actuator portion of the SSAP was derived as discussed in TR-71-20, Section III. Figure 21 gives the SSAP secondary actuator no load speed as a function of the percent pulse width. As shown in Figure 21, the secondary actuator operates very much like a contactor control system in that any input command which is large enough to produce movement causes the development of a no load speed which is 91% of the maximum available. The SSAP main ram velocity is presented in Figure 22 as a function of master control valve position. The slope of this curve represents the gain, K_3, called out in the block diagram of Figure 20.

An all digital six-degree-of-freedom large angle simulation was used to evaluate the stability and response characteristics of the airframe and control system combination including the SSAP. A large number of responses were obtained using a variety of input commands and disturbances at several flight conditions. The inputs included: step inputs of stick force with varying magnitudes, one cycle of a large amplitude sinusoidal input of stick force; continuous sinusoidal inputs of stick force, and large amplitude wind gusts. These inputs were applied in both straight ahead symmetrical flight and during high bank angle turns. Stability and performance characteristics were determined by evaluating the transient response characteristics and comparing these responses to those obtained using the Phase IIA actuator configuration. This technique for determining system stability was used in preference to the usual phase and gain margin measurements due to the presence of several nonlinearities and the high order of the control loop.

Results of the simulation indicate little or no degradation in response characteristics for most flight conditions as a result of using the SSAP in the control loop. Typical time history responses are presented in Figures 23 and 24 to illustrate the similarity of transient responses using the two actuator configurations.

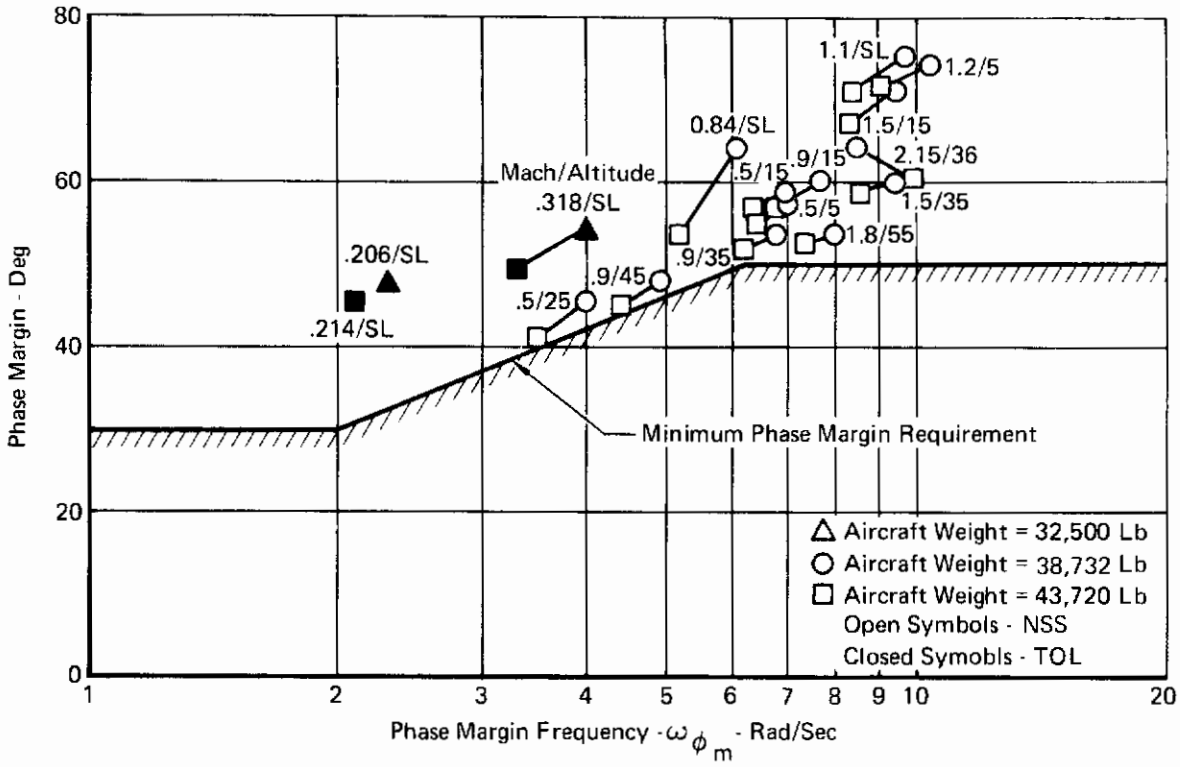

FIGURE 18
PHASE MARGIN
Adaptive Gain

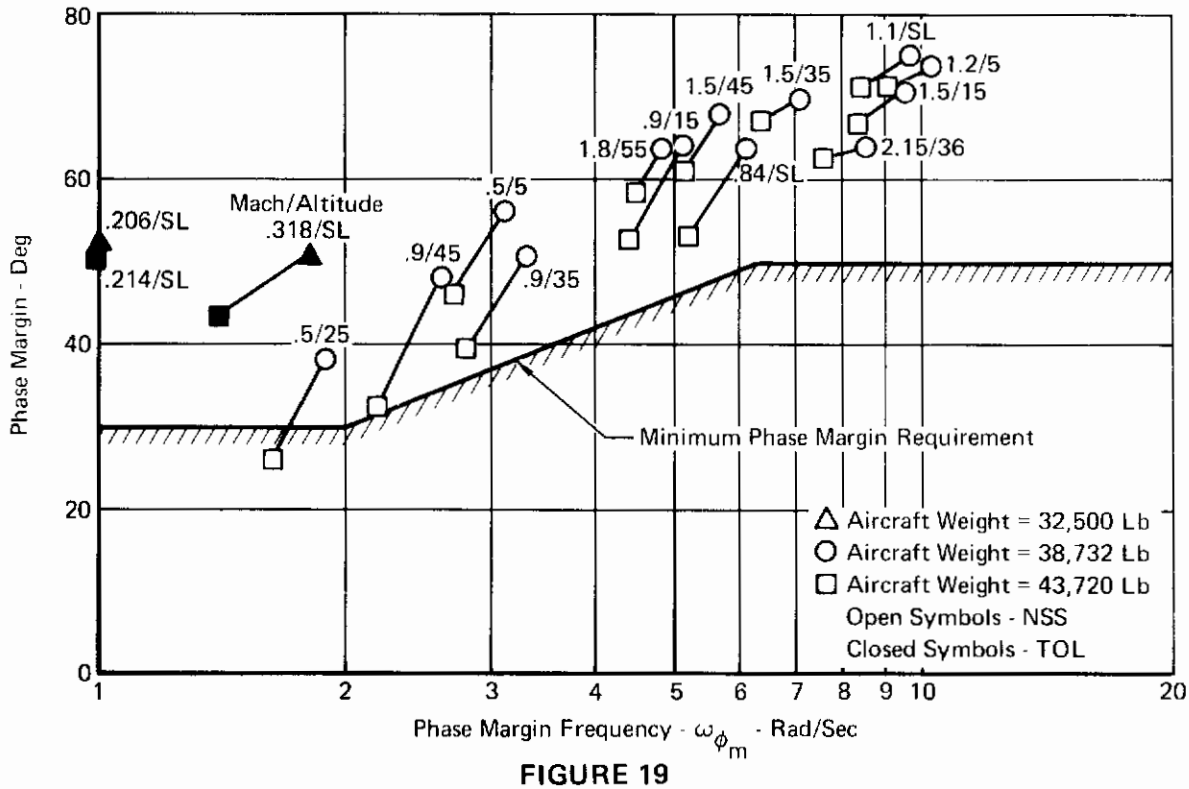

FIGURE 19
PHASE MARGIN
Fixed Gain

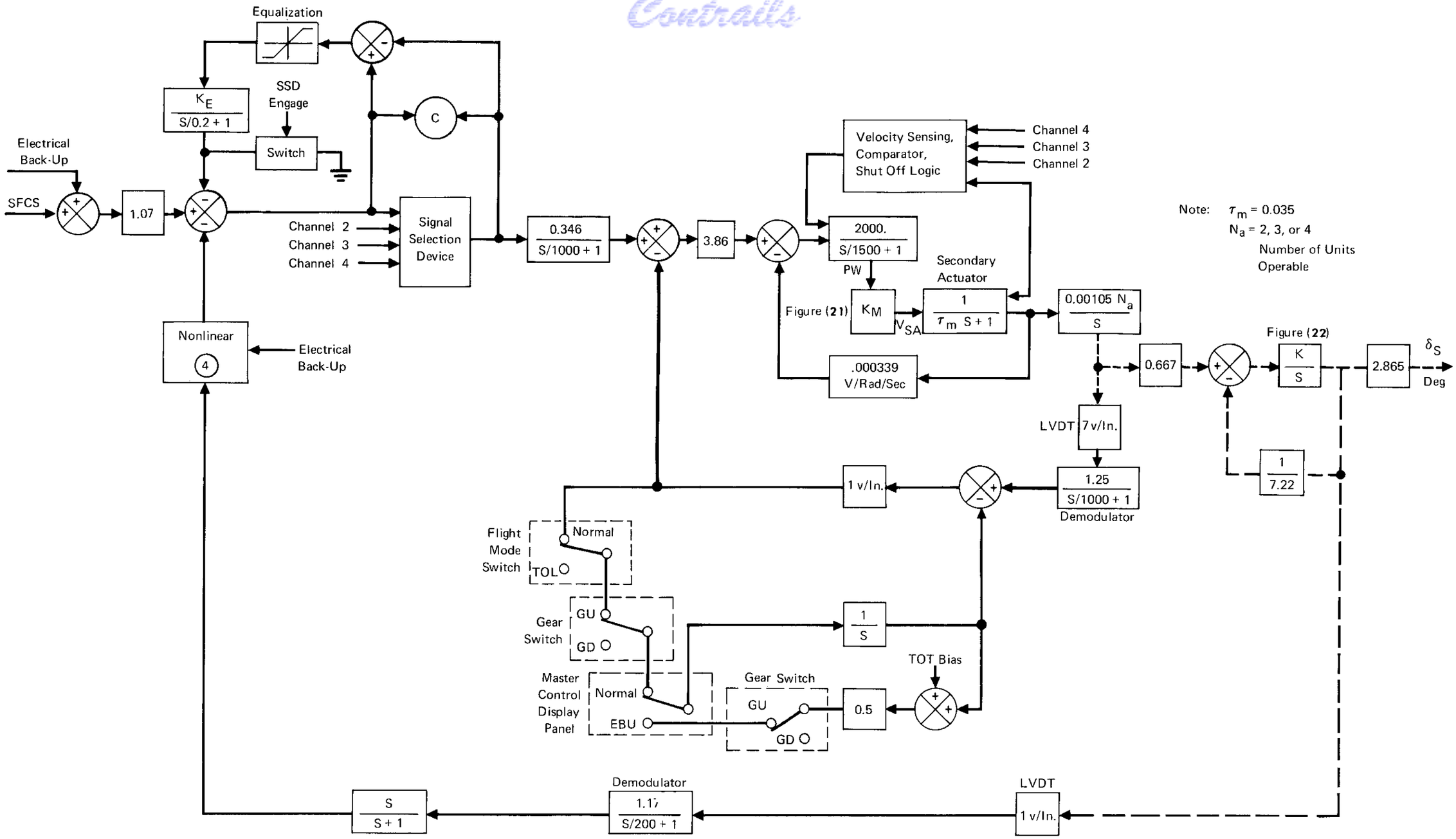

Note: Dashed lines denote mechanical paths. Solid lines denote electrical paths.

FIGURE 20
SURVIVABLE STABILATOR ACTUATOR PACKAGE FUNCTIONAL BLOCK DIAGRAM

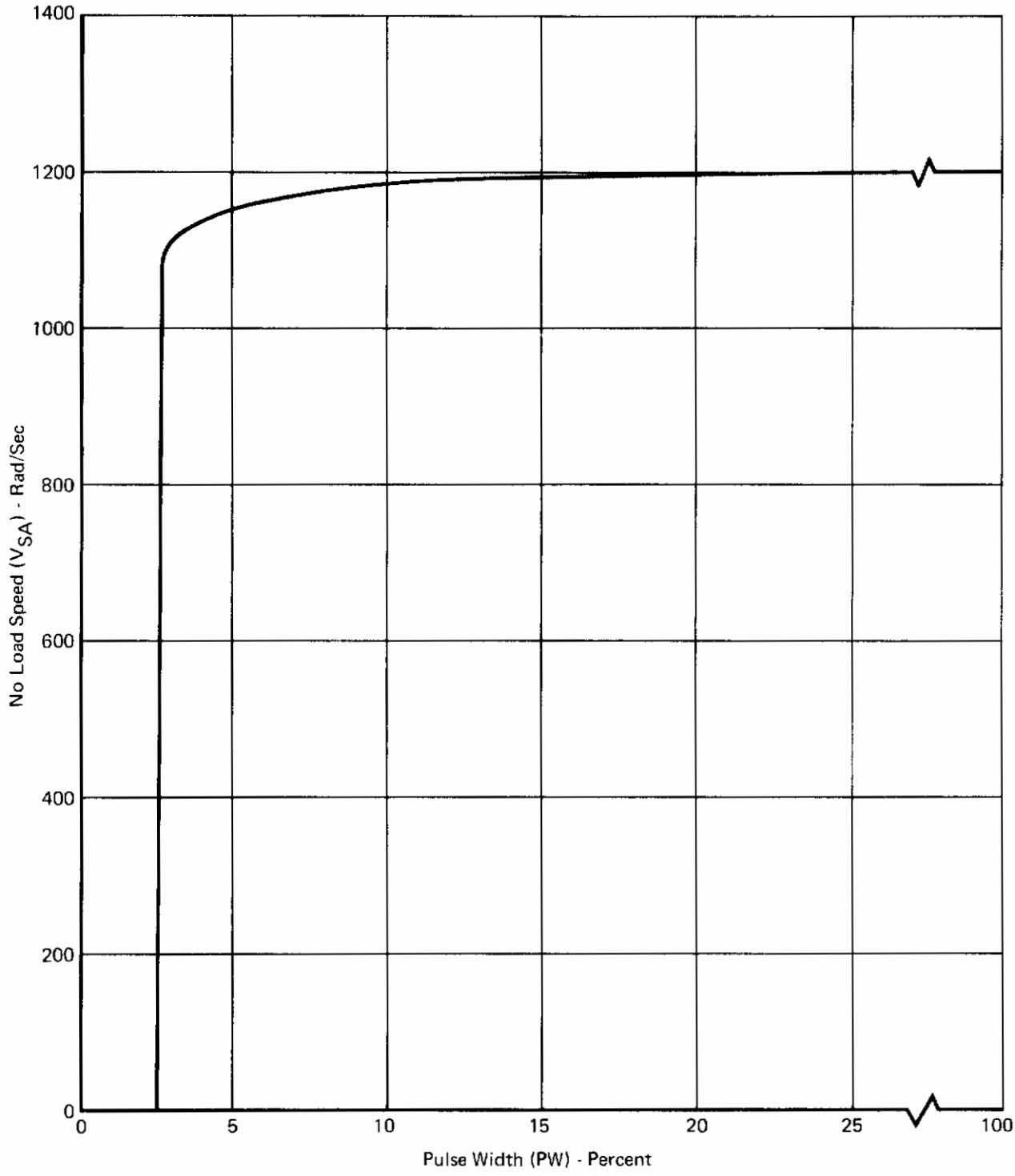

FIGURE 21

NO LOAD SPEED vs PULSE WIDTH

SSAP Secondary Actuator Servo Motors

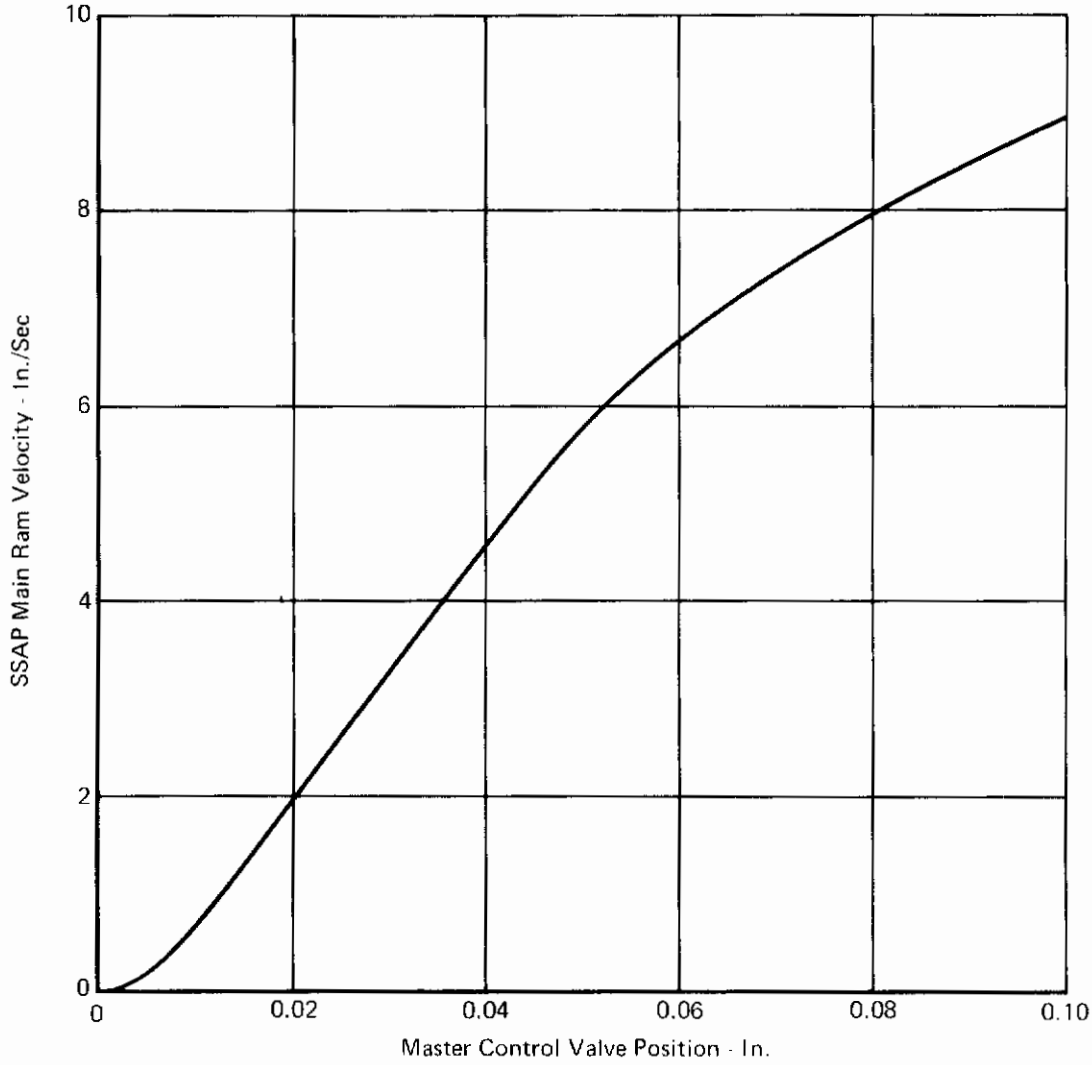

FIGURE 22

SSAP MAIN RAM VELOCITY vs MASTER CONTROL VALVE POSITION

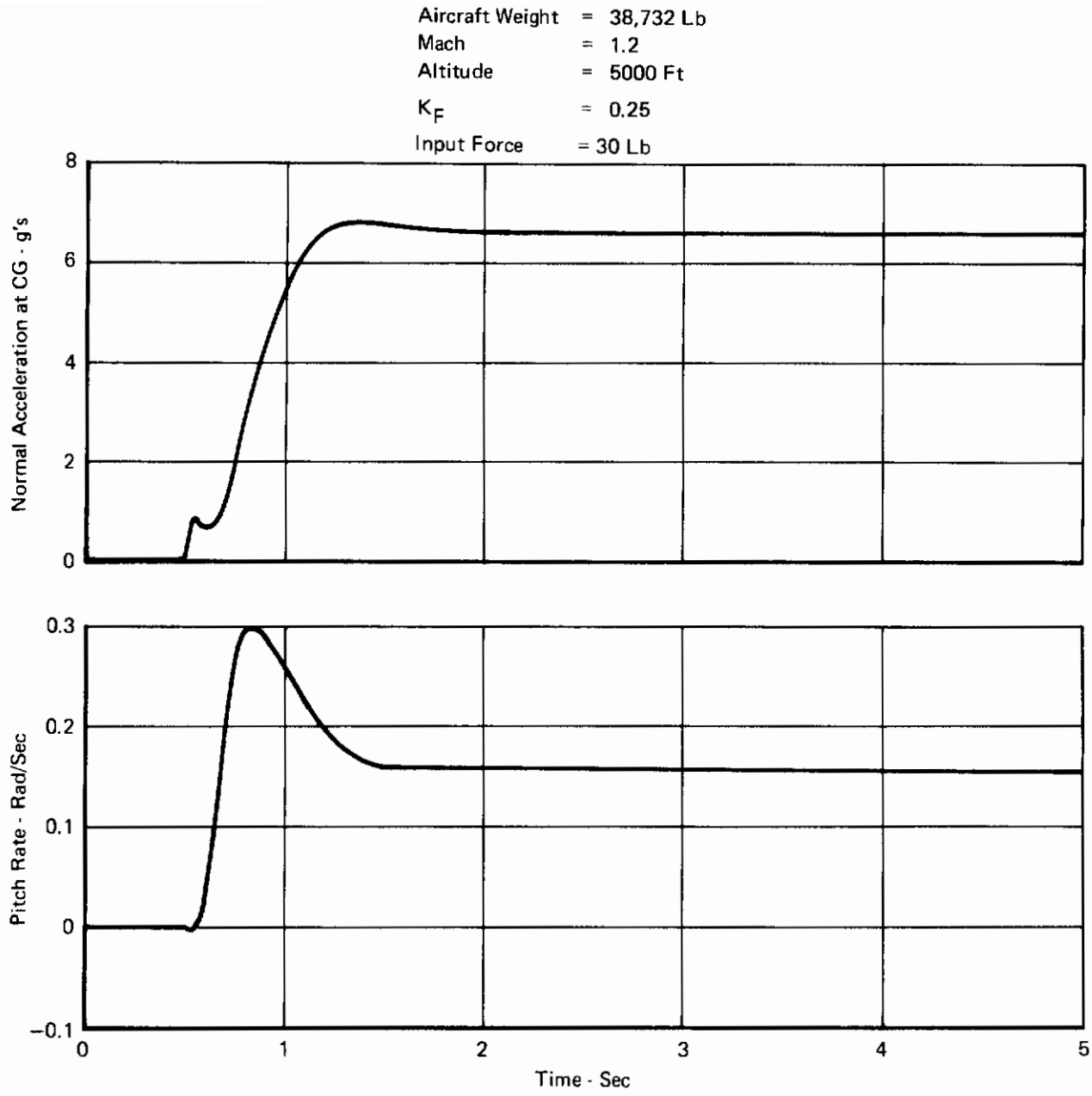

FIGURE 23
AIRCRAFT RESPONSES WITH PHASE IIA, B ACTUATOR FOR STICK FORCE STEP INPUT

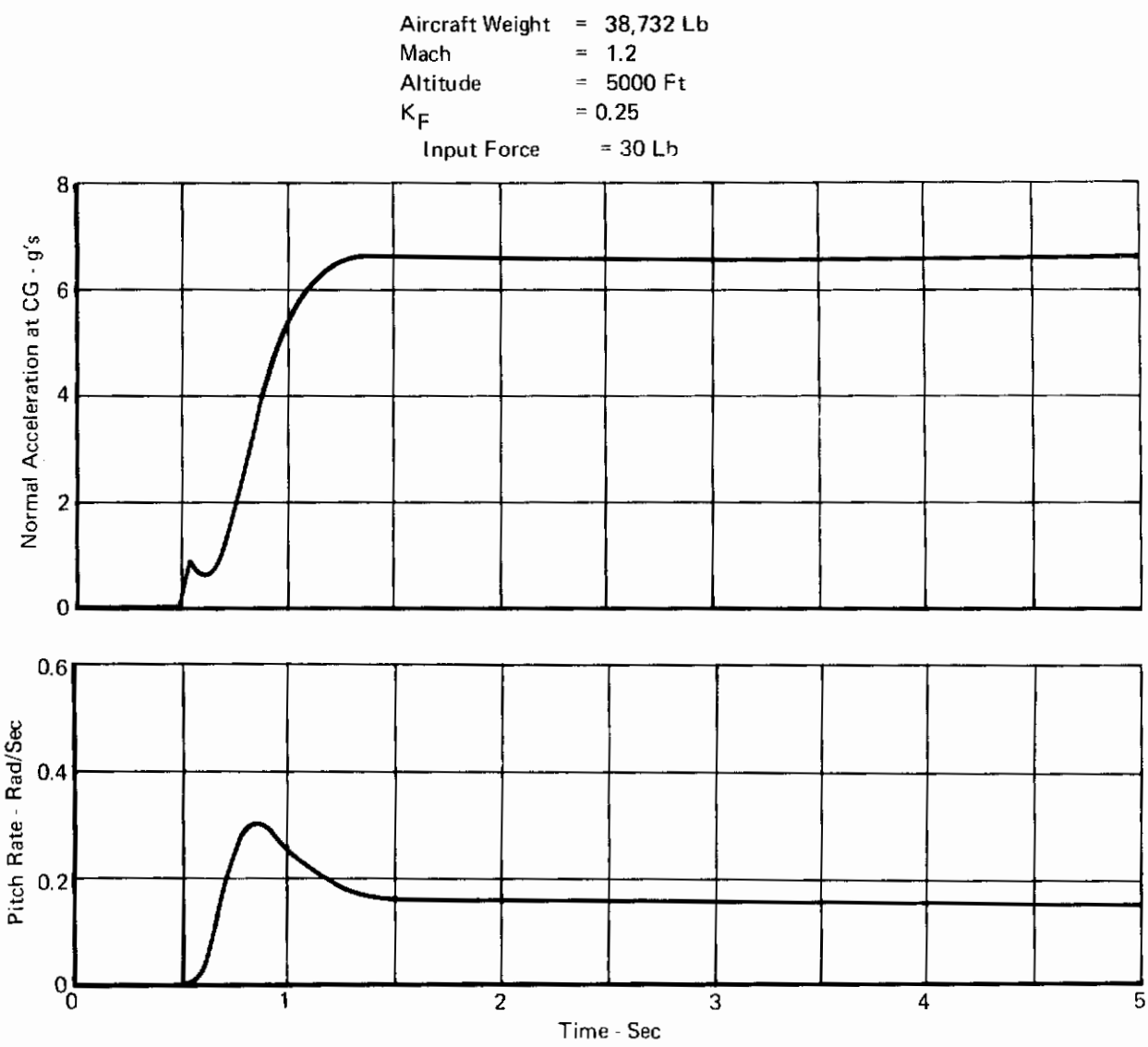

FIGURE 24
AIRCRAFT RESPONSE WITH SSAP ACTUATOR FOR STICK FORCE STEP INPUT

Use of the SSAP math model resulted in instability when large step inputs of stick force were applied and held at two simulated low $\bar{q}$ flight conditions. Figure 25 shows one of these responses for the 0.5 Mach number at 5,000 feet flight condition. A comparable response using the Phase IIA actuator is provided in Figure 26. While the response using the SSAP indicates an actual instability, not present with the Phase IIA actuator, the validity of the large step input of stick force is somewhat questionable. Actual step inputs of stick force cannot be achieved in practice and high stick forces would not be held in the presence of oscillating normal acceleration. Using a more realistic large amplitude sinusoidal input of stick force (one cycle) results in the transient response shown in Figure 27. This response is considered adequate in view of the large amplitude 40 pound input used.

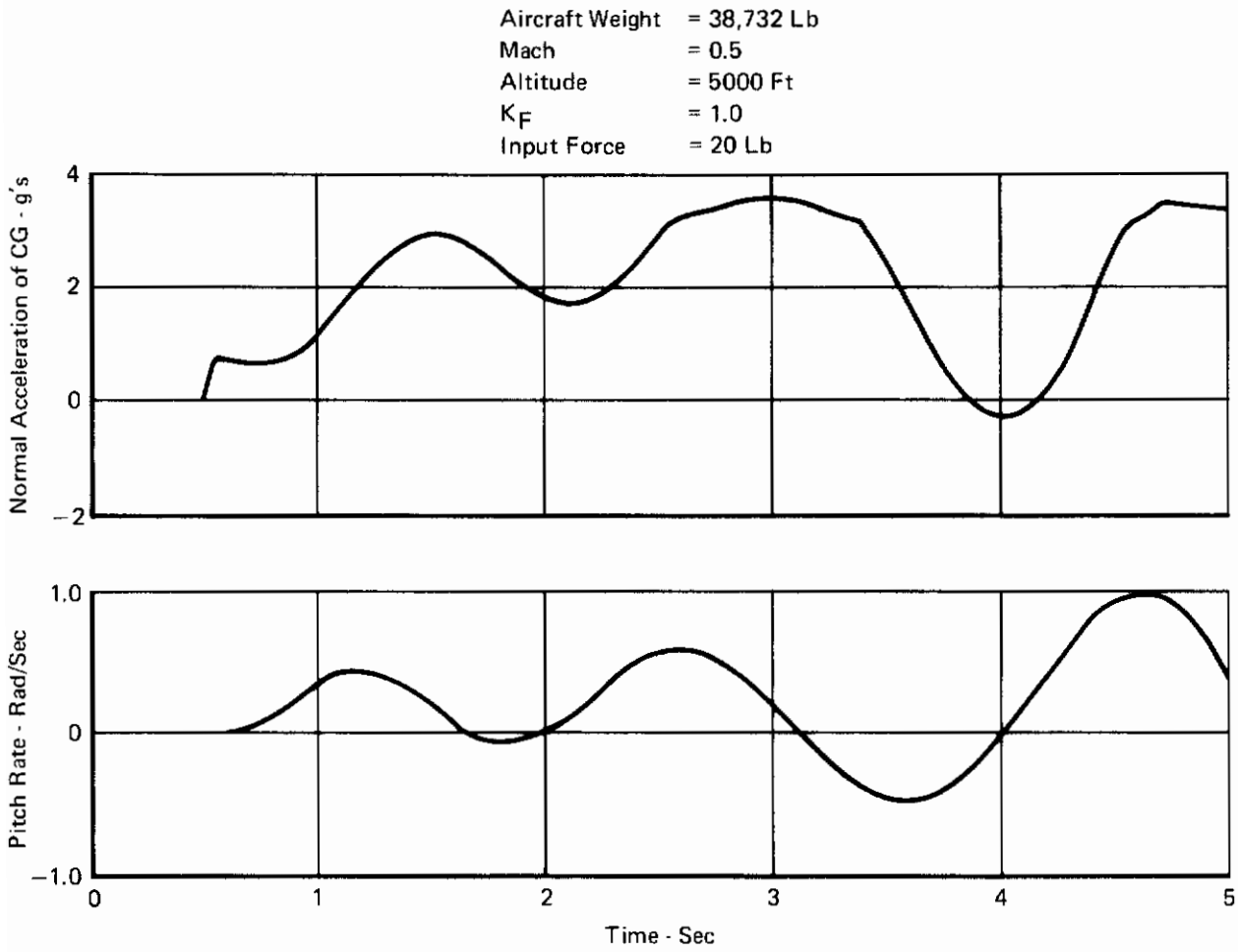

FIGURE 25
AIRCRAFT RESPONSE WITH SSAP ACTUATOR FOR STICK FORCE STEP INPUT

Transient response analyses using the SSAP are continuing in an effort to determine whether any other problem areas exist. At this time it appears that the SSAP characteristics are adequate for use with the SFCS.

(2) Structural Mode Stability

Bode frequency response and root locus techniques were employed in determining the stability characteristics of the longitudinal SFCS structural modes. Structural mode data were obtained for eleven flight conditions and two aircraft weight configurations. The open loop frequency responses were computed for all flight

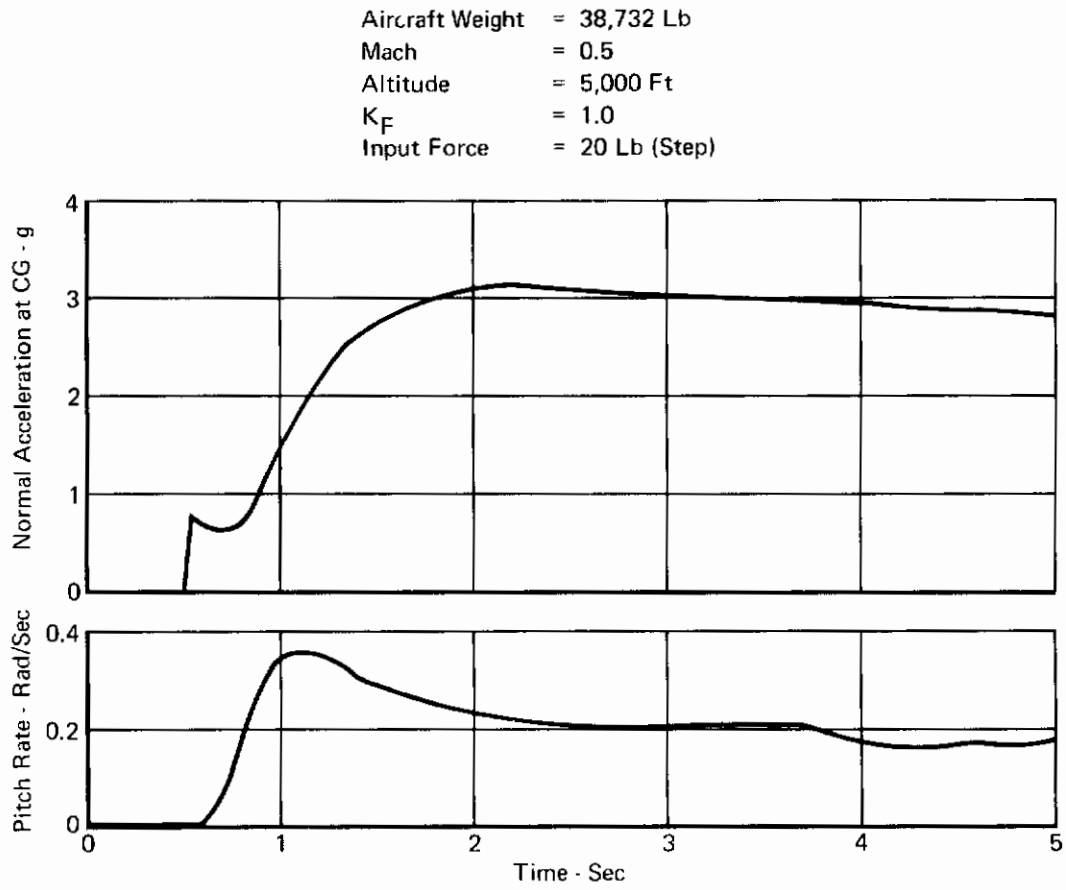

FIGURE 26
AIRCRAFT RESPONSE WITH PHASE IIA ACTUATOR FOR STICK FORCE STEP INPUT

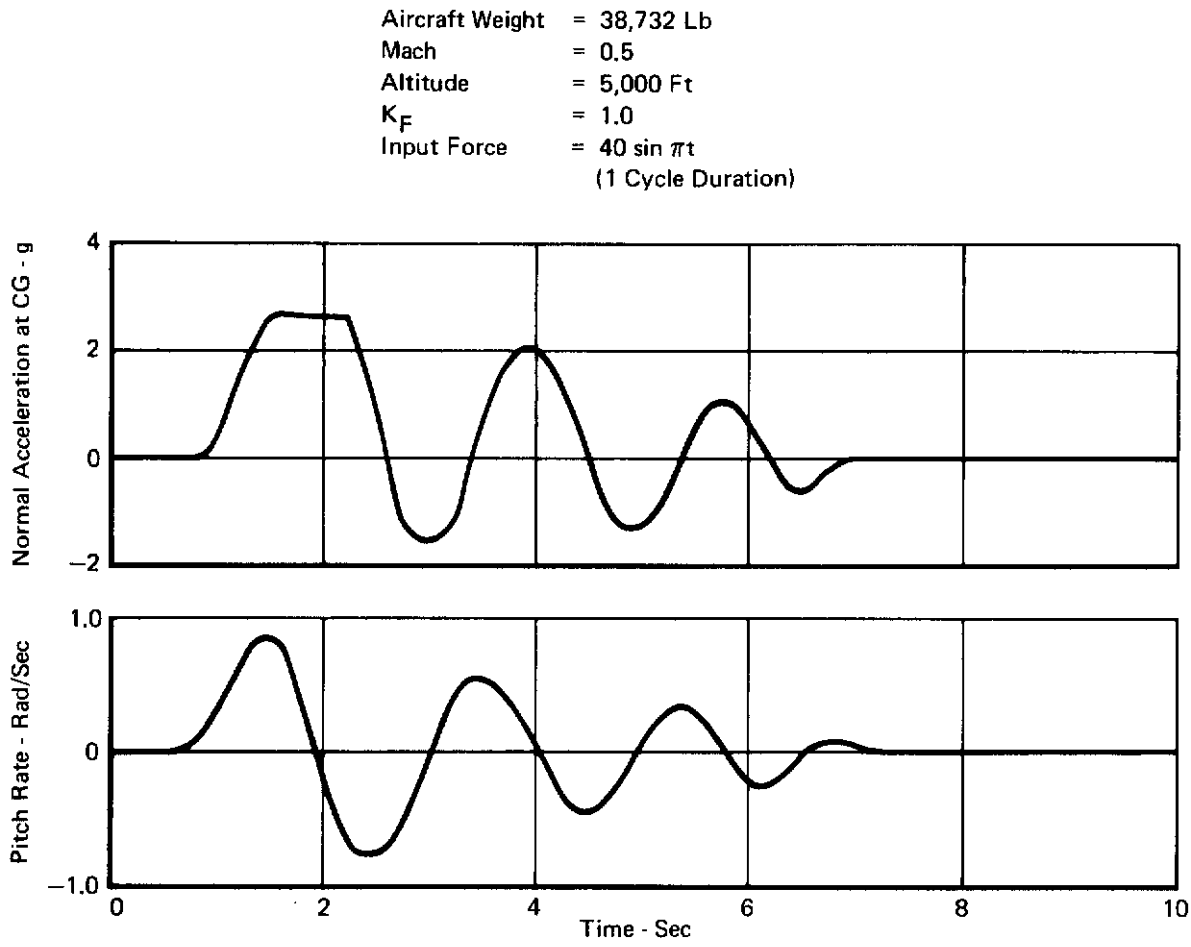

FIGURE 27
AIRCRAFT RESPONSE WITH SSAP ACTUATOR
FOR ONE CYCLE OF A SINUSOIDAL INPUT OF STICK FORCE

conditions as discussed in Appendix III. The open loop peak gain amplitudes corresponding to each of the three structural modes were used to obtain the minimum attenuation at each structural mode. The structural mode attenuation is given in Table IV. As can be seen from Table IV, the attenuation is at least -6 dB for all flight conditions investigated. Also,

TABLE IV
STRUCTURAL MODE ATTENUATION
(Adaptive Gains)

Mach	Altitude (Ft)	Weight (Lb)	Function (NSS/TOL)	K_F	Stabilator Bending		First Vertical Bending		Stabilator Rotation	
					Freq (Rad/Sec)	Attenuation (dB)	Freq (Rad/Sec)	Attenuation (dB)	Freq (Rad/Sec)	Attenuation (dB)
0.5	5,000	38,732	NSS	1.0	71	−22	88	−11	139	−11
0.5	5,000	43,720	NSS	1.0	71	−22	88	−11	139	−10
0.5	25,000	38,732	NSS	1.0	68	− 9	87	−10	142	− 7
0.5	25,000	43,720	NSS	1.0	68	− 9	87	−10	142	− 8
0.9	15,000	38,732	NSS	0.5	76	−17	90	−28	139	−26
0.9	15,000	43,720	NSS	0.5	76	−17	90	−28	139	−27
0.9	35,000	38,732	NSS	1.0	70	−20	87	−12	139	−10
0.9	35,000	43,720	NSS	1.0	70	−20	87	−12	139	−10
0.9	45,000	38,732	NSS	1.0	69	−10	88	−11	140	− 8
0.9	45,000	43,720	NSS	1.0	69	−10	88	−11	140	− 8
1.2	5,000	38,732	NSS	0.25	81	−16	98	− 6	160	−15
1.2	5,000	43,720	NSS	0.25	81	−14	98	− 6	160	−16
1.5	15,000	38,732	NSS	0.25	80	−16	96	−11	160	−18
1.5	15,000	43,720	NSS	0.25	80	−16	96	−11	160	−19
1.5	35,000	38,732	NSS	0.5	74	−20	90	−22	149	−30
1.5	35,000	43,720	NSS	0.5	75	−21	90	−22	149	−29
1.5	45,000	38,732	NSS	0.5	73	−24	88	−18	145	−19
1.5	45,000	43,720	NSS	0.5	73	−24	88	−18	145	−18
1.8	55,000	38,732	NSS	1.0	70	−18	88	−11	144	−16
1.8	55,000	43,720	NSS	1.0	70	−18	88	−11	144	−16
2.15	36,000	38,732	NSS	0.25	76	−27	90	−20	148	−25
2.15	36,000	43,720	NSS	0.5	76	−21	90	−20	148	−24

the desired attenuation of -9 dB for the stabilator bending and first vertical bending modes for subsonic flight conditions has been maintained. The structural mode attenuation will be greater for fixed low gain operation by 6 to 12 dB.

(3) Phugoid Stability

The desired goal of stable phugoid characteristics at all flight conditions was not attained. At six of the 30 conditions investigated using small perturbation three-degree-of-freedom aircraft motion equations, the SFCS exhibited unstable phugoid characteristics. The times to double amplitude for the six conditions vary from 50 to 33,393 seconds for operation with adaptive gains, and all except the Mach=.5, Alt.=25,000 feet, heavy weight condition meet the MIL-F-8785B(ASG) Level 3 requirement. The standard F-4E has unstable phugoid characteristics at these six flight conditions with times to double amplitude which vary from 7 to 203 seconds. As shown in Table V the phugoid is very well damped for the other 24 cases, and are well within the MIL-F-8785B (ASG) Level 1 requirement.

The six-degree-of-freedom simulation, which was employed during the manned simulation program, was used to obtain time history plots of velocity and altitude following a throttle doublet command. Figure 28 shows a 60 second time history for three flight conditions, two of which are not stable and one which is stable. As can be seen from these data, the two unstable conditions, (Mach = .5, Alt. = 25,000 ft. and Mach = .9, Alt. = 45,000 ft.) do not exhibit characteristics which could be considered dangerous; nor, in fact, does there appear to be any indication that normal pilot attention would not correct the mildly divergent phugoid condition. This conclusion was verified during the manned simulation program. MCAIR pilots who participated in the manned simulation program were requested to attempt to excite the phugoid mode from the simulator cockpit and provide comments on the degree of acceptability of the phugoid characteristics. Their comments were that the phugoid, if present, was not readily detectable.

b. Response Characteristics

(1) C* and dC*/dt Criteria

Time history responses of seven aircraft parameters are provided in Appendix II for a number of flight conditions. Summary plots of the C* and dC*/dt responses are given in Figures 29 through 32 for the nonterminal flight conditions and two aircraft weight configurations. All flight conditions compare favorably with the evaluation criteria. The responses for Mach .5, Alt.=25,000 feet and Mach 2.15, Alt.=36,000 feet do not fall entirely within the envelopes. These two flight conditions represent extreme points on the flight envelope which were included in the analysis primarily to investigate achievable

TABLE V

PHUGOID CHARACTERISTICS (PHASE IIA, B)

(Adaptive Gains)

Mach	Altitude (Ft)	Weight (Lb)	Function (NSS/TOL)	Damping (ζ_{PH})	Time to Double Amplitude (Sec)
0.206	SL	32,500	TOL	0.76	–
0.214	SL	43,720	TOL	0.55	–
0.318	SL	32,500	TOL	>1.0	–
0.318	SL	43,720	TOL	0.95	–
0.5	5,000	38,732	NSS	>1.0	–
0.5	5,000	43,720	NSS	–	1427.0
0.5	25,000	38,732	NSS	–	72.0
0.5	25,000	43,720	NSS	–	50.0
0.84	SL	38,732	NSS	>1.0	–
0.84	SL	43,720	NSS	–	33,393.0
0.9	15,000	38.732	NSS	>1.0	–
0.9	15,000	43,720	NSS	>1.0	–
0.9	35,000	38,732	NSS	>1.0	–
0.9	35,000	43,720	NSS	>1.0	–
0.9	45,000	38,732	NSS	–	152.0
0.9	45,000	43,720	NSS	–	198.0
1.1	SL	38,732	NSS	> 1.0	–
1.1	SL	43,720	NSS	> 1.0	–
1.2	5,000	38,732	NSS	>1.0	–
1.2	5,000	43,720	NSS	>1.0	–
1.5	15,000	38,732	NSS	>1.0	–
1.5	15,000	43,720	NSS	>1.0	–
1.5	35,000	38,732	NSS	>1.0	–
1.5	35,000	43,720	NSS	>1.0	–
1.5	45,000	38,732	NSS	0.68	–
1.5	45,000	43,720	NSS	0.66	–
1.8	55,000	38,732	NSS	0.61	–
1.8	55,000	43,720	NSS	0.59	–
2.15	36,000	38,732	NSS	>1.0	–
2.15	36,000	43,720	NSS	>1.0	–

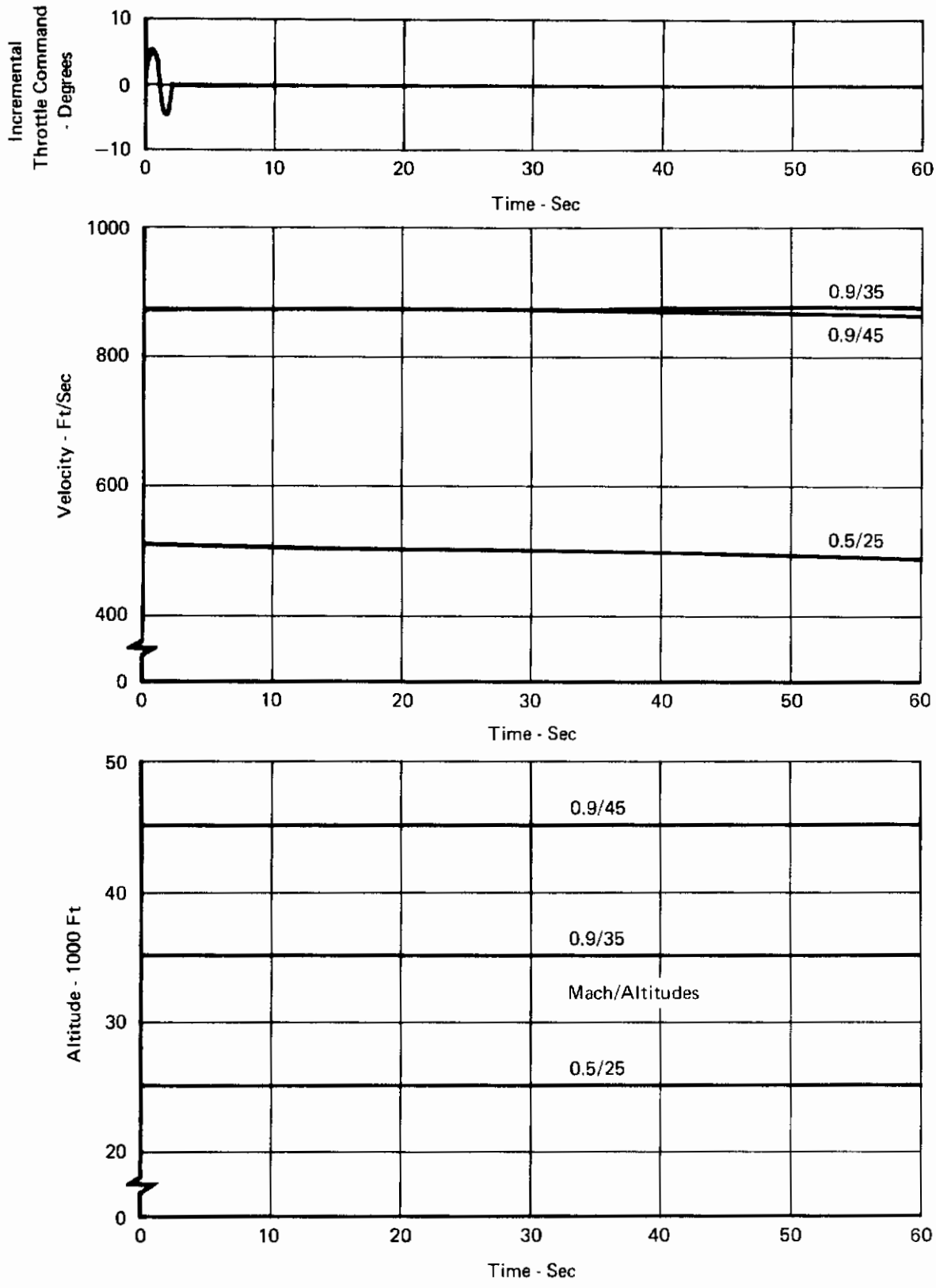

FIGURE 28
AIRCRAFT RESPONSE TO THROTTLE DOUBLET COMMAND

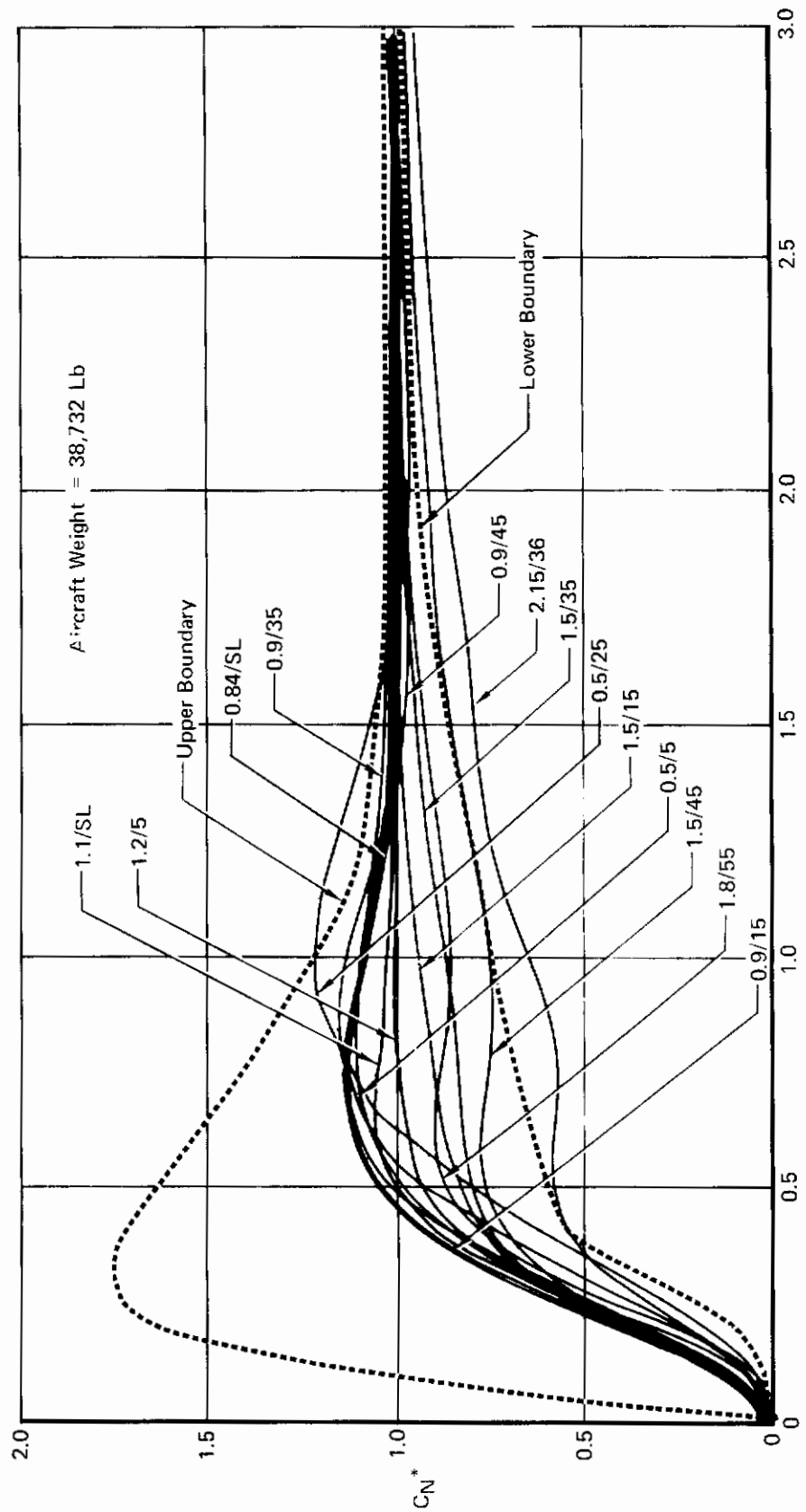

FIGURE 29
LONGITUDINAL SFCS TIME HISTORY C* CRITERIA COMPLIANCE
Adaptive Gains - NSS

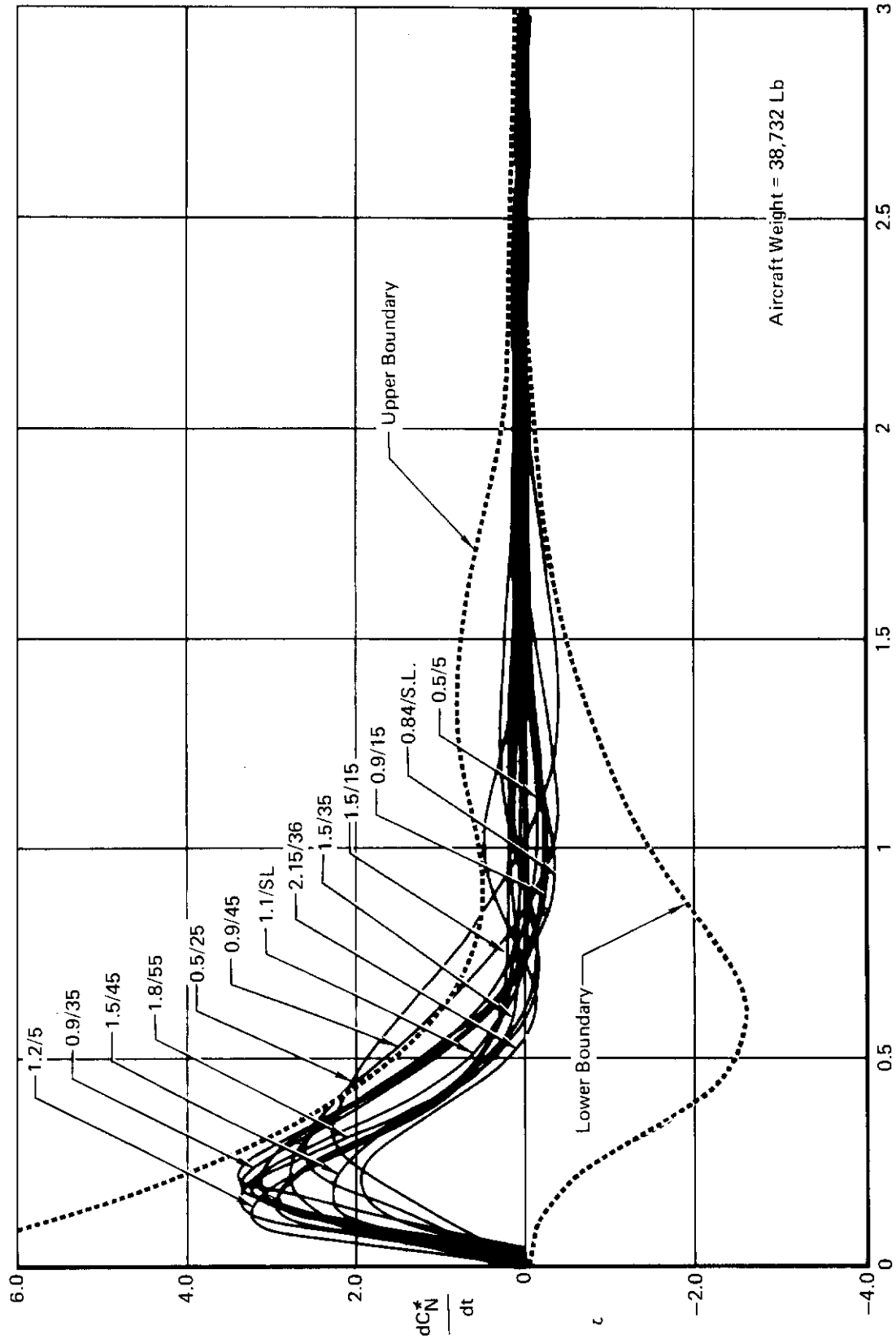

FIGURE 30
LONGITUDINAL SFCS TIME HISTORY $\frac{dC^*}{dt}$ CRITERIA COMPLIANCE
Adaptive Gains - NSS

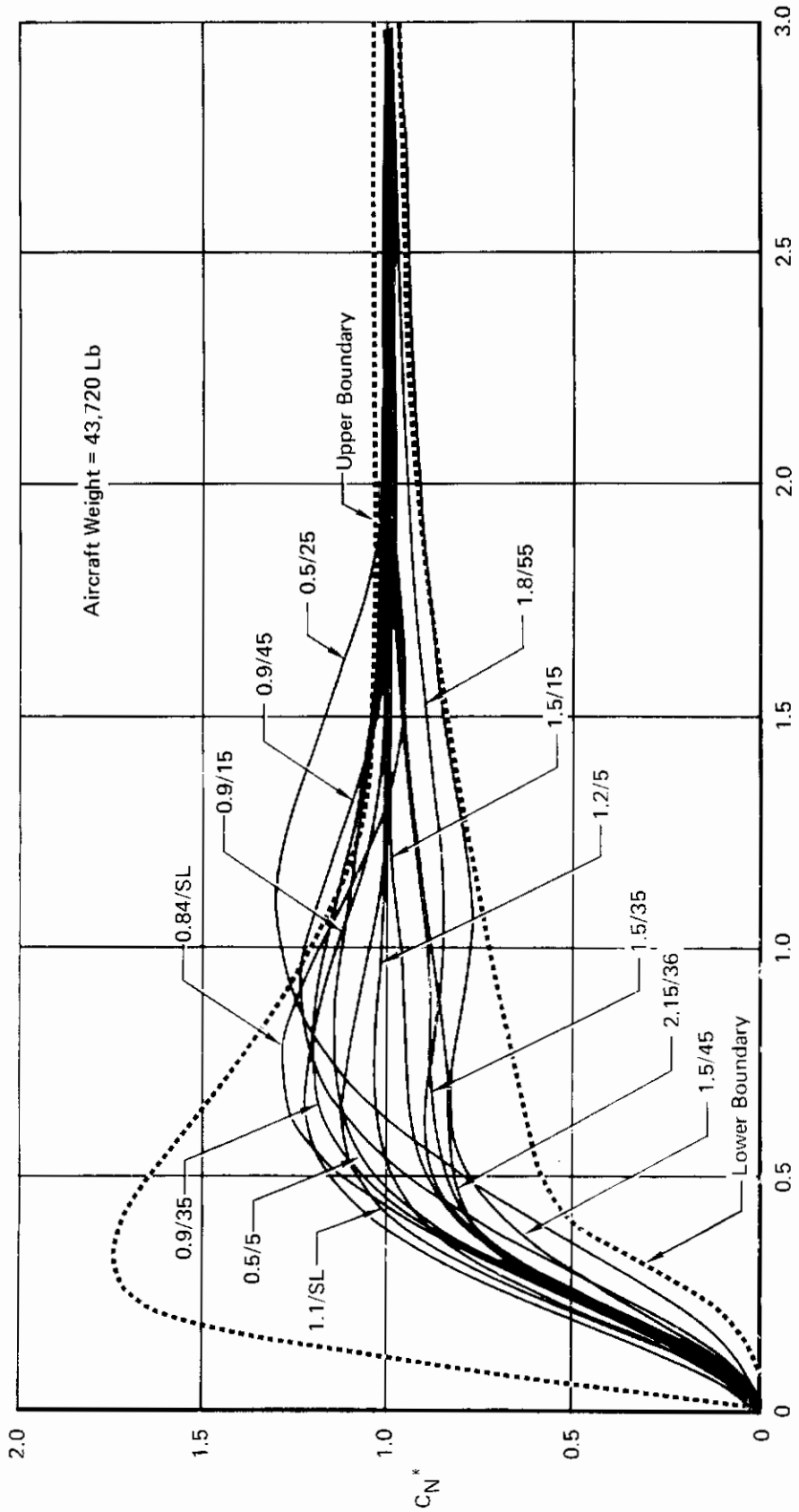

FIGURE 31
LONGITUDINAL SFCS TIME HISTORY C* CRITERIA COMPLIANCE
Adaptive Gains - NSS

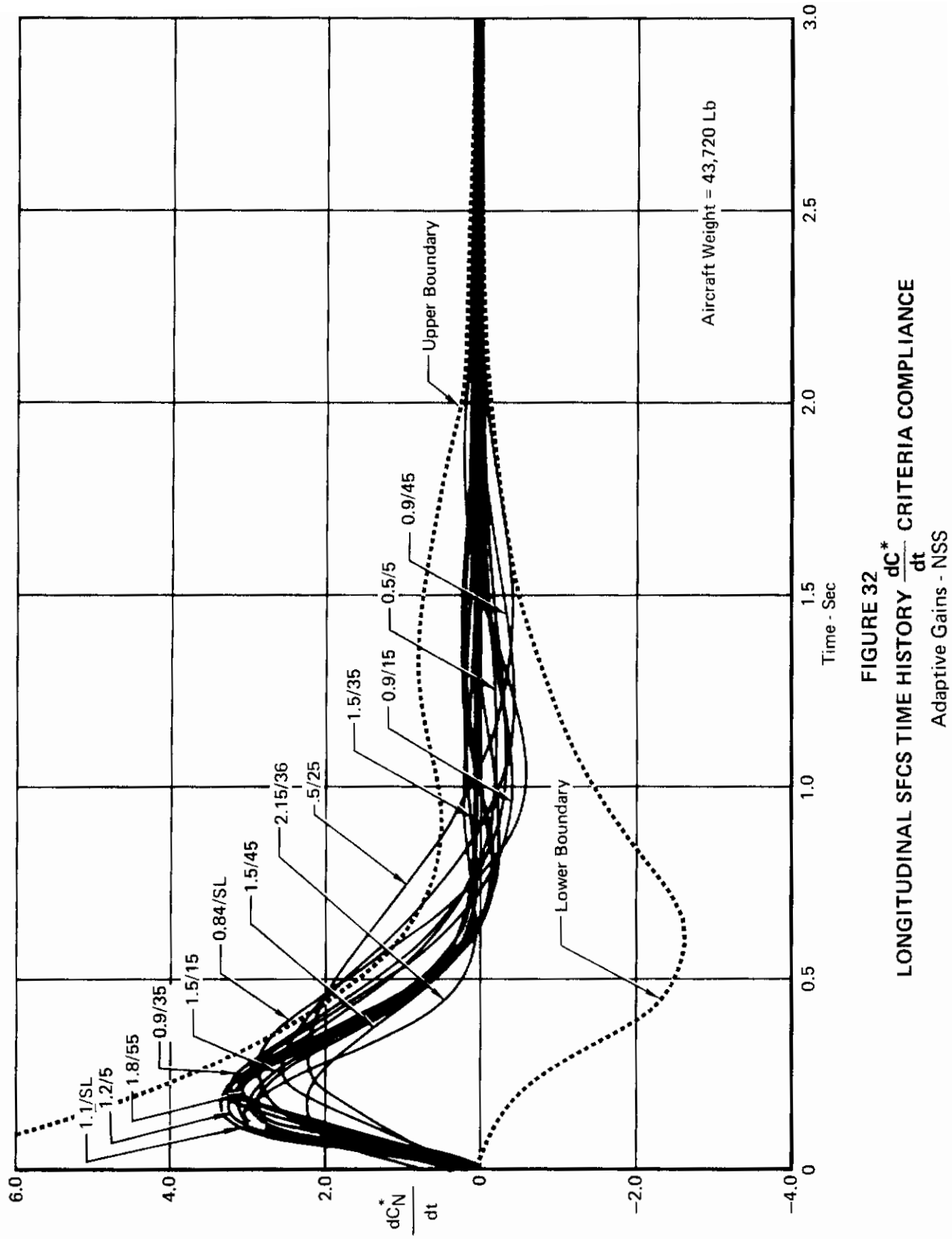

FIGURE 32
LONGITUDINAL SFCS TIME HISTORY $\frac{dC^*}{dt}$ CRITERIA COMPLIANCE
Adaptive Gains - NSS

stability margins. The significance of the response shapes is decreased since at these conditions any maneuver produces speed and/or altitude changes. This effect tends to mask any undesirable characteristics in the load factor and pitch rate response. For this reason, attempts to obtain pilot comments for simulated flight at conditions near the flight envelope boundary were frustrated during the manned simulation program. Evaluation of response characteristics in actual flight are expected to be similarly masked by changes in flight condition. Precise compliance with the handling qualities requirement at these flight conditions is therefore considered relatively unimportant. An increase in the forward loop gain would correct the response characteristics so that the criteria could be met. However, reduction in structural mode attenuation would result unless additional structural filtering was also incorporated. The increased phase lag which would accompany additional structural filtering would deteriorate the stability margins at other flight conditions. The penalties associated with reconfiguring the SFCS control laws to comply with the C* and dC*/dt response criteria at these flight conditions exceed any advantage which might be obtained through improvement in the response characteristics.

(2) Frequency and Damping

Root locus data for the longitudinal SFCS were computed for fifteen flight conditions and two aircraft weights for the purpose of documenting the frequency and damping of the aircraft short period and phugoid modes. Representative root locus plots are provided in Appendix II.

The frequency and damping of the closed loop roots which eminate from the basic aircraft short period poles were compiled for the adaptive gain at each flight condition. These roots represent the predominant oscillatory modes. Figures 33 and 34 present the Level 1 short period frequency requirements of MIL-F-8785B (ASG), Paragraph 3.2.2.1.1 for Category A and C flight phases. The SFCS closed loop short period frequency for each flight condition are superimposed on the requirement envelope and are seen to be within the required values for all flight conditions.

The damping ratios for all flight conditions documented are provided in Figures 35 and 36 and are shown in comparison with the stick force per g and damping ratio boundary contour of Reference 2. The Reference 2 boundary is described in Section III, Paragraph 2.a.(1) of this report. As can be seen, the SFCS short period damping ratios at 29 of the 30 conditions documented are within the Level 1 range, $.35 \leq \zeta \leq 1.3$, specified in MIL-F-8785B (ASG), Paragraph 3.2.2.1.2 for Category A and C flight phases. The one point at which the damping ratio is below the required .35 (Mach 2.15, Alt.=36,000 feet, Wt.=38,732 lb.) is a flight condition on the edge of the

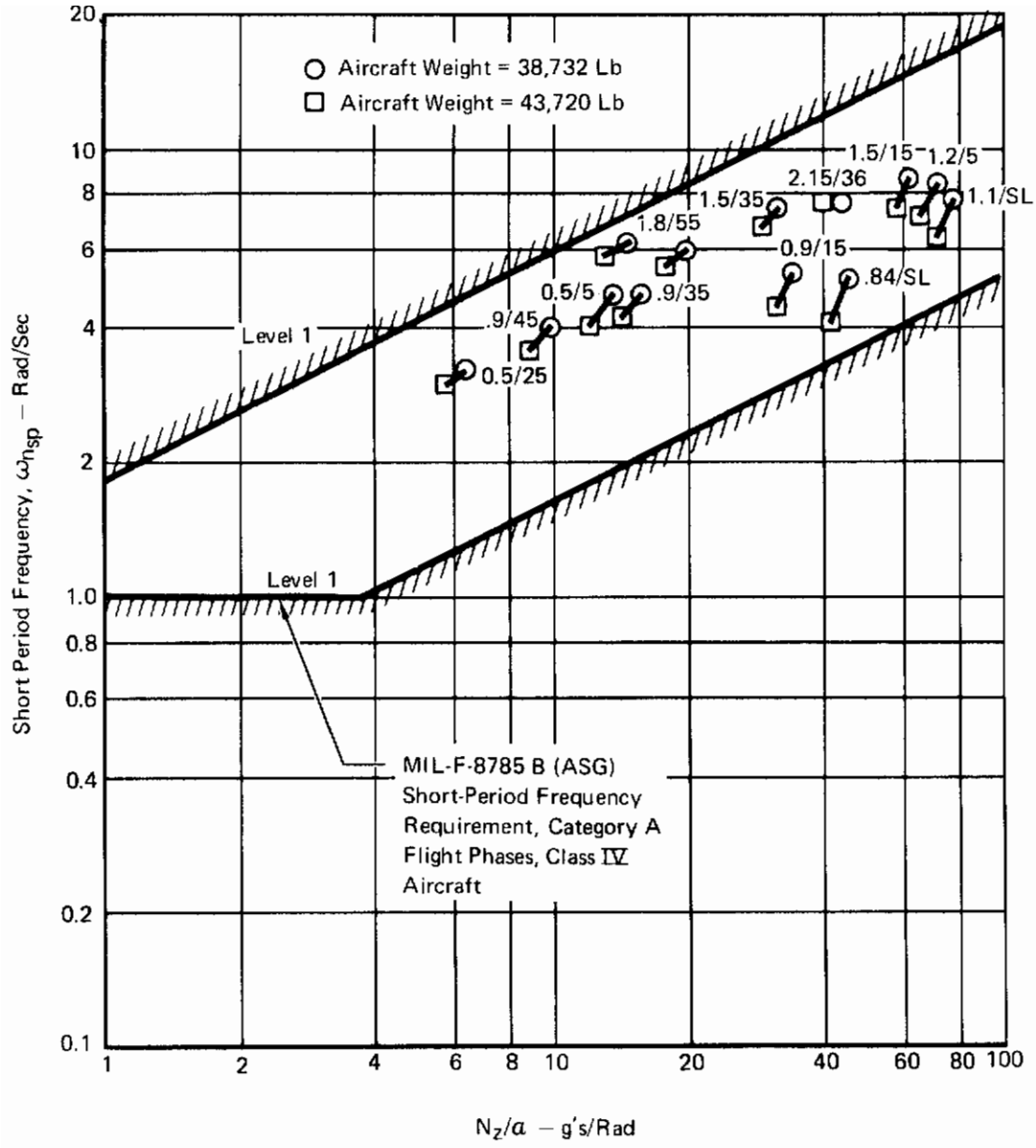

FIGURE 33
SHORT-PERIOD FREQUENCIES FOR CATEGORY A FLIGHT PHASES
Adaptive Gains
NSS

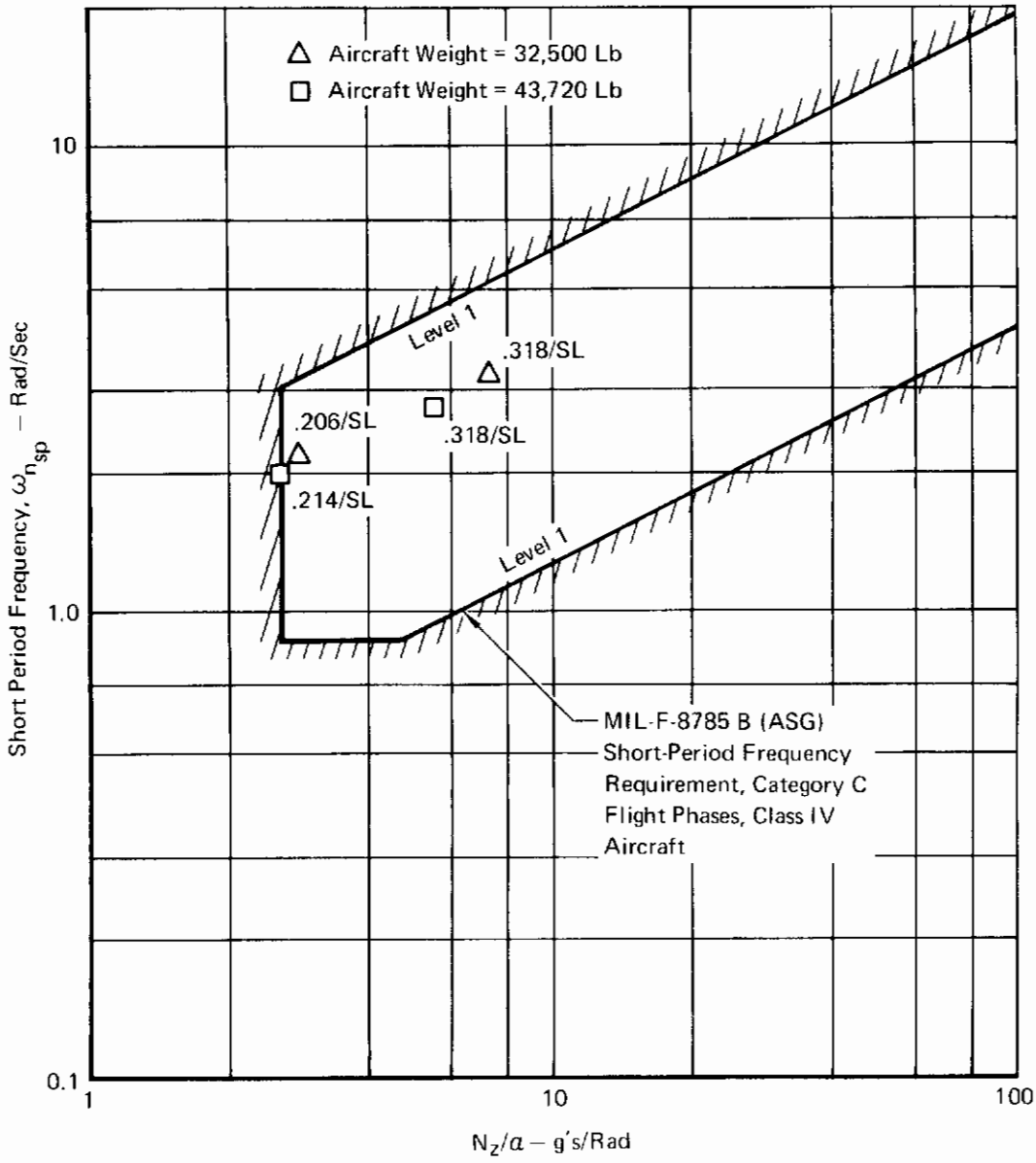

FIGURE 34
SHORT PERIOD FREQUENCIES FOR CATEGORY C FLIGHT PHASES
Adaptive Gains
TOL

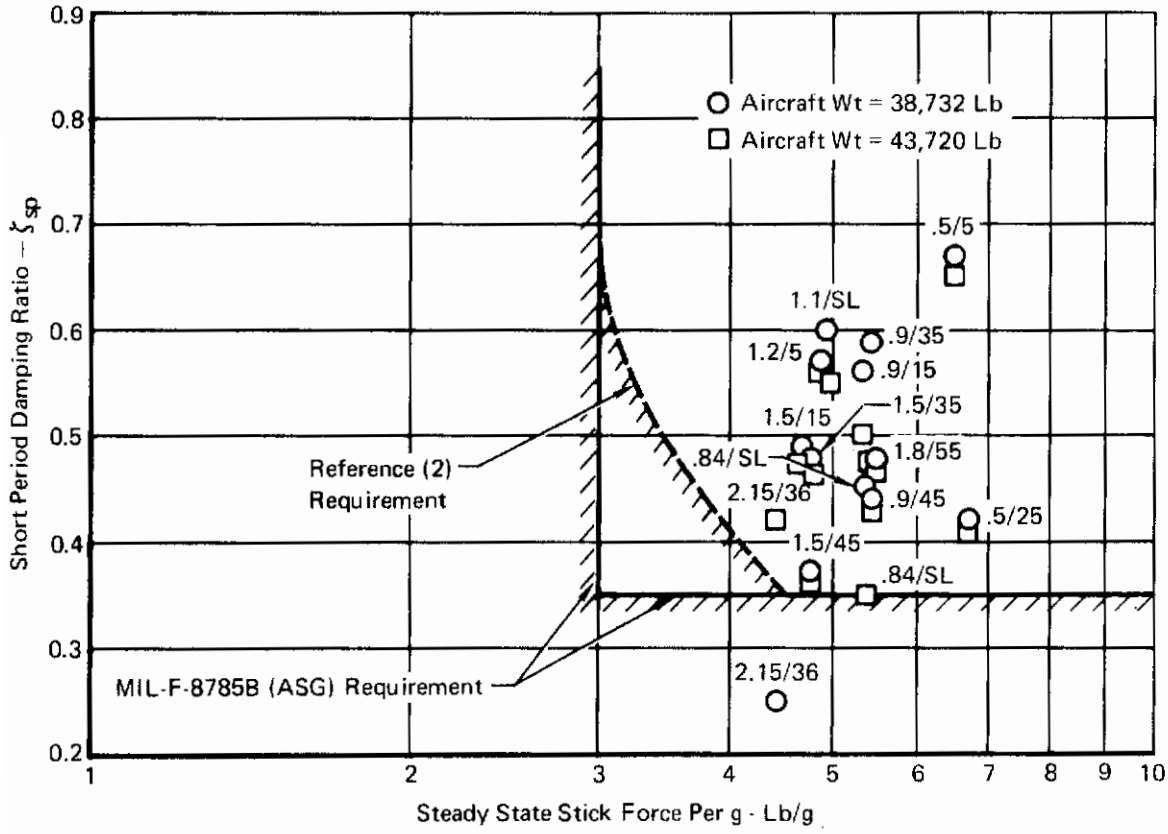

FIGURE 35
SHORT PERIOD DAMPING RATIO FOR CATEGORY A FLIGHT PHASE
Adaptive Gains
NSS

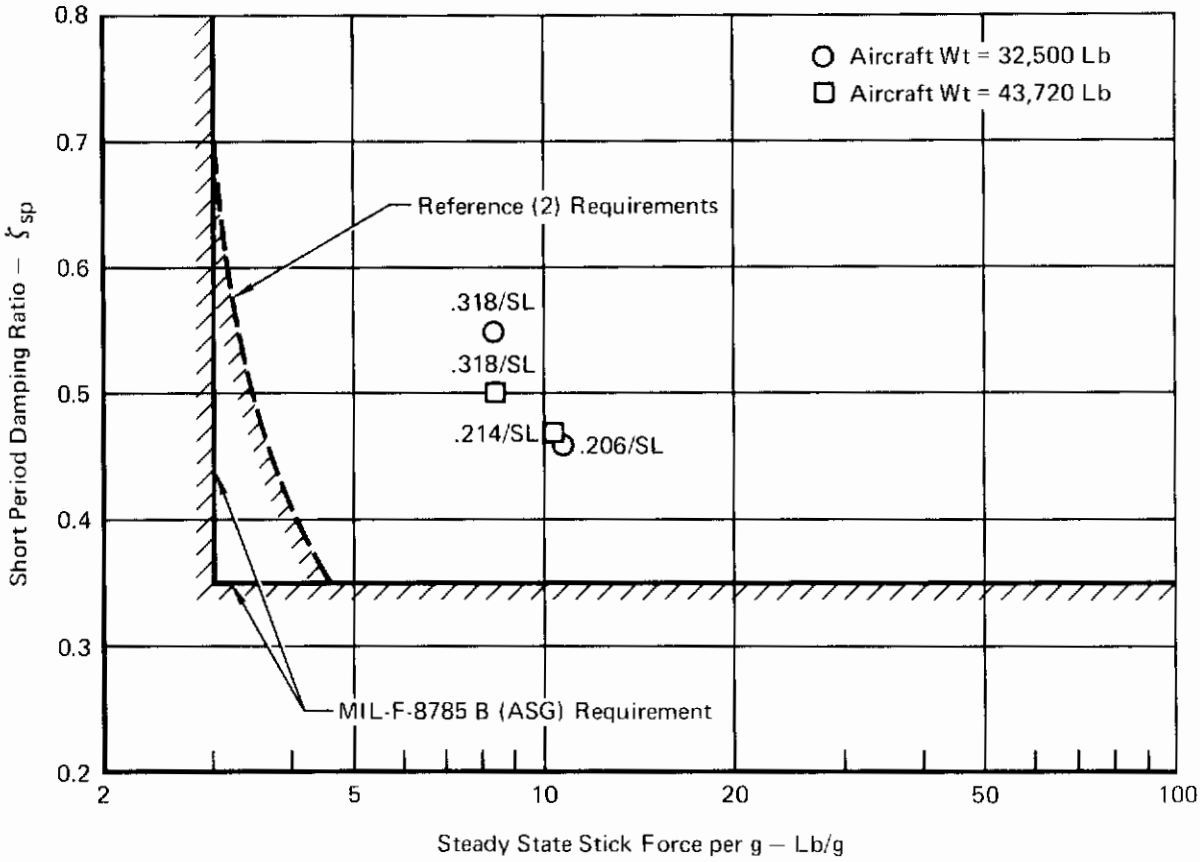

FIGURE 36
SHORT PERIOD DAMPING RATIO FOR CATEGORY C FLIGHT PHASE
Adaptive Gains
TOL

flight envelope. Sustained, maneuvering flight is impossible at this flight condition, since the drag created when a maneuver is initiated results in rapid loss of airspeed.

(3) Maneuvering Force Gradient

The center stick sensitivity was set to provide a minimum maneuvering force gradient of four pounds per g at the high $\bar{q}$ flight conditions. The electrical gains were appropriately distributed to allow pilot commanded limit load factor without voltage saturation in the SFCES.

The center stick maneuvering force gradients for the longitudinal SFCS are presented in Figure 37 for 15 flight conditions and two aircraft weights. All flight conditions investigated exhibited stick force per g characteristics in compliance with the Level 1 requirements of MIL-F-8785B (ASG) Paragraph 3.2.2.2.1.

Provisions were made in the SFCES to vary the center stick sensitivity through a range of 50% to 150% of the nominal value. The sidestick controller longitudinal sensitivity was selected and evaluated during the man-in-the-loop simulation program. Figure 38 shows a comparison of the center stick and sidestick output commands as a function of pilot applied force. The sidestick has a breakout of 1.75 pounds followed by dual linear gradients. The breakout was originally set at 2.5 pounds; however, it was found during the man-in-the-loop simulation that this value was too high. Consequently, the breakout was adjusted down to 1.75 pounds at which point favorable pilot comments were received for simulated flight with the sidestick. Dual gradients were provided in the SSC to permit fine control of pitch attitude or normal acceleration with low force inputs while retaining limit load factor capability with higher forces. Evaluation of the SSC during the flight simulation program indicated that satisfactory gradients have been chosen. A capability to adjust the location of the gradient brake point has been included in the system design.

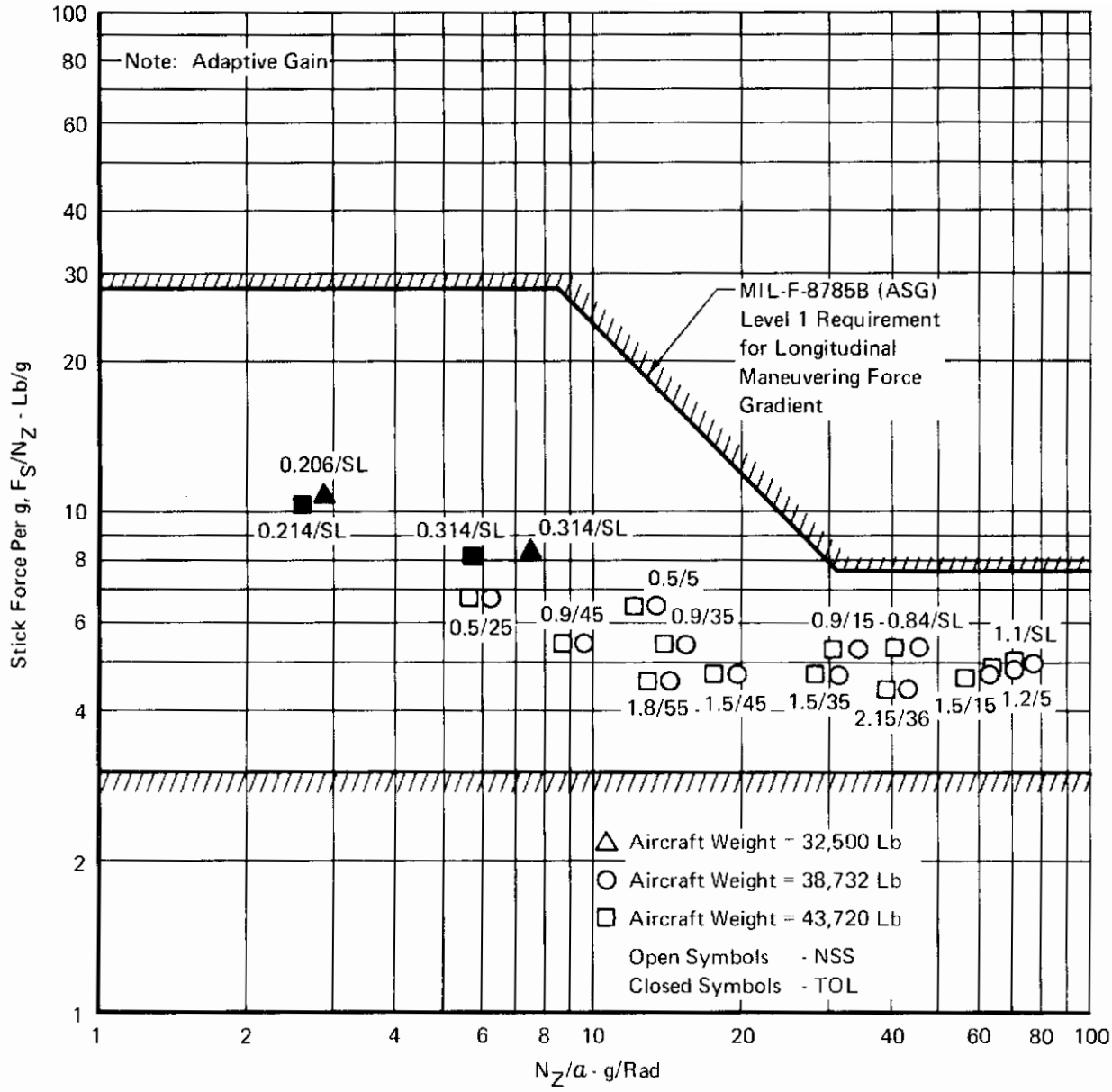

FIGURE 37
STICK FORCE PER g

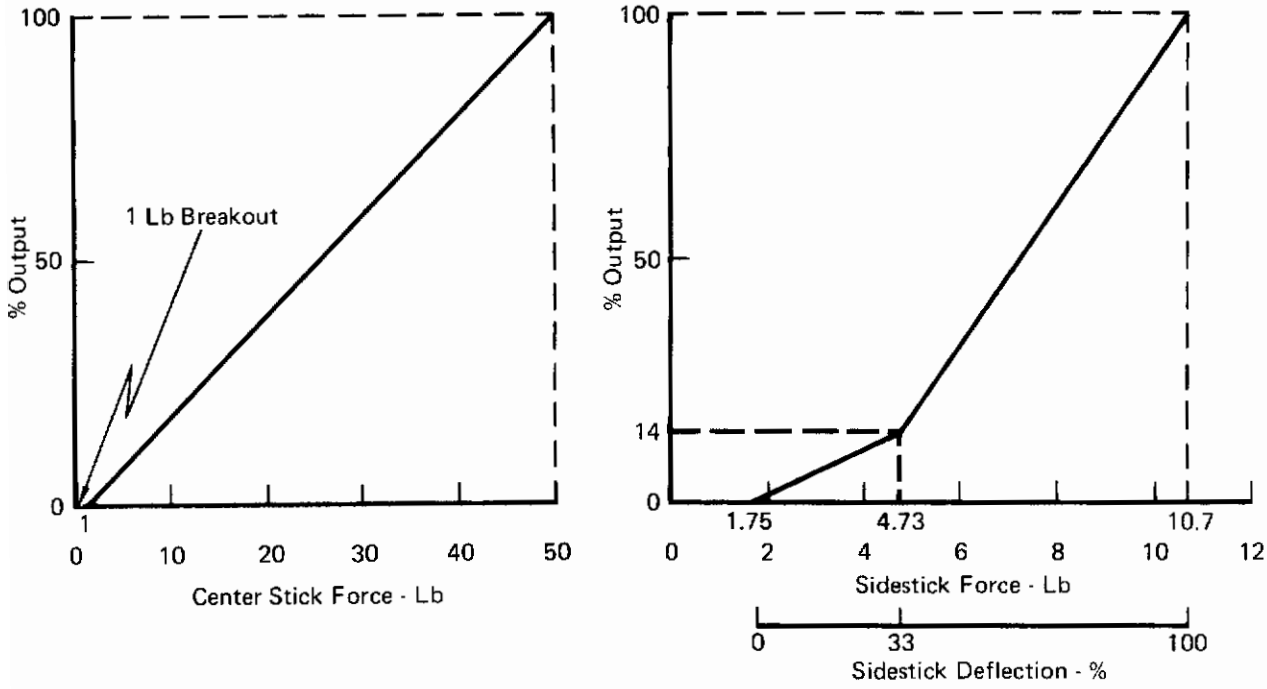

FIGURE 38
LONGITUDINAL CONTROL SYSTEM COMMAND vs STICK FORCE

SECTION IV

LATERAL-DIRECTIONAL

CONTROL LAW DEVELOPMENT

1. SYSTEM DESCRIPTION

This section describes the overall mechanization of the lateral and directional control laws as presently planned. Further details of the actuator control loops and trim mechanization are presented in TR-71-20, Section III.

a. Lateral Axis

A functional block diagram of the lateral axis is shown in Figure 39 . This figure shows only one channel of the lateral axis. The other three channels are identical with the exception of failure insertion circuitry which is part of the "yellow" channel only. Crossfeed from one channel to another is provided at the Signal Selection Device (SSD) only.

The lateral axis utilizes a fly-by-wire mechanization from the outset of Phase IIA. No mechanical back-up system is used. The axis has two major modes of operation: a Normal mode which is a fixed gain closed loop mode with roll to yaw crossfeed, and an open loop Electrical Back-Up (EBU) mode. The Normal mode incorporates a high gain model following technique to achieve a nearly constant roll rate time constant and roll rate to stick force sensitivity throughout the flight envelope. The high gain tends to mask the basic airframe response, forcing it to follow the prefilter response which is under the designer's control.

The lateral axis operation is comprised of the following major signal paths and shaping networks. The center stick force transducer signal, after shaping by a special network consisting of a dead zone followed by a dual gradient, is passed through the prefilter model, gain adjusted by the gear position sensing network, and summed with roll rate feedback to become the lateral axis forward loop command signal. The prefilter model output signal also commands yaw rate (for turn coordination) through the roll to yaw crossfeed network. A second signal from the stick force signal shaping network bypasses the prefilter model and, after proper scaling, is applied to the SSD. This second command signal path serves both as the EBU mode signal path and as part of the Normal mode forward path. The forward and aft side stick lateral position signals, after summing, demodulation, and shaping, are added to the correspondingly shaped center stick signals. The side stick position signals perform the identical function as the center stick force signals and provide parallel paths for lateral control.

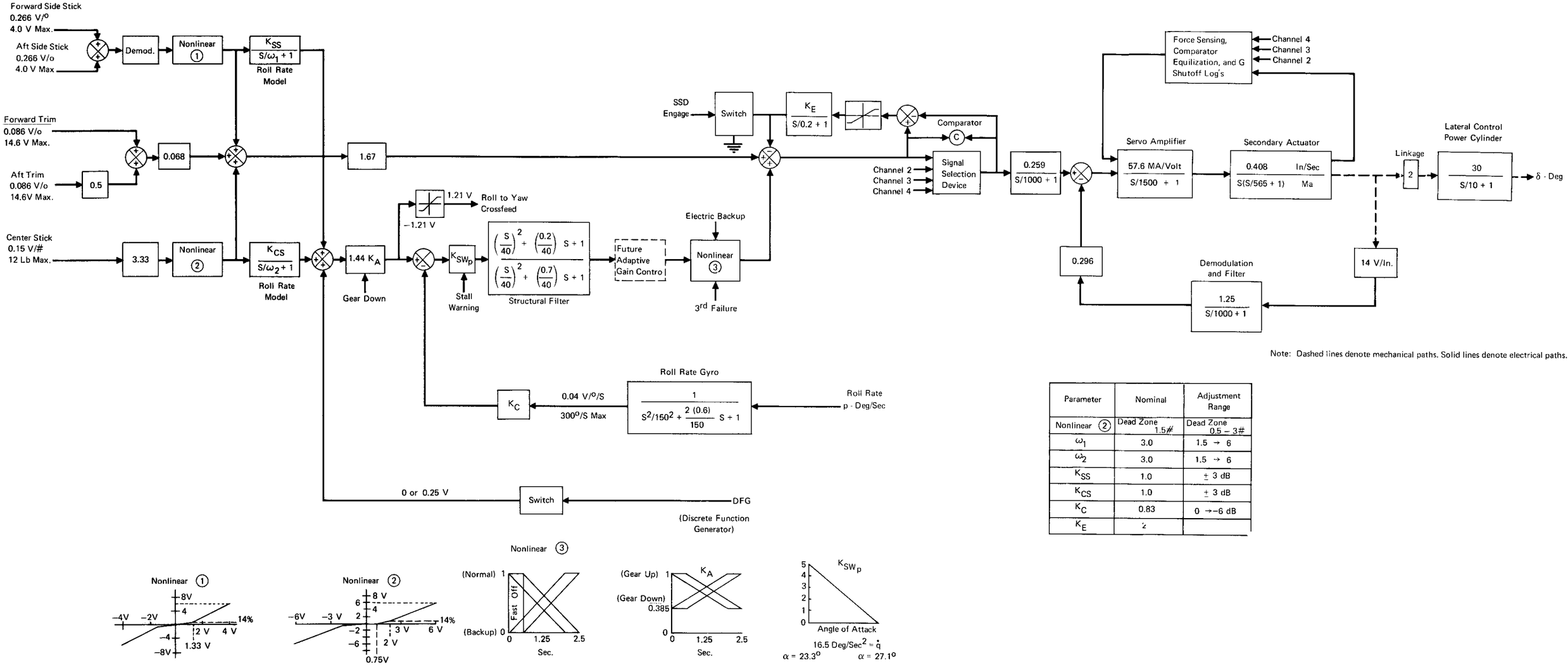

Note: Dashed lines denote mechanical paths. Solid lines denote electrical paths.

Parameter	Nominal	Adjustment Range
Nonlinear ②	Dead Zone 1.5#	Dead Zone 0.5 – 3#
ω_1	3.0	1.5 → 6
ω_2	3.0	1.5 → 6
K_{SS}	1.0	± 3 dB
K_{CS}	1.0	± 3 dB
K_C	0.83	0 → −6 dB
K_E	'	

FIGURE 39
SFCS PHASE IIA LATERAL AXIS FUNCTIONAL BLOCK DIAGRAM

The Normal mode forward loop command signal is shaped by the stall warning computer adjusted gains, a structural mode notch filter, and the Normal to back-up mode switching network before entering the SSD. The output of the SSD is applied to the summing amplifier of the minor loops around the secondary actuators in each wing. These minor loops consist of a servoamplifier, feedback filter and demodulator, and summing amplifier which sums actuator commands with actuator position feedback.

Other functions included in the lateral axis are the forward and aft trim and a discrete function generator. Provisions to accept signals from additional lateral axis modes and/or an adaptive gain control in the future are also included. The lateral axis trim operates through the EBU path and therefore is available during both Normal and EBU mode operation. The discrete function generator is a Normal mode provision only, and is utilized to obtain discrete inputs for data correlation between simulator and flight test results.

b. Directional Axis

A directional axis functional block diagram is presented in Figure 40. This figure shows only one channel of the directional axis. The other three channels are identical with the exception of failure insertion circuitry which is part of the "yellow" channel only. Crossfeed from one channel to another is provided at the SSD only.

The directional axis includes a mechanical back-up capability in Phase IIA resulting in three major modes of operation: a fly-by-wire Normal mode, an open loop EBU mode and a mechanical back-up mode. Switching from the fly-by-wire modes to the mechanical back-up mode is accomplished through the Mechanical Isolation Mechanism (MIM). The pilot has the option, while in mechanical back-up mode, to engage the normal F-4 yaw Stability Augmentation System (SAS).

The EBU mode is an open loop mode and provides rudder position commands only. The Normal mode is a closed loop, employing yaw rate and lateral acceleration feedback to improve aircraft Dutch Roll damping and turn coordination. The rudder pedal force transducer signal, after shaping, is summed with shaped yaw rate, lateral acceleration, and the roll to yaw crossfeed signals to become the directional axis command signal. Yaw rate feedback is shaped by a washout network and a variable gain. Lateral acceleration feedback is shaped by a fixed gain and a first order lag to attenuate the high frequency body bending pickup. Roll to yaw crossfeed uses a variable lag-lead and washout network. Both pilot selectable and adaptive gain control is provided for the yaw rate feedback and roll to yaw crossfeed networks. The gain levels are as shown in Figure 40.

As in the lateral axis, the directional EBU signal bypasses the low pass filter and adds into the forward loop at the SSD. The EBU

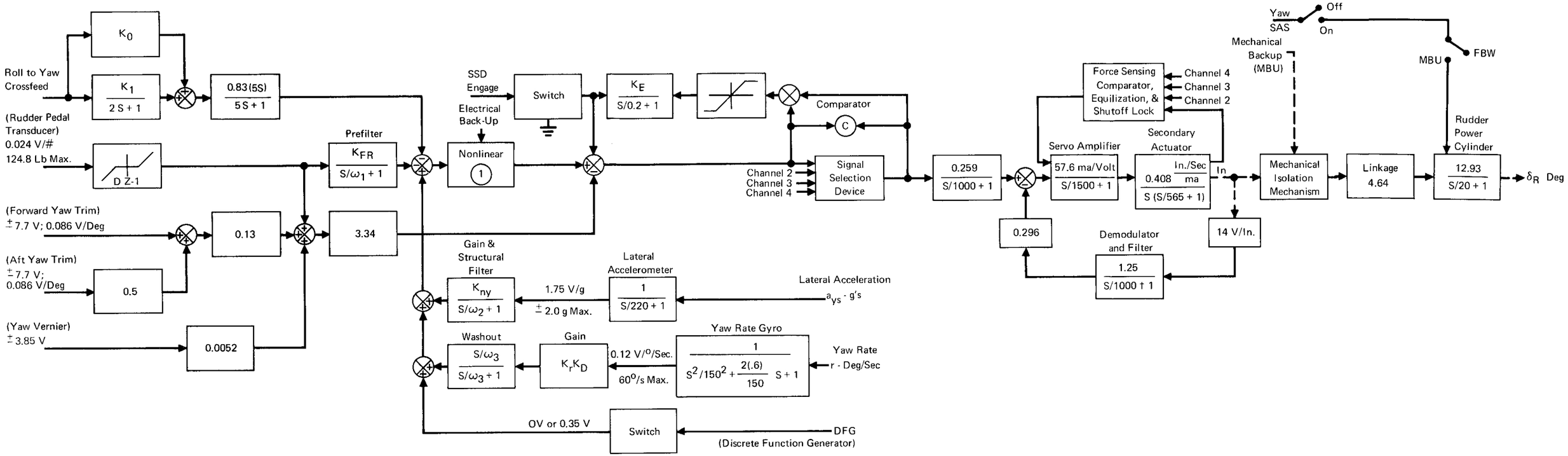

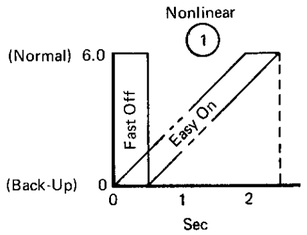

Level / Gain	Gear Up: Adaptive $M_\delta < 6$	Gear Up: Adaptive $6 < M_\delta < 10$	Gear Up: Adaptive $10 < M_\delta < 30$	Gear Up: Adaptive $M_\delta > 30$	Gear Up: Manual Switch Position High	Gear Up: Manual Switch Position Med	Gear Up: Manual Switch Position Low	Gear Down
K_0	0.325	0.15	0.0	0.0	0.325	0.0	0.0	0.35
K_1	0.0	0.05	0.2	0.0	0.0	0.2	0.0	0.2
K_r	0.83	1.67	1.67	3.33	0.83	1.67	3.33	0.83

Note: Gain Change Time = 2 Sec.

Parameter	Nominal	Adjust Range
K_{FR}	0.278	
ω_1	3.0	1.5 – 6.0
ω_2	40.0	
ω_3	0.5	0.25 – 1.0
K_{ny}	0.815	±3.0 dB
K_D	0.42	±3.0 dB
K_E	20.0	
DZ-1	5.0 #	2.4 – 5.5 #

FIGURE 40
SFCS PHASE IIA DIRECTIONAL AXIS FUNCTIONAL BLOCK DIAGRAM

signal path is used at all times, and is in parallel with the Normal mode signal path, rather than being switched in and out.

The directional forward loop contains the Normal to back-up mode switching network, SSD, MIM and a minor loop around the secondary actuator identical to those in the lateral axis. The directional yaw vernier and the forward and aft trim sum into the EBU path and are available during both Normal and EBU mode operation. The directional DFG operates in the Normal mode only and is utilized to obtain discrete inputs for data correlation between simulator and flight test results.

2. SYSTEM SYNTHESIS

a. Introduction

The SFCS lateral-directional control laws were developed initially using the linearized three-degree-of-freedom equations of motion. The resulting control system was then programmed into the man-in-the-loop, fixed base, control system evaluation simulation for evaluation and modification. This later effort is detailed in Section V of this supplement. Pertinent aircraft physical data and the equations of motion coefficients relating to the flight conditions employed in the three-degree-of-freedom analysis are presented in Appendix I.

The lateral-directional three-degree-of-freedom model included linearized secondary actuator, power cylinder and sensor models in the control loops. The airload limits on aileron, spoiler, and rudder deflection were introduced into the overall model when considering maximum maneuvers. The aileron and spoiler systems were considered as a single moment producing surface with their combined effect being represented by a single coefficient in each equation of motion. An equivalent limit was calculated for the combined aileron and spoiler surface description for those flight conditions at which the aileron or spoiler deflections were airload limited. Rudder flexibility effects resulting from the spring effect in the rudder torque tube were maintained constant during each flight condition and included in the directional axis forward loop. The result of rudder flexibility is a reduction in directional loop gain and effective rudder authority as $\bar{q}$ increases.

The objectives of the lateral-directional control law design were:

To utilize advanced control techniques available with the use of a fly-by-wire system to improve on the F-4 basic handling qualities and performance, and

- to comply with the criteria of MIL-F-8785B (ASG) in applicable areas.

In addition, the SFCS system performance was evaluated with respect to the handling qualities criteria reported in TR-71-20, Supplement 1.

The method of approach employed in the development of the lateral-directional control laws was to develop the lateral loop first based on the single-degree-of-freedom roll equation. The synthesis then proceeded to the directional loop and the roll to yaw crossfeed network. Parallel studies were performed on sensor location and structural dynamic effects as sufficient structural data became available. As the synthesis progressed, the control laws were incorporated into the six-degree-of-freedom man-in-the-loop simulation for pilot evaluation. Figure 41 is a simplified lateral-directional control law block diagram.

b. Sensor Placement

The location of the aircraft motion sensors is guided by the desire to sense only appropriate rigid body motion and to suppress undesirable sensing of structural mode oscillations. An analysis of the structural mode pickup as a function of sensor placement is presented in Appendix V.

The roll rate and yaw rate gyros will sense pitch, roll and yaw rates due to gyro inclination effects. To minimize cross axis sensing, the roll and yaw rate gyro sensitive axes are located parallel to and perpendicular to the average longitudinal principal axis, respectively. The F-4s longitudinal principal axis orientation with respect to the aircraft waterline varies with both weight and configuration but has an average value of 1.5 degrees below a waterline.

Since roll rates are normally much greater than yaw rates, the tolerances on the roll rate gyro axis inclination are not critical. The yaw rate gyro sensitive axis inclination is much more critical. If the yaw rate gyro sensitive axis is rotated to obtain an angle less than 90° relative to the positive longitudinal principal axis, positive roll rate will be sensed and a rolling maneuver can cause a significant increase in adverse sideslip. Rotating the yaw rate gyro sensitive axis to obtain an angle greater than 90° relative to the positive longitudinal principal axis causes an increase in proverse sideslip at high $\bar{q}$ low angle-of-attack flight conditions and is generally accompanied by a decrease in Dutch Roll damping.

The location of the lateral accelerometer is mainly a function of the structural mode pickup. However, its location with respect to the longitudinal principal axis is also of some importance. If the lateral accelerometer is significantly displaced from the longitudinal principal axis a considerable amount of rolling acceleration pickup can result. This additional acceleration feedback will contribute adverse sideslip if the accelerometer is below the longitudinal principal axis and proverse sideslip if it is above the longitudinal principal axis.

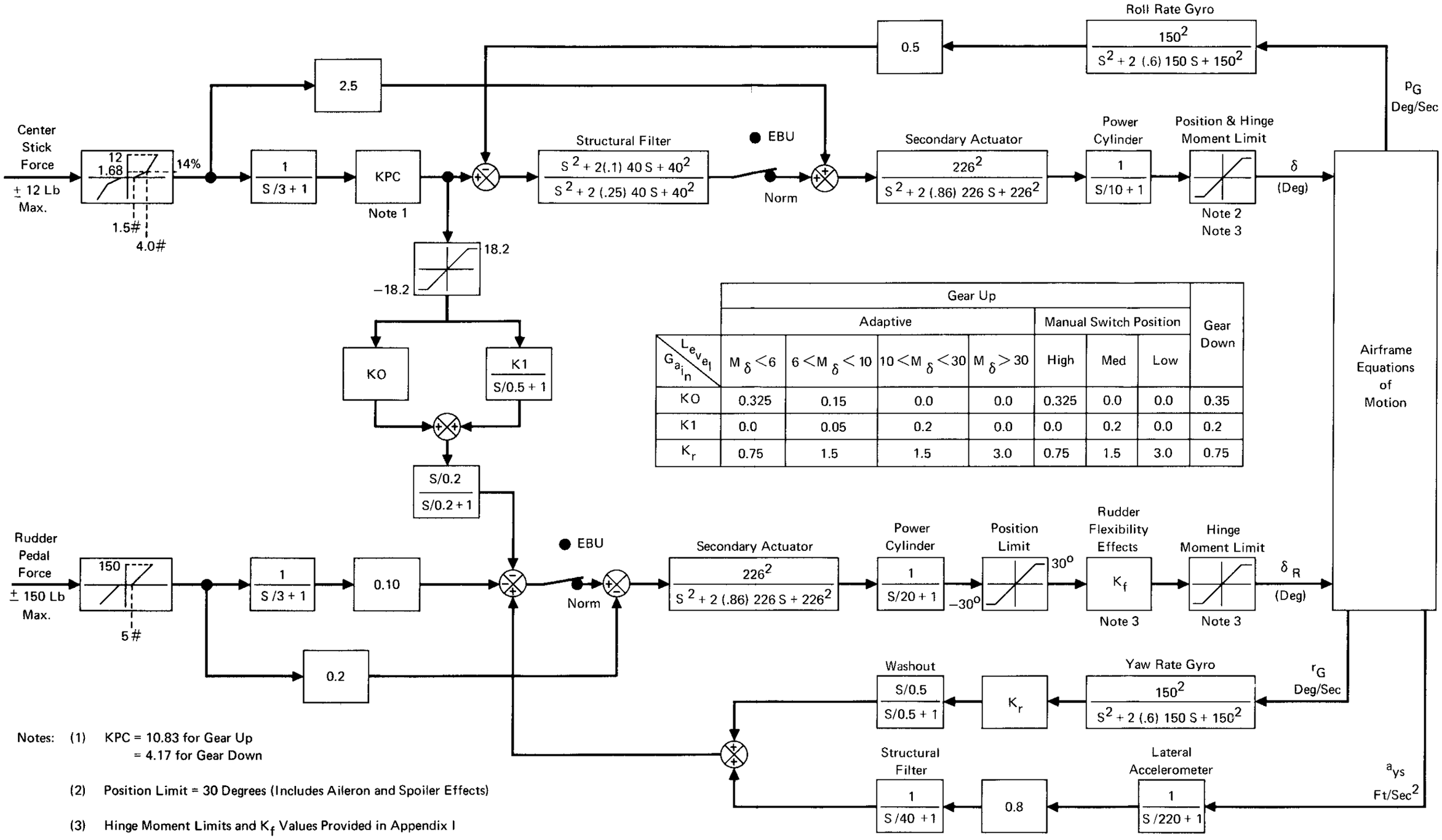

Gain \ Level	Gear Up: Adaptive $M_\delta < 6$	Gear Up: Adaptive $6 < M_\delta < 10$	Gear Up: Adaptive $10 < M_\delta < 30$	Gear Up: Adaptive $M_\delta > 30$	Gear Up: Manual Switch Position High	Gear Up: Manual Switch Position Med	Gear Up: Manual Switch Position Low	Gear Down
KO	0.325	0.15	0.0	0.0	0.325	0.0	0.0	0.35
K1	0.0	0.05	0.2	0.0	0.0	0.2	0.0	0.2
K_r	0.75	1.5	1.5	3.0	0.75	1.5	3.0	0.75

Notes: (1) KPC = 10.83 for Gear Up
= 4.17 for Gear Down

(2) Position Limit = 30 Degrees (Includes Aileron and Spoiler Effects)

(3) Hinge Moment Limits and K_f Values Provided in Appendix I

FIGURE 41

LATERAL-DIRECTIONAL CONTROL LAW BLOCK DIAGRAM

c. Lateral Axis

A roll rate command system was considered fundamental to a control system designed to improve lateral performance. The aims of the SFCS lateral control design were to provide a nearly constant roll rate time constant and roll rate to stick force sensitivity throughout the flight envelope, in addition to complying with the requirements in MIL-F-8785B (ASG).

The major rolling response criteria specified in MIL-F-8785B (ASG) are the time to bank, the roll mode time constant and the maximum allowable Dutch Roll oscillations coupled into the roll mode. A fixed gain in the lateral loop suffices to comply with the last two criteria, and a loop gain of 0.5 radians per radian per second was selected. Single-degree-of-freedom roll rate loop root loci presented in Figures 42 and 43 show that the 0.5 loop gain decreases the roll mode time constant for the low roll power flight conditions while avoiding the introduction of a lightly damped oscillatory roll mode at high roll power flight conditions. In addition to introducing a roll mode oscillation, higher values of lateral loop gain were avoided due to the additional structural mode filtering required. Appendix V includes a discussion of the structural mode pickup through the roll rate gyro.

Using the F-4, it is not possible to comply with the MIL-F-8785B (ASG) time to bank requirements for Level 1 Categories A and C at all flight conditions. The original F-4 design was not required to provide the high roll power capability at all flight conditions needed to comply with this time to bank criteria. Modification in the F-4 lateral control system to meet these updated requirements is beyond the scope of this program. The SFCS roll power and the related time to bank are therefore limited to that achieved with maximum aileron and spoiler deflection. Figures 44 and 45 show the presently estimated F-4E maximum steady state roll rates and the bank angle achievable at one second following a full lateral surface step deflection command. These estimated data show that the maximum F-4 roll power prevents compliance with the aforementioned MIL-F-8785B (ASG) time to bank criteria. There is good general agreement between this estimated data and flight test data except at low to medium altitude, high subsonic Mach numbers where the estimates of maximum roll rates are low. Flight test data show that the maximum roll rate of 260 degrees per second can be achieved at 0.9 Mach at 15,000 ft. altitude.

The SFCS roll rate command to stick force gain (KPC), as shown in Figure 41 , was compiled using the following equation to provide the 260 degrees per second maximum roll rate capability at full stick force:

$$KPC = \frac{260(deg/sec)0.5}{12(lbs)} = 10.83 \left(\frac{deg/sec}{lb}\right)$$

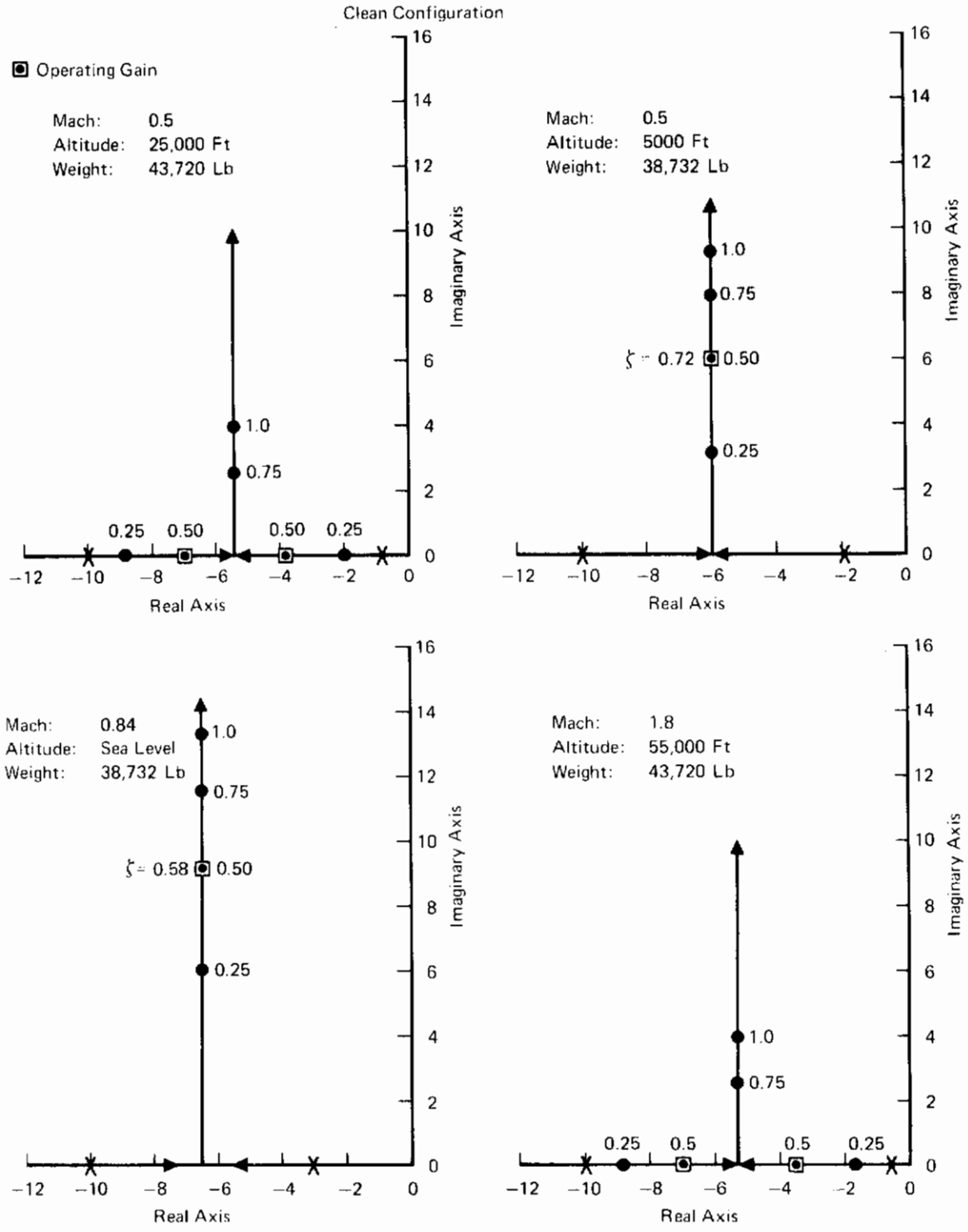

FIGURE 42
ROLL-RATE LOOP ROOT LOCUS
(Single Degree of Freedom)

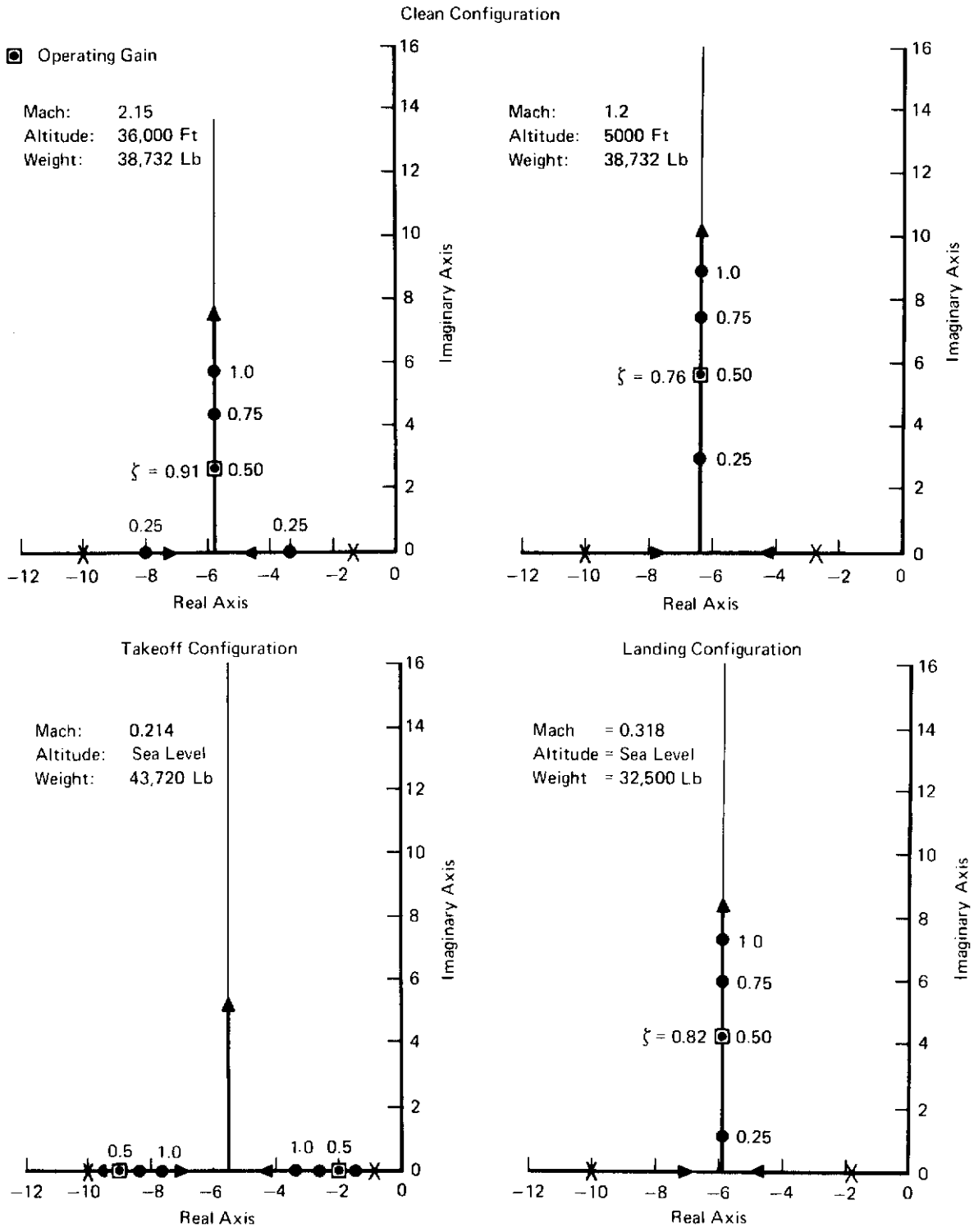

FIGURE 43
ROLL-RATE LOOP ROOT LOCUS
(Single Degree of Freedom)

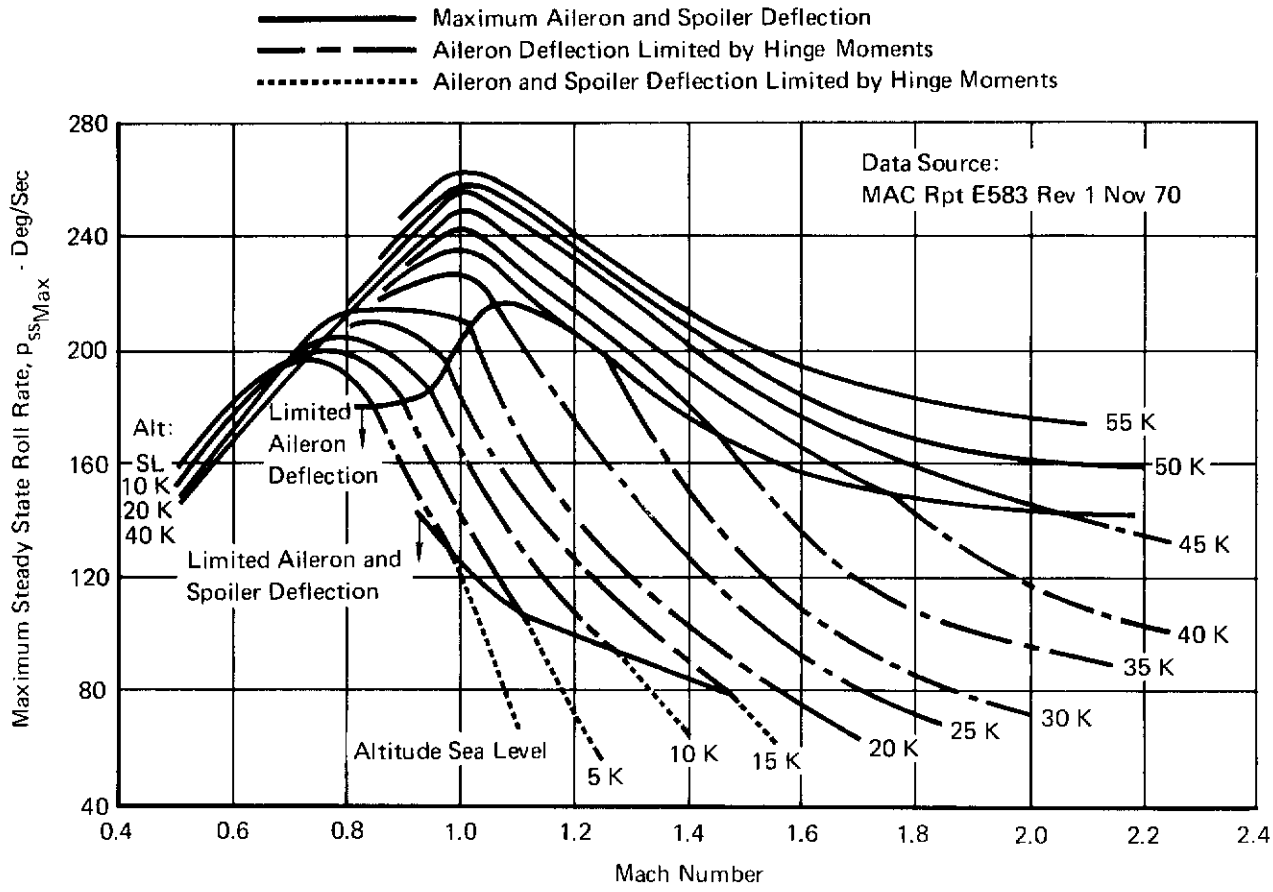

FIGURE 44

MAXIMUM STEADY STATE ROLL RATES

Weight = 38,924 Lb CG at 28.9% $\bar{c}$

Clean Configuration

$N_{Z_{Entry}}$ = 1.0g

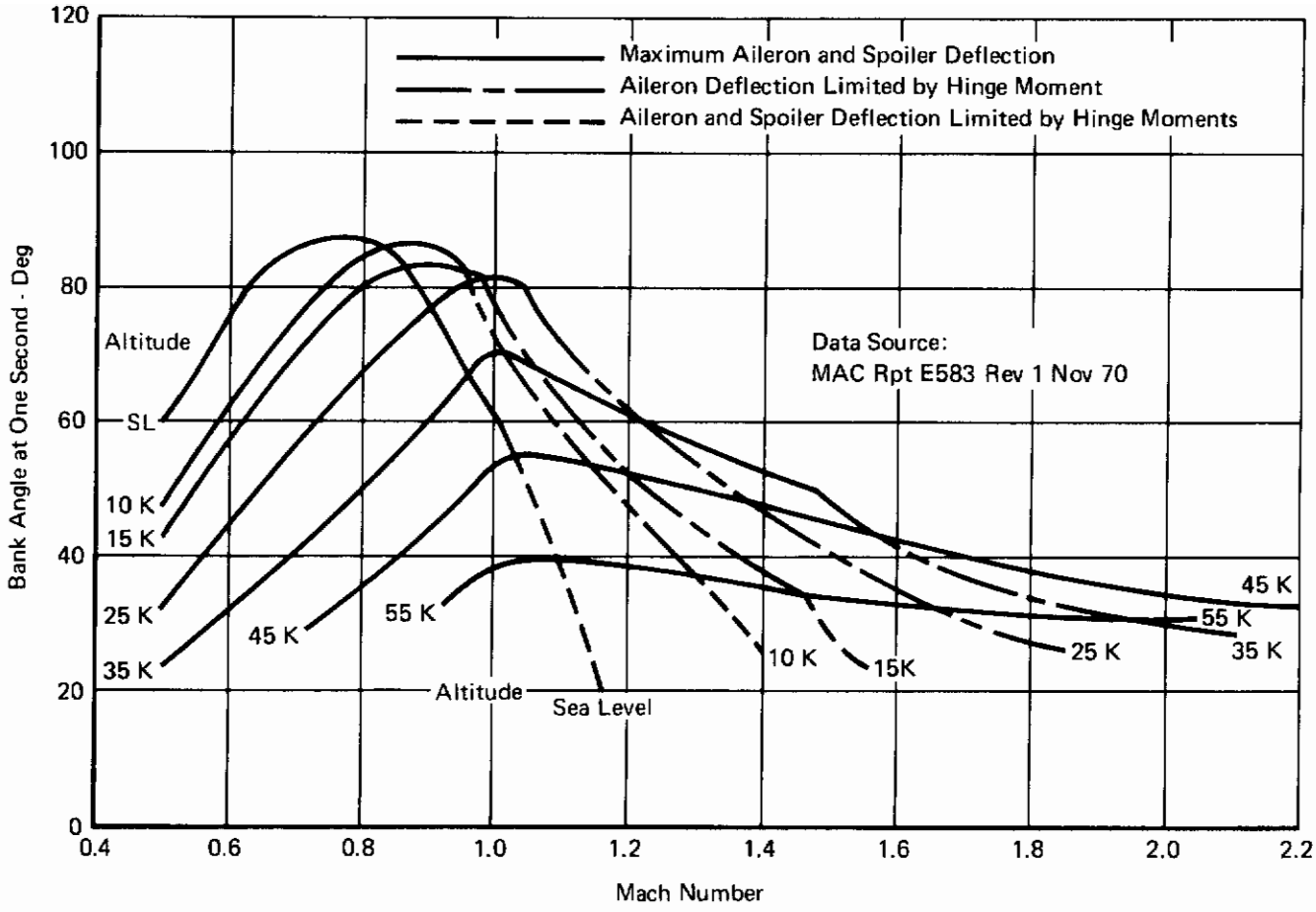

FIGURE 45
BANK ANGLE AT ONE SECOND
Weight = 38,924 Lb
I_X = 25,000 Slug-Ft^2
0.1 Sec Control System Lag Included

The EBU mode command path is used as part of the Normal mode and provides the aileron position commands necessary to maintain this maximum roll rate. The EBU mode gain was also selected for maximum surface deflection capability at maximum stick force. To provide the pilot with lower sensitivity at approach, the roll rate command gain (KPC) is reduced to 4.16($\frac{\text{deg/sec}}{\text{lb}}$) by the gear down switch.

The lateral stick force transducer signal is shaped by a special network consisting of a dead zone followed by a dual gradient. This nonlinearity maintains good control characteristics by providing for a lower roll rate to stick force sensitivity around neutral while allowing for high roll rate commands without excessive stick force. The dual gradient was evaluated during the man-in-the-loop simulation and found to improve handling qualities and performance. Figure 46 shows the lateral stick force nonlinearity for both the center and side stick controllers. These nonlinearities provide 14% of the maximum roll rate command at 33% of maximum center stick force or side stick displacement.

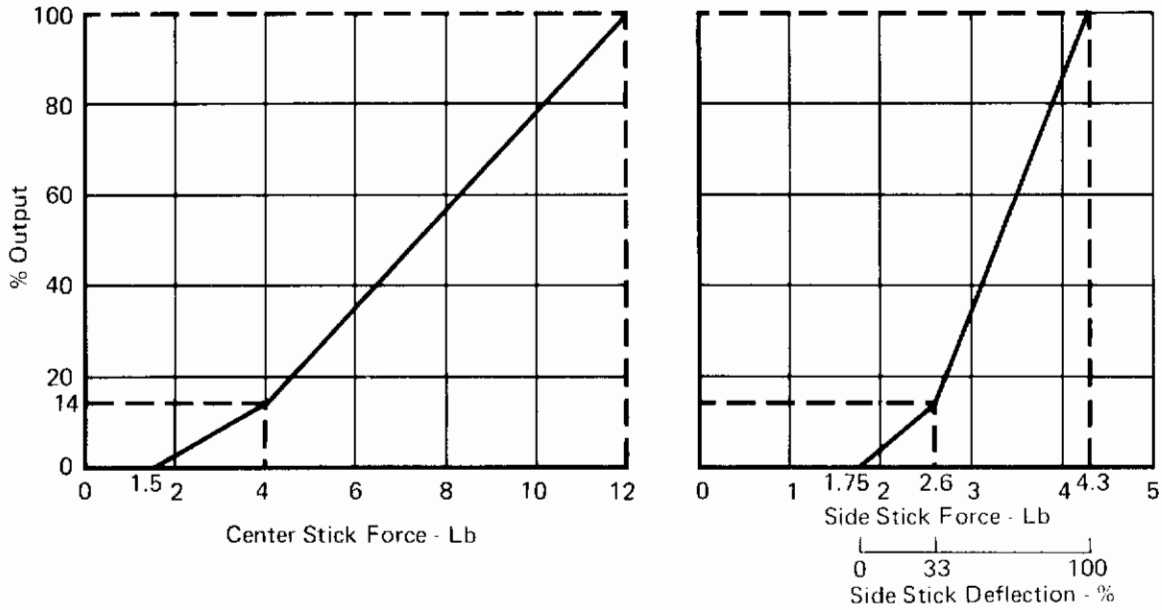

FIGURE 46

ROLL RATE COMMAND vs LATERAL STICK FORCE CHARACTERISTICS

A three radian per second prefilter is included in the Normal mode command pitch to shape the roll rate response. The SFCS hardware design includes provisions for changing the prefilter over a range from 1.5 radians per second to 6 radians per second. The 3 radian per second filter was found to be satisfactory during the man-in-the-loop simulation program.

The roll rate command signal also improves turn coordination at low and medium $\bar{q}$ flight conditions through the roll to yaw crossfeed network. Details of this network are presented in Paragraph e.

The use of ailerons at or near stall on a high performance aircraft can precipitate spin. To avoid an aileron induced spin, a signal from the stall warning computer reduces effective roll rate feedback to zero as a function of pitch rate and angle of attack at high angles of attack.

d. Directional Axis

The major requirements for the directional axis are to provide Dutch Roll mode damping and to keep the sideslip excursions in rolling maneuvers sufficiently small so as to provide good tracking performance. The MIL-F-8785B (ASG) damping requirements used in the SFCS design were augmented by the tracking performance Figure of Merit (FOM) shown in Figure 47. This FOM curve resulted from previous MCAIR precision flying studies

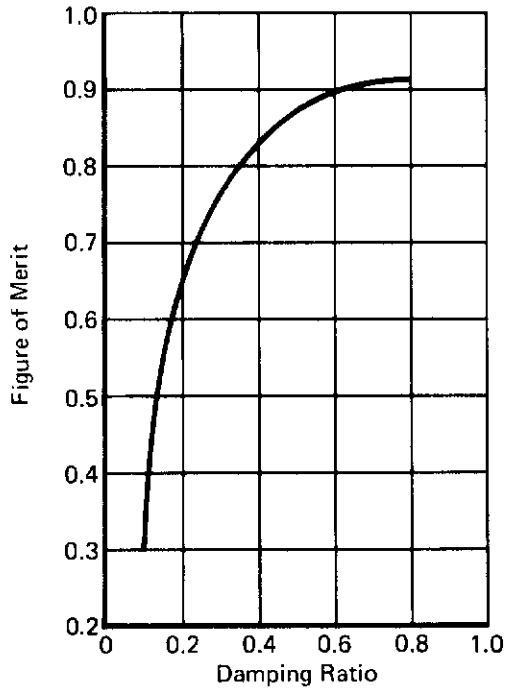

FIGURE 47
EFFECTS OF DUTCH ROLL DAMPING ON TRACKING PERFORMANCE

conducted to determine the effects of various control parameters including Dutch Roll damping on the pilot's ability to accurately track an airborne target. The study was performed with a pilot evaluated six-degree-of-freedom man-in-the-loop moving target simulation. The tracking performance FOM is a measure of tracking accuracy and was calculated from histograms of tracking error obtained during the simulation. These histograms showed the function of tracking time that falls into each five milliradian increment from zero to fifty milliradians of total tracking error. The FOM associated with each histogram is the normalized weighted average of that histogram and is computed as follows:

$$FOM = \sum_{i=1}^{10} \left(\frac{11-i}{10}\right) h_i$$

where i = 1 for the 0 - 5 Mil increment, i = 2 for the 5 - 10 Mil increment, etc., and h_i is the fraction of tracking time that falls into the ith increment of the histogram. The resulting FOM data plotted as a function of Dutch Roll mode damping shows that a distinct increase in precision tracking capability may be realized by increasing the Dutch Roll mode damping beyond the Level 1 Category A requirements of MIL-F-8785B (ASG). The curve shows that tracking performance rapidly increases as the Dutch Roll damping ratio is increased up to 0.4, at which time 90% of the realizable return is reached. Above a damping ratio of 1.0 there is essentially no change in tracking accuracy and the pilots indicated that such high damping ratios made the aircraft "sluggish" and therefore difficult to acquire a target.

To achieve good damping and minimize sideslip excursions, a combination of yaw rate and lateral acceleration feedback is employed in the directional axis. The high lateral loop gain alone prevents the roll to sideslip coupling in the Dutch Roll mode from exceeding maximums allowable. Yaw rate to rudder feedback augments the airframe Dutch Roll damping. A washout network in this feedback loop prevents opposing rudder deflection during steady state turn maneuvers. Lateral acceleration aids in reducing sideslip and provides turn coordination, especially at high dynamic pressure flight conditions. Turn coordination at low and mid dynamic pressure flight conditions is augmented by the roll to yaw crossfeed network. Details of this network are presented in Paragraph e.

The increase in turn coordination provided by lateral accelerometer feedback is obtained at the expense of a higher rms g environment experienced by the pilot during gusts, and possible feedback of structural modes. In consideration of these factors, the lateral accelerometer gain was set at the rather low value of 0.014 radians per foot per second squared. Appendix V includes an analysis of structural mode pickup through the lateral accelerometer.

To some extent, the yaw rate to rudder feedback causes adverse yaw which can produce considerable sideslip. This effect results from roll rate being coupled into the yaw axis, and is especially noticeable at high angle-of-attack flight conditions where considerable amounts of roll may be detected by the yaw rate gyro. The resulting rudder deflection produces additional adverse sideslip. Therefore, it is desirable to maintain the yaw rate feedback gain low at low $\bar{q}$ flight conditions but retain sufficient gain for damping considerations. The rudder flexibility gain reduces the directional loop gain at high $\bar{q}$ by a factor of 4 over that at low $\bar{q}$ and thus adds the requirement for high yaw rate feedback gain to achieve acceptable damping at high $\bar{q}$ flight conditions.

Root loci for the yaw rate loop closure, with the roll rate loop and the lateral acceleration loop closed at their fixed gain values, are shown in Figures 48 through 55 . These data show that the yaw rate feedback gain must be variable to maintain both low yaw rate feedback at low $\bar{q}$ flight conditions and sufficient Dutch Roll damping at medium and high $\bar{q}$ flight conditions. A three value variable gain is therefore included in the yaw rate feedback loop. This gain is both pilot selectable and controllable by the adaptive gain changer as a function of the longitudinal M_δ parameter. The three gains of 0.75, 1.5 and 3.0 radians per radian per second, as shown in Figures 48 through 55, provide for higher Dutch Roll mode damping at some flight conditions than desired. This higher damping resulted from a requirement to relocate the lateral accelerometer to reduce structural pickup after the yaw rate gains had been selected. The structural mode considerations which led to relocation of the lateral accelerometer are presented in Appendix V. At the new location (F.S.186.3) the lateral accelerometer causes less degradation in Dutch Roll damping than previously. Provisions are included in the SFCS to reduce the yaw rate gain by 3 dB.

The directional axis EBU mode is utilized during Normal mode operation with overall gains selected to provide full rudder authority at maximum rudder pedal force. The Normal mode command gain is selected to offset the feedback signals at low $\bar{q}$ where full rudder deflection may be desired. A three radian filter is included in this command path to reduce the initial command gradiant and prevent oversensitivity of the rudder pedals due to the added gain.

e. Roll to Yaw Crossfeed

The directional axis yaw rate and lateral acceleration feedback provide satisfactory Dutch Roll mode damping, but do not provide for sufficient improvement in turn coordination. Severe sideslip excursion resulting from rolling maneuvers can exist at several flight conditions. Since increasing lateral acceleration feedback is not feasible due to its degrading effect on Dutch Roll damping, the higher rms g environment experienced by the pilot during random gusts, and structural mode feedback, another method needed to be found.

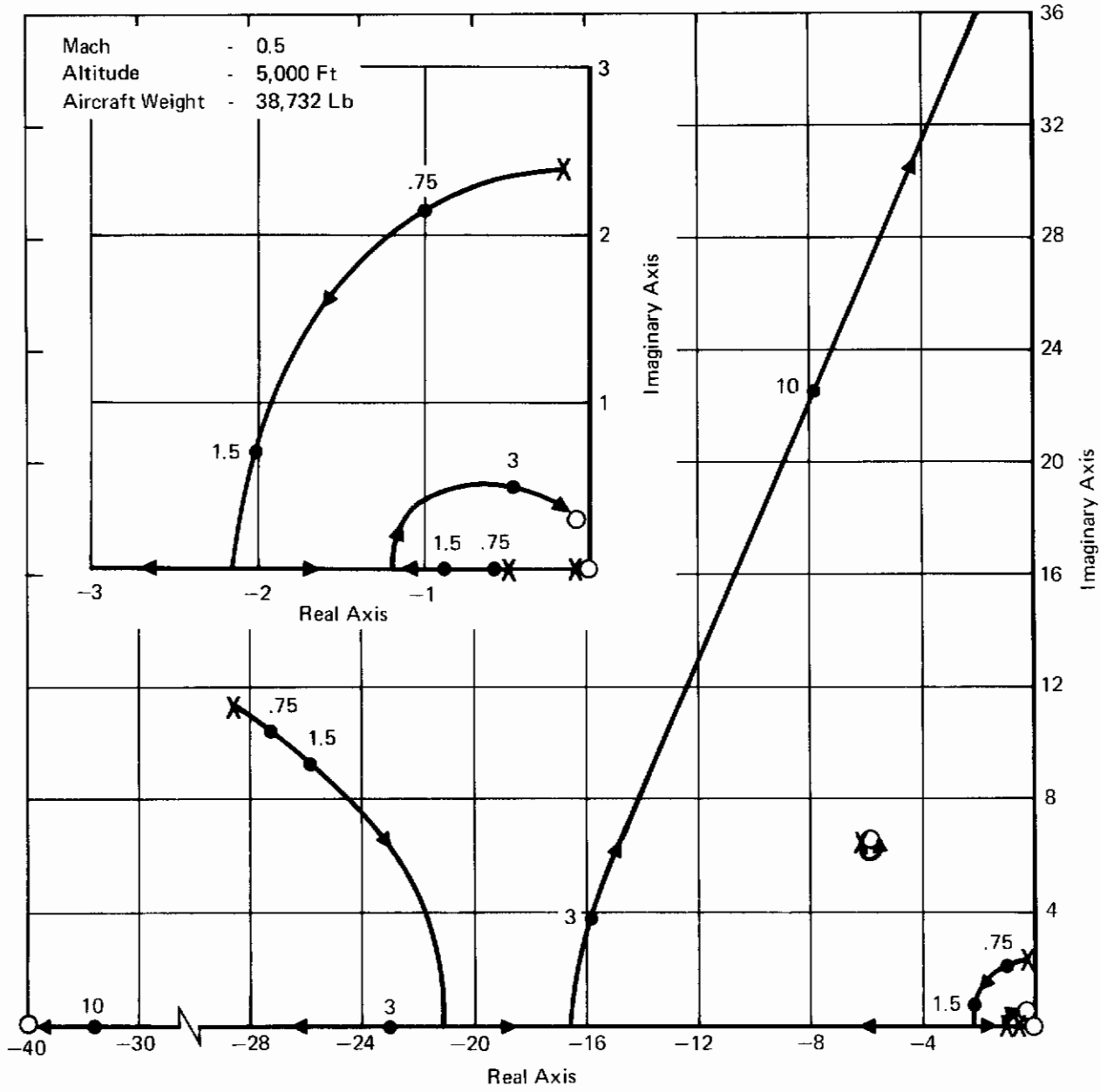

FIGURE 48
YAW RATE LOOP ROOT LOCUS

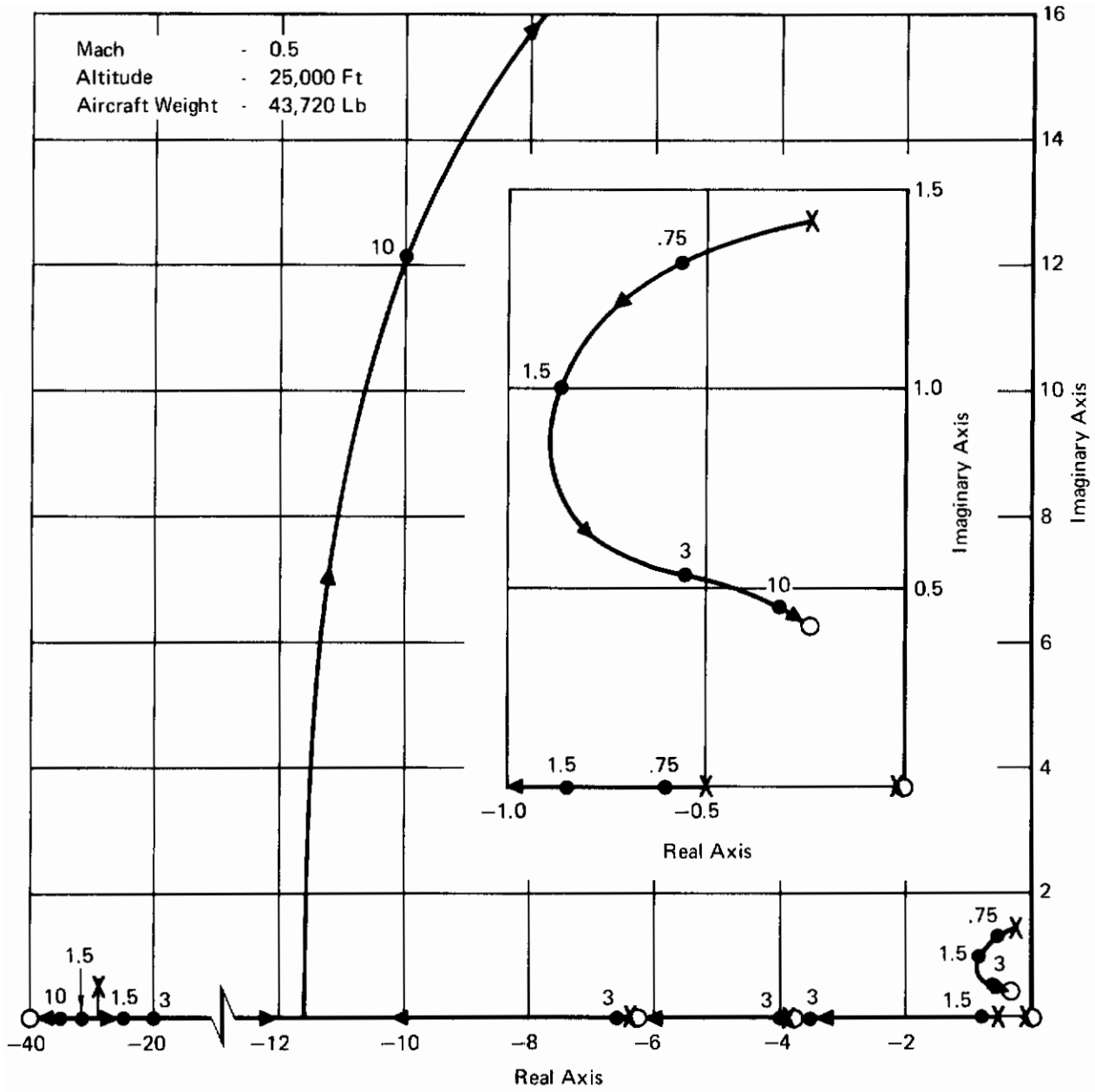

FIGURE 49
YAW RATE LOOP ROOT LOCUS

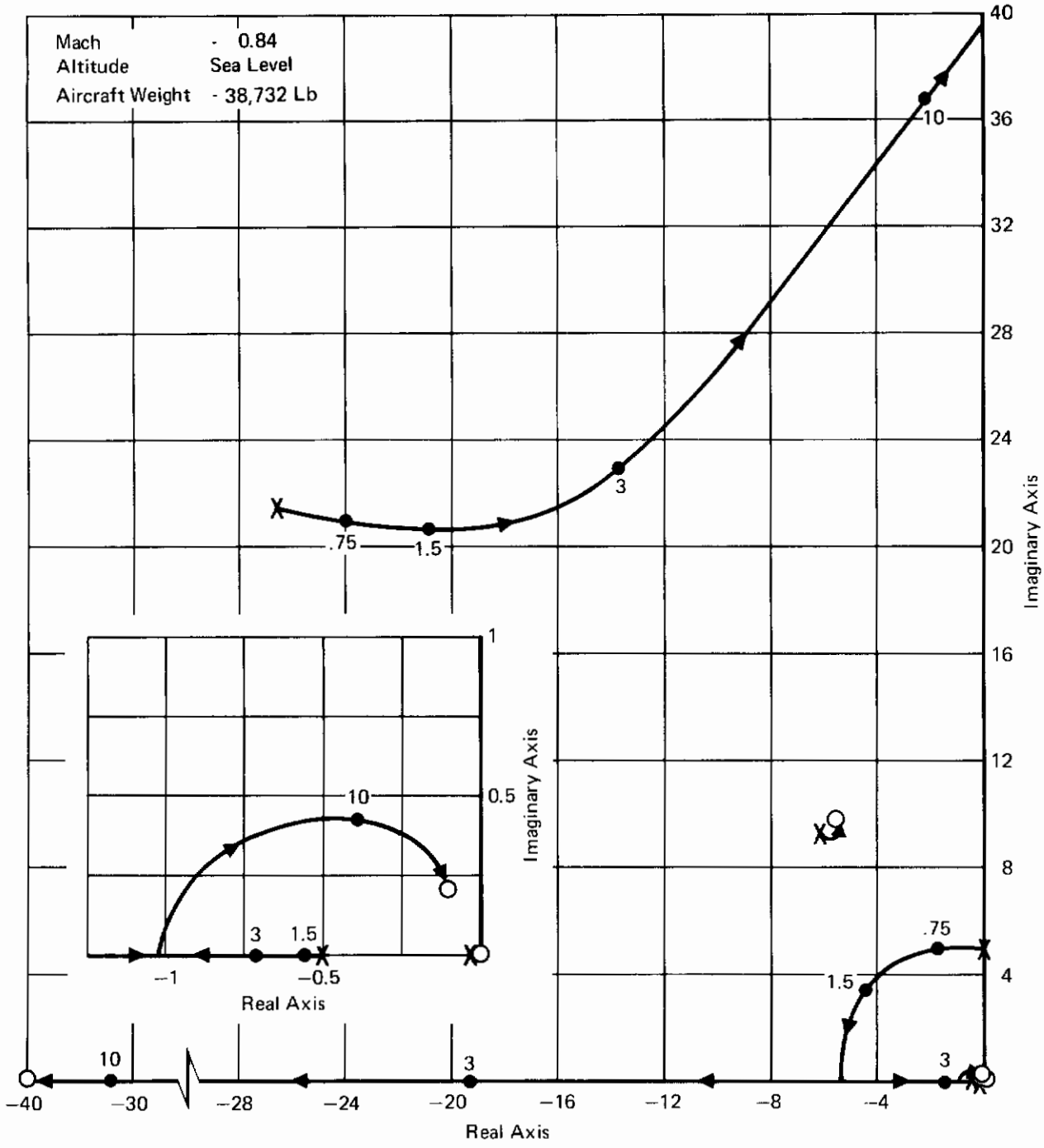

FIGURE 50
YAW RATE LOOP ROOT LOCUS

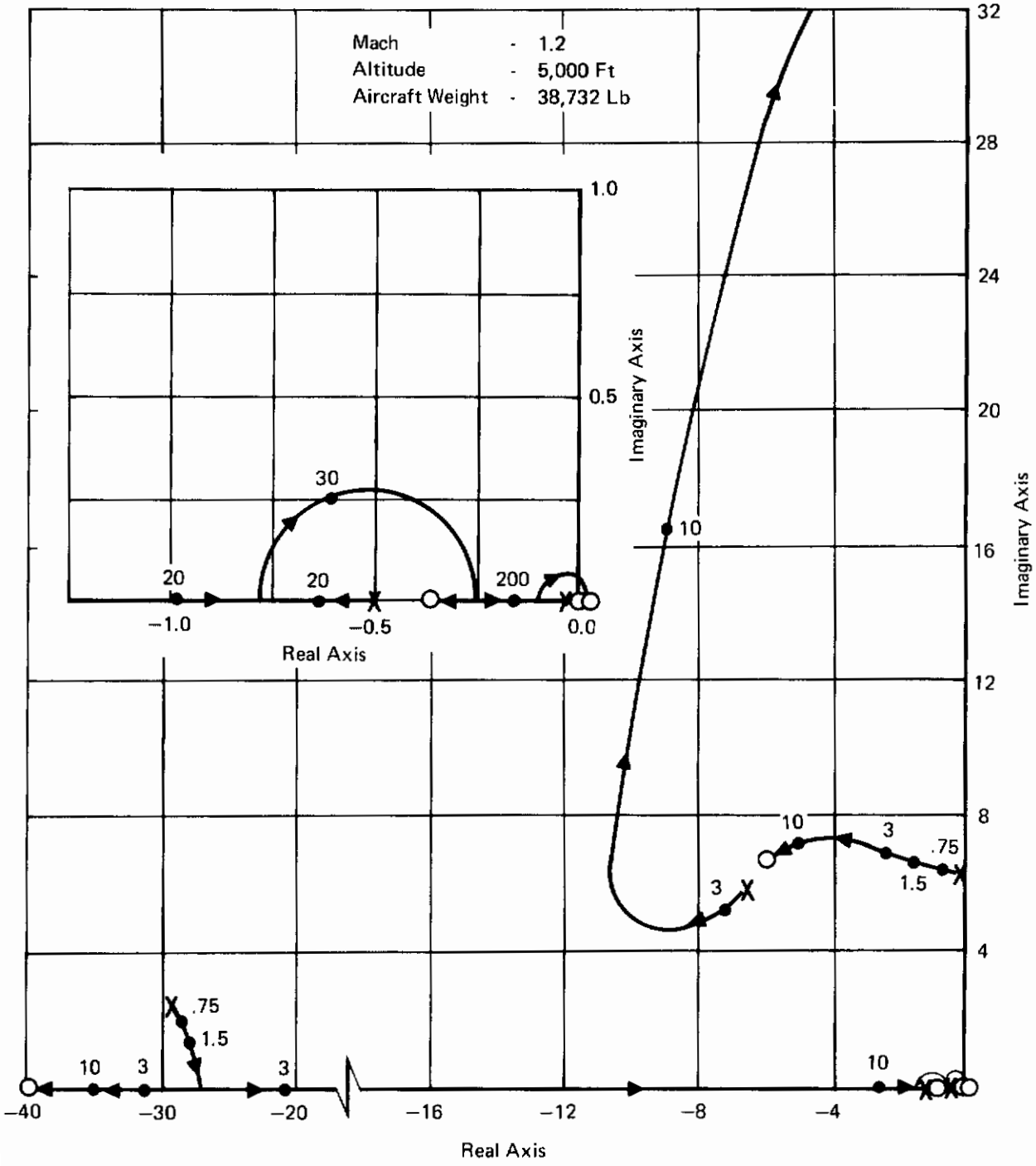

FIGURE 51
YAW RATE LOOP ROOT LOCUS

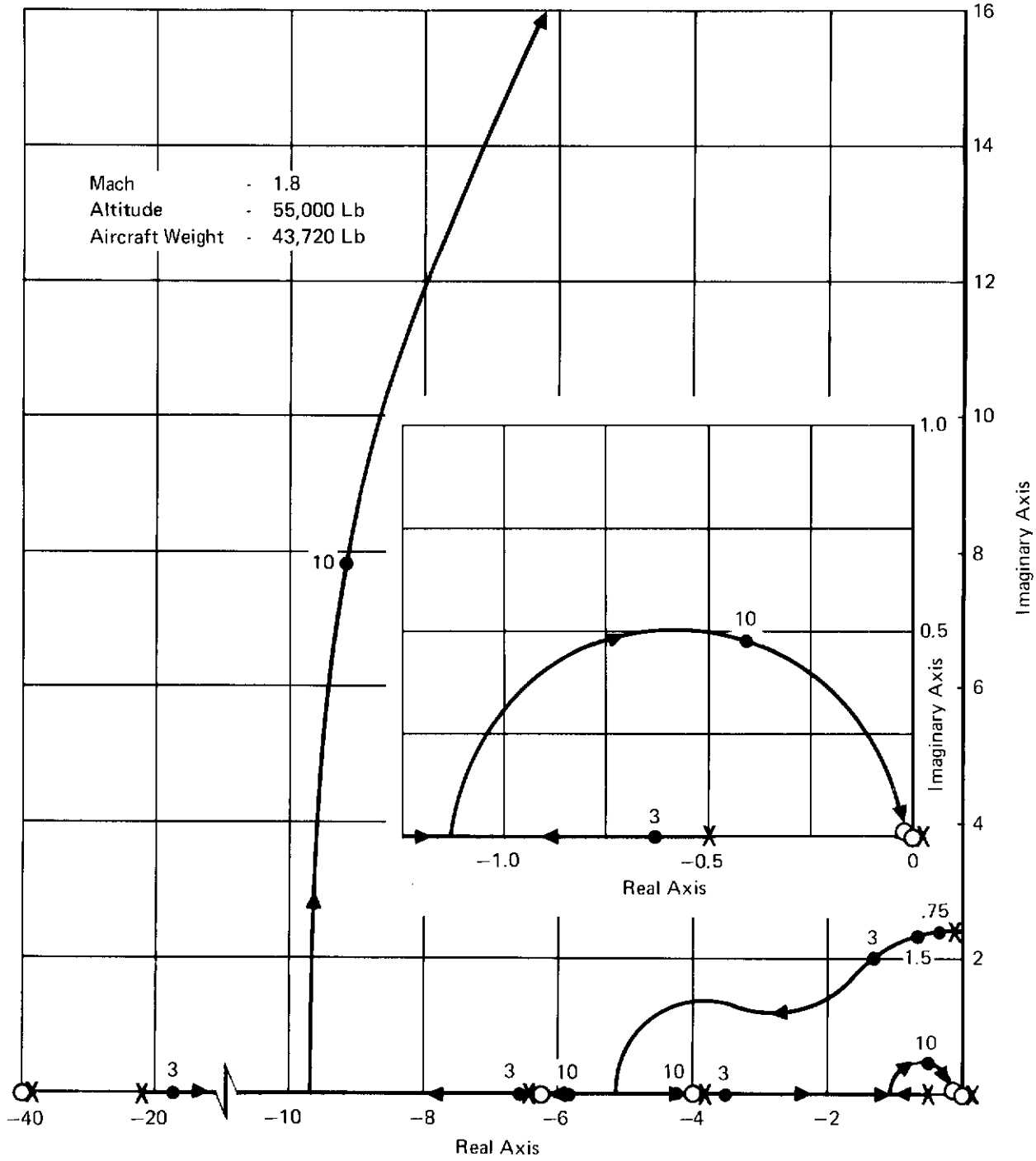

FIGURE 52
YAW RATE LOOP ROOT LOCUS

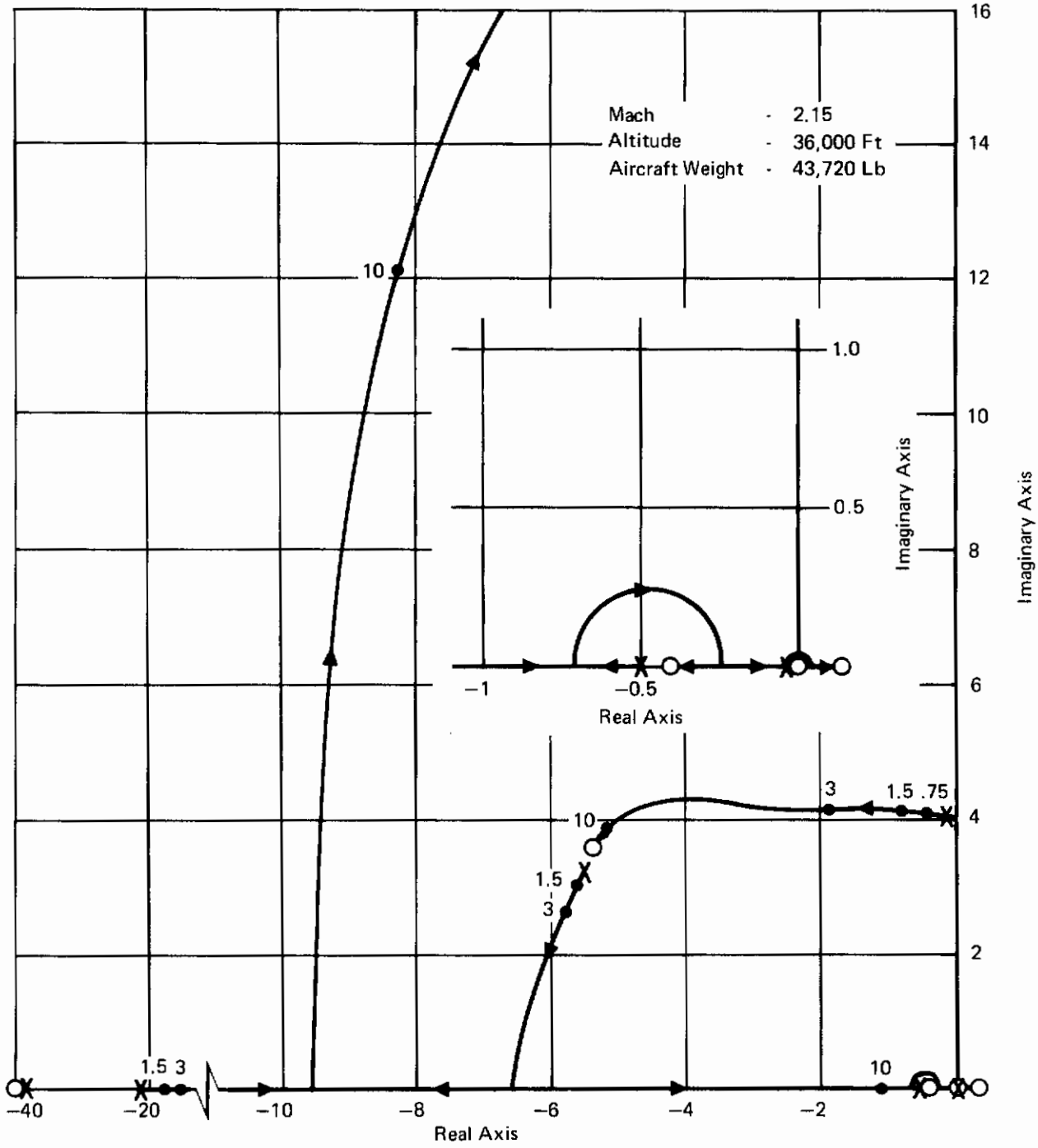

FIGURE 53
YAW RATE LOOP ROOT LOCUS

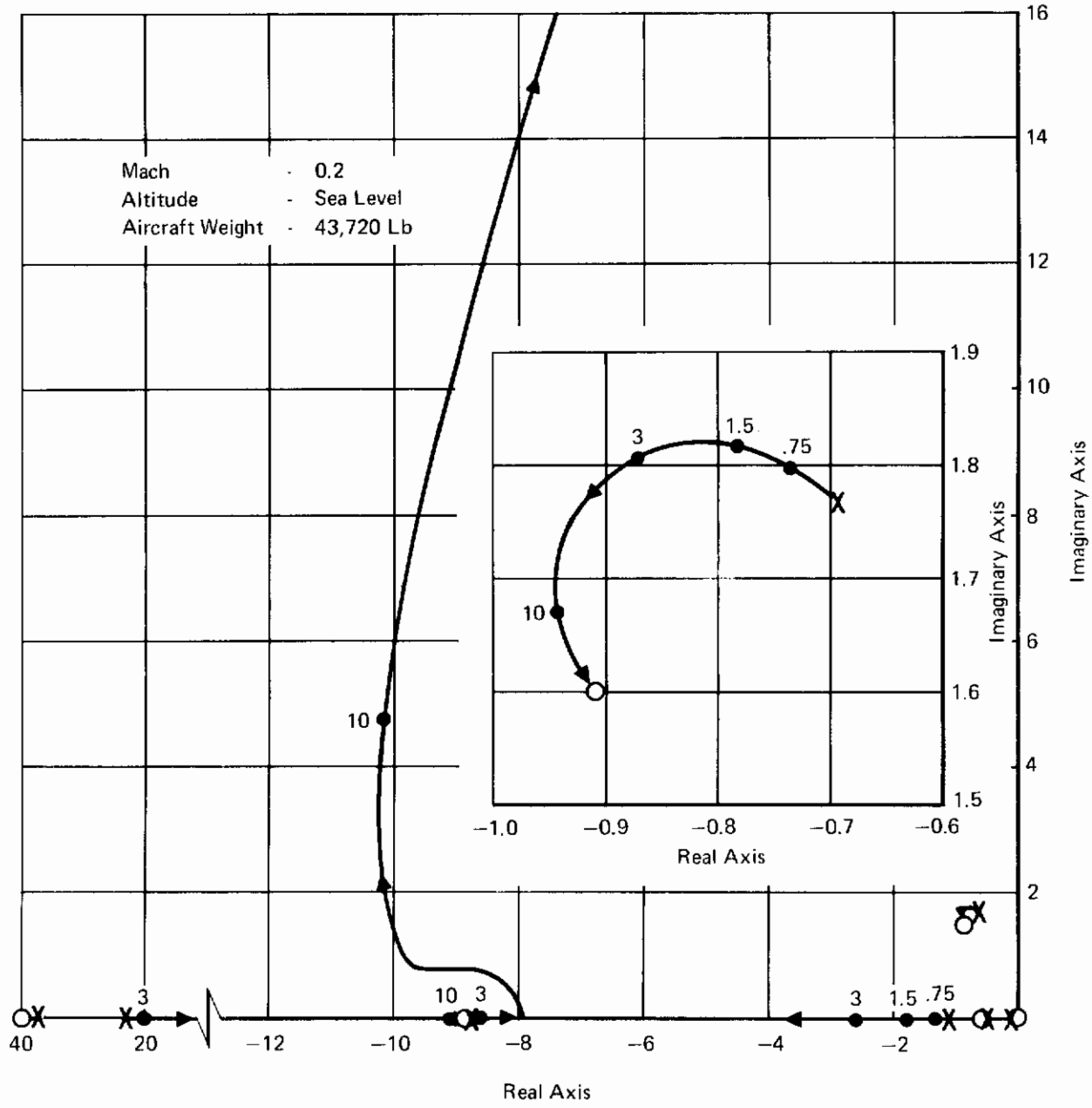

FIGURE 54
YAW RATE LOOP ROOT LOCUS

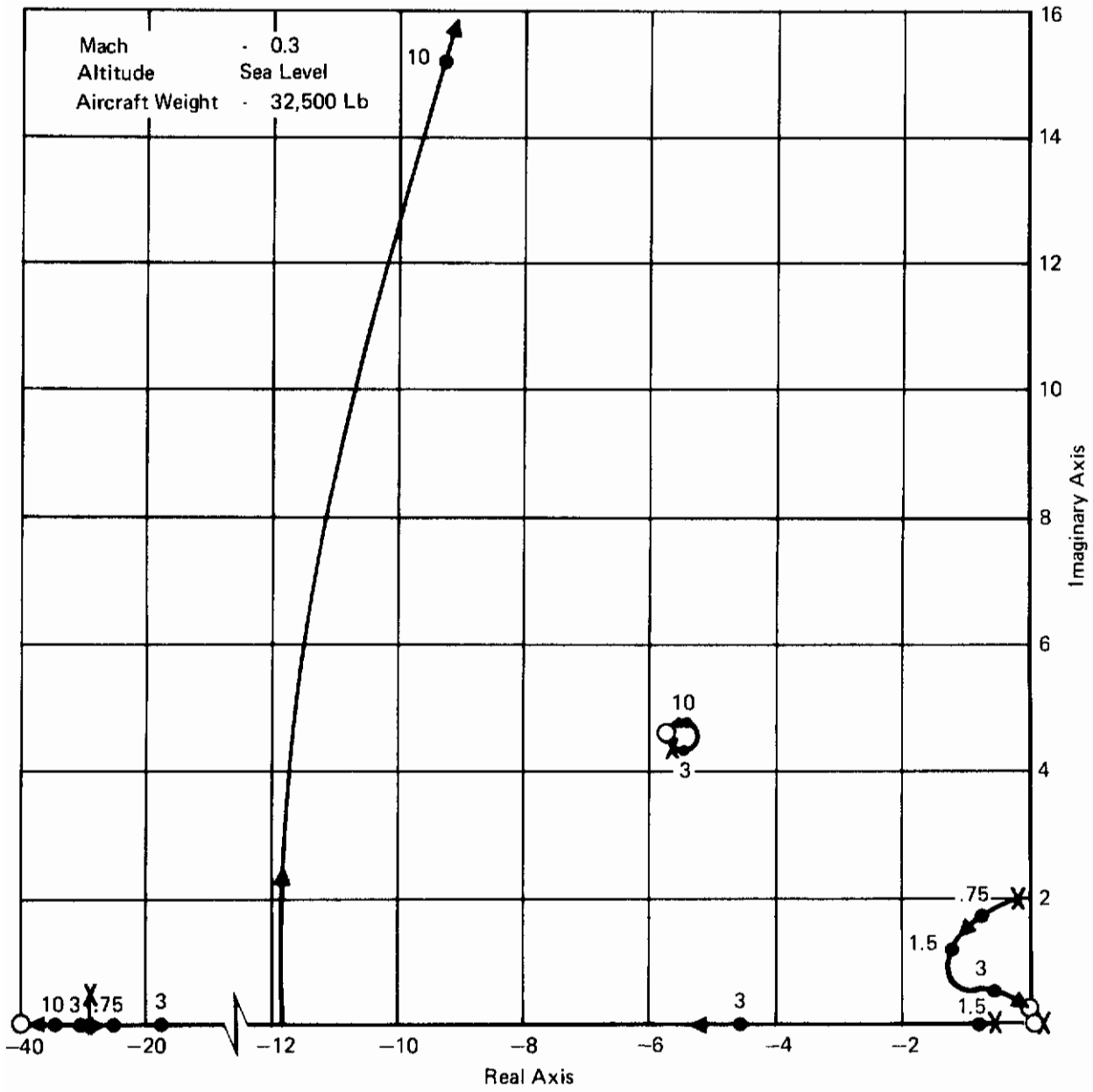

FIGURE 55
YAW RATE LOOP ROOT LOCUS

Of the methods considered for providing increased turn coordination, the use of a crossfeed from the lateral axis to the directional axis seems the most straightforward. The features of a crossfeed network are to reduce the roll induced sideslip resulting from aileron induced (N_δ) and roll rate induced (N_p) yawing moments. Two methods of roll to yaw crossfeed, one from the aileron secondary actuator position, and one from the roll rate command signal were investigated. Since neither scheme directly senses sideslip (the parameter that is to be controlled) the effectiveness of both schemes depends totally on the ability to predict the sideslip which will result from a rolling maneuver at each flight condition of interest. Roll to yaw crossfeed from the roll rate command signal was selected for the SFCS since it does not affect loop dynamics.

An analysis of the F-4's roll induced sideslip shows that sideslip varies from highly adverse at high angle of attack to proverse at low angle of attack flight conditions. A fixed network crossfeed would, therefore, not be sufficient. A crossfeed with ideal characteristics would command a rudder induced sideslip that varied in time with equal magnitude and opposite phase to the roll maneuver induced sideslip. This ideal crossfeed for the SFCS lateral-directional mechanization is a complex sixth order over sixth order transfer function, which would require both extensive gain and network parameter scheduling as a function of flight condition.

The SFCS roll to yaw crossfeed represents a compromise between the ideal and a network that is relatively uncomplicated and adequate to provide a significant reduction in sideslip. The network incorporates two variable gains which are changed automatically as a function of M_δ by the adaptive gain changer, or manually by the directional axis manual gain select switch. Four sets of gains, varying from high gains at low M_δ to zero gain at high M_δ, are provided through the adaptive gain changer. A fifth set of gains is used with gear down. A 5 second washout is included in the crossfeed network to provide aircraft "de-crab" ability. A capability to "de-crab" the airplane during landing approach is essential.

The roll to yaw crossfeed signal limiter is set equal to the crossfeed signal developed at 14% of maximum roll rate command. This value is the breakpoint between the roll rate to stick force low and high gradients. The effect of the limiter is to avoid excessive crossfeed commands at low roll power flight conditions.

f. Structural Modes

Three structural modes have been identified as factors to be considered in the design of the lateral-directional control system. The three modes are:

- o the fuselage first torsion mode,
- o the wing first asymmetric bending mode, and
- o the fuselage first lateral bending mode.

The grounds for selecting these modes, the development of the equations describing them and the computational methods employed in obtaining the equation coefficients are presented in TR-71-20, Section III. Appendix V presents the analysis of the structural modes performed to assess their possible influence on the SFCS performance and to develop means of minimizing this influence.

The Appendix V analysis shows that surface excited structural modes will be present at significant levels in both the lateral and directional loops. The lateral loop is primarily sensitive to the fuselage first torsion mode. The low frequency and the high sensitivity of this mode to aileron deflection, coupled with the high SFCS lateral loop gain, required that a 10 dB 40 radian notch filter be provided in the lateral loop. The directional axis is primarily sensitive to the fuselage first lateral bending mode through the lateral accelerometer pickup. This mode frequency varies between 80 and 103 radians per second and its magnitude can limit the upper value of accelerometer gain or require filtering. Sufficient attenuation of this structural mode in the SFCS is provided by the 0.014 radian per foot per second gain and the 40 radian lag filter in the lateral acceleration feedback loop. No filter for structural modes is required in the yaw rate loop.

Table VI shows the attenuation of the structural modes in both the SFCS lateral and directional loops.

3. SYSTEM PERFORMANCE

a. Introduction

Performance of the lateral-directional axes of the SFCS has been verified throughout the F-4 flight envelope using a three-degree-of-freedom small perturbation simulation and a six-degree-of-freedom man-in-the-loop simulation. The manned simulation is described in Section V.

The small perturbation evaluation employed digital computer computation of gains and phase margins, Dutch Roll mode frequency and damping, roll to sideslip coupling, and spiral mode stability. Analog computer and digital computer time history programs were employed in obtaining time responses to pilot step inputs of lateral stick and rudder pedal force and steps of lateral wind gust.

Six small perturbation equations were used with analog and digital computer programs when calculating phase margins, gain margins and structural mode attenuation. Three of these equations are required to describe rigid body motion. The additional three equations were needed to describe the structural modes that are presented in Appendix V. The results from the structural mode analysis are summarized in Table VI.

Table VI shows that adequate phase margins, gain margins, and structural mode attenuation have been achieved using the proposed lateral-directional SFCS. The minimum lateral axis stability margins

TABLE VI

LATERAL-DIRECTIONAL GAIN AND PHASE MARGINS

Flight Condition Mach/Alt	Yaw Rate Gain (K_r)	Lateral Loop**							Directional Loop***						
		Phase Margin		Gain Margin		Gain (dB) at Flexible Modes			Phase Margin		Gain Margin		Gains (dB) at Flexible Modes		
		γ (Deg)	$\omega_\phi \left(\frac{\text{Rad}}{\text{Sec}}\right)$	a (dB)	$\omega_c \left(\frac{\text{Rad}}{\text{Sec}}\right)$	η_4	η_5	η_6	γ (Deg)	$\omega_\phi \left(\frac{\text{Rad}}{\text{Sec}}\right)$	a (dB)	$\omega_c \left(\frac{\text{Rad}}{\text{Sec}}\right)$	η_4	η_5	η_6
0.5/5K	1.5*	80.8	4.38	19.3	19.4	−24.5	−36.5	−34.1	90.1	4.5	26.0	49.5	−22.0	−42.3	−17.3
0.5/25K	0.75*	96.5	2.61	26.6	19.5	−32.0	−45.0	−39.0	116.2	1.85	37.5	54.5	−30.4	−53.0	−22.3
	1.5	98.0	2.55	25.6	18.4	−32.0	−45.0	−39.0	101.3	2.52	32.3	50.0	−28.3	−48.0	−22.9
	3.0	98.8	2.51	25.6	18.5	−32.0	−45.0	−39.0	89.1	4.0	26.7	45.3	−24.9	−37.0	−24.2
0.84/SL	0.75	63.3	6.9	15.4	20.5	−14.1	−27.0	−17.0	80.4	6.6	22.9	57.5	−15.4	−22.5	−13.4
	1.5*	61.1	7.3	15.4	20.5	−14.1	−25.4	−17.1	77.2	10.8	17.8	52.2	−13.4	−21.7	−14.0
	3.0	63.2	7.2	15.1	20.0	−14.2	−25.4	−17.2	53.7	17.8	12.4	47.0	−10.3	−19.9	−15.0
0.9/15K	1.5*	66.3	6.03	16.4	19.6	−17.6	−28.0	−20.2	82.3	7.9	20.1	52.5	−15.0	−26.2	−15.0
0.9/35K	1.5*	75.4	4.13	19.6	18.6	−25.7	−34.8	−26.8	89.7	4.25	27.2	51.5	−22.9	−41.8	−19.7
0.9/45K	0.75	82.5	2.96	23.1	18.0	−30.0	−38.0	−30.5	107.3	2.12	38.0	54.5	−30.5	−48.6	−22.2
1.2/5K	0.75*	85.5	4.57	21.7	20.0	−11.4	−22.2	− 9.1	102.4	6.2	37.0	53.4	−27.3	−24.7	−21.1
	1.5	87.9	4.42	21.4	19.6	−11.4	−22.2	− 9.1	82.7	6.9	30.8	49.2	−25.8	−25.0	−21.6
	3.0*	89.7	4.3	21.4	19.4	−11.4	−22.3	− 9.3	73.1	8.13	24.8	45.0	−22.8	−28.4	−22.7
1.5/15K	3.0*	100.5	3.25	22.8	19.3	−14.8	−24.8	−11.7	80.1	6.55	30.2	42.0	−30.0	−29.7	−22.1
1.5/35K	1.5*	82.7	3.55	21.0	19.0	−21.2	−30.0	−16.2	82.7	4.6	32.7	44.0	−31.1	−34.5	−20.3
1.5/45K	1.5*	87.3	3.0	22.2	18.4	−25.4	−32.0	−19.8	89.3	3.9	33.9	43.0	−32.8	−39.0	−21.3
1.8/55K	1.5*	95.0	2.0	24.9	18.0	−27.7	−33.0	−21.0	88.7	3.0	34.7	33.7	−38.5	−35.6	−20.7
2.15/36K	1.5*	99.6	2.48	24.0	18.3	−16.3	−26.0	−11.4	58.3	4.39	29.4	26.5	−43.9	−27.1	−17.9

η_4 First fuselage torsional mode - 40 Rad/Sec
η_5 Unsymmetric wing bending mode - 68 Rad/Sec
η_6 First lateral bending mode - 80 to 104 Rad/Sec

* Adaptive gain value
** Based on a frequency response of the open lateral loop with the directional loop closed
*** Based on a frequency response of the open directional loop with the lateral loop closed

are 61 degrees of phase and 15 dB of gain. The minimum directional axis stability margins are 54 degrees of phase and 12 dB of gain. These data are for the most critical flight condition, Mach 0.84 at sea level. All structural mode amplitudes are less than -10 dB at the structural mode resonant frequency.

b. Lateral Axis

The salient features of the SFCS lateral axis are the improved roll rate time constant and roll rate to stick force gradient, lower roll rate overshoot and a reduction in roll oscillation.

Figure 56 shows a comparison between the roll mode time constant of the basic F-4 and the F-4 with the SFCS. The SFCS values are the time to reach 63% of the average roll rate in response to a step of stick force as measured from time history responses. The SFCS time constants vary between 0.35 and 0.7 seconds with the more typical values being 0.5 seconds. Although the response does not follow the 0.33 second prefilter time constant exactly, the improvement over the unaugmented F-4 is substantial.

The roll rate to stick force ratio is shown in Figure 57. At 15,000 feet altitude, the variation in roll rate to stick force with Mach number is about 3 to 1 for the F-4 with yaw SAS. The F-4 with SFCS has about a 1.35 to 1 variation under the same conditions. In addition, the SFCS provides a lower sensitivity for small roll maneuvers for precise tracking, and higher sensitivity for more rapid roll maneuvers.

Figure 58 shows that the relatively high SFCS roll rate feedback gain effectively suppresses the Dutch Roll oscillations in the roll rate response to a step of stick force. The parameter, P_{OSC}/P_{AV}, is a measure of the ratio of the oscillatory component of the roll rate to the average component of roll rate following a rudder-pedals-free step of lateral stick force. Figure 58 shows this parameter to be well below the MIL-F-8785B (ASG) level 1 requirements and near zero for most flight conditions. P_{OSC}/P_{AV} was calculated as per MIL-F-8785B (ASG).

An evaluation of lateral response in terms of the normalized roll rate response criteria is presented in Figures 59 through 62. The flight conditions shown represent the slowest and the fastest responding conditions at both subsonic and supersonic velocities. These curves show the improvement in the F-4 SFCS lateral response over that of the F-4 with yaw SAS. Additional time history responses to stick force are presented in Appendix IV.

c. Directional Axis

The basic directional axis performance is measured in terms of Dutch Roll frequency and damping, spiral stability, and turn coordination. Turn coordination is discussed in Paragraph d below.

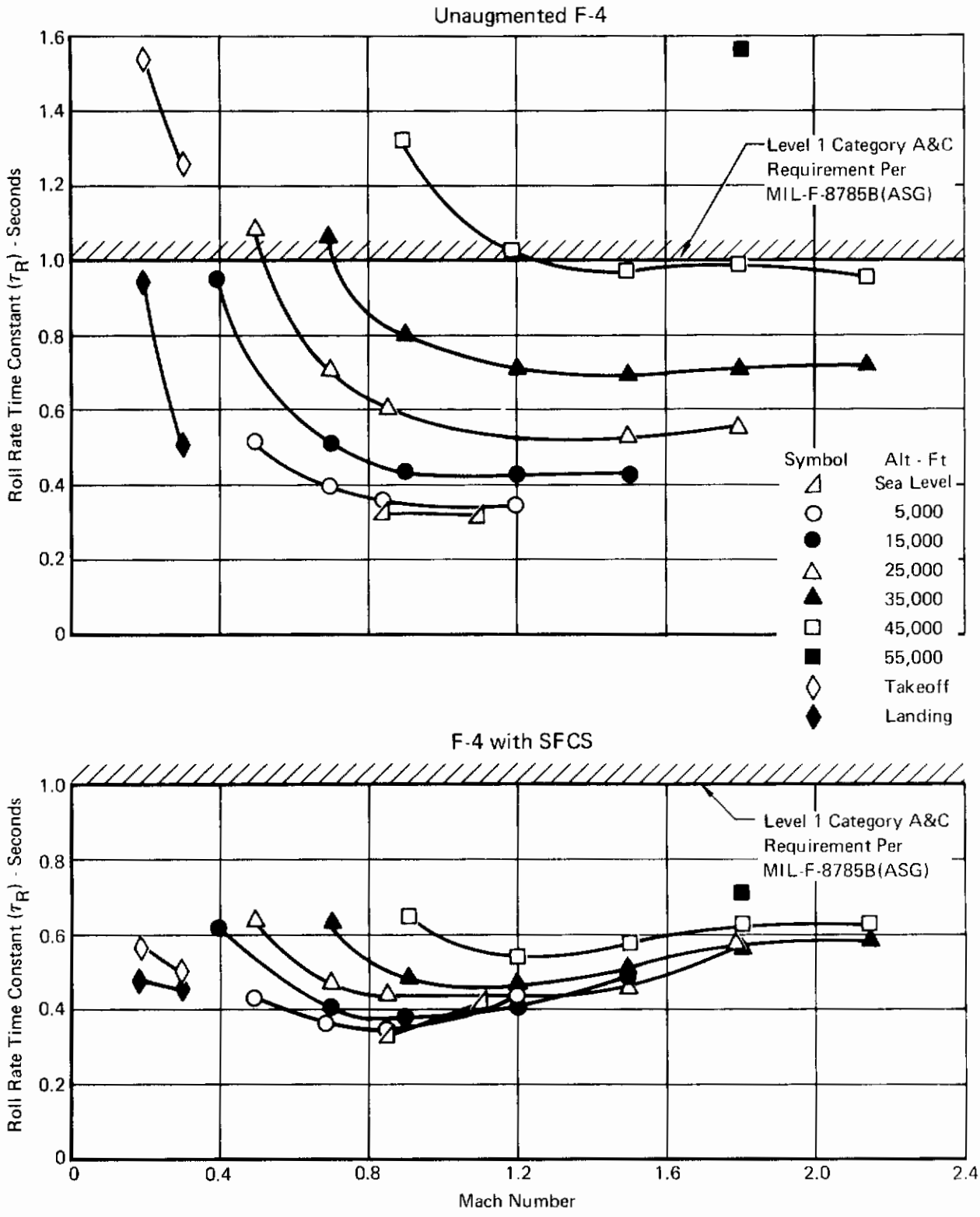

FIGURE 56
ROLL RATE TIME CONSTANT

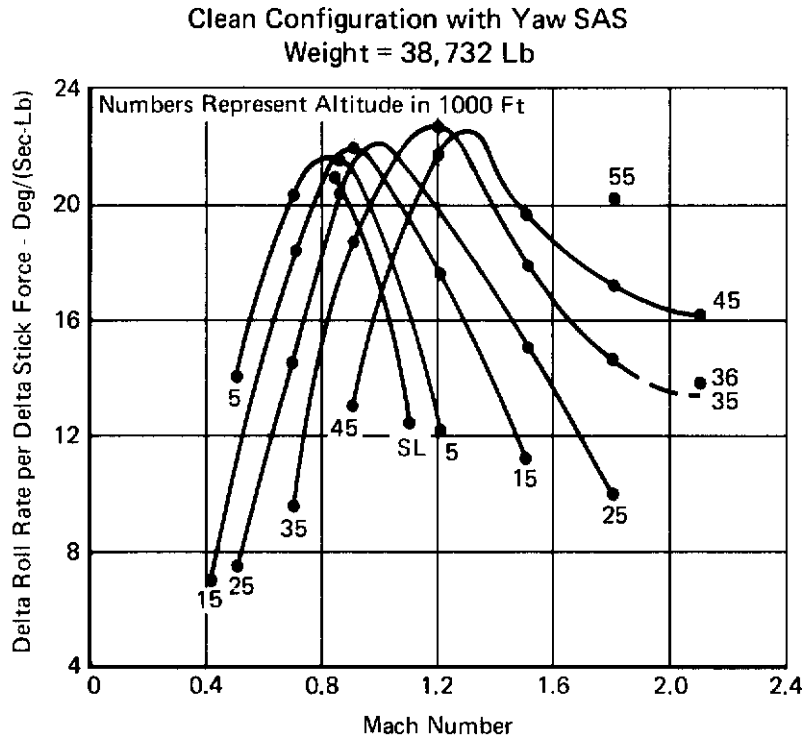

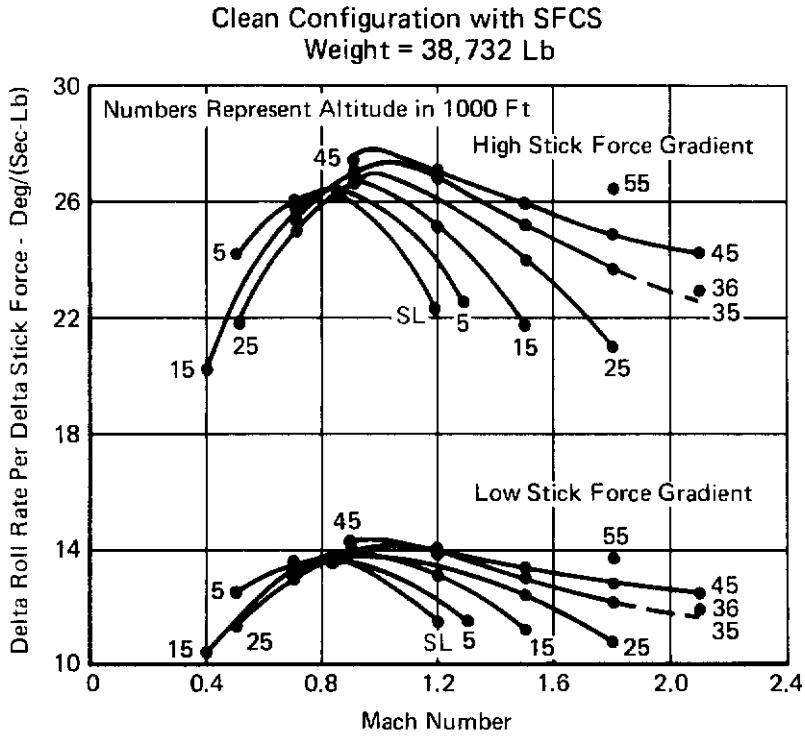

FIGURE 57
ROLL RATE PER STICK FORCE

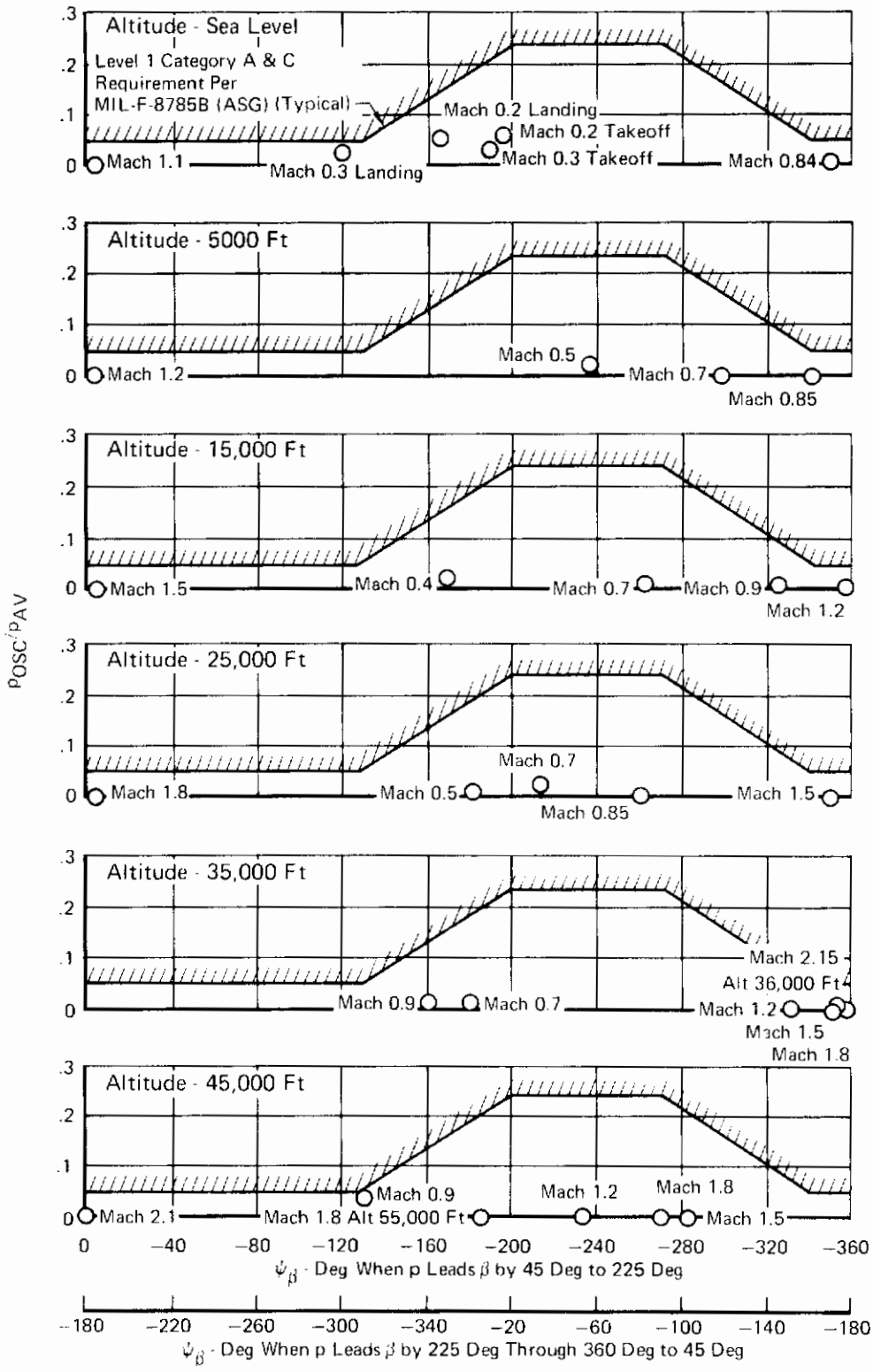

FIGURE 58
ROLL RATE OSCILLATIONS

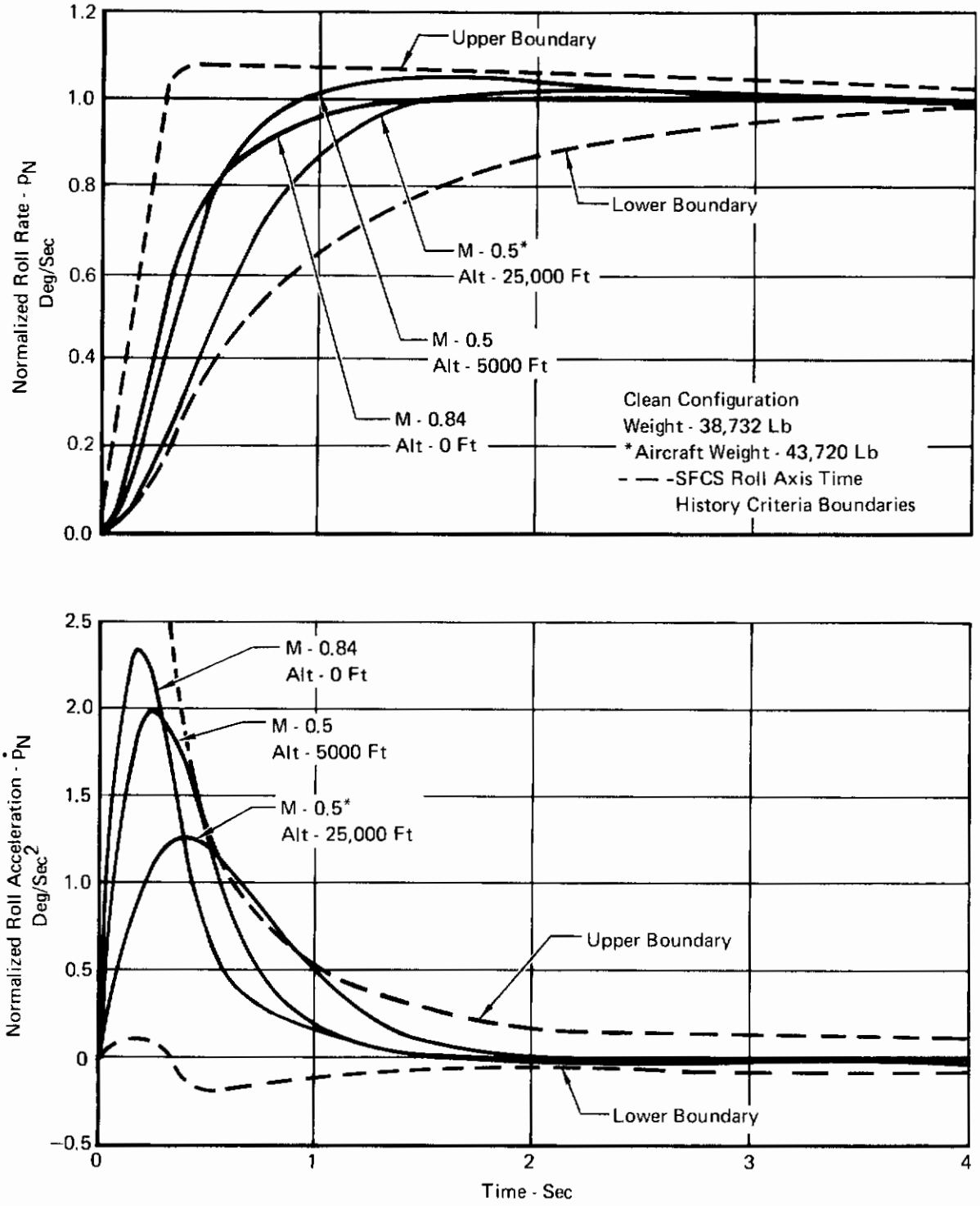

FIGURE 59

NORMALIZED ROLL RESPONSE

F-4 with SFCS

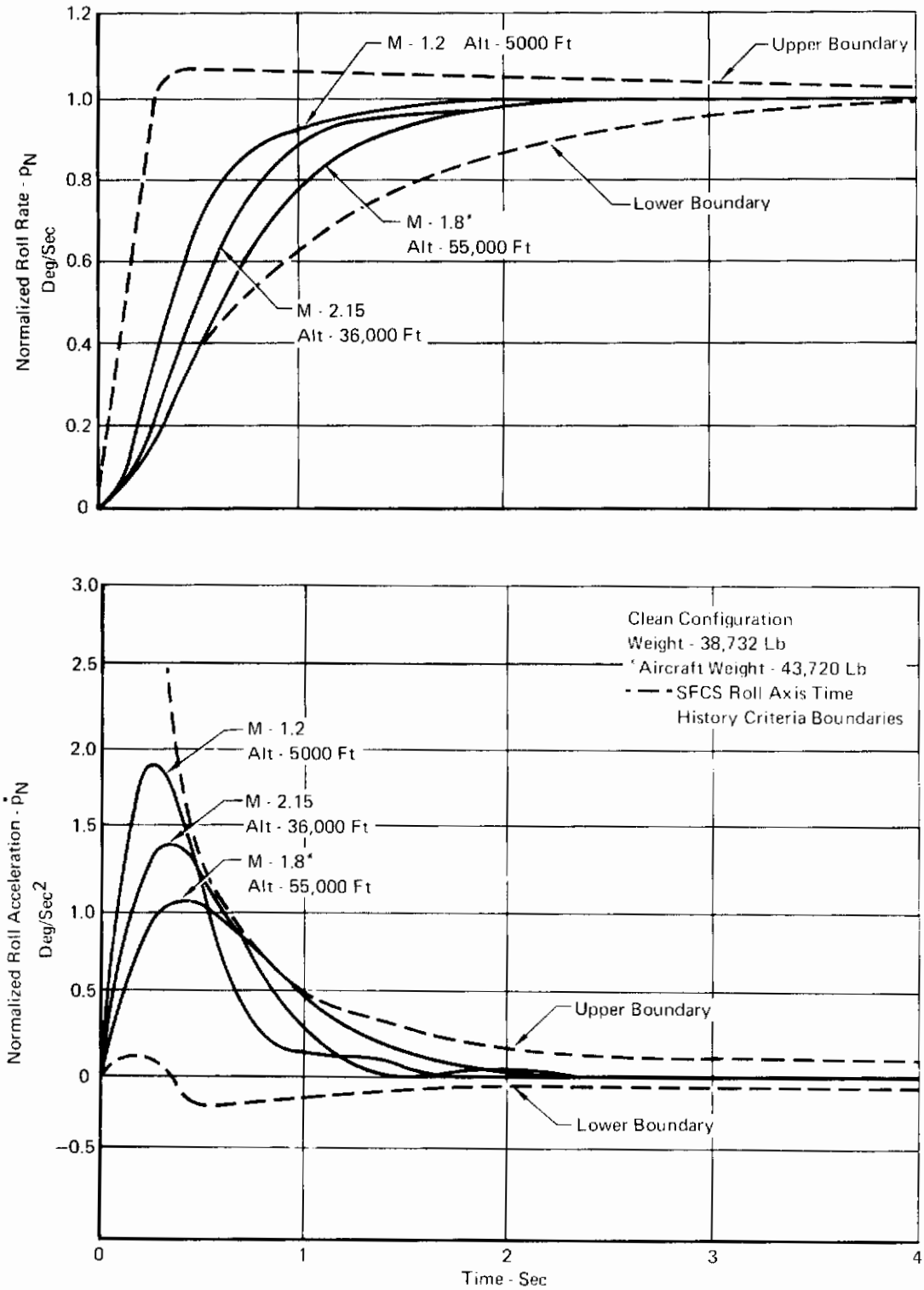

FIGURE 60
NORMALIZED ROLL RESPONSE
F-4 with SFCS

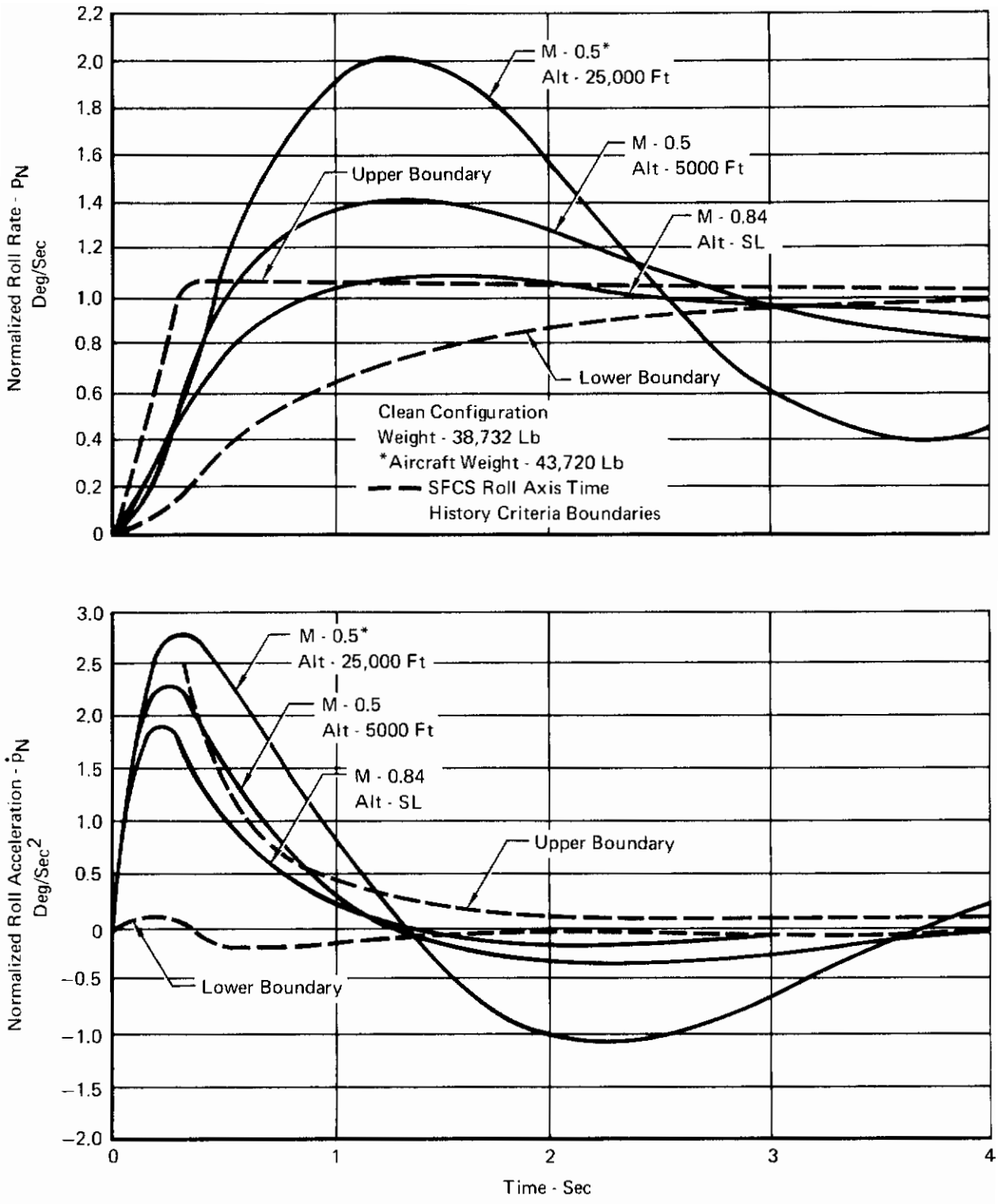

FIGURE 61

NORMALIZED ROLL RESPONSE

F-4 with Yaw SAS

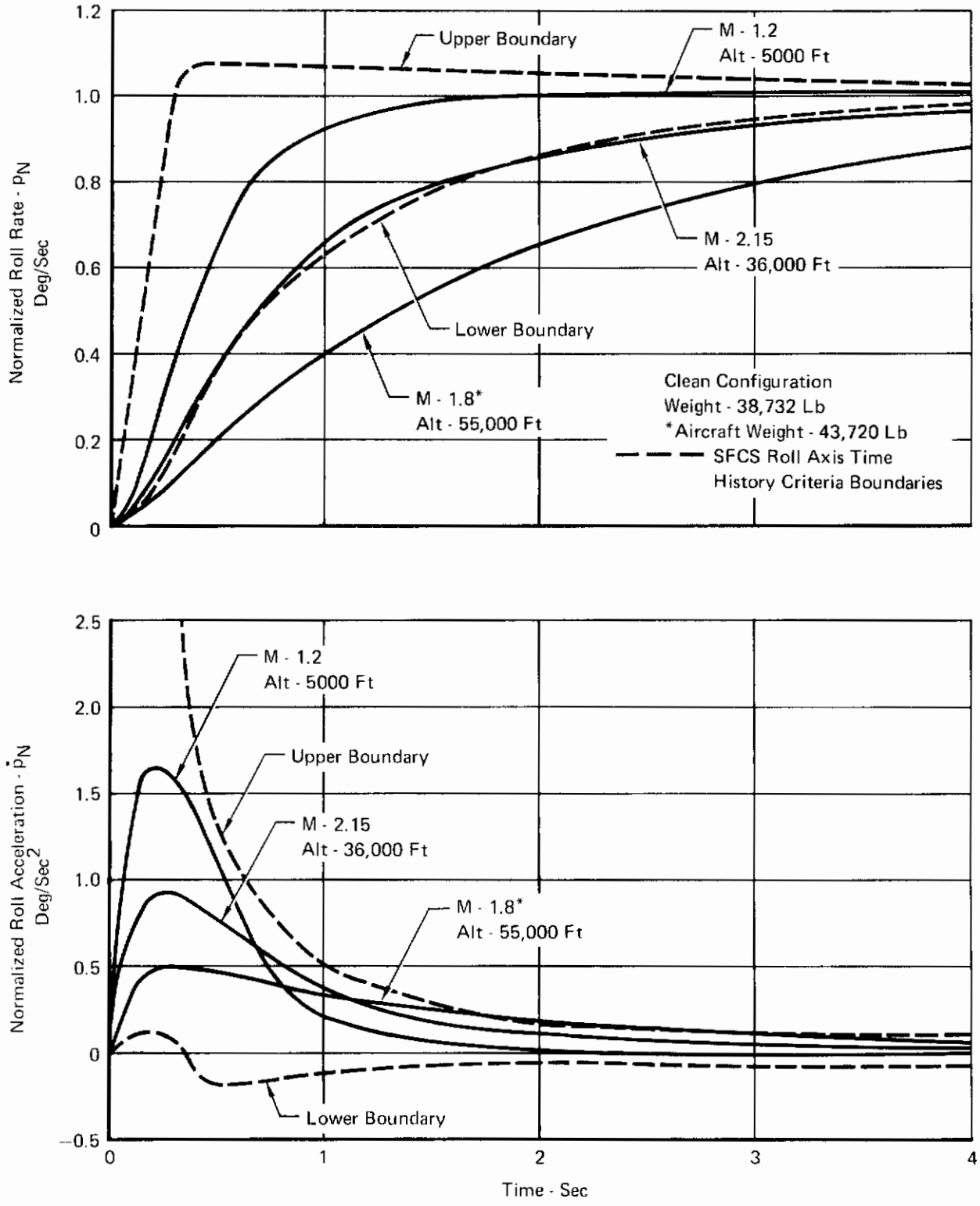

FIGURE 62

NORMALIZED ROLL RESPONSE
F-4 with Yaw SAS

The F-4 SFCS Dutch Roll frequency and damping characteristics are presented in Figures 63 and 64 at the proper adaptive value of yaw rate feedback gain. Figures 65 and 66 show the variation in Dutch Roll frequency and damping as a function of all three adaptive or pilot selectable gain values. At the proper adaptive gain setting, all flight conditions are within MIL-F-8785B (ASG) requirements.

At the high M_δ flight conditions, the SFCS generally has a damping ratio between 0.3 and 0.5. At the low M_δ flight conditions, damping ranges between 0.3 and 0.4. The mid range M_δ flight conditions show a 0.75 to 0.95 damping ratio for subsonic flight and 0.2 to 0.35 for supersonic flight. These data were obtained from a digital computer analysis of the Dutch Roll root only. However, in a highly augmented system there are generally other complex roots which may reduce overall damping slightly at the highly damped flight conditions.

Figures 63 and 64 also show the roll to sideslip coupling ($|\phi/\beta|$) in the Dutch Roll mode. The MIL-F-8785B (ASG) requirement is that this parameter have a value less than the $|\phi/\beta|$ curve corresponding to its particular frequency and damping. The relatively high lateral axis loop gain reduces the coupling to well within the requirements.

The SFCS spiral stability characteristics are shown in Figure 67 in terms of the inverse of time to double amplitude for an unstable spiral mode and the inverse of time to half amplitude for a stable spiral mode. These data show that the SFCS has both slightly stable and slightly unstable spiral mode characteristics depending on flight condition. However, the spiral stability characteristics are well within the requirements for all flight conditions.

d. Turn Coordination

The turn coordination performance for the F-4 SFCS with the adaptive roll to yaw crossfeed gains is summarized in Figure 68 in terms of the MIL-F-8785B(ASG)sideslip requirement. For many flight conditions the system Dutch Roll damping does not allow for the calculation of the angle Ψ_β as defined in the military specification. The Ψ_β values used are based on values of the unaugmented airframe and on the general nature of the sideslip angle time history response. Generally, flight conditions with all adverse sideslip have a Ψ_β between -180 and -280 degrees; flight conditions with both adverse and proverse sideslip have Ψ_β values between -140 and -180 degrees or -280 and -340 degrees; and flight conditions exhibiting all proverse sideslip have Ψ_β values less than -140 and greater than -340 degrees. This same Ψ_β was used in the p_{OSC}/p_{AV} curves in Figure 58. Figure 68 shows sideslip to be within the requirements except at the very low $\bar{q}$ and very high $\bar{q}$ flight conditions.

An evaluation of the SFCS with respect to the lateral-directional $D\Psi$ criteria is presented in Figures 69 and 70 for three subsonic and supersonic flight conditions.

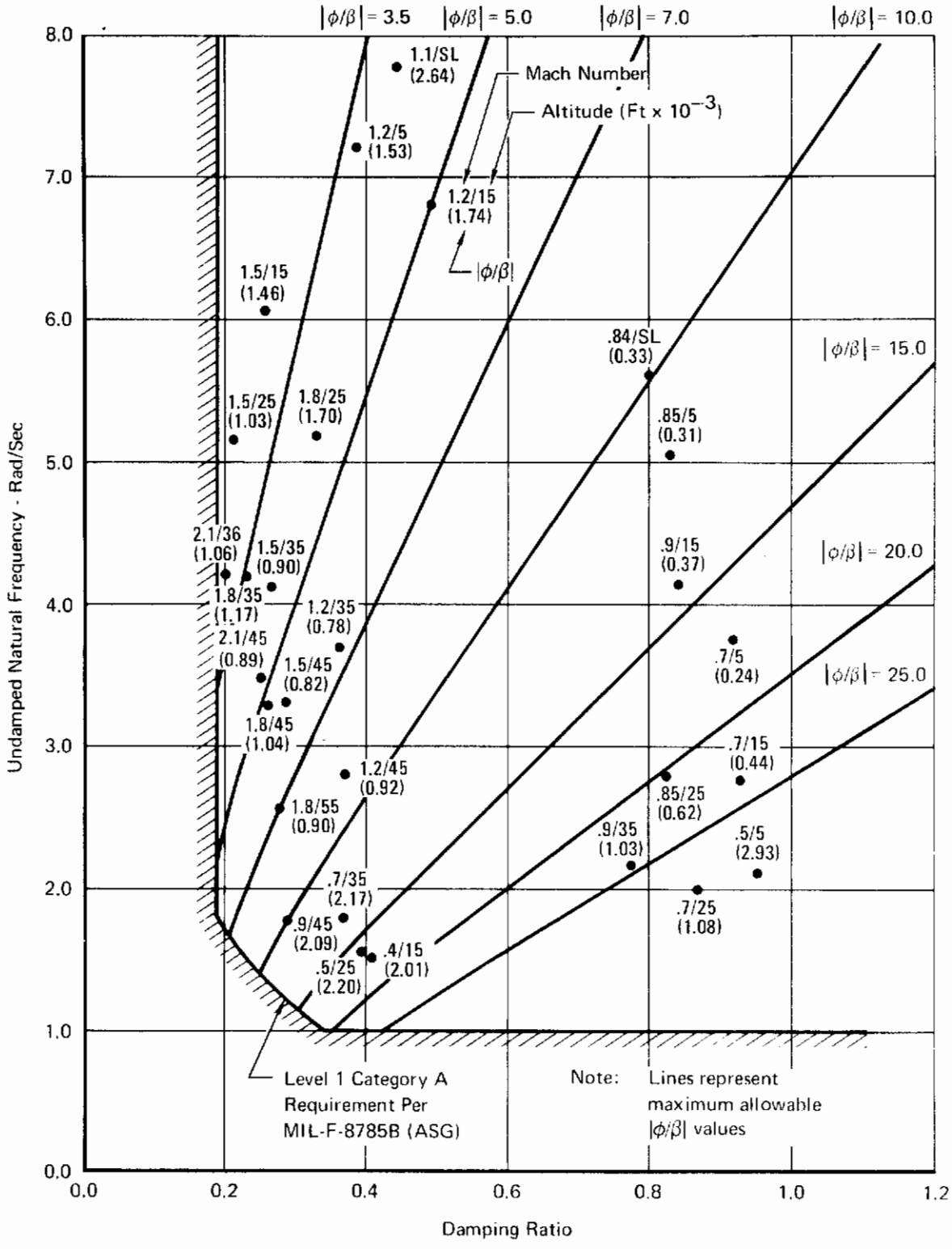

FIGURE 63

· DUTCH ROLL FREQUENCY AND DAMPING FOR ADAPTIVE MODE GAINS

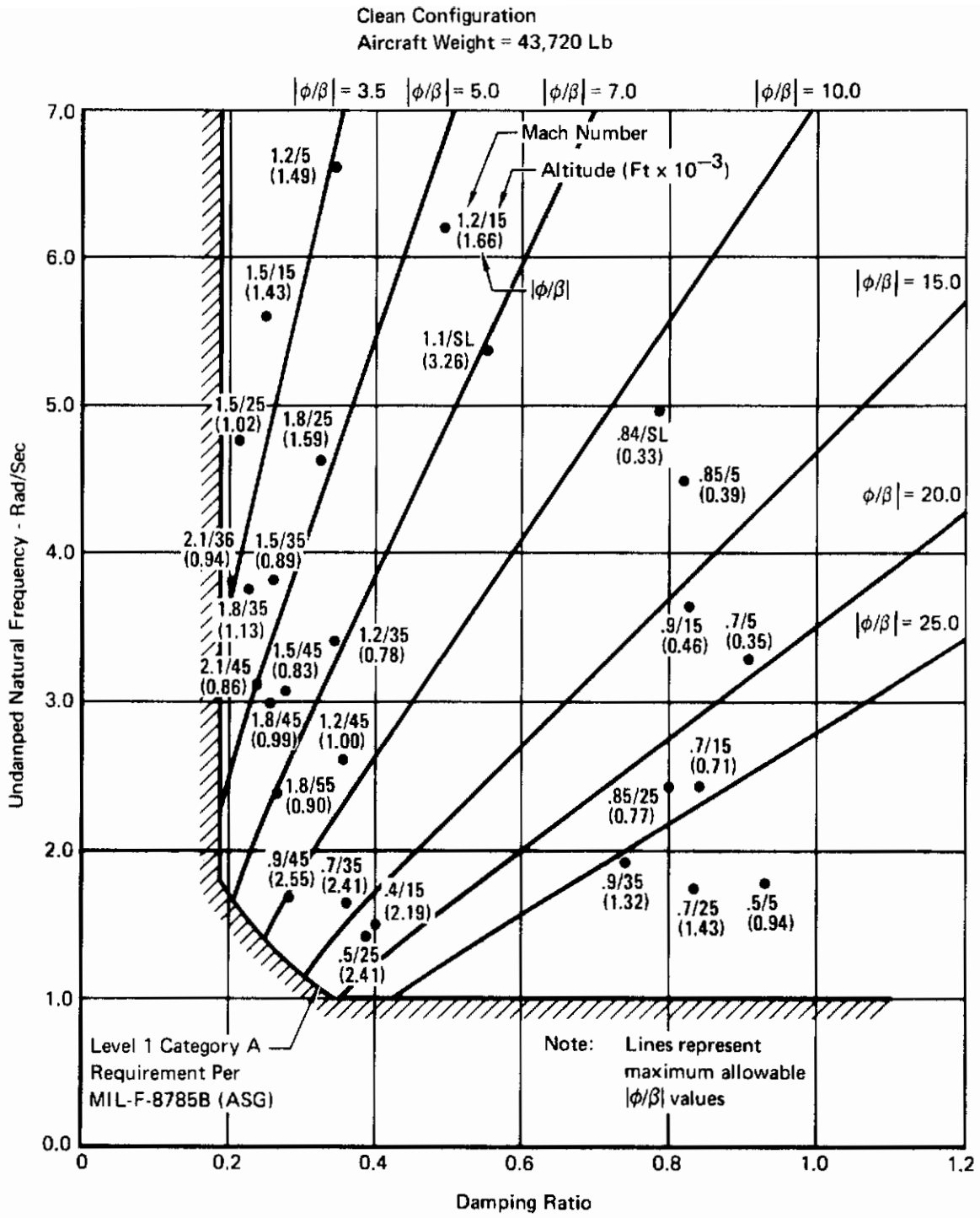

FIGURE 64
DUTCH ROLL FREQUENCY AND DAMPING FOR ADAPTIVE MODE GAINS

Clean Configuration
Weight: 38,732 Lb
*Takeoff Weight: 43,720 Lb
**Landing Weight: 32,500 Lb

Note: △ KR = 0.75
▲ KR = 1.5
● KR = 3.0

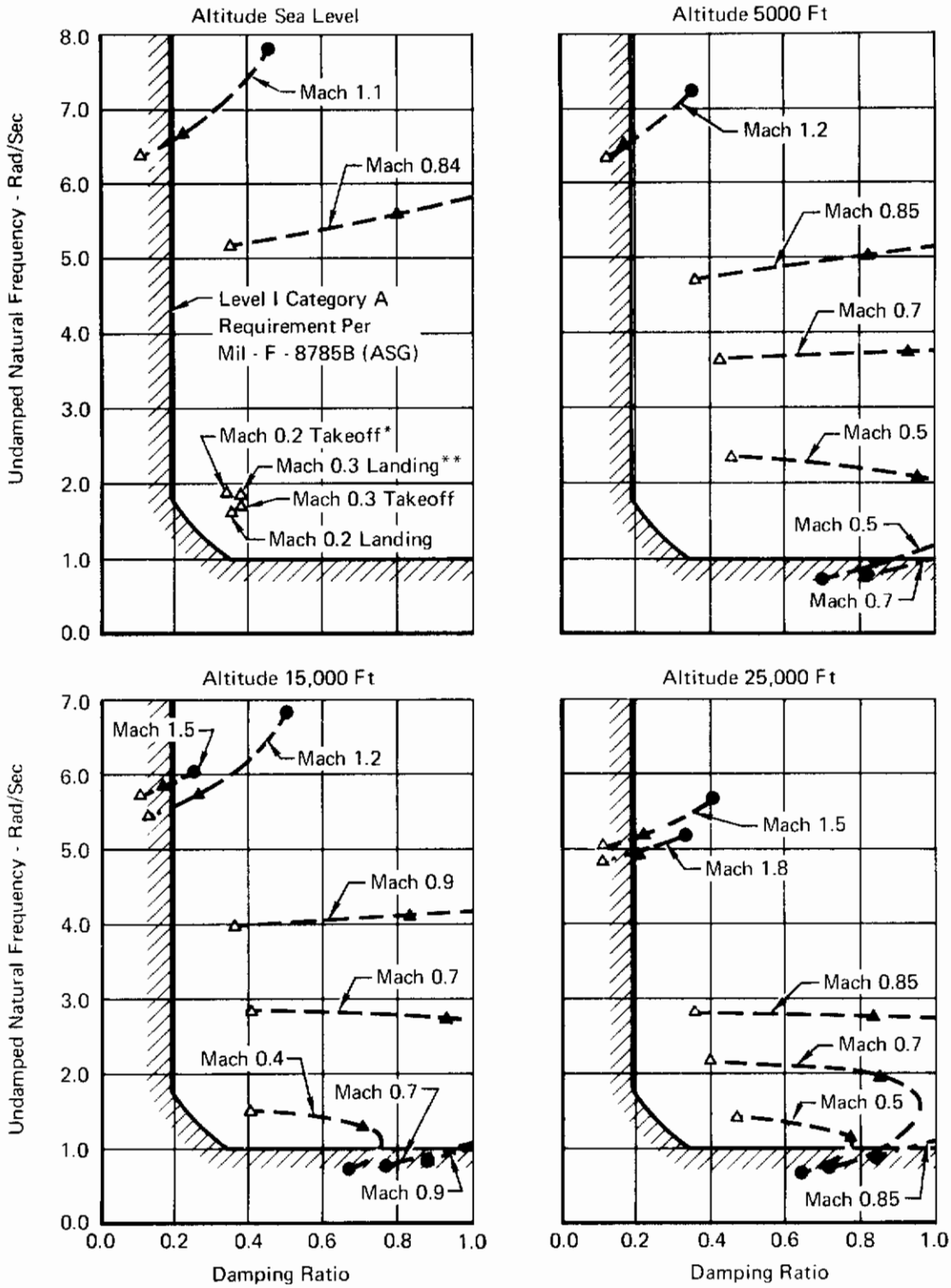

FIGURE 65
DUTCH ROLL FREQUENCY AND DAMPING AS A FUNCTION OF YAW RATE GAIN (KR)

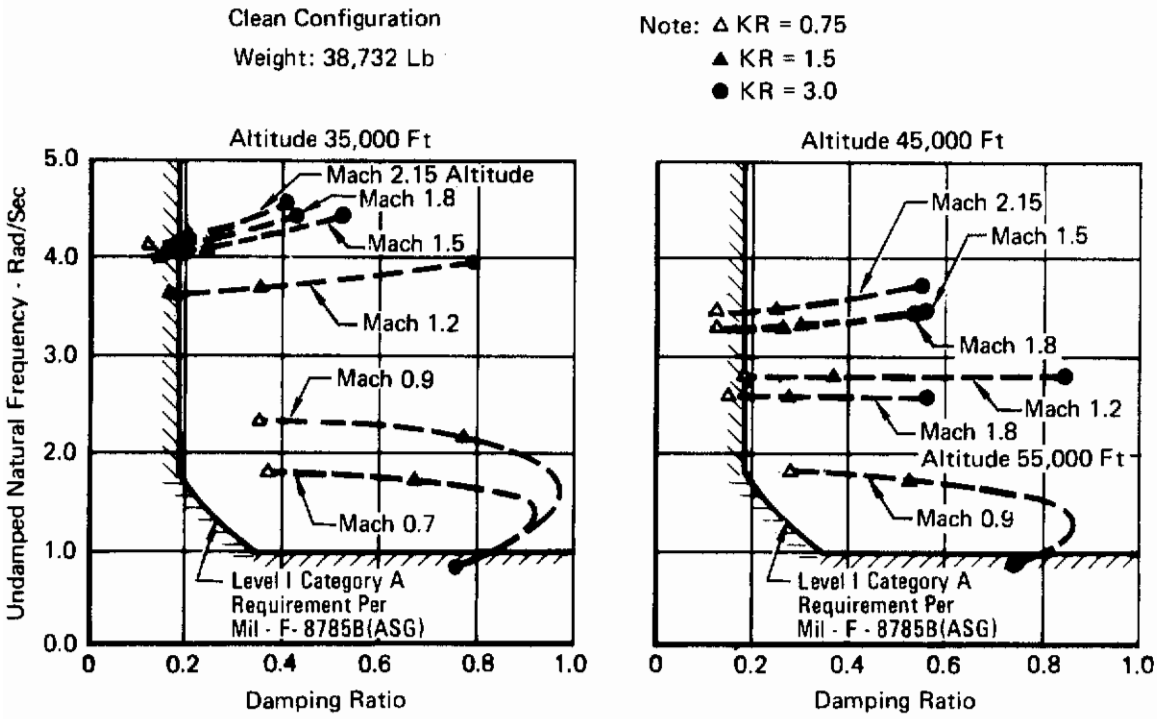

FIGURE 66

DUTCH ROLL FREQUENCY AND DAMPING AS A FUNCTION OF YAW RATE GAIN (KR)

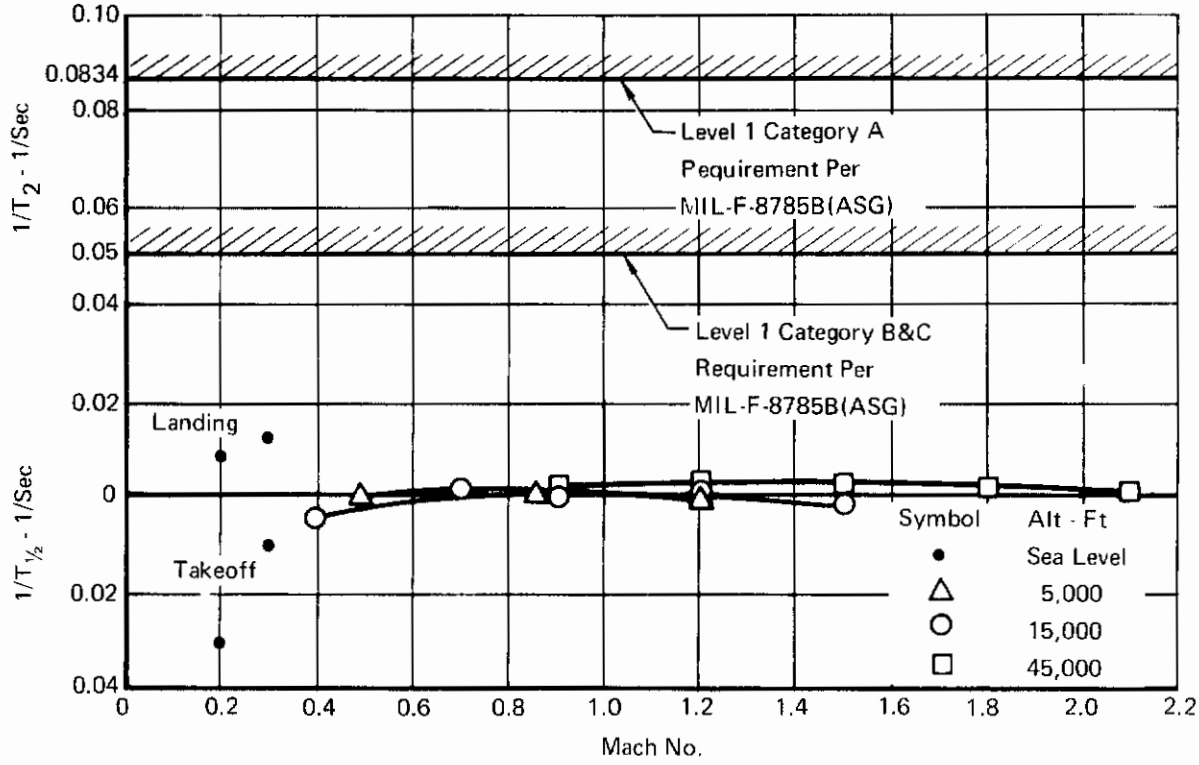

FIGURE 67
SPIRAL STABILITY CHARACTERISTICS

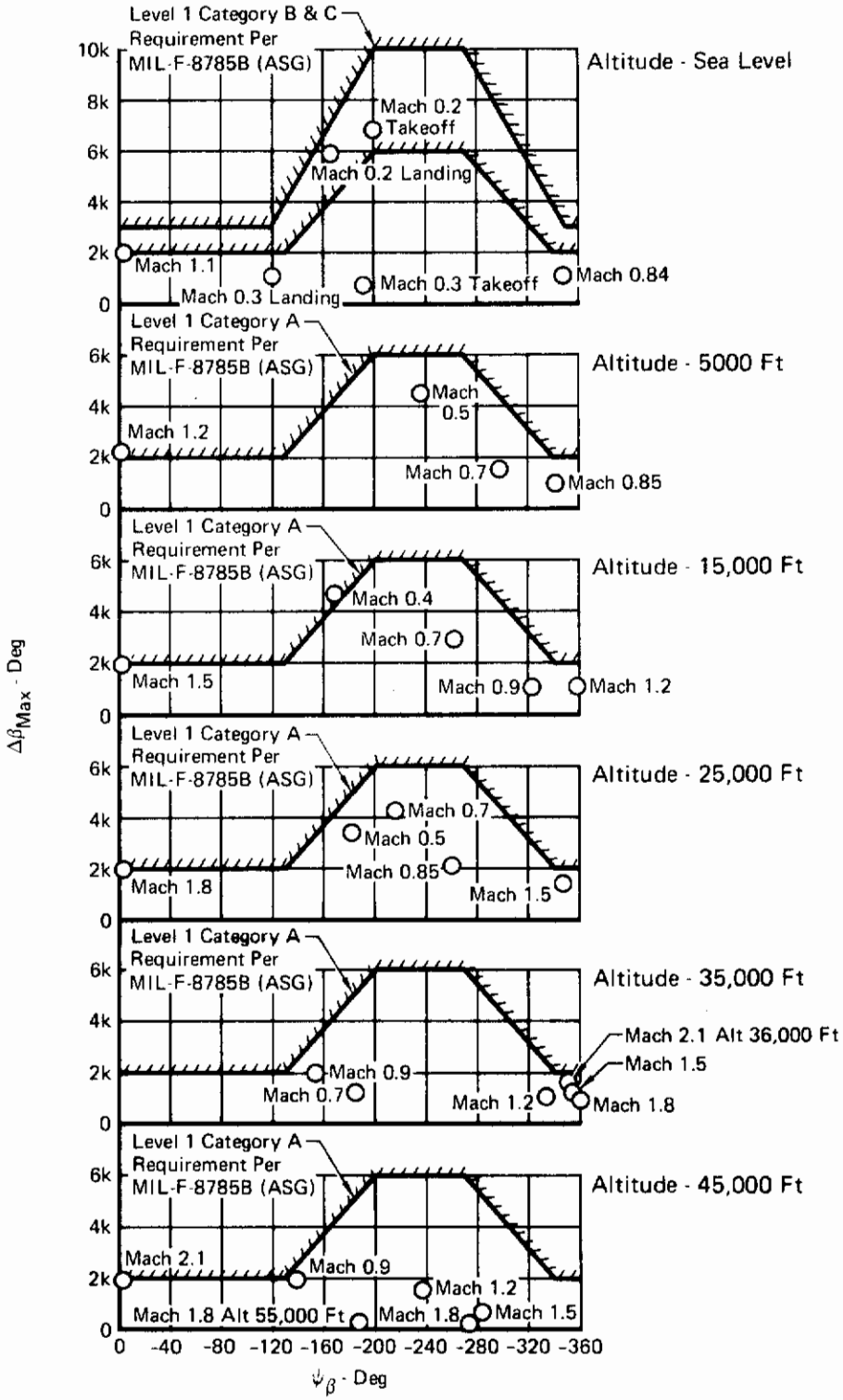

FIGURE 68
SFCS SIDESLIP EXCURSION

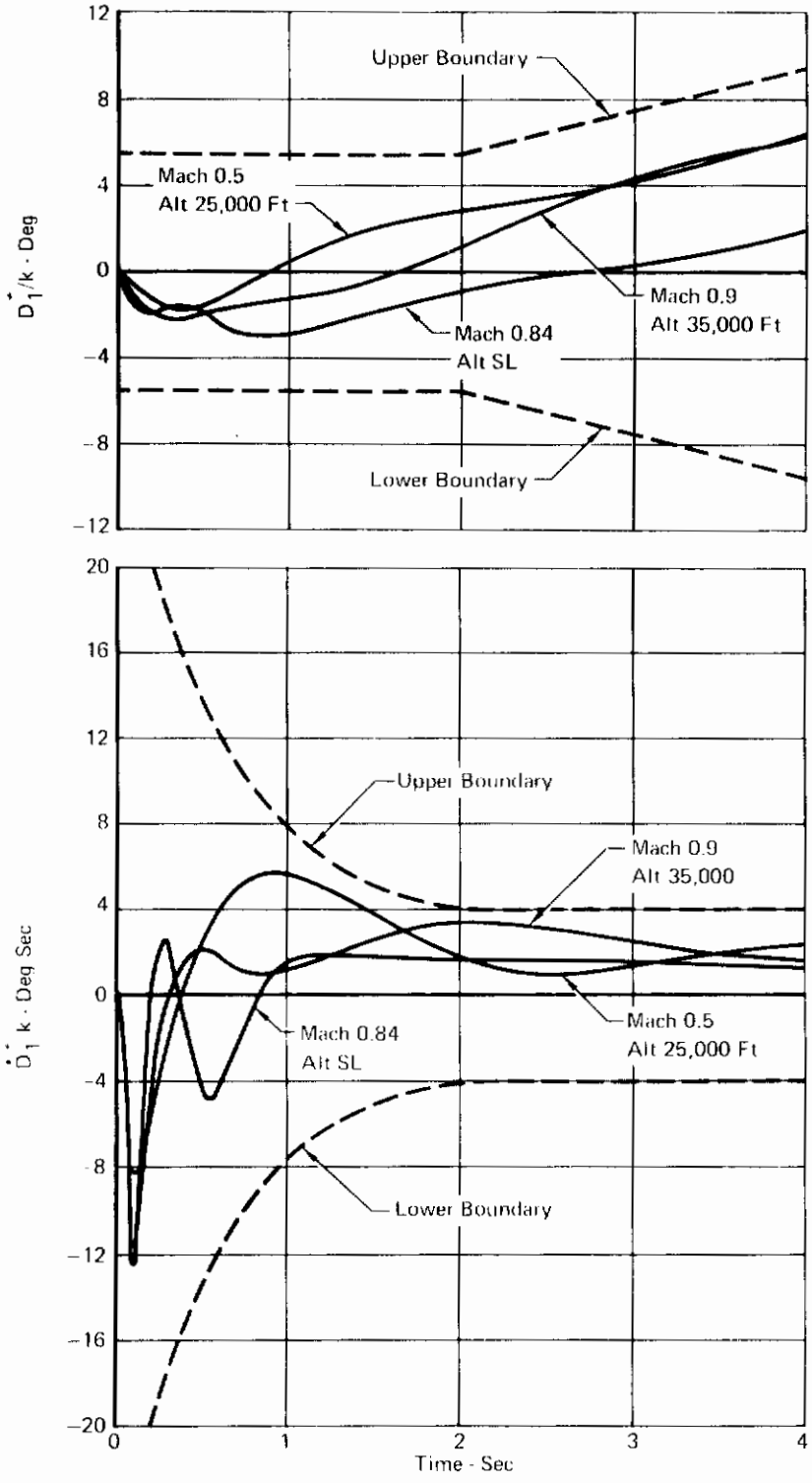

FIGURE 69
SFCS LATERAL DIRECTIONAL D_1^* RESPONSE

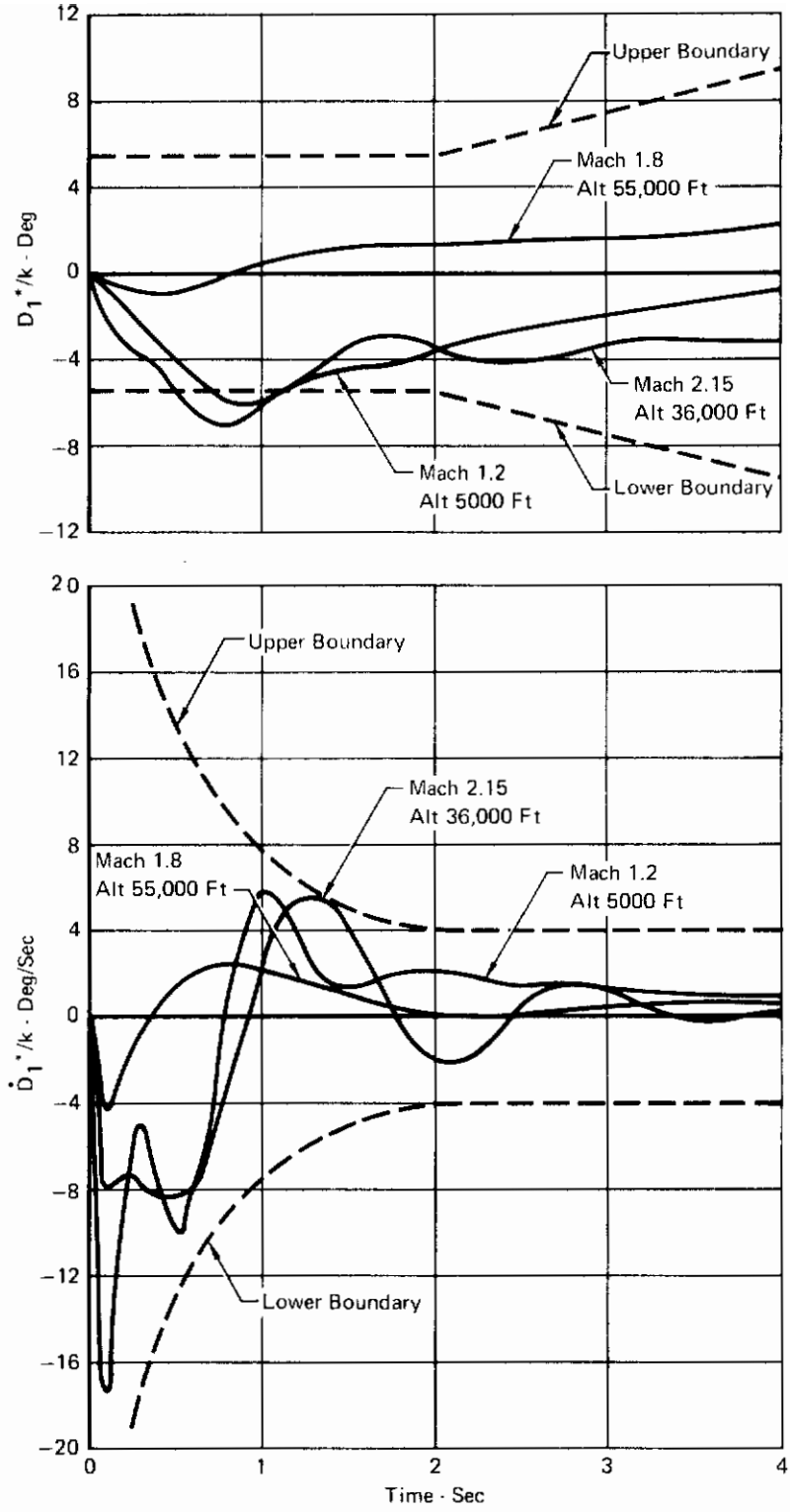

FIGURE 70

SFCS LATERAL DIRECTIONAL D_1^* RESPONSE

The D_1^* parameter recorded in Figures 69 and 70 is in response to a step of lateral stick force and is a combination of sideslip and lateral acceleration at the pilot seat as expressed by the following equation.

$$D_1^* = \beta - .513\, a_{y_p} \quad \text{(deg)}$$

where: β (sideslip) in degrees

a_{y_p} (lateral acceleration at the pilot seat) in feet/second^2

The development and discussion of the D_1^* criteria is presented in TR-71-20, Supplement 1. Additional D_1^* data are presented in Appendix IV. The SFCS meets the D_1^* criteria at all flight conditions except some low $\bar{q}$ and some very high $\bar{q}$ and high Mach number flight conditions. At these flight conditions, the aircraft response will slightly exceed the boundary value for a short period of time. The effect of failure to exactly comply with the D* and $\dot{D}$* criteria at the edge of the envelope flight conditions will probably not be noticeable to the pilots and is not expected to degrade system performance.

Figure 71 shows the sideslip for the F-4 with yaw SAS for many of the same flight conditions. A comparison between Figures 68 and 71 shows the improvement obtained with the SFCS.

Figure 72 shows the time history response of the D_1^* parameter for the Mach 0.9 at 35,000 feet altitude flight condition for the pilot selectable roll to yaw crossfeed gain values. The figure shows that gain settings which provide crossfeed gains less than the proper adaptive gain value result in excess adverse sideslip, and those gain settings providing crossfeed gains in excess of the proper adaptive gain value result in excessive proverse sideslip.

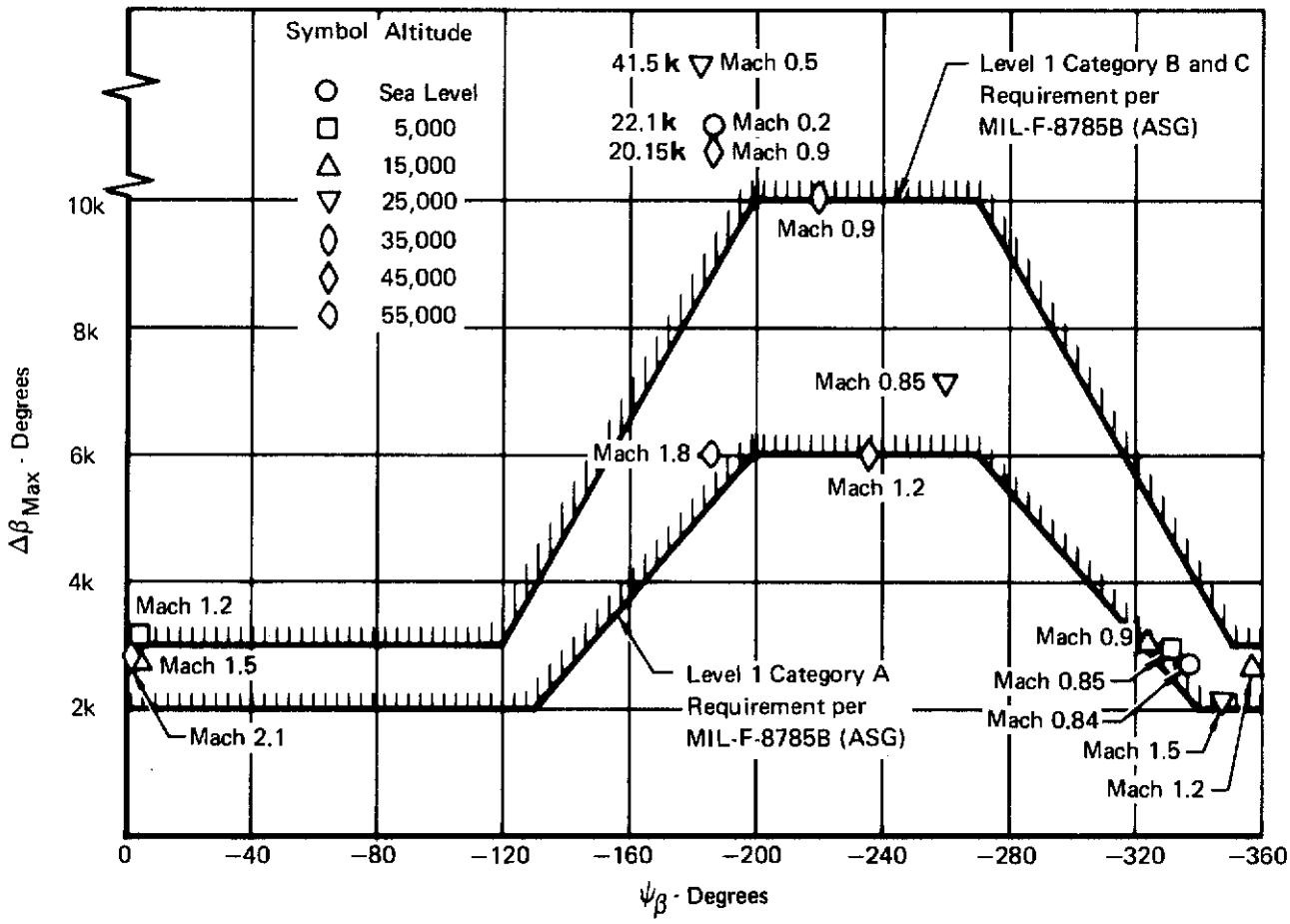

FIGURE 71
SIDESLIP EXCURSION - F-4 WITH YAW SAS

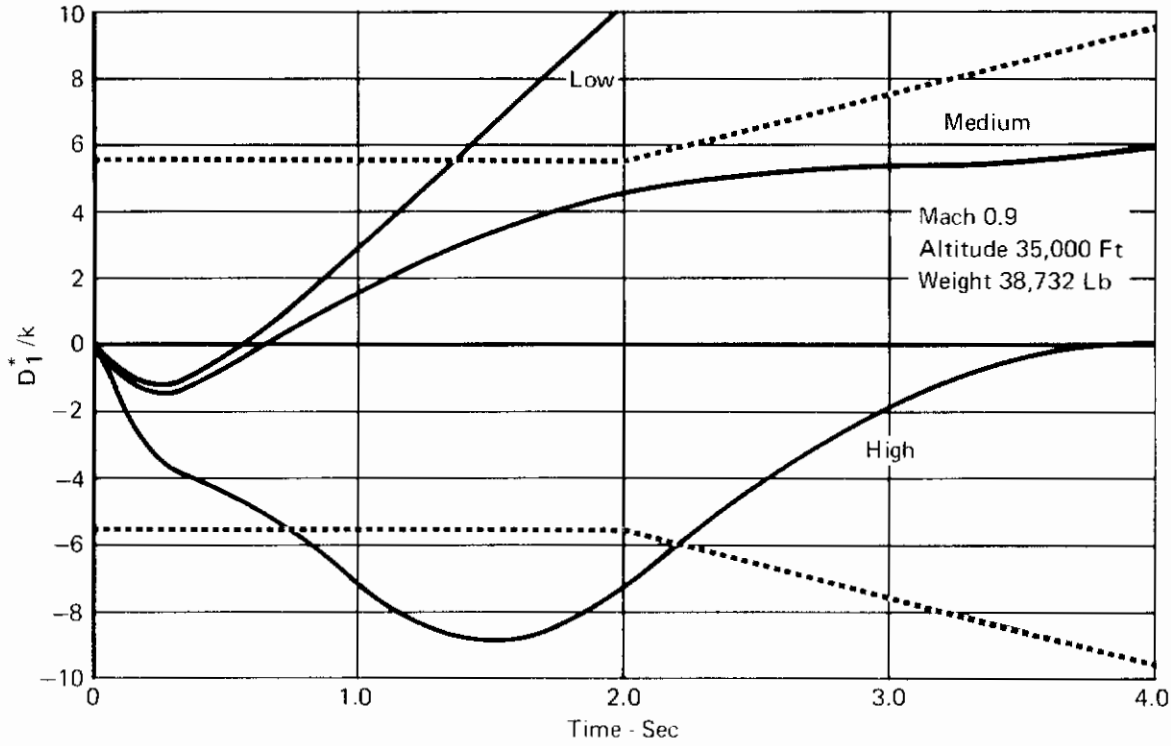

FIGURE 72
D_1^* RESPONSE VARIATIONS WITH SELECTABLE GAINS

SECTION V

CONTROL SYSTEM EVALUATION SIMULATION

1. INTRODUCTION

A fixed base flight simulator program was conducted to evaluate the selected SFCS in order to reveal any design problems or necessary modifications. A complete three axis single channel SFCS math model was programmed on the hybrid computer along with aircraft flight dynamics representing the F-4E. The entire flight envelope could be flown including power approach, stall entry, and post stall recovery. The simulator crew station was equipped with all necessary controls for the pilot to fly the aircraft and change the SFCS operating mode during flight. The following paragraphs describe the simulator set-up, the evaluation approach and the resulting SFCS modifications.

2. OBJECTIVES

The following objectives for the subject simulation were established:

a. SFCS handling qualities and operating characteristics

The simulator pilot shall be able to fly the SFCS throughout the entire F-4E flight envelope so as to evaluate the SFCS operating characteristics.

b. In-flight parameter and gain variations

The effect of SFCS parameter and gain variations on system performance will be determined.

c. In-flight failure simulation

The effect of failures inserted during simulated flight with the SFCS will be determined.

d. SFCS mode transitions

The controllability of the F-4E when switching between the available modes will be established.

e. Establish flight test procedures

Test procedures for use during the Phase II flight test program will be developed.

3. HYBRID FACILITY

The SFCS manned simulator program utilized the MCAUTO simulation facility which has been assembled expressly for hybrid simulation. Use

of digital computing techniques on the CDC 6600 permitted large variations in flight parameters while retaining the precision required for simulation accuracy. An analog computer served as a buffer to the cockpit equipment, visual display equipment and time history recorders. Peripheral equipment, consisting of closed circuit TV, terrain map, gimballed target model and horizon generator, provided a more realistic environment in which to evaluate the selected SFCS. A description of this computing and display equipment is presented in Appendix VI.

4. SOFTWARE DESCRIPTION

A math model representing the complete SFCS (single channel) was programmed on the hybrid computer. The SSAP mechanization was not included in the subject simulation due to the incomplete state of the available mathematical models of the actuator. The SSAP will be evaluated during future simulations.

Aerodynamic derivatives for the entire flight envelope were included so that the SFCS could be evaluated at all flight conditions including landing and stall. Operating logic for the SFCS was controlled from the crewstation providing for pilot selection of parameter and gain variations and SFCS modes during flight. Close coordination was maintained with the control law development studies so that any system modification would be reviewed by both. A complete description of the selected SFCS evaluated during this simulation is presented in Sections III and IV. Special operating characteristics not discussed in Sections III and IV are presented in Appendix VII.

5. EVALUATION APPROACH

a. General Flight Maneuvering

A detailed run schedule was prepared so that the simulation objectives would be accomplished in an orderly manner. The pilots were provided with a briefing sheet as shown in Figure 73 for use in evaluating the SFCS. This form listed the SFCS modes to be evaluated and recommended maneuvers which would test the full SFCS capability. Following the simulator flight, each pilot completed a questionnaire to obtain a qualitative measure of the system performance. The questions related to the responsiveness of the SFCS to control inputs, phugoid stability, feel-trim characteristics, ARI operation, PIO tendencies and mode transitions. A Cooper rating was assigned and comments were solicited for each mode of operation.

b. Performance Tasks

The pilots performed special tasks to obtain a quantitative measure of the SFCS performance. An air-to-air tracking problem demonstrated

I. Objectives - The following objectives for the subject simulation are designated in the SFCS statement of work.
- Evaluate the controllability, tracking, operating characteristics, and general pilot acceptance of the SFCS over the entire F-4E flight envelope.
- Evaluate the effects of in-flight parameter variations on the SFCS. The manner of adaptive gain changing is of primary interest.
- Evaluate the failure transients as applied to the quad-redundant SFCS.
- Evaluate transitions between mechanical backup and FBW modes.
- Establish flight test procedures which will later be used to generate comparative data between the 680-J flight test program and this simulation.

II. Man-in-the-Loop Evaluation Procedure - A detailed run schedule will be used during the selected control system evaluation to assure that the simulation objectives are met. The following tasks will be performed.
- General maneuvering throughout the F-4E (clean configuration) flight envelope. The following modes and functions will be examined.

Mechanical Back-Up	Normal Adaptive Gain
Electrical Back-Up	Normal Fixed Gain (Lo) with TOL selected
Normal Fixed Gain (Lo)	

- General maneuvering throughout the entire F-4E flight envelope to include the following flight conditions:

0.5 M at 25,000 ft ($\bar{q}$ Low)	1.5 M at 15,000 ft
0.9 M at 15,000 ft	2.15 M at 36,000 ft (V Max.)
1.2 M at 5,000 ft ($\bar{q}$ Max.)	1.8 M at 55,000 ft
0.9 M at 35,000 ft (Cruise)	

III. Include the maneuvers when applicable:
- Accels and decels at sea level, 20,000 ft, and 40,000 ft.
- Maximum power climbs and dives from 0.9 M at sea level to 1.2 M at 30,000 ft and back to 0.9 M at sea level using split S to return.
- From trim 0.7 M at 35,000 ft perform split S and observe lateral/directional handling in comparison with the high $\bar{q}$ split S performed above.
- Snap aileron rolls and barrel rolls at high and low $\bar{q}$ flight conditions.
- Pull-up and push-over cycling at high and low $\bar{q}$ flight conditions.
- Terrain following task at end of run.
- Cycle MIM while in SFCS normal fixed (Lo) and in electrical back-up going to mechanical back-up. Select 0.7 M at 15,000 ft and cycle during:
  (a) Level flight
  (b) Normal maneuvering
  (c) High "g"; 3 axes maneuvering
- Aerial tracking pursuing a target aircraft which performs a set of programmed maneuvers.
- Landing approach and takeoff using the high lift F-4E configuration.
- Stall entry and recovery with the SFCS operating using special high alpha and beta aerodynamic data.

IV. A questionaire will be filled out following each flight concerning:
- Short period handling qualities
- Phugoid stability
- Feel/trim characteristics
- ARI operation
- PIO tendencies
- MIM operation (when applicable)

FIGURE 73

PILOT BRIEFING SHEET

the relative effectiveness of the SFCS modes while pursuing a target performing evasive maneuvers. The tracking error between the pursuit aircraft's fixed reticle and the target aircraft was tabulated for the duration of the run. Following each run a cumulative distribution plot of the error signal was formulated to show per cent tracking accuracy. A terrain following task was performed as another performance measurement of the SFCS. Similar cumulative distribution data of the command needle error were tabulated for this task.

The SFCS was evaluated in the power approach configuration by the pilots while performing a landing approach. An out-the-window terrain display, described in Appendix VI, provided visual cues to the pilot for maintaining the aircraft on glide slope and centerline of the runway. The gear and flaps could be retracted to perform a missed approach. The pilots completed a questionnaire evaluating the PA handling qualities at the end of this evaluation task.

c. Stall entry and post stall recovery

Special aerodynamic data describing the F-4E in the stall and post stall region were programmed for the subject simulation. This provided a means of evaluating the SFCS recoverability from a stall and the effectiveness of the stall warning system. The pilots were asked to enter both one g and accelerated stalls. All SFCS modes were evaluated for the stall recovery task including reversion to the back-up modes at stall entry. Pilot comment on the SFCS operation during the stall entry and post stall condition added to the system evaluation.

d. Failure Analysis

Wave forms representing worse case single channel failures were applied to the pitch, roll and yaw channels. The pilot's ability to control the resultant transient was determined. The nature of these wave forms is presented in Appendix VII. Further discussion of the failure analysis is given in TR-71-20, Section III.

6. EVALUATION OF SELECTED SFCS

The various modes of the selected SFCS were evaluated in accordance with the test plan outlined in Paragraph 5 above. The resulting hybrid data and pilot comments obtained from this evaluation were analyzed in order to reveal problem areas in system design. Scheduled inputs were applied to the SFCS simulation to generate data which could be compared to the control law small perturbation study results to assure no differences in system response existed between the various simulations. Figures 74 and 75 present airframe responses to force inputs which compare with those found in Sections III and IV above. The results of the subject simulation are discussed in the following paragraphs.

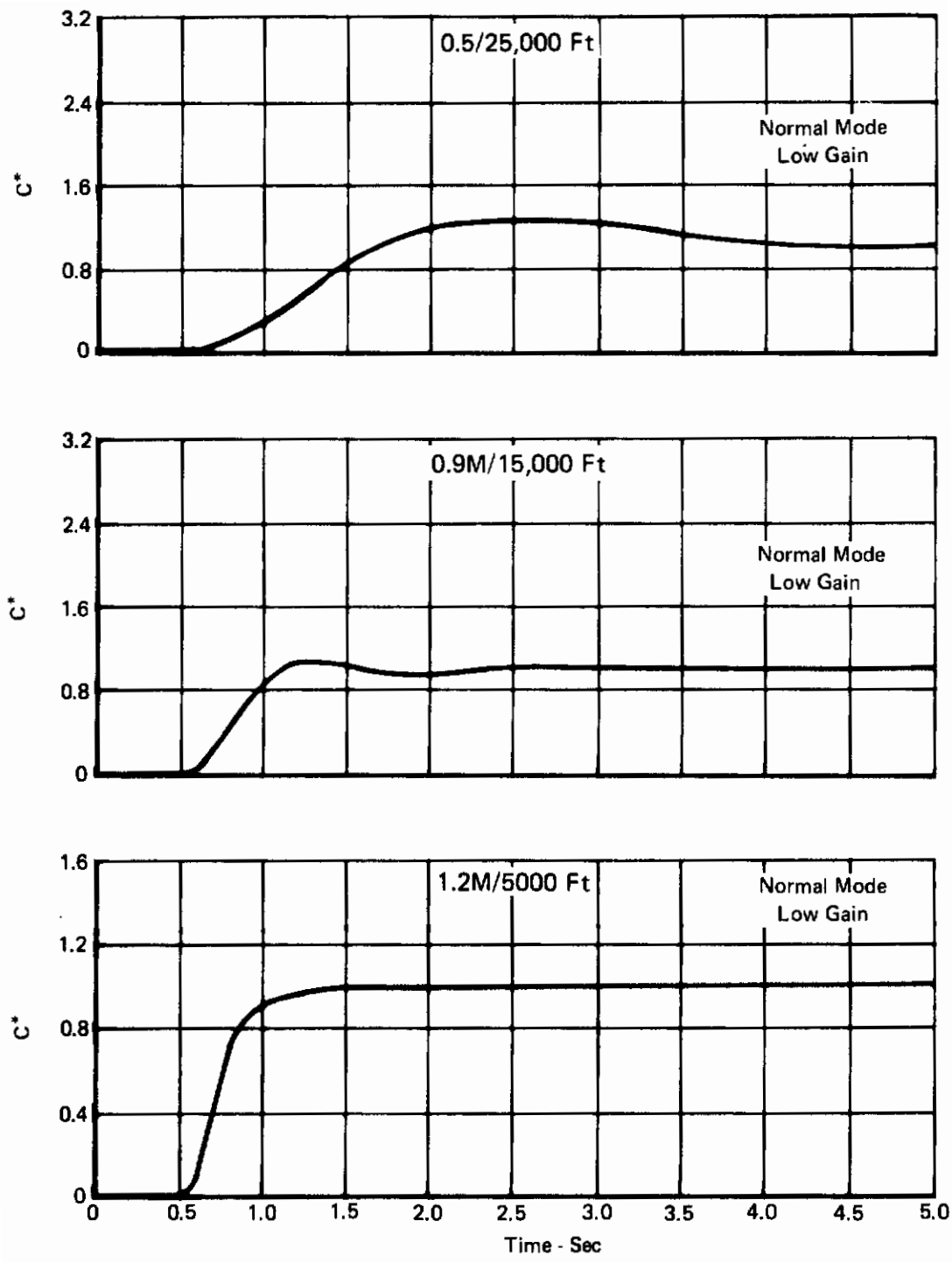

FIGURE 74
LONGITUDINAL AIRFRAME RESPONSE TO 5 POUND STICK INPUT

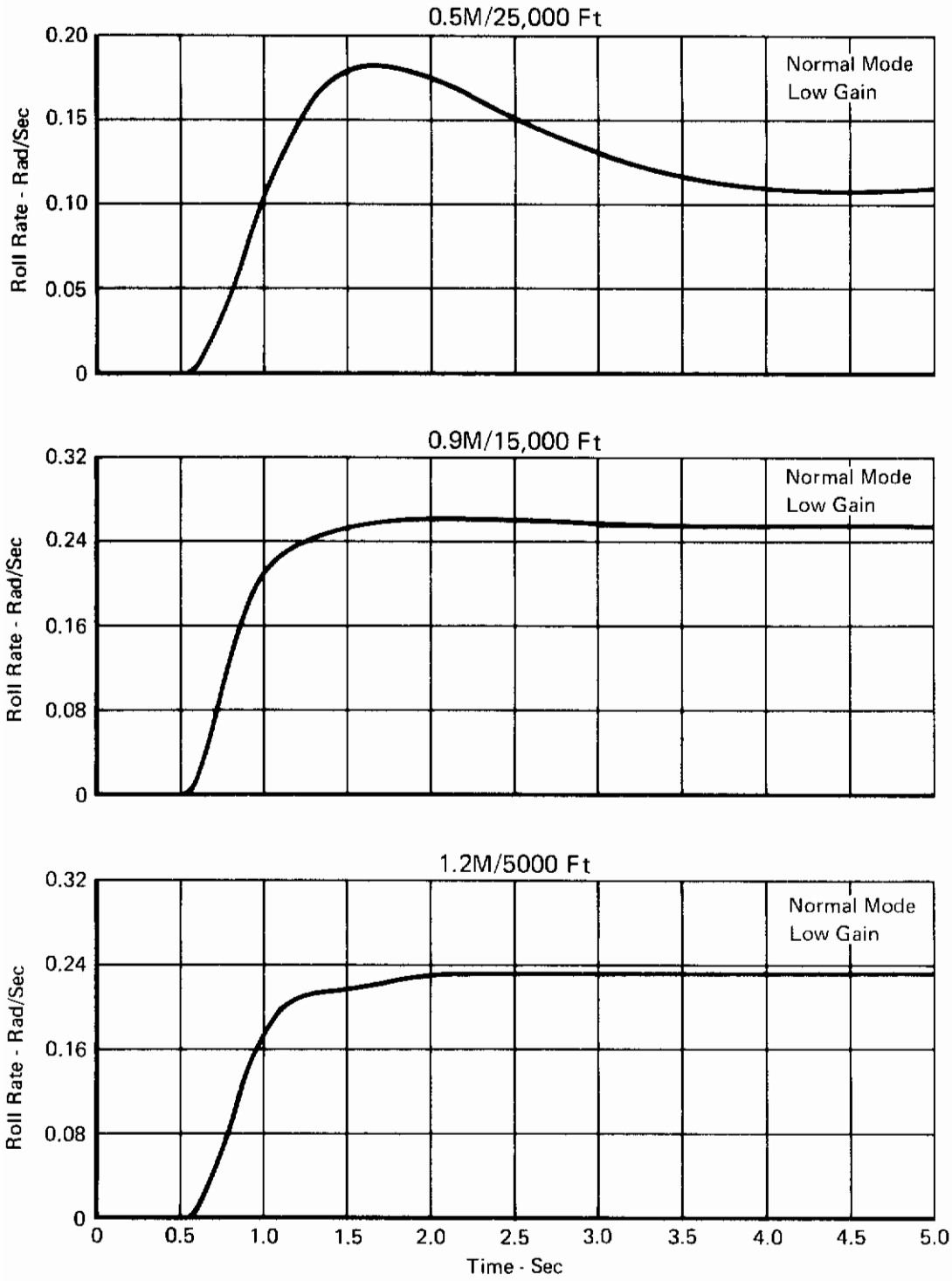

FIGURE 75
LATERAL AIRFRAME RESPONSE TO 3 POUND STICK INPUT

a. SFCS Modes

(1) Mechanical Back-Up (MBU)

No control problems were found with the pitch and yaw MBU mode. The F-4E damper mode was operative with MBU selected, providing handling qualities quite similar to the F-4E. The slight differences resulted from the use of the SFCS feel system in place of the $\bar{q}$ bellows system found in the production F-4E. The roll channel operated in electrical back-up mode since no lateral mechanical back-up exists. The lateral feel system did receive unfavorable pilot comment due to the original design having a $\pm$20 pound maximum lateral center stick force. This high force level led to pilot fatigue while flying. Reduced forces were evaluated and maximum force levels of $\pm$12 pounds were found to be more desirable by the pilots.

(2) Electrical Back-Up (EBU)

Control harmony between the pitch and roll axes was found to be a problem in the EBU mode. Pitch sensitivity is high at high M_δ flight conditions due to the use of a direct electrical link to the stabilator. Methods are currently being evaluated to eliminate the high pitch axis sensitivity through the use of a dual gradient in the EBU signal path. The roll axis has an apparent low roll response to small stick inputs caused by the dual gradient used in the lateral axis. The low responsiveness becomes more apparent in the PA configuration. The pilots considered these roll axis characteristics acceptable for the EBU mode.

A longitudinal stick lightening was seen by the pilots when a constant load factor was commanded. The high passed stabilator feedback signal in the EBU mode was removed to eliminate this problem. No apparent problems were found with the directional channel in the EBU mode.

(3) Normal (NSS) Mode

The handling qualities of the Normal mode were found to be quite satisfactory by all pilots evaluating the SFCS simulator and received an average Cooper rating of 2. The Normal mode SFCS responded well to pilot commands and showed good damping throughout the flight envelope. The neutral speed stability (NSS) function performed satisfactorily during accelerations and decelerations. Essentially no effort was required by the pilots to maintain speed or altitude thus

indicating acceptable phugoid characteristics. The effectiveness of the Normal mode in performing tasks such as air-to-air tracking of a maneuvering target and terrain following is discussed in subsequent paragraphs. Formation flying and aerial refueling were not investigated since the pilot effort required for these did not differ significantly from the chosen tasks. The purpose of the NSS function is to eliminate the need for the pilot to retrim for a change in airspeed. This characteristic may be desirable in reducing pilot work load during in-flight refueling. The stabilator position change, which accompanies the weight increase and CG shift during in-flight refueling, will be automatically provided in the Normal mode. Judgement as to the total acceptability of neutral speed stability must ultimately be based upon flight experience.

(4) Adaptive Gain Select

The pilots found no apparent change in aircraft response between adaptive and fixed gain operation except for low $\bar{q}$ and landing flight conditions. The gain changer operated with sufficient accuracy with the pitch adaptive function selected, provided the pilot generated inputs sufficient to excite the airframe in the 4 Hz frequency range. Without the pitch adaptive switch engaged, the computed M_δ did not agree or track the actual stabilator effectiveness. The gain changer did not compute M_δ accurately enough to select the correct gain levels for the roll to yaw crossfeed. The results obtained through use of the original parameter identifier design programmed for the subject simulation indicated that a redesign was required. Further discussion on the gain changer design development is presented in TR-71-20, Section III.

(5) Normal (TOL) Mode

The selection of TOL operation with the Normal SFCS mode engaged caused no apparent change in aircraft response. The similarity between the characteristics obtained with the TOL function selected and the normal (NSS) function selected is due to the inherent neutral speed stability characteristics of the basic airframe at mid and high $\bar{q}$ flight conditions. The positive speed stability characteristics of the TOL function were noticeable at low $\bar{q}$ flight conditions.

b. Trim

Pitch and roll trim changes were made for each mode of the SFCS. Pilots inadvertently used the mechanical trim switch located at the top of the center stick when in the Normal and EBU modes. Operation of this switch has no effect on aircraft trim but does change stick position. Inadvertent operation of the trim switch

caused a mismatch between stick and surface position and caused an undesirable transient on reversion to the MBU mode. To remove this problem, the center stick trim button was disabled during Normal and EBU mode operation.

The longitudinal electrical trim authority was found to be excessive. At high M_δ flight conditions maximum load factor could be commanded with partial movement of the trim thumbwheel. A reduction of the EBU trim authority from a range of -14° to 3° of stabilator to $\pm 1^\circ$ for clean and $\pm 5^\circ$ for PA was found necessary. The amount of longitudinal trim available in the Normal mode was reduced by one half. The pilots felt that the capability to trim into a 60° banked level turn at 360 Knots-sea level was not necessary. The roll trim authority was also reduced by one half for Normal and EBU. The original 33 1/3% lateral surface authority was too sensitive for small roll rate corrections. No problem was found with the directional trim.

c. Mode Transitions

The possibility existed for a catastrophic transient when changing modes before the modifications to the longitudinal trim circuits were made. A mistrimmed stabilator could occur for the MBU mode due to the inadvertent trimming of the center stick while in FBW operation. Disengagements from Normal to EBU with full longitudinal trim applied caused an uncontrollable transient at high $\bar{q}$ flight conditions. This transition was made acceptable by the reduction of the Normal and EBU trim authorities and by doubling the time constant of the longitudinal easy-on easy-off network from 2.5 seconds to 5.0 seconds. Figure 76 presents time histories of transitions from Normal to EBU modes with one half the original trim authority (-7° δ_s) applied. Transition from Normal to EBU with the final $\pm 1^\circ$ stabilator trim authority is shown in Figure 77. It can be seen from these figures that less pilot action is needed with the final electrical trim definition. Figure 78 presents transitions from EBU to MBU with an aft center stick position obtained prior to the disablement of the mechanical trim in FBW modes. Reversion to MBU from either Normal or EBU caused no control problem after the mechanical trim switch was disabled. A slight change of stick force was needed to maintain the same load factor maneuver due to the difference of stick force per g between modes. Figures 79 and 80 present time history traces obtained for transition between Normal and MBU and between EBU modes with no trim applied.

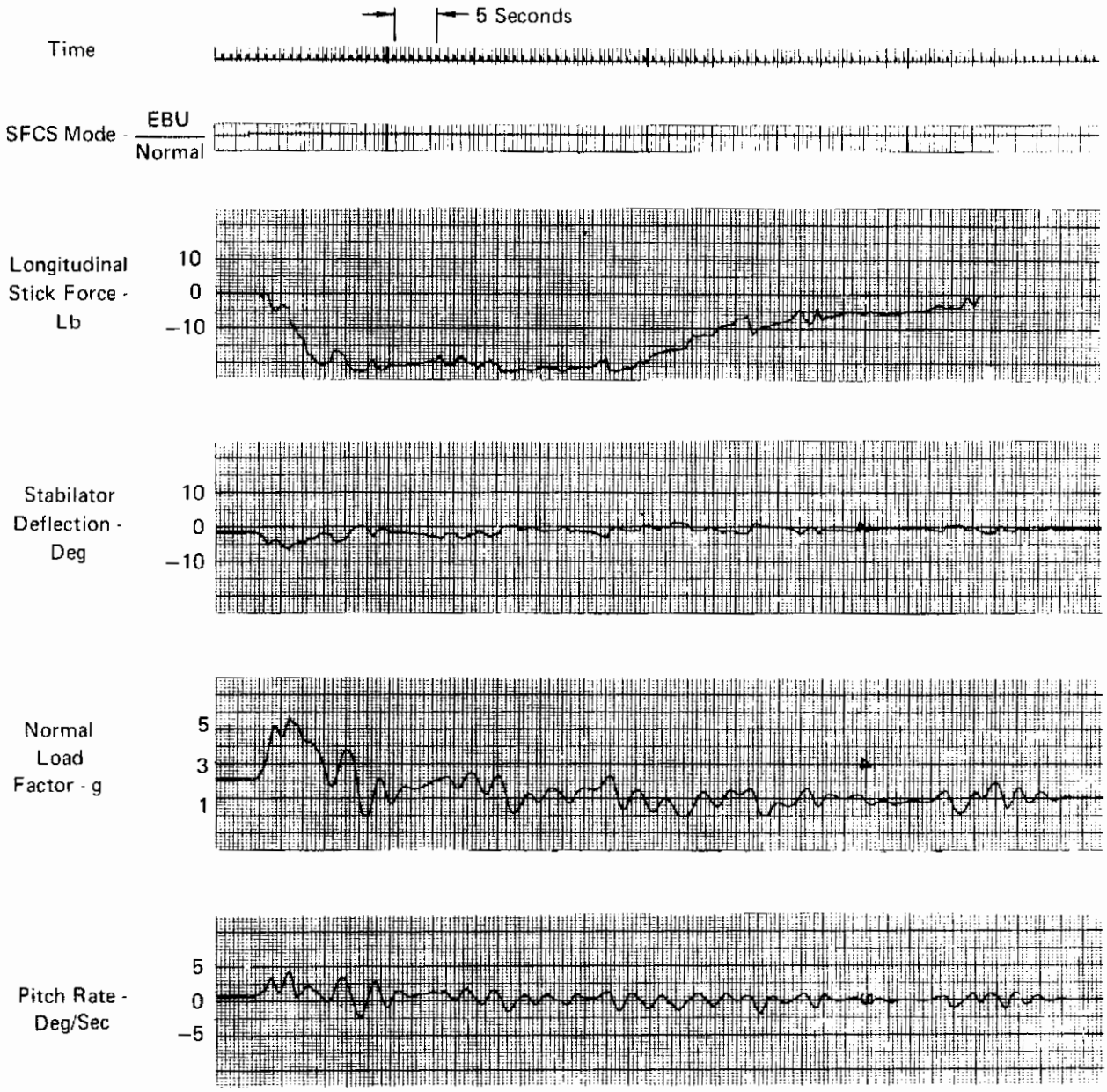

FIGURE 76

TRANSITION FROM SFCS NORMAL MODE TO ELECTRICAL BACK-UP

$\pm 7^{O}$ Trim Authority

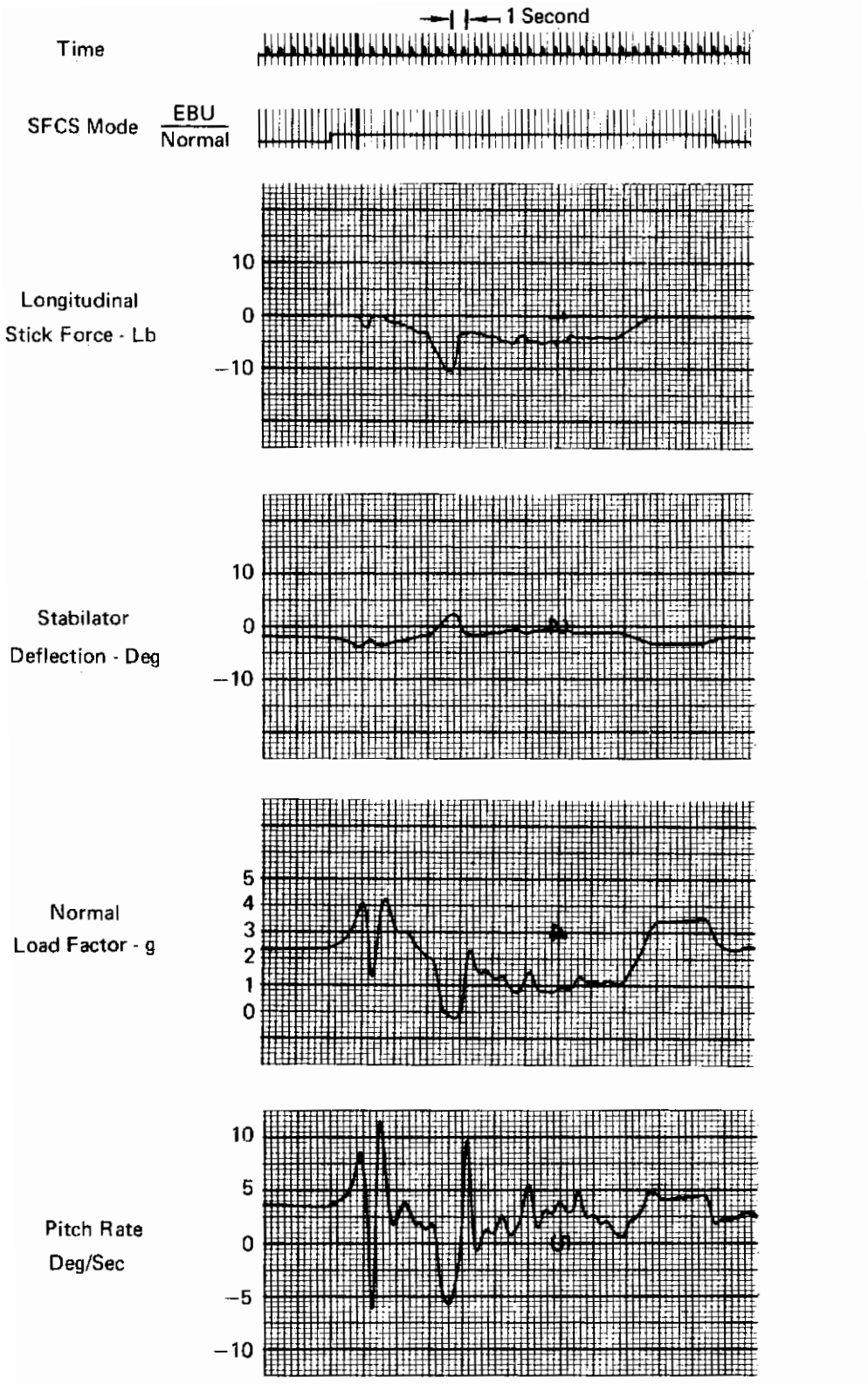

FIGURE 77

TRANSITION FROM SFCS NORMAL MODE TO ELECTRICAL BACK-UP

$\pm 1^{o}$ Trim Authority

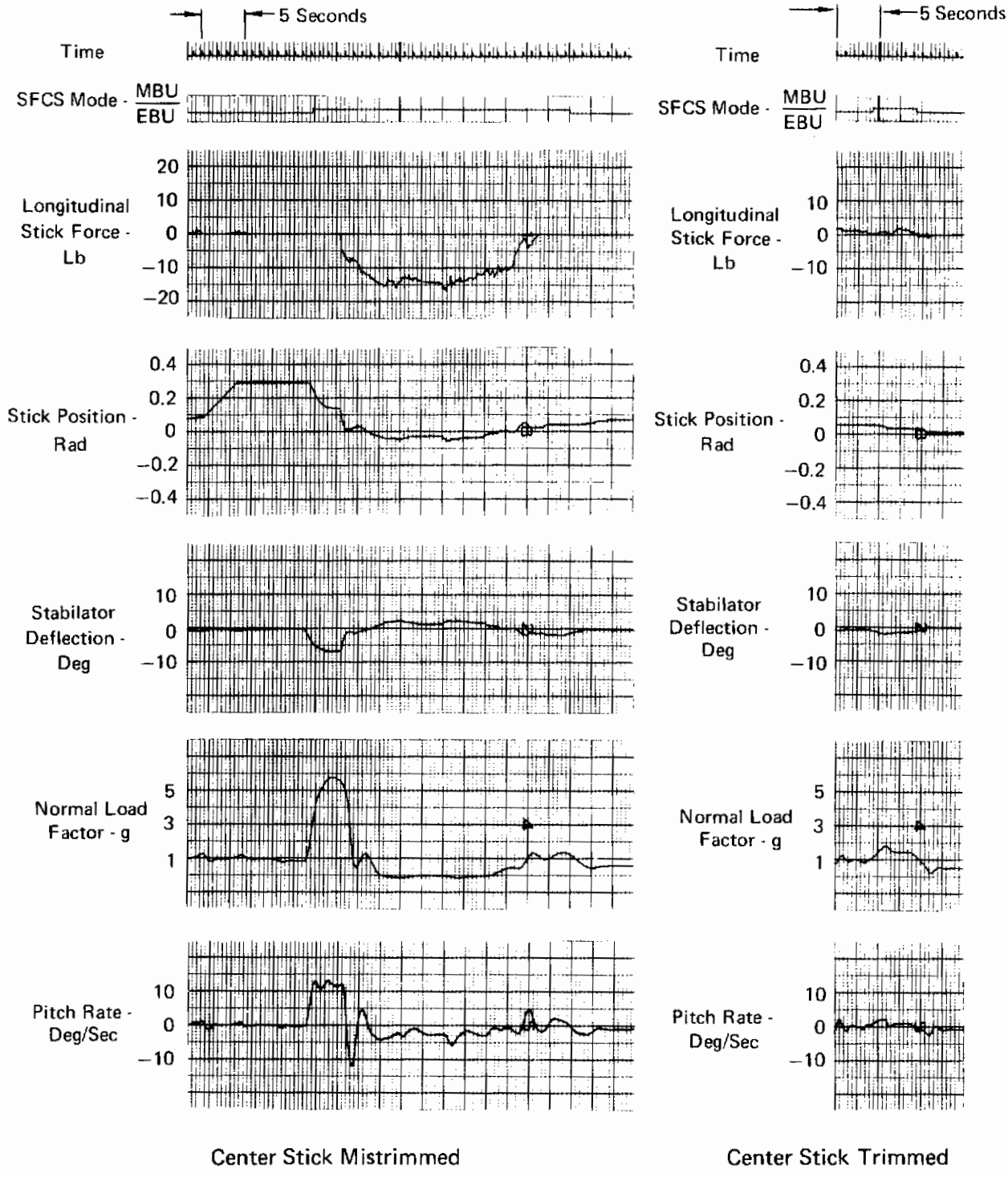

FIGURE 78

TRANSITION FROM SFCS ELECTRICAL BACK-UP MODE TO MECHANICAL BACK-UP MODE

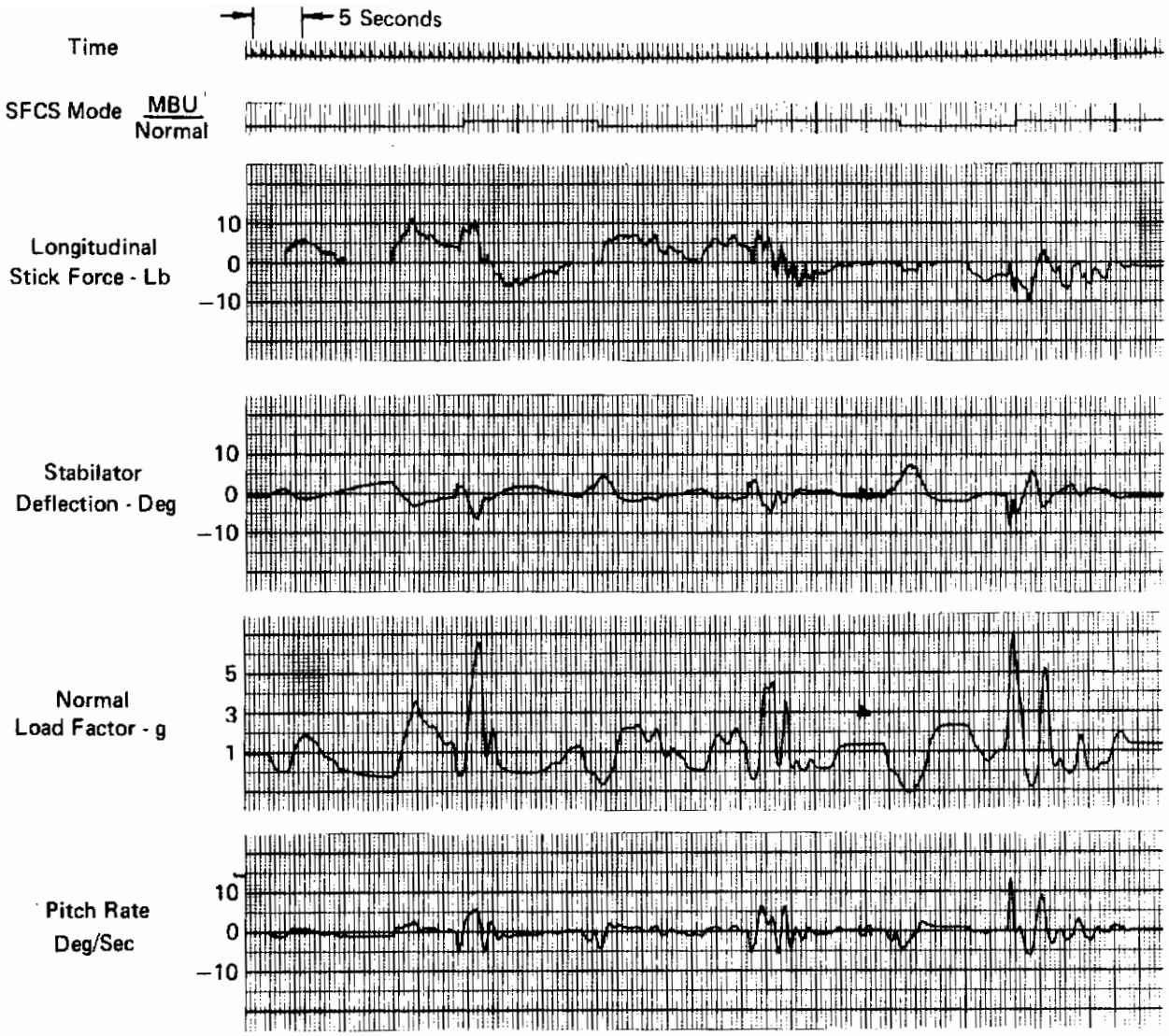

FIGURE 79
TRANSITIONS BETWEEN SFCS NORMAL AND MECHANICAL BACK-UP MODES

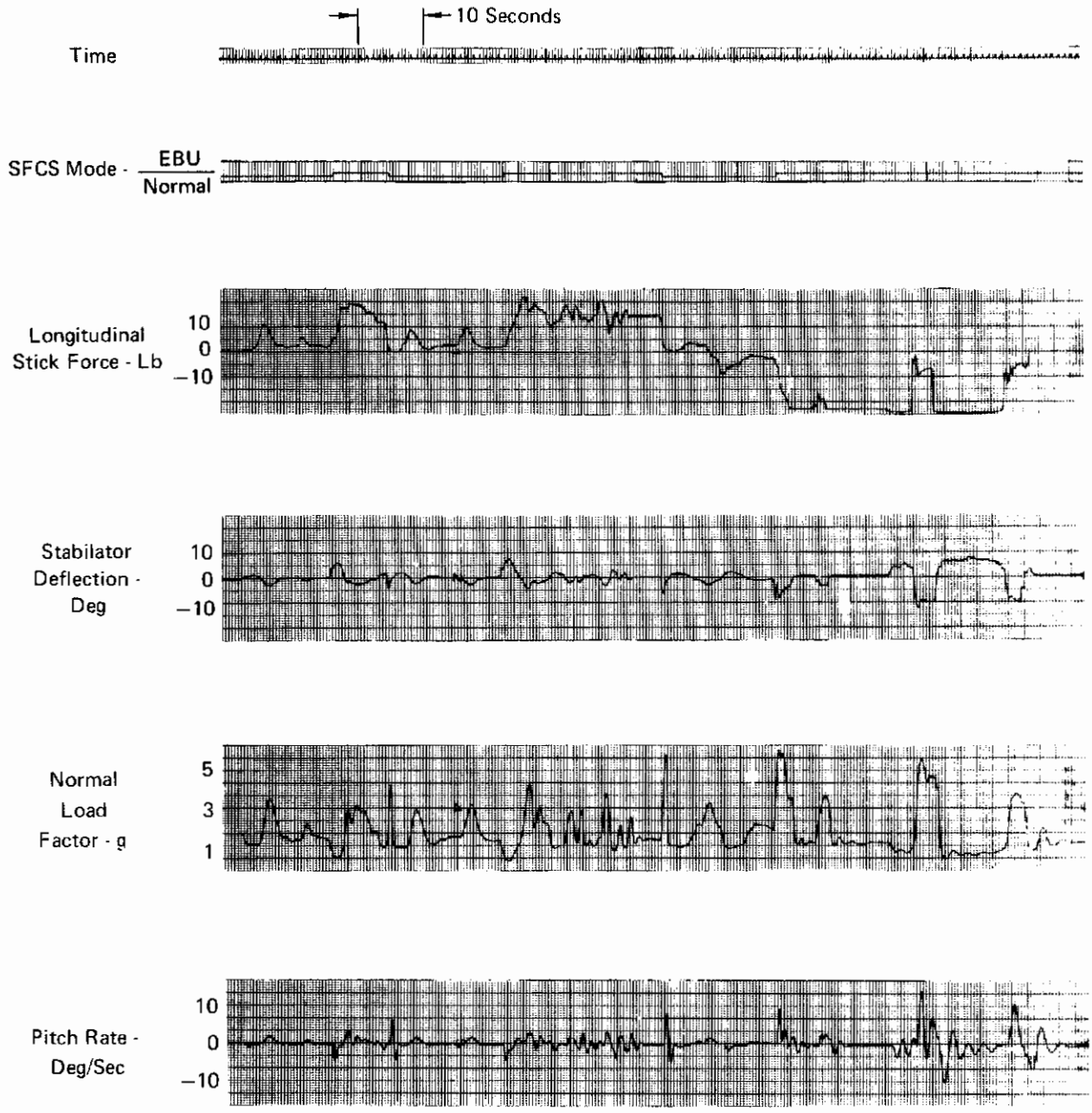

FIGURE 80
TRANSITIONS BETWEEN SFCS NORMAL AND ELECTRICAL BACK-UP MODES

d. In-Flight Failure Simulation

Wave forms(described in Appendix VII)representing single channel failures were applied to the forward loops of the SFCS with and without the pilot's knowledge. Figures 81, 82, and 83 show the resulting aircraft response to the applied failures with no pilot action taken. The pilots found no difficulty in correcting for the small effect caused by these failures. The failure signals were first individually applied to the SFCS with the pilot observing the resultant transient. The transients caused by these failures were insignificant relative to the mode transition transients prior to the trim system modifications. Quantitative data were then taken during the air-to-air tracking and terrain following tasks and the resultant cumulative distribution data with and without failures applied showed no significant deterioration in performance due to the simulated single channel failures.

e. Performance Data

(1) Air-To-Air Tracking

Quantitative and qualitative data were obtained for the air-to-air tracking task for all SFCS modes. Pilot comment indicated

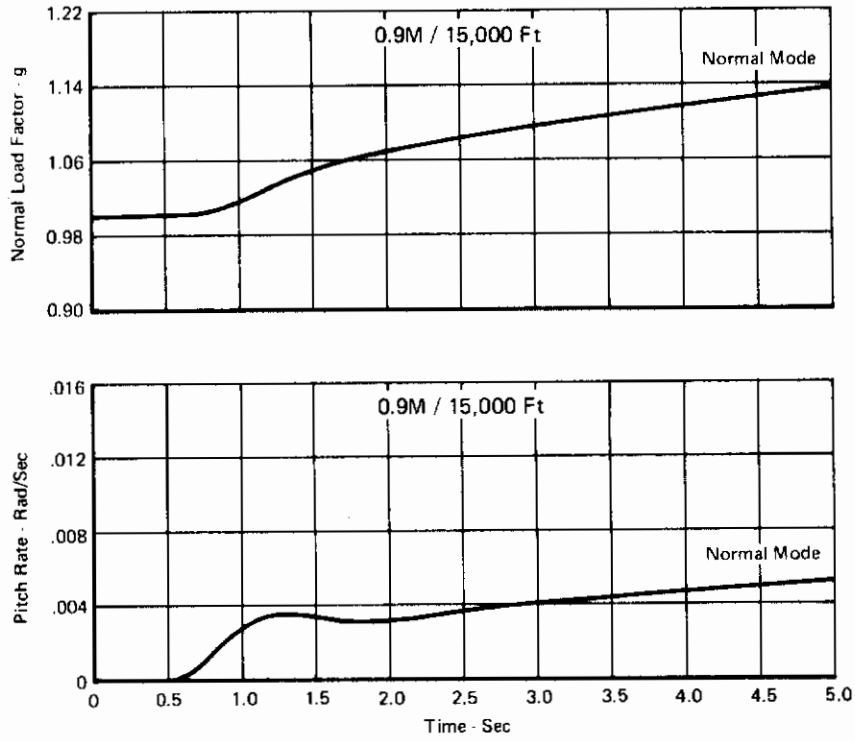

FIGURE 81
PITCH AXIS SINGLE CHANNEL FAILURE

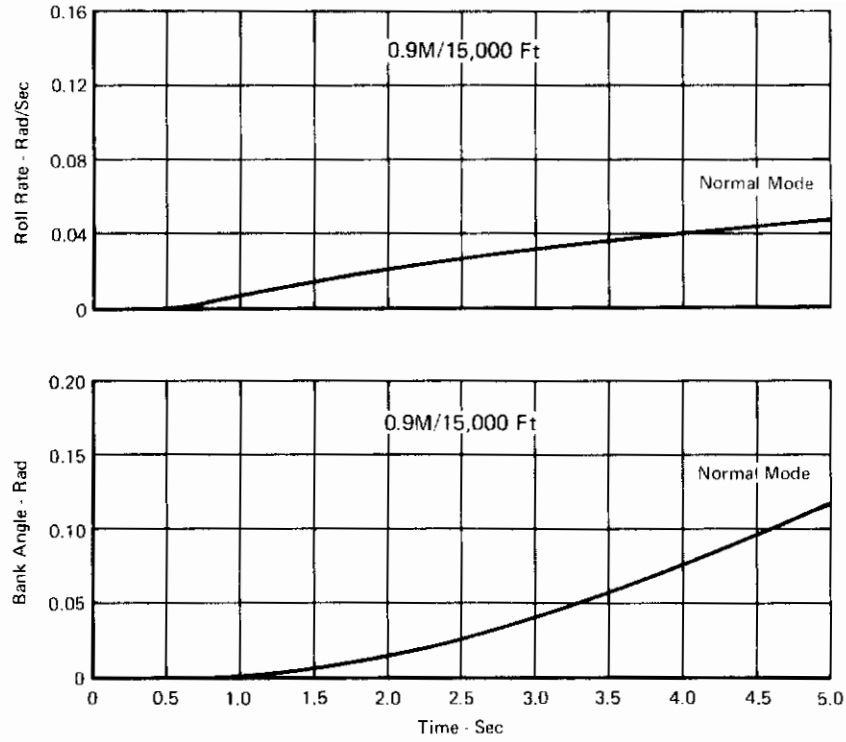

FIGURE 82
ROLL AXIS SINGLE CHANNEL FAILURE

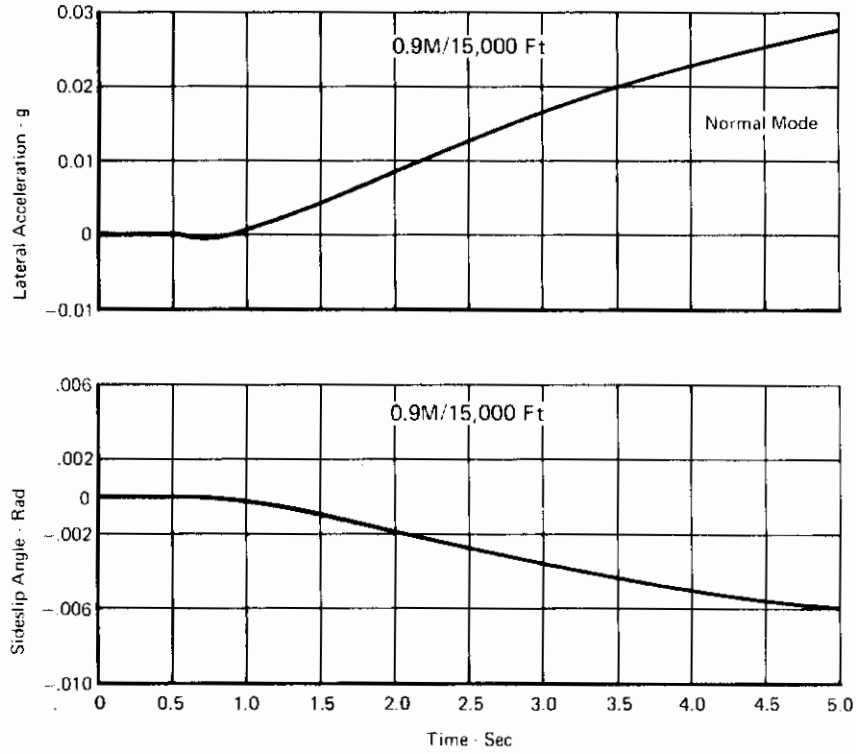

FIGURE 83
YAW AXIS SINGLE CHANNEL FAILURE

tracking was easiest to perform in the Normal mode followed by the MBU then EBU. The adaptive gain operation, even though selecting the proper gains, did not appreciably improve the pilot's tracking ability. Figure 84 presents cumulative distribution plots of the angular tracking error measured relative to a fixed reticle for the SFCS modes evaluated. The curves in Figure 84 show the percentage of time that the tracking error when firing is within a specified value. This figure shows that for 7 percent of the firing time the error was zero milliradians for the Normal mode and at no time was the error less than 2.5 milliradians for the EBU mode. This cumulative distribution plot also shows that for 81.5 percent of the firing time the error was 20 milliradians or less for the Normal mode while the EBU mode error when firing was 20 milliradians or less for 46 percent of the time. The higher percentage of firing time with a smaller tracking error for the Normal mode shows the Normal mode to be best.

(2) Terrain Following (TF)

Results of the terrain following task led to similar pilot comment on the relative performance of the SFCS modes. This task requires less high g maneuvering than the air-to-air tracking. However, more precise inputs were required to null the needle commands. Cumulative distribution plots of the pitch needle signal are presented in Figure 85 for the SFCS modes. These cumulative distribution plots show that the pilot was able to maintain tracking errors, represented by the needle signal, smallest for the greatest percent of time with the Normal mode selected.

(3) Landing Approach

The SFCS modes were evaluated for the power approach (PA) configuration. The Normal mode again was found to be the most desirable mode of operation. As previously mentioned, EBU showed poor lateral control due to the dual force gradient. The pitch axis was poorly damped in EBU due to the absence of rate damping. MBU was similar to the production F-4E in this configuration. Time history traces of aircraft parameters recorded during the approach using the Normal mode are presented in Figure 86 for the high, medium, and low gains. It can be seen that the pilot was able to maintain the aircraft on glide slope best with the medium gain selected, which reflected the pilot's comment that the medium gain was easiest to fly in the PA configuration. Evaluation of the Normal mode was accomplished using the three fixed gain levels in the pitch channel and adaptive gains. Further discussion of the selectable gains for PA configuration is found in TR-71-20, Section III.

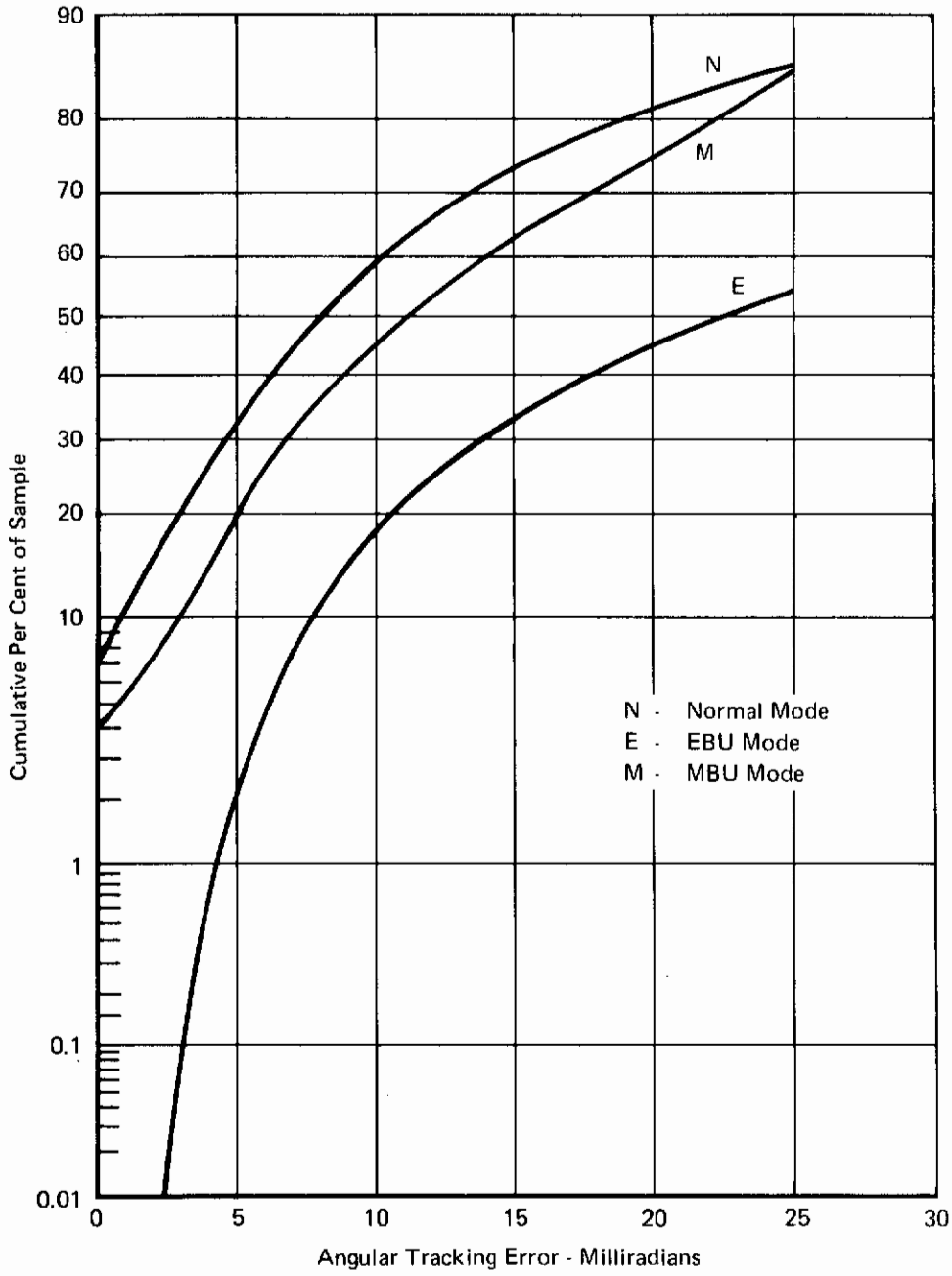

FIGURE 84
CUMULATIVE DISTRIBUTION OF TRACKING ERROR (WHILE FIRING) FOR SFCS AIR-TO-AIR TASK

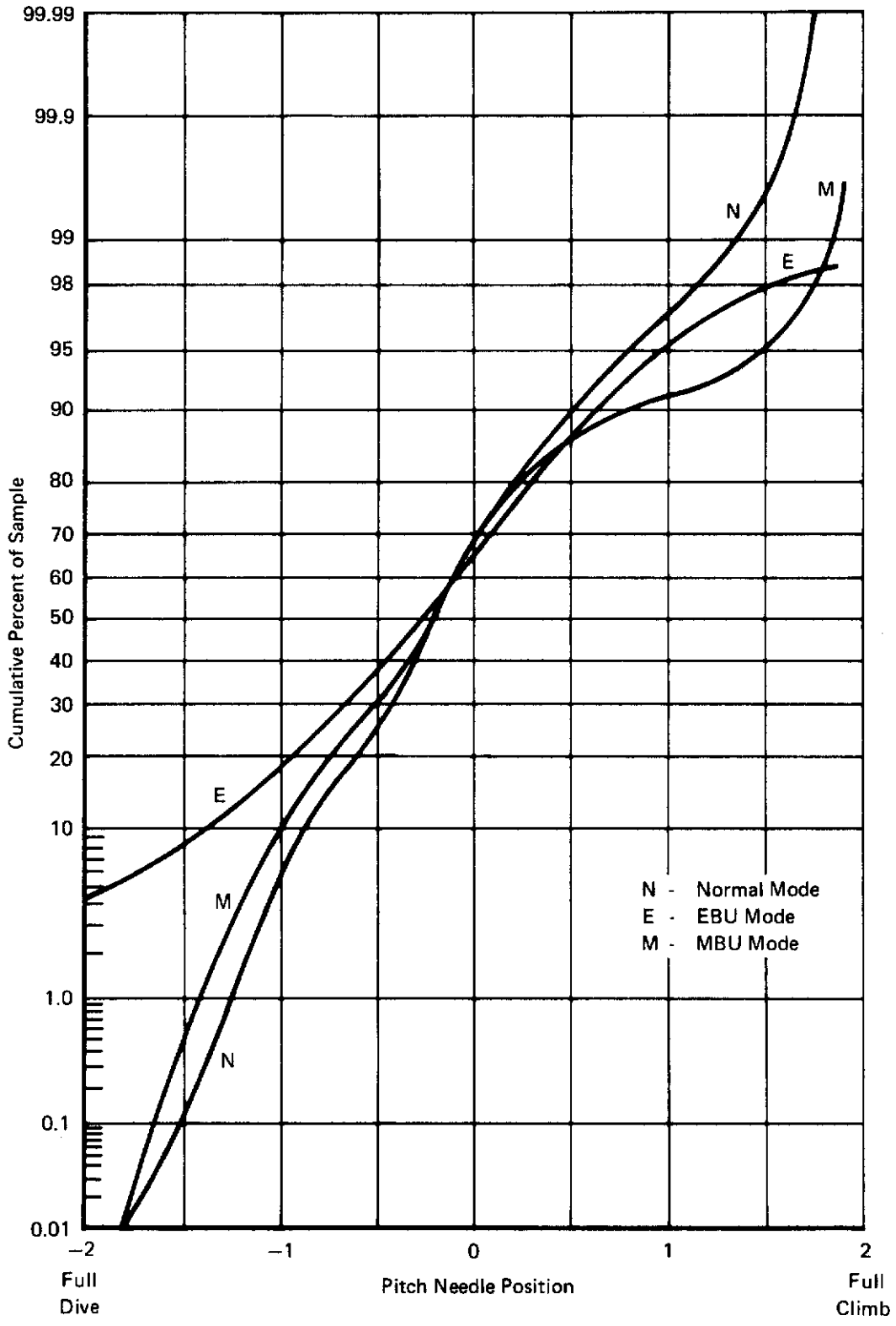

FIGURE 85
CUMULATIVE DISTRIBUTION FOR SFCS TERRAIN FOLLOWING

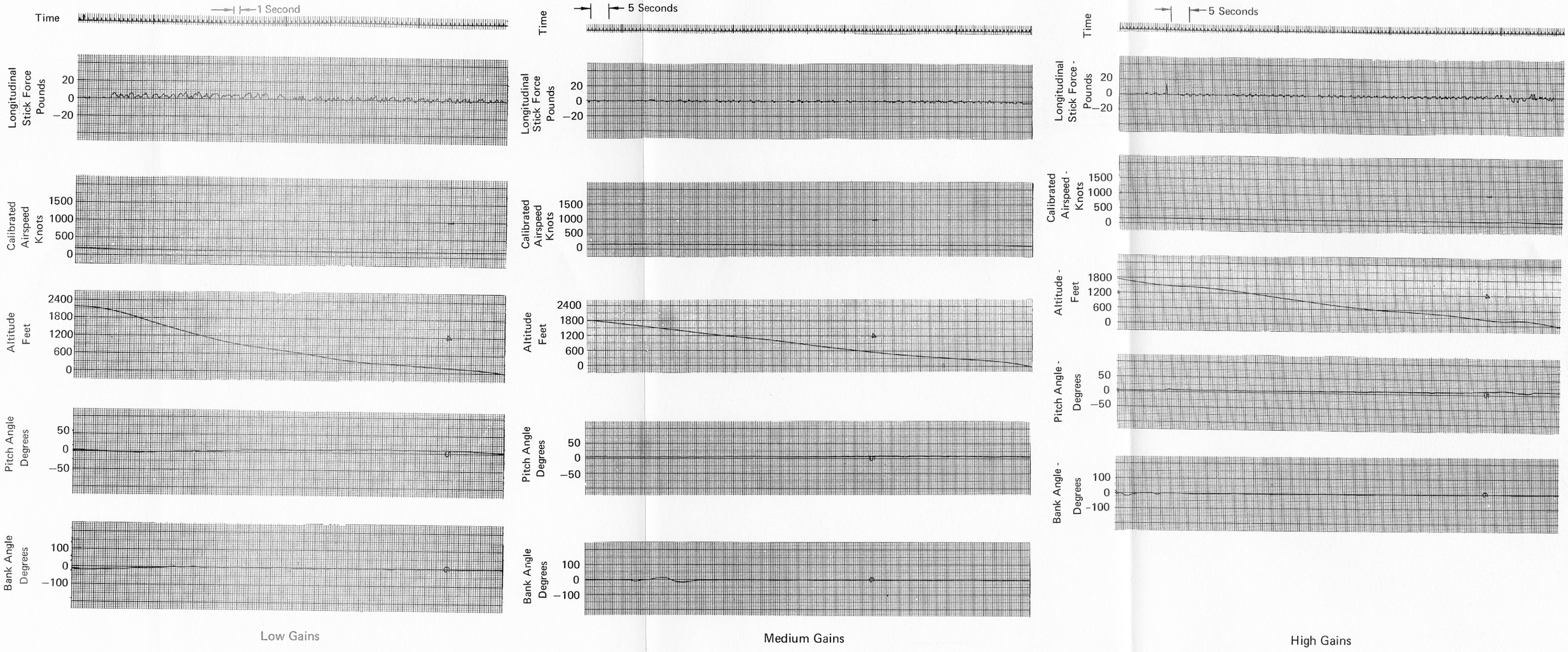

FIGURE 86
LANDING APPROACH IN SFCS NORMAL MODE

Mode transitions were performed during final approach to landing. The results of these runs led to modifications in the trim networks and actuator control loops. A large negative pitch rate developed during transitions from Normal to EBU mode as a result of automatic synchronization to the takeoff trim (TOT) position. This control problem was corrected by disabling the circuit in the secondary actuator feedback loop which returns the integrator to the TOT position on engagement of the EBU mode when the landing gear are extended.

f. Stall Entry and Post Stall Recovery

Results of the stall evaluation showed the aircraft was recoverable in all SFCS modes. The pilots found recovery easiest and stall entry most difficult in the Normal mode. The action of the stall warning network, to increase the stick force gradient as high angles of attack were reached, received favorable comments from the pilots. The SFCS stall warning did not warn the pilot of an imminent one g stall. The lack of one g stall warning was not considered to be a problem by the evaluation pilots. The audio tone generator will provide adequate warning for the one g stall. The aircraft was allowed to enter a fully developed spin during the stall evaluation. Even under the worse case conditions the pilots had no problem recovering the aircraft in the Normal mode. Figure 87 presents time history traces of aircraft parameters recorded during a stall entry and post stall recovery with the EBU and the Normal modes selected.

g. Side Stick Evaluation

A mockup of the LSI side stick controller was evaluated during the subject simulation. It was used to perform the various tasks and found to be an acceptable flight controller. The pilots felt the breakout forces of $\pm$2.5 pounds were too high. A reduction to $\pm$1.75 pounds was found more desirable. More time for familiarization with the actual side stick hardware during flight tests will be required before valid comparisons between the controllers can be made. A time history of a landing approach using the side stick controller in the Normal mode is presented in Figure 88. Cumulative distribution plots indicating a slight variation in performance with the center and side stick controllers are presented in Figure 89. This plot shows that the side stick is an effective flight controller for landing approach. The pilots used the side stick for the other tasks and found it useable in all cases. Only during the rapid attitude changes required during the air-to-air tracking did the pilots tend to over control with the side stick.

7. SFCS MODIFICATIONS

Eight modifications to the SFCS resulted from the subject simulation. These modifications reduced pilot workload, improved SFCS effectiveness, and reduced the possibility of catastrophic transients caused by inadvertant pilot action. The required modifications were as follows:

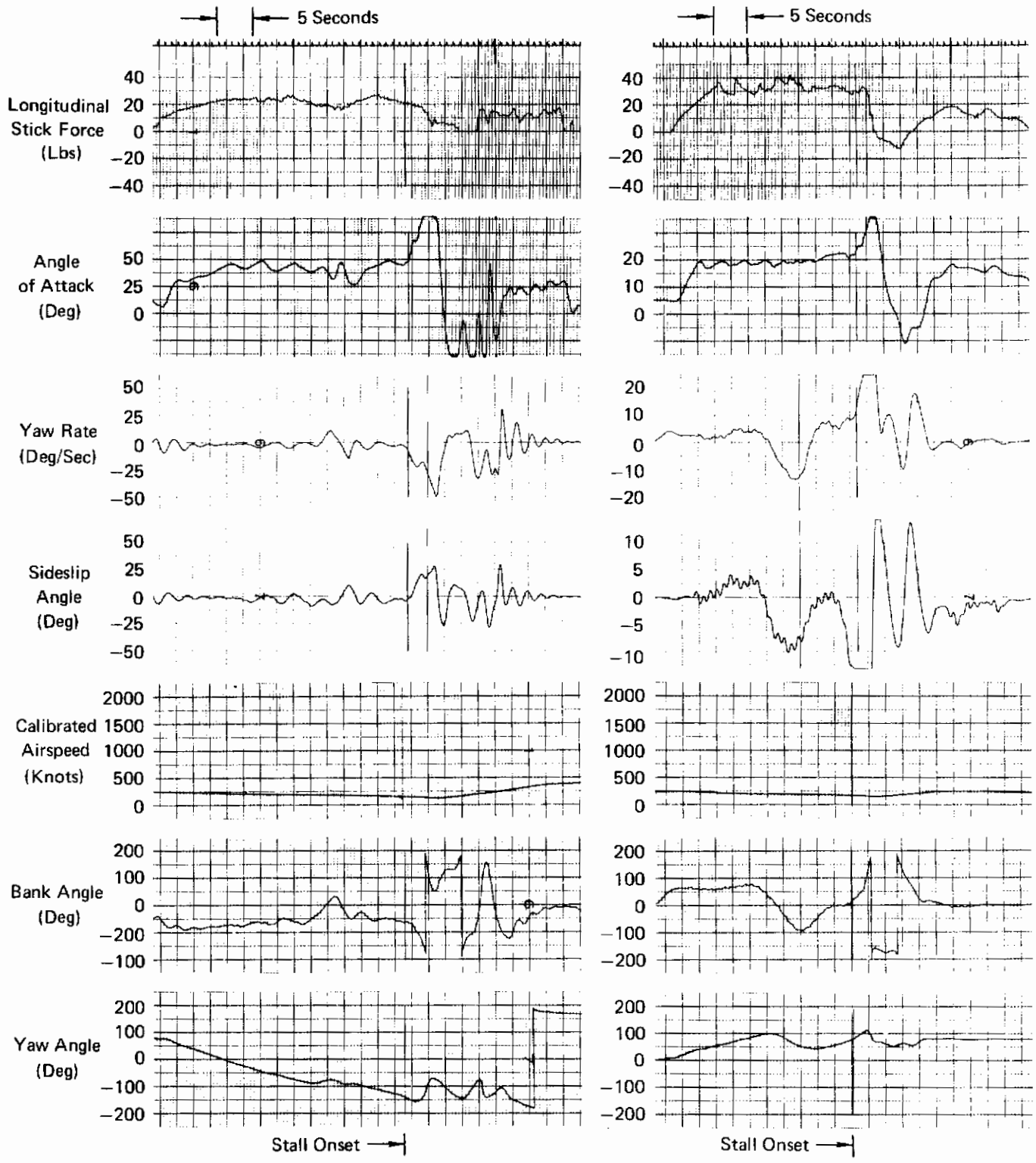

FIGURE 87
STALL ENTRY AND RECOVERY

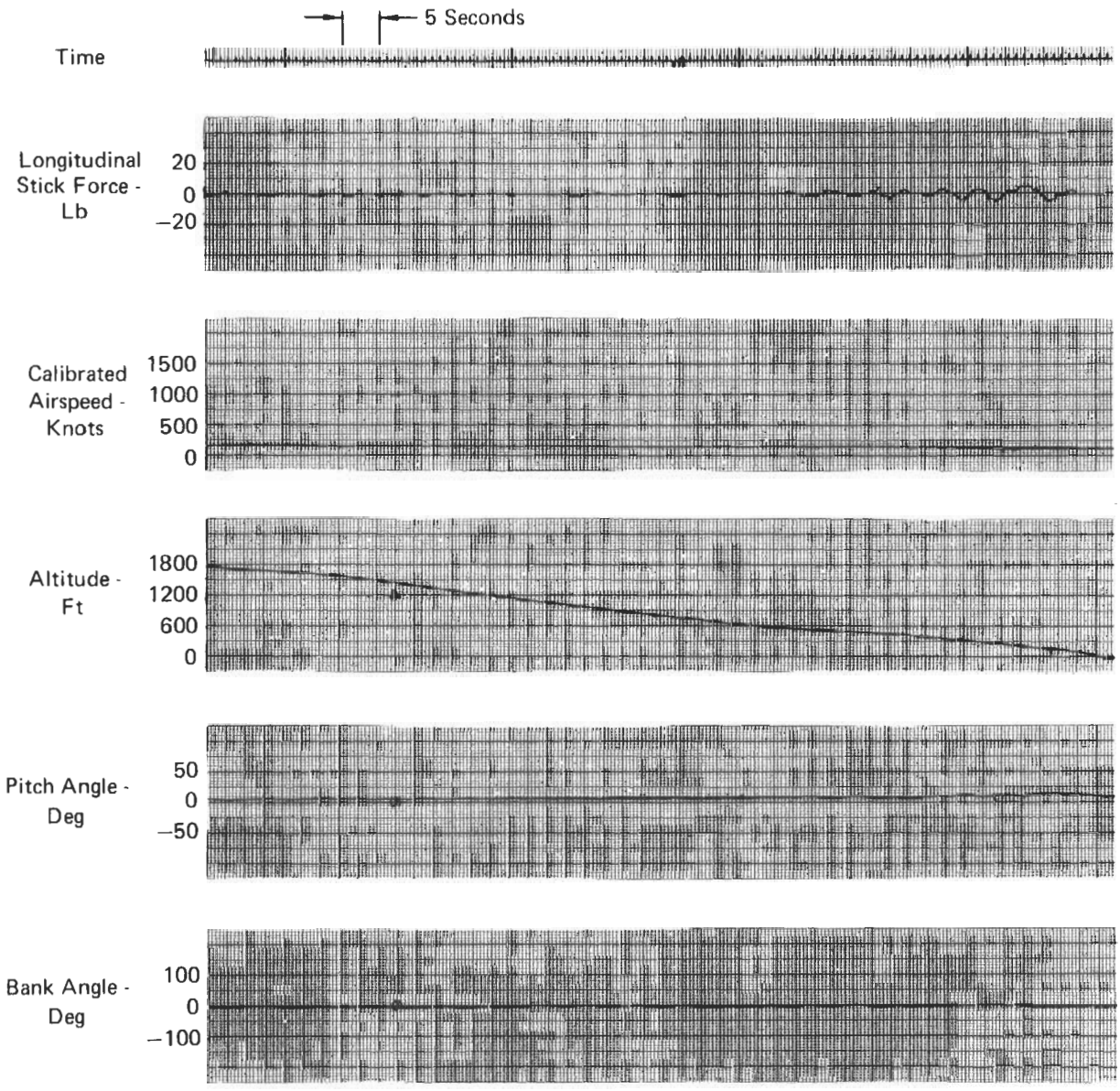

FIGURE 88
LANDING APPROACH USING SIDE STICK CONTROLLER

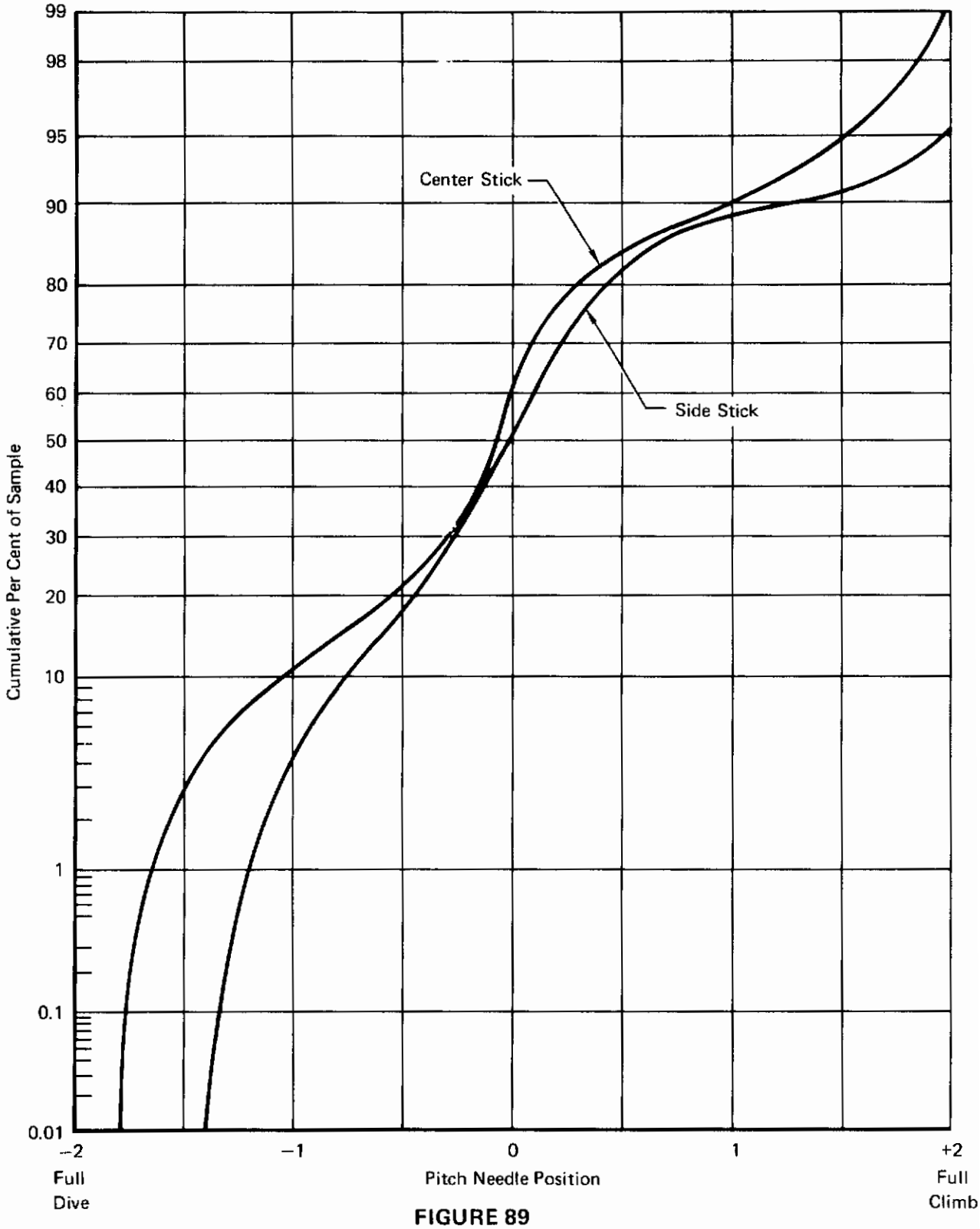

FIGURE 89
TERRAIN FOLLOWING TASK
CUMULATIVE DISTRIBUTION FOR SFCS
USING CENTER STICK vs SIDE STICK CONTROLLER

- Disable mechanical trim switch on the center stick grip when the fly-by-wire modes are engaged.

- Reduce the maximum lateral roll force from ± 20 pounds to ± 12 pounds.

- Eliminate the high passed stabilator position feedback for the EBU mode.

- Disable the circuit in the secondary actuator feedback loop which returns the integrator to the take-off trim position on the engagement of electrical back-up mode when the landing gear are extended.

- Reduce the roll electrical trim authority from ±33 1/3% of full lateral surface to ±16 2/3% of full authority.

- Reduce the pitch electrical trim authority in the EBU mode to ±1° δ_s with an additional ±4° of stabilator with gear down. The ±1° portion is also used as the fly-by-wire trim authority and allows trimming into a 45° banked level turn at 360 Knots-sea level.

- Reduce the side stick breakout forces from ±2.5 pounds to ±1.75 pounds.

- Increase the easy-on easy-off switching time in the pitch axis from 2.5 seconds to 5.0 seconds.

All the modifications listed above have been incorporated in the SFCS design.

SECTION VI

CONCLUSIONS

As a result of the studies and simulation reported herein, the following conclusions can be drawn:

- The SFCS will provide adequate stability and good performance characteristics in the Normal mode.
- The electrical back-up mode will provide for safe return and landing in the event of inaccessibility of the Normal mode.
- The longitudinal SFCS, operating in the Normal mode throughout the F-4E flight envelope, provides airframe responses which compare favorably with the C* and $\dot{C}$* criteria.
- The phugoid mode, although not convergent at all flight conditions, does not present control problems with the Normal mode selected since the time to double amplitude is large.
- The side stick is an effective controller for the tasks performed. However, additional flight test evaluation of the hardware SSC is required before valid comparisons between the controllers can be made.
- The longitudinal stick force per g provides improved handling qualities and meets the applicable criteria.
- The lateral SFCS, while operating in the Normal mode throughout the F-4E flight envelope, provides improved airframe roll response which meets applicable requirements at most flight conditions.
- The directional SFCS, while operating in the Normal mode throughout the F-4E flight envelope, provides Dutch Roll damping which meets the applicable requirements at most flight conditions.
- The spiral mode, although not convergent at all flight conditions, does not present control problems with the Normal mode selected, since the time to double amplitude is large.
- The Roll to Yaw Crossfeed provides improved turn coordination which meets the applicable requirements except for some very low $\bar{q}$ and very high Mach number flight conditions.
- An adaptive gain changer function is provided for the SFCS which allows automatic in-flight gain variations based upon the proper identification of the stabilator effectiveness, M_δ.
- The pitch axis control law provides a selectable neutral speed stability function which allows the pilot to change flight condition without having to apply trim commands. This characteristic could prove helpful in reducing pilot workload during in-flight refueling by automatically compensating for the substantial trim stabilator

change which accompanies the weight increase and cg shift during in-flight refueling. The inherent lack of stick force cues during airspeed changes was not objectionable to any of the pilots for the missions evaluated in the man-in-the-loop simulation program. Judgment as to the total acceptibility of neutral speed stability for all missions and flight modes must ultimately be based upon flight experience.

- No deterioration in SFCS performance is caused by gear reaction while landing with the Normal mode selected.

- The stall warning mechanization provides good indication of the approach to stall. The aircraft is recoverable using the SFCS following stall, even in the event of a fully developed spin.

- Adequate structural mode stability margins for stable operation are provided by the three axis SFCS through the correct placement of feedback sensors and utilization of structural filters.

The results of the studies and simulations indicate that the SFCS will provide improvement over the production F-4E when both are evaluated relative to the following criteria:

- C* and $\dot{C}$* criteria

- D* and $\dot{D}$* criteria

- MIL-F-8785B (ASG) level 1 requirement for longitudinal short period damping ratio

- MIL-F-8785B (ASG) level 1 requirement for phugoid mode stability

- MIL-F-8785B (ASG) level 1 requirement for maneuvering force gradient

- MIL-F-8785B (ASG) level 1 requirement for roll response time constant

- MIL-F-8785B (ASG) level 1 requirement for Dutch Roll damping ratio

- MIL-F-8785B (ASG) level 1 requirement for turn coordination

APPENDIX I

PHYSICAL PARAMETERS AND AERODYNAMIC CHARACTERISTICS

The physical and aerodynamic characteristics describing the F-4E airplane are contained in the following paragraphs. These data were used during the control law development studies. The linearized (small perturbation) three-degree-of-freedom longitudinal and lateral-directional equations appear in Figure 90. The axis system shown in Figure 91 describes the coordinates applicable to these equations and the aerodynamic coefficients.

The flight conditions chosen for analyses are shown superimposed on the F-4E flight envelope in Figure 92. Aircraft weights corresponding to a maximum internal fuel load configuration and a combat configuration are also shown in Figure 92. Aircraft weight and inertia data and motion sensor locations are presented in Figure 93.

The longitudinal and lateral-directional coefficients of the equations of motion for selected flight conditions measured about the stability axis are presented in Tables VII and VIII respectively. These coefficients apply to the small perturbation equations and were dimensionalized using the physical data of the F-4E shown in Figure 93. Due to the hinge moment limits imposed on the lateral and directional control surfaces and the rudder flexure characteristics, the data shown in Tables IX and X were needed along with the aerodynamic coefficients to analyze the small perturbation lateral-directional aircraft response.

Three-Degrees-of-Freedom Longitudinal Equations

$$\ddot{\theta} = M_q \dot{\theta} + M_u \left(\frac{\Delta u}{v}\right) + M_{\dot{\alpha}} \dot{\alpha} + M_\alpha \Delta\alpha + M_h \left(\frac{\Delta h}{v}\right) + M\delta \, \Delta\delta$$

$$\frac{\dot{u}}{v} = (g/v) \, \Delta\theta + x_u \left(\frac{\Delta u}{v}\right) + X_\alpha \Delta\alpha + X_h \left(\frac{\Delta h}{v}\right)$$

$$\dot{\alpha} = (1 + Zq) \, \dot{\theta} + Z_u \left(\frac{\Delta u}{v}\right) + Z_\alpha \Delta\alpha + Z_h \left(\frac{\Delta h}{v}\right) + Z_\delta \Delta\delta$$

$$\frac{\dot{h}}{v} = \Delta\theta - \Delta\alpha \qquad N_{Z_{cg}} = \frac{v}{g} \ddot{h} \qquad N_{Z_A} = N_{Z_{cg}} + \frac{\ell_A}{32.2} \ddot{\theta}$$

$\dot{\theta} = q \cos\phi - r \sin\phi$, since $\phi = o$ for this representation, $\dot{\theta} = q$

Two-Degrees-of-Freedom Longitudinal Equations

The three-degree-of-freedom equations given above can be modified to provide two-degree-of-freedom representation by equating to zero the terms M_u, M_h, Z_u, and Z_h and deleting the $\dot{u}/v$ equation.

Three-Degrees-of-Freedom Lateral-Directional Equations

$$\dot{p} = L_p p + L_r r + L_\beta \beta + L_{\delta_A} \delta_A + L_{\delta_R} \delta_R$$

$$\dot{r} = N_p p + N_r r + N_\beta \beta + N_{\delta_A} \delta_A + N_{\delta_R} \delta_R$$

$$\dot{\beta} = Y_p p + Y_r r + Y_\beta \beta + Y_\delta \delta + Y_{\delta_R} \delta_R + Y_\phi \phi$$

FIGURE 90
SMALL PERTURBATION EQUATIONS OF MOTION

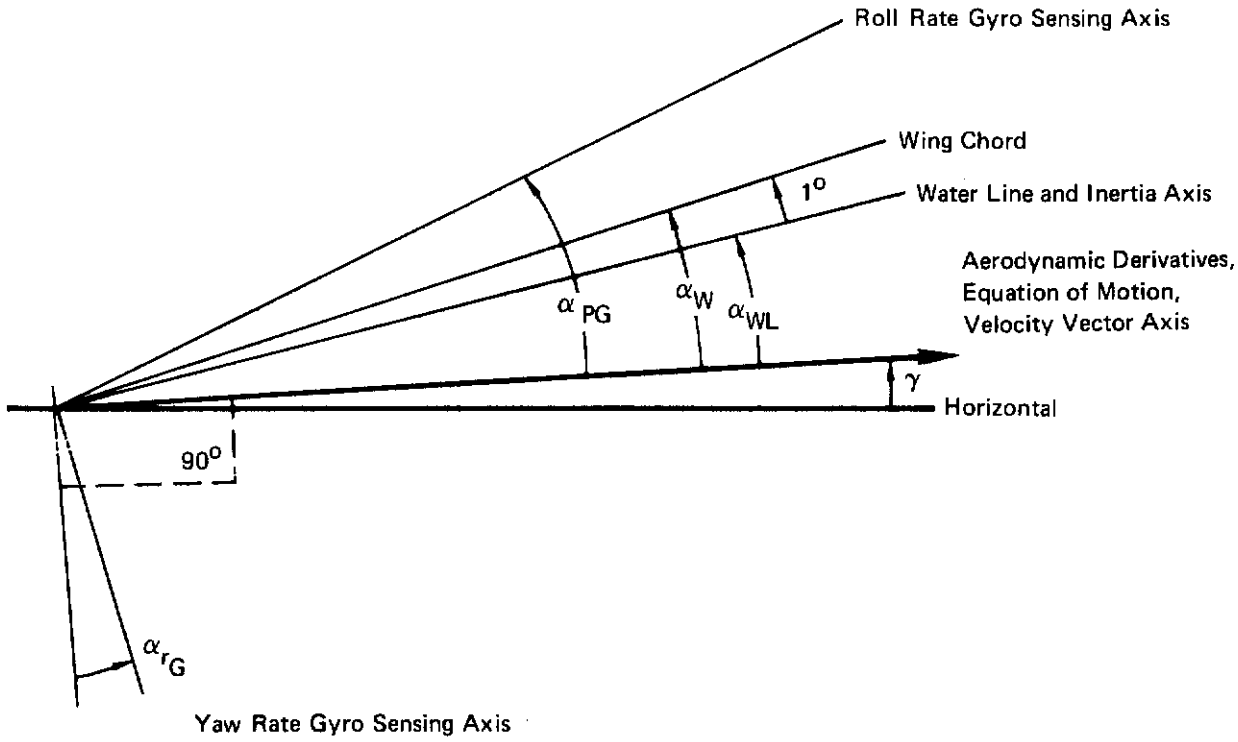

All angles are shown in the positive sense.

FIGURE 91
DEFINITION OF AXIS SYSTEMS FOR SMALL PERTURBATION EQUATIONS

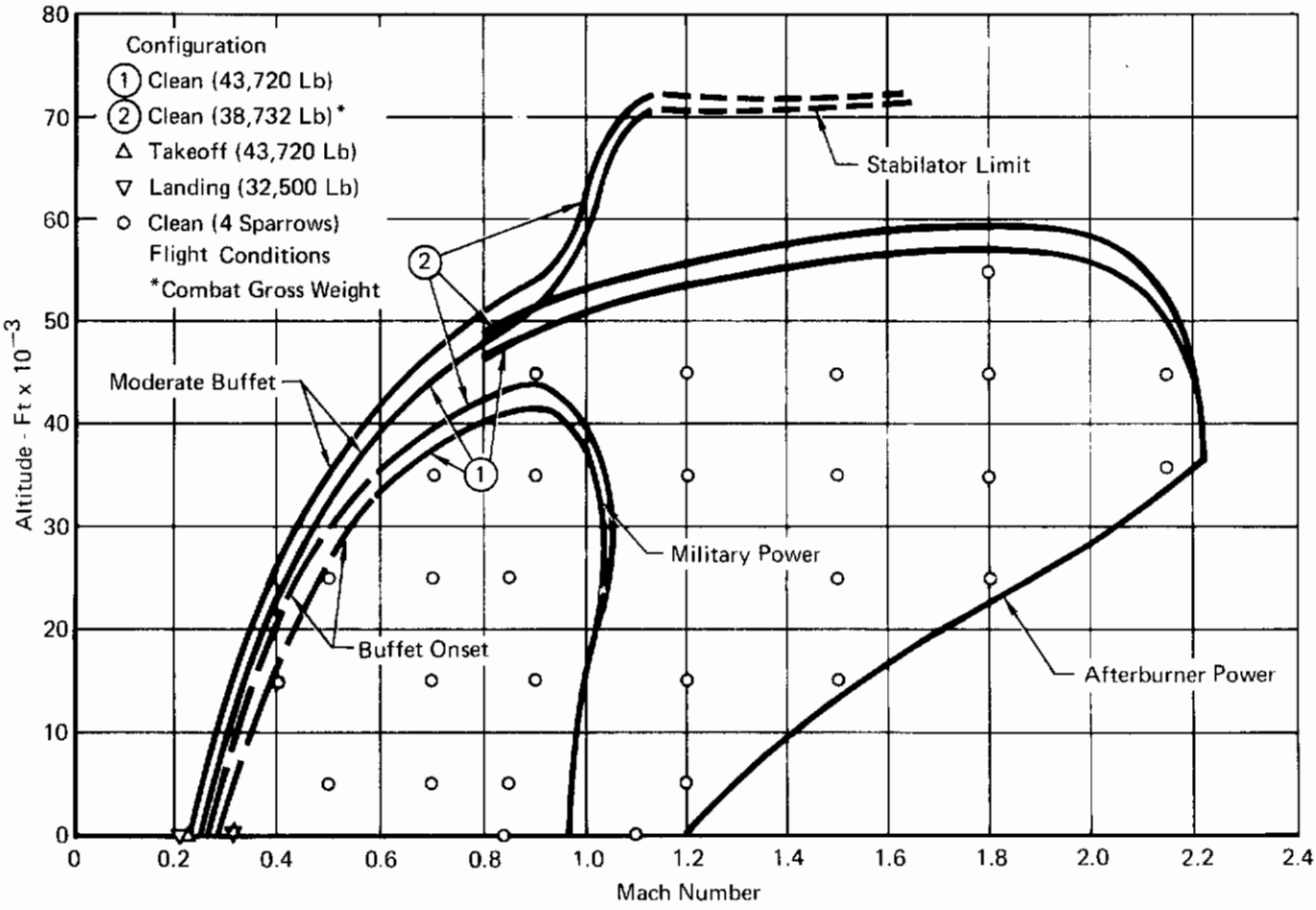

FIGURE 92
YF-4E (A.F. SN 62-12200) OPERATIONAL FLIGHT ENVELOPE

WEIGHT, INERTIA AND CENTER OF GRAVITY LOCATION

Takeoff Configuration - Gear Down

Weight = 43,720 Lb

CG = 34%$\bar{c}$
CG (FS) = 326.55 In.
CG (WL) = 27.6 In.

I_x = 31,002 Slug-Ft^2
I_y = 166,651 Slug-Ft^2
I_z = 186,801 Slug-Ft^2
I_{xz} = 7,043 Slug-Ft^2

Landing Configuration - Gear Down

Weight = 32,500 Lb

CG = 30.4%$\bar{c}$
CG (FS) = 319.62 In.
CG(WL) = 25.2 In.

I_x = 23,756 Slug-Ft^2
I_y = 135,859 Slug-Ft^2
I_z = 152,735 Slug-Ft^2
I_{xz} = 3,532 Slug-Ft^2

Clean Configuration

100% Internal Fuel

Weight = 43,720 Lb

CG = 34%$\bar{c}$
CG(FS) = 326.55 In.
CG(WL) = 29.0 In.

I_x = 28,478 Slug-Ft^2
I_y = 164,258 Slug-Ft^2
I_z = 184,136 Slug-Ft^2
I_{xz} = 6,899 Slug-Ft^2

60% Internal Fuel

Weight = 38,732 Lb*

CG = 30.6%$\bar{c}$
CG(FS) = 320.00 In.
CG(WL) = 27.65 In.

I_x = 24,873 Slug-Ft^2
I_y = 152,495 Slug-Ft^2
I_z = 169,824 Slug-Ft^2
I_{xz} = 4,820 Slug-Ft^2

*Combat gross weight

SFCS Sensor Locations

Sensor	Fuselage Station	Water Line	Butt Line	Direction of Sensing Axis
Pitch Rate Gyro	383	6	47.5L	Parallel to the y-axis, positive aircraft nose up
Roll Rate Gyro	77	11.5	00	Forward in the X-Z plane and 1.5 degrees below water line
Yaw Rate Gyro	383	6	47.5R	Down, parallel to X-Z plane and perpendicular to the roll rate gyro sensing axis
Lateral Accelerometer	186.3	19.8	00	Perpendicular to X-Z plane, positive to pilot's right
Normal Accelerometer	77	22.5	00	Perpendicular to the water line, positive up

FIGURE 93
F-4E PHYSICAL DATA

TABLE VII
COEFFICIENTS FOR LONGITUDINAL SMALL PERTURBATION EQUATIONS OF MOTION

Wt. (lb)	43720	43720	43720	43720	43720	43720	43720	43720	43720	43720
Mach	0.214	0.318	0.4	0.5	0.5	0.7	0.7	0.7	0.7	0.84
Alt. (ft)	0	0	15000	5000	25000	5000	15000	25000	35000	0
$\bar{q}$ (lb/ft^2)	67.7	150.0	133.1	308.4	137.4	603.9	409.6	269.4	170.8	1045.1
V (ft/sec)	238.8	354.9	423.1	548.8	508.2	768.3	740.5	711.5	681.3	937.8
X_h (sec^{-2})	−0.0000464	−0.0000659	−0.0000301	−0.0000438	−0.0000285	−0.0000447	−0.0000343	−0.0000281	−0.0000241	−0.0000652
X_u (sec^{-1})	−0.0548	−0.0518	−0.01240	−0.01753	−0.0114	−0.0167	−0.01189	−0.00977	−0.00844	−0.01956
X_α (sec^{-1})	0.01669	0.0254	−0.07873	−0.00329	−0.0570	−0.000699	−0.00192	−0.00689	−0.02261	−0.003043
Z_h (sec^{-2})	0.000765	0.000824	0.00102	−0.000767	0.00100	0.000976	0.001076	0.00113	0.001149	0.000739
Z_u (sec^{-1})	−0.2046	−0.5549	−0.1389	−0.10082	−0.11181	−0.09915	−0.10306	−0.10172	−0.0960	−0.09128
Z_α (sec^{-1})	−0.3483	−0.5193	−0.4215	−0.7276	−0.3628	−1.00	−0.7337	−0.51614	−0.3479	−1.4475
Z_q (non dim)	−0.00847	−0.00953	−0.00589	−0.00761	−0.00421	−0.00749	−0.00547	−0.00403	−0.002878	−0.007993
Z_δ (sec^{-1})	−0.04755	−0.0650	−0.0481	−0.0842	−0.04082	−0.1102	−0.0804	−0.0560	−0.0374	−0.14562
M_h (sec^{-3})	0.000076	0.000122	−0.00122	0.0	0.0	−0.00382	−0.00399	−0.003904	−0.00376	−0.00757
M_u (sec^{-2})	0.09048	0.09718	0.1839	−0.1596	−0.1280	−0.17164	−0.08228	−0.00661	0.0306	−2.2718
M_α (sec^{-2})	0.00345	0.0	−0.4605	−2.3747	−0.44027	−3.266	−2.2828	−2.0668	−0.9102	−8.0160
$M_{\dot{\alpha}}$ (sec^{-1})	−0.1131	−0.1658	−0.14267	−0.2442	−0.13504	−0.3266	−0.22985	−0.16591	−0.1154	−0.3932
M_q (sec^{-1})	−0.2386	−0.3649	−0.31714	−0.5511	−0.2877	−0.7621	−0.5357	−0.37591	−0.2552	−1.0200
M_δ (sec^{-2})	−1.830	−3.834	−3.8491	−9.1127	−4.090	−16.005	−11.245	−7.5813	−4.875	−26.936

Wt. (lb)	32500	32500	38732	38732	38732	38732	38732	38732	38732	38732
Mach	0.206	0.318	0.4	0.5	0.5	0.7	0.7	0.7	0.7	0.84
Alt. (ft)	0	0	15000	5000	25000	5000	15000	25000	35000	0
$\bar{q}$ (lb/ft^2)	63.0	150	133.1	308.4	137.4	603.9	409.6	269.4	170.8	1045.1
V (ft/sec)	229.9	354.9	423.1	548.8	508.2	768.3	740.5	711.5	681.3	937.75
X_h (sec^{-2})	−0.0000589	−0.0000865	−0.0000339	−0.0000495	−0.0000321	−0.0000505	−0.0000388	−0.0000317	−0.0000272	−0.0000736
X_u (sec^{-1})	−0.0725	−0.0679	−0.013993	−0.019791	−0.01286	−0.01746	−0.01343	−0.01103	−0.00953	−0.02208
X_α (sec^{-1})	0.0210	0.02572	−0.071603	−0.003711	−0.06429	−0.000518	−0.001306	−0.005725	−0.01596	−0.00343
Z_h (sec^{-2})	0.000962	0.00102	0.001058	0.000866	0.00113	0.000998	0.00111	0.00117	0.001199	0.000834
Z_u (sec^{-1})	−0.2645	−0.1783	−0.14254	−0.11380	−0.12620	−0.10183	−0.1066	−0.105697	−0.1007	−0.10303
Z_α (sec^{-1})	−0.4026	−0.6830	−0.47510	−0.82134	−0.40957	−1.1290	−0.8278	−0.5822	−0.3924	−1.6339
Z_q (non dim)	−0.0114	−0.00128	−0.006654	−0.008587	−0.00475	−0.00846	−0.00617	−0.00455	−0.00325	−0.00902
Z_δ (sec^{-1})	−0.0566	−0.0794	−0.05447	−0.094998	−0.04608	−0.1245	−0.09082	−0.06338	−0.04240	−0.16437
M_h (sec^{-3})	0.0000828	0.00015	0.000732	0.0	0.0	−0.000434	−0.000405	−0.000291	−0.000238	−0.008156
M_u (sec^{-2})	0.1049	0.1164	−0.07704	−0.17190	−0.13790	−0.53123	−0.43994	−0.3442	−0.27145	−2.4470
M_α (sec^{-2})	−0.0339	−0.7509	−1.4207	−4.497	−1.3706	−7.3535	−5.1626	−3.834	−2.0083	−15.230
$M_{\dot{\alpha}}$ (sec^{-1})	−0.1350	−0.2057	−0.16119	−0.26304	−0.1454	−0.36903	−0.25969	−0.18744	−0.13038	−0.42353
M_q (sec^{-1})	−0.2848	−0.4458	−0.35284	−0.59366	−0.30989	−0.84663	−0.59588	−0.41801	−0.28361	−1.09869
M_δ (sec^{-2})	−2.1484	−4.975	−4.2569	−9.8156	−4.4053	−17.667	−12.4148	−8.3742	−5.38666	−29.0143

Wt. (lb)	43720	43720	43720	43720	43720	43720	43720	43720	43720	43720
Mach	0.85	0.85	0.9	0.9	0.9	1.1	1.2	1.2	1.2	1.2
Alt. (ft)	5000	25000	15000	35000	45000	0	5000	15000	35000	45000
$\bar{q}$ (lb/ft^2)	890.5	397.2	677.1	282.33	174.6	1793.8	1774.8	1203.7	501.9	310.4
V (ft/sec)	932.5	863.6	952.0	876.0	871.6	1228.6	1317.	1269.3	1167.9	1162.2
X_h (sec^{-2})	−0.0000596	−0.0000359	−0.0000805	−0.0000490	0.0	−0.000316	−0.000210	−0.0000684	−0.0000277	0.0
X_u (sec^{-1})	−0.0177	−0.01031	−0.021084	−0.01383	−0.009765	−0.069485	−0.04205	−0.01406	−0.00545	−0.00323
X_α (sec^{-1})	−0.00372	−0.00448	−0.00472	−0.01195	−0.02969	−0.05695	−0.02628	−0.02404	−0.02766	−0.02969
Z_h (sec^{-2})	0.000745	0.000897	0.000832	0.001069	0.001484	0.00131	0.00142	0.001295	0.00154	0.001614
Z_u (sec^{-1})	−0.08939	−0.0933	−0.08877	−0.0943	−0.09453	−0.00790	0.0	−0.00740	−0.021791	−0.02396
Z_α (sec^{-1})	−1.2961	−0.67629	−1.0803	−0.5280	−0.33045	−1.9533	−1.6977	−1.313	−0.6789	−0.4406
Z_q (non dim)	−0.00711	−0.00406	−0.00559	−0.00294	−0.00189	−0.907993	−0.00551	−0.004487	−0.003085	−0.002106
Z_δ (sec^{-1})	−0.12812	−0.0682	−0.10043	−0.04966	−0.03148	−0.18503	−0.16767	−0.12946	−0.06856	−0.04448
M_h (sec^{-3})	−0.00783	−0.00452	−0.008410	−0.00672	0.0	0.012998	0.03399	0.02305	0.00883	0.0
M_u (sec^{-2})	−2.350	−1.2745	−3.2590	−1.8557	−1.5180	2.5995	6.9167	4.5976	1.6885	0.9638
M_α (sec^{-2})	−8.001	−3.8255	−7.3942	−2.712	−1.7068	−28.604	−34.161	−28.8251	−16.033	−10.1664
$M_{\dot{\alpha}}$ (sec^{-1})	−0.3948	−0.2257	−0.3614	−0.17900	−0.11980	−0.72909	−0.5801	−0.46920	−0.22191	−0.13446
M_q (sec^{-1})	−0.91401	−0.49864	−76.1601	−0.3698	−0.23162	−1.6012	−1.5394	−1.16394	−0.5614	−0.35360
M_δ (sec^{-2})	−23.596	−11.614	−18.8534	−8.577	−5.4122	−44.0897	−43.539	−32.395	−15.794	−10.2002

TABLE VII (CONTINUED)

COEFFICIENTS FOR LONGITUDINAL SMALL PERTURBATION EQUATIONS OF MOTION (CONTINUED)

Wt (lb)	38732	38732	38732	38732	38732	38732	38732	38732	38732	38732
Mach	0.85	0.85	0.9	0.9	0.9	1.1	1.2	1.2	1.2	1.2
Alt. (ft)	5000	25000	15000	35000	45000	0.0	5000	15000	35000	45000
$\bar{q}$ (lb/ft^2)	890.5	397.2	677.1	282.3	174.6	1793.8	1774.8	1203.7	501.9	310.4
V (ft/sec)	932.5	863.6	952.0	876.0	871.6	1228.6	1317.0	1269.3	1167.9	1162.2
X_h (sec^{-2})	−0.0000672	−0.0000405	−0.0000908	−0.0000553	0.0	−0.000357	−0.000237	−0.0000772	−0.0000312	0.0
X_u (sec^{-1})	−0.01997	−0.01164	−0.0238	−0.01561	−0.01102	−0.07843	−0.0475	−0.01587	−0.00615	−0.00364
X_α (sec^{-1})	−0.00420	−0.00506	−0.00532	−0.013481	−0.03351	−0.06428	−0.02967	−0.02714	−0.03122	−0.03351
Z_h (sec^{-2})	0.000841	0.00101	0.000939	0.00121	0.001675	0.001478	0.00160	0.001461	0.00174	0.00182
Z_u (sec^{-1})	−0.10090	−0.10530	−0.10021	−0.10643	−0.1067	−0.00836	0.0	−0.00835	−0.0246	−0.02704
Z_α (sec^{-1})	−1.4630	−0.7634	−1.23066	−0.59500	−0.37301	−2.2049	−1.9164	−1.4822	−0.76631	−0.49734
Z_q (nom dim)	−0.00803	−0.00459	−0.00631	−0.00331	−0.002134	−0.009022	−0.006214	−0.005065	−0.00348	−0.00238
Z_δ (sec^{-1})	−0.14462	−0.07694	−0.1134	−0.05605	−0.03554	−0.20886	−0.18926	−0.14613	−0.07739	−0.05020
M_h (sec^{-3})	−0.00844	−0.00487	−0.00906	−0.00724	0.0	0.01400	0.03661	0.02483	0.00951	0.0
M_u (sec^{-2})	−2.5317	−1.3728	−3.5104	−1.999	−1.63504	2.800	7.45022	4.9522	1.8188	1.03814
M_α (sec^{-2})	−14.4953	−6.9592	−13.0075	−5.205	−3.238	−42.471	−47.660	−39.148	−21.1231	−13.283
$M_{\dot{\alpha}}$ (sec^{-1})	−0.42523	−0.24306	−0.3892	−0.19281	−0.129041	−0.78533	−0.62480	−0.5054	−0.23903	−0.14483
M_q (sec^{-1})	−0.98452	−0.53711	−0.82013	−0.39830	−0.2495	−1.7247	−1.6581	−1.2537	−0.60469	−0.3809
M_δ (sec^{-2})	−25.4164	−12.5101	−20.3077	−9.2389	−5.8297	−47.491	−46.8978	−39.894	−17.0126	−10.987

Wt. (lb)	43720	43720	43720	43720	43720	43720	43720	43720	43720	43720
Mach	1.5	1.5	1.5	1.5	1.8	1.8	1.8	1.8	2.15	2.15
Alt. (ft)	15000	25000	35000	45000	25000	35000	45000	55000	36000	45000
$\bar{q}$ (lb/ft^2)	1880.0	1236.9	784.3	485.0	1781.1	1129.3	698.3	432.0	1538.4	996.3
V (ft/sec)	1586.6	1524.6	1459.9	1452.7	1829.5	1751.9	1743.9	1743.2	2081.3	2081.3
X_h (sec^{-2})	−0.0001387	−0.0000728	−0.0000335	0.0	−0.000221	−0.0000850	0.0	0.0	0.0	0.0
X_u (sec^{-1})	−0.02150	−0.011392	−0.00545	−0.00325	−0.03024	−0.01154	−0.006725	−0.003866	−0.02335	−0.014377
X_α (sec^{-1})	−0.009247	−0.01424	−0.01781	−0.02083	−0.02453	−0.02343	−0.02525	−0.01450	−0.01153	−0.00934
Z_h (sec^{-2})	0.001387	0.001645	0.001676	0.00165	0.003096	0.00266	0.00265	0.001614	0.00202	0.001624
Z_u (sec^{-1})	0.0374	0.01266	0.00210	−0.00651	−0.04491	−0.03464	−0.02880	−0.01643	−0.04036	−0.03174
Z_α (sec^{-1})	−1.2668	−0.9778	−0.70191	−0.44921	−0.9691	−0.67365	−0.4352	−0.27935	−0.69191	−0.4481
Z_q (non dim)	−0.00269	−0.00236	−0.00196	−0.00137	−0.00136	−0.001125	−0.000829	−0.000587	−0.000689	−0.000540
Z_δ (sec^{-1})	−0.12252	−0.09145	−0.06495	−0.04258	−0.08135	−0.05771	−0.0383	−0.02455	−0.0493	−0.0344
M_h (sec^{-3})	0.03504	0.02753	0.0203	0.0	0.004527	0.002227	0.0	0.0	0.0	0.0
M_u (sec^{-2})	5.5484	4.2891	3.2472	2.50991	4.361	3.1374	2.5847	1.38624	1.1943	1.1344
M_α (sec^{-2})	−36.0941	−30.529	−23.871	−16.0484	−34.922	−27.635	−19.9541	−13.1089	−35.208	−25.741
$M_{\dot{\alpha}}$ (sec^{-1})	−0.39063	−0.25155	−0.15497	−0.09048	−0.08675	−0.05167	−0.03271	−0.02129	0.05093	0.03497
M_q (sec^{-1})	−1.2021	−0.8577	−0.58666	−0.37454	−0.74781	−0.50713	−0.32575	−0.21612	−0.46266	−0.30798
M_δ (sec^{-2})	−38.352	−27.527	−18.712	−12.1932	−28.201	−19.1226	−12.609	−8.4516	−20.223	−14.1287

Wt. (lb)	38732	38732	38732	38732	38732	38732	38732	38732	38732	38732
Mach	1.5	1.5	1.5	1.5	1.8	1.8	1.8	1.8	2.15	2.15
Alt. (ft)	15000	25000	35000	45000	25000	35000	45000	55000	36000	45000
$\bar{q}$ (lb/ft^2)	1880.8	1236.9	784.3	485.0	1781.1	1129.3	698.3	432.0	1538.4	996.3
V (ft/sec)	1586.6	1524.6	1459.9	1452.7	1829.5	1751.9	1743.9	1743.2	2081.3	2081.3
X_h (sec^{-2})	−0.000157	−0.0000822	−0.0000378	0.0	−0.000249	−0.000096	0.0	0.0	0.0	0.0
X_u (sec^{-1})	−0.02427	−0.01286	−0.006149	−0.00367	−0.03413	−0.013022	−0.00759	−0.00436	−0.02636	−0.016228
X_α (sec^{-1})	−0.01044	−0.016073	−0.02010	−0.02352	−0.024531	0.0	−0.04570	−0.01637	−0.01302	−0.01053
Z_h (sec^{-2})	0.00157	0.00186	0.001892	0.001867	0.00328	0.002815	0.001749	0.001822	0.002278	0.001834
Z_u (sec^{-1})	0.03653	0.01429	0.00237	−0.00735	−0.04856	−0.03719	−0.04035	−0.01855	−0.04556	−0.03583
Z_α (sec^{-1})	−1.4300	−1.1037	−0.79231	−0.50706	−1.0935	−0.76008	−0.49260	−0.3153	−0.78101	−0.50581
Z_q (non dim)	−0.003034	−0.002668	−0.002209	−0.00155	−0.001538	−0.00127	−0.000935	−0.000663	−0.000777	−0.000609
Z_δ (sec^{-1})	−0.13830	−0.10323	−0.07332	−0.04806	−0.091227	−0.06515	−0.04327	−0.02771	−0.05565	−0.003878
M_h (sec^{-3})	0.03775	0.02965	0.02186	0.0	0.03064	0.02358	0.0314	0.0	0.0	0.0
M_u (sec^{-2})	5.9764	4.61992	3.4976	2.7035	4.1368	2.9471	3.2953	1.4932	1.2864	1.22193
M_α (sec^{-2})	−48.6503	−40.1243	−30.6918	−20.4576	−49.2839	−36.9291	−25.130	−16.4851	−44.922	−32.259
$M_{\dot{\alpha}}$ (sec^{-1})	−0.42877	−0.270957	−0.166925	−0.09746	−0.098005	−0.05837	−0.03695	−0.02294	0.05486	0.03767
M_q (sec^{-1})	−1.29478	−0.92386	−0.63191	−0.40343	−0.82452	−0.55974	−0.35984	−0.23279	−0.49835	−0.33174
M_δ (sec^{-2})	−41.3108	−29.6502	−20.1551	−13.1391	−31.1002	−21.0892	−13.9095	−9.10353	−21.7835	−15.2186

TABLE VIII

LATERAL-DIRECTIONAL RIGID EQUATIONS OF MOTION COEFFICIENTS

		Takeoff Configuration CG = 34% $\bar{c}$ CG (FS) = 326.55 In. CG (WL) = 27.6 In. W = 43,720 Lb I_x = 31,002 (Slug - Ft^2) I_z = 186,801 (Slug - Ft^2) I_{xz} = 7,043 (Slug - Ft^2)		Landing Configuration CG = 30.4% $\bar{c}$ CG (FS) = 319.62 In. CG (WL) = 25.2 In. W = 32,500 Lb I_x = 23,756 (Slug - Ft^2) I_z = 152,735 (Slug - Ft^2) I_{xz} = 3,532 (Slug - Ft^2)	
Mach Number		0.214	0.318	0.206	0.318
Altitude (Ft)		0.0	0.0	0.0	0.0
Velocity (Ft/Sec)		238.8	354.90	229.00	354.5
Dynamic Pressure (Lb/Ft^2)		67.70	156.59	62.326	156.59
α_{wL} (Deg)		18.0	7.000	12.90	0.9800
L_p	$\times 10^1$	−0.9773	−1.350	−1.177	−1.888
L_r	$\times 10^1$	9.884	6.795	11.29	13.10
L_β	$\times 10^{-1}$	−1.190	−1.163	−0.9863	−0.8307
L_δ	$\times 10^{-1}$	1.600	4.740	2.969	7.027
L_{δ_R}	$\times 10^{-1}$	−0.4013	1.783	0.3184	1.945
N_p	$\times 10^2$	23.80	10.75	17.95	1.333
N_r	$\times 10^1$	−4.347	−3.523	−4.184	−3.079
N_β	$\times 10^1$	4.102	3.267	3.410	3.138
N_δ	$\times 10^1$	−4.458	−3.205	−5.321	1.203
N_{δ_R}	$\times 10^1$	−0.4691	−1.348	−0.6790	−1.503
Y_p	$\times 10^3$	10.40	6.891	14.91	6.905
Y_r	$\times 10^1$	−9.935	−9.949	−9.915	−9.946
Y_β	$\times 10^1$	−0.7729	−1.282	−0.9296	−1.583
Y_δ	$\times 10^3$	−3.538	−6.023	−5.062	−7.250
Y_{δ_R}	$\times 10^2$	1.371	2.134	1.775	2.860
Y_ϕ	$\times 10^2$	13.47	9.066	14.05	9.076

TABLE VIII (CONTINUED)

LATERAL-DIRECTIONAL RIGID EQUATIONS OF MOTION COEFFICIENTS

Clean Configuration

100% Internal Fuel
CG = 34% c
CG (FS) = 326.55 In.
CG (WL) = 29.0 In.

W = 43,720 Lb
I_x = 28,478 Slug Ft^2
I_z = 184,136 Slug Ft^2
I_{xz} = 6899 Slug Ft^2

Mach Number	0.4	0.5	0.5	0.7	0.7	0.7	0.7	0.84	0.85	0.85	0.9	0.9	0.9	1.1
Altitude (Ft)	15,000	5000	25,000	5000	15,000	25,000	35,000	0	5000	25,000	15,000	35,000	45,000	0
Velocity (Ft/Sec)	423.09	548.76	508.19	768.27	740.41	711.47	681.29	937.75	932.51	863.57	951.96	875.95	871.62	1228.6
Dynamic Pressure (Lb/Ft^2)	133.75	308.36	137.43	603.92	409.60	269.37	170.80	104.51	890.47	397.18	677.10	282.33	174.58	1792.4
α_{W_L} (Deg)	9.369	3.660	9.240	1.456	2.611	4.540	7.574	0.3300	1.410	2.090	0.7500	3.190	6.110	−0.2807
L_P	−0.9928	−1.668	−0.8416	−2.132	−1.626	−1.180	−0.8021	−2.658	−2.391	−1.374	−1.920	−0.9949	−0.5909	−2.770
$L_r \times 10^1$	2.077	3.506	2.868	5.561	5.333	4.839	4.162	6.294	6.147	4.391	5.023	4.065	3.562	6.207
$L_\beta \times 10^{-1}$	−0.7998	−1.331	−0.8637	−1.878	−1.598	−1.396	−1.171	−2.668	−2.477	−1.534	−2.029	−1.354	−1.206	−4.237
L_δ	3.706	9.167	3.702	14.31	11.06	7.744	4.778	16.91	15.95	10.31	13.38	7.976	4.725	8.933
L_{δ_R}	0.4149	1.417	0.4000	3.165	2.095	1.228	0.5235	5.471	5.523	2.123	3.595	1.345	0.5500	6.770
$N_P \times 10^2$	10.16	−0.6472	8.235	−4.606	−2.305	1.144	4.646	−6.538	−2.588	−2.469	−4.798	−1.007	1.851	−0.2406
$N_r \times 10^1$	−1.664	−2.728	−1.538	−3.811	−2.723	−1.966	−1.488	−5.583	−4.866	−2.330	−3.623	−1.707	−1.199	−7.566
N_β	2.384	4.050	2.505	7.234	5.176	3.865	3.080	12.43	11.04	5.192	8.522	4.019	3.075	26.07
$N_\delta \times 10^1$	−4.803	−2.180	−4.734	2.493	−0.4589	−3.056	−4.572	7.626	4.413	0.7457	4.821	−0.9675	−3.157	14.95
N_{δ_R}	−1.225	−2.659	−1.210	−5.213	−3.502	−2.342	−1.367	−8.710	−7.519	−3.016	−5.741	−2.249	−1.119	−6.186
$Y_P \times 10^3$	1.969	1.634	1.388	0.6962	0.8885	0.9798	0.9457	0.2381	0.2516	0.5400	0.2746	0.5438	0.5643	−0.1736
$Y_r \times 10^1$	−9.985	−9.977	−9.989	−9.977	−9.983	−9.988	−9.992	−9.972	−9.975	−9.987	−9.982	−9.991	−9.995	−9.969
$Y_\beta \times 10^1$	−0.7204	−1.381	−0.6258	−2.031	−1.412	−0.9470	−0.6071	−2.983	−2.555	−1.210	−1.900	−0.8403	−0.5043	−4.180
$Y_\delta \times 10^3$	−1.812	−3.221	−1.550	−4.506	−3.171	−2.170	−1.437	−6.389	−5.474	−2.636	−4.077	−1.848	−1.148	−8.370
$Y_{\delta_R} \times 10^2$	1.448	2.704	1.281	3.818	2.646	1.675	1.160	5.315	4.567	2.128	3.147	1.383	0.6446	2.967
$Y_\phi \times 10^2$	7.605	5.863	6.331	4.188	4.345	4.522	4.723	3.431	3.450	3.726	3.380	3.673	3.691	2.619

TABLE VIII (CONTINUED)
LATERAL-DIRECTIONAL RIGID EQUATIONS OF MOTION COEFFICIENTS

Clean Configuration

100% Internal Fuel — W = 43,720 Lb
CG = 34% c — I_x = 28,478 Slug Ft^2
CG (FS) = 326.55 In. — I_z = 184,136 Slug Ft^2
CG (WL) = 29.0 In. — I_{xz} = 6899 Slug Ft^2

Mach Number	1.2	1.2	1.2	1.2	1.5	1.5	1.5	1.5	1.8	1.8	1.8	1.8	2.15	2.15
Altitude (Ft)	5000	15,000	35,000	45,000	15,000	25,000	35,000	45,000	25,000	35,000	45,000	55,000	36,000	45,000
Velocity (Ft/Sec)	1317.0	1269.3	1167.9	1162.0	1586.6	1524.6	1459.9	1452.7	1829.5	1751.9	1743.9	1743.2	2081.3	2081.3
Dynamic Pressure (Lb/Ft^2)	1774.8	1203.7	501.93	310.37	1880.8	1236.9	784.26	484.96	1781.1	1129.3	698.3	432.0	1538.4	996.32
α_{W_L} (Deg)	0.0500	0.3700	1.780	3.380	0.4000	0.8300	1.450	2.760	0.9093	1.552	2.622	3.770	0.9300	1.660
L_P	−2.413	−1.993	−1.193	−0.8092	−1.977	−1.605	−1.236	−0.880	−1.571	−1.232	−0.8902	−0.5500	−1.194	−0.9084
$L_r \times 10^1$	6.024	4.692	2.808	2.126	6.34	5.235	4.002	2.910	5.412	4.200	2.959	2.037	2.799	2.085
$L_\beta \times 10^{-1}$	−2.857	−2.157	−1.183	−0.9407	−2.918	−1.775	−1.109	−0.7685	−1.711	−1.197	−0.7658	−0.4999	−0.5278	−0.4226
L_δ	7.956	10.13	8.681	6.452	6.154	7.323	6.701	5.536	4.551	5.315	4.768	3.845	4.623	4.369
L_{δ_R}	5.402	5.168	1.792	1.093	3.555	3.472	2.391	1.371	3.551	2.649	1.607	0.8971	3.278	2.159
$N_P \times 10^2$	−2.997	−3.919	−2.641	−1.590	−1.106	−1.718	−1.467	−0.5111	1.596	0.2625	0.7625	1.049	0.3592	0.5273
$N_r \times 10^1$	−9.191	−6.833	−2.966	−1.889	−7.941	−5.616	−3.740	−2.373	−4.867	−3.405	−2.223	−1.417	−3.100	−2.023
N_β	29.85	21.66	9.952	6.422	24.12	18.13	12.12	8.509	14.95	11.06	7.463	5.352	10.37	7.644
$N_\delta \times 10^1$	13.27	9.851	2.983	−0.097	7.459	5.068	2.653	0.0295	2.659	1.192	−0.3811	−1.273	2.637	0.5953
N_{δ_R}	−4.907	−4.370	−2.437	−1.634	−2.662	−2.857	−2.230	−1.554	−2.279	−1.961	−1.413	−1.034	−1.851	−1.470
$Y_P \times 10^3$	−0.1341	−0.0420	0.1916	0.2659	−0.1147	−0.0249	0.0661	0.1145	−0.0642	−0.0138	0.0237	0.0655	−0.0775	−0.0407
$Y_r \times 10^1$	−9.968	−9.976	−9.987	−9.992	−9.978	−9.983	−9.988	−9.992	−9.986	−9.990	−9.994	−9.996	−9.992	−9.995
$Y_\beta \times 10^1$	−3.989	−2.929	−1.343	−0.8260	−3.495	−2.465	−1.663	−1.033	−2.654	−1.747	−1.082	−0.6703	−1.793	−1.172
$Y_\delta \times 10^3$	−7.726	−5.437	−2.464	−1.531	−4.670	−3.196	−2.116	−1.315	−2.195	−1.453	−0.9028	−0.5626	−1.023	−0.6628
$Y_{\delta_R} \times 10^2$	2.349	2.082	1.190	0.7822	1.452	1.547	1.207	0.8346	1.394	1.182	0.8325	0.5674	1.058	0.7972
$Y_\phi \times 10^2$	2.443	2.535	2.755	2.768	2.028	2.110	2.204	2.215	1.759	1.837	1.845	1.846	1.546	1.546

TABLE VIII (CONTINUED)
LATERAL-DIRECTIONAL RIGID EQUATIONS OF MOTION COEFFICIENTS
Clean Configuration

60% Internal Fuel
CG = 30.6% c
CG (FS) = 320.0 In.
CG (WL) = 27.65 In.

W = 38,732 Lb
I_X = 24,873 Slug Ft^2
I_z = 169,824 Slug Ft^2
I_{xz} = 4820 Slug Ft^2

Mach Number	0.4	0.5	0.5	0.7	0.7	0.7	0.7	0.84	0.85	0.85	0.9	0.9	0.9	1.1
Altitude (Ft)	15,000	5000	25,000	5000	15,000	25,000	35,000	0	5000	25,000	15,000	35,000	45,000	0
Velocity (Ft/Sec)	423.09	548.76	508.19	768.27	740.41	711.47	681.29	937.8	932.51	863.57	951.96	875.95	871.62	1228.6
Dynamic Pressure (Lb/Ft^2)	133.75	308.36	137.43	603.92	409.60	269.37	170.80	1045.1	890.47	397.18	677.1	282.33	174.58	1792.4
α_{W_L} (deg)	8.524	3.298	8.168	1.207	2.242	4.010	6.791	0.261	0.4330	1.980	0.662	2.725	4.959	−0.3662
L_p	−1.142	−1.890	−0.9793	−2.426	−1.849	−1.338	−0.9377	−3.033	−2.725	−1.566	−2.192	−1.142	−0.6993	−3.164
$L_r \times 10^1$	2.121	4.076	3.034	6.209	5.846	5.376	4.661	7.407	6.820	5.063	5.838	4.436	3.716	7.441
$L_\beta \times 10^{-1}$	−0.9495	−1.480	−1.029	−2.107	−1.765	−1.526	−1.343	−3.081	−2.768	−1.759	−2.334	−1.482	−1.249	−4.923
L_δ	4.456	10.51	4.522	16.27	12.55	8.928	5.664	19.26	18.19	11.74	15.24	9.127	5.673	10.09
L_{δ_R}	0.6129	1.845	0.6117	4.009	2.695	1.633	0.7802	6.833	5.942	2.658	4.509	1.762	0.8336	8.277
$N_P \times 10^2$	10.11	−0.1574	7.837	−3.596	−1.569	1.369	4.694	−5.060	−4.616	−1.599	−3.741	−0.7081	1.596	1.196
$N_r \times 10^1$	−1.825	−3.043	−1.676	−4.254	−3.042	−2.196	−1.646	−6.216	−5.342	−2.616	−4.044	−1.906	−1.299	−8.396
N_β	2.828	4.785	2.950	8.618	6.126	4.503	3.594	14.88	12.86	6.215	10.18	4.719	3.400	30.79
$N_\delta \times 10^1$	−5.391	−2.714	−5.184	2.214	−0.7411	−3.412	−5.042	7.341	6.108	0.0868	4.451	−1.118	−3.033	14.44
N_{δ_R}	−1.370	−2.963	−1.354	−5.796	−3.900	−2.605	−1.532	−9.689	−8.316	−3.371	−6.377	−2.500	−1.244	−6.619
$Y_P \times 10^3$	2.261	1.726	1.594	0.685	0.8874	1.020	1.064	0.2319	0.2918	0.5841	0.2839	0.5399	0.5437	−0.2309
$Y_r \times 10^1$	−9.983	−9.974	−9.987	−9.974	−9.981	−9.986	−9.991	−9.968	−9.972	−9.986	−9.980	−9.990	−9.994	−9.965
$Y_\beta \times 10^1$	−0.8191	−1.565	−0.7134	−2.298	−1.600	−1.075	−0.6909	−3.370	−2.883	−1.368	−2.147	−0.9540	−0.5778	−4.708
$Y_\delta \times 10^3$	−2.046	−3.636	−1.750	−5.086	−3.580	−2.450	−1.622	−7.211	−6.179	−2.976	−4.602	−2.086	−1.296	−9.440
$Y_{\delta_R} \times 10^2$	1.635	3.053	1.446	4.310	2.986	1.891	1.309	6.000	5.155	2.402	3.553	1.561	0.7276	3.346
$Y_\phi \times 10^2$	7.605	5.863	6.331	4.188	4.345	4.522	4.723	3.431	3.450	3.726	3.380	3.673	3.691	2.619

TABLE VIII (CONTINUED)

LATERAL-DIRECTIONAL RIGID EQUATIONS OF MOTION COEFFICIENTS

Clean Configuration

60% Internal Fuel
CG = 30.6% c
CG (FS) = 320.0 In.
CG (WL) = 27.65 In.

W = 38,732 Lb
I_x = 24,873 Slug Ft^2
I_z = 169,824 Slug Ft^2
I_{xz} = 4820 Slug Ft^2

Mach Number	1.2	1.2	1.2	1.2	1.5	1.5	1.5	1.5	1.8	1.8	1.8	1.8	2.15	2.15
Altitude (Ft)	5000	15,000	35,000	45,000	15,000	25,000	35,000	45,000	25,000	35,000	45,000	55,000	36,000	45,000
Velocity (Ft/Sec)	1317.0	1269.3	1167.9	1162.2	1586.6	1524.6	1459.9	1452.7	1829.5	1751.9	1743.9	1743.2	2081.3	2081.3
Dynamic Pressure (Lb/Ft^2)	1774.8	1203.7	501.93	310.37	1880.8	1236.9	784.26	484.96	1781.1	1129.3	698.3	432.01	1538.4	996.3
α_{W_L} (Deg)	−0.198	0.0890	1.349	2.610	−0.083	0.2610	0.834	1.98	0.7902	1.367	2.364	3.011	0.318	1.063
L_P	−2.754	−2.273	−1.360	−0.9231	−2.255	−1.838	−1.410	−1.003	−1.794	−1.406	−1.016	−0.6272	−1.361	−1.036
$L_r \times 10^1$	6.983	5.593	3.247	2.408	7.627	5.982	4.564	3.263	6.422	4.949	3.461	2.324	3.196	2.365
$L_\beta \times 10^{-1}$	−3.284	−2.535	−1.358	−1.038	−3.261	−2.000	−1.267	−0.8624	−2.005	−1.400	−0.8939	−0.5544	−0.6494	−0.4700
L_δ	9.040	11.53	9.894	7.355	7.005	8.3501	7.640	6.311	5.171	6.087	5.425	4.381	5.289	4.991
L_{δ_R}	6.387	5.299	2.443	1.292	4.081	4.046	2.755	1.583	4.275	3.235	2.040	1.106	4.098	2.543
$N_P \times 10^2$	−2.084	−3.421	−2.349	−1.605	−1.058	−7.115	−1.653	−0.6824	2.980	1.204	1.566	1.168	0.3032	0.5972
$N_r \times 10^1$	−10.08	−7.095	−3.255	−2.065	−8.971	−6.146	−4.092	−2.591	−5.412	−3.790	−2.476	−1.555	−3.411	−2.228
N_β	33.65	24.42	11.19	7.172	27.44	20.41	13.23	9.534	18.32	13.40	8.927	5.991	12.11	8.772
$N_\delta \times 10^1$	14.41	10.45	3.149	0.1158	7.892	5.765	3.031	0.5077	2.900	1.183	−0.5561	−1.201	4.108	1.854
N_{δ_R}	−5.407	−4.820	−2.679	−1.794	−2.945	−3.147	−2.455	−1.709	−2.571	−2.206	−1.551	−1.144	−2.042	−1.690
$Y_P \times 10^3$	−0.1730	−0.0632	0.1991	0.2798	−0.1327	−0.0337	0.07778	0.1224	−0.0792	−0.0230	0.0184	0.09736	−0.08798	−0.0511
$Y_r \times 10^1$	−9.964	−9,973	−9.986	−9.991	−9.975	−9.981	−9.986	−9.991	−9.985	−9.989	−9.993	−9.995	−9.991	−9.994
$Y_\beta \times 10^1$	−4.557	−3.277	−1.517	−0.9359	−3.946	−2.782	−1.883	−1.170	−2.923	−1.987	−1.234	−0.7627	−2.034	−1.328
$Y_\delta \times 10^3$	−8.722	−6.137	−2.781	−1.728	−5.271	−3.608	−2.389	−1.484	−2.477	−1.640	−1.019	−0.6350	−1.155	−0.7482
$Y_{\delta_R} \times 10^2$	2.652	2.351	1.343	0.8830	1.639	1.747	1.362	0.9421	1.573	1.334	0.9400	0.6405	1.194	0.9000
$Y_\phi \times 10^2$	2.443	2.535	2.755	2.768	2.028	2.110	2.204	2.215	1.759	1.837	1.845	1.846	1.546	1.546

TABLE IX
AILERON AND RUDDER DEFLECTION LIMITATIONS DUE TO POSITION AND HINGE MOMENT LIMITS

Mach No.	Altitude (Ft)	Aileron Limit*	Rudder Limit
0.206	SL	30°	30°
0.318	SL	30°	30°
0.400	15,000	30°	30°
0.500	5,000	30°	15°
0.500	25,000	30°	30°
0.700	5,000	30°	8°
0.700	15,000	30°	11.6°
0.700	25,000	30°	16.6°
0.700	35,000	30°	24.3°
0.840	SL	29.2°	4.9°
0.850	5,000	30°	5.9°
0.850	25,000	30°	11.9°
0.900	15,000	30°	7.2°
0.900	35,000	30°	16.1°
0.900	45,000	30°	23.8°
1.100	SL	20.8°	1.6°
1.200	5,000	22.7°	1.0°
1.200	15,000	24.6°	1.5°
1.200	35,000	30°	3.5°
1.200	45,000	30°	5.6°
1.500	15,000	25.1°	1.0°
1.500	25,000	24.7°	1.9°
1.500	35,000	30°	2.9°
1.500	45,000	30°	4.5°
1.800	25,000	24.6°	1.5°
1.800	35,000	26.7°	2.5°
1.800	45,000	30°	3.9°
1.800	55,000	30°	5.5°
2.15	36,000	25.1°	2.0°
2.15	45,000	30°	3.5°

*Includes effect of ailerons and spoilers

TABLE X
RUDDER FLEXURE EFFECTS

Flight Conditions Mach - Alt (Ft)	Rudder Flexure (K_f) Gain	dB	Flight Conditions Mach - Alt (Ft)	Rudder Flexure (K_f) Gain	dB
0.206 – SL	0.9680	– 0.2825	1.100 – SL	0.3675	– 8.695
0.318 – SL	0.9270	– 0.6584	1.200 – 5,000	0.2721	– 11.305
0.400 – 15,000	0.9340	– 0.5931	1.200 – 15,000	0.3551	– 8.993
0.500 – 5,000	0.8600	– 1.31	1.200 – 35,000	0.5692	– 4.895
0.500 – 25,000	0.9323	– 0.6089	1.200 – 45,000	0.6810	– 3.337
0.700 – 5,000	0.7580	– 2.407	1.500 – 15,000	0.2874	– 10.830
0.700 – 15,000	0.8220	– 1.703	1.500 – 25,000	0.3802	– 8.400
0.700 – 25,000	0.8760	– 1.150	1.500 – 35,000	0.4914	– 6.171
0.700 – 35,000	0.9170	– 0.753	1.500 – 45,000	0.6095	– 4.301
0.840 – SL	0.6444	– 3.817	1.800 – 25,000	0.3670	– 8.707
0.850 – 5,000	0.6800	– 3.350	1.800 – 35,000	0.4770	– 6.130
0.850 – 25,000	0.8265	– 1.655	1.800 – 45,000	0.5960	– 4.495
0.900 – 15,000	0.7367	– 2.654	1.800 – 55,000	0.7009	– 3.085
0.900 – 35,000	0.8700	– 1.210	2.150 – 36,000	0.5037	– 5.957
0.900 – 45,000	0.9160	– 0.7621	2.150 – 45,000	0.6105	– 4.286

APPENDIX II

LONGITUDINAL RESPONSE AND ROOT LOCUS ANALYSIS

Longitudinal axis stability characteristics were investigated using frequency response, time history, and root locus data. These data are presented in this appendix.

1. FREQUENCY RESPONSE

Bode plots were obtained for the SFCS longitudinal control system in the fixed gain mode, K_F=.25. A linearized Secondary Actuator model with an actuator gain K_{MR}=163 and a high pass network in the feedback was used to provide the NSS function. The aircraft was represented by the small perturbation, two-degree-of-freedom equations-of-motion of Appendix I for thirteen flight conditions and two aircraft weight configurations. These frequency responses are shown in Figures 94 through 119. In addition, frequency responses were computed for four take-off and landing configurations. These data are shown in Figures 120 through 123. Gain and phase margins for the longitudinal SFCS control system were obtained from these data.

2. ROOT LOCUS PLOTS

Root locus data were computed in order to determine the damping and frequency for the SFCS short period and phugoid modes. The frequency and damping ratio of the closed loop roots which eminate from the basic aircraft short period poles were compiled for the adaptive gain at each flight condition. A typical root locus for these roots and others within its vicinity are shown in Figure 124. Figure 125 presents a typical root locus of the phugoid roots. It should be noted that while all the SFCS open loop poles and zeros are not shown on these plots, all the poles and zeros which significantly affect the locus of the roots are included in computation of the loci presented.

3. TIME HISTORIES

The short period small perturbation longitudinal equations of motion and the SFCS control system with a nonlinear actuator model were programmed on an analog computer. Time histories for a simulated step of pilot applied stick force were obtained for thirteen clean configuration flight conditions and four take-off and landing flight conditions for two weight configurations. For each flight condition and weight configuration considered, time histories were obtained for all values of forward loop gain, K_F=.25, .5, and 1.0. The time histories for the adaptive gain cases are shown in Figures 126 through 128.

Figures 129 and 130 present time history responses for cases where the accelerometer lag break frequency, ω_3, was varied from 1 to 20 rad/sec.

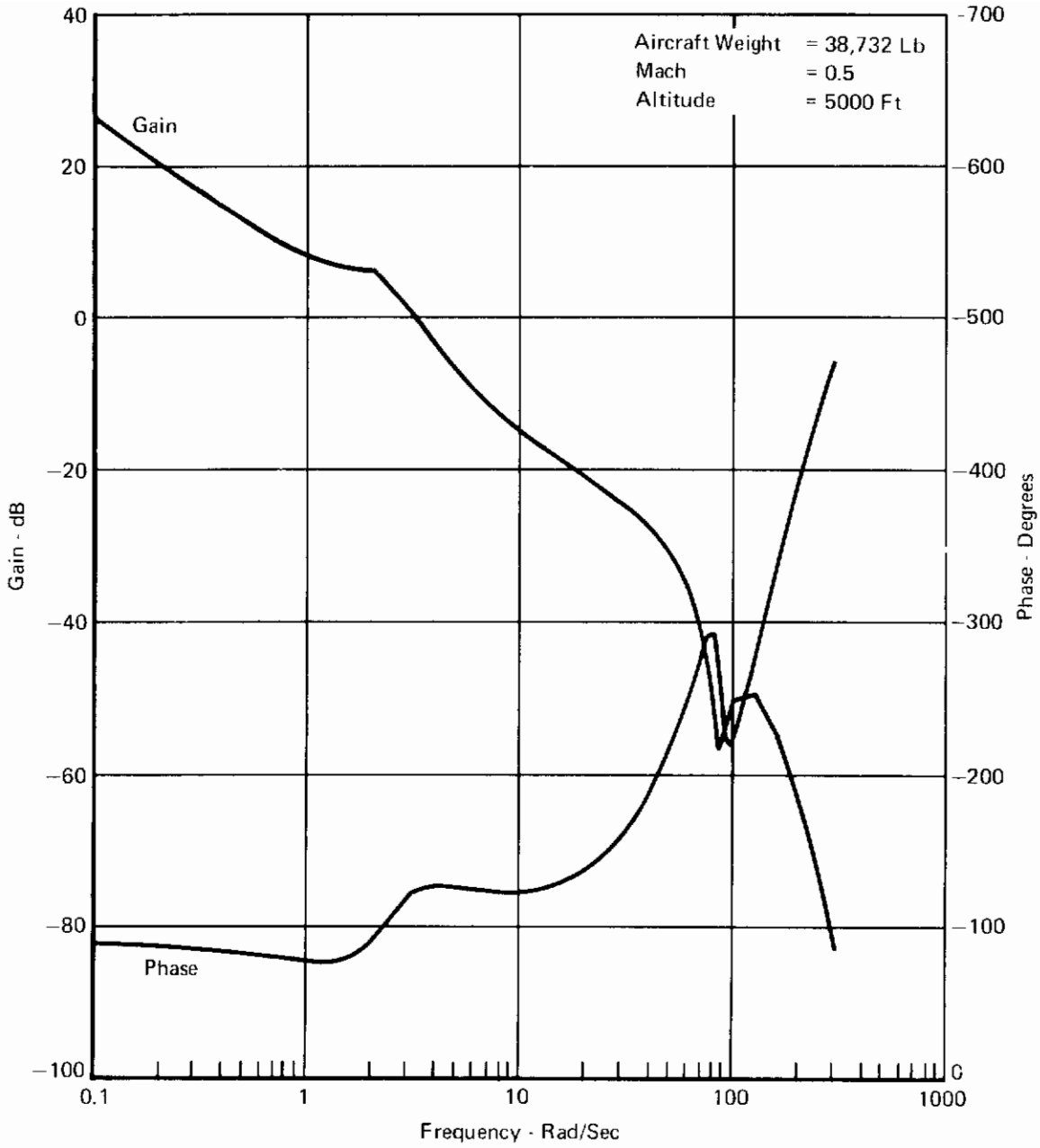

FIGURE 94
OPEN LOOP FREQUENCY RESPONSE (PHASE IIA, B)
NSS, $K_F = 0.25$

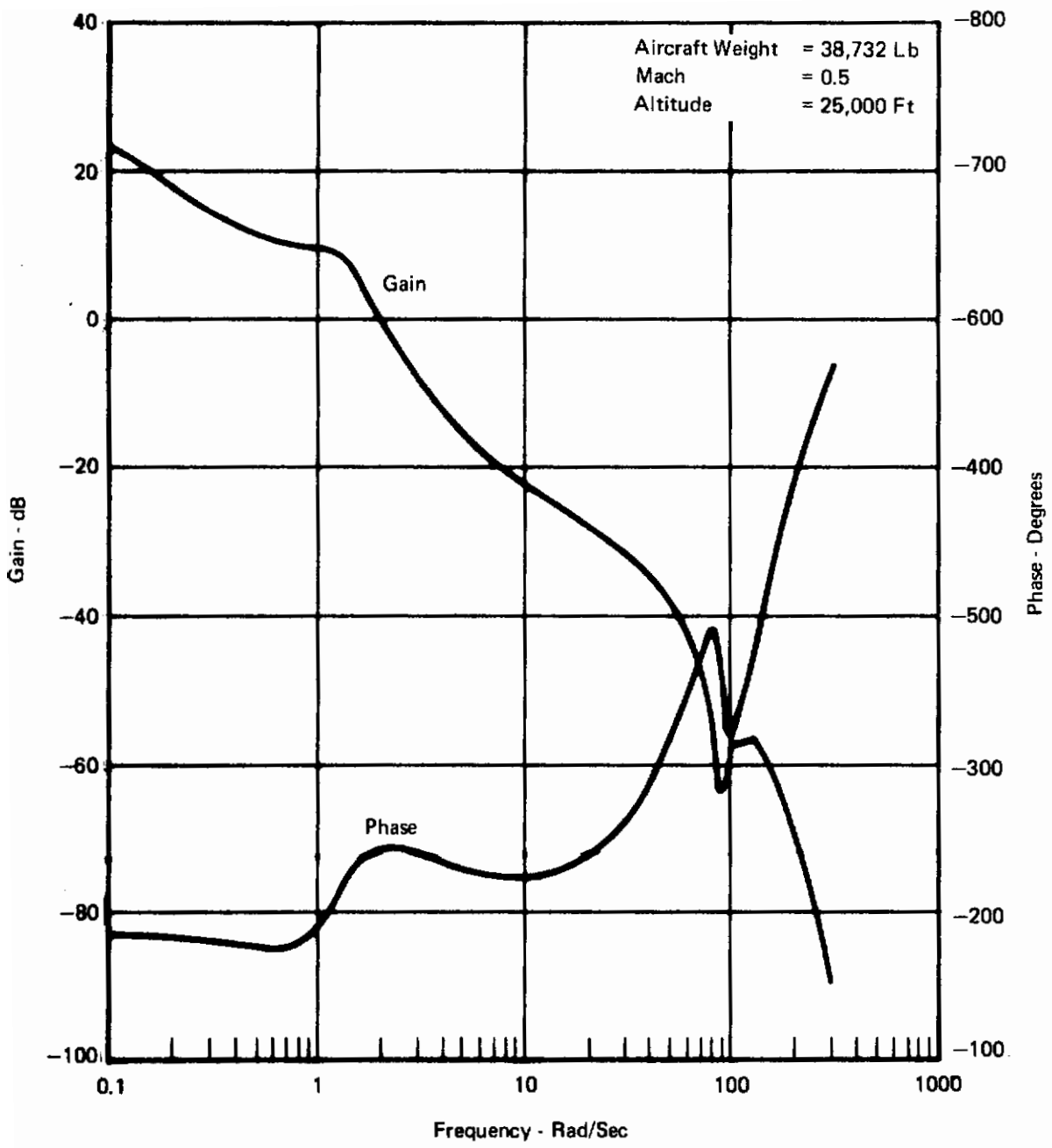

FIGURE 95
OPEN LOOP FREQUENCY RESPONSE (PHASE IIA, B)
NSS, $K_F = 0.25$

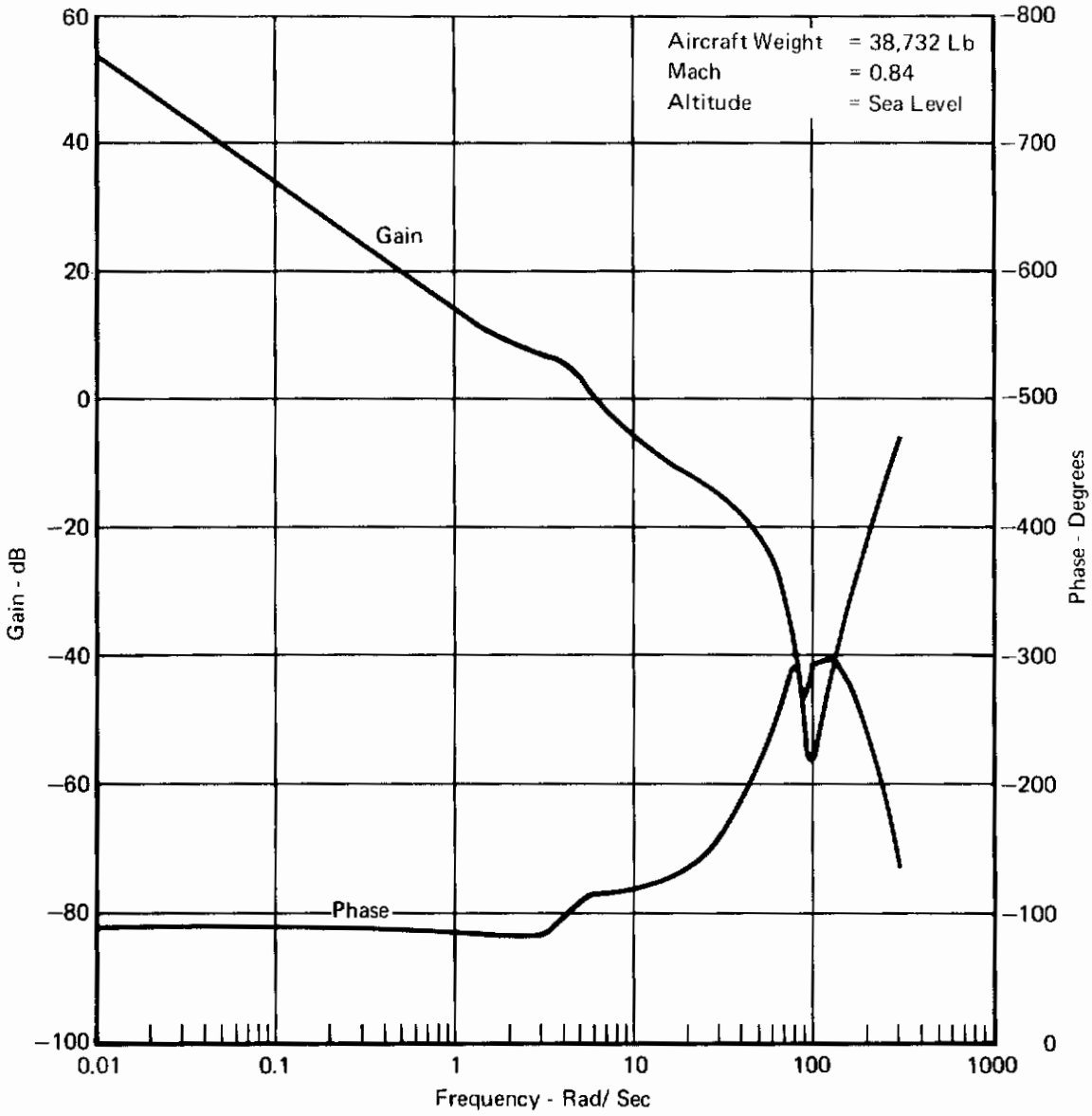

FIGURE 96
OPEN LOOP FREQUENCY RESPONSE (PHASE IIA, B)
NSS, $K_F = 0.25$

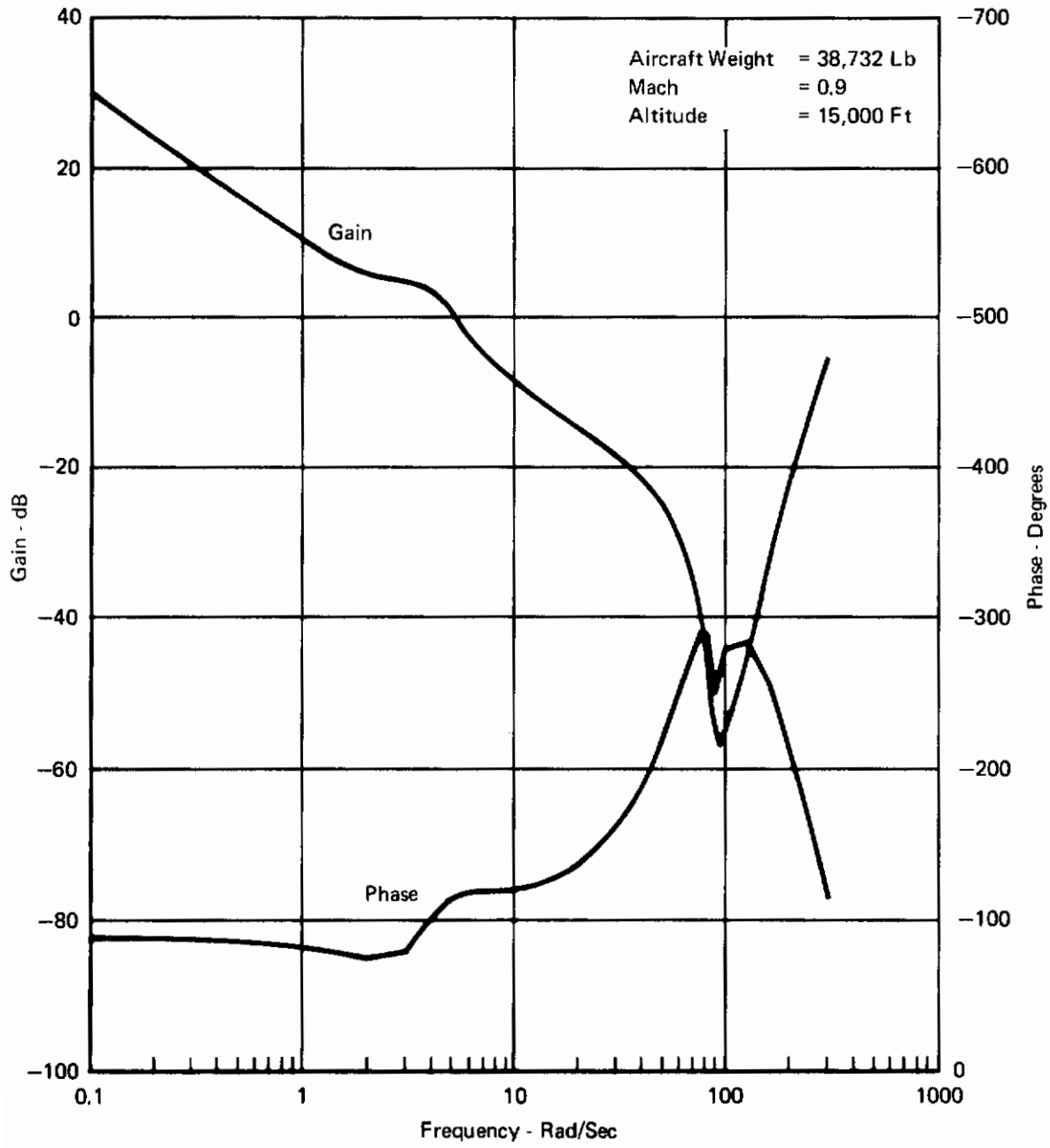

FIGURE 97

OPEN LOOP FREQUENCY RESPONSE (PHASE IIA, B)

NSS, $K_F = 0.25$

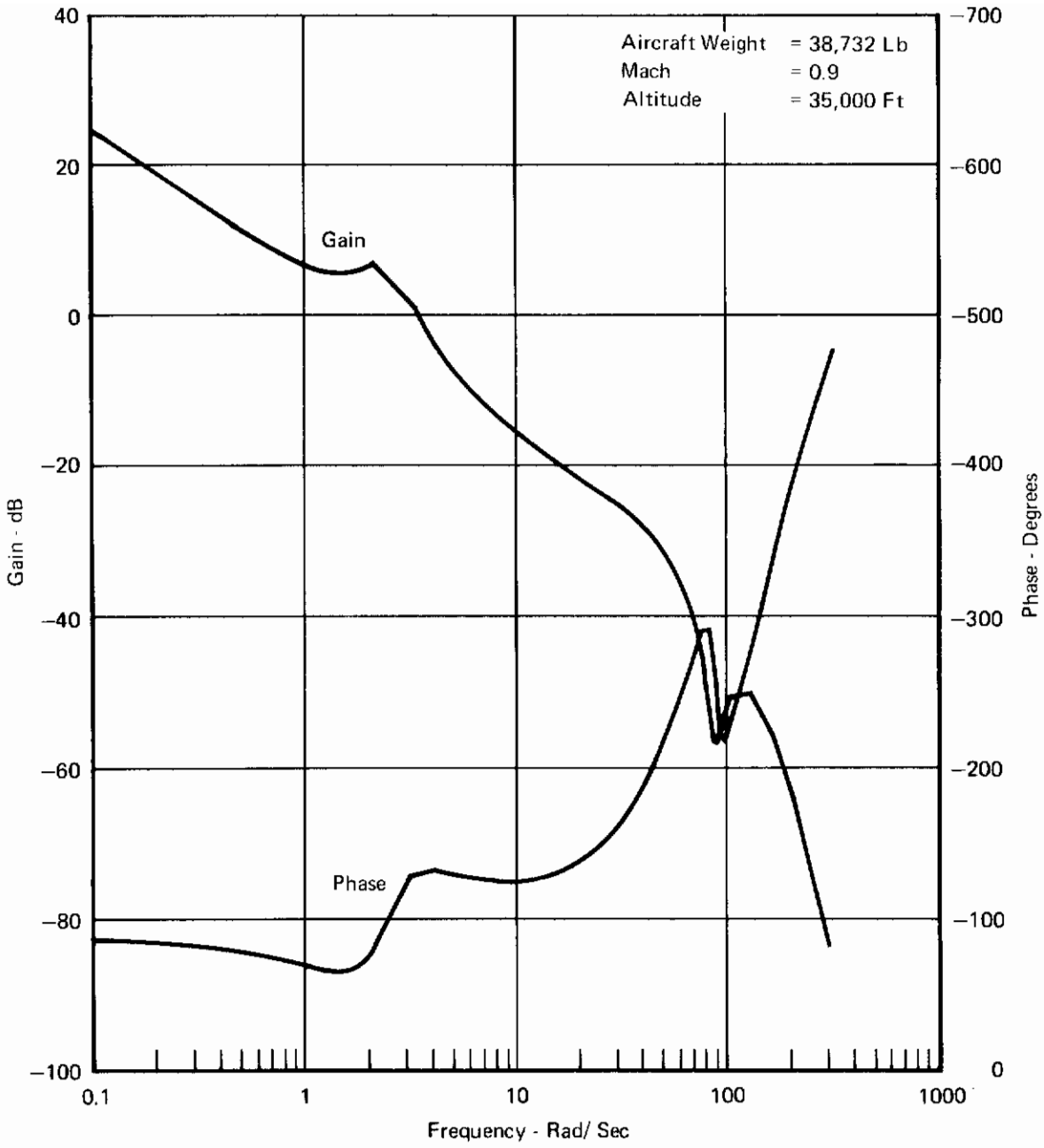

FIGURE 98

OPEN LOOP FREQUENCY RESPONSE (PHASE IIA, B)

NSS, $K_F = 0.25$

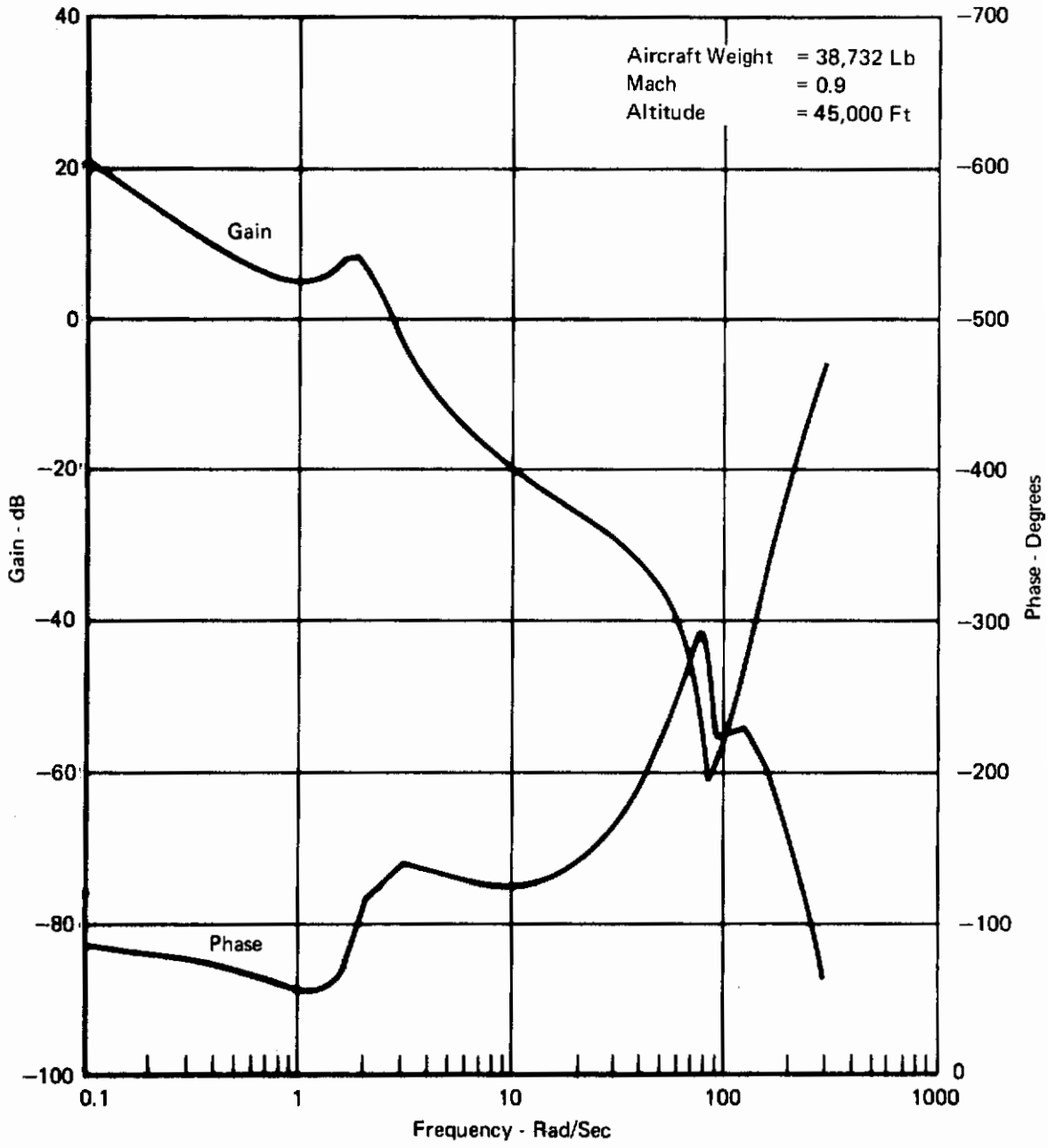

FIGURE 99
OPEN LOOP FREQUENCY RESPONSE (PHASE IIA, B)
NSS, $K_F = 0.25$

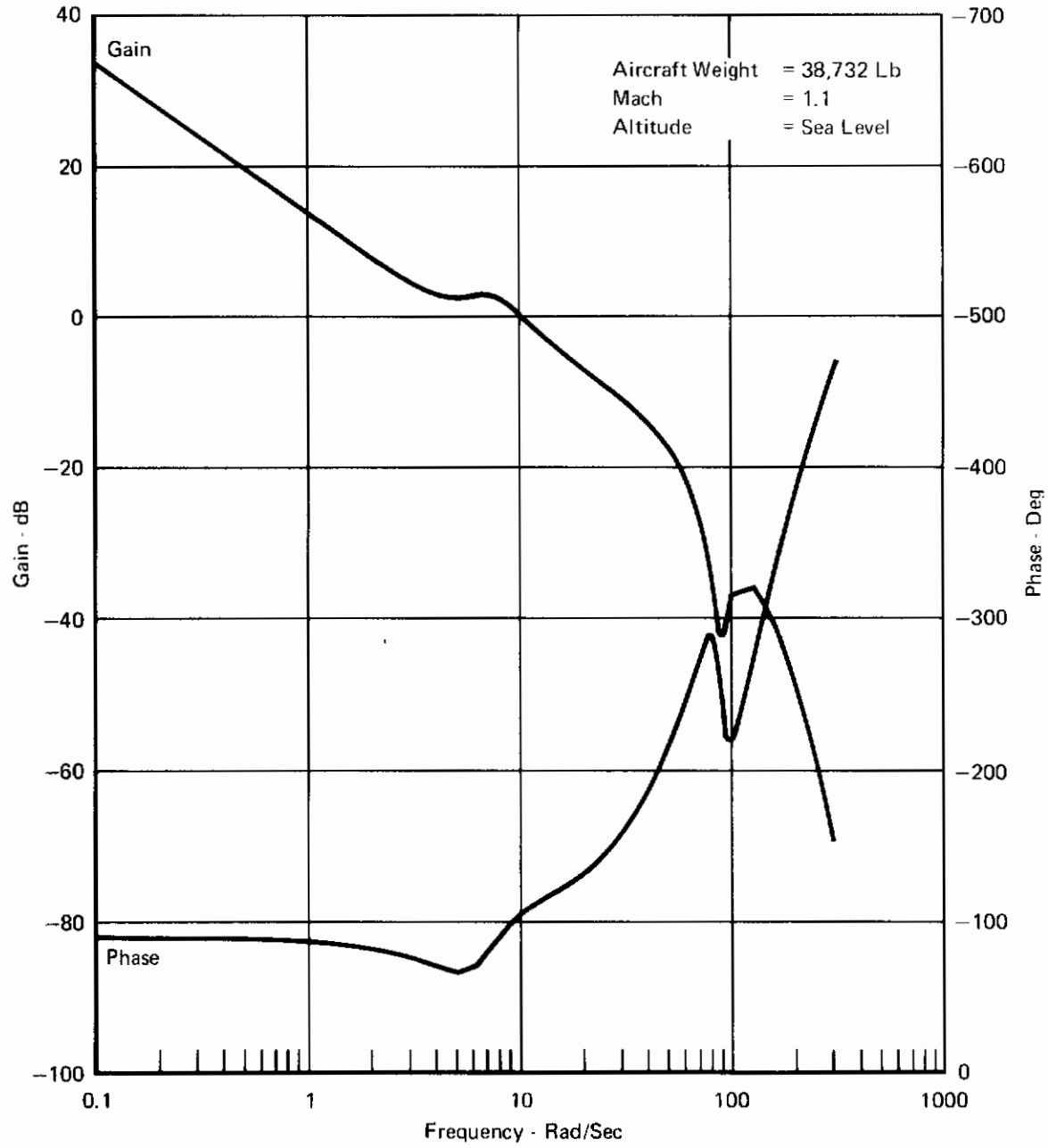

FIGURE 100
OPEN LOOP FREQUENCY RESPONSE (PHASE IIA, B)
NSS, $K_F = 0.25$

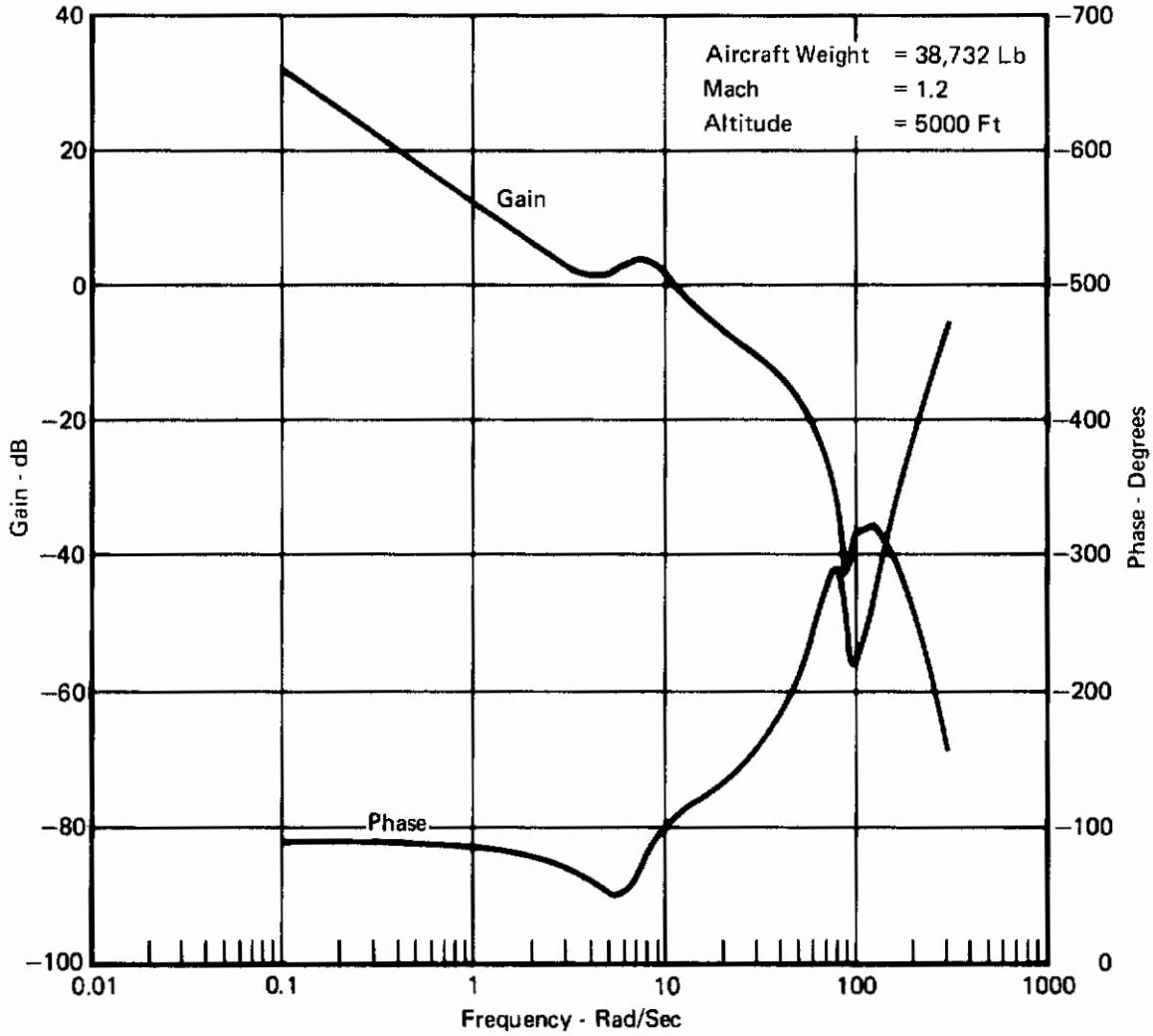

FIGURE 101
OPEN LOOP FREQUENCY RESPONSE (PHASE IIA,B)
NSS, $K_F = 0.25$

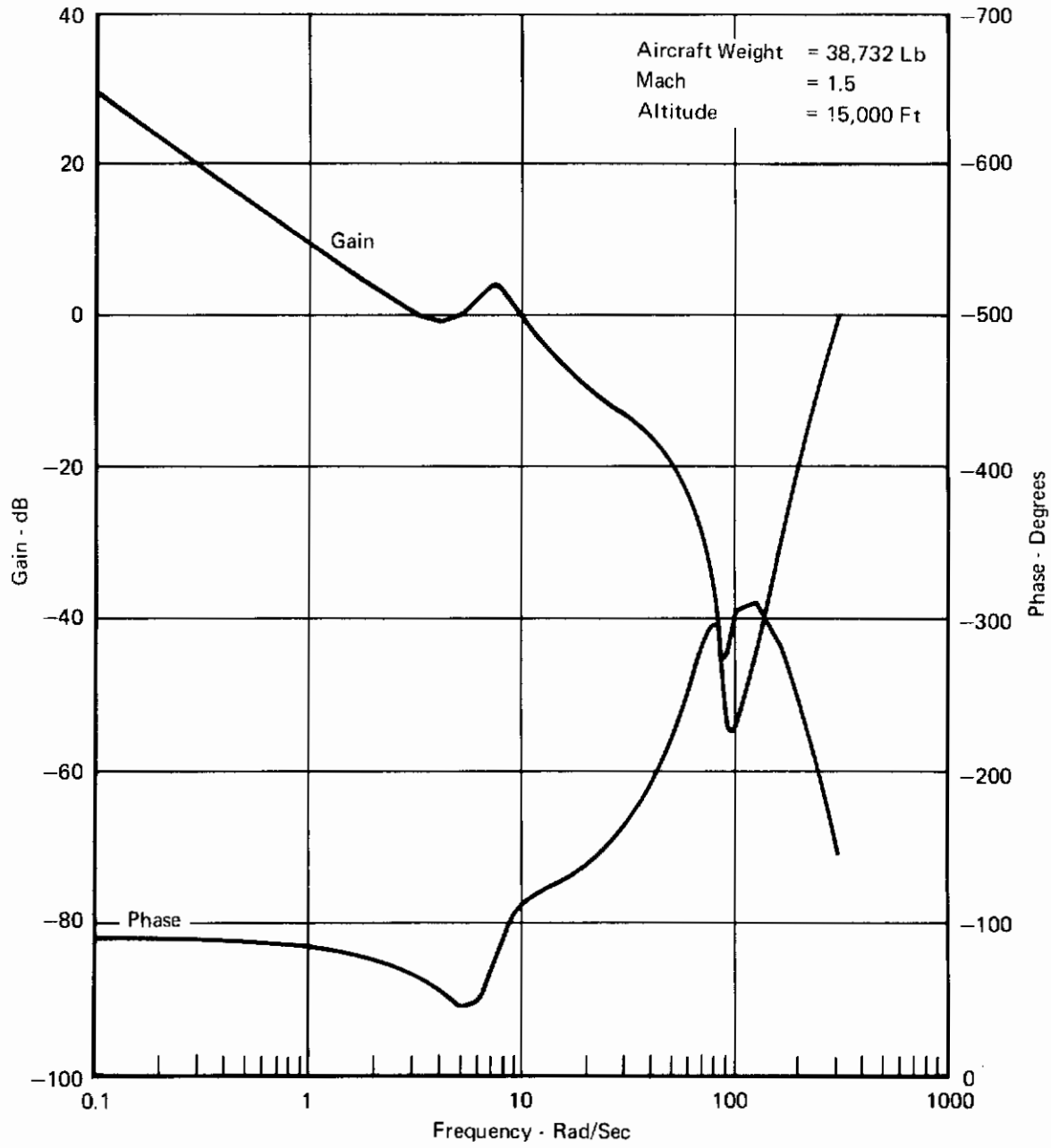

FIGURE 102
OPEN LOOP FREQUENCY RESPONSE (PHASE IIA, B)
NSS, $K_F = 0.25$

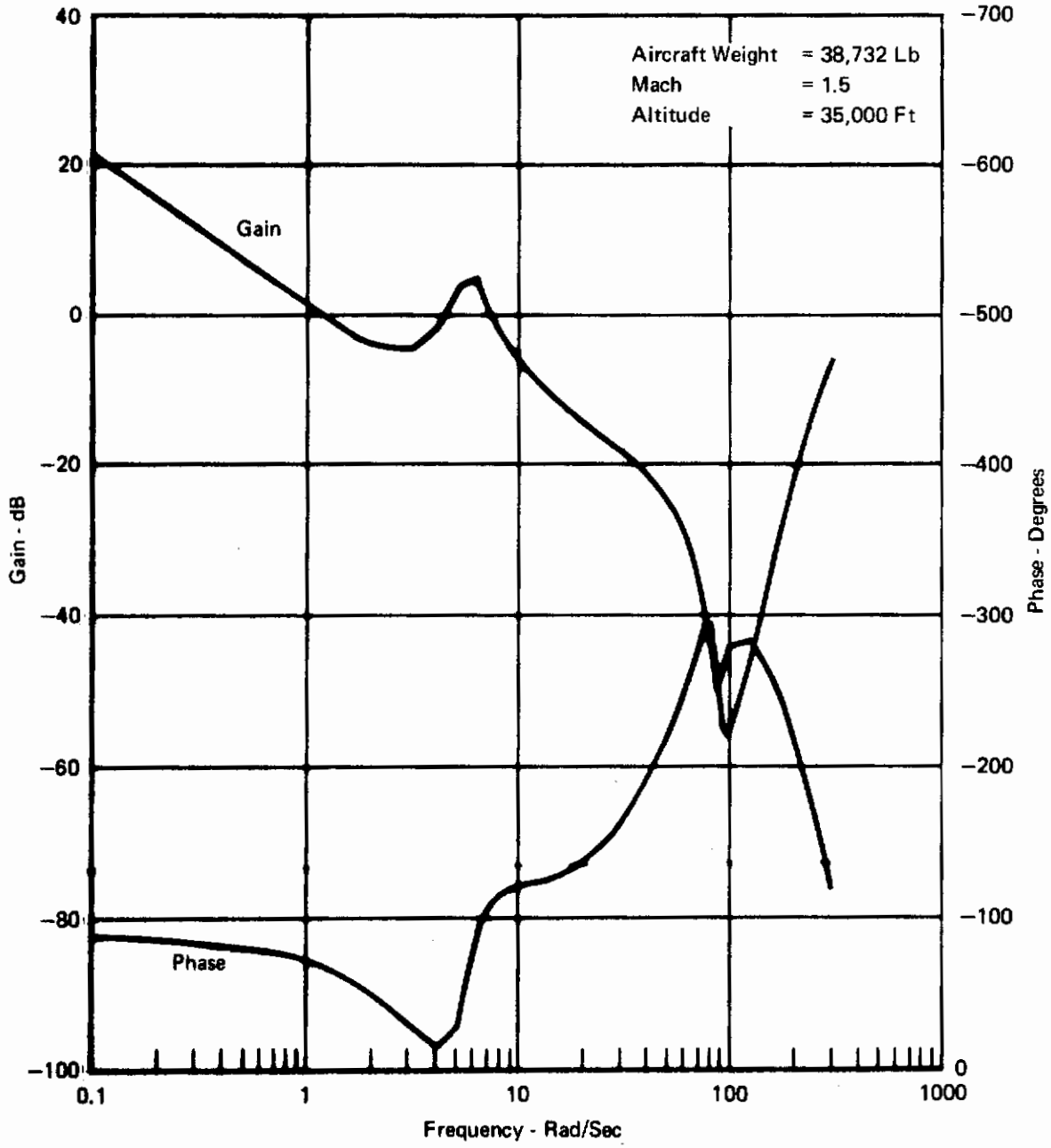

FIGURE 103
OPEN LOOP FREQUENCY RESPONSE (PHASE IIA, B)
NSS, $K_F = 0.25$

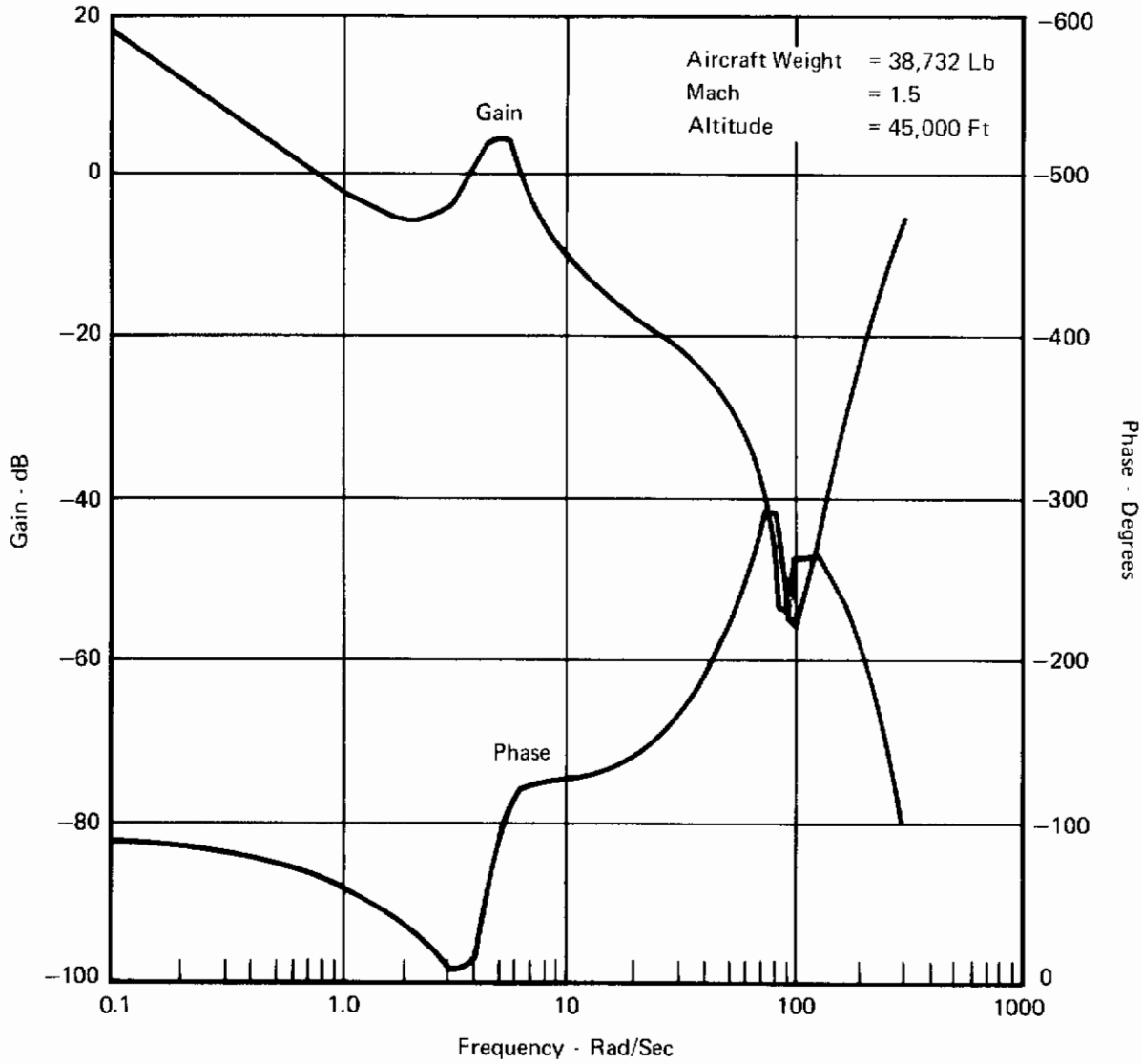

FIGURE 104
OPEN LOOP FREQUENCY RESPONSE (PHASE IIA, B)
NSS, $K_F = 0.25$

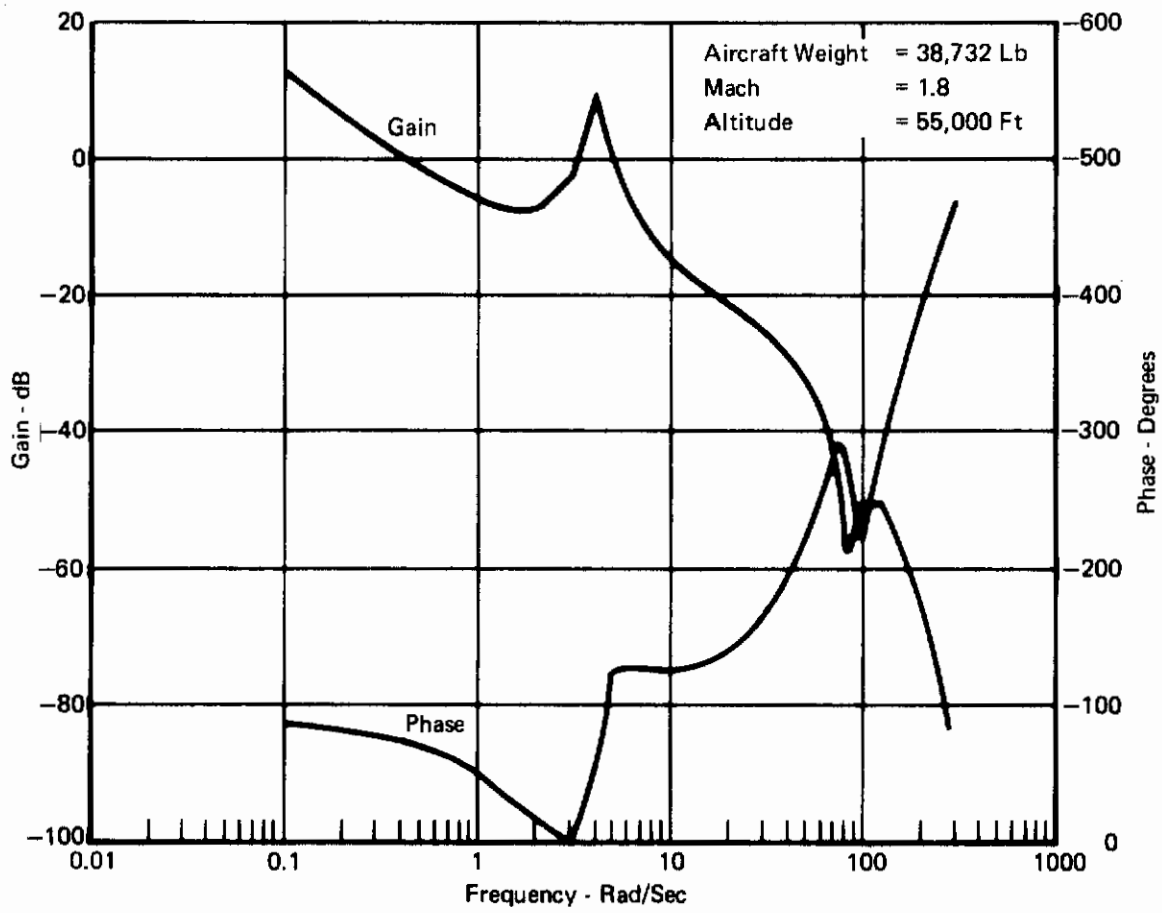

FIGURE 105
OPEN LOOP FREQUENCY RESPONSE (PHASE IIA,B)
NSS, K_F = 0.25

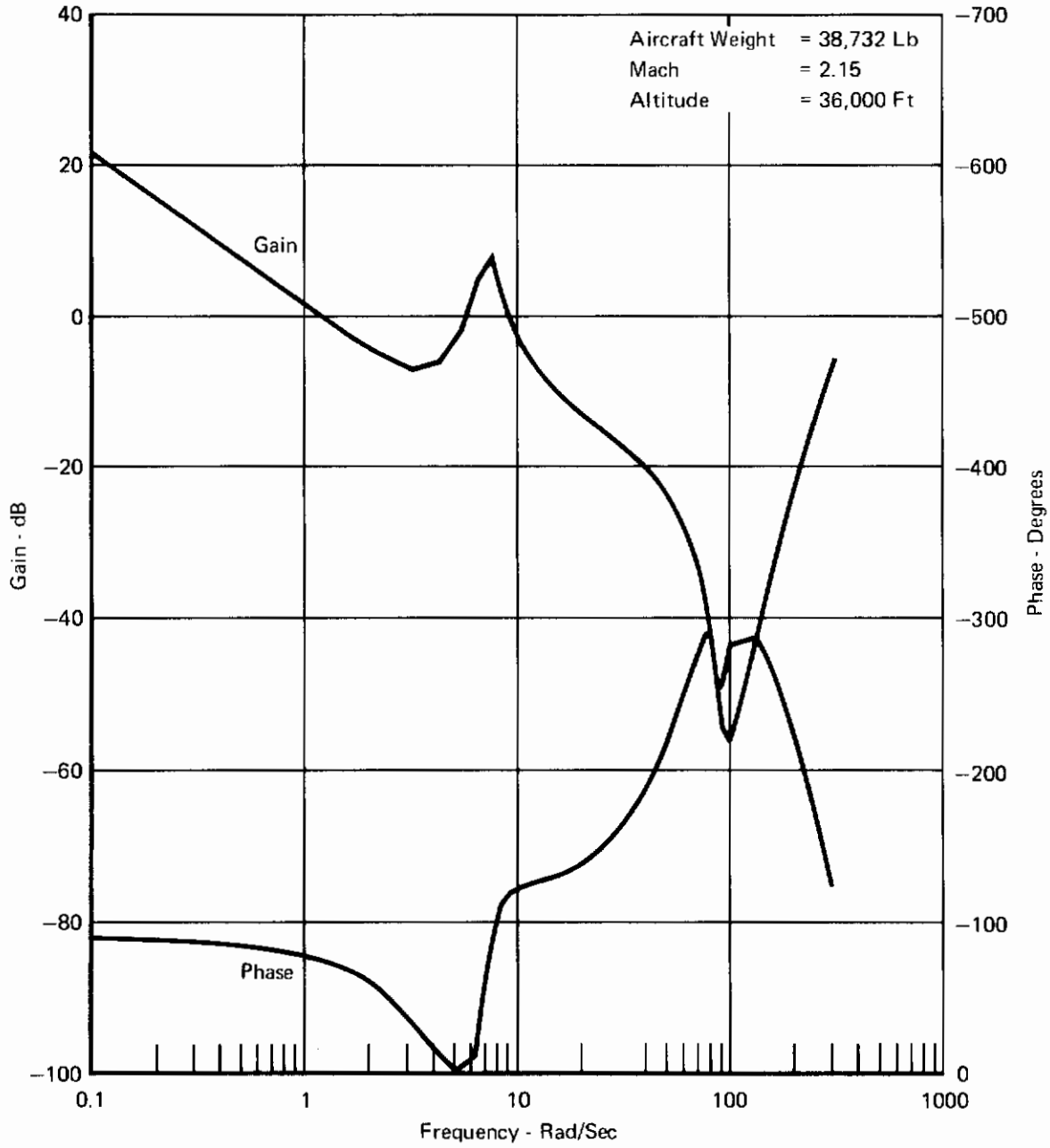

FIGURE 106
OPEN LOOP FREQUENCY RESPONSE (PHASE IIA,B)
NSS, $K_F = 0.25$

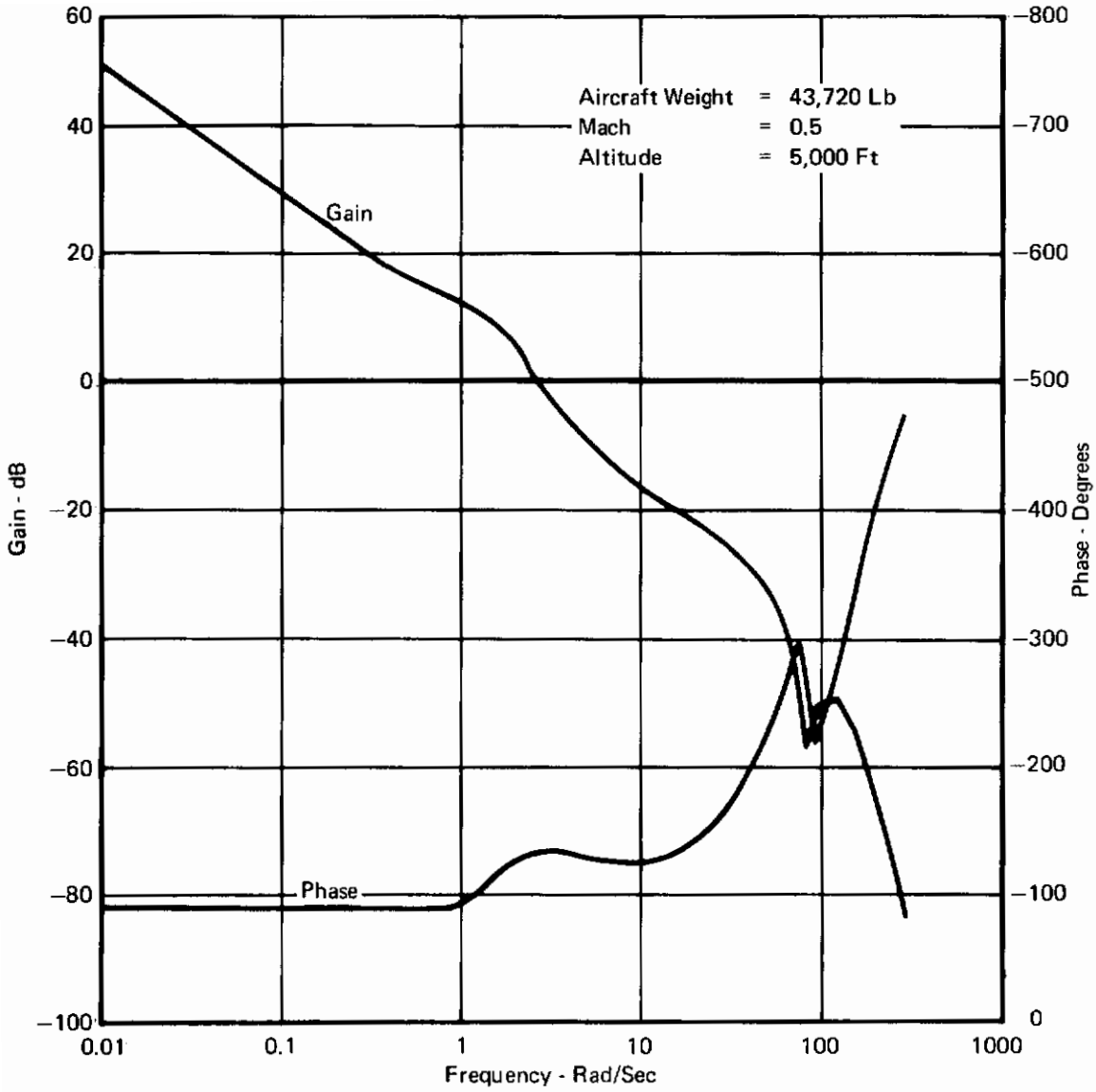

FIGURE 107
OPEN LOOP FREQUENCY RESPONSE (PHASE IIA, B)
NSS, $K_F = 0.25$

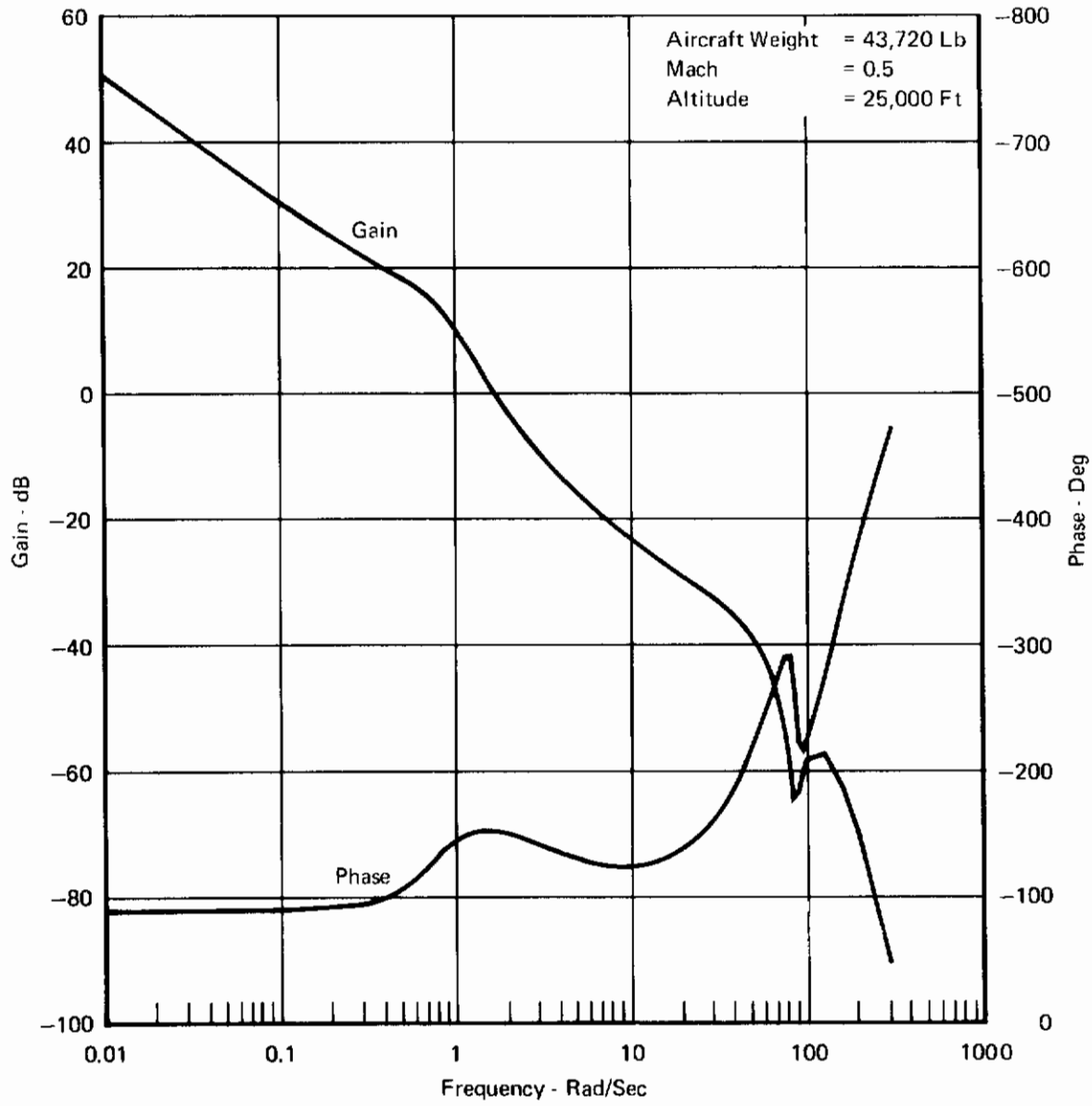

FIGURE 108
OPEN LOOP FREQUENCY RESPONSE (PHASE IIA, B)
NSS, $K_F = 0.25$

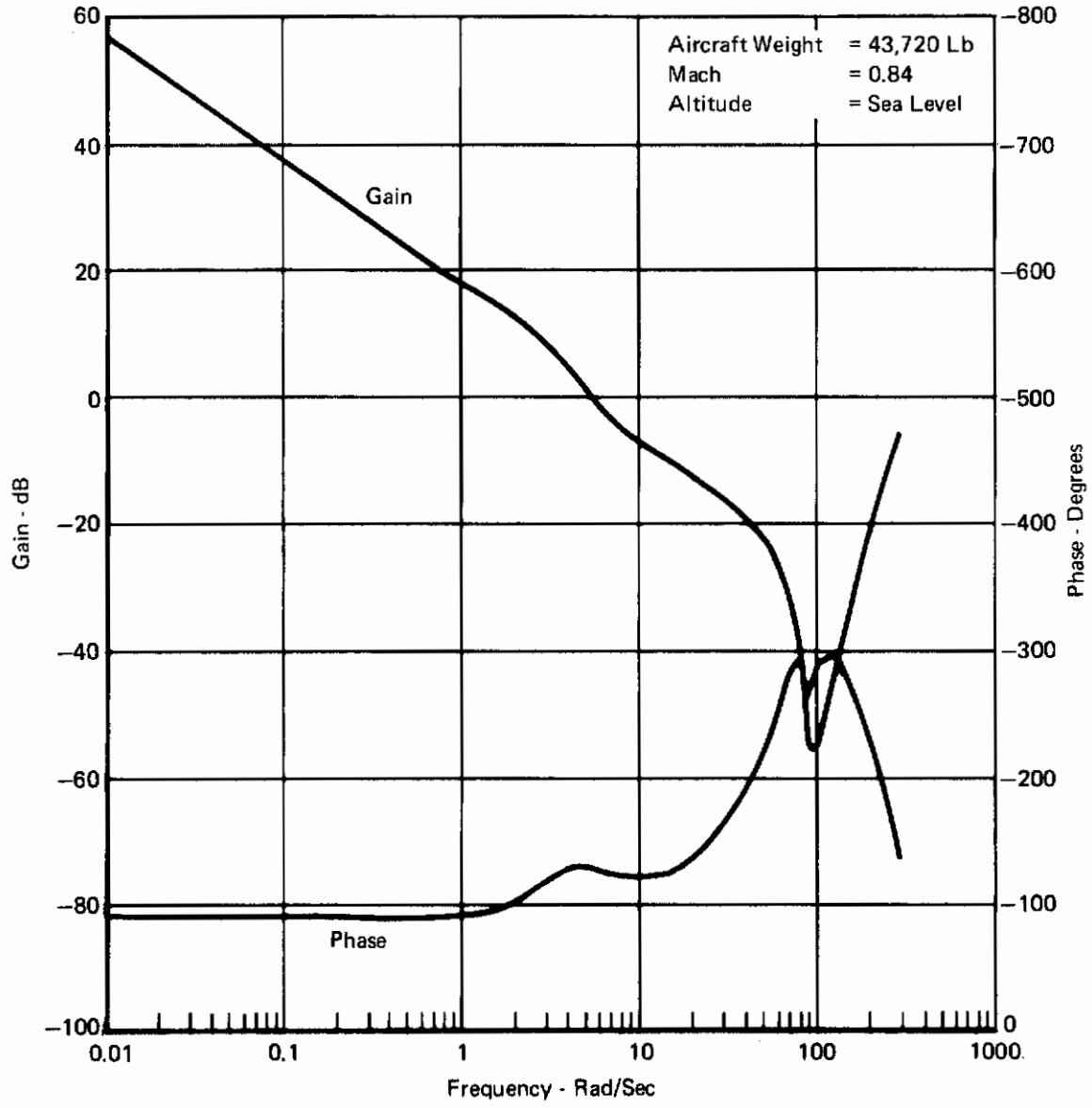

FIGURE 109
OPEN LOOP FREQUENCY RESPONSE (PHASE IIA, B)
NSS, $K_F = 0.25$

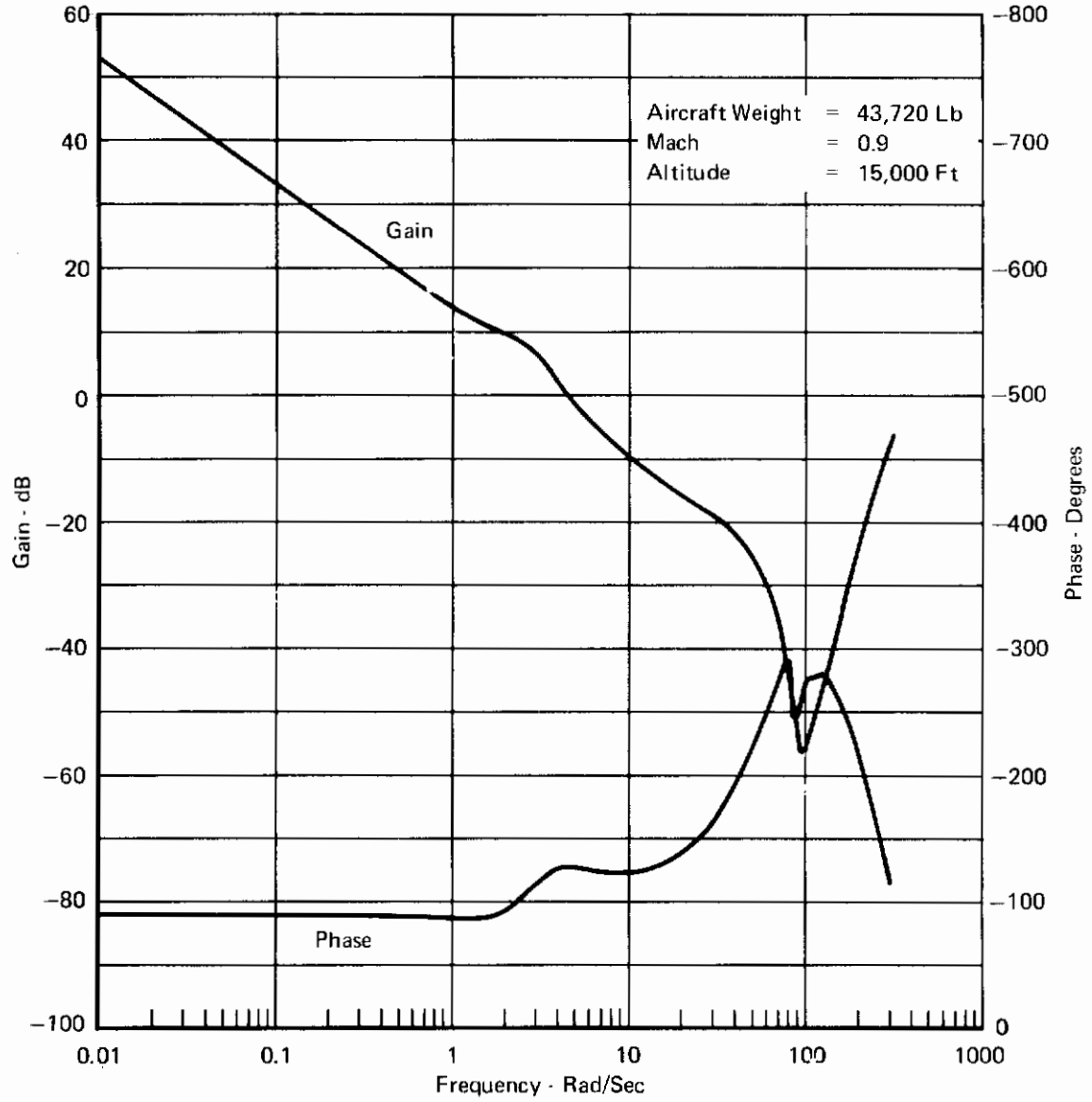

FIGURE 110
OPEN LOOP FREQUENCY RESPONSE (PHASE IIA, B)
NSS, $K_F = 0.25$

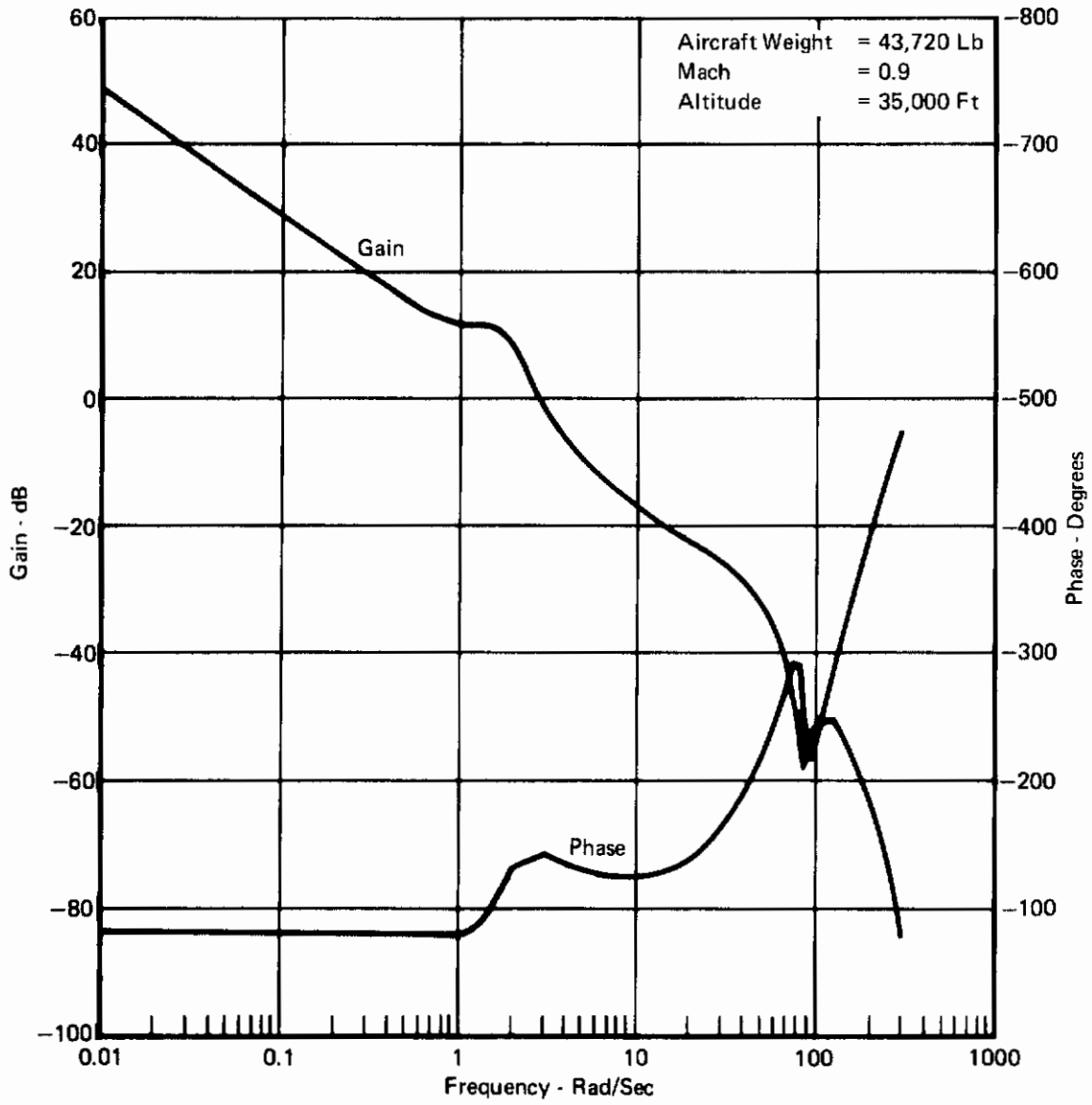

FIGURE 111
OPEN LOOP FREQUENCY RESPONSE (PHASE IIA,B)
NSS, $K_F = 0.25$

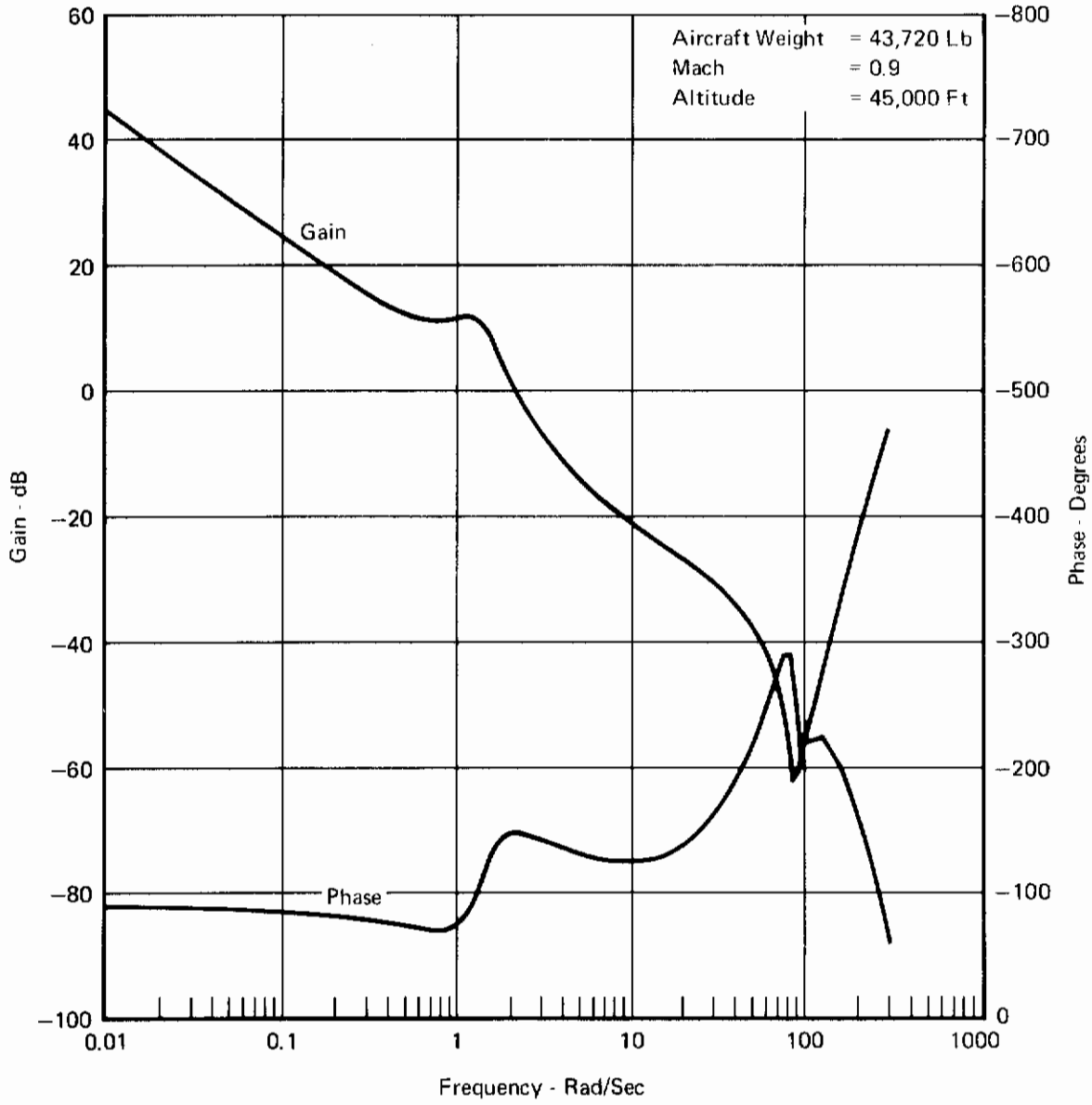

FIGURE 112
OPEN LOOP FREQUENCY RESPONSE (PHASE IIA,B)
NSS, $K_F = 0.25$

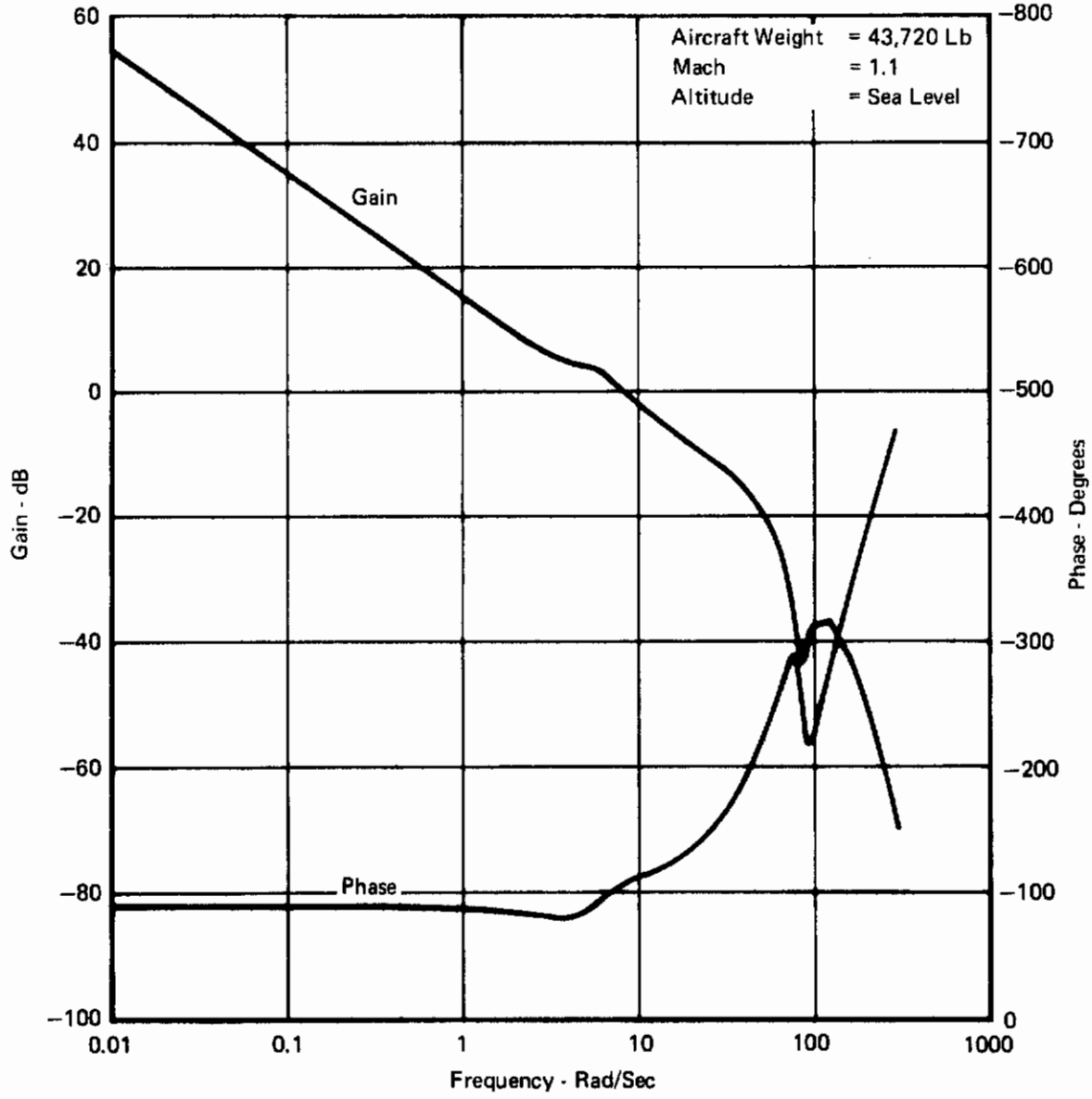

FIGURE 113
OPEN LOOP FREQUENCY RESPONSE (PHASE IIA, B)
NSS, $K_F = 0.25$

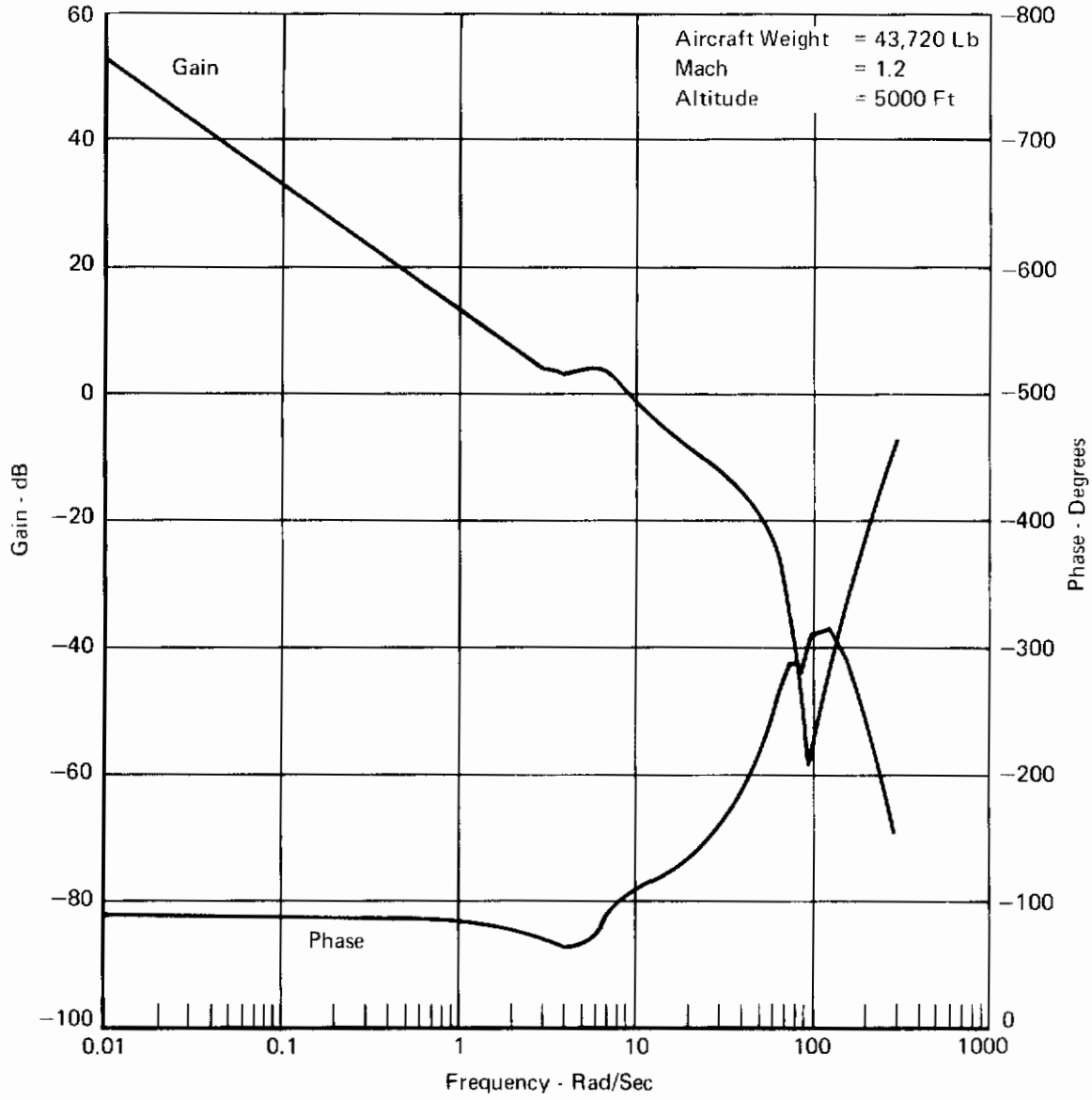

FIGURE 114
OPEN LOOP FREQUENCY RESPONSE (PHASE IIA,B)
NSS, $K_F = 0.25$

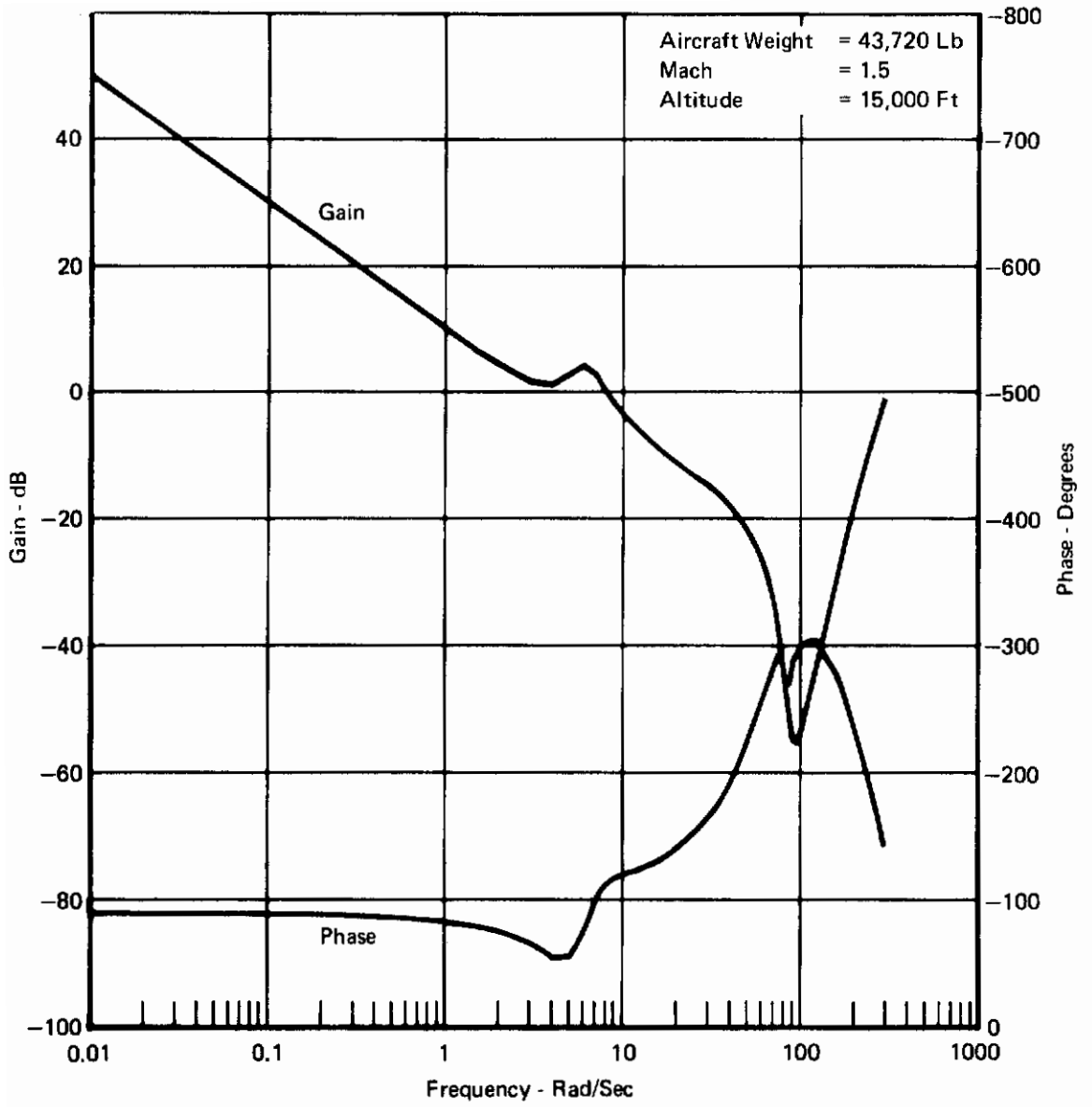

FIGURE 115
OPEN LOOP FREQUENCY RESPONSE (PHASE IIA, B)
NSS, $K_F = 0.25$

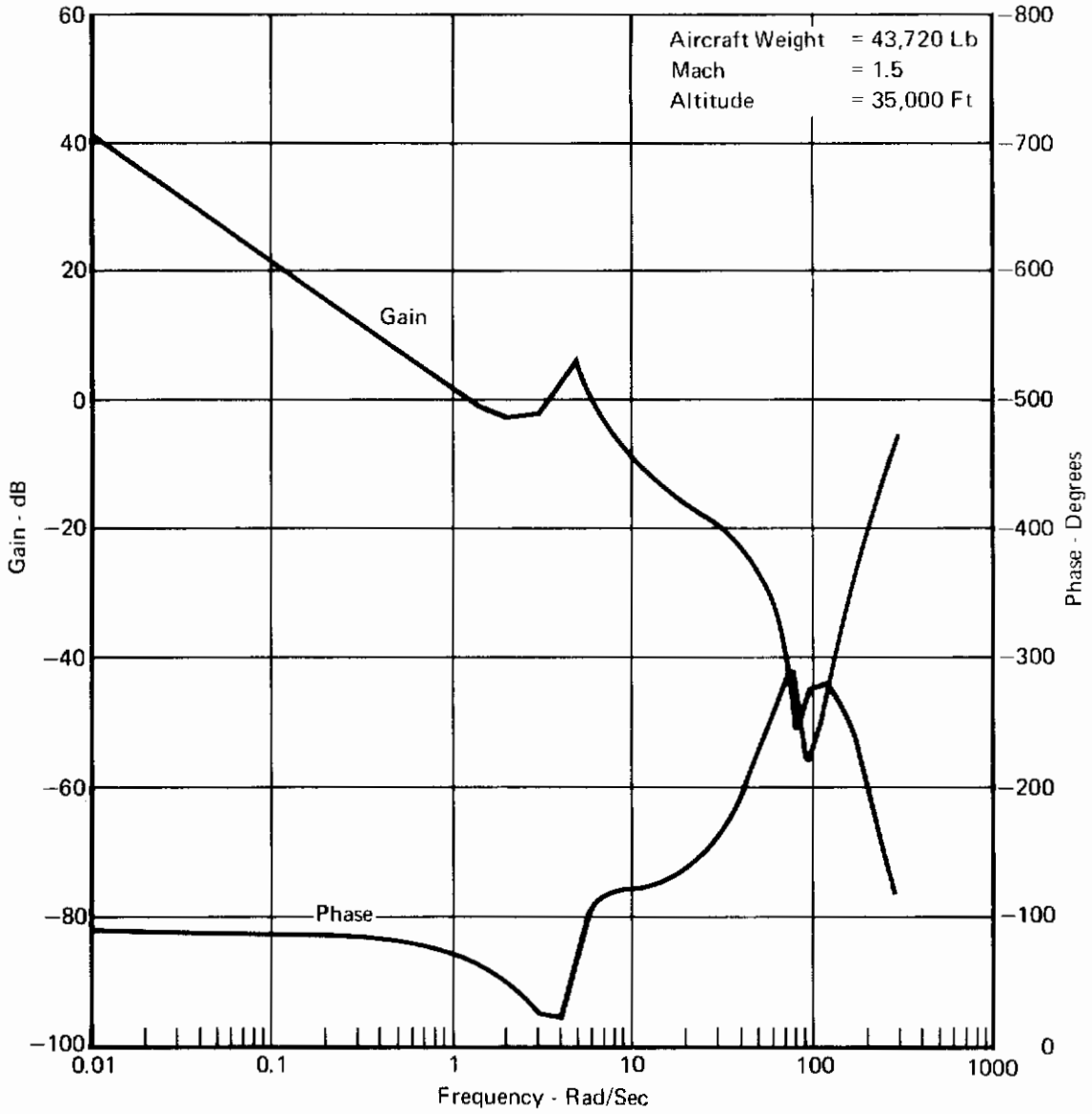

FIGURE 116
OPEN LOOP FREQUENCY RESPONSE (PHASE IIA, B)
NSS, $K_F = 0.25$

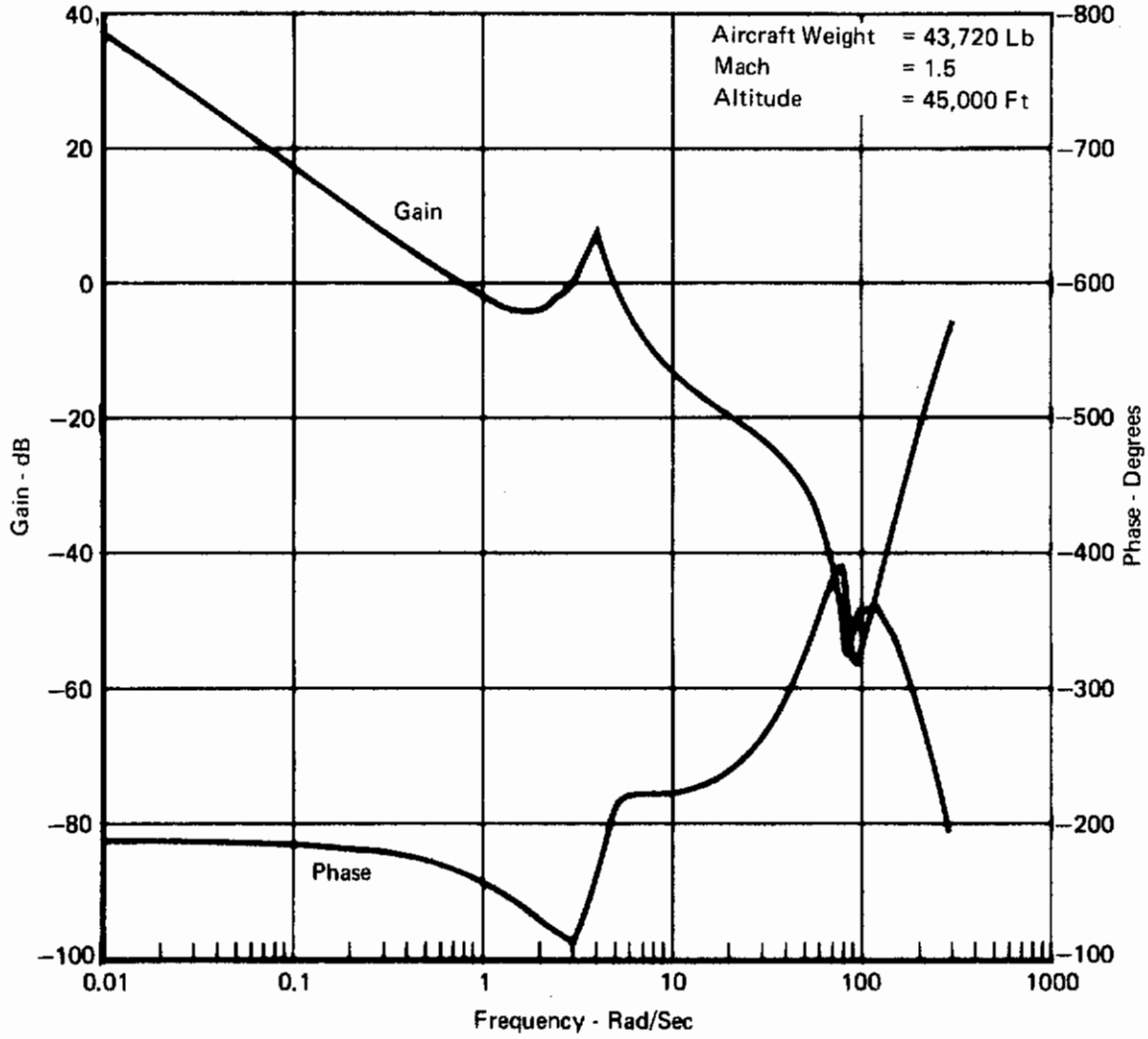

FIGURE 117
OPEN LOOP FREQUENCY RESPONSE (PHASE IIA, B)
NSS, $K_F = 0.25$

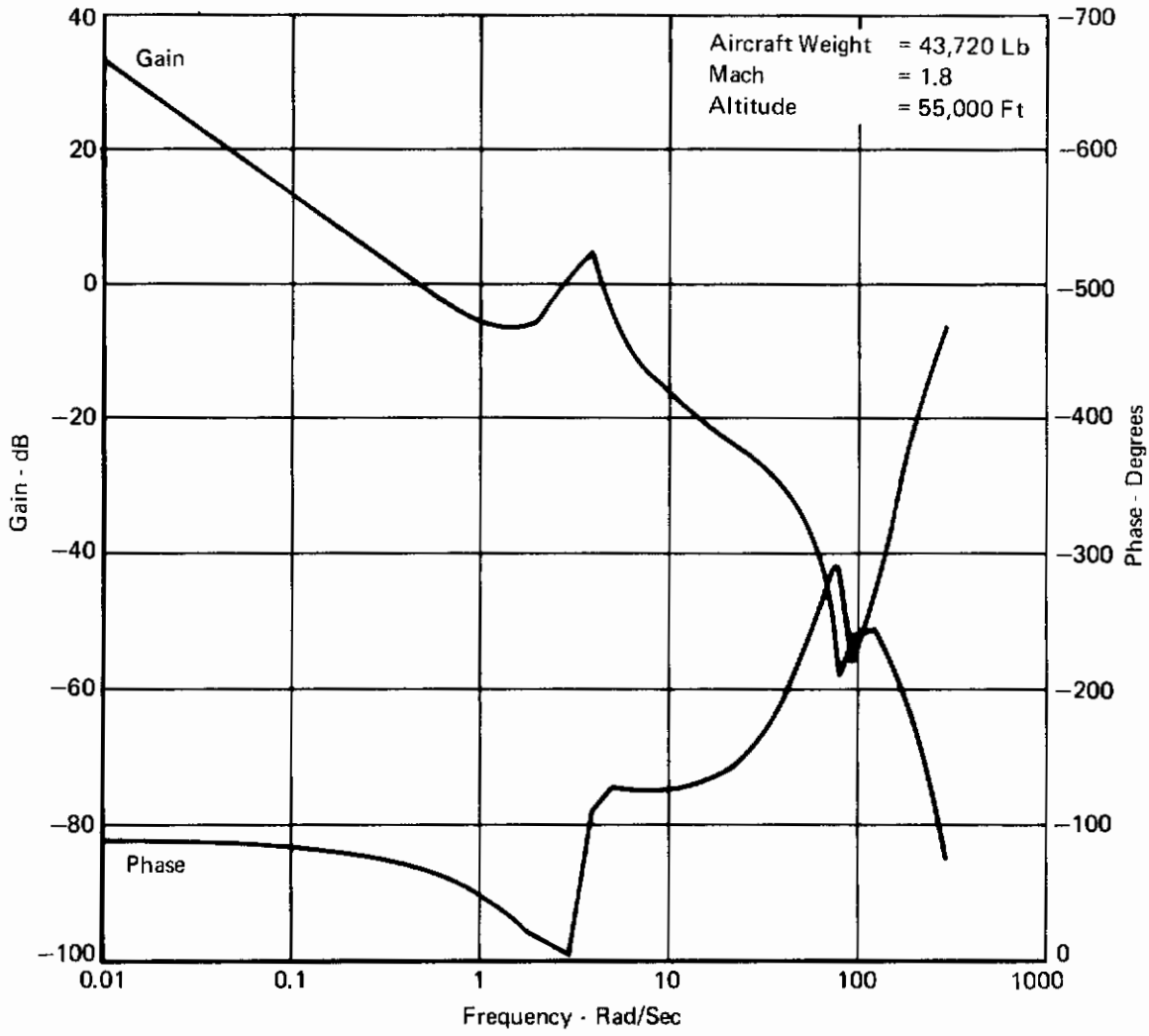

FIGURE 118
OPEN LOOP FREQUENCY RESPONSE (PHASE IIA,B)
NSS, $K_F = 0.25$

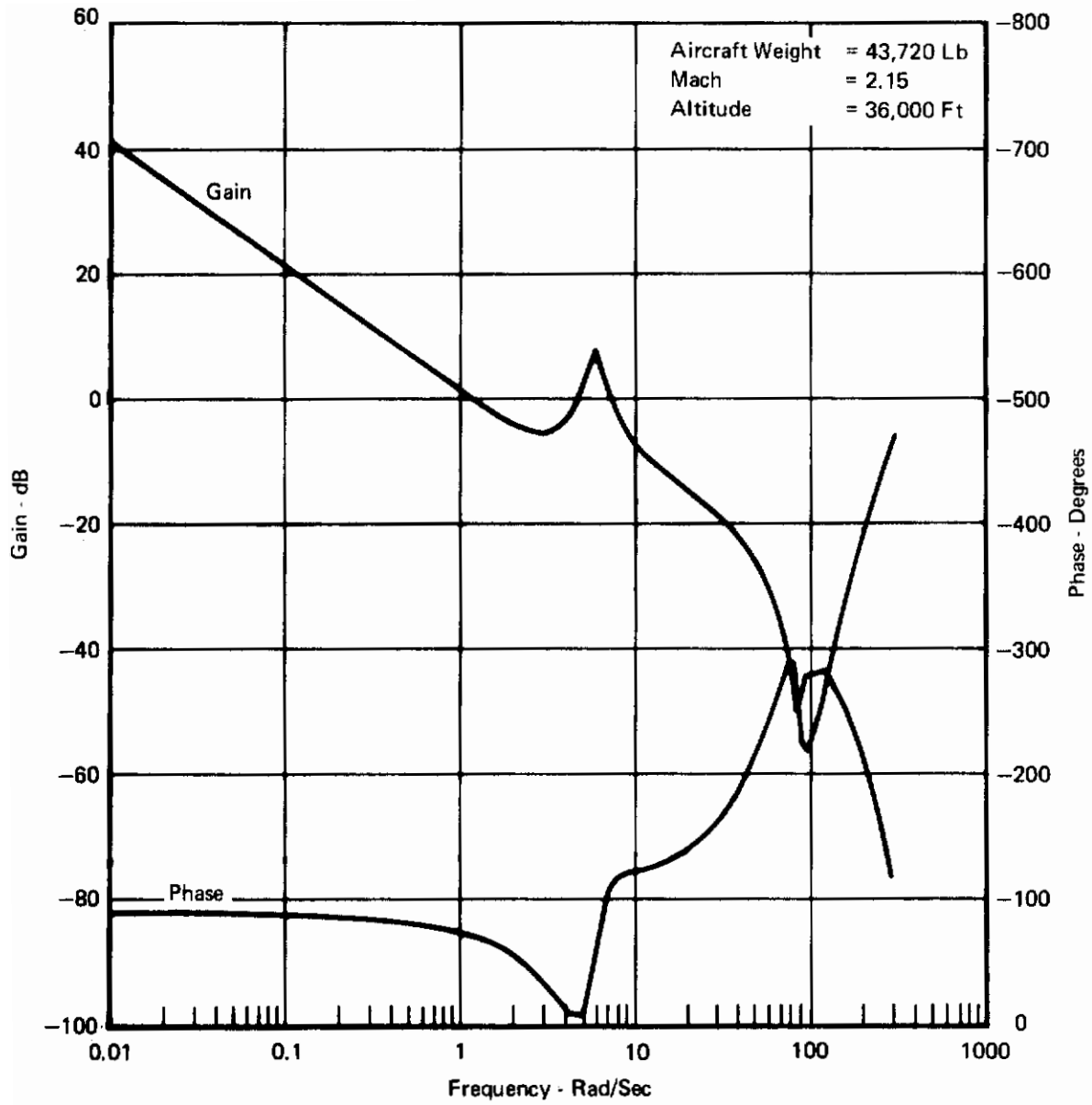

FIGURE 119
OPEN LOOP FREQUENCY RESPONSE (PHASE IIA,B)
NSS, $K_F = 0.25$

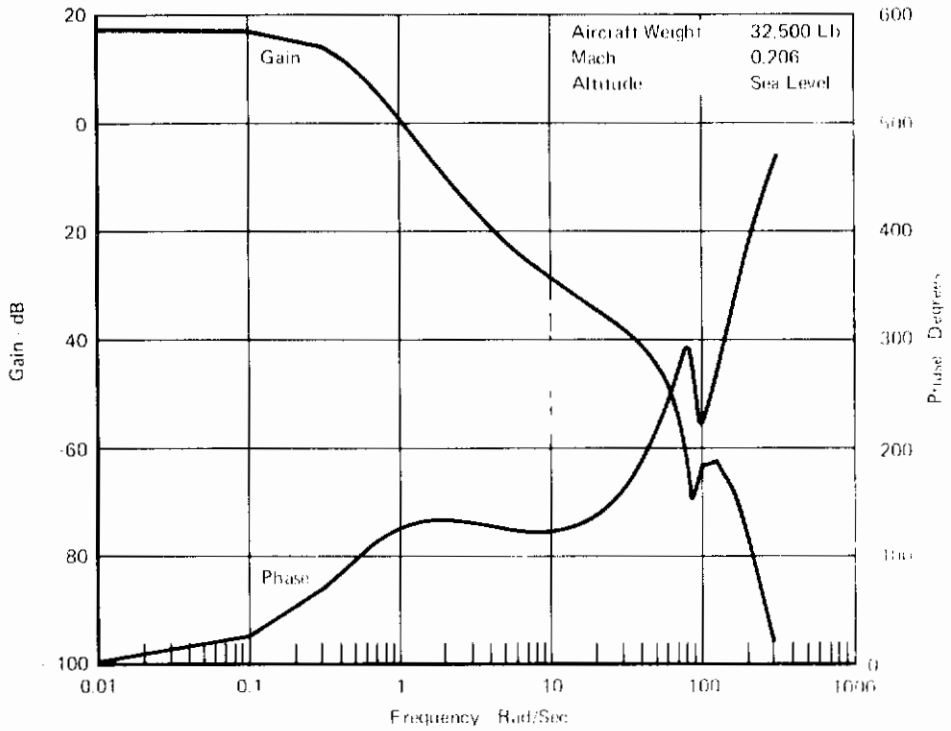

FIGURE 120
OPEN LOOP FREQUENCY RESPONSE (PHASE IIA, B)
TOL, $K_F = 0.25$

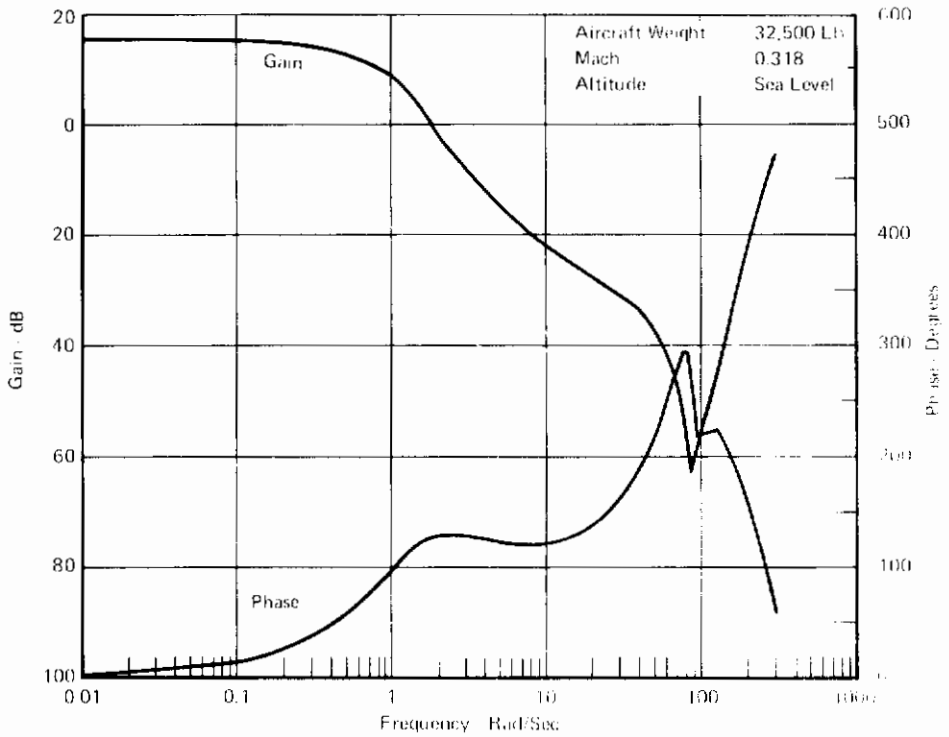

FIGURE 121
OPEN LOOP FREQUENCY RESPONSE (PHASE IIA, B)
TOL, $K_F = 0.25$

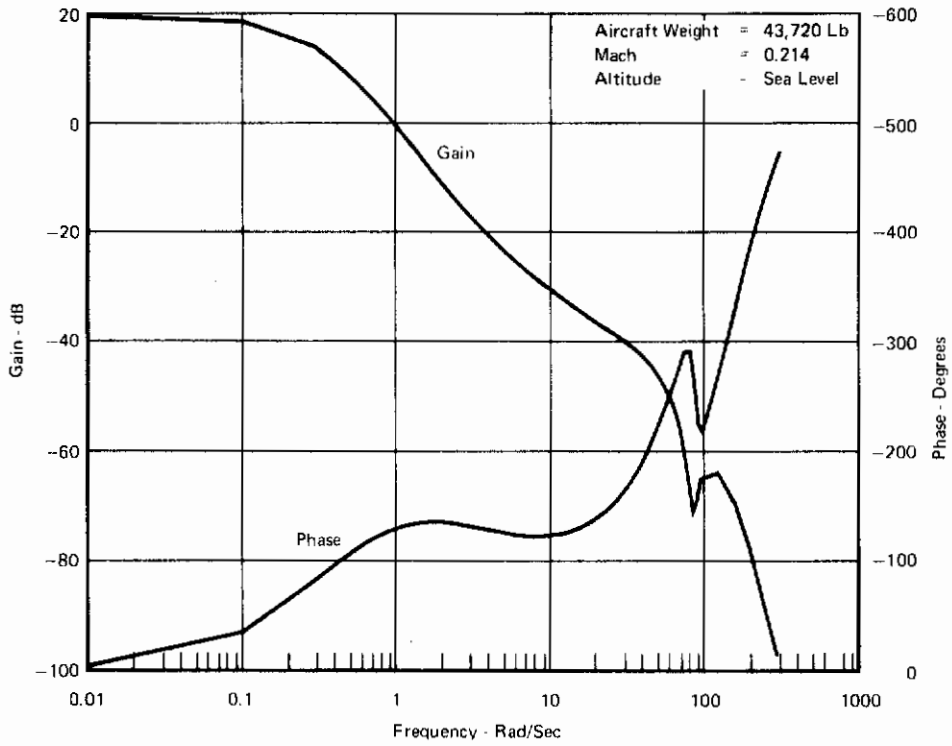

FIGURE 122
OPEN LOOP FREQUENCY RESPONSE (PHASE IIA, B)
TOL, K_F = 0.25

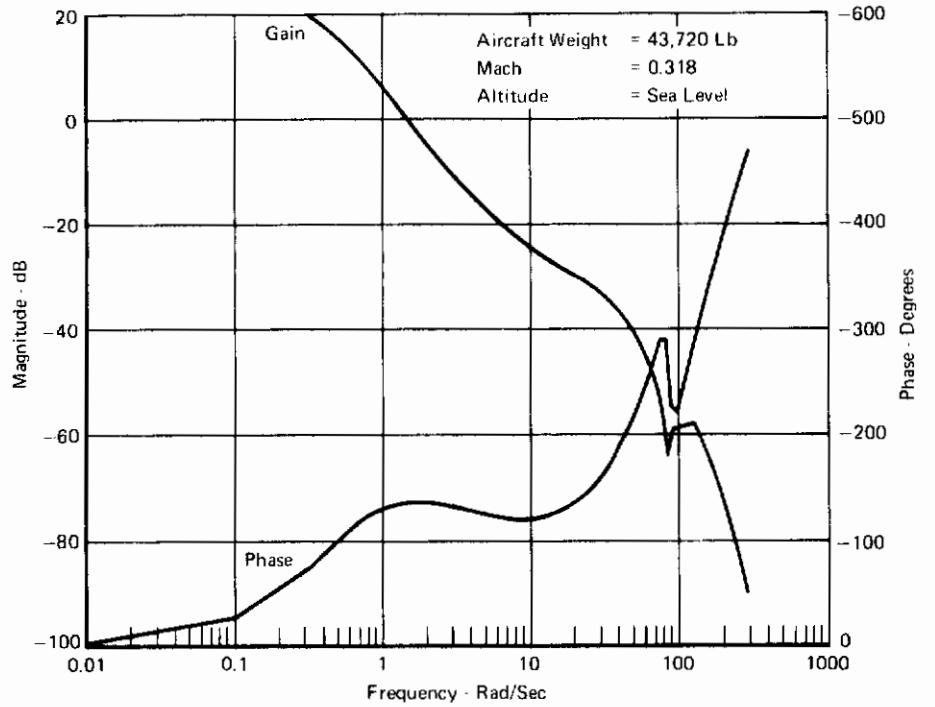

FIGURE 123
OPEN LOOP FREQUENCY RESPONSE (PHASE IIA, B)
TOL, K_F = 0.25

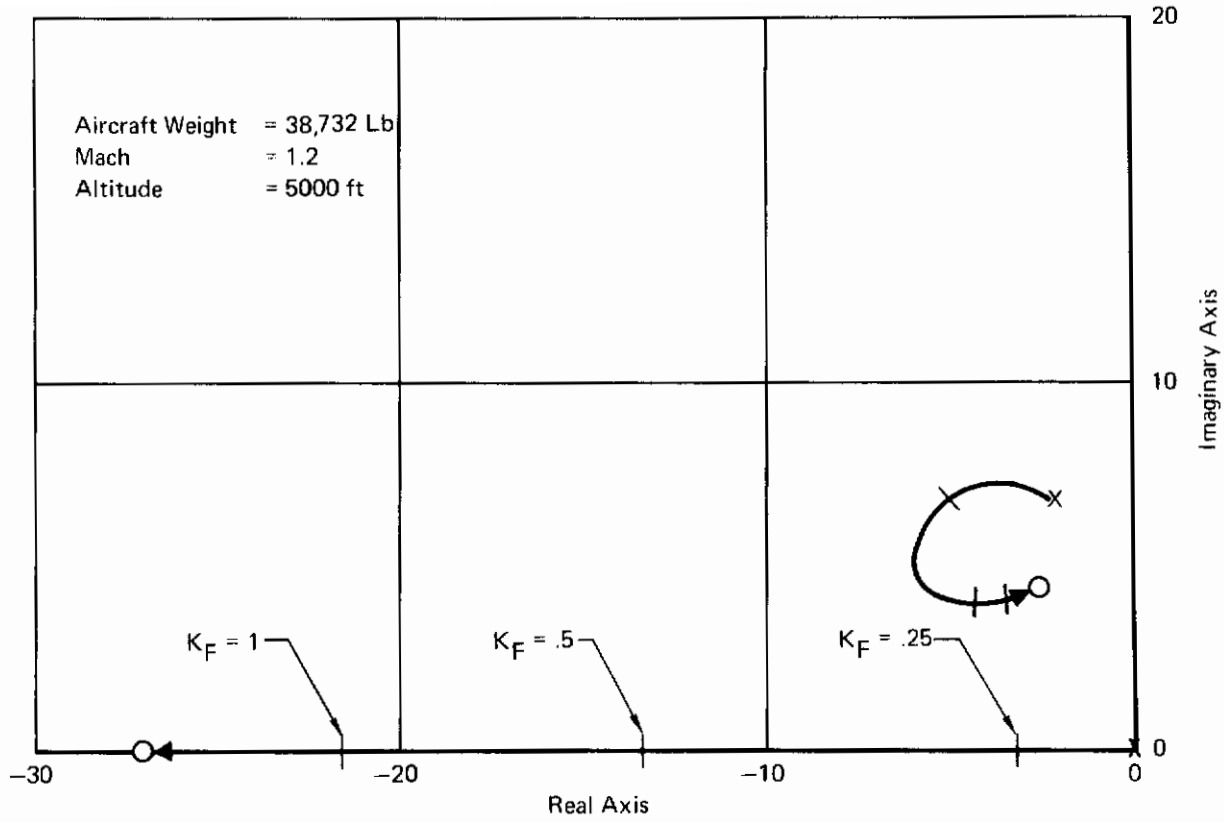

FIGURE 124
SHORT PERIOD ROOT LOCUS (PHASE II A, B)
Adaptive Gains
NSS

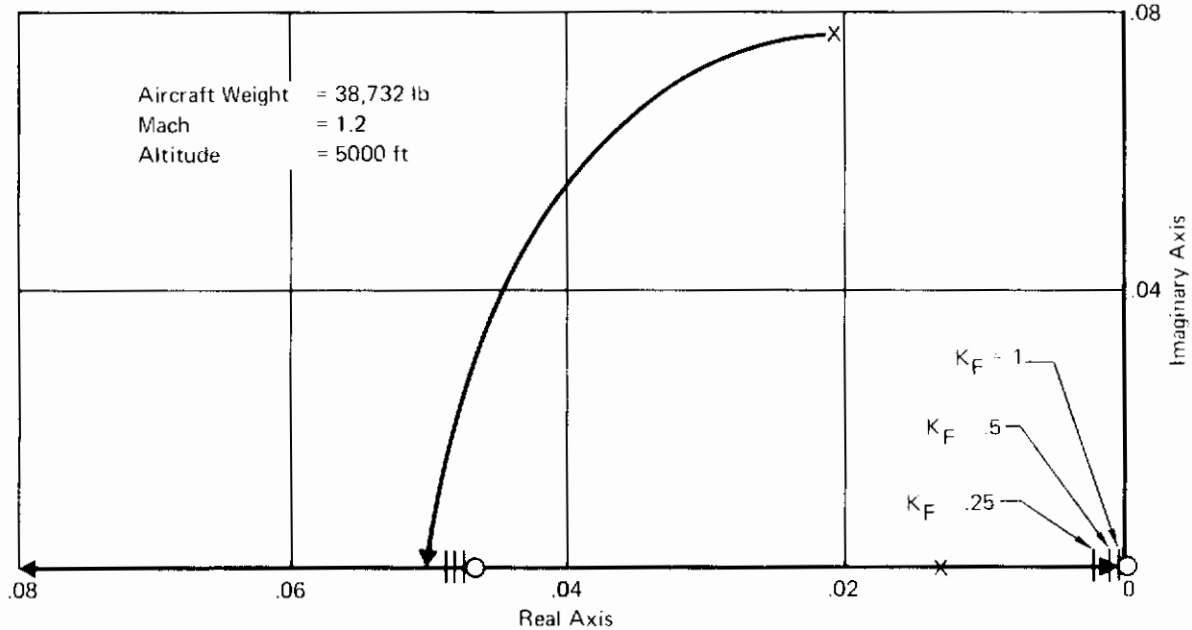

FIGURE 125
PHUGOID ROOT LOCUS (PHASE II A, B)
Adaptive Gains
NSS

Aircraft Weight = 38,732 Lb
Adaptive Gains
NSS

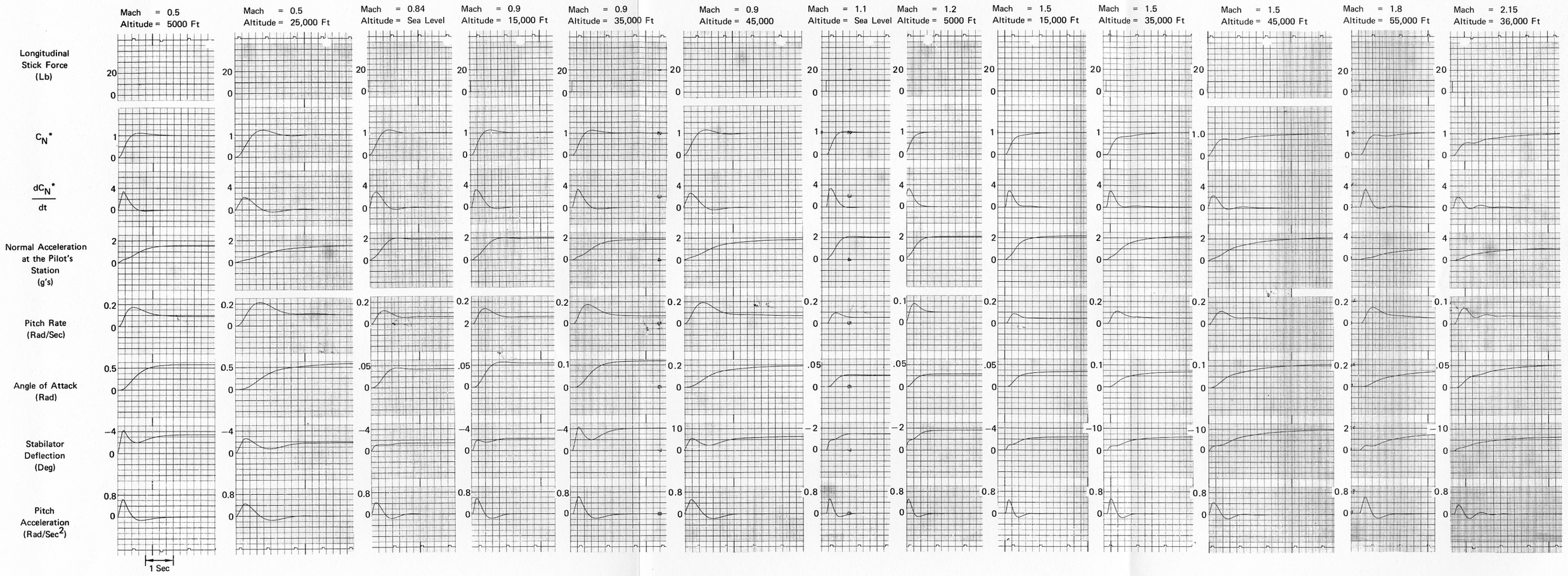

FIGURE 126
SFCS LONGITUDINAL CONTROL SYSTEM RESPONSE TO A STEP OF STICK FORCE

Aircraft Weight = 43,720 Lb
Adaptive Gains
NSS

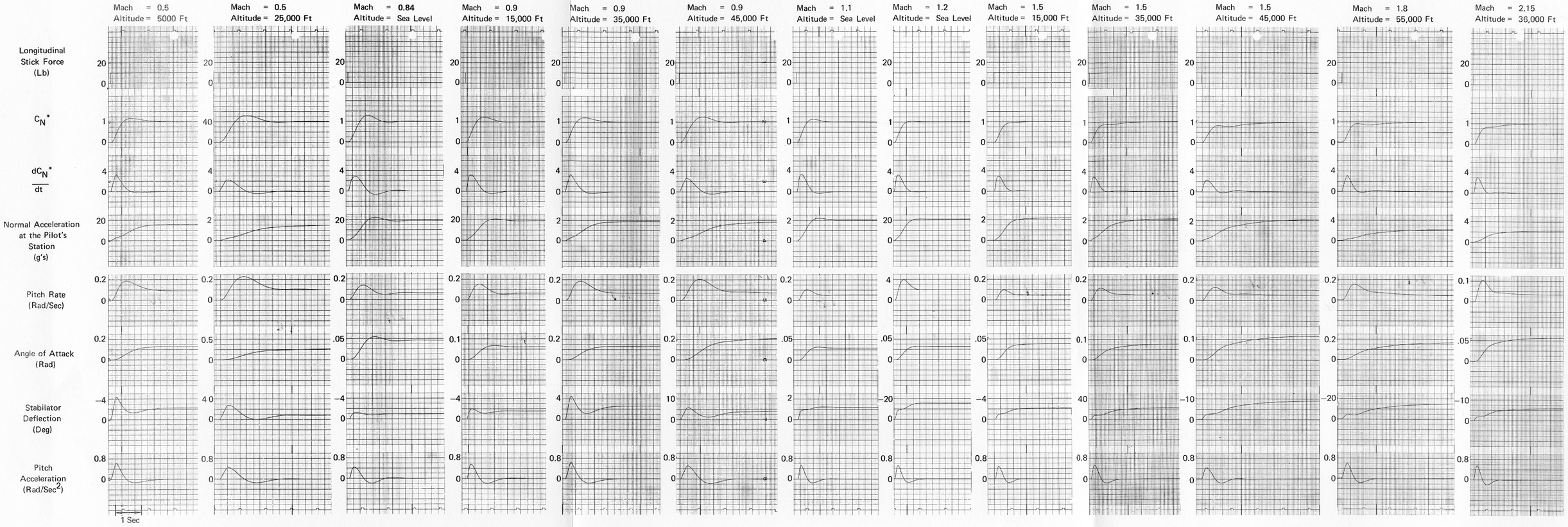

FIGURE 127
SFCS LONGITUDINAL CONTROL SYSTEM RESPONSE TO A STEP OF STICK FORCE

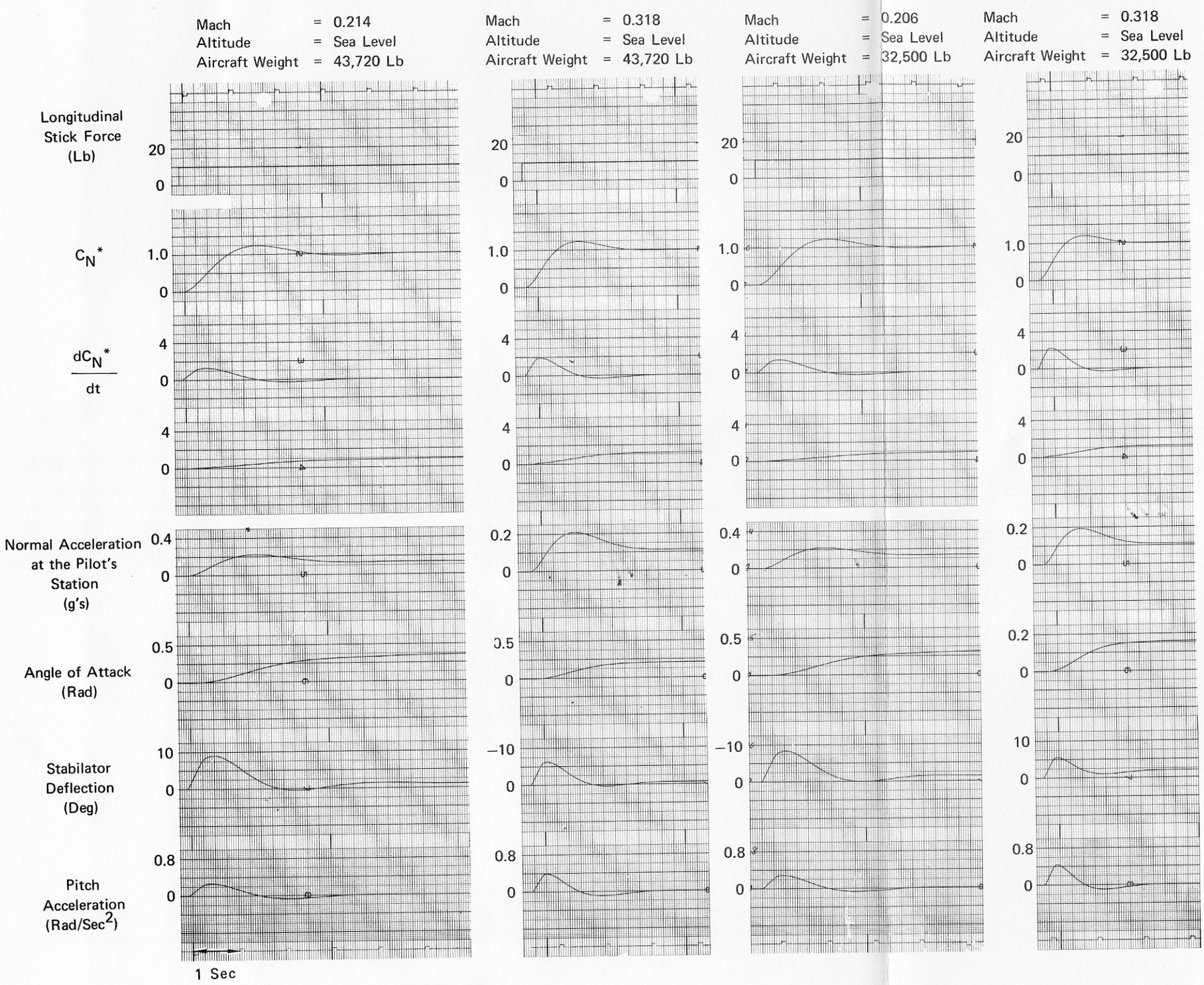

FIGURE 128
SFCS LONGITUDINAL CONTROL SYSTEM RESPONSE TO A STEP OF STICK FORCE

Aircraft Weight = 38,732 Lb
Altitude = 5000 Ft
Mach = 0.5
Fixed Gain
K_F = 0.25

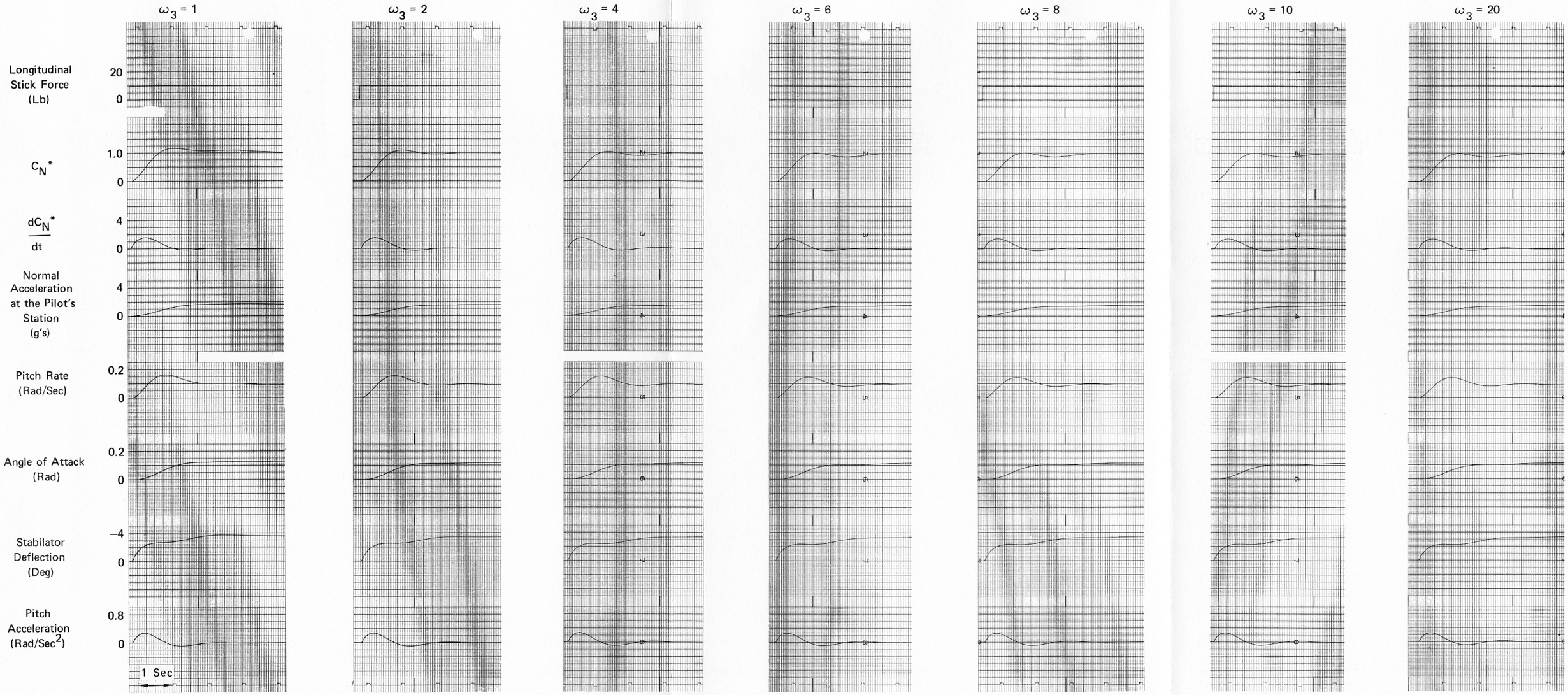

FIGURE 129
RESPONSES FOR VARIATIONS IN THE ACCELEROMETER LAG FILTER BREAK FREQUENCY

Aircraft Weight = 38,732 Lb
Altitude = 5000 Ft
Mach = 1.2
Fixed Gain
$K_F = 0.25$

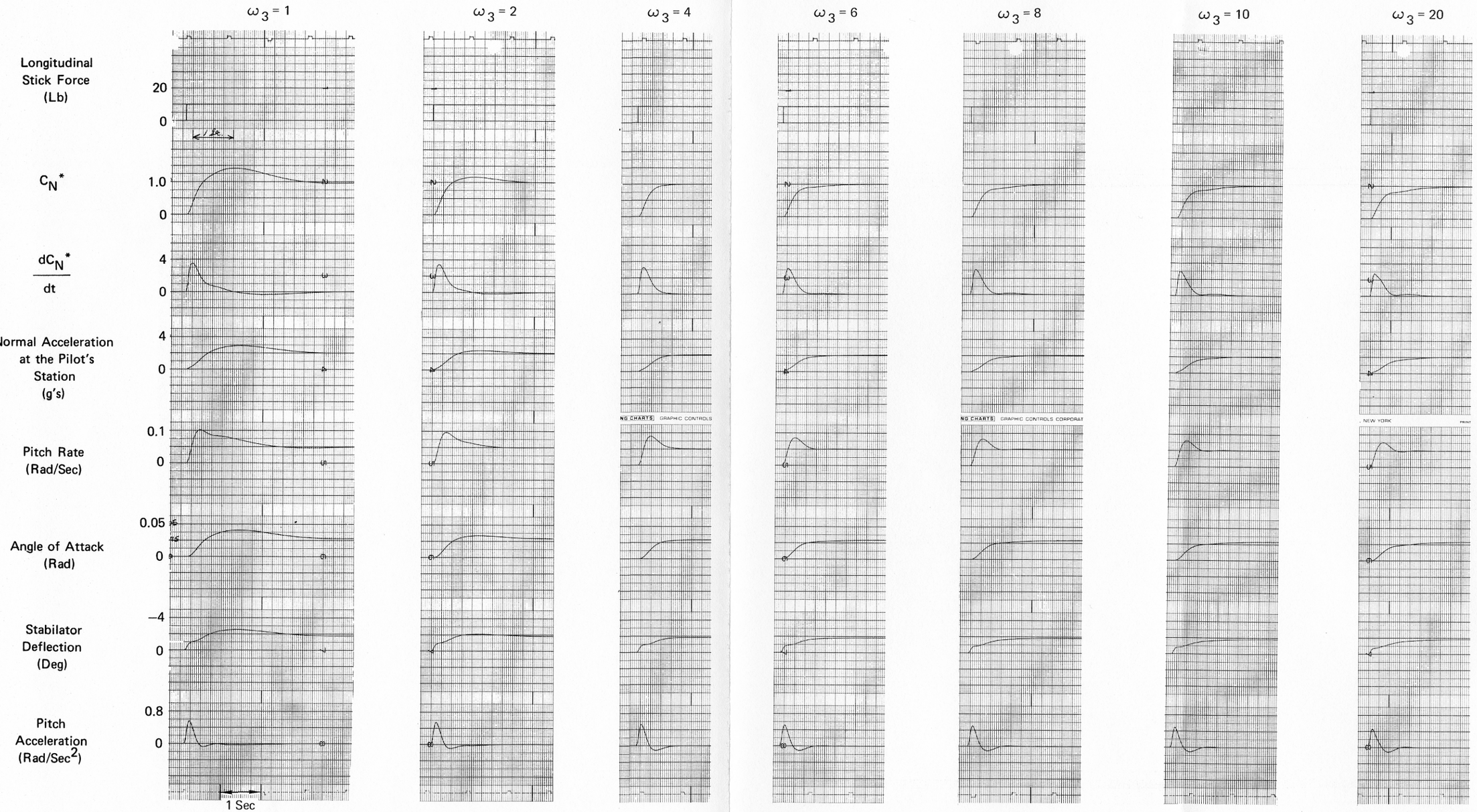

FIGURE 130
RESPONSES FOR VARIATIONS IN THE ACCELEROMETER LAG FILTER BREAK FREQUENCY

APPENDIX III

LONGITUDINAL STRUCTURAL STABILITY ANALYSIS

1. AEROELASTIC EQUATIONS OF MOTION

The Aeroelastic Equations of Motion are presented in Figure 131. The equations describe aircraft pitch axis motion and the significant structural body bending for small perturbation of the aircraft from straight and level flight. Equations (1) and (2) represent the two-degree-of-freedom, short period dynamic characteristics and include aeroelastic coupling. Equations (3), (4) and (5) are the structural body bending equations. Equations (6) and (7) provide for computation of aircraft pitch rate and normal acceleration that will be sensed at the locations of the pitch rate gyro and normal accelerometer. The coefficients for the equations of motion are presented in Table XI.

Since the motion of the aircraft with respect to its body axis is sensed by the pitch rate gyro and normal accelerometer, structural coupling with the rigid airframe exists when these devices detect structural modes at frequencies below the cut-off frequency of the aircraft control system. The effects of aeroelastic coupling due to the intermingling of the structural frequencies with the rigid body control frequencies could produce extraneous control signals which degrade aircraft handling qualities and controllability if these effects were not considered in the system design.

From equations (6) and (7), it is seen that the adverse effects of structural coupling may be reduced by careful selection of the control system's sensor locations; that is, selection of locations which tend to reduce the variables ϕ_1, ϕ_2, and ϕ_3 for normal acceleration and the derivatives $\frac{\partial \phi_1}{\partial x}$, $\frac{\partial \phi_2}{\partial x}$, and $\frac{\partial \phi_3}{\partial x}$ for pitch rate. The variables ϕ_1, ϕ_2, are the mode shapes of the significant structural modes of the aircraft and $\frac{\partial \phi_1}{\partial x}$, $\frac{\partial \phi_2}{\partial x}$, $\frac{\partial \phi_3}{\partial x}$ represent rate of change of ϕ_1, ϕ_2, and ϕ_3. A plot of normalized ϕ_1, ϕ_2, and ϕ_3 versus fuselage station is shown in Figure 132. If the assumption is made that the structural mode shapes may be represented by simple harmonic motion, then a reduction of structural mode coupling may be obtained by locating the accelerometers on nodal points, and the rate gyros on antinodal points. Based on this consideration and space available on the test aircraft, three locations for the pitch rate gyro, F.S. (Fuselage Station, in inches) 179, 313, and 383, were selected for study. The locations chosen for the accelerometer were F.S. 77 and F.S. 24.

The derivatives $\partial\phi_1/\partial x$, $\partial\phi_2/\partial x$, $\partial\phi_3/\partial x$ and the variables ϕ_1, ϕ_2, and ϕ_3 are presented in Figure 133. From these data, F.S. 383 appears to be the best location for the pitch rate gyro since the slope, $\partial\phi_1/\partial x$, is zero at this location. This means that the lowest frequency structural mode, Stabilator Bending, should not add appreciably to the rigid body pitch rate signal. Similarly, F.S. 77 appears to be the better location for the normal accelerometer since the variables ϕ_1, ϕ_2, and ϕ_3 are less than their respective values at F.S. 24. The data in

(1) $\dot{\alpha} - \dot{\theta} = Z_{\alpha}\,\alpha + Z_{\dot{\theta}}\,\dot{\theta} + Z_{\dot{\eta}_1}\,\dot{\eta}_1 + Z_{\eta_1}\,\eta_1 + Z_{\dot{\eta}_2}\,\dot{\eta}_2 + Z_{\eta_2}\,\eta_2 + Z_{\dot{\eta}_3}\,\dot{\eta}_3 + Z_{\eta_3}\,\eta_3 + Z_{\ddot{\delta}}\,\ddot{\delta} + Z_{\dot{\delta}}\,\dot{\delta} + Z_{\delta}\,\delta$

(2) $\ddot{\theta} = M_{\alpha}\,\alpha + M_{\dot{\alpha}}\,\dot{\alpha} + M_{\dot{\theta}}\,\dot{\theta} + M_{\dot{\eta}_1}\,\dot{\eta}_1 + M_{\eta_1}\,\eta_1 + M_{\dot{\eta}_2}\,\dot{\eta}_2 + M_{\eta_2}\,\eta_2 + M_{\dot{\eta}_3}\,\dot{\eta}_3 + M_{\eta_3}\,\eta_3 + M_{\ddot{\delta}}\,\ddot{\delta} + M_{\dot{\delta}}\,\dot{\delta} + M_{\delta}\,\delta$

(3) $\ddot{\eta}_1 = F_{\alpha}\,\alpha + F_{\dot{\theta}}\,\dot{\theta} + F_{\dot{\eta}_1}\,\dot{\eta}_1 + F_{\eta_1}\,\eta_1 + F_{\dot{\eta}_2}\,\dot{\eta}_2 + F_{\eta_2}\,\eta_2 + F_{\dot{\eta}_3}\,\dot{\eta}_3 + F_{\eta_3}\,\eta_3 + F_{\ddot{\delta}}\,\ddot{\delta} + F_{\dot{\delta}}\,\dot{\delta} + F_{\delta}\,\delta$

(4) $\ddot{\eta}_2 = G_{\alpha}\,\alpha + G_{\dot{\theta}}\,\dot{\theta} + G_{\dot{\eta}}\,\dot{\eta}_1 + G_{\eta_1}\,\eta_1 + G_{\dot{\eta}_2}\,\dot{\eta}_2 + G_{\eta_2}\,\eta_2 + G_{\dot{\eta}_3}\,\eta_3 + G_{\eta_3}\,\eta_3 + G_{\ddot{\delta}}\,\ddot{\delta} + G_{\dot{\delta}}\,\dot{\delta} + G_{\delta}\delta$

(5) $\ddot{\eta}_3 = H_{\alpha}\,\alpha + H_{\dot{\theta}}\,\dot{\theta} + H_{\dot{\eta}_1}\,\dot{\eta}_1 + H_{\eta_1}\,\eta_1 + H_{\dot{\eta}_2}\,\dot{\eta}_2 + H_{\eta_2}\,\eta_2 + H_{\dot{\eta}_3}\,\dot{\eta}_3 + H_{\eta_3}\,\eta_3 + H_{\ddot{\delta}}\,\ddot{\delta} + H_{\dot{\delta}}\,\dot{\delta} + H_{\delta}\,\delta$

(6) $\dot{\theta}_{M_j} = \dot{\theta} + [\partial\phi_1/\partial X]_j\,\dot{\eta}_1 + [\partial\phi_2/\partial X]_j\,\eta_2 + [\partial\phi_3/\partial X]_j\,\eta_3$

(7) $N_{Z_i} = \left\{ V(\dot{\theta} - \dot{\alpha}) + [(\ell_{cg} - i)/12]\,\ddot{\theta} - [\phi_1]_i\,\ddot{\eta}_1 - [\phi_2]_i\,\ddot{\eta}_2 - [\phi_3]_i\,\ddot{\eta}_3 \right\} \frac{1}{32.2}$

i = Accelerometer Fuselage Station Location

j = Pitch Rate Gyro Fuselage Station Location

FIGURE 131

LONGITUDINAL AEROELASTIC EQUATIONS OF MOTION

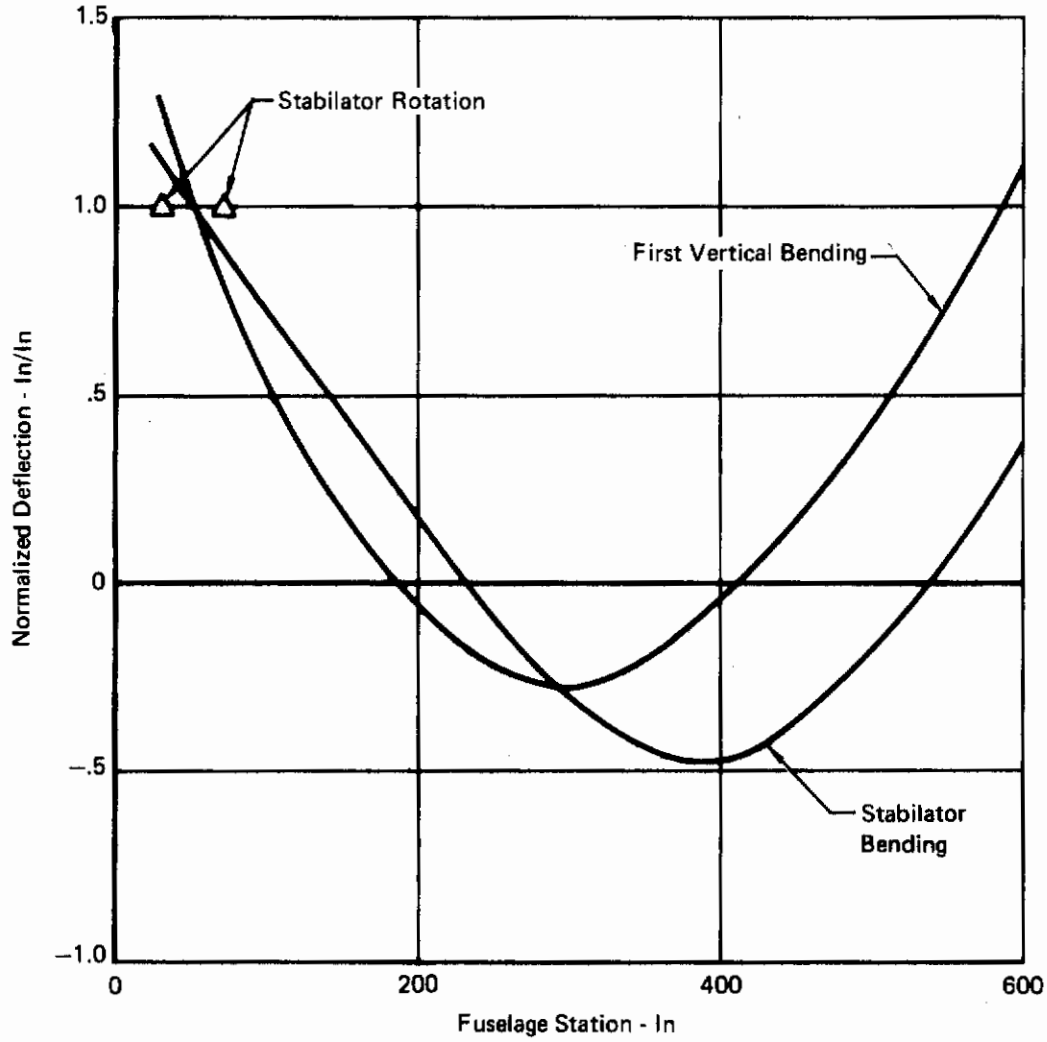

FIGURE 132
LONGITUDINAL STRUCTURAL MODE SHAPES

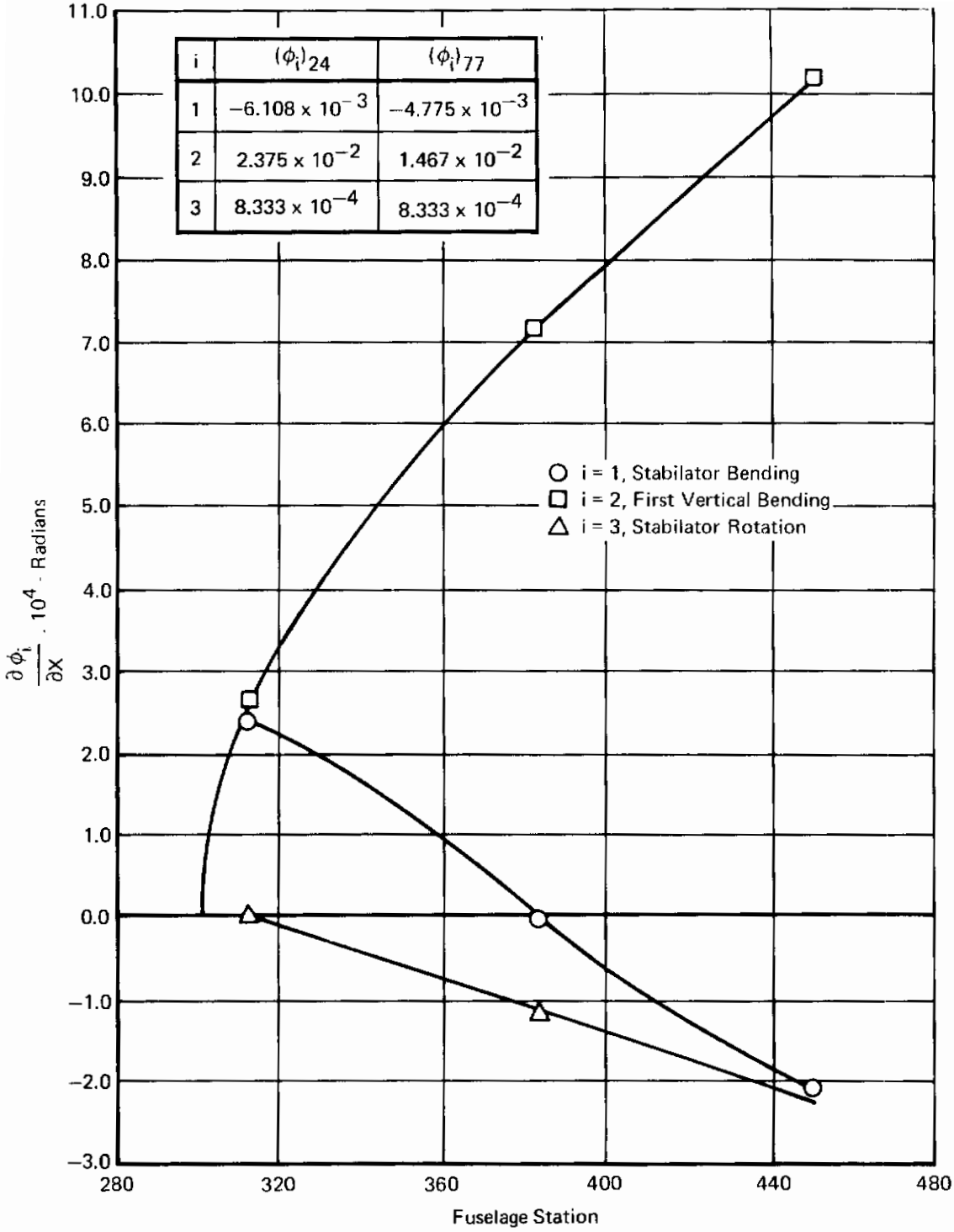

FIGURE 133
BENDING MODE SLOPE vs FUSELAGE STATION

TABLE XI

COEFFICIENTS FOR LONGITUDINAL EQUATIONS OF MOTION

Dimension		Z_a 1/Sec	$Z_{\dot\theta}$ Dimensionless	$Z_{\dot\eta_1}$ Dimensionless	Z_{η_1} 1/Sec	$Z_{\dot\eta_2}$ Dimensionless	Z_{η_2} 1/Sec	$Z_{\dot\eta_3}$ Dimensionless	Z_{η_3} 1/Sec	$Z_{\dot\delta_e^*}$ Sec	$Z_{\dot\delta}$ Dimensionless	Z_δ 1/Sec	M_a 1/Sec^2	$M_{\dot a}$ 1/Sec	$M_{\dot\theta}$ 1/Sec	$M_{\dot\eta_1}$ 1/Sec	M_{η_1} 1/Sec^2	$M_{\dot\eta_2}$ 1/Sec	M_{η_2} 1/Sec^2	$M_{\dot\eta_3}$ 1/Sec	M_{η_3} 1/Sec^2	M_δ 1/Sec^2	$M_{\dot\delta}$ 1/Sec	$M_{\dot\delta_e^*}$ Dimensionless	F_a 1/Sec^2	F_θ 1/Sec	$F_{\dot\eta_1}$ 1/Sec	F_{η_1} 1/Sec^2	$F_{\dot\eta_2}$ 1/Sec	F_{η_2} 1/Sec^2	$F_{\dot\eta_3}$ 1/Sec	F_{η_3} 1/Sec^2
0.5M - 5K	38,732 Lb	−.8213	-8.587×10^{-3}	-3.834×10^{-7}	-6.076×10^{-4}	-1.711×10^{-7}	-7.056×10^{-4}	-1.488×10^{-6}	-5.653×10^{-3}	-5.918×10^{-6}	-3.455×10^{-5}	−.1025	−4.497	−.2630	−.5937	-4.298×10^{-5}	−.06727	-2.062×10^{-5}	−.07896	-1.688×10^{-4}	−.6144	−11.02	-3.910×10^{-3}	-8.999×10^{-4}	-3.360×10^{3}	−180.5	−1.719	-5.039×10^{3}	−.2808	-7.901×10^{2}	−1.115	-4.193×10^{3}
	43,720 Lb	−.7276	-7.607×10^{-3}	-3.396×10^{-7}	-5.383×10^{-4}	-1.516×10^{-7}	-6.252×10^{-4}	-1.318×10^{-6}	-5.008×10^{-3}	-5.244×10^{-6}	-3.061×10^{-5}	−.09078	−2.375	−.2442	−.5511	-3.970×10^{-5}	−.06215	-1.906×10^{-5}	−.07295	-1.560×10^{-4}	−.5676	−10.18	-3.612×10^{-3}	-8.221×10^{-4}	-3.360×10^{3}	−180.5	−1.719	-5.039×10^{3}	−.2808	-7.901×10^{2}	−1.115	-4.193×10^{3}
0.5M - 25K	38,732 Lb	−.4096	-4.754×10^{-3}	-2.761×10^{-7}	-2.923×10^{-4}	-1.233×10^{-7}	-3.394×10^{-4}	-1.072×10^{-6}	-2.719×10^{-3}	-6.390×10^{-6}	-2.489×10^{-5}	−.04929	−1.371	−.1454	−.3099	-2.867×10^{-5}	−.02997	-1.376×10^{-5}	−.03518	-1.127×10^{-4}	−.2737	−4.909	-2.609×10^{-3}	-8.999×10^{-4}	-2.076×10^{3}	−120.4	−1.590	-4.705×10^{3}	−.1874	−352.0	−.7441	-1.868×10^{3}
	43,720 Lb	−.3628	-4.211×10^{-3}	-2.447×10^{-7}	-2.589×10^{-4}	-1.092×10^{-7}	-3.007×10^{-4}	-9.495×10^{-7}	-2.409×10^{-3}	-5.661×10^{-6}	-2.205×10^{-5}	−.04367	−.4403	−.1350	−.2877	-2.649×10^{-5}	−.02923	-1.271×10^{-5}	−.03250	-1.041×10^{-4}	−.2529	−4.535	-2.410×10^{-3}	-8.221×10^{-4}	-2.076×10^{3}	−120.4	−1.590	-4.705×10^{3}	−.1874	−352.0	−.7441	-1.868×10^{3}
0.9M - 15K	38,732 Lb	−1.231	-6.305×10^{-3}	-3.316×10^{-7}	-7.826×10^{-4}	-1.470×10^{-7}	-9.089×10^{-4}	-1.278×10^{-6}	-7.277×10^{-3}	-3.414×10^{-6}	-2.975×10^{-5}	−.1319	−13.01	−.3824	−.8201	-6.451×10^{-5}	−.1503	-3.077×10^{-5}	−.1765	-2.518×10^{-4}	−1.373	−24.62	-5.840×10^{-3}	-8.999×10^{-4}	-8.789×10^{3}	−271.8	−1.914	-5.785×10^{3}	−.4206	-1.766×10^{3}	−1.664	-9.370×10^{3}
	43,720 Lb	−1.090	-5.586×10^{-3}	-2.938×10^{-7}	-6.934×10^{-4}	-1.303×10^{-7}	-8.053×10^{-4}	-1.133×10^{-6}	-6.451×10^{-3}	-3.022×10^{-6}	-2.636×10^{-5}	−.1169	−7.394	−.3614	−.7614	-5.947×10^{-5}	−.1389	-2.843×10^{-5}	−.1630	-2.326×10^{-4}	−1.268	−22.75	-5.395×10^{-3}	-8.221×10^{-4}	-8.784×10^{3}	−271.8	−1.914	-5.785×10^{3}	−.4206	-1.766×10^{3}	−1.664	-9.370×10^{3}
0.9M - 35K	38,732 Lb	−.5960	-3.313×10^{-3}	-2.328×10^{-7}	-3.547×10^{-4}	-1.032×10^{-7}	-4.119×10^{-4}	-8.975×10^{-7}	-3.300×10^{-3}	-3.708×10^{-6}	-2.087×10^{-5}	−.05981	−5.205	−.1928	−.3983	-4.165×10^{-5}	−.06269	-1.987×10^{-5}	−.07359	-1.626×10^{-4}	−.5725	−10.27	-3.771×10^{-3}	-8.999×10^{-4}	-5.221×10^{3}	−175.5	−1.708	-4.998×10^{3}	−.2716	−736.3	−1.075	-3.907×10^{3}
	43,720 Lb	−.5280	-2.935×10^{-3}	-2.062×10^{-7}	-3.143×10^{-4}	-9.144×10^{-8}	-3.650×10^{-4}	-7.951×10^{-7}	-2.924×10^{-3}	-3.285×10^{-6}	-1.850×10^{-5}	−.05299	−2.712	−.1790	−.3698	-3.848×10^{-5}	−.05792	-1.836×10^{-5}	−.06798	-1.502×10^{-4}	−.5289	−9.486	-3.484×10^{-3}	-8.221×10^{-4}	-5.221×10^{3}	−175.5	−1.708	-4.998×10^{3}	−.2716	−736.3	−1.075	-3.907×10^{3}
0.9M - 45K	38,732 Lb	−.3730	-2.134×10^{-3}	-1.830×10^{-7}	-2.200×10^{-4}	-8.116×10^{-8}	-2.555×10^{-4}	-7.057×10^{-7}	-2.047×10^{-3}	-3.719×10^{-6}	-1.642×10^{-5}	−.03711	−3.238	−.1290	−.2495	-3.265×10^{-5}	−.03877	-1.558×10^{-5}	−.04551	-1.275×10^{-4}	−.3541	−6.351	-2.956×10^{-3}	-8.999×10^{-4}	-4.081×10^{3}	−137.6	−1.627	-4.784×10^{3}	−.2129	−455.4	−.8425	-2.416×10^{3}
	43,720 Lb	−.3304	-1.890×10^{-3}	-1.622×10^{-7}	-1.949×10^{-4}	-7.190×10^{-8}	-2.264×10^{-4}	-6.252×10^{-7}	-1.813×10^{-3}	-3.295×10^{-6}	-1.454×10^{-5}	−.03287	−1.707	−.1198	−.2316	-3.016×10^{-5}	.03521	-1.439×10^{-5}	−.04205	-1.177×10^{-4}	−.3271	−5.867	-2.731×10^{-3}	-8.221×10^{-4}	-4.081×10^{3}	−137.6	−1.627	-4.784×10^{3}	−.2129	−455.4	−.8425	-2.416×10^{3}
1.2M - 5K	38.732 Lb	−1.916	-6.214×10^{-3}	-4.046×10^{-7}	-1.639×10^{-3}	-1.686×10^{-7}	-1.928×10^{-3}	-1.059×10^{-6}	-1.387×10^{-2}	-2.466×10^{-6}	-2.742×10^{-5}	−.2756	−47.66	−.6248	−1.658	-1.117×10^{-4}	−.4503	-4.941×10^{-5}	−.5344	-2.955×10^{-4}	−3.759	−73.89	-7.665×10^{-3}	-8.999×10^{-4}	-2.267×10^{4}	−487.4	−2.351	-8.466×10^{3}	−.7135	-5.284×10^{3}	−1.919	-2.608×10^{4}
	43,720 Lb	−1.698	-5.505×10^{-3}	-3.585×10^{-7}	-1.452×10^{-3}	-1.494×10^{-7}	-1.708×10^{-3}	-9.380×10^{-7}	-1.229×10^{-2}	-2.185×10^{-6}	-2.429×10^{-5}	−.2442	−34.16	−.5800	−1.539	-1.032×10^{-4}	−.4160	-4.565×10^{-5}	−.4937	-2.730×10^{-4}	−3.473	−68.27	-7.081×10^{-3}	-8.221×10^{-4}	-2.267×10^{4}	−487.4	−2.351	-8.466×10^{3}	−.7135	-5.284×10^{3}	−1.919	-2.608×10^{4}
1.5M - 15K	38,732 Lb	−1.430	-3.033×10^{-3}	-2.874×10^{-7}	-1.121×10^{-3}	-1.326×10^{-7}	-1.320×10^{-3}	-8.765×10^{-7}	-9.494×10^{-3}	-2.048×10^{-6}	-2.164×10^{-5}	−.1886	−48.65	−.4288	−1.295	-9.550×10^{-5}	−.3711	-4.637×10^{-5}	−.4404	-2.941×10^{-4}	−3.103	−60.90	-7.264×10^{-3}	-8.999×10^{-4}	-2.187×10^{4}	−397.2	−2.194	-7.757×10^{3}	−.6285	-4.355×10^{3}	−1.888	-2.153×10^{4}
	43,720 Lb	−1.267	-2.688×10^{-3}	-2.546×10^{-7}	-9.936×10^{-4}	-1.175×10^{-7}	-1.169×10^{-3}	-7.766×10^{-7}	-8.411×10^{-3}	-1.814×10^{-6}	-1.914×10^{-5}	−.1671	−36.09	−.3981	−1.202	-8.823×10^{-5}	−.3429	-4.284×10^{-5}	−.4068	-2.717×10^{-4}	−2.867	−56.26	-6.771×10^{-3}	-8.221×10^{-4}	-2.187×10^{4}	−397.2	−2.194	-7.757×10^{3}	−.6285	-4.355×10^{3}	−1.888	-2.153×10^{4}
1.5M - 35K	38,732 Lb	−.7923	-2.209×10^{-3}	-2.014×10^{-7}	-5.080×10^{-4}	-9.292×10^{-8}	-5.977×10^{-4}	-6.143×10^{-7}	-4.300×10^{-3}	-2.224×10^{-6}	-1.516×10^{-5}	−.08543	−30.69	−.1669	−.6319	-6.161×10^{-5}	−.1547	-2.991×10^{-5}	−.1836	-1.897×10^{-4}	−1.294	−25.39	-4.686×10^{-3}	-8.999×10^{-4}	-1.299×10^{4}	−256.2	−1.888	-5.821×10^{3}	−.4054	-1.816×10^{3}	−1.218	-8.978×10^{3}
	43,720 Lb	−.7019	-1.957×10^{-3}	-1.785×10^{-7}	-4.501×10^{-4}	-8.232×10^{-8}	-5.296×10^{-4}	-5.442×10^{-7}	-3.810×10^{-3}	-1.971×10^{-6}	-1.343×10^{-5}	−.07569	−23.87	−.1550	−.5866	-5.692×10^{-5}	−.1429	-2.764×10^{-5}	−.1696	-1.753×10^{-4}	−1.195	−23.46	-4.329×10^{-3}	-8.221×10^{-4}	-1.299×10^{4}	−256.2	−1.888	-5.821×10^{3}	−.4054	-1.816×10^{3}	−1.218	-8.978×10^{3}
1.5M - 45K	38,732 Lb	−.5071	-1.550×10^{-3}	-1.590×10^{-7}	-3.156×10^{-4}	-7.334×10^{-8}	-3.714×10^{-4}	-4.848×10^{-7}	-2.672×10^{-3}	-2.235×10^{-6}	-1.197×10^{-5}	−.05309	−20.46	−.09746	−.4034	-4.839×10^{-5}	−09569	-2.350×10^{-5}	−.1135	-1.49×10^{-4}	−.8002	−15.70	-3.681×10^{-3}	-8.999×10^{-4}	-1.015×10^{4}	−201.3	−1.769	-5.292×10^{3}	−.3184	-1.123×10^{3}	−.9568	-5.552×10^{3}
	43,720 Lb	−.4492	-1.373×10^{-3}	-1.408×10^{-7}	-2.796×10^{-4}	-6.497×10^{-8}	-3.291×10^{-4}	-4.295×10^{-7}	-2.367×10^{-3}	-1.980×10^{-6}	-1.060×10^{-5}	−.04703	−16.05	−.09048	−.3745	-4.470×10^{-5}	−.08840	-2.171×10^{-5}	−.1049	-1.377×10^{-4}	−.7392	−14.51	-3.401×10^{-3}	-8.221×10^{-4}	-1.015×10^{4}	−201.3	−1.769	-5.292×10^{3}	−.3184	-1.123×10^{3}	−.9568	-5.552×10^{3}
1.8M - 55K	38,732 Lb	−.3153	-6.626×10^{-4}	-1.039×10^{-7}	-1.786×10^{-4}	-5.350×10^{-8}	-2.101×10^{-4}	-3.711×10^{-7}	-1.512×10^{-3}	-1.863×10^{-6}	-8.762×10^{-6}	−.03003	−16.48	−.02293	−.2328	-3.791×10^{-5}	−.06495	-2.038×10^{-5}	−.07704	-1.366×10^{-4}	−.5442	−10.66	-3.224×10^{-3}	-8.999×10^{-4}	-8.765×10^{3}	−148.2	−1.670	-5.017×10^{3}	−.2582	−761.8	−.8679	-3.777×10^{3}
	43,720 Lb	−.2793	-5.870×10^{-4}	-9.202×10^{-8}	-1.582×10^{-4}	-4.740×10^{-8}	-1.862×10^{-4}	-3.288×10^{-7}	-1.339×10^{-3}	-1.651×10^{-6}	-7.763×10^{-6}	−.02661	−13.11	−.02129	−.2161	-3.502×10^{-5}	−.06000	-1.883×10^{-5}	−.07117	-1.262×10^{-4}	−.5028	−9.846	-2.978×10^{-3}	-8.221×10^{-4}	-8.765×10^{3}	−148.2	−1.670	-5.017×10^{3}	−.2582	−761.8	−.8679	-3.777×10^{3}
2.15M-36K	38,732 Lb	−.7810	-7.774×10^{-4}	-1.374×10^{-7}	-3.994×10^{-4}	-7.931×10^{-8}	-4.700×10^{-4}	-5.739×10^{-7}	-3.381×10^{-3}	-1.560×10^{-6}	-1.303×10^{-5}	−.06717	−44.92	.05486	−.4983	-5.985×10^{-5}	−.1734	-3.578×10^{-5}	−.2056	-2.519×10^{-4}	−1.458	−28.46	-5.711×10^{-3}	-8.999×10^{-4}	-1.483×10^{4}	−216.9	−1.857	-5.988×10^{3}	−.4237	-2.038×10^{3}	−1.586	-1.012×10^{4}
	43,720 Lb	−.6919	-6.887×10^{-4}	-1.217×10^{-7}	-3.539×10^{-4}	-7.027×10^{-8}	-4.164×10^{-4}	-5.084×10^{-7}	-2.995×10^{-3}	-1.382×10^{-6}	-1.156×10^{-5}	−.05951	−35.21	.05093	−.4627	-5.529×10^{-5}	−.1610	-3.305×10^{-5}	−.1928	-2.328×10^{-4}	−1.367	−26.69	-5.287×10^{-3}	-8.221×10^{-4}	-1.483×10^{4}	−216.9	−1.857	-5.988×10^{3}	−.4237	-2.033×10^{3}	−1.586	-1.012×10^{4}

Dimension		$F_{\dot\delta_e^*}$ Dimensionless	$F_{\dot\delta}$ 1/Sec	F_δ 1/Sec^2	G_a 1/Sec^2	$G_{\dot\theta}$ 1/Sec	$G_{\dot\eta_1}$ 1/Sec	G_{η_1} 1/Sec^2	$G_{\dot\eta_2}$ 1/Sec	G_{η_2} 1/Sec^2	$G_{\dot\eta_3}$ 1/Sec	G_{η_3} 1/Sec^2	$G_{\dot\delta_e^*}$ Dimensionless	$G_{\dot\delta}$ 1/Sec	G_δ 1/Sec^2	H_a 1/Sec^2	$H_{\dot\theta}$ 1/Sec	$H_{\dot\eta_1}$ 1/Sec	H_{η_1} 1/Sec^2	$H_{\dot\eta_2}$ 1/Sec	H_{η_2} 1/Sec^2	$H_{\dot\eta_3}$ 1/Sec	H_{η_3} 1/Sec^2	$H_{\dot\delta_e^*}$ Dimensionless	$H_{\dot\delta}$ 1/Sec	H_δ 1/Sec^2	$(\partial\phi_1/\partial X)_{383}$ Dimensionless	$(\partial\phi_2/\partial X)_{383}$ Dimensionless	$(\partial\phi_3/\partial X)_{383}$ Dimensionless	$(\phi_1)_{77}$ Ft	$(\phi_2)_{77}$ Ft	$(\phi_3)_{77}$ Ft	ℓ_{cg} Inches
0.5M - 5K	38,732 Lb	−22.799	−28.60	-7.383×10^{4}	−166.6	−9.926	−.05595	−86.07	−3.657	-7.652×10^{3}	−.05236	−236.5	−5.612	−2.386	-3.662×10^{3}	880.6	36.45	.03041	103.8	−.01180	124.9	−16.51	-2.00×10^{4}	−23.43	−3.356	1.935×10^{4}	0	7.11×10^{-4}	-1.143×10^{-4}	-4.475×10^{-3}	1.666×10^{-2}	8.33×10^{-4}	320.4
	43,720 Lb	−22.799	−28.60	-7.383×10^{4}	−166.6	−9.926	−.05595	−86.07	−3.657	-7.652×10^{3}	−.05236	−236.5	−5.612	−2.386	-3.662×10^{3}	880.6	36.45	.03041	103.8	−.01180	124.9	−16.51	-2.00×10^{4}	−23.43	−3.356	1.935×10^{4}	0	7.11×10^{-4}	-1.143×10^{-4}	-4.475×10^{-3}	1.666×10^{-2}	8.33×10^{-4}	326.9
0.5M - 25K	38,732 Lb	−22.799	−19.08	-3.289×10^{4}	−102.9	−6.623	−.03733	−38.35	−3.634	-7.578×10^{3}	−.03493	−105.4	−5.612	−1.592	-1.631×10^{3}	544.2	24.32	.02029	46.25	-7.875×10^{-3}	55.67	−16.42	-2.043×10^{4}	−23.43	−2.239	8.623×10^{3}	0						320.4
	43,720 Lb	−22.799	−19.08	-3.289×10^{4}	−102.9	−6.623	−.03733	−38.35	−3.634	-7.578×10^{3}	−.03493	−105.4	−5.612	−1.592	-1.631×10^{3}	544:2	24.32	.02029	46.25	-7.875×10^{-3}	55.67	−16.42	-2.043×10^{4}	−23.43	−2.239	8.623×10^{3}	0						326.9
0.9M - 15K	38,732 Lb	−22.799	−42.80	-1.650×10^{5}	−435.8	−14.96	−.08414	−192.3	−3.690	-7.820×10^{3}	−.07855	−528.3	−5.612	−3.594	-8.184×10^{3}	2.303×10^{3}	55.10	.04634	232.0	−.01728	279.0	−16.64	-1.906×10^{4}	−23.43	−4.918	4.325×10^{4}	0						320.4
	43,720 Lb	−22.799	−42.80	-1.650×10^{5}	−435.8	−14.96	−.08414	−192.3	−3.690	-7.820×10^{3}	−.07855	−528.3	−5.612	−3.594	-8.184×10^{3}	2.303×10^{3}	55.10	.04634	232.0	−.01728	279.0	−16.64	-1.906×10^{4}	−23.43	−4.918	4.325×10^{4}	0						326.9
0.9M - 35K	38,732 Lb	−22.799	−27.63	-6.880×10^{4}	−258.9	−9.661	−.05433	−80.21	−3.655	-7.644×10^{3}	−.05072	−220.3	−5.612	−2.320	-3.413×10^{3}	1.368×10^{3}	35.58	.02992	96.73	−.01116	116.3	−16.49	-2.005×10^{4}	−23.43	−3.175	1.803×10^{4}	0						320.4
	43,720 Lb	−22.799	−27.63	-6.880×10^{4}	−258.9	−9.661	−.05433	−80.21	−3.655	-7.644×10^{3}	−.05072	−220.3	−5.612	−2.320	-3.413×10^{3}	1.368×10^{3}	35.58	.02992	96.73	−.01116	116.3	−16.49	-2.005×10^{4}	−23.43	−3.175	1.803×10^{4}	0						326.9
0.9M - 45K	38,732 Lb	−22.799	−21.66	-4.255×10^{4}	−202.4	−7.574	−.04259	−49.61	−3.641	-7.596×10^{3}	−.03976	−136.2	−5.612	−1.819	-2.111×10^{3}	1.070×10^{3}	27.89	.02346	59.83	-8.749×10^{-3}	71.97	−16.44	-2.032×10^{4}	−23.43	−2.489	1.115×10^{4}	0						320.4
	43,720 Lb	−22.799	−21.66	-4.255×10^{4}	−202.4	−7.574	−.04259	−49.61	−3.641	-7.596×10^{3}	−.03976	−136.2	−5.612	−1.819	-2.111×10^{3}	1.070×10^{3}	27.89	.02346	59.83	-8.749×10^{-3}	71.97	−16.44	-2.032×10^{4}	−23.43	−2.489	1.115×10^{4}	0						326.9
1.2M - 5K	38,732 Lb	−22.799	−60.36	-4.983×10^{5}	-1.288×10^{3}	−30.80	−.1521	−581.0	−3.766	-8.414×10^{3}	−.08180	-1.745×10^{3}	−5.612	−6.528	-2.830×10^{4}	-2.520×10^{3}	−66.88	−.1312	−451.0	−.08229	−526.8	−17.22	-2.558×10^{4}	−23.43	−19.43	-5.536×10^{4}	0						320.4
	43,720 Lb	−22.799	−60.36	-4.983×10^{5}	-1.288×10^{3}	−30.80	−.1521	−581.0	−3.766	-8.414×10^{3}	−.08180	-1.745×10^{3}	−5.612	−6.528	-2.830×10^{4}	-2.520×10^{3}	−66.88	−.1312	−451.0	−.08229	−526.8	−17.22	-2.558×10^{4}	−23.43	−19.43	-5.536×10^{4}	0						326.9
1.5M - 15K	38,732 Lb	−22.799	−55.05	-4.107×10^{5}	-1.242×10^{3}	−24.77	−.1262	−478.9	−3.738	-8.257×10^{3}	−.07364	-1.447×10^{3}	−5.612	−5.327	-2.332×10^{4}	-2.431×10^{3}	−56.50	−.1152	−371.2	−.07645	−426.8	−17.20	-2.503×10^{4}	−23.43	−18.49	-4.562×10^{4}	0						320.4
	43,720 Lb	−22.799	−55.05	-4.107×10^{5}	-1.242×10^{3}	−24.77	−.1262	−478.9	−3.738	-8.257×10^{3}	−.07364	-1.447×10^{3}	−5.612	−5.327	-2.332×10^{4}	-2.431×10^{3}	−56.50	−.1152	−371.2	−.07645	−426.8	−17.20	-2.503×10^{4}	−23.43	−18.49	-4.562×10^{4}	0						326.9
1.5M - 35K	38,732 Lb	−22.799	−35.51	-1.712×10^{5}	−737.8	−15.98	−.08142	−199.7	−3.685	-7.826×10^{3}	−.04751	−603.3	−5.612	−3.436	-9.725×10^{3}	-1.444×10^{3}	−36.45	−.07433	−154.8	−.04932	−177.9	−16.86	-2.254×10^{4}	−23.43	−11.93	-1.902×10^{4}	0						320.4
	43,720 Lb	−22.799	−35.51	-1.712×10^{5}	−737.8	−15.98	−.08142	−199.7	−3.685	-7.826×10^{3}	−.04751	−603.3	−5.612	−3.436	-9.725×10^{3}	-1.444×10^{3}	−36.45	−.07433	−154.8	−.04932	−177.9	−16.86	-2.254×10^{4}	−23.43	−11.93	-1.902×10^{4}	0						326.9
1.5M - 45K	38,732 Lb	−22.799	−27.89	-1.059×10^{5}	−576.7	−12.55	−.06395	−123.5	−3.665	-7.709×10^{3}	−.03731	−373.1	−5.612	−2.699	-6.014×10^{3}	-1.129×10^{3}	−28.63	−.05838	−95.72	−.03874	−110.0	−16.73	-2.186×10^{4}	−23.43	−9.368	-1.176×10^{4}	0						320.4
	43,720 Lb	−22.799	−27.89	-1.059×10^{5}	−576.7	−12.55	−.06393	−123.5	−3.665	-7.709×10^{3}	−.03731	−373.1	−5.612	−2.699	-6.014×10^{3}	-1.129×10^{3}	−28.63	−.05838	−95.72	−.03874	−110.0	−16.73	-2.186×10^{4}	−23.43	−9.368	-1.176×10^{4}	0						320.9
1.8M - 55K	38,732 Lb	−22.799	−23.50	-7.187×10^{4}	−497.8	−9.082	−.04824	−83.82	−3.647	-7.647×10^{3}	−.03100	−255.3	−5.612	−1.992	-4.081×10^{3}	−974.1	−22.10	−.04715	−64.83	−.03326	−72.87	−16.68	-2.158×10^{4}	−23.43	−8.238	-7.983×10^{3}	0						320.4
	43,720 Lb	−22.799	−23.50	-7.187×10^{4}	−497.8	−9.082	−.04824	−83.82	−3.647	-7.647×10^{3}	−.03100	−255.3	−5.612	−1.992	-4.081×10^{3}	−974.1	−22.10	−.04715	−64.83	−.03326	−72.87	−16.68	-2.158×10^{4}	−23.43	−8.238	-7.983×10^{3}	0						326.9
2.15M-36K	38,732 Lb	−22.799	−40.11	-1.919×10^{5}	−842.2	−12.97	−.07280	−223.8	−3.679	-7.863×10^{3}	−.05217	−689.5	−5.612	−2.921	-1.090×10^{4}	-1.648×10^{3}	−34.28	−.07704	−172.6	−.05782	−187.8	−17.05	-2.323×10^{4}	−23.43	−14.64	-2.131×10^{4}	0						320.4
	43,720 Lb	−22.799	−40.11	-1.919×10^{5}	−842.2	−12.97	−.07280	−223.8	−3.679	-7.863×10^{3}	−.05217	−689.5	−5.612	−2.921	-1.090×10^{4}	-1.648×10^{3}	−34.28	−.07704	−172.6	−.05782	−187.8	−17.05	-2.323×10^{4}	−23.43	−14.64	-2.131×10^{4}	0						326.9

Figure 133, along with the Aeroelastic Aerodynamic Data in Table XI were used to compute transfer functions and frequency responses of $\dot{\theta}_{M_{313}}/\delta_s$, $\dot{\theta}_{M_{179}}/\delta_s$, $N_{z_{77}}/\delta_s$, and $N_{z_{24}}/\delta_s$ for two aircraft weight configurations at eleven flight conditions. Representative frequency response plots, one high $\bar{q}$ and one low $\bar{q}$ flight condition, for each of these sensor locations are shown in Figures 134 through 139. Table XII presents a summary of these data. The results, in terms of structural peak magnitudes for the three locations show that F.S. 383 is the best location for pitch rate gyro and F.S. 77 is the best location for the normal accelerometer.

2. STRUCTURAL FILTER

Prior to the completion of the analysis of the aeroelastic math model, the exact amplitudes of the structural modes were not known. It was assumed that proper placement of the sensors would not entirely eliminate the structural peaking and that a structural filter would be needed to provide further structural peak attenuation. A filter was designed for inclusion in the earliest control law studies in order that its effect upon system stability could be taken into consideration. The design of this filter was based upon the following ground rules:

- The filter would consist of a second order notch and first order lag.
- The filter would provide 20 dB attenuation at 80 radians per second.
- The damping ratios for the notch numerator and denominator would be greater than .1.

Use of a notch filter for mode reduction required a trade-off between the relative width, notch depth, and phase lag. A notch filter has the form:

$$\frac{S^2/\omega_N^2 + 2(\zeta_N/\omega_N)S + 1}{S^2/\omega_D^2 + 2(\zeta_D/\omega_D)S + 1}$$

The notch depth and relative width are primarily controlled by the ratio ζ_N/ζ_D. As this ratio becomes smaller, the depth of the notch increases while its width narrows. Conversely, an increase in the ratio produces the opposite effect, less depth and wider notch. The tuned frequency is governed by the frequency ω_N and ω_D. If the notch filter is symmetrical, then the tuned frequency is $\omega_N = \omega_D$. If the notch filter is asymmetrical, $\omega_N \neq \omega_D$, then the tuned frequency is determined by ω_N if $\zeta_N < \zeta_D$. A ratio of $\zeta_N/\zeta_D = 1/7$ gives the filter an attenuation of approximately -17 dB at its tuned frequency of 80 rad/sec. An 80 rad/sec first order lag was added to the notch filter to provide roll-off at the high frequencies and an additional -3 dB attenuation at 80 rad/sec. The transfer function for the filter is

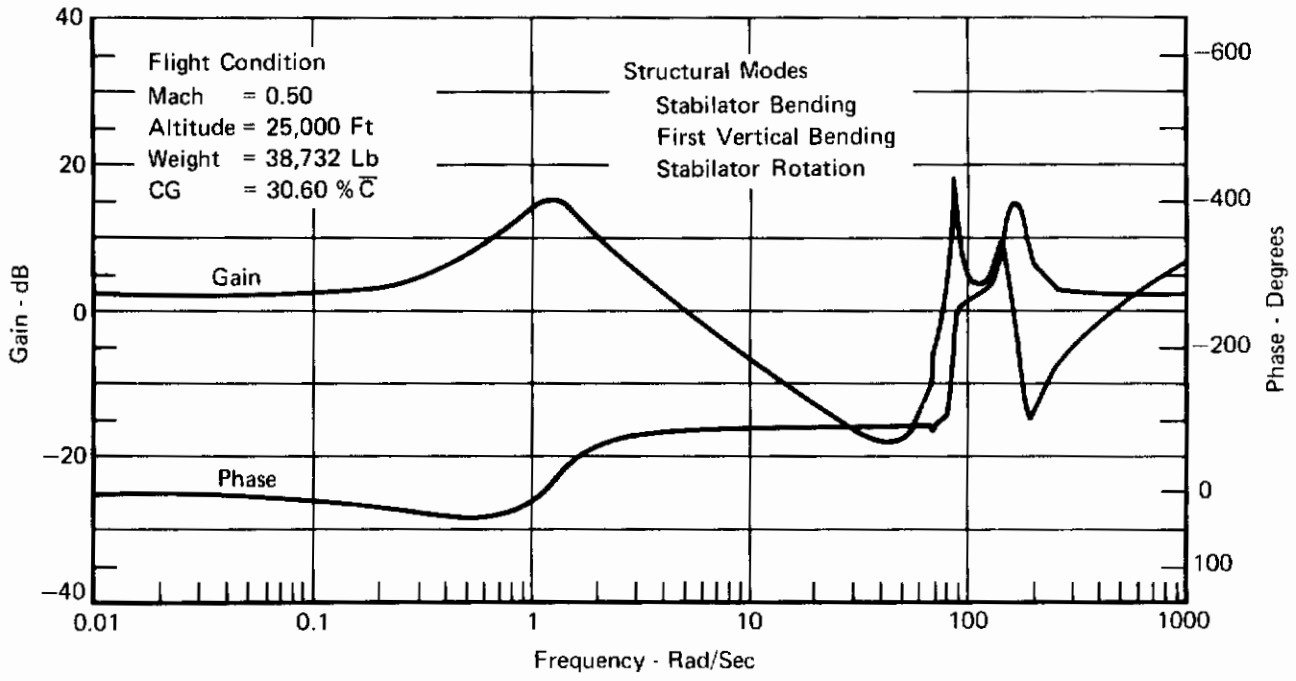

FIGURE 134
FREQUENCY RESPONSE OF $\dot{\theta}_{M_{383}}/\delta_S$ TRANSFER FUNCTION

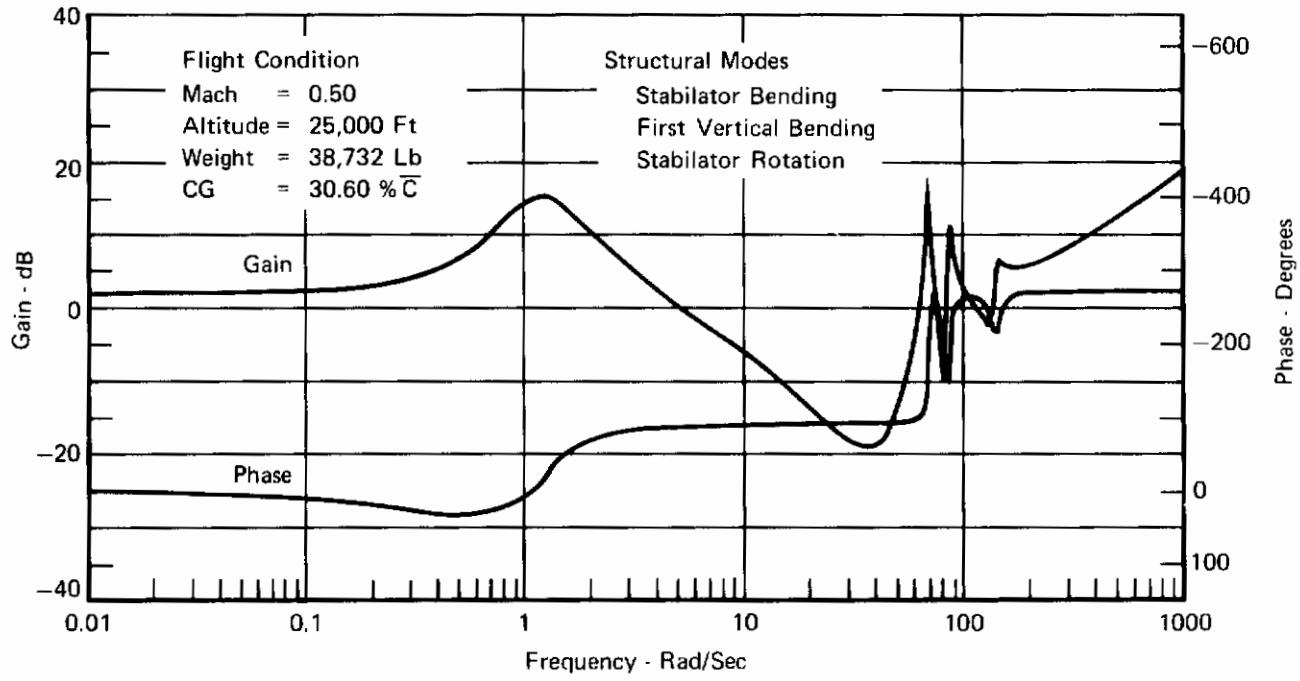

FIGURE 135
FREQUENCY RESPONSE OF $\dot{\theta}_{M_{313}}/\delta_S$ TRANSFER FUNCTION

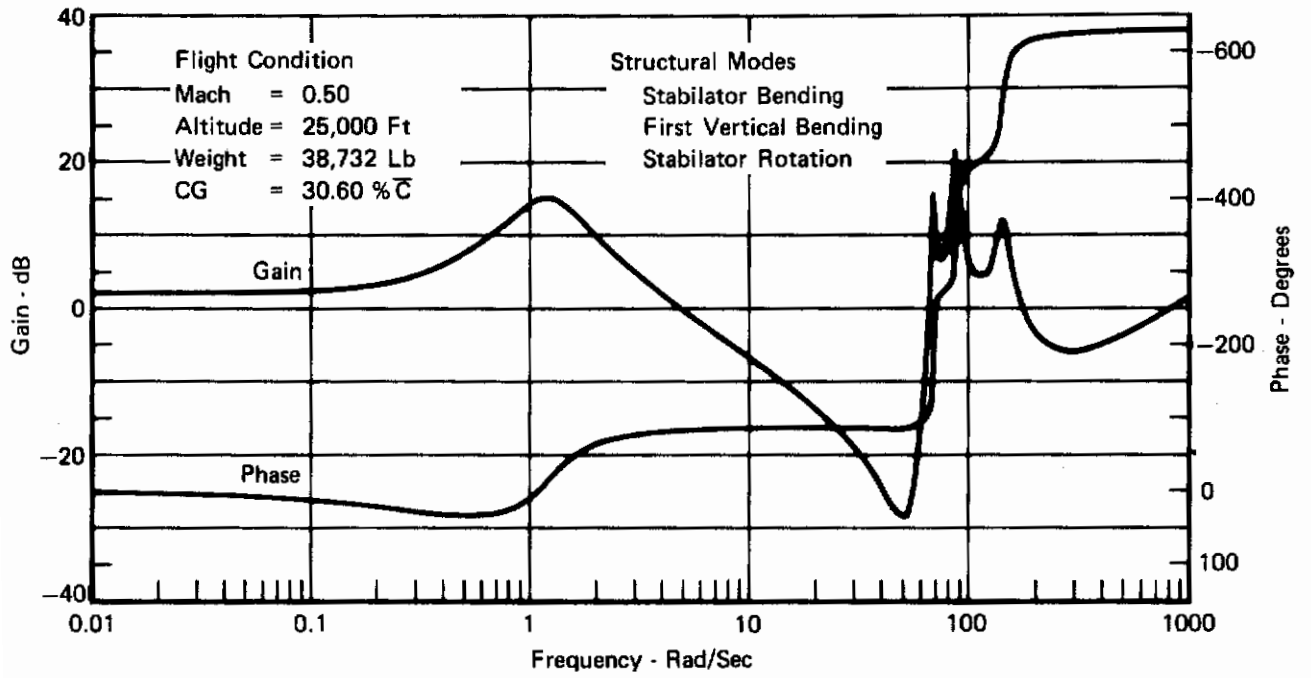

FIGURE 136

FREQUENCY RESPONSE OF $\dot{\theta}_{M_{179}}/\delta_S$ TRANSFER FUNCTION

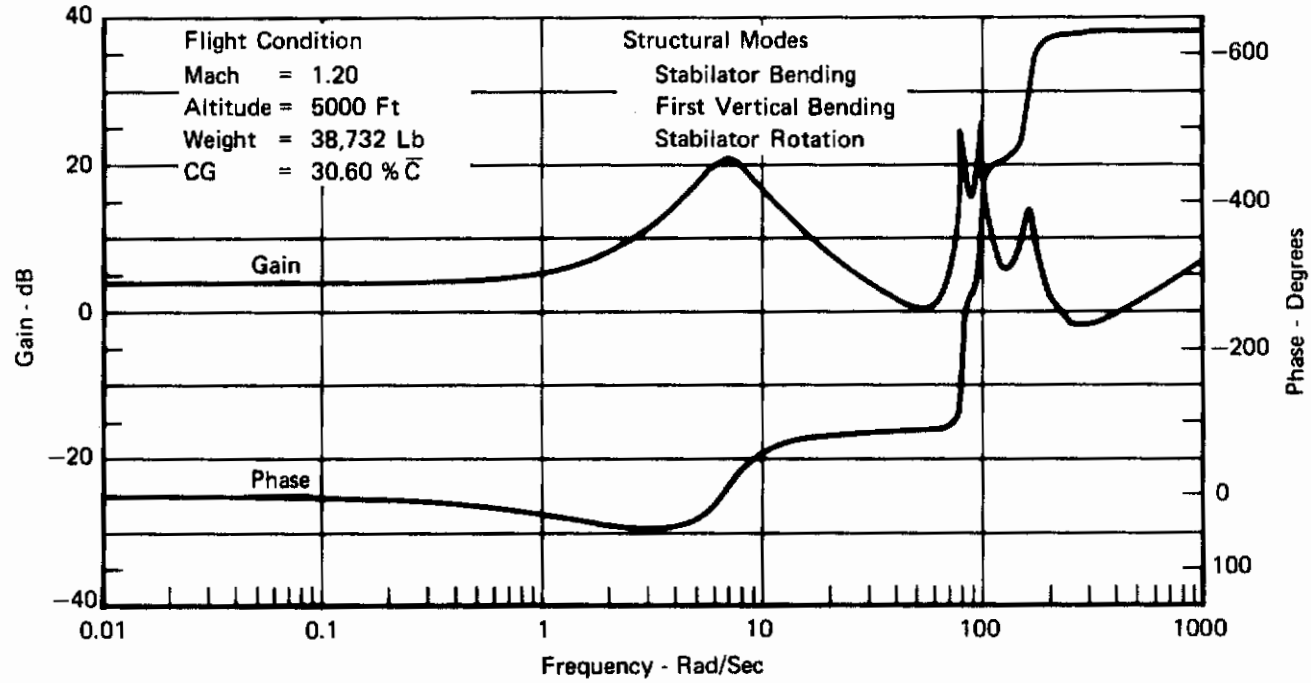

FIGURE 137

FREQUENCY RESPONSE OF $\dot{\theta}_{M_{383}}/\delta_S$ TRANSFER FUNCTION

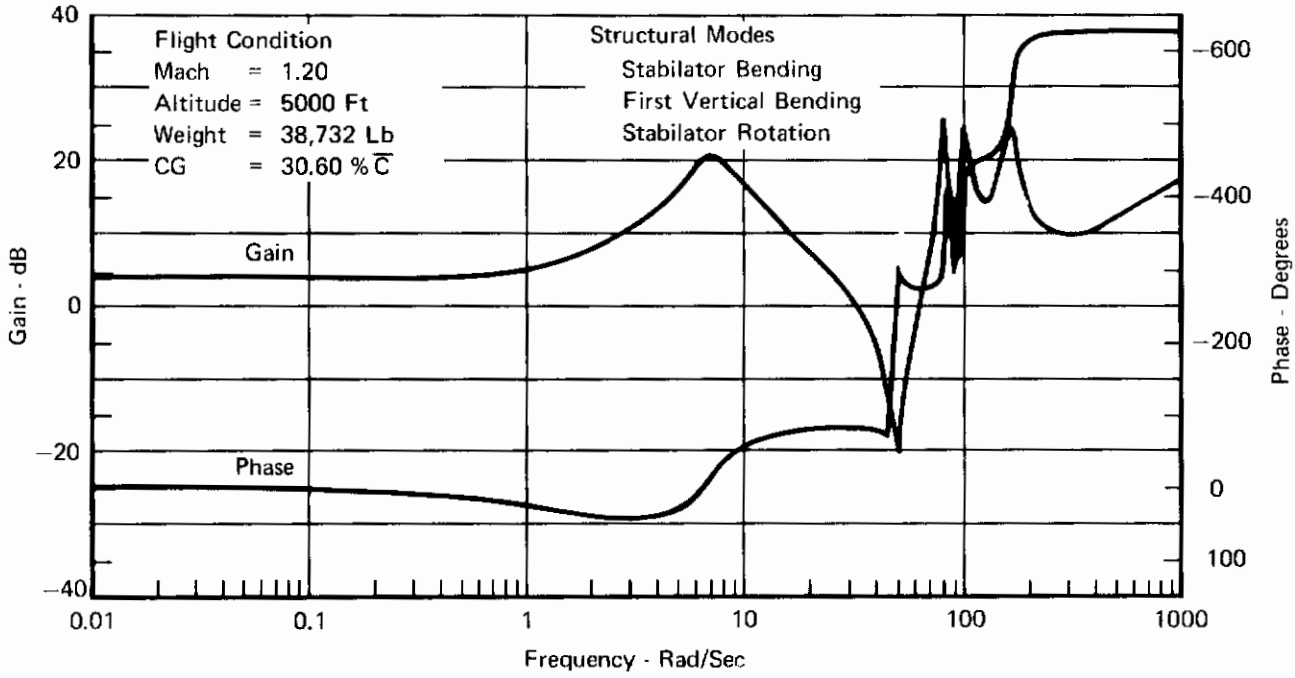

FIGURE 138

FREQUENCY RESPONSE OF $\dot{\theta}_{M_{313}}/\delta_S$ TRANSFER FUNCTION

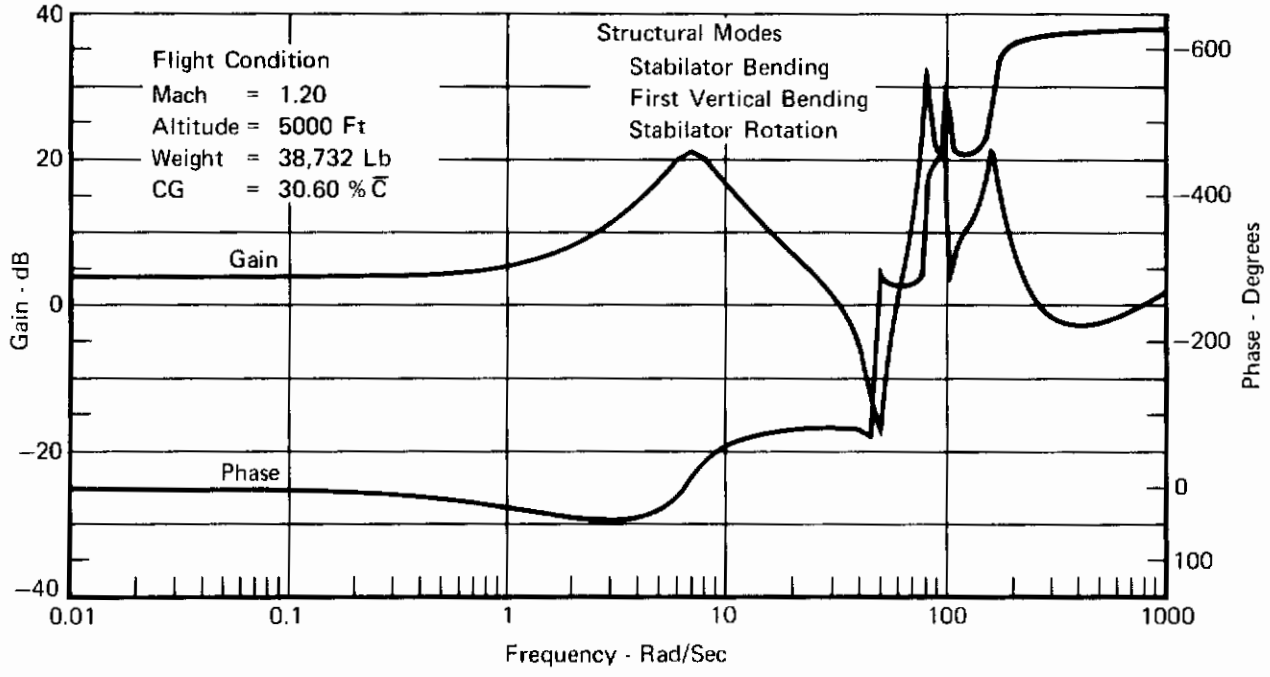

FIGURE 139

FREQUENCY RESPONSE OF $\dot{\theta}_{M_{179}}/\delta_S$ TRANSFER FUNCTION

TABLE XII
COMPARISON OF SENSED PITCH RATE AMPLITUDE

Mach	Altitude	Weight	$\dot{\theta}_{M_{383}}/\delta_S$ Stabilator Bending		$\dot{\theta}_{M_{383}}/\delta_S$ First Vertical Bending		$\dot{\theta}_{M_{383}}/\delta_S$ Stabilator Rotation		$\dot{\theta}_{M_{313}}/\delta_S$ Stabilator Bending		$\dot{\theta}_{M_{313}}/\delta_S$ First Vertical Bending		$\dot{\theta}_{M_{313}}/\delta_S$ Stabilator Rotation		$\dot{\theta}_{M_{179}}/\delta_S$ Stabilator Bending		$\dot{\theta}_{M_{179}}/\delta_S$ First Vertical Bending		$\dot{\theta}_{M_{179}}/\delta_S$ Stabilator Rotation	
			$\omega(\frac{\text{Rad}}{\text{Sec}})$	Magnitude (dB)	$\omega(\frac{\text{Rad}}{\text{Sec}})$	Magnitude (dB)	$\omega(\frac{\text{Rad}}{\text{Sec}})$	Magnitude (dB)	$\omega(\frac{\text{Rad}}{\text{Sec}})$	Magnitude (dB)	$\omega(\frac{\text{Rad}}{\text{Sec}})$	Magnitude (dB)	$\omega(\frac{\text{Rad}}{\text{Sec}})$	Magnitude (dB)	$\omega(\frac{\text{Rad}}{\text{Sec}})$	Magnitude (dB)	$\omega(\frac{\text{Rad}}{\text{Sec}})$	Magnitude (dB)	$\omega(\frac{\text{Rad}}{\text{Sec}})$	Magnitude (dB)
0.5	5,000	38,732	71	–6	88	17	139	7	71	–3	88	11	139	10	71	–4	88	20	139	14
0.5	5,000	43,720	71	–6	88	17	139	7	71	–3	88	11	139	10	71	–4	88	20	139	14
0.5	25,000	38,732	68	–6	87	18	142	10	68	18	87	11	142	9	68	16	87	21	142	12
0.5	25,000	43,720	68	–6	87	18	142	10	68	18	87	11	142	9	68	16	87	21	142	12
0.9	15,000	38,732	76	11	90	5	138	–3	76	26	90	9	138	17	76	28	90	9	138	17
0.9	15,000	43,720	76	12	90	5	138	–3	76	26	90	9	138	17	76	28	90	9	138	17
0.9	35,000	38,732	70	–6	88	17	140	7	70	–5	88	11	140	9	70	14	88	20	140	14
0.9	35,000	43,720	70	–6	88	17	140	7	70	–5	88	11	140	9	70	14	88	20	140	14
0.9	45,000	38,732	69	–7	87	18	141	9	69	19	87	11	141	6	69	13	87	21	141	12
0.9	45,000	43,720	69	–7	87	18	141	9	69	19	87	11	141	6	69	13	87	21	141	12
1.2	5,000	38,732	81	25	98	26	160	14	81	26	98	27	160	25	81	34	98	23	160	21
1.2	5,000	43,720	81	25	98	26	160	14	81	26	98	27	160	25	81	34	98	23	160	21
1.5	15,000	38,732	80	23	95	22	160	11	80	26	95	22	160	23	80	33	95	22	160	20
1.5	15,000	43,720	80	23	95	22	160	11	80	26	95	22	160	23	80	33	95	22	160	20
1.5	35,000	38,732	74	6	90	11	148	0.4	74	22	89	9	148	15	74	23	90	14	148	16
1.5	35,000	43,720	75	6	90	11	148	0.4	75	22	89	9	148	15	75	23	90	14	148	16
1.5	45,000	38,732	73	–6	88	16	146	5	73	12	88	11	146	12	73	12	88	19	146	14
1.5	45,000	43,720	73	–6	88	16	146	5	73	12	88	11	146	12	73	12	88	19	146	14
1.8	55,000	38,732	70	–6	88	17	144	8	70	11	88	11	144	9	70	3	88	20	144	13
1.8	55,000	43,720	70	–6	88	17	144	8	70	11	88	11	144	9	70	3	88	20	144	13
2.15	36,000	38,732	76	10	90	12	148	3	76	23	90	10	148	14	76	25	90	14	148	17
2.15	36,000	43,720	76	10	90	12	148	3	76	23	90	10	148	14	76	25	90	14	148	17

$$\frac{S^2/(80)^2 + (2(.1)/80)S + 1}{[S^2/(80)^2 + (2(.7)/80)S+1]\ (S/80 + 1)}$$

As seen in Table XII strategic placement of the sensors is not sufficient to reduce the possibility of structural mode feedback; therefore, the basic assumption that structual filtering would be needed is justified.

Analysis revealed that the originally assumed filter was unacceptable for three reasons: (1) the notch was not deep enough to provide sufficient structural mode attenuation at high $\bar{q}$ flight conditions; (2) the restriction that the damping ratios be greater than .1 proved to be unjustified, causing excessive phase lag at the short period airframe frequencies; and (3) the tuned frequency was low by 6 rad/sec.

The data in Table XII for a pitch rate gyro placement at F.S. 383 show that the most likely structural modes that might affect the aircraft control system are the first two (Stabilator Bending and First Vertical Bending). The frequency of the first mode ranges from 71 rad/sec to 81 rad/sec, and the frequency of the second mode ranges from 87 rad/sec to 98 rad/sec. Open loop frequency responses of the longitudinal SFCS were computed with the original structural filter deleted so that the attenuation from other system components and the structure modes passed through the normal accelerometer would be included. Figure 140 presents a composite plot of these frequency responses for eleven flight conditions. Although individual responses for each flight condition are not readily distinguishable on this plot, the frequencies at which structural mode peaks occur and the amplitudes of the peaks are easily seen. The largest peak is 13 dB and occurs at 88 rad/sec.

Using these data, the filter was redesigned. The transfer function for the redesigned filter is:

$$\frac{S^2/(86)^2 + (.1/86)S + 1}{[S^2/(84)^2 + (1.2/84)S + 1]\ [(S/120) + 1]}$$

Open loop frequency responses for eleven flight conditions and two aircraft weights were computed and are presented in Figures 141 through 146. These frequency responses are representative for low fixed gain operation (K_F = .25). For adaptive gains, the gain curve is shifted up by 6 or 12 dB for those flight conditions where the adaptive gain is .5 or 1.0 respectively. From these plots the attenuation of each structural mode for the adaptive gains was obtained and tabulated in Table XIII.

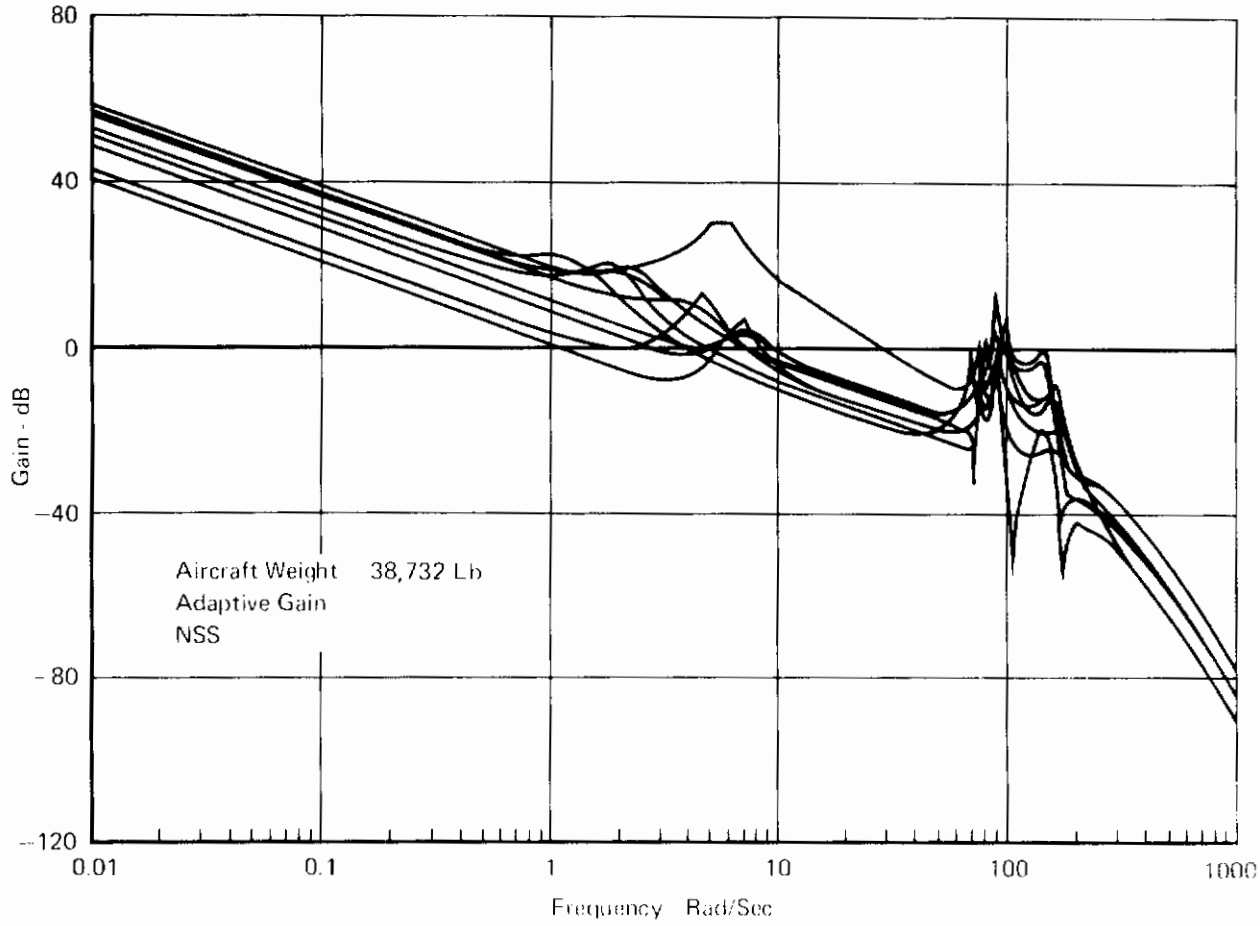

FIGURE 140

OPEN LOOP FREQUENCY RESPONSES WITHOUT STRUCTURAL NOTCH FILTER (PHASE II A, B)

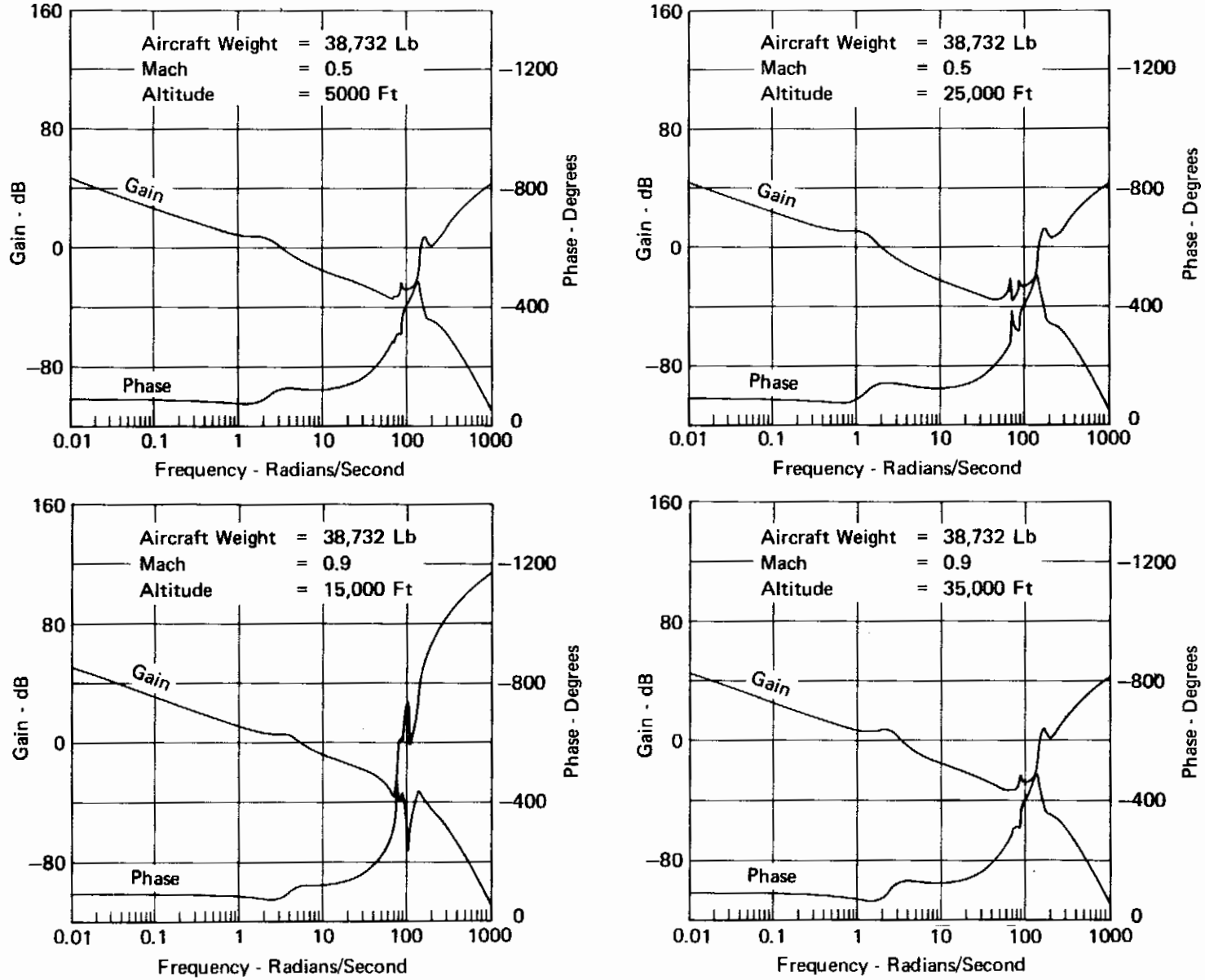

FIGURE 141

OPEN LOOP FREQUENCY RESPONSE WITH STRUCTURAL BENDING MODES INCLUDED

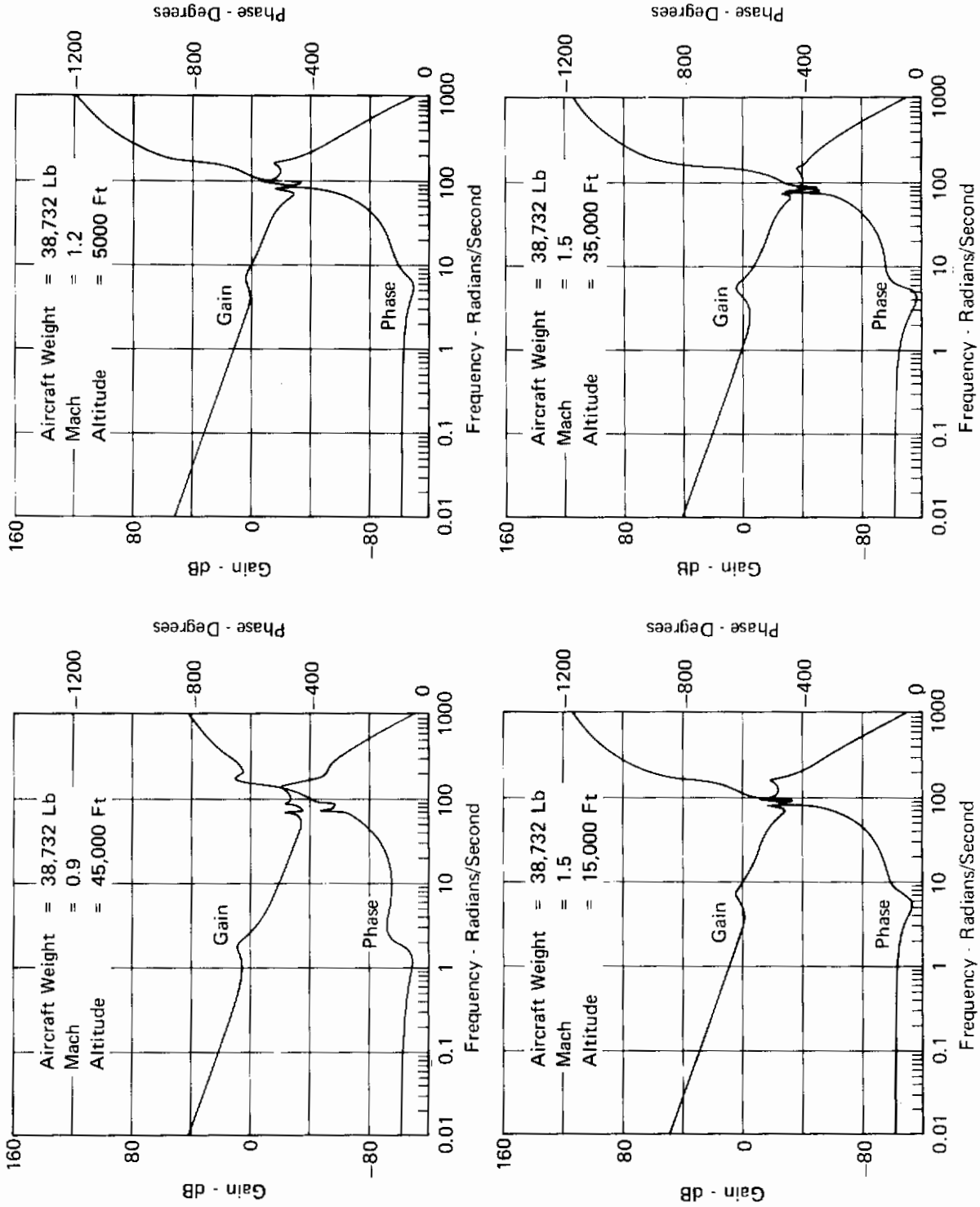

FIGURE 142

OPEN LOOP FREQUENCY RESPONSE WITH STRUCTURAL BENDING MODES INCLUDED

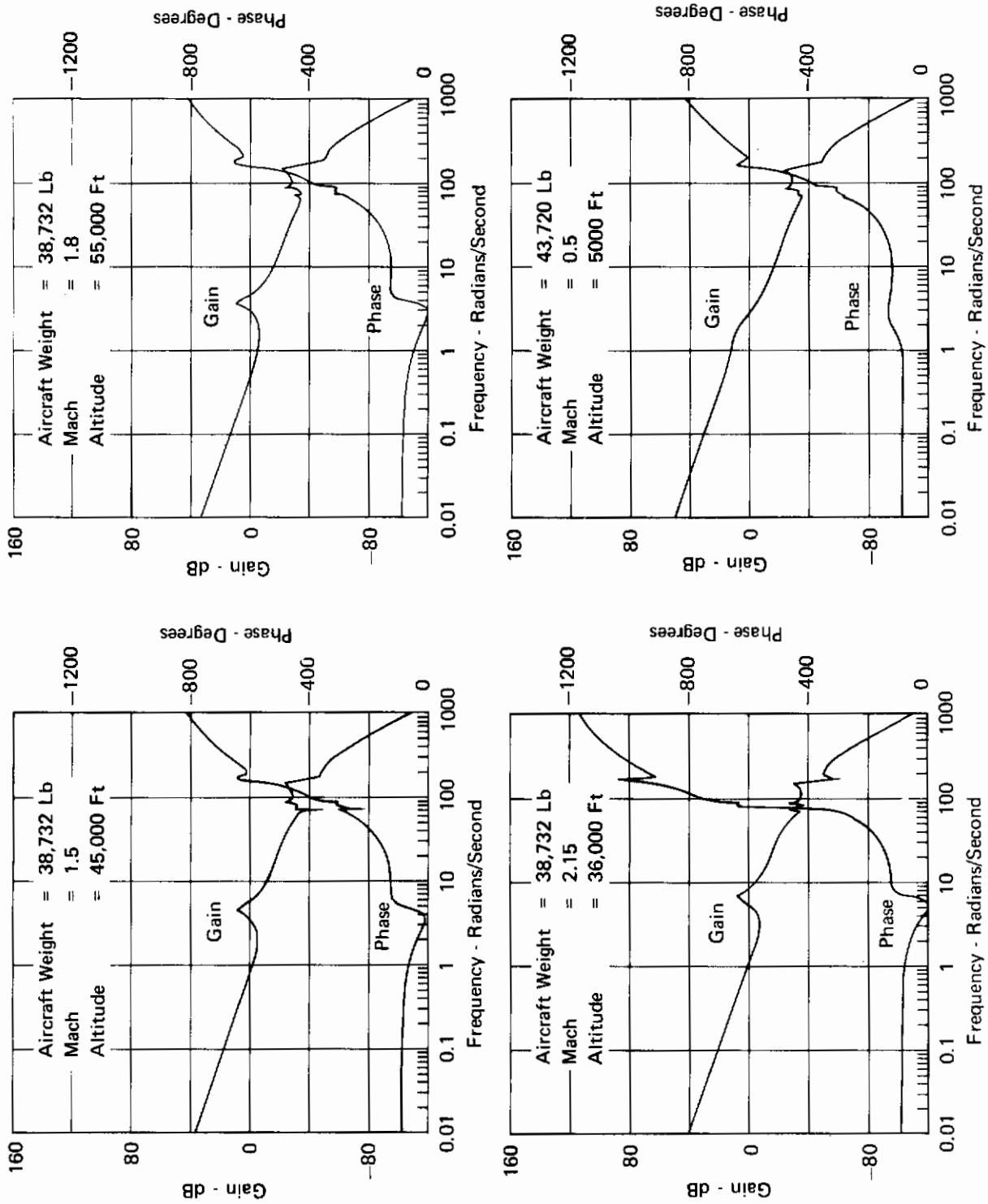

FIGURE 143

OPEN LOOP FREQUENCY RESPONSE WITH STRUCTURAL BENDING MODES INCLUDED

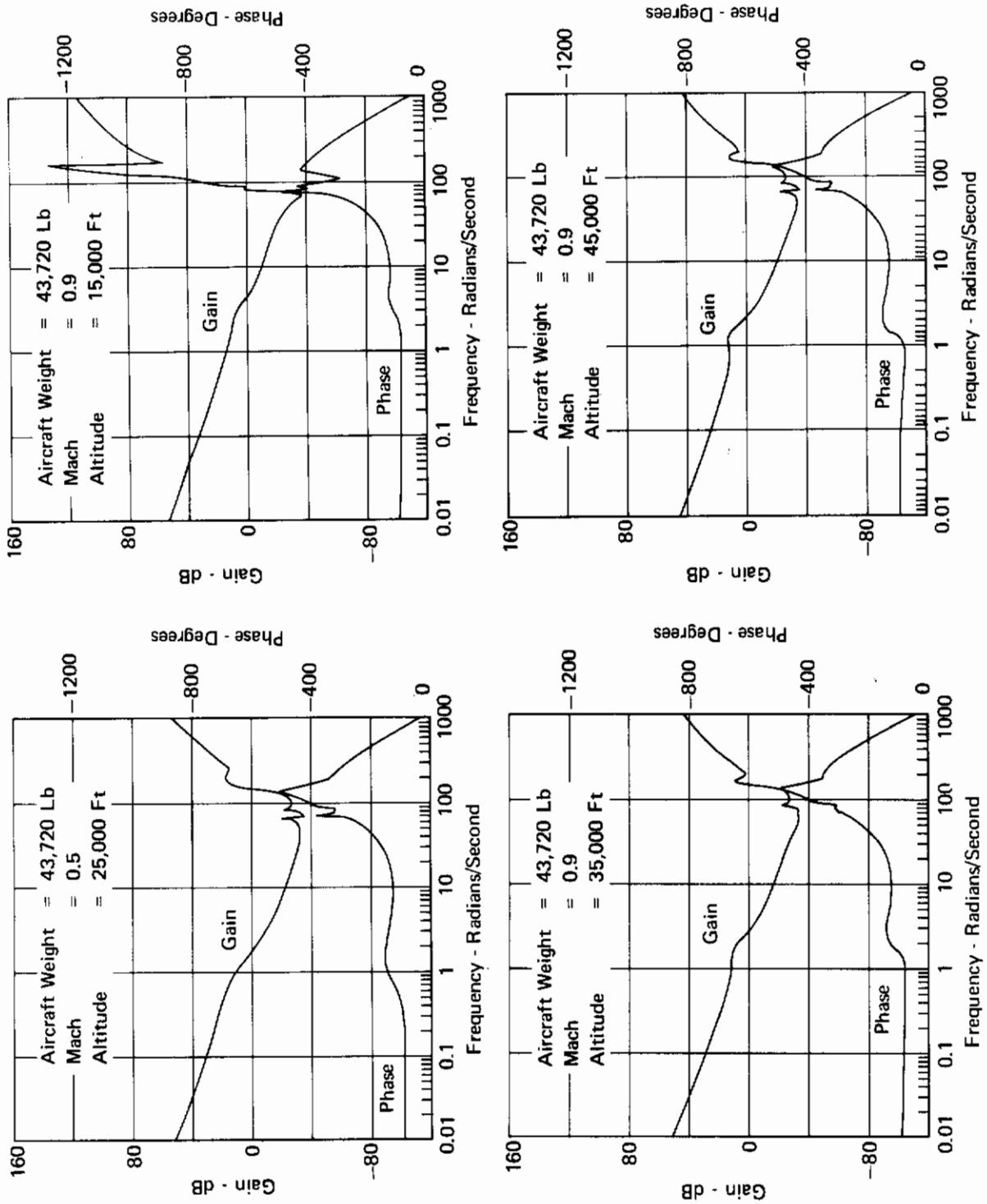

FIGURE 144

OPEN LOOP FREQUENCY RESPONSE WITH STRUCTURAL BENDING MODES INCLUDED

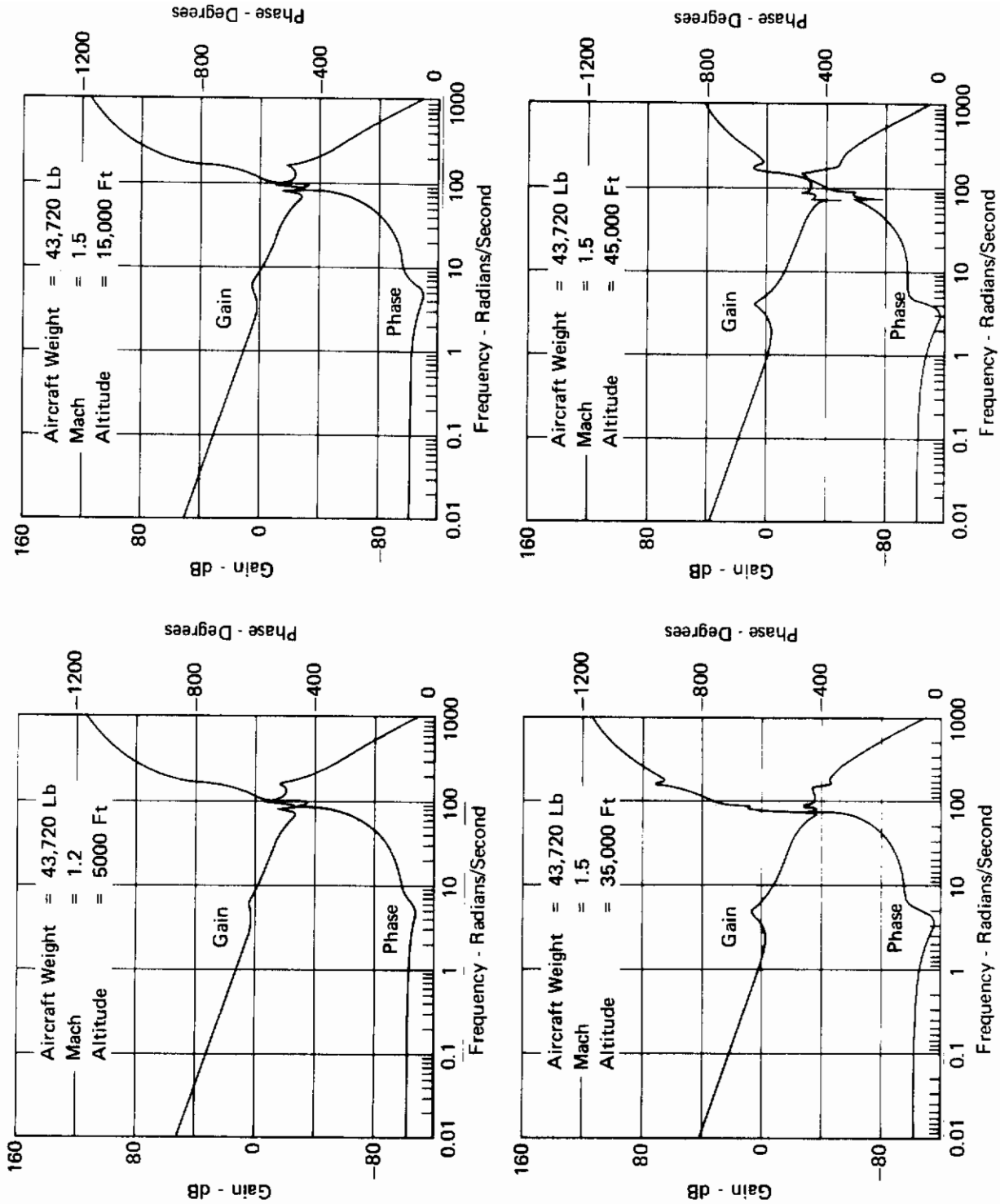

FIGURE 145

OPEN LOOP FREQUENCY RESPONSE WITH STRUCTURAL BENDING MODES INCLUDED

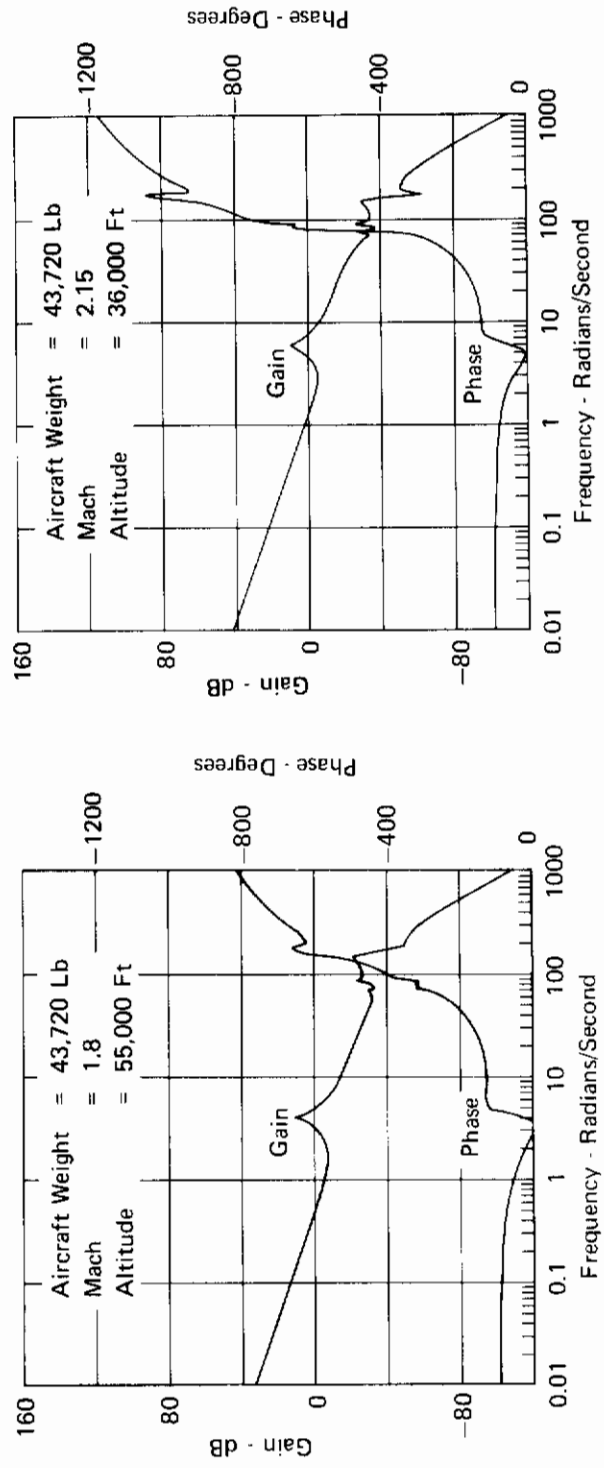

FIGURE 146

OPEN LOOP FREQUENCY RESPONSE WITH STRUCTURAL BENDING MODES INCLUDED

TABLE XIII
STRUCTURAL MODE ATTENUATION
(Adaptive Gains)

Mach	Altitude (Ft)	Weight (Lb)	Function (NSS/TOL)	K_F	Stabilator Bending		First Vertical Bending		Stabilator Rotation	
					Freq (Rad/Sec)	Attenuation (dB)	Freq (Rad/Sec)	Attenuation (dB)	Freq (Rad/Sec)	Attenuation (dB)
0.5	5,000	38,732	NSS	1.0	71	−22	88	−11	139	−11
0.5	5,000	43,720	NSS	1.0	71	−22	88	−11	139	−10
0.5	25,000	38,732	NSS	1.0	68	− 9	87	−10	142	− 7
0.5	25,000	43,720	NSS	1.0	68	− 9	87	−10	142	− 8
0.9	15,000	38,732	NSS	0.5	76	−17	90	−28	139	−26
0.9	15,000	43,720	NSS	0.5	76	−17	90	−28	139	−27
0.9	35,000	38,732	NSS	1.0	70	−20	87	−12	139	−10
0.9	35,000	43,720	NSS	1.0	70	−20	87	−12	139	−10
0.9	45,000	38,732	NSS	1.0	69	−10	88	−11	140	− 8
0.9	45,000	43,720	NSS	1.0	69	−10	88	−11	140	− 8
1.2	5,000	38,732	NSS	0.25	81	−16	98	− 6	160	−15
1.2	5,000	43,720	NSS	0.25	81	−14	98	− 6	160	−16
1.5	15,000	38,732	NSS	0.25	80	−16	96	−11	160	−18
1.5	15,000	43,720	NSS	0.25	80	−16	96	−11	160	−19
1.5	35,000	38,732	NSS	0.5	74	−20	90	−22	149	−30
1.5	35,000	43,720	NSS	0.5	75	−21	90	−22	149	−29
1.5	45,000	38,732	NSS	0.5	73	−24	88	−18	145	−19
1.5	45,000	43,720	NSS	0.5	73	−24	88	−18	145	−18
1.8	55,000	38,732	NSS	1.0	70	−18	88	−11	144	−16
1.8	55,000	43,720	NSS	1.0	70	−18	88	−11	144	−16
2.15	36,000	38,732	NSS	0.25	76	−27	90	−20	148	−25
2.15	36,000	43,720	NSS	0.5	76	−21	90	−20	148	−24

Root locus plots were obtained for 4 flight conditions and are presented for reference purposes in Figures 147 through 152.

The aeroelastic math model was included in a small perturbation analog simulation and representative time history response recordings obtained for 5 flight conditions. These data are presented in Figures 153 through 157.

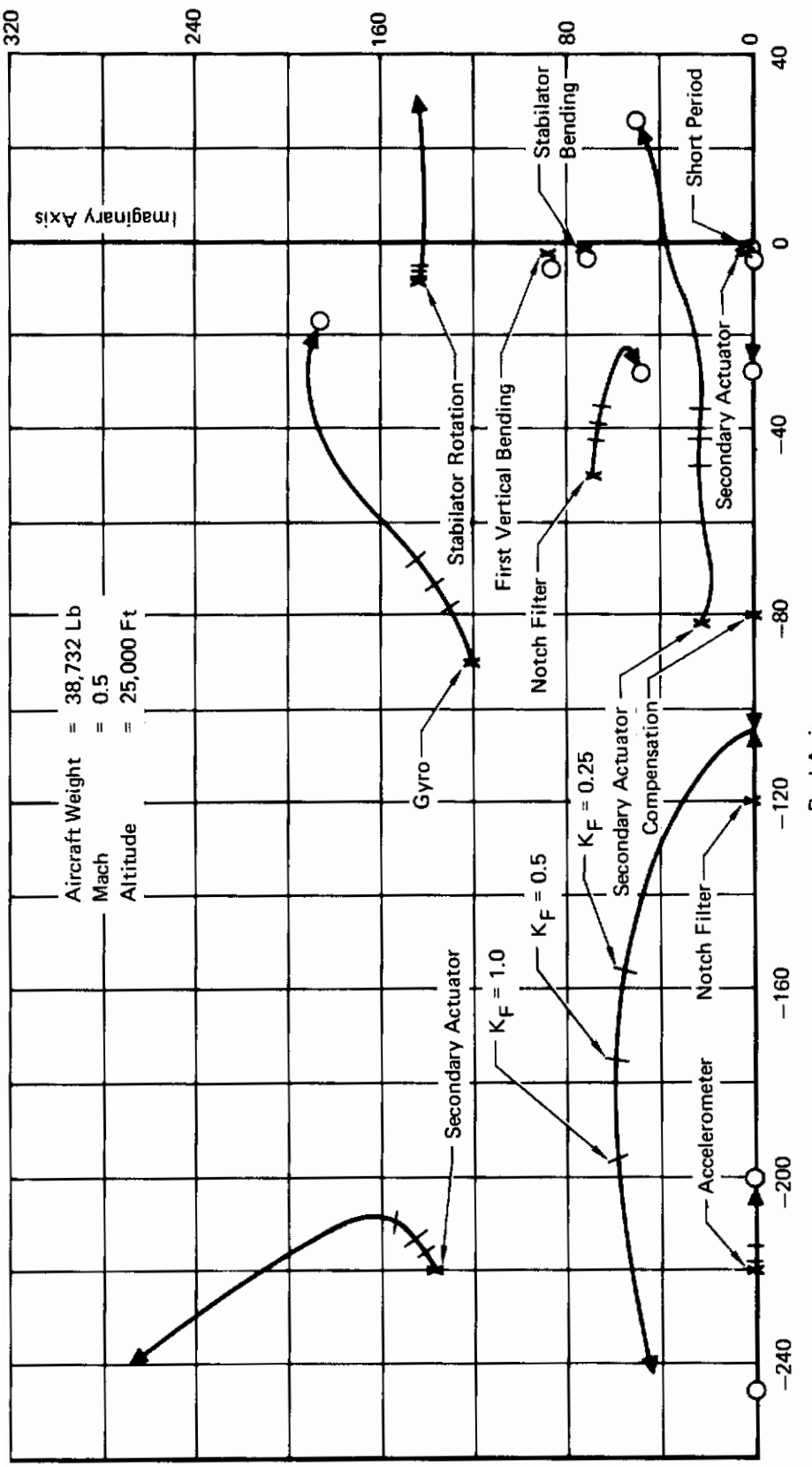

FIGURE 147
LONGITUDINAL SFCS ROOT LOCUS

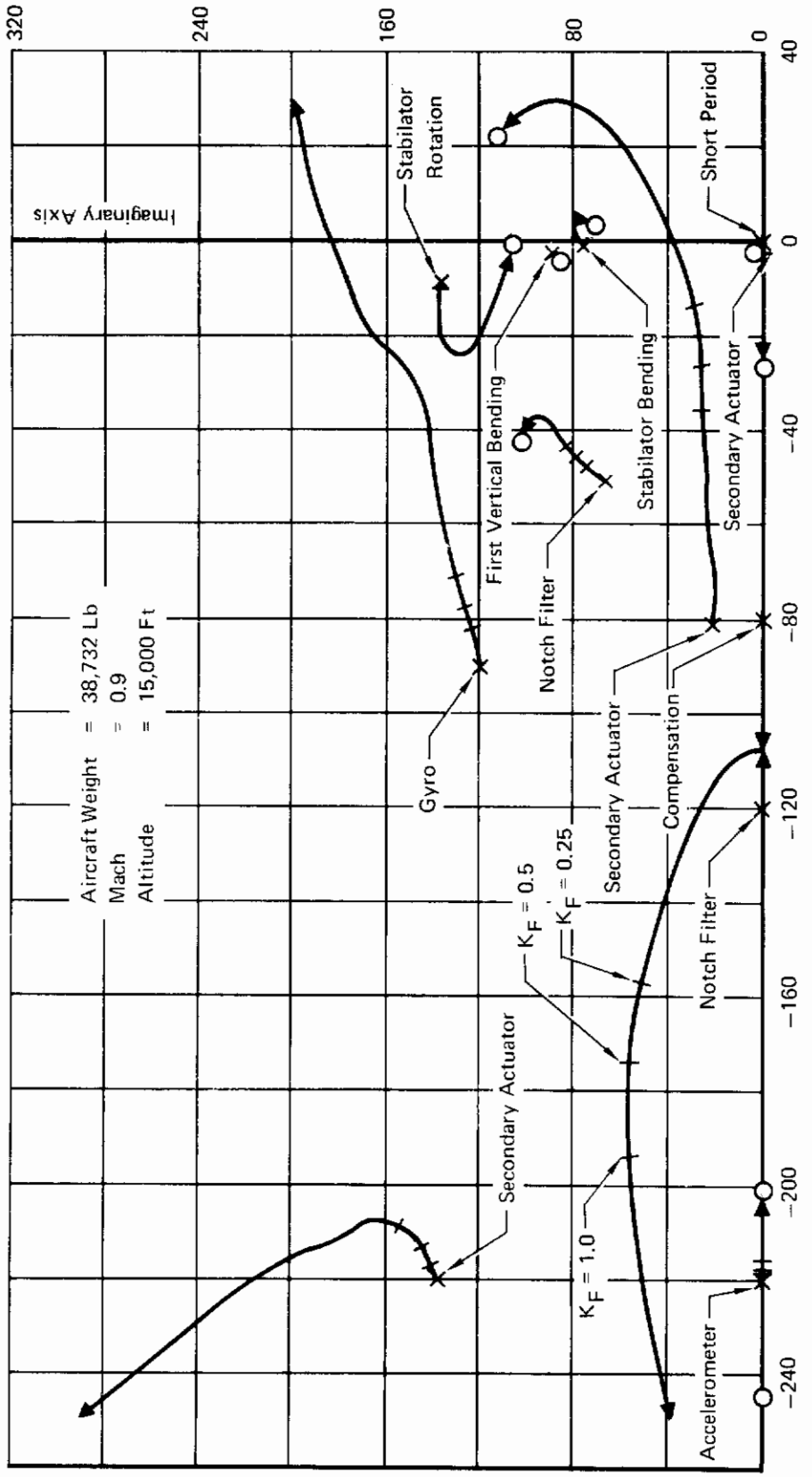

FIGURE 148
LONGITUDINAL SFCS ROOT LOCUS

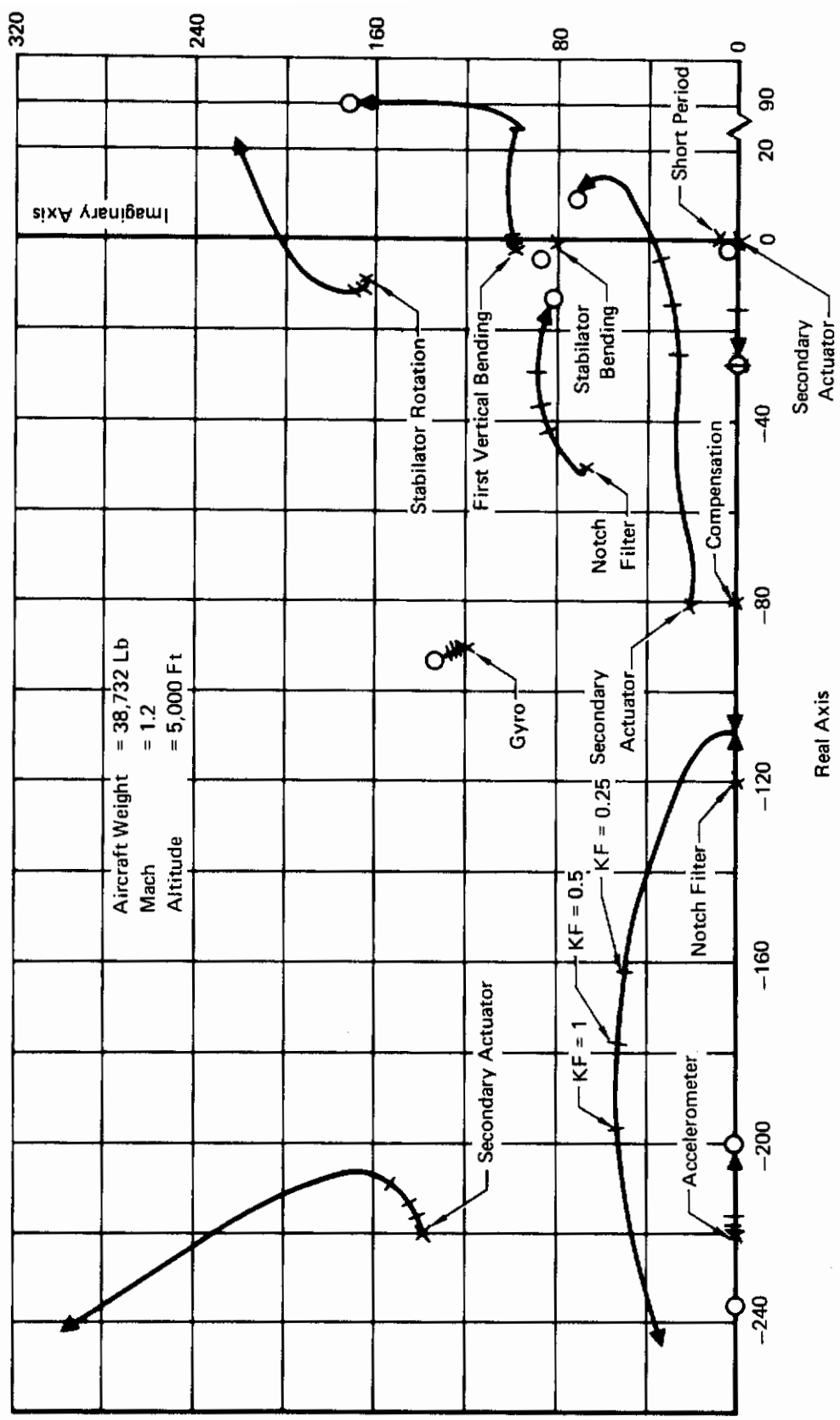

FIGURE 149
LONGITUDINAL SFCS ROOT LOCUS

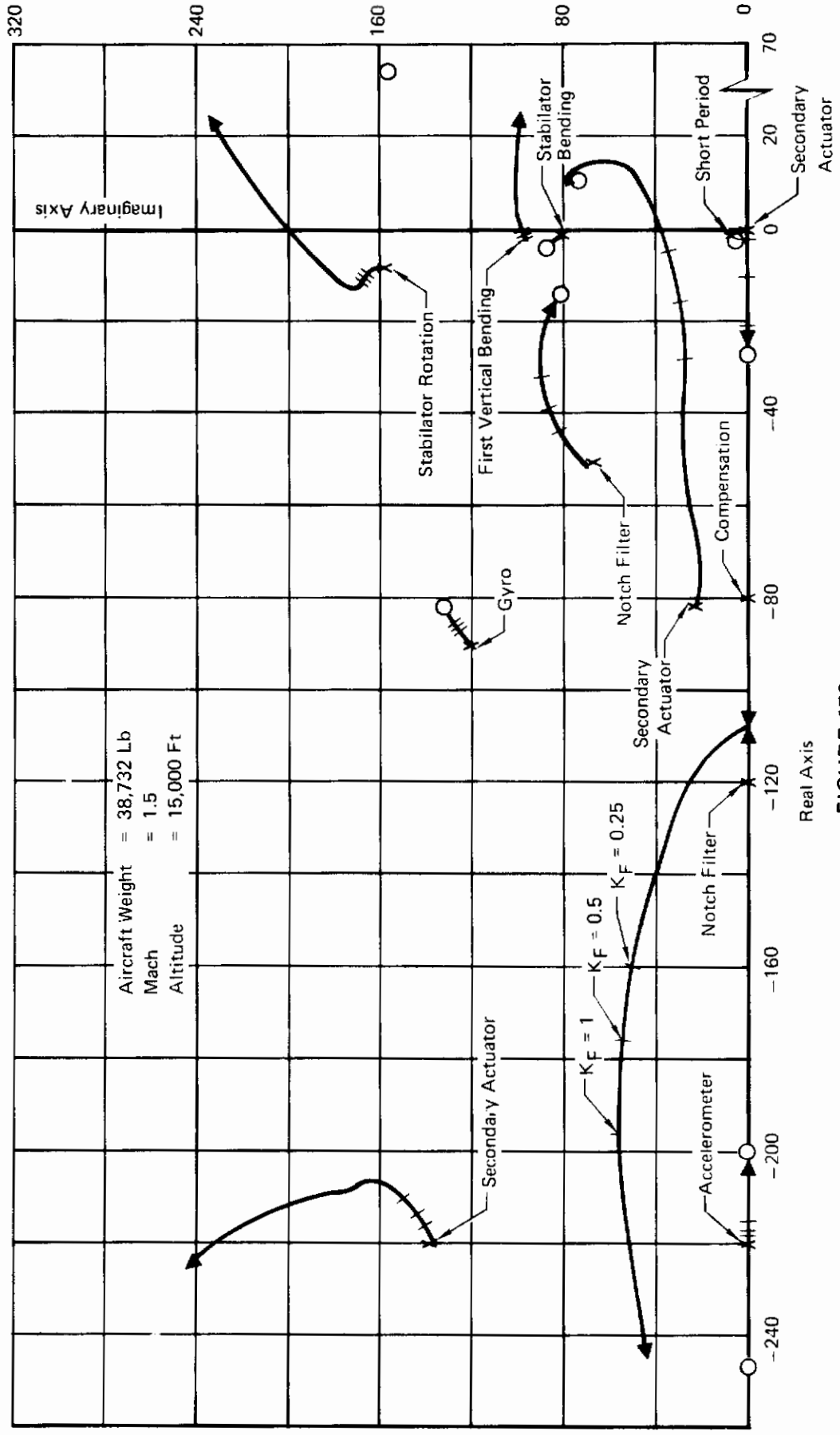

FIGURE 150
LONGITUDINAL SFCS ROOT LOCUS

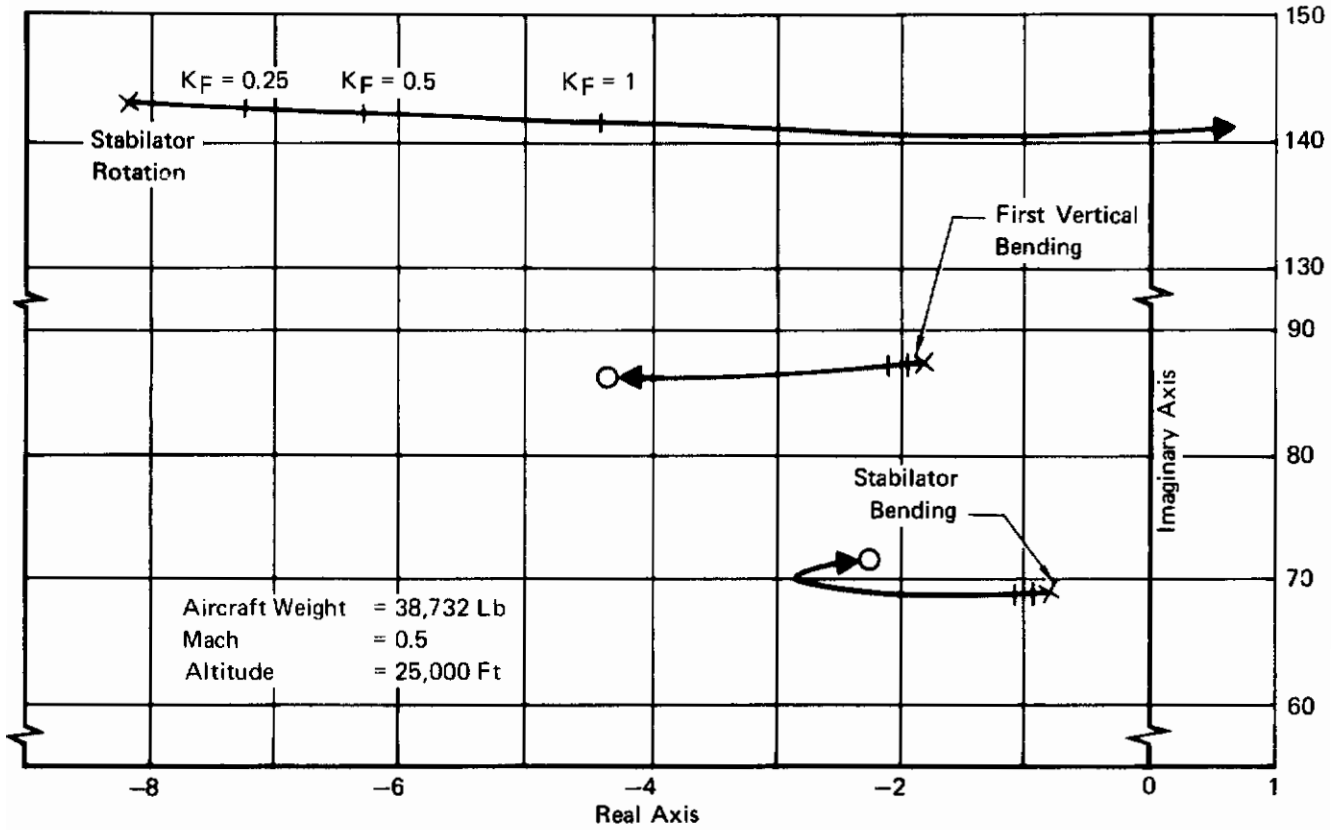

FIGURE 151
LONGITUDINAL SFCS ROOT LOCUS
(Detail Structural Roots)

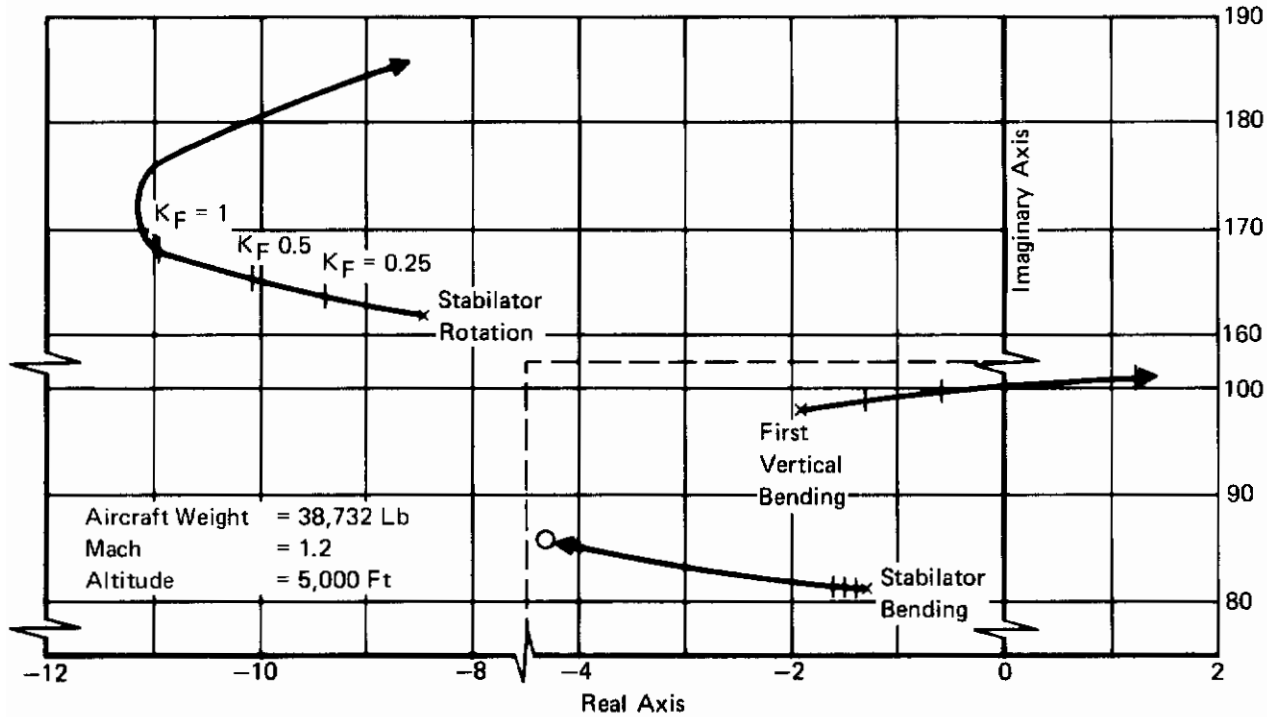

FIGURE 152
LONGITUDINAL SFCS ROOT LOCUS
(Detail Structural Roots)

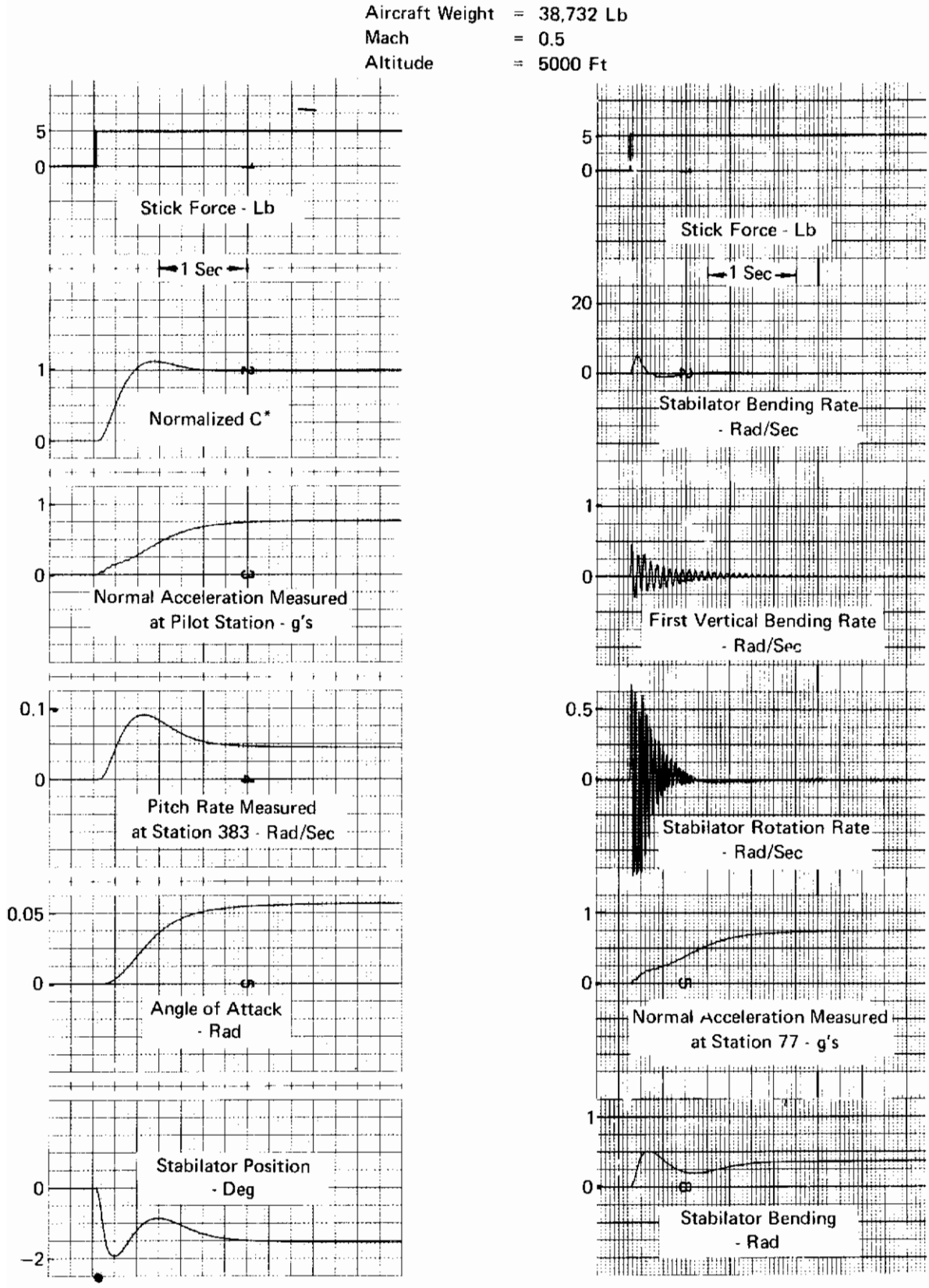

FIGURE 153
AEROELASTIC RESPONSE FOR STEP INPUT OF STICK FORCE
NSS, $K_F = 1.0$

Aircraft Weight = 38,732 Lb
Mach = 0.5
Altitude = 25,000 Ft

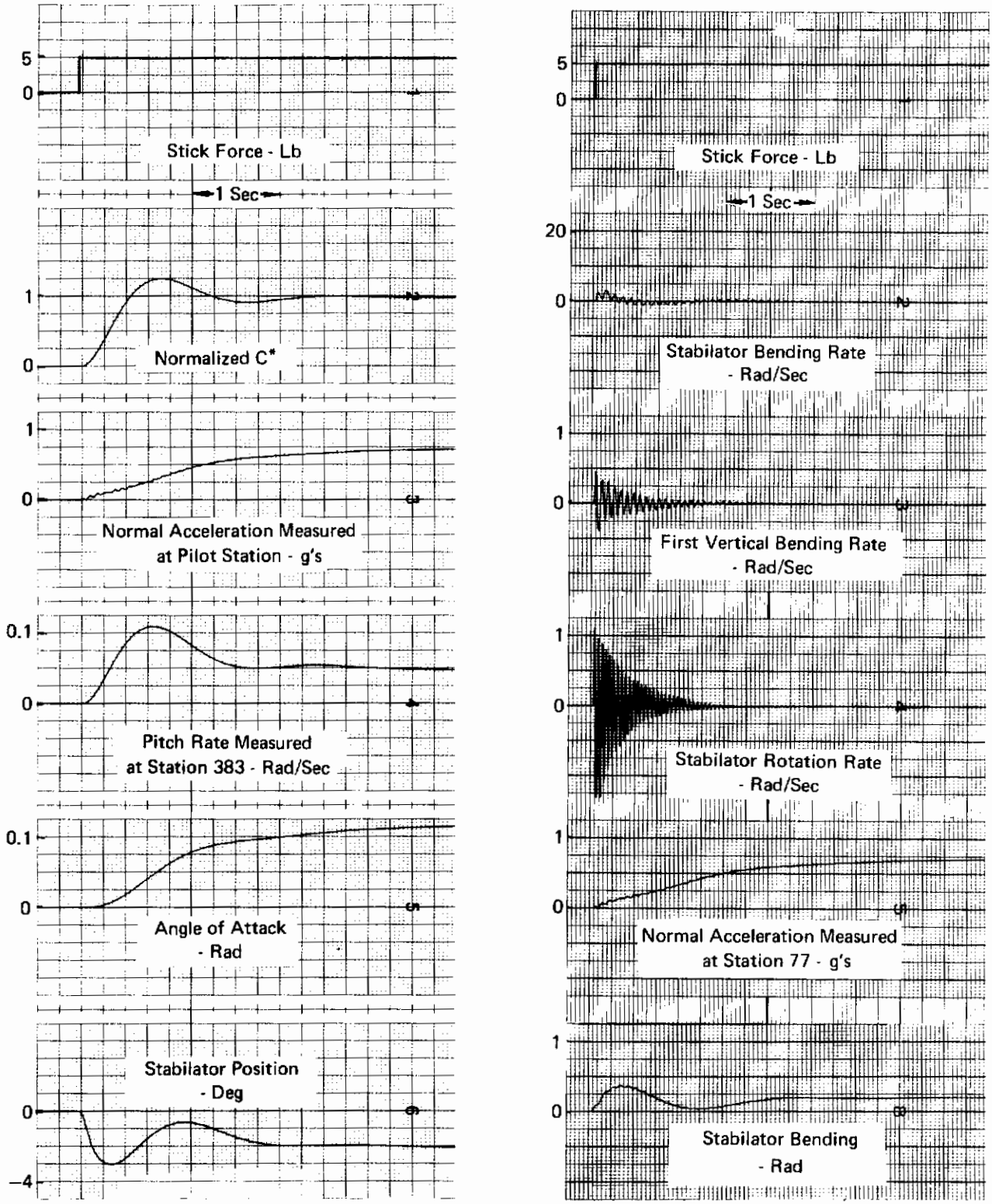

FIGURE 154
AEROELASTIC RESPONSE FOR STEP INPUT OF STICK FORCE
NSS, $K_F = 1.0$

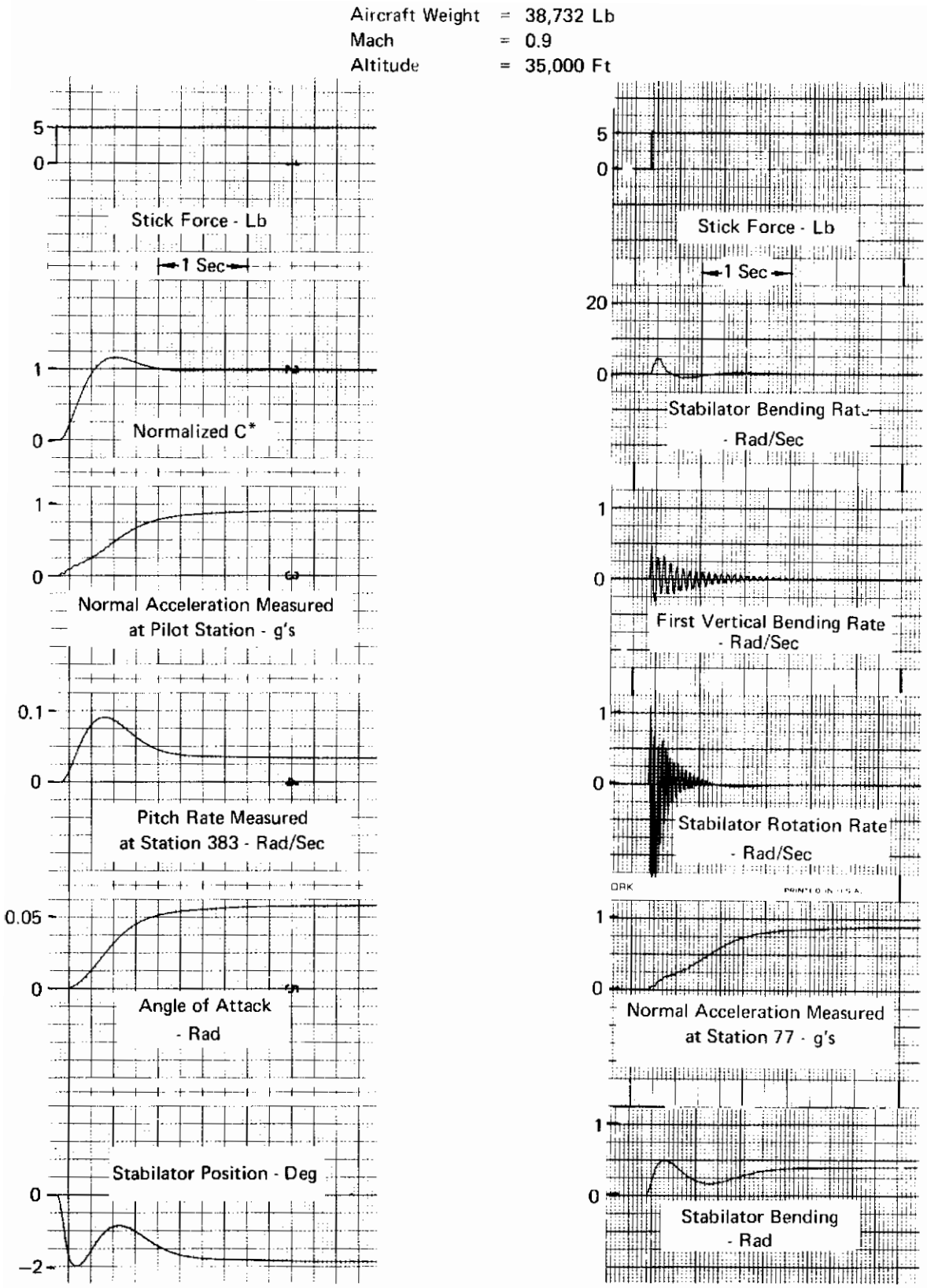

FIGURE 155
AEROELASTIC RESPONSE FOR STEP INPUT OF STICK FORCE
NSS, $K_F = 1.0$

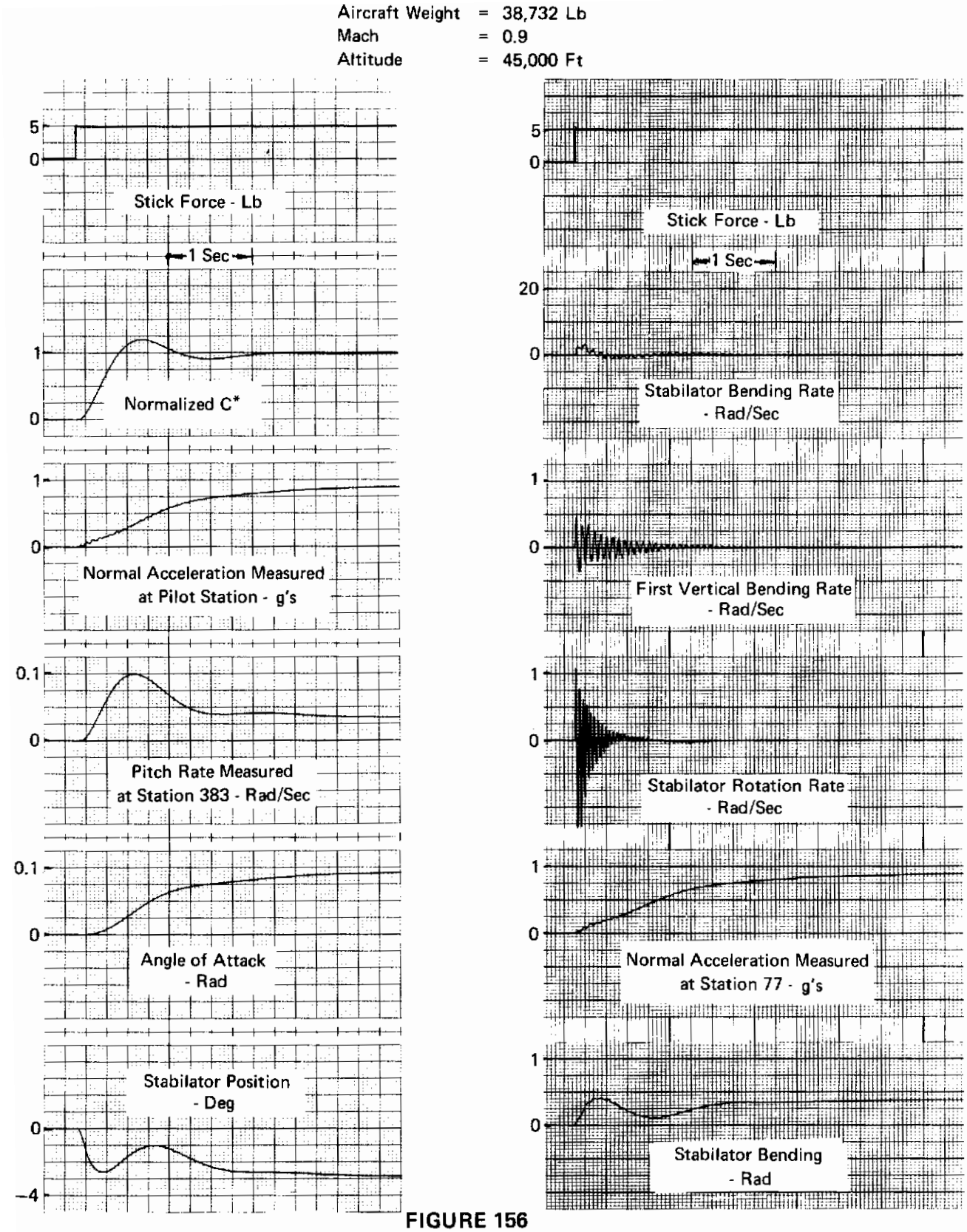

FIGURE 156
AEROELASTIC RESPONSE FOR STEP INPUT OF STICK FORCE
NSS, $K_F = 1.0$

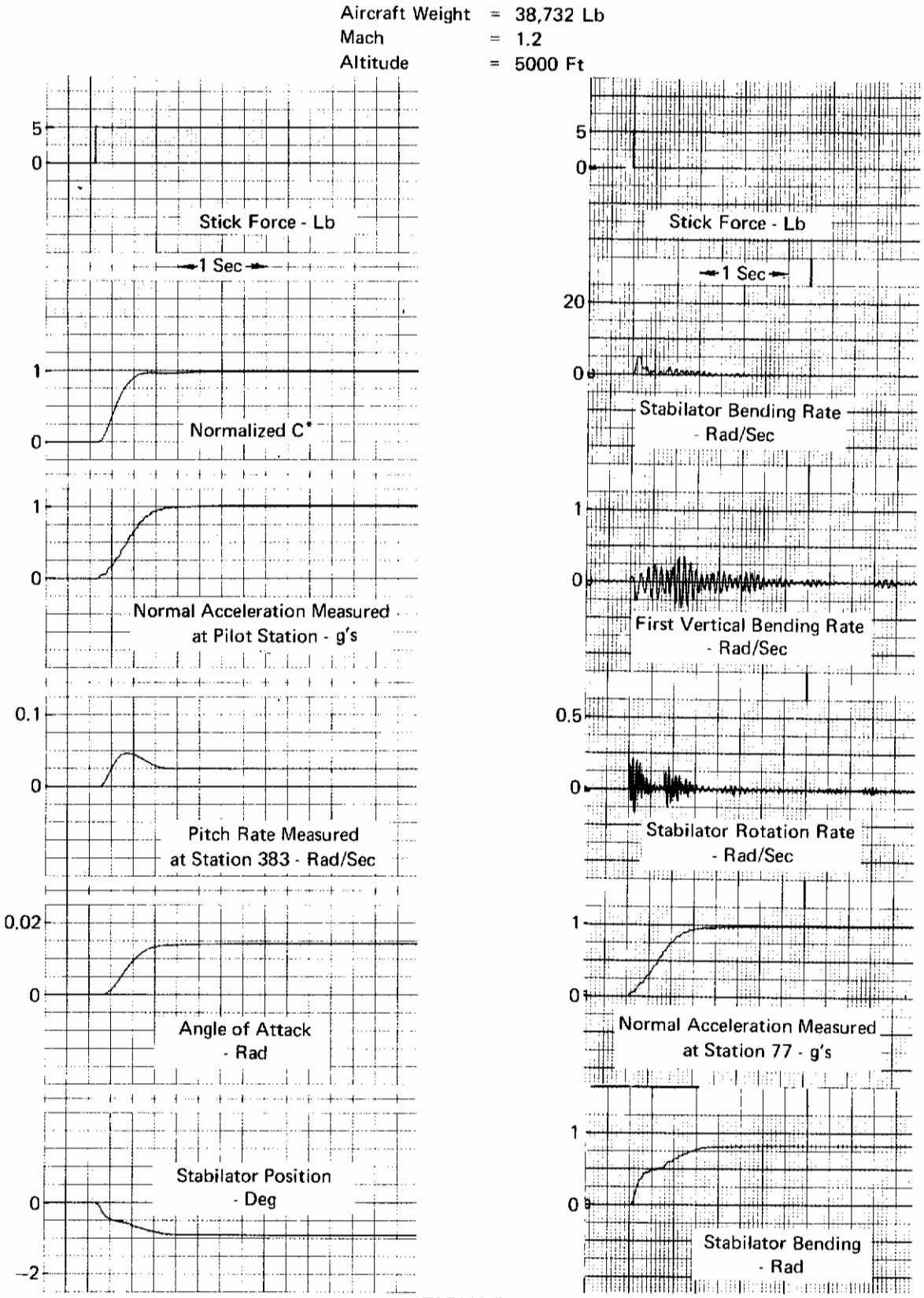

FIGURE 157

AEROELASTIC RESPONSE FOR STEP INPUT OF STICK FORCE

NSS, $K_F = 0.25$

APPENDIX IV

LATERAL-DIRECTIONAL TIME HISTORY RESPONSES

Time history responses showing system performance with the adaptive yaw rate and roll to yaw crossfeed gains are presented in this appendix for 12 clean configuration flight conditions and one each landing and takeoff flight conditions. Figures 158 through 172 show the response to a pilot step input of lateral stick force. Figures 173 through 186 show the responses to a pilot step input of rudder pedal force, and Figures 187 through 200 show lateral-directional system response to a step of lateral wind gust.

The lateral stick force responses have the D_I^* criteria boundary superimposed on the D_I^* trace.

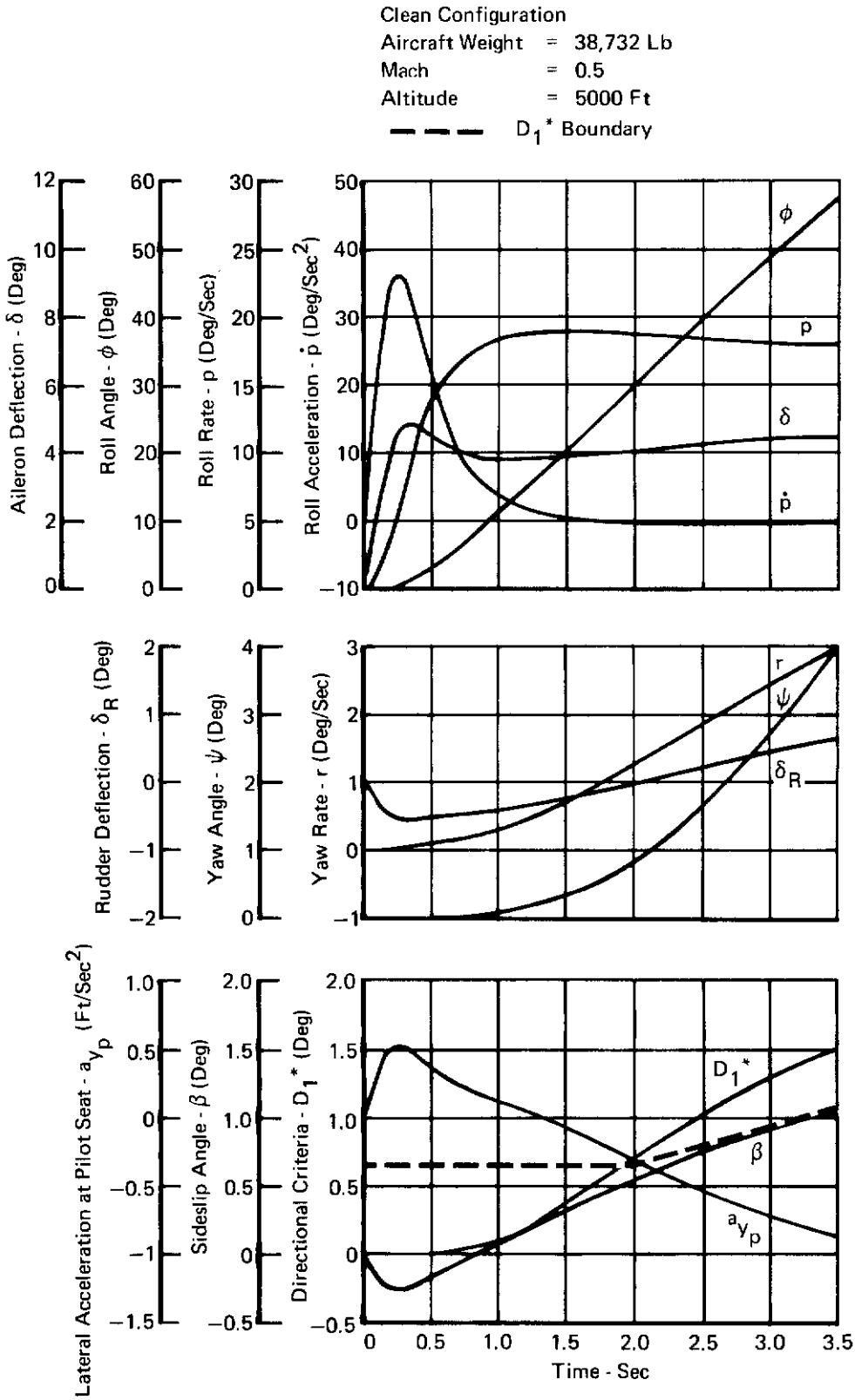

FIGURE 158
DYNAMIC RESPONSE TO A 3 LB STEP OF CENTER STICK FORCE

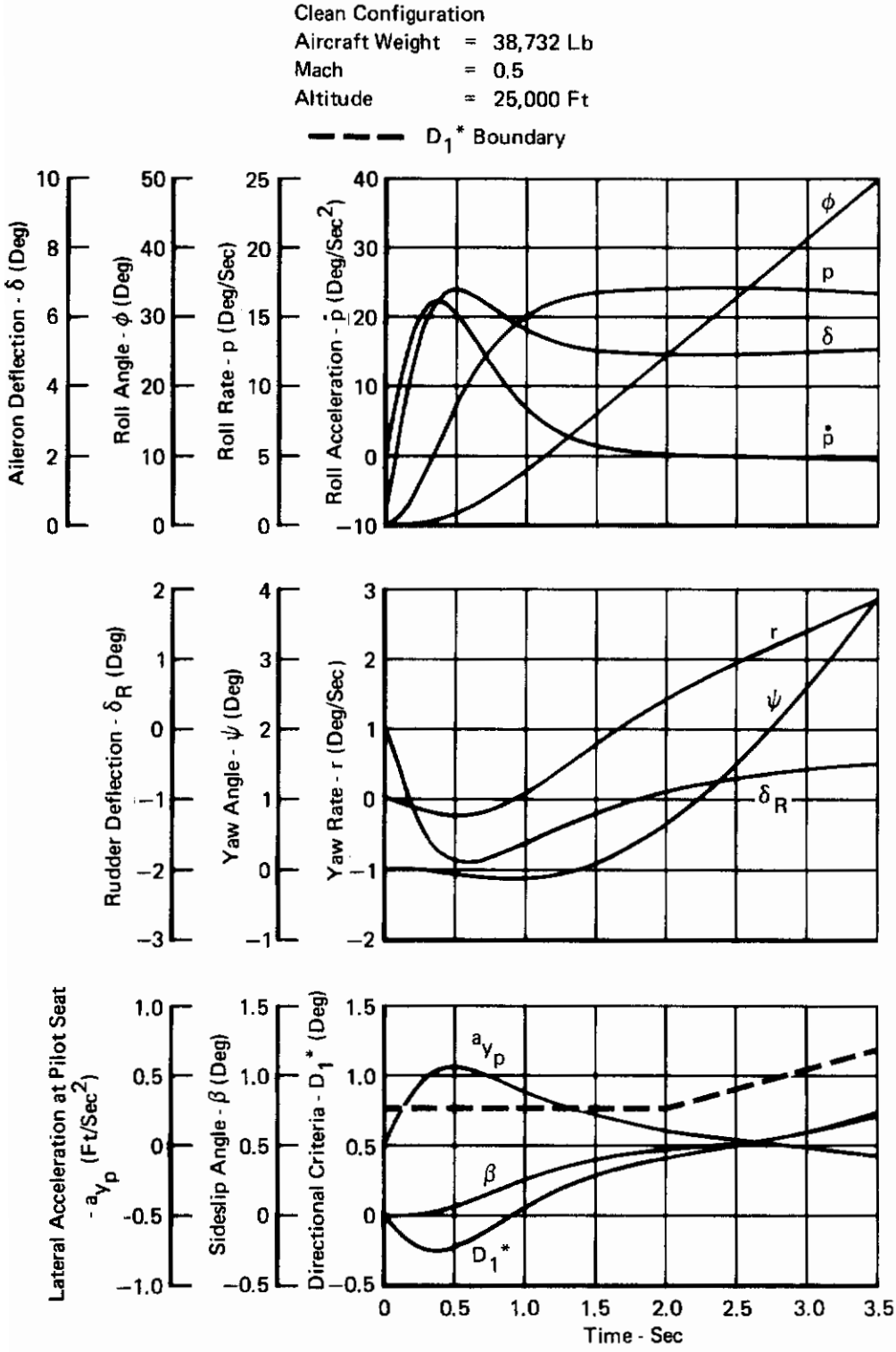

FIGURE 159
DYNAMIC RESPONSE TO A 3 LB STEP OF CENTER STICK FORCE

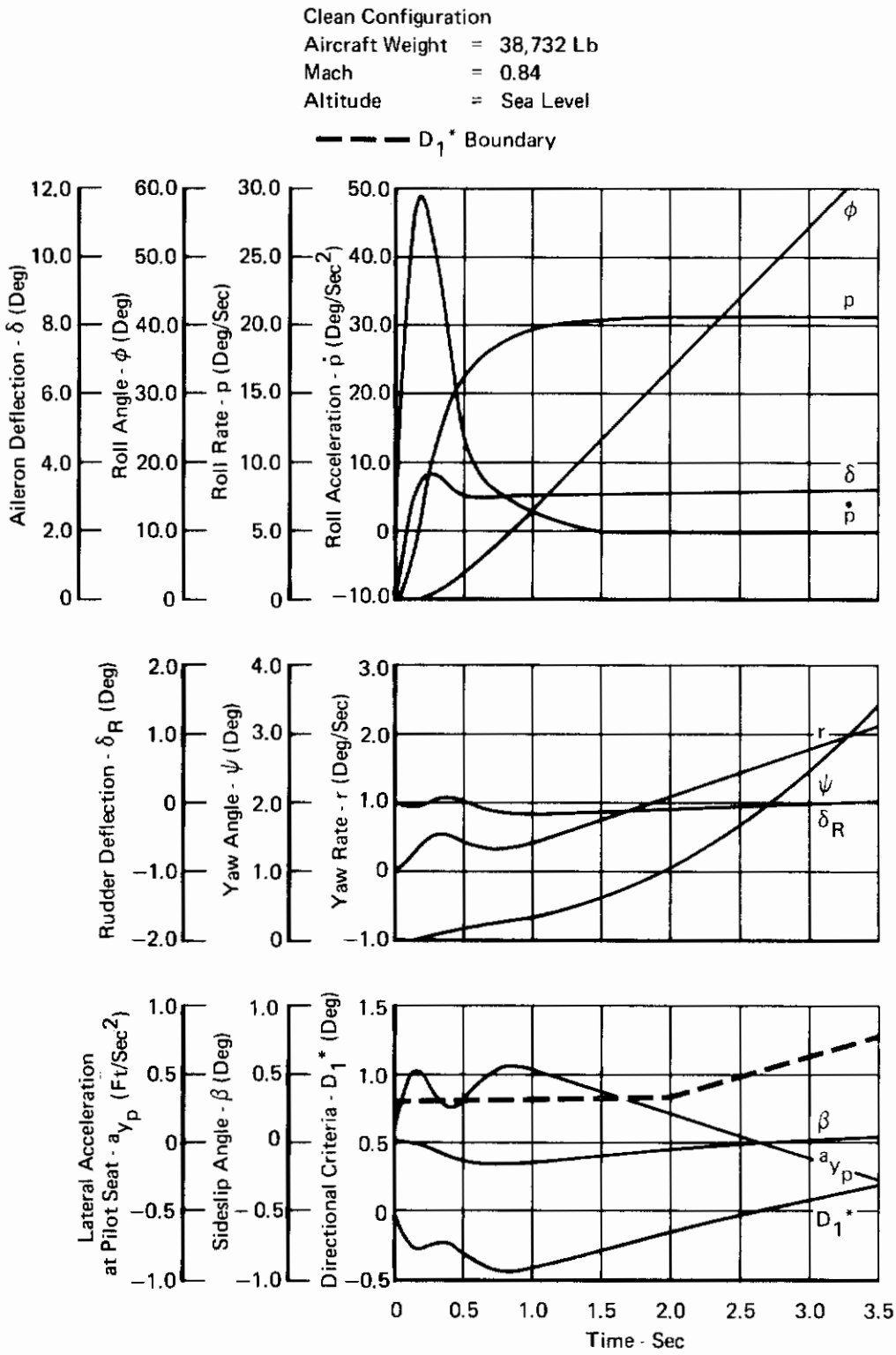

FIGURE 160
DYNAMIC RESPONSE TO A 3 LB STEP OF CENTER STICK FORCE

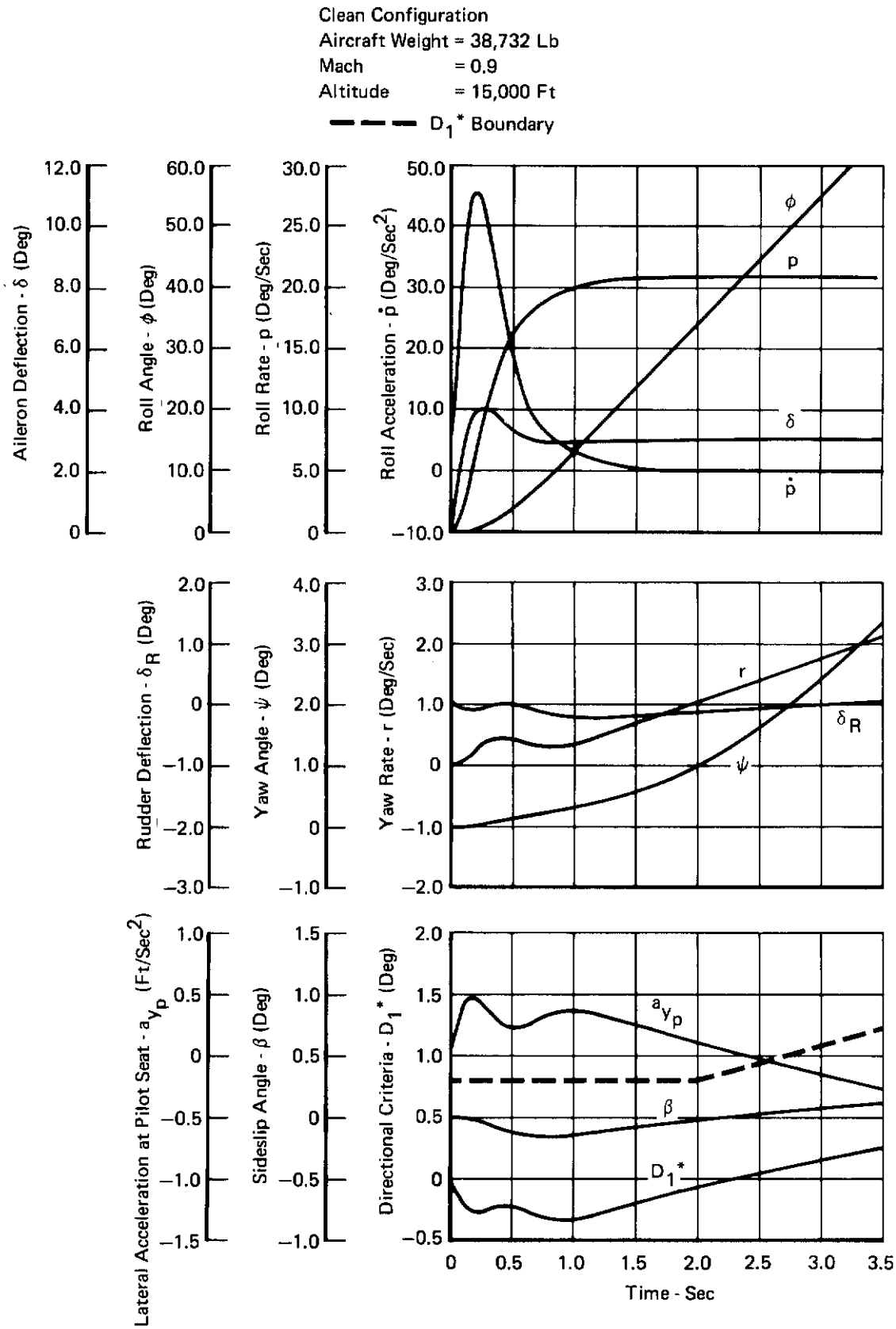

FIGURE 161
DYNAMIC RESPONSE TO A 3 LB STEP OF CENTER STICK FORCE

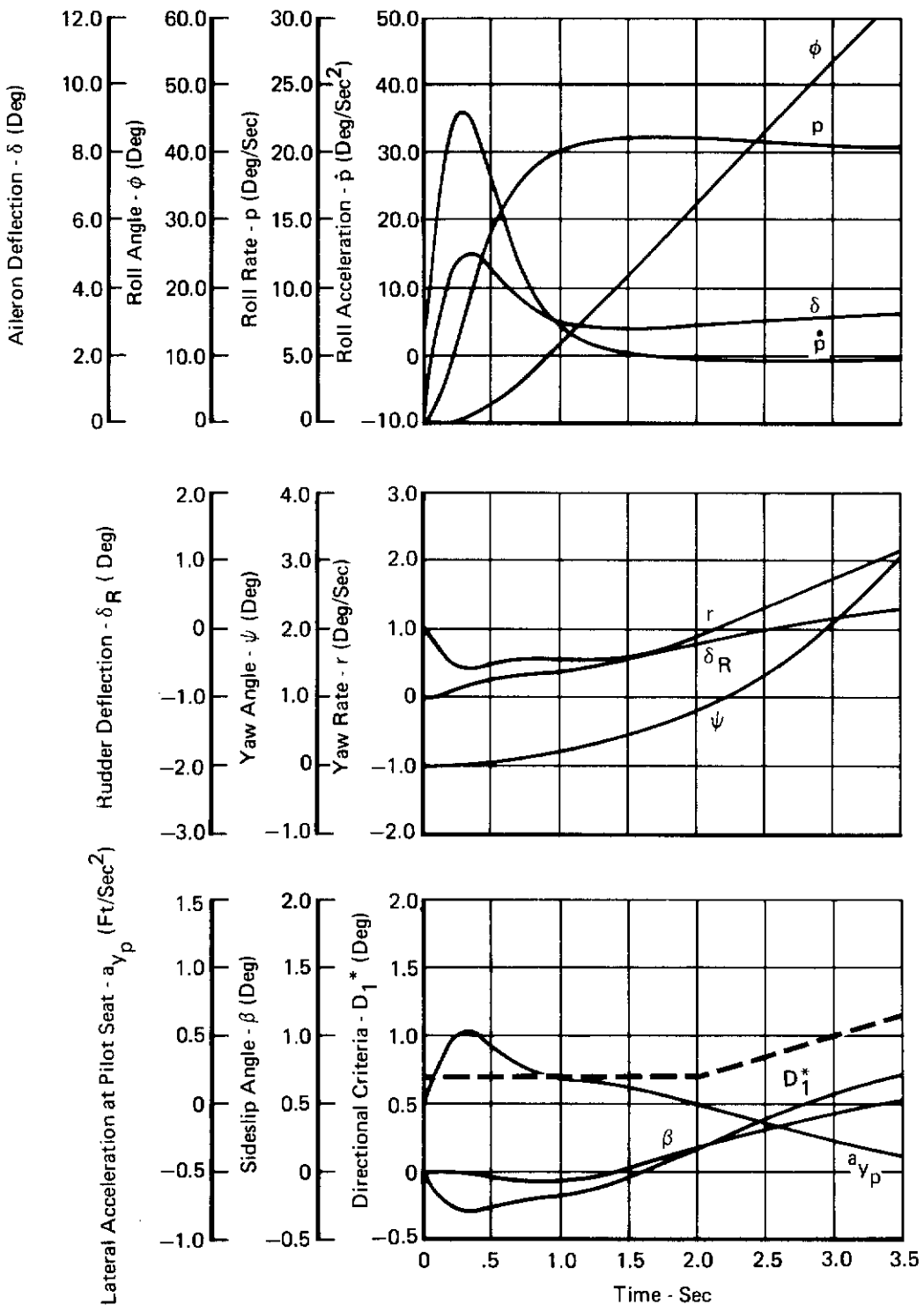

FIGURE 162
DYNAMIC RESPONSE TO A 3 LB STEP OF CENTER STICK FORCE

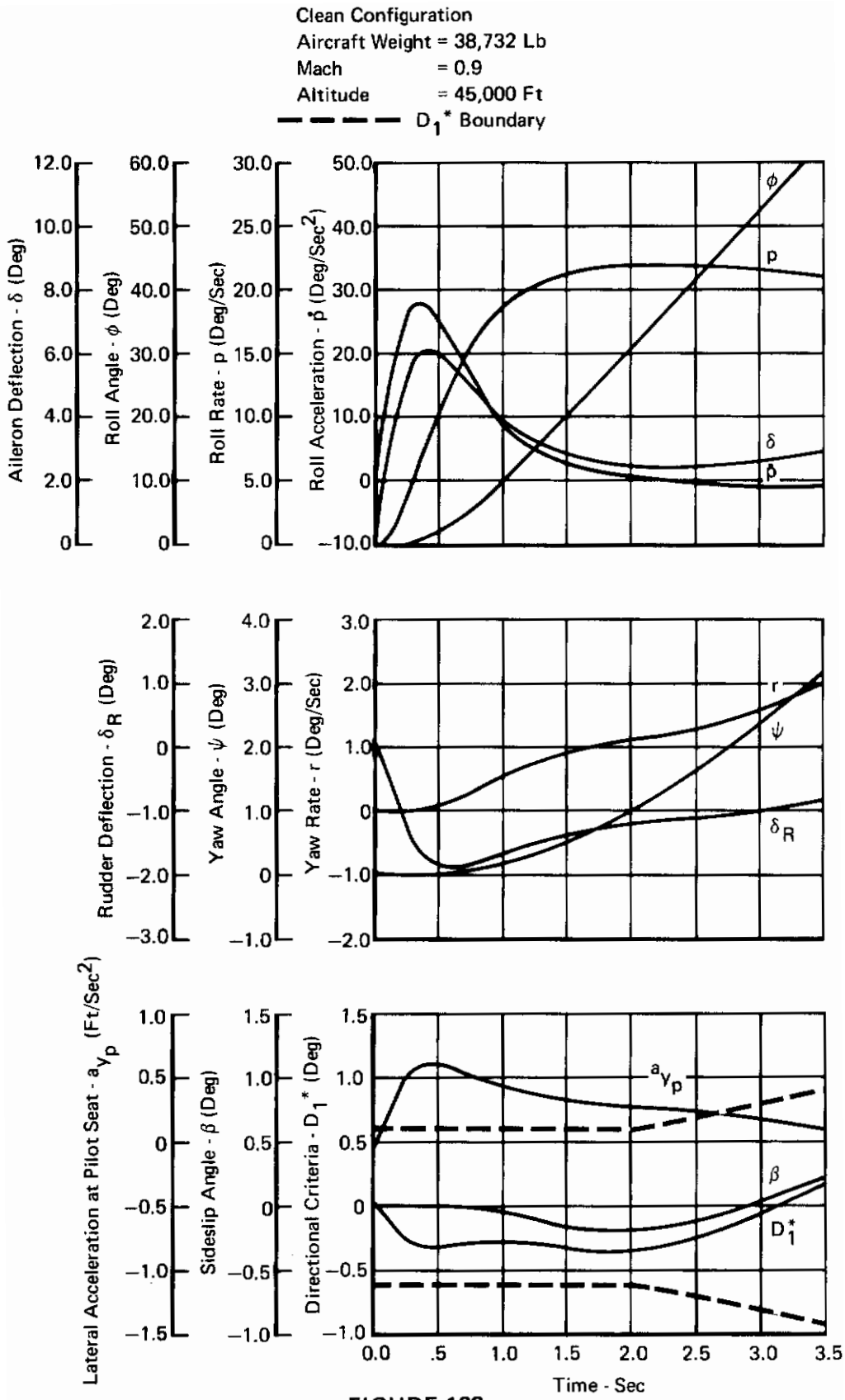

FIGURE 163
DYNAMIC RESPONSE TO A 3 LB STEP OF CENTER STICK FORCE

Clean Configuration
Aircraft Weight = 38,732 Lb
Mach = 1.2
Altitude = 5000 Ft
D_1^* Boundary

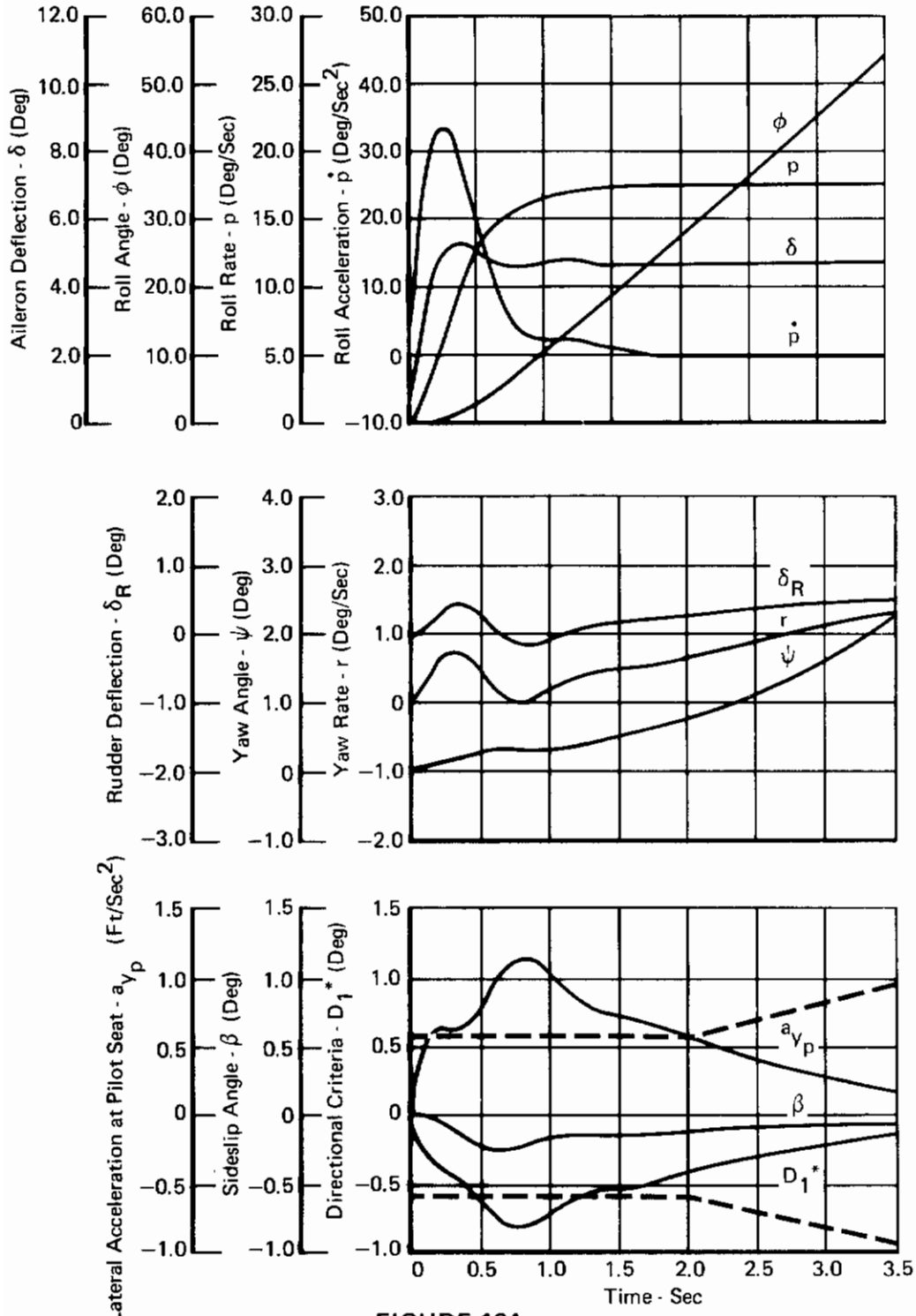

FIGURE 164
DYNAMIC RESPONSE TO A 3 LB STEP OF CENTER STICK FORCE

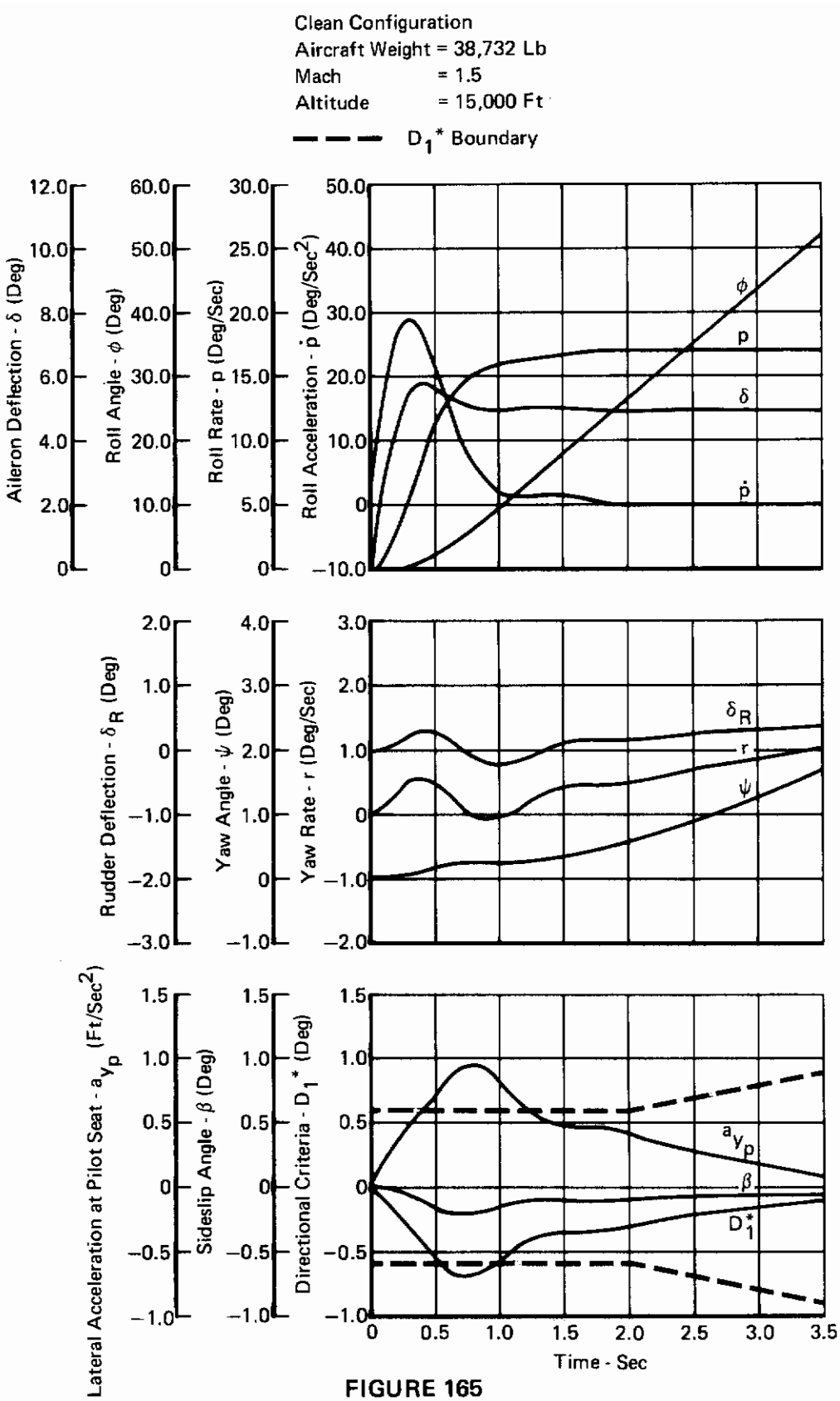

FIGURE 165

DYNAMIC RESPONSE TO A 3 LB STEP OF CENTER STICK FORCE

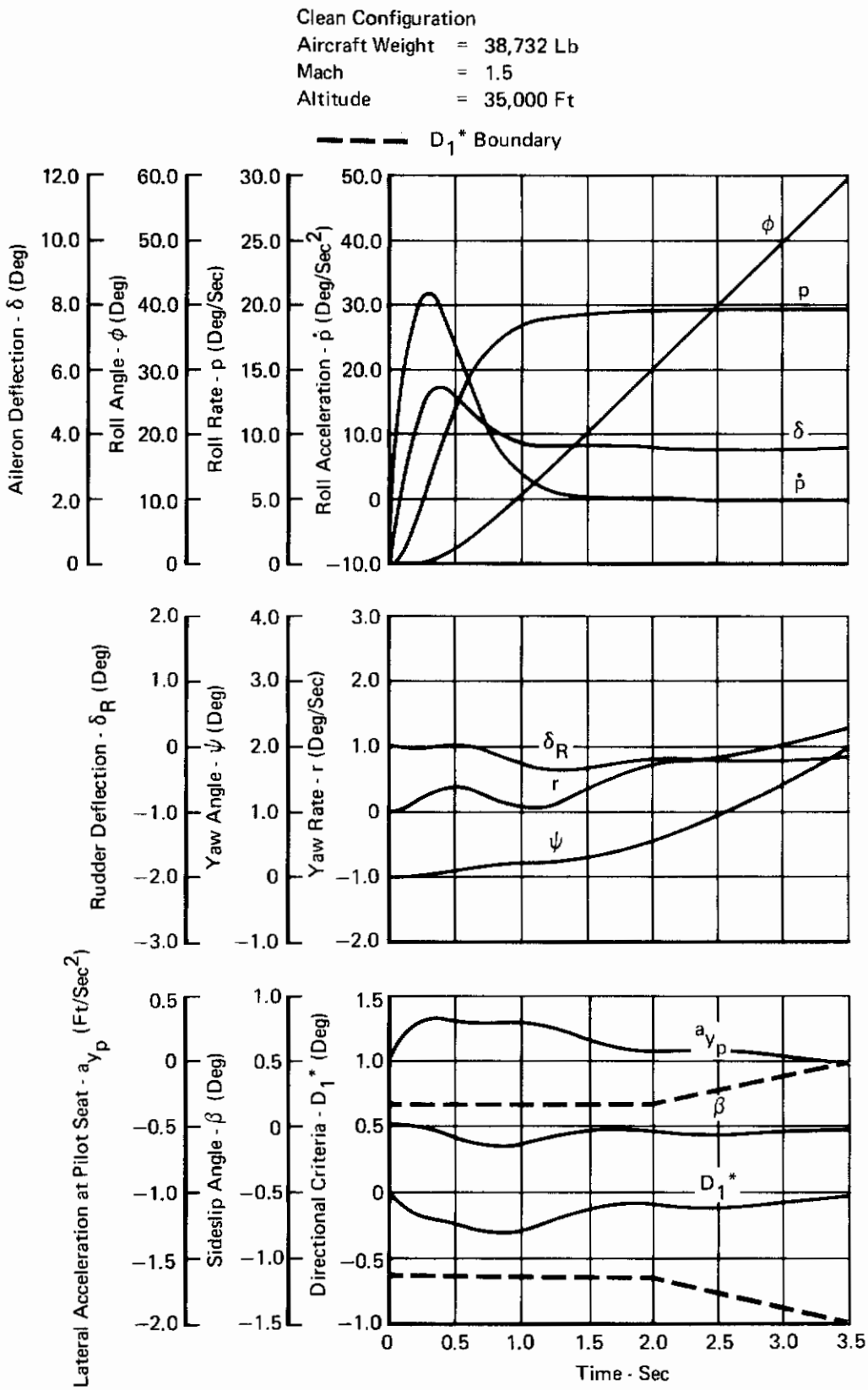

FIGURE 166
DYNAMIC RESPONSE TO A 3 LB STEP OF CENTER STICK FORCE

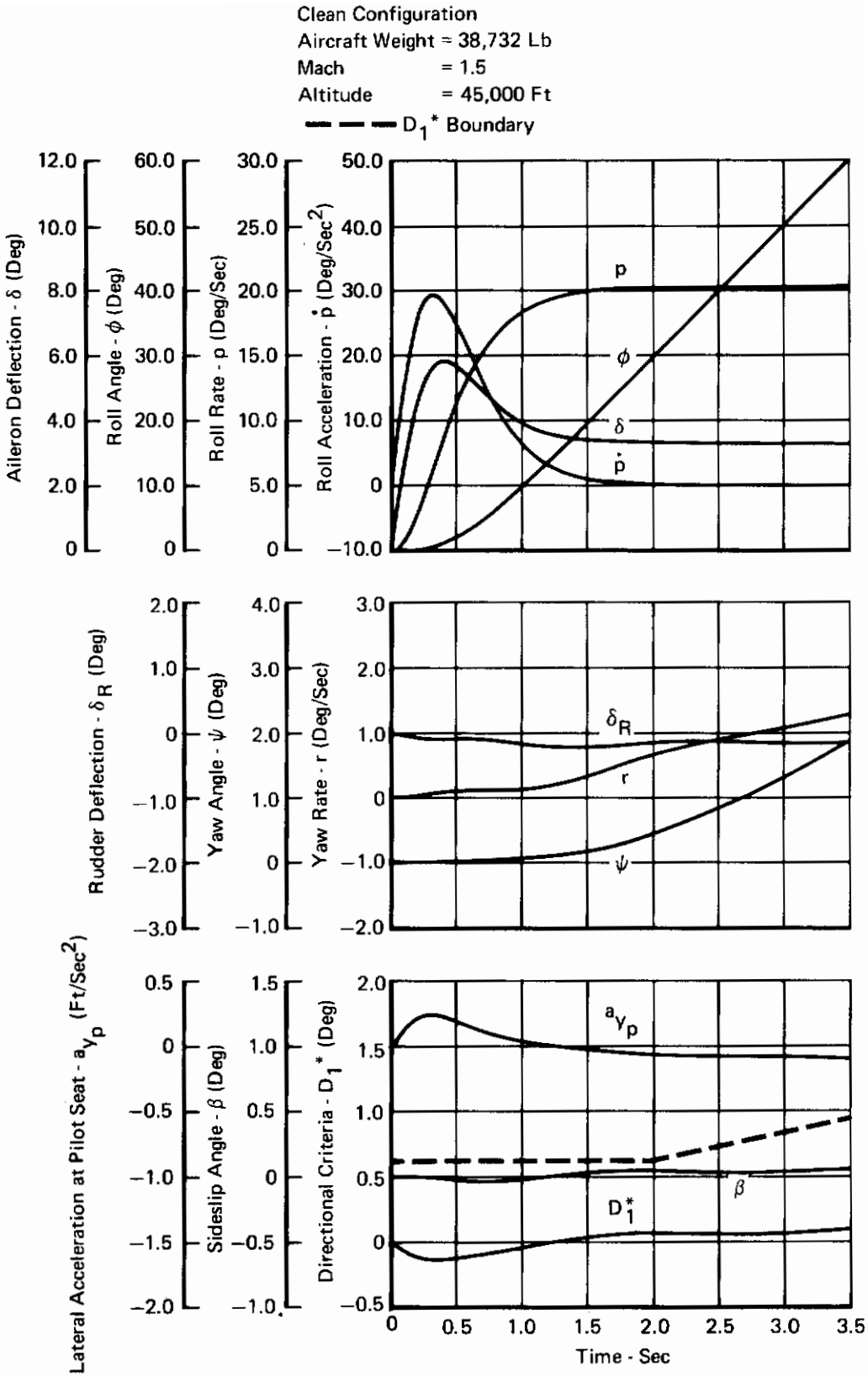

FIGURE 167

DYNAMIC RESPONSE TO A 3 LB STEP OF CENTER STICK FORCE

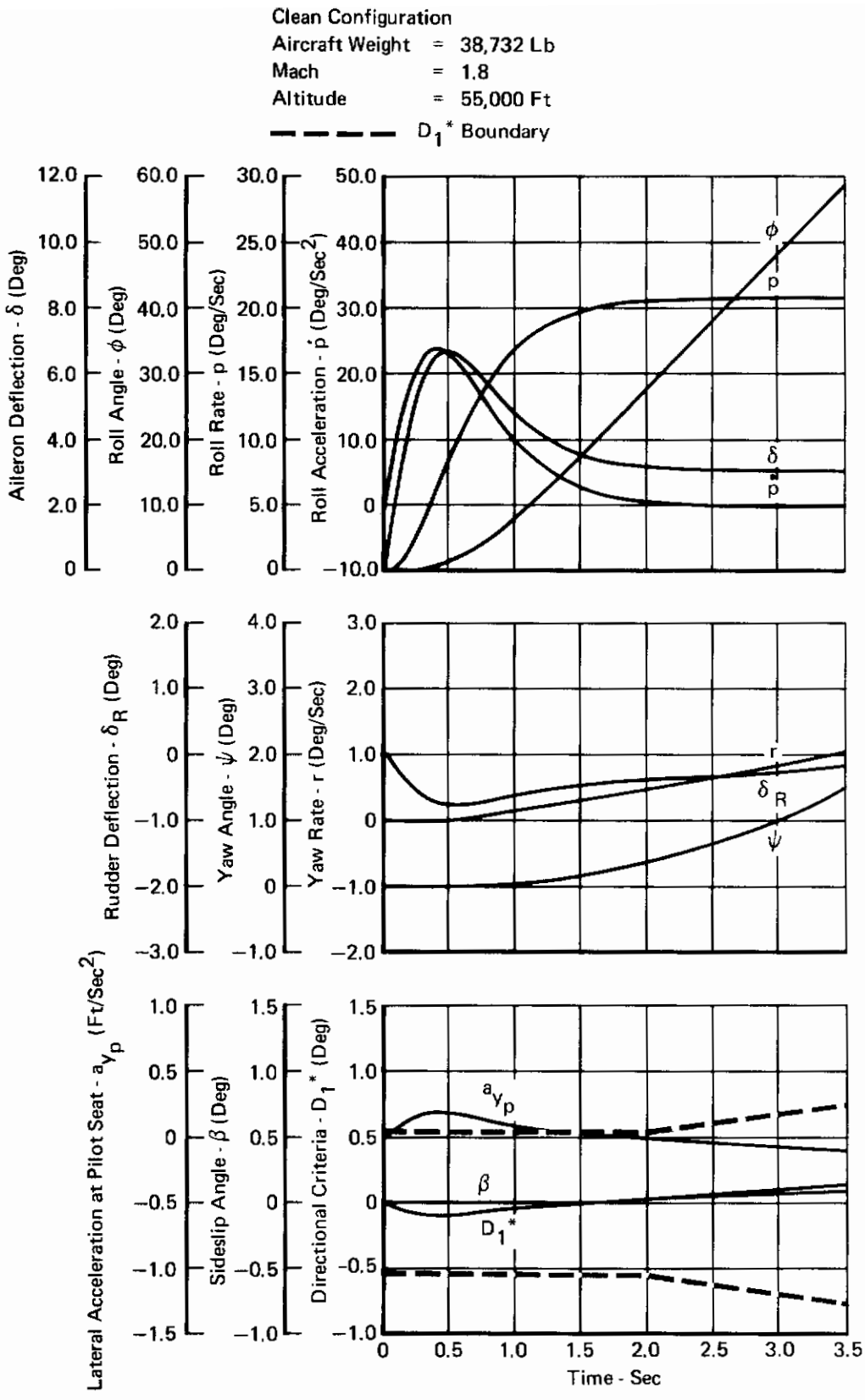

FIGURE 168
DYNAMIC RESPONSE TO A 3 LB STEP OF CENTER STICK FORCE

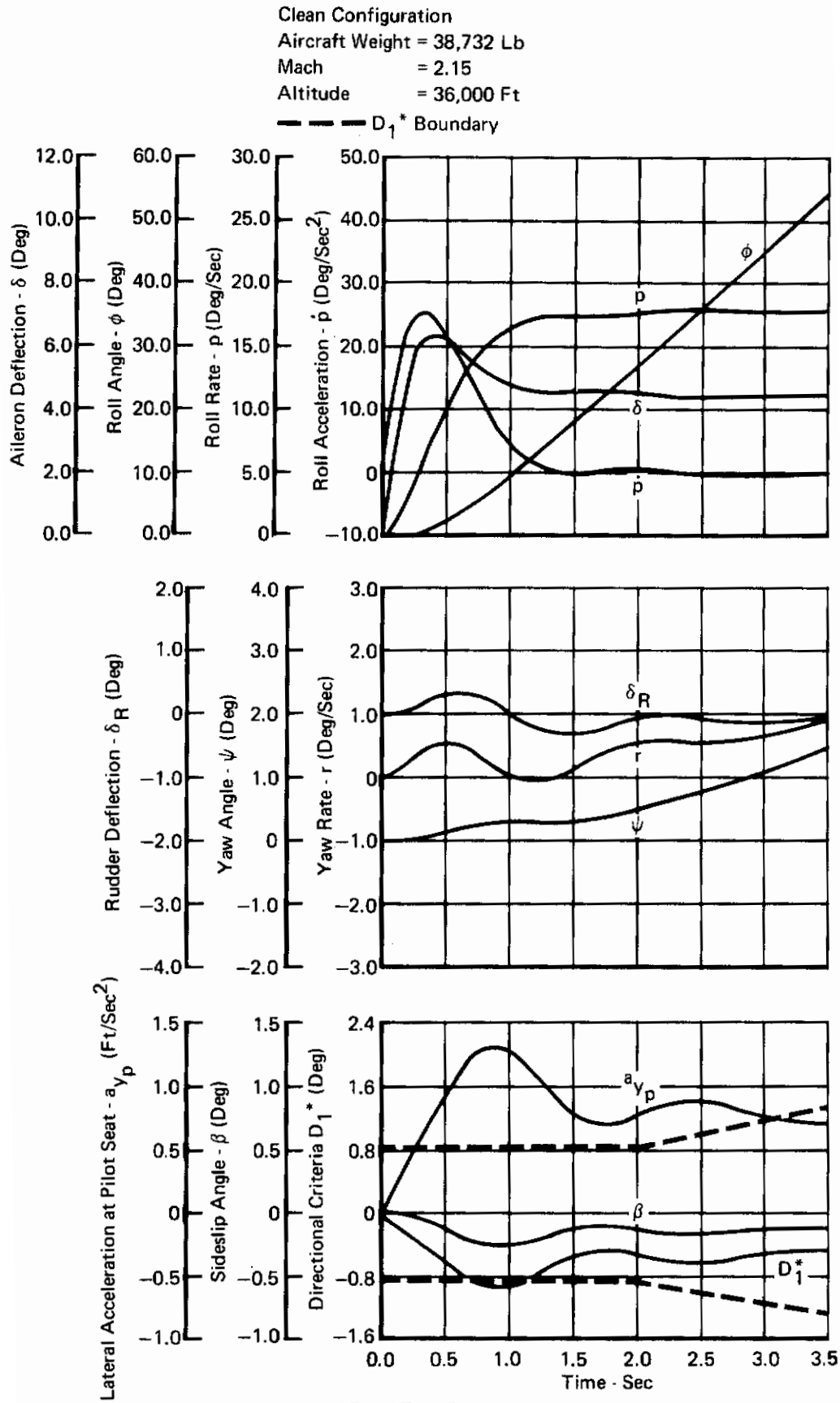

FIGURE 169
DYNAMIC RESPONSE TO A 3 LB STEP OF CENTER STICK FORCE

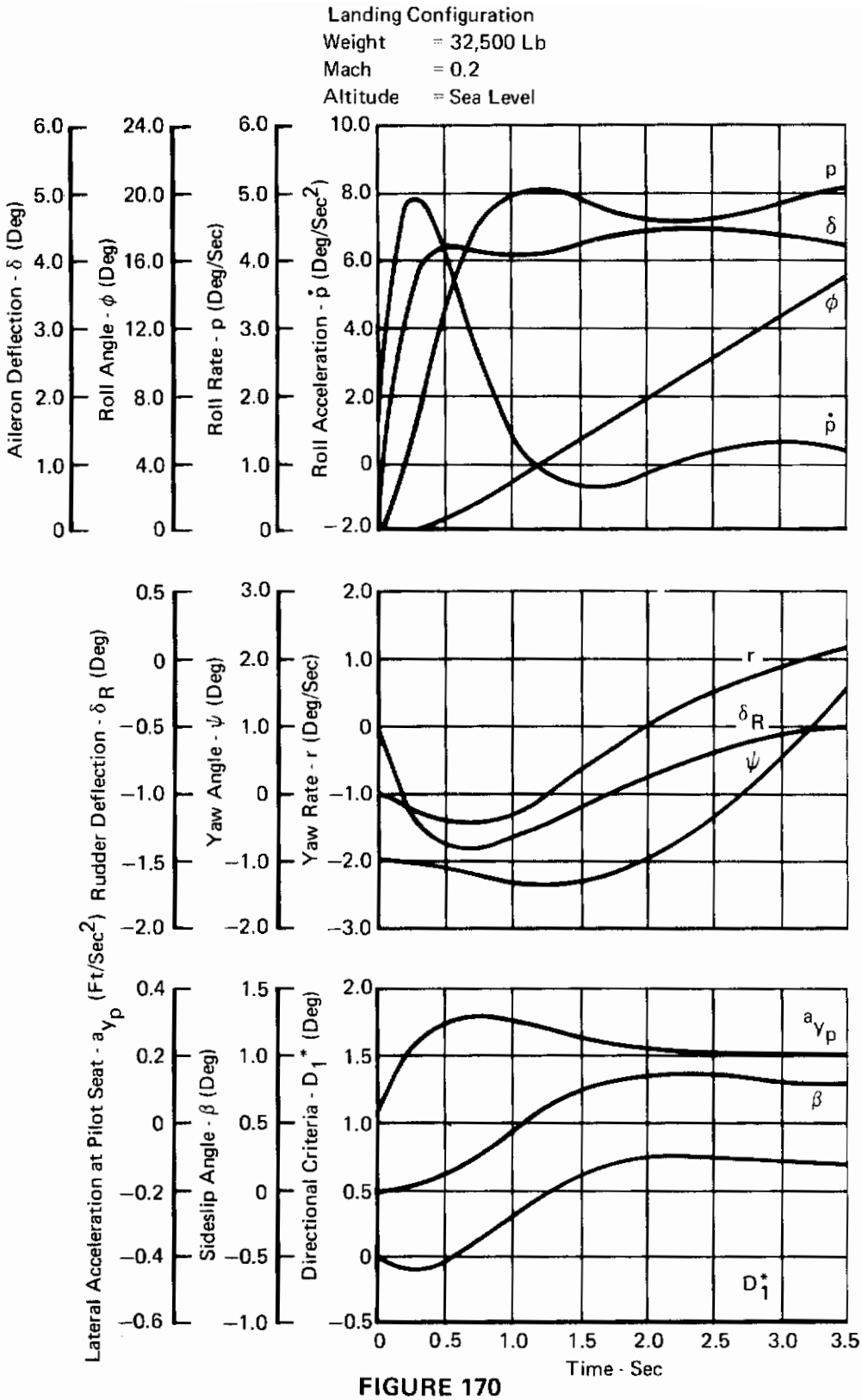

FIGURE 170

DYNAMIC RESPONSE TO A 3 LB STEP OF CENTER STICK FORCE

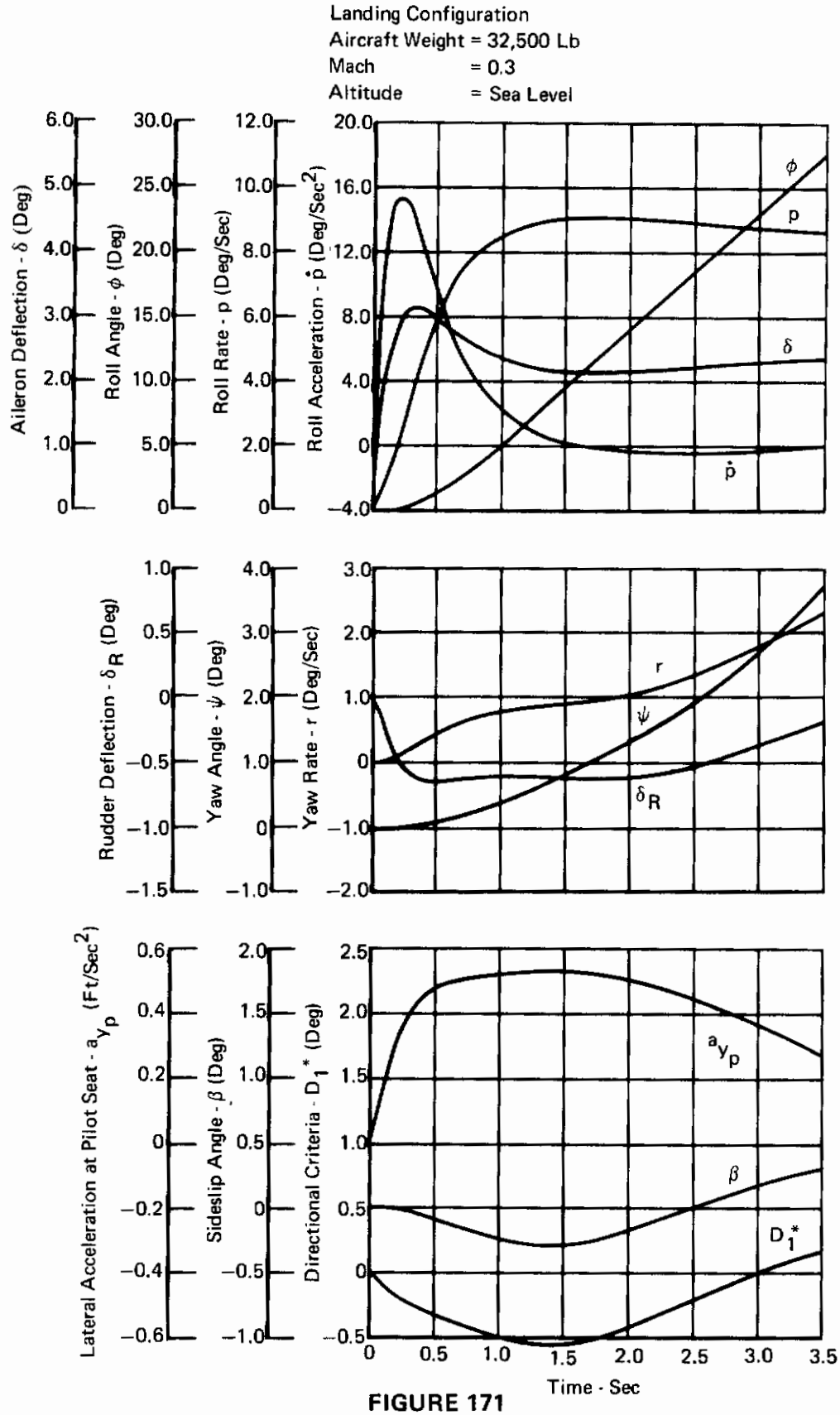

FIGURE 171

DYNAMIC RESPONSE TO A 3 LB STEP OF CENTER STICK FORCE

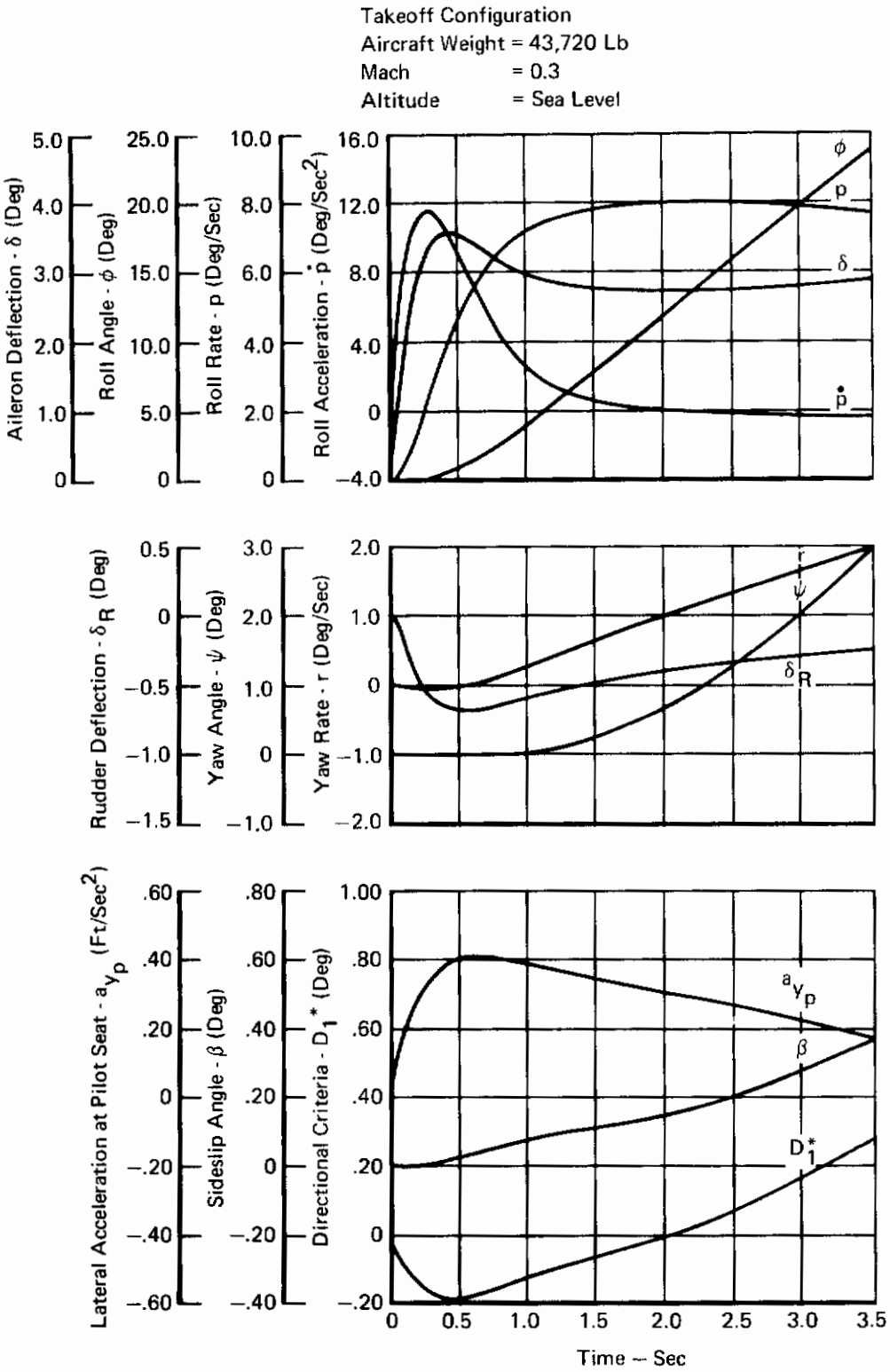

FIGURE 172
DYNAMIC RESPONSE TO A 3 LB STEP OF CENTER STICK FORCE

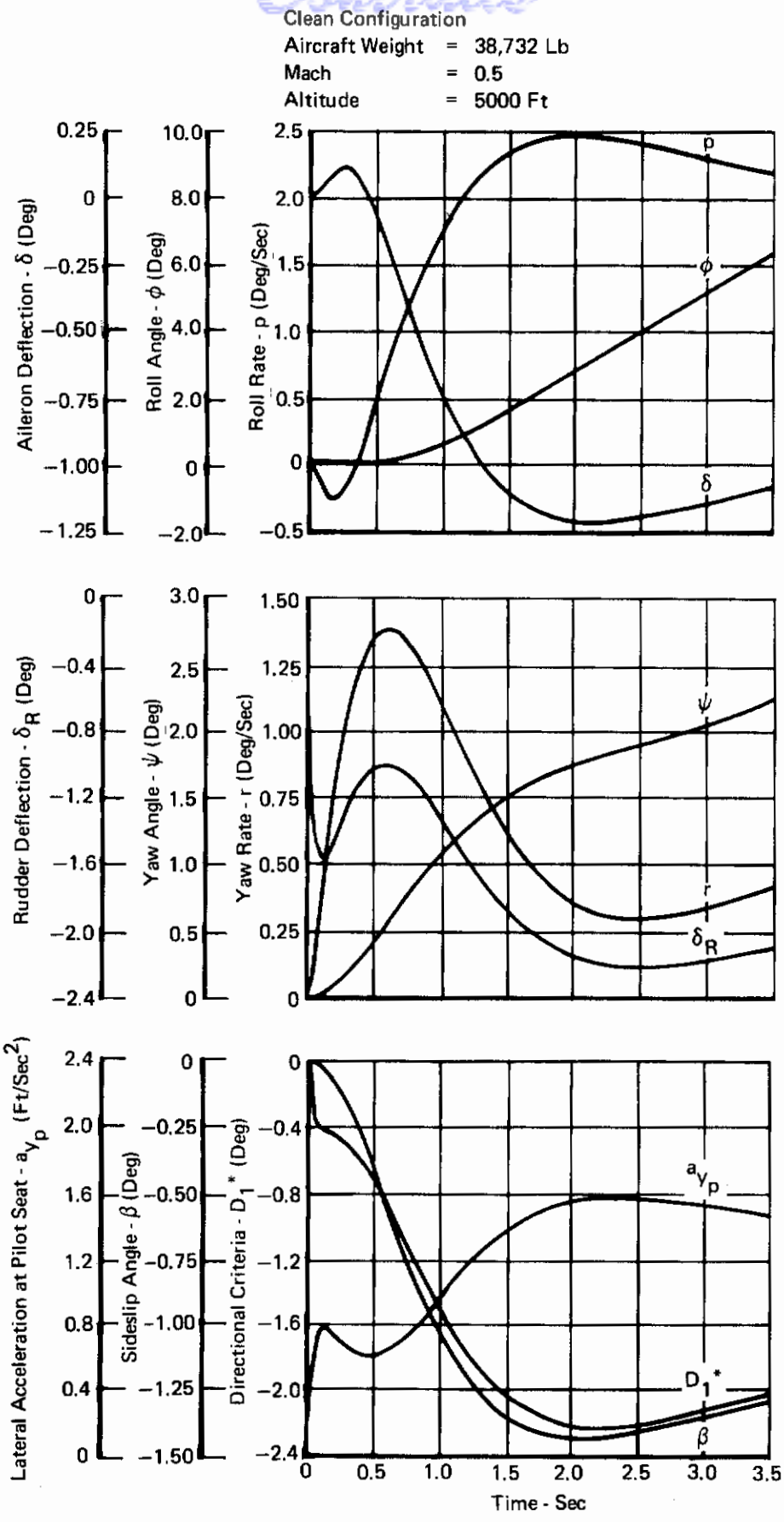

FIGURE 173
DYNAMIC RESPONSE TO A 16.5 LB STEP OF RUDDER PEDAL FORCE

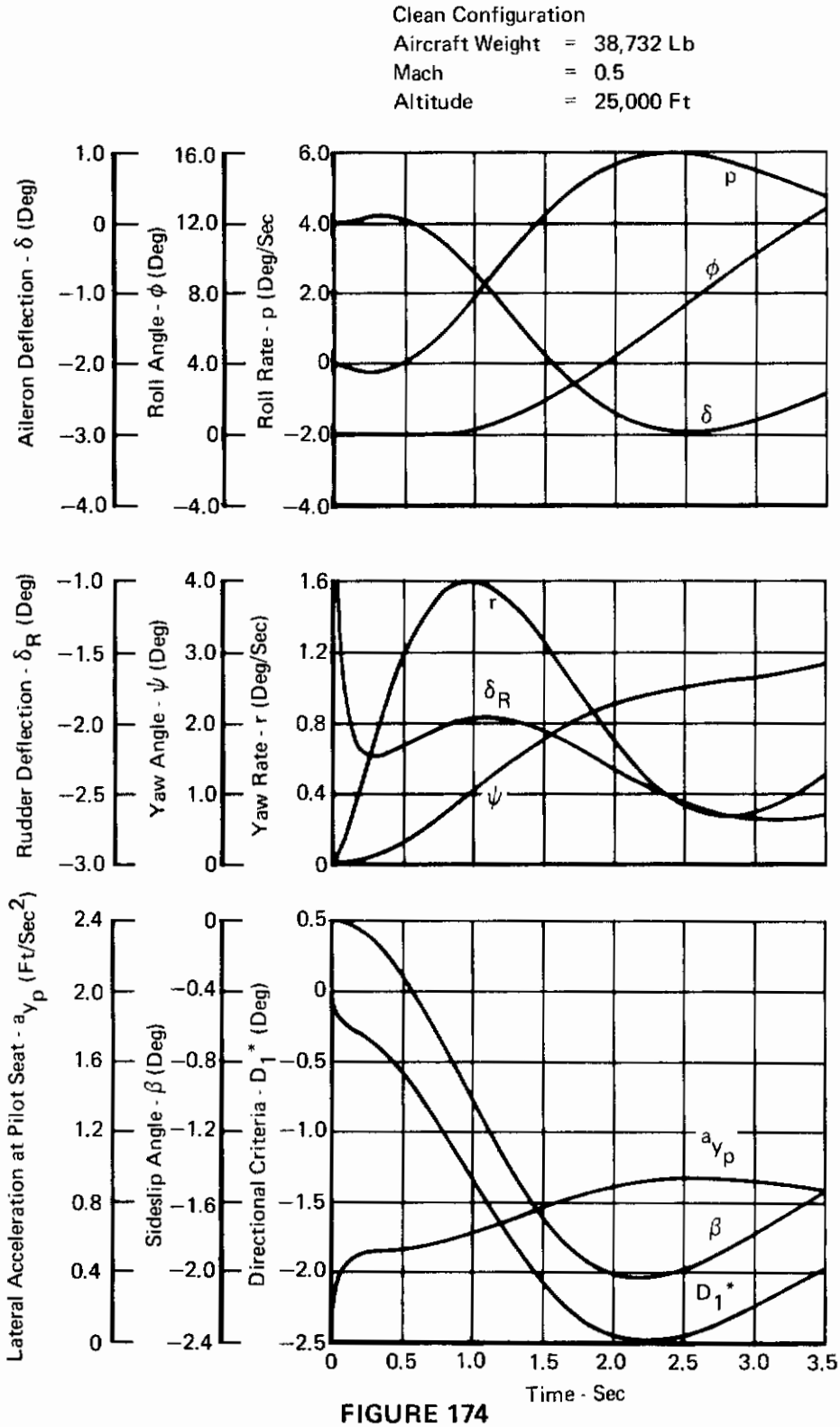

FIGURE 174
DYNAMIC RESPONSE TO A 16.5 LB STEP OF RUDDER PEDAL FORCE

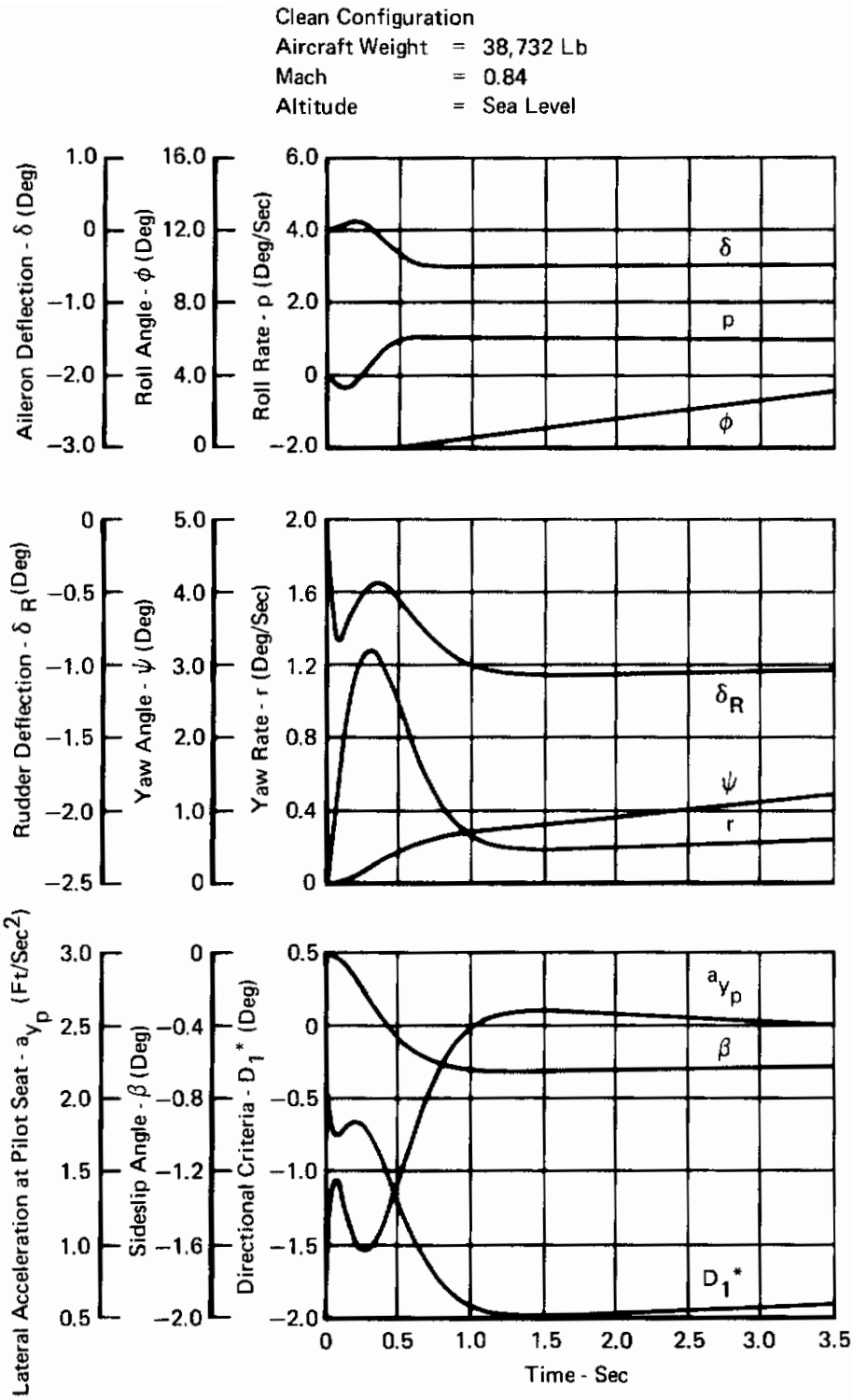

FIGURE 175
DYNAMIC RESPONSE TO A 16.5 LB STEP OF RUDDER PEDAL FORCE

Clean Configuration
Aircraft Weight = 38,732 Lb
Mach = 0.9
Altitude = 15,000 Ft

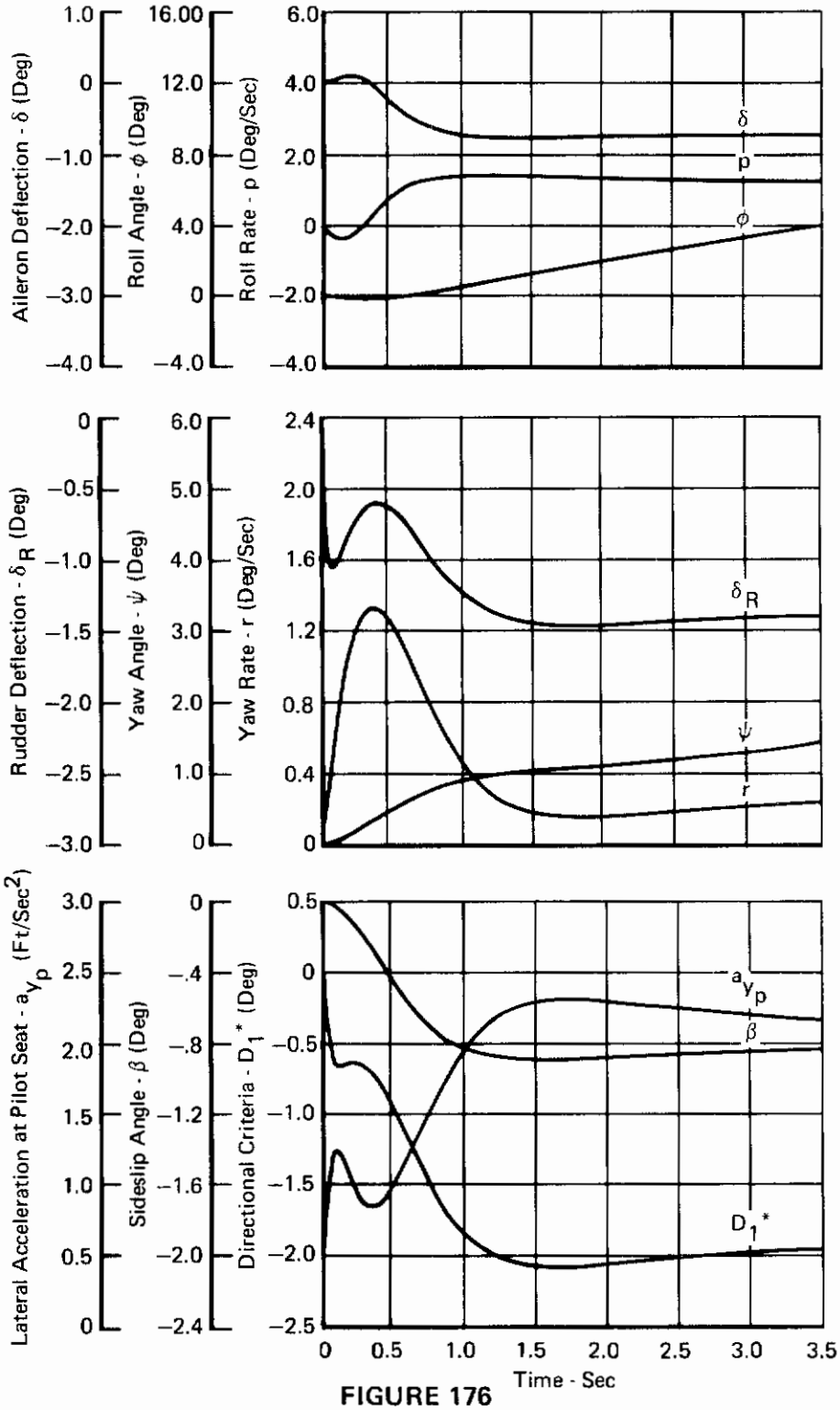

FIGURE 176
DYNAMIC RESPONSE TO A 16.5 LB STEP OF RUDDER PEDAL FORCE

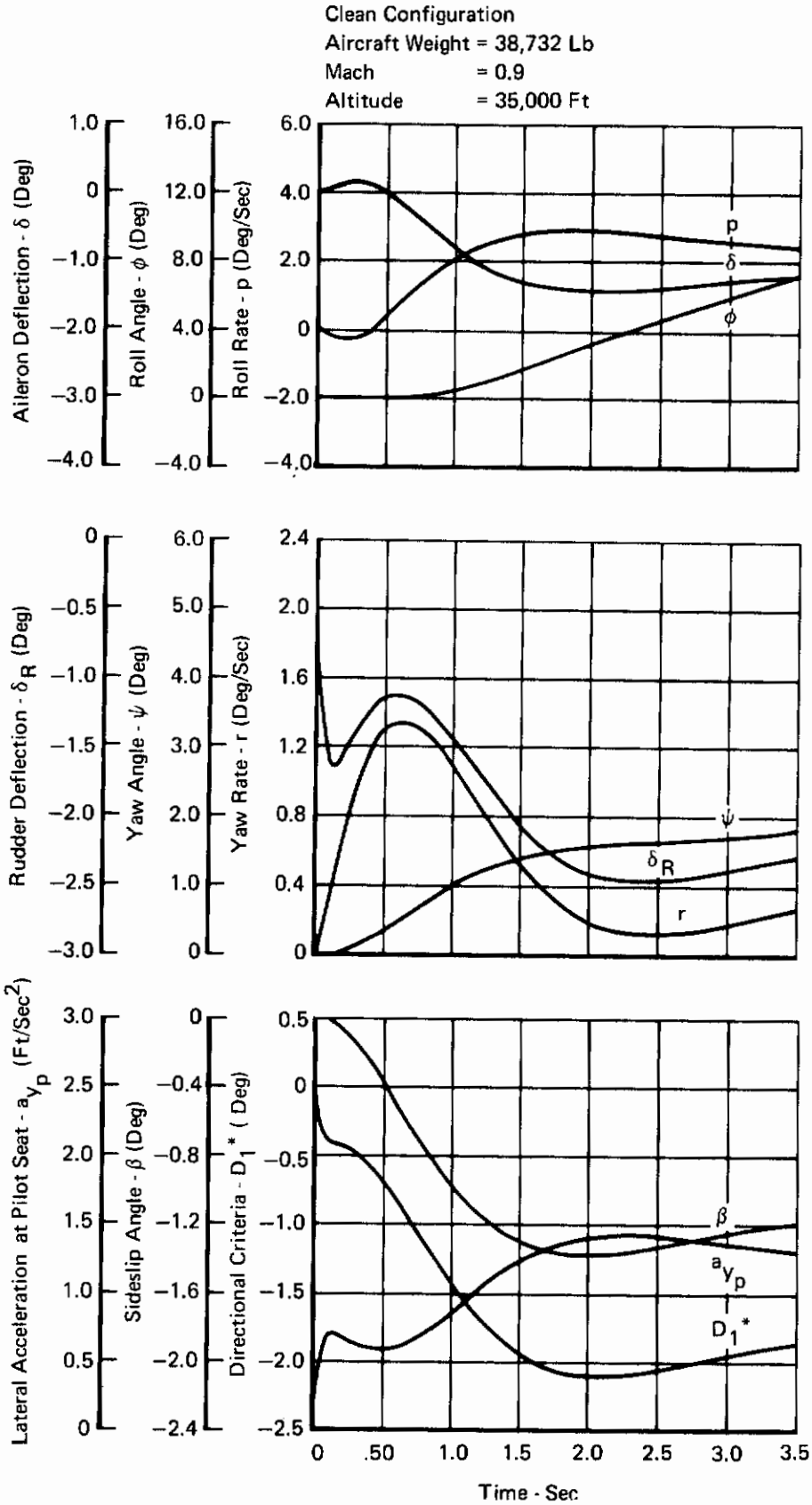

FIGURE 177
DYNAMIC RESPONSE TO A 16.5 LB STEP OF RUDDER PEDAL FORCE

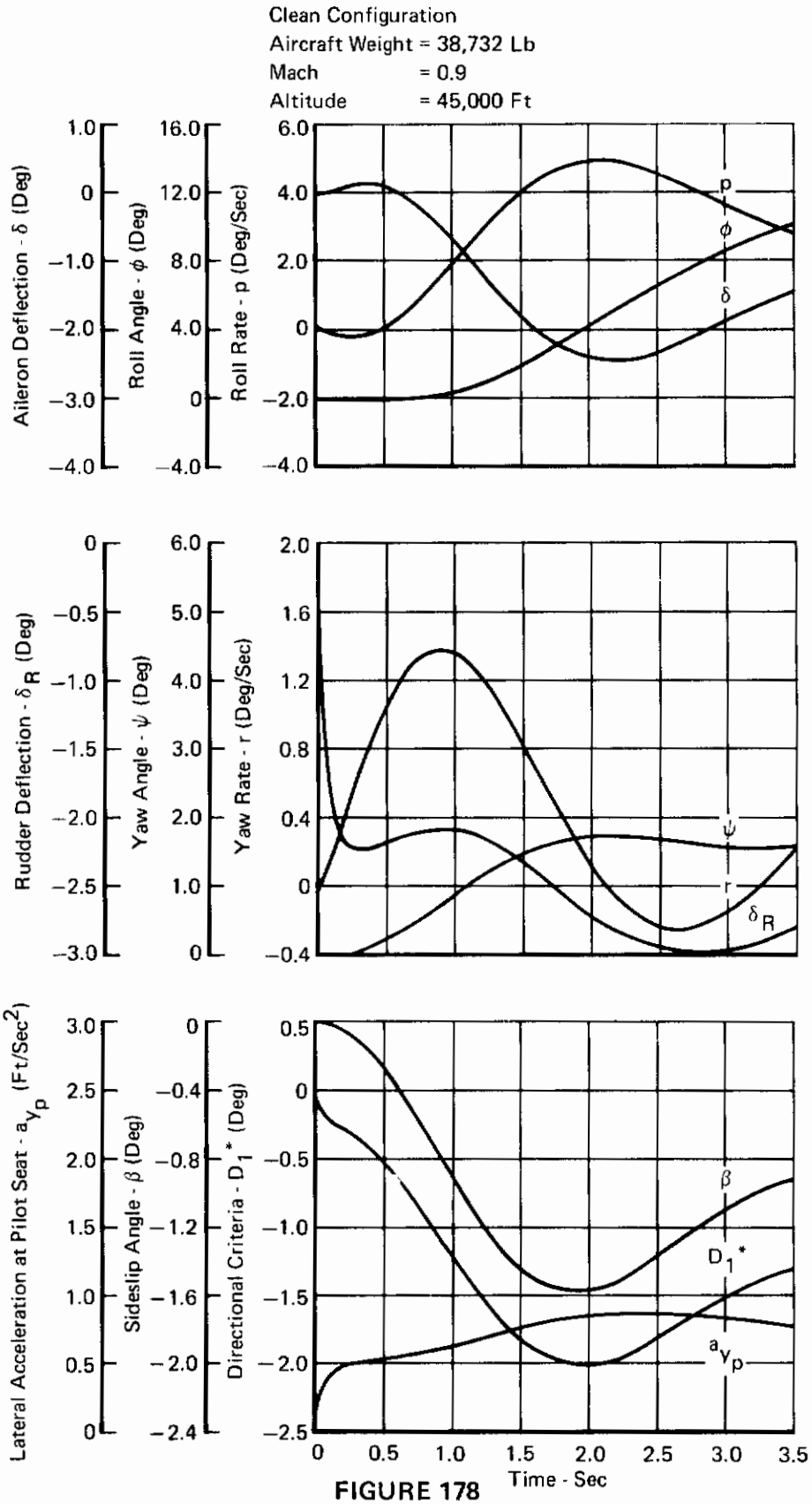

FIGURE 178
DYNAMIC RESPONSE TO A 16.5 LB STEP OF RUDDER PEDAL FORCE

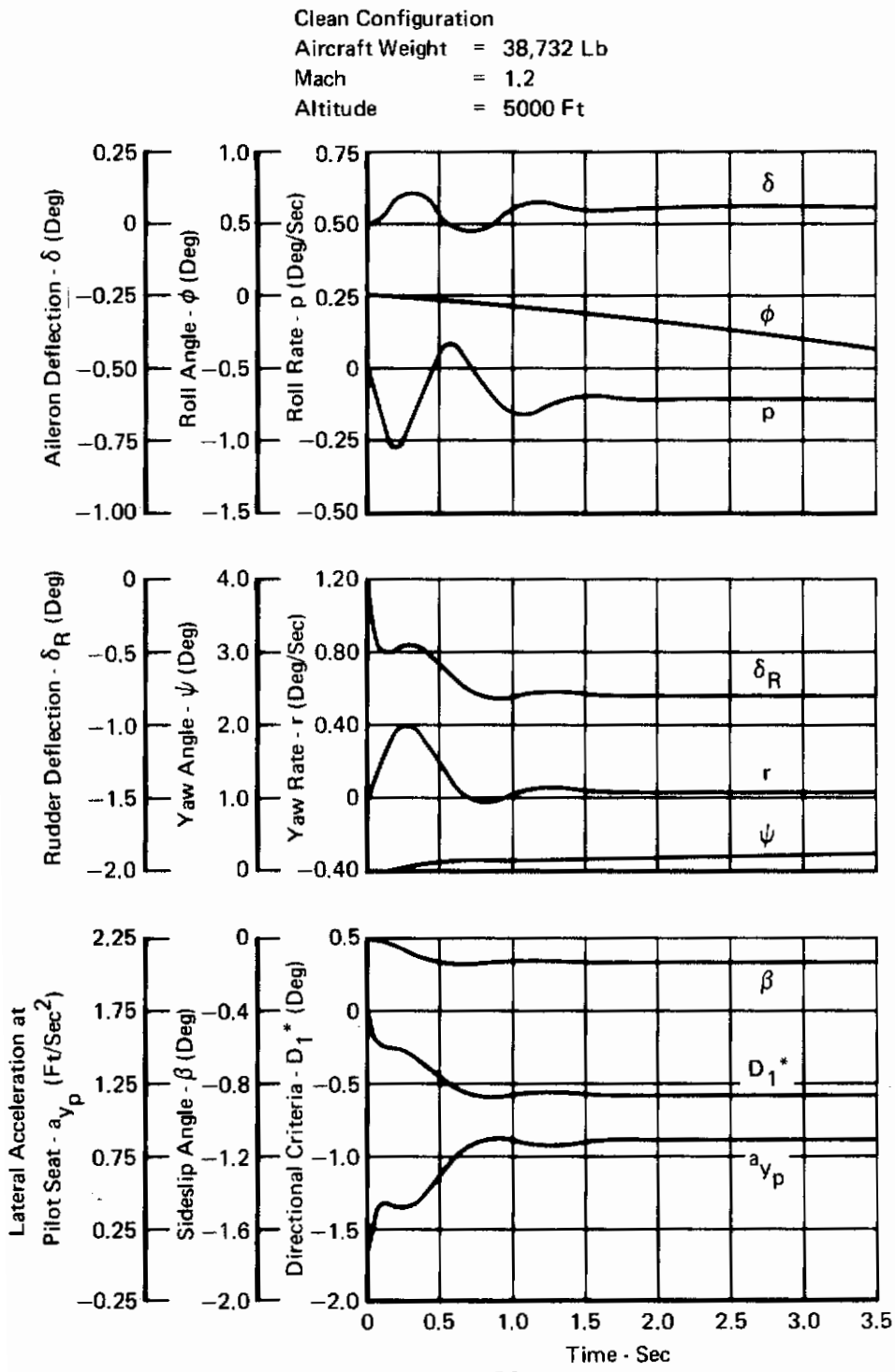

FIGURE 179
DYNAMIC RESPONSE TO A 16.5 LB STEP OF RUDDER PEDAL FORCE

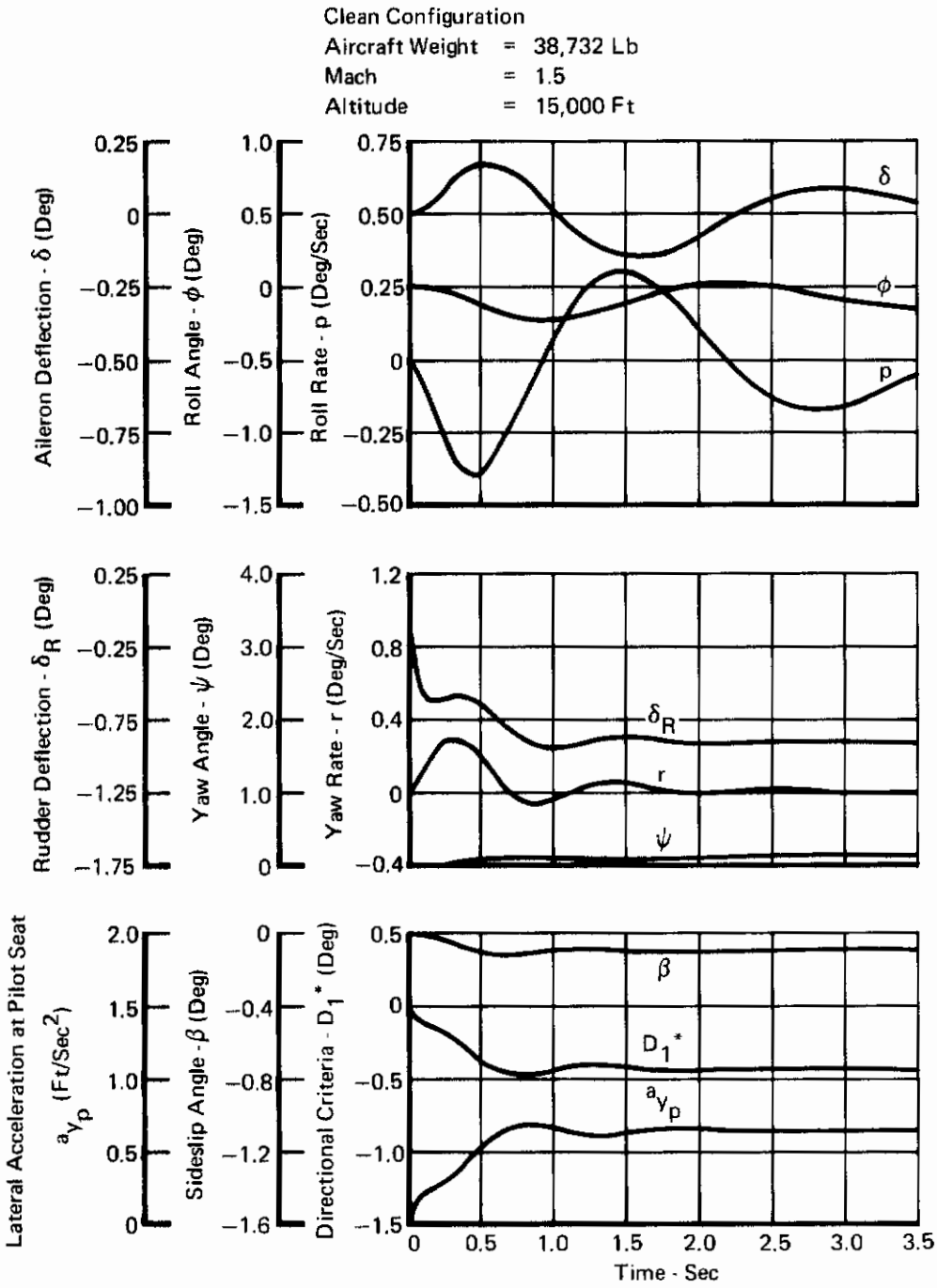

FIGURE 180

DYNAMIC RESPONSE TO A 16.5 LB STEP OF RUDDER PEDAL FORCE

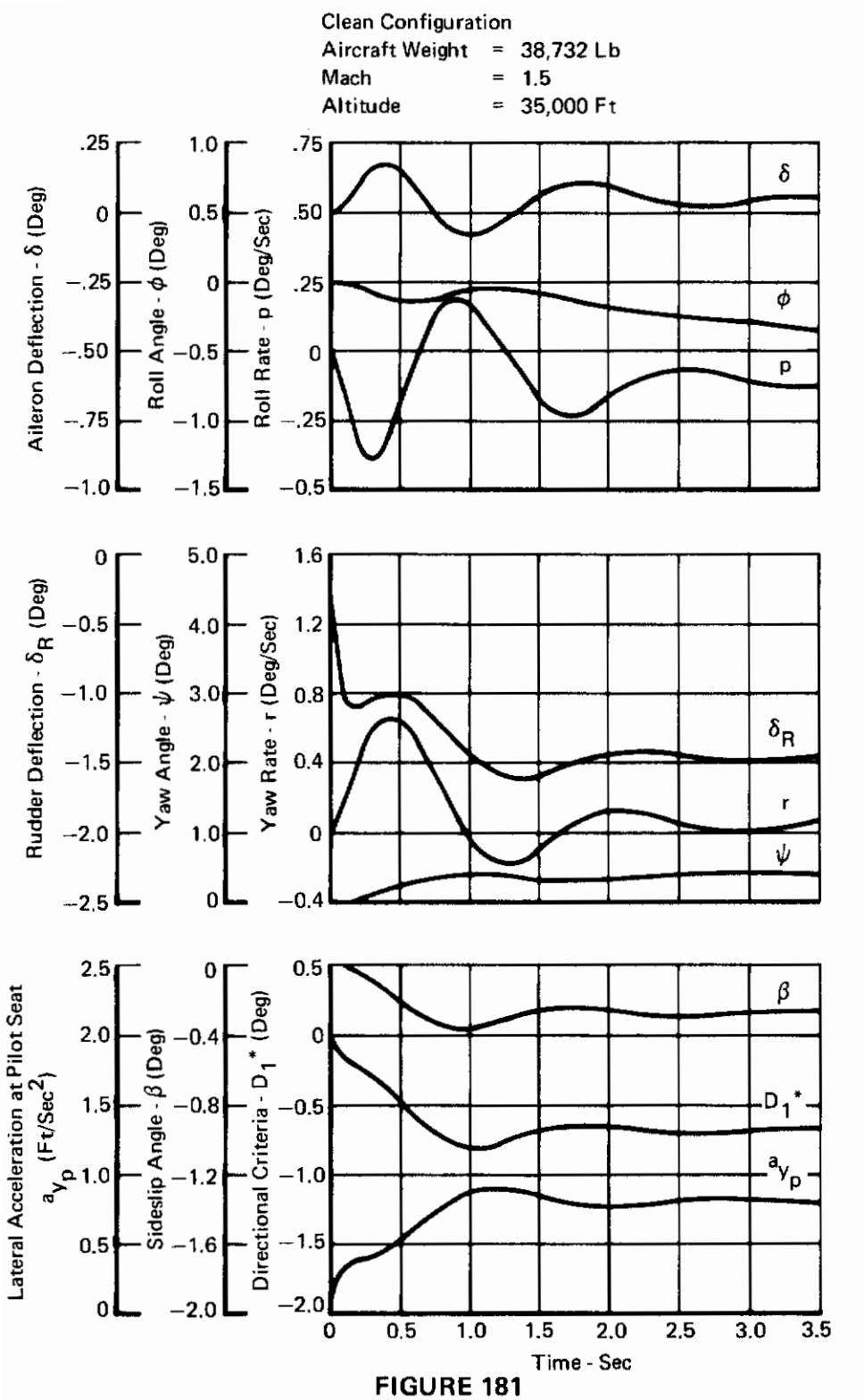

FIGURE 181

DYNAMIC RESPONSE TO A 16.5 LB STEP OF RUDDER PEDAL FORCE

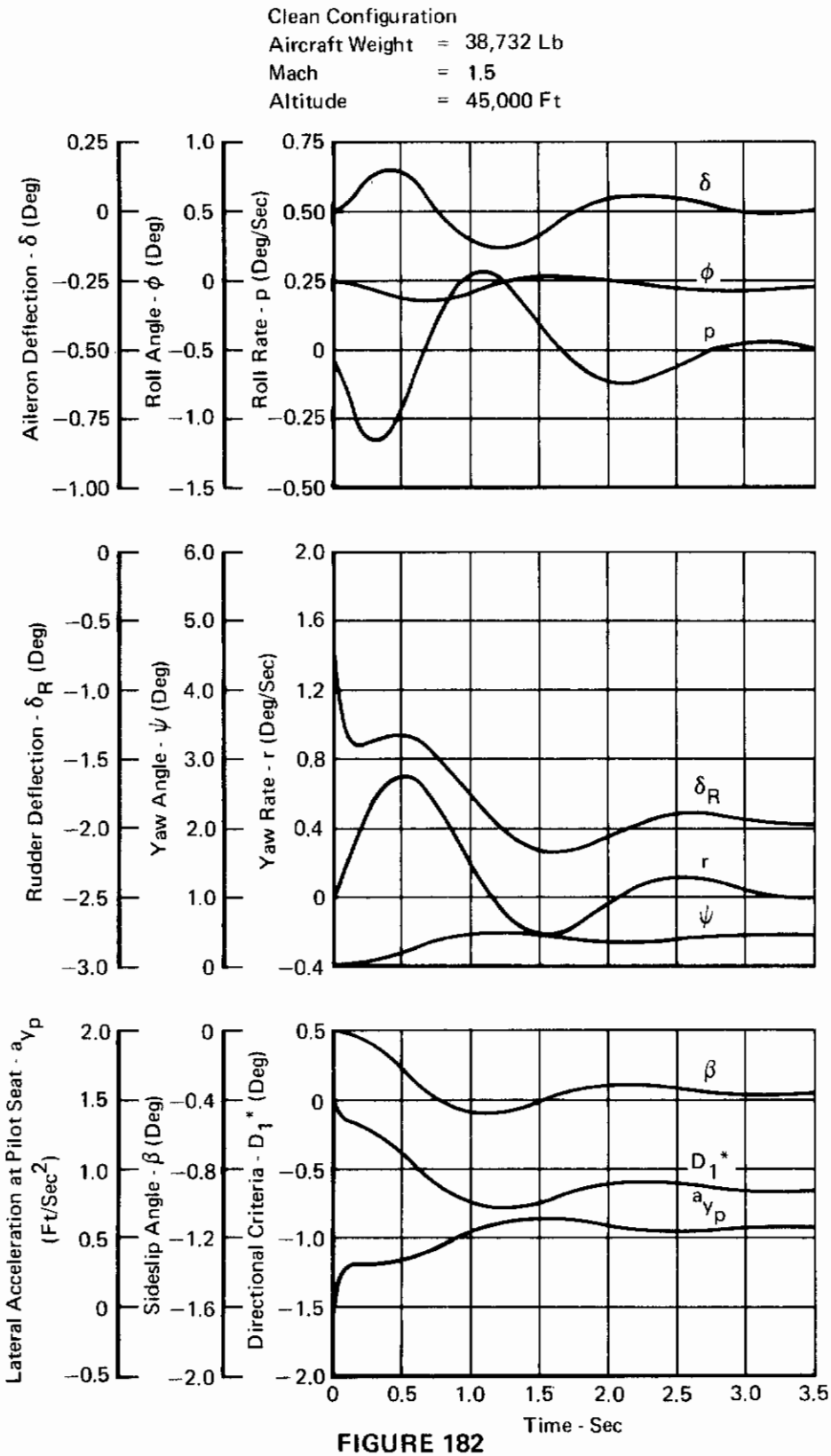

FIGURE 182
DYNAMIC RESPONSE TO A 16.5 LB STEP OF RUDDER PEDAL FORCE

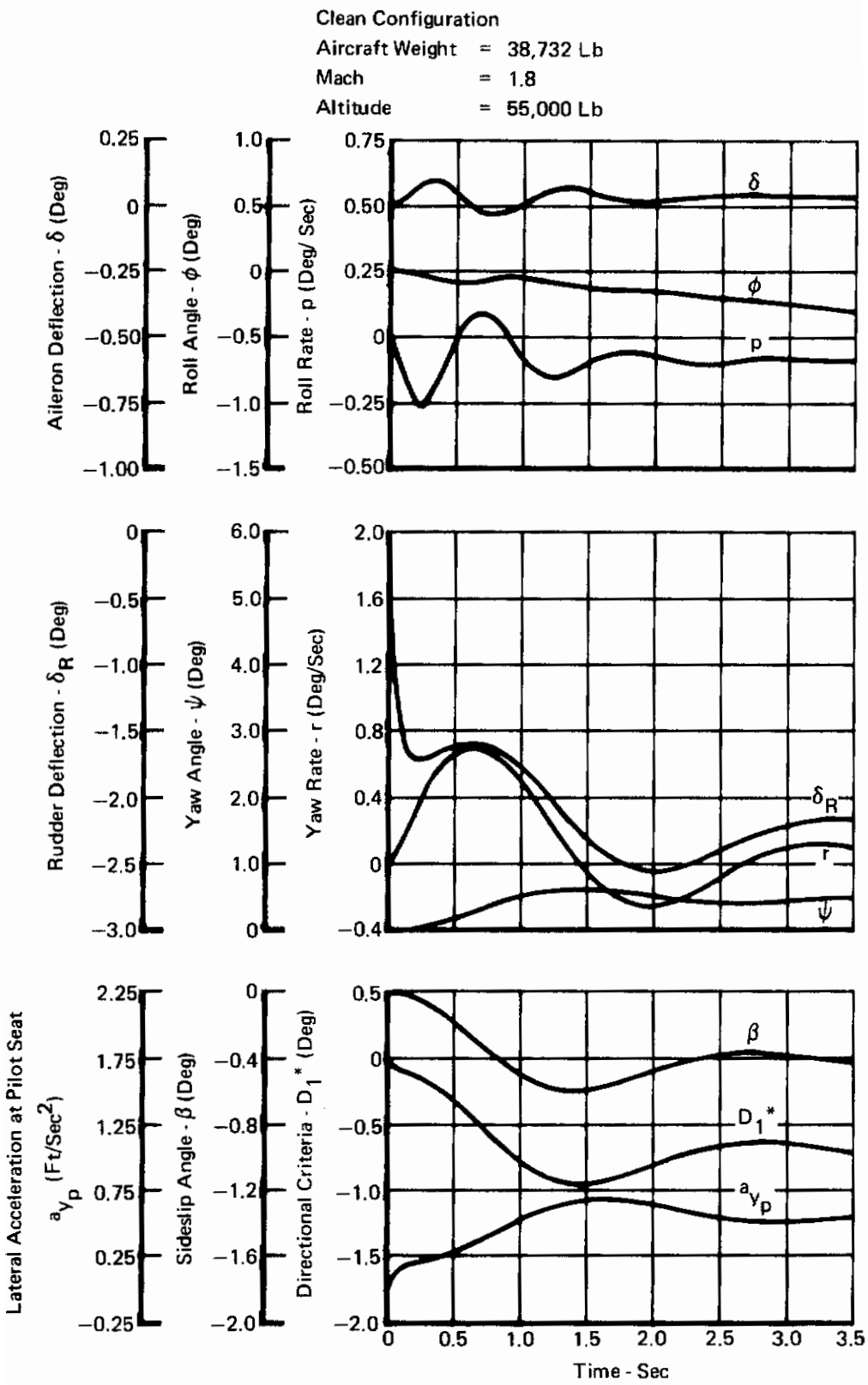

FIGURE 183
DYNAMIC RESPONSE TO A 16.5 LB STEP OF RUDDER PEDAL FORCE

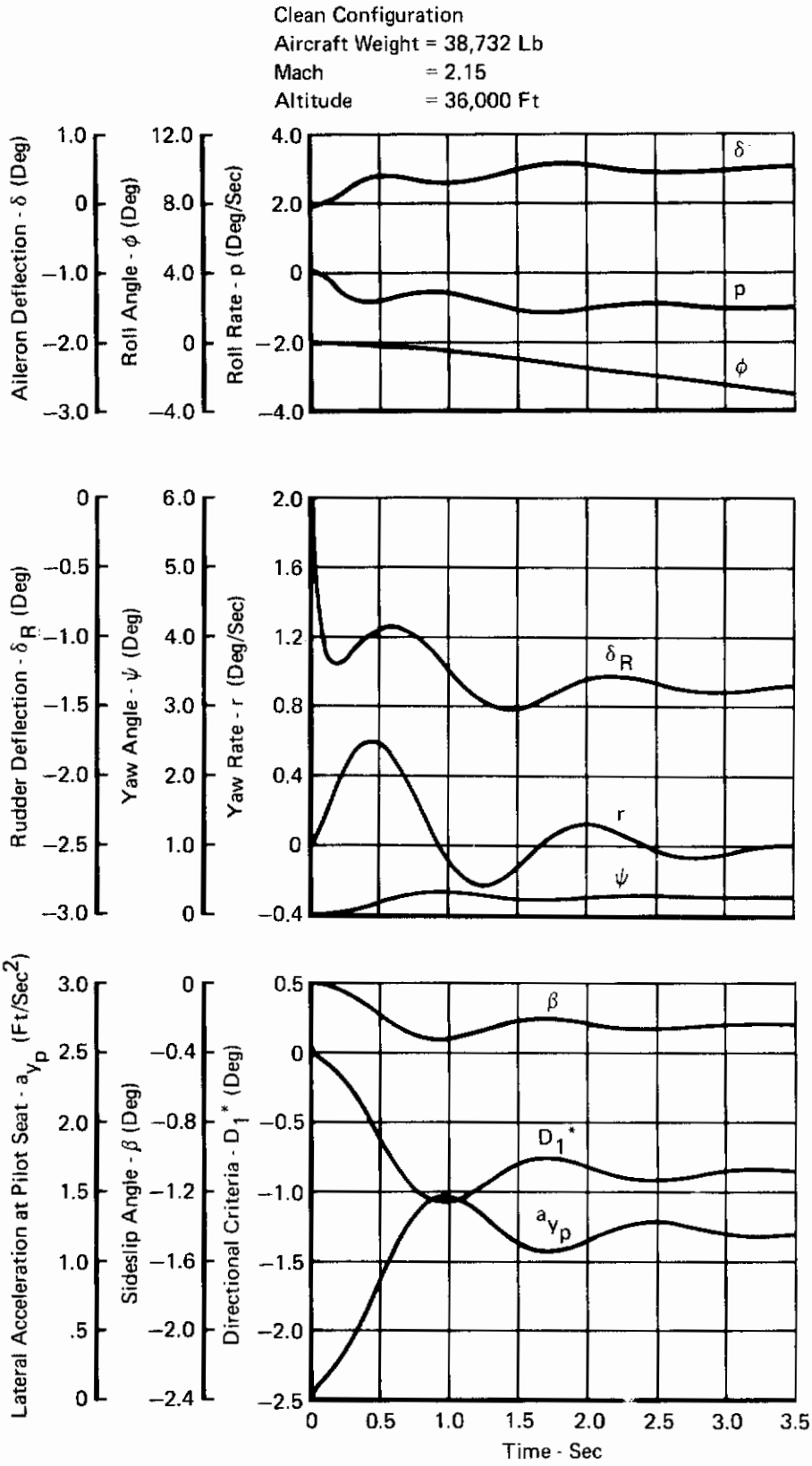

FIGURE 184
DYNAMIC RESPONSE TO A 16.5 LB STEP OF RUDDER PEDAL FORCE

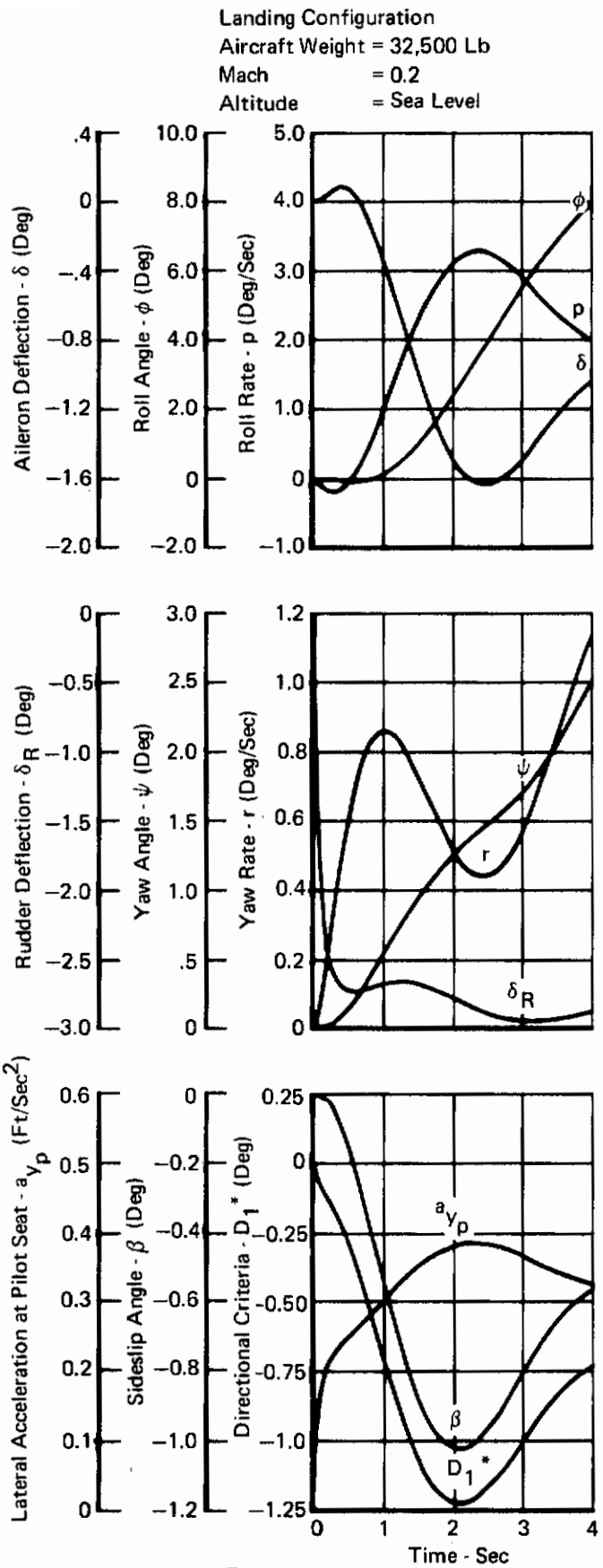

FIGURE185

DYNAMIC RESPONSE TO A 16.5 LB STEP OF RUDDER PEDAL FORCE

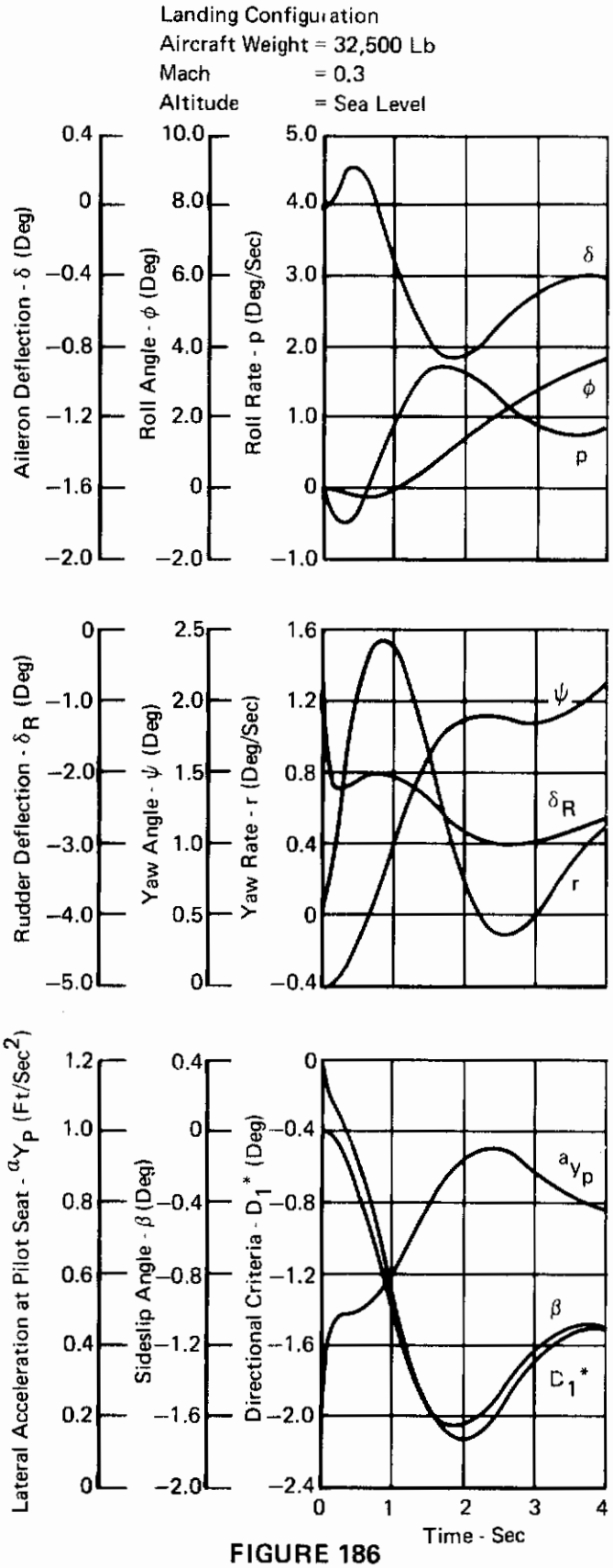

FIGURE 186

DYNAMIC RESPONSE TO A 16.5 LB STEP OF RUDDER PEDAL FORCE

Clean Configuration
Aircraft Weight = 38,732 Lb
Mach = 0.5
Altitude = 5000 Ft

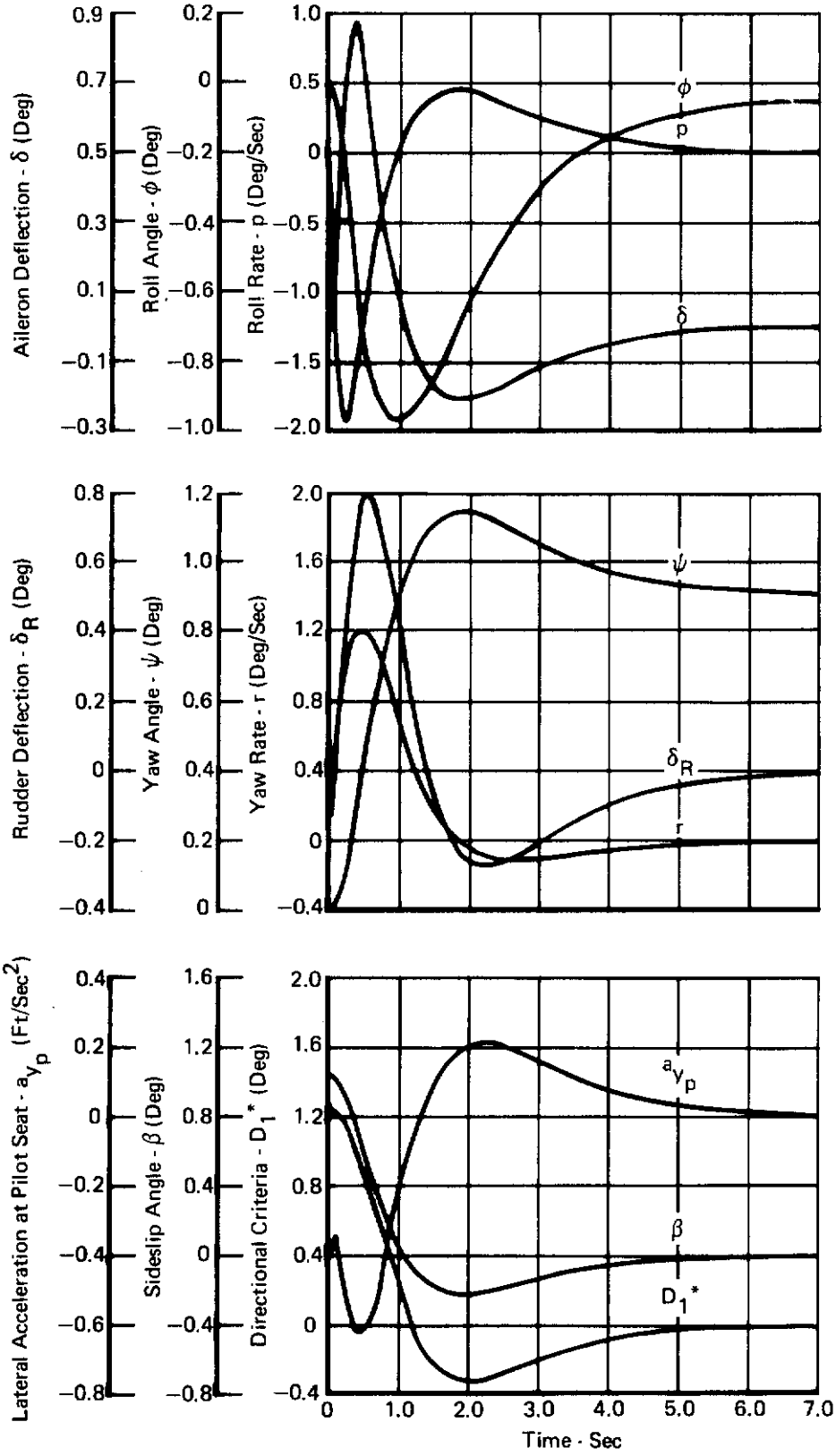

FIGURE 187
DYNAMIC RESPONSE TO A 10 FT/SEC SHARP EDGED WIND GUST

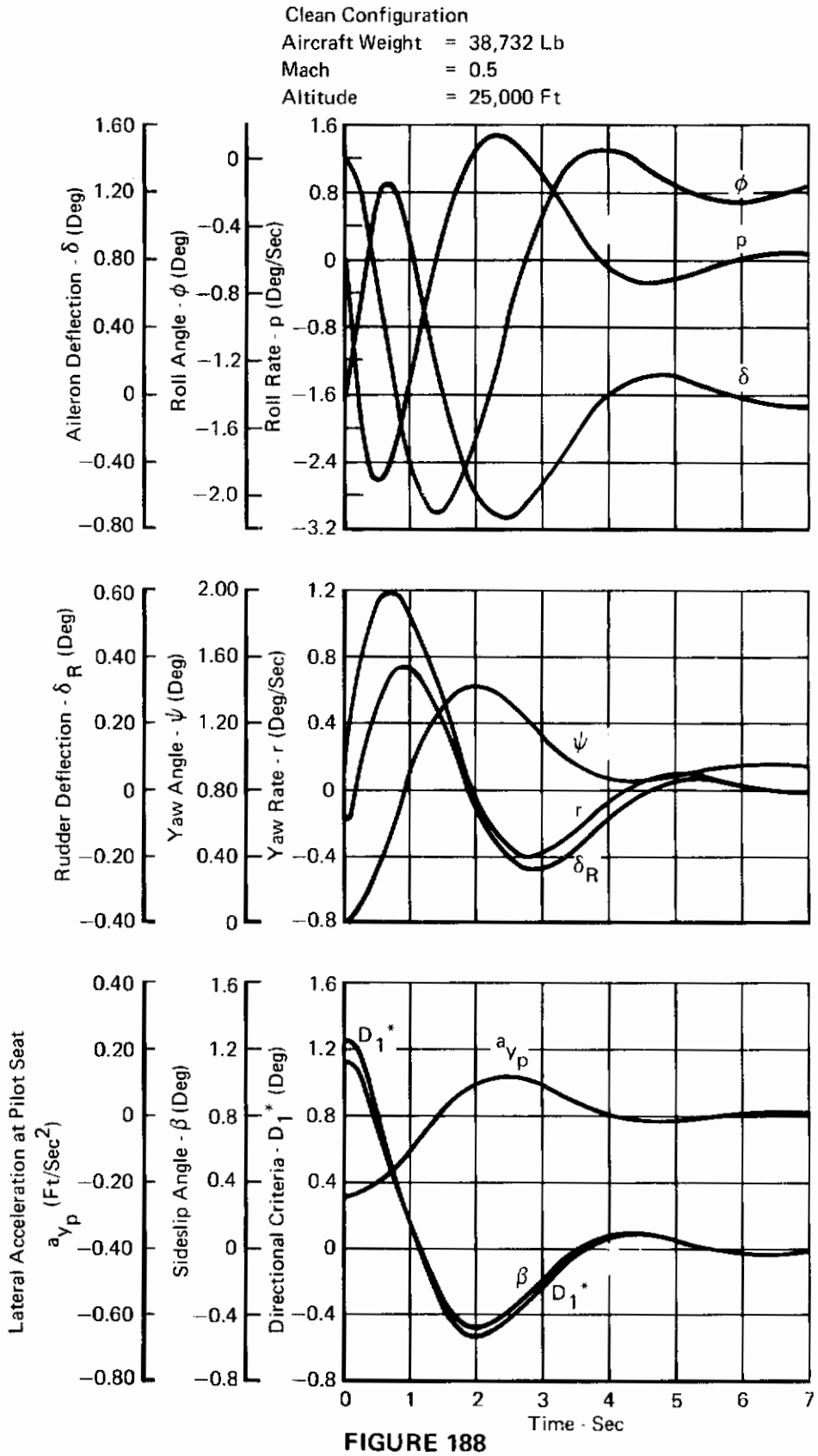

FIGURE 188

DYNAMIC RESPONSE TO A 10 FT/SEC SHARP EDGED WIND GUST

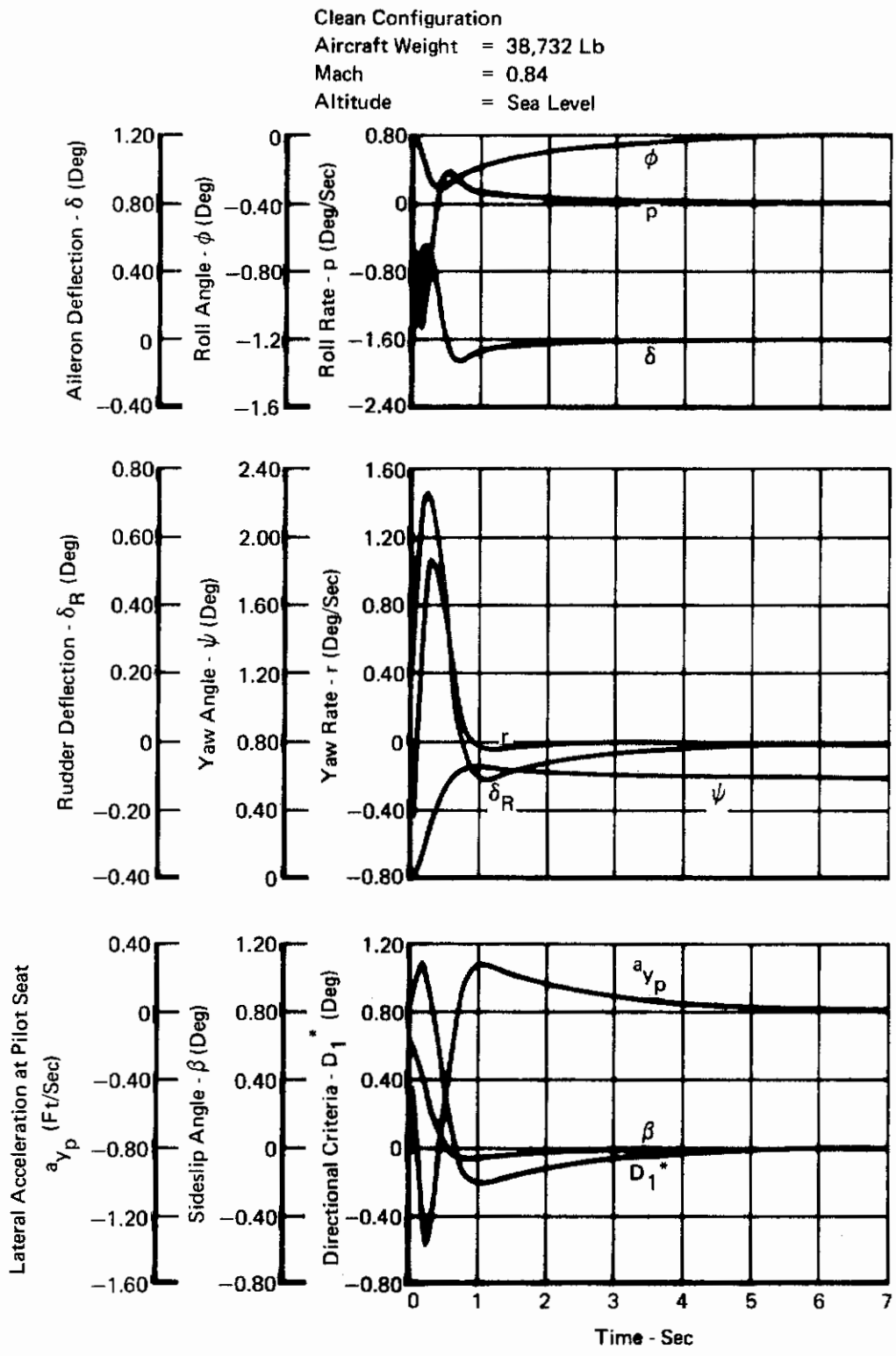

FIGURE 189
DYNAMIC RESPONSE TO A 10 FT/SEC SHARP EDGED WIND GUST

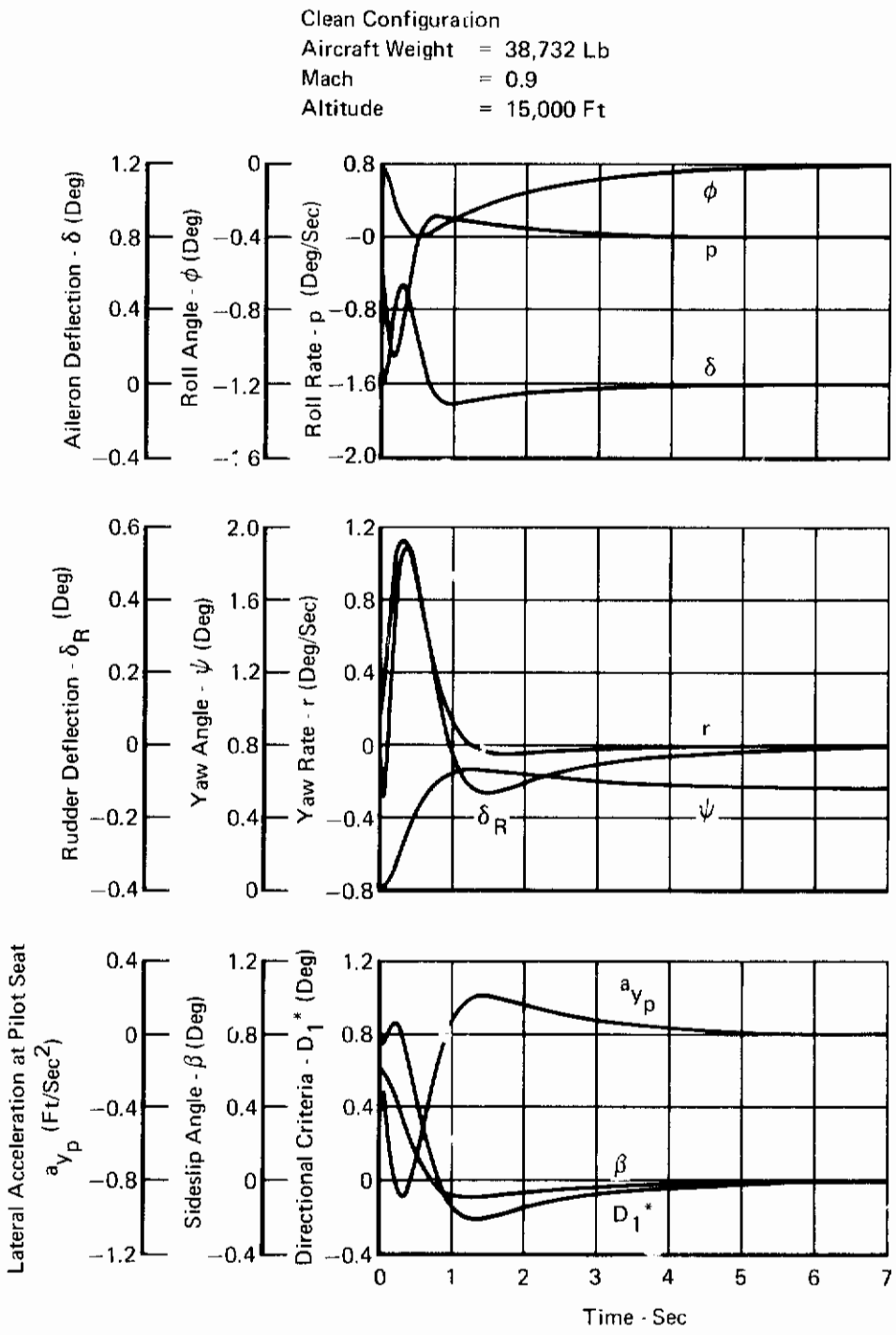

FIGURE 190
DYNAMIC RESPONSE TO A 10 FT/SEC SHARP EDGED WIND GUST

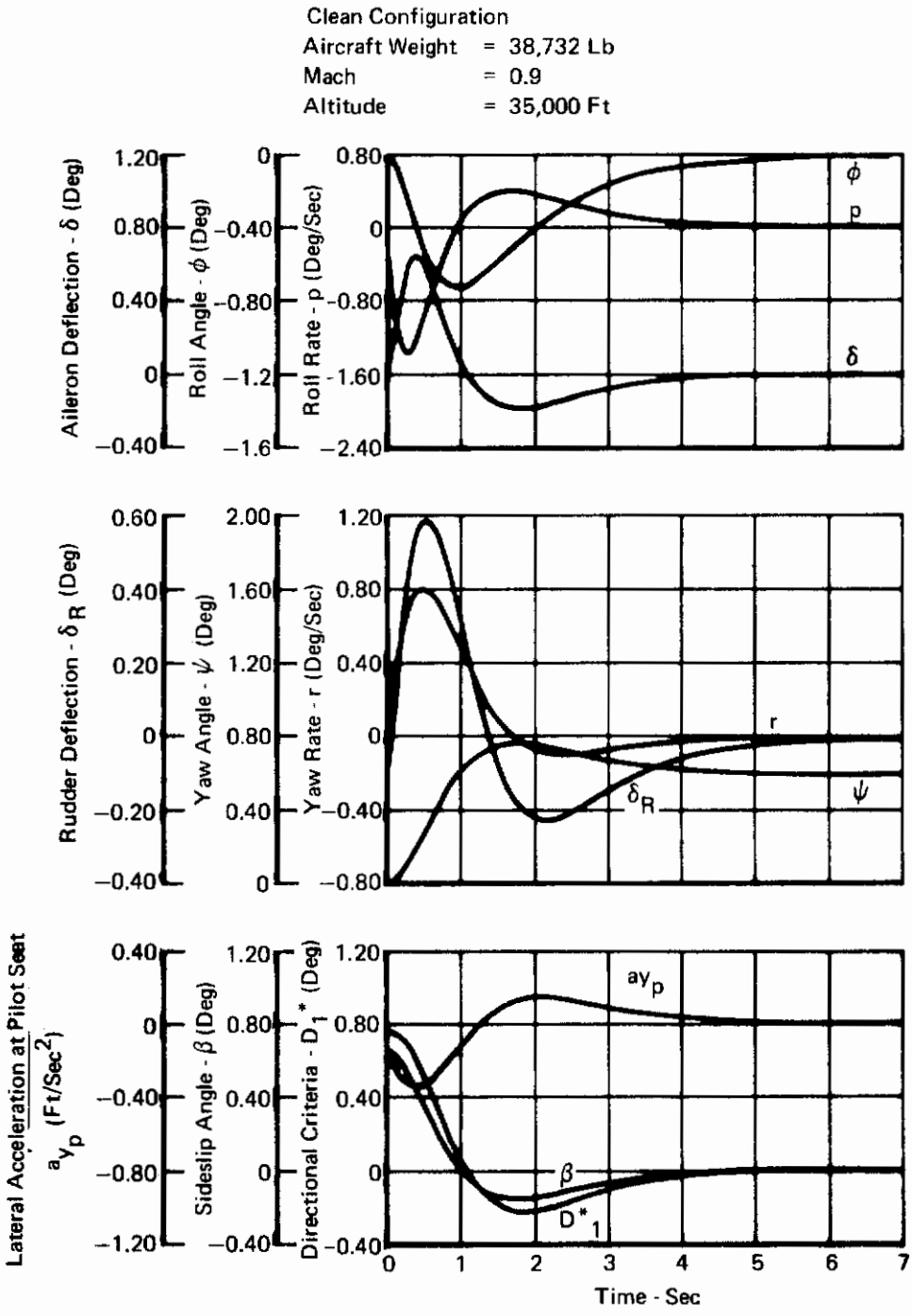

FIGURE 191
DYNAMIC RESPONSE TO A 10 FT/SEC SHARP EDGED WIND GUST

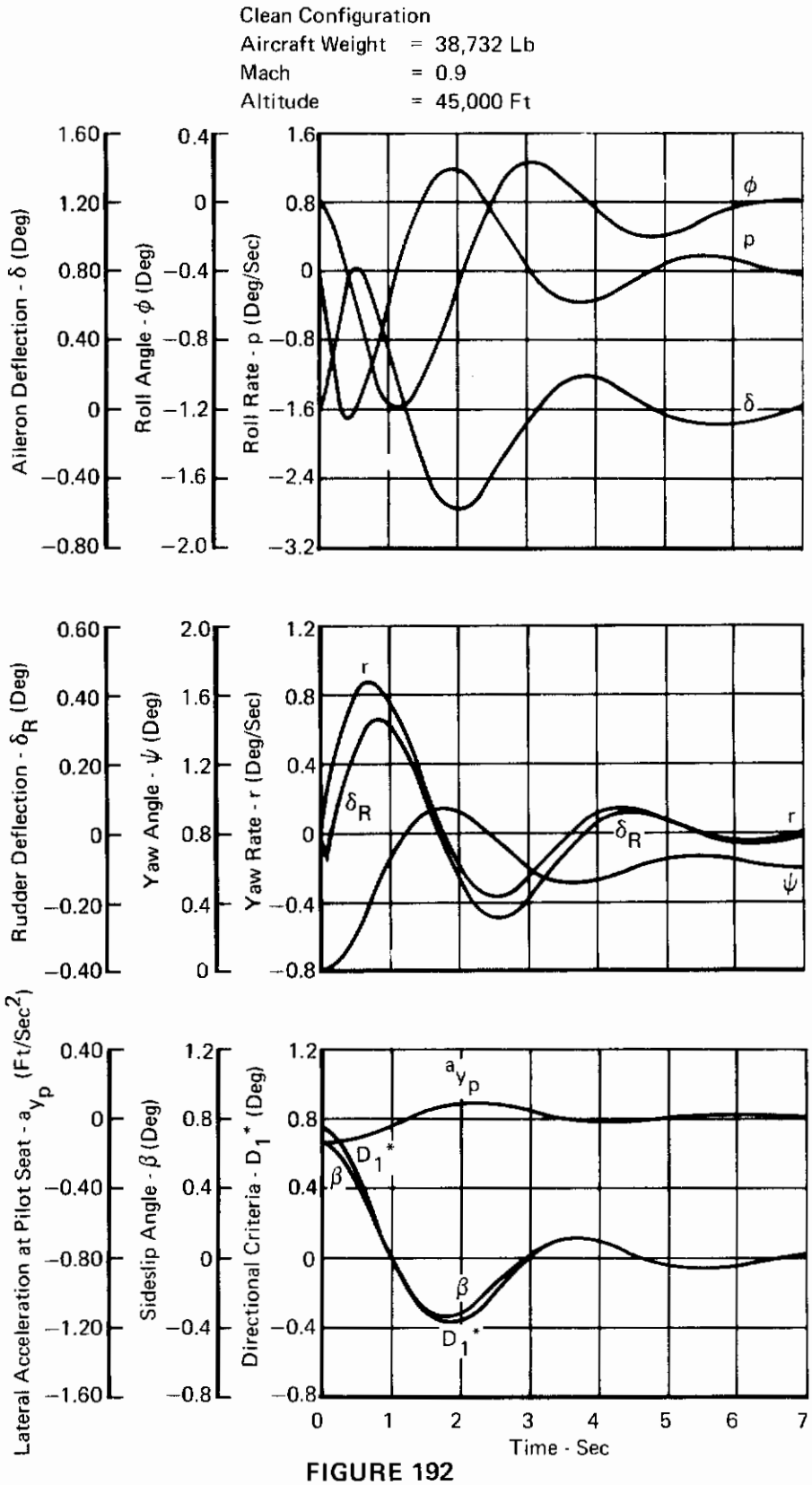

FIGURE 192
DYNAMIC RESPONSE TO A 10 FT/SEC SHARP EDGED WIND GUST

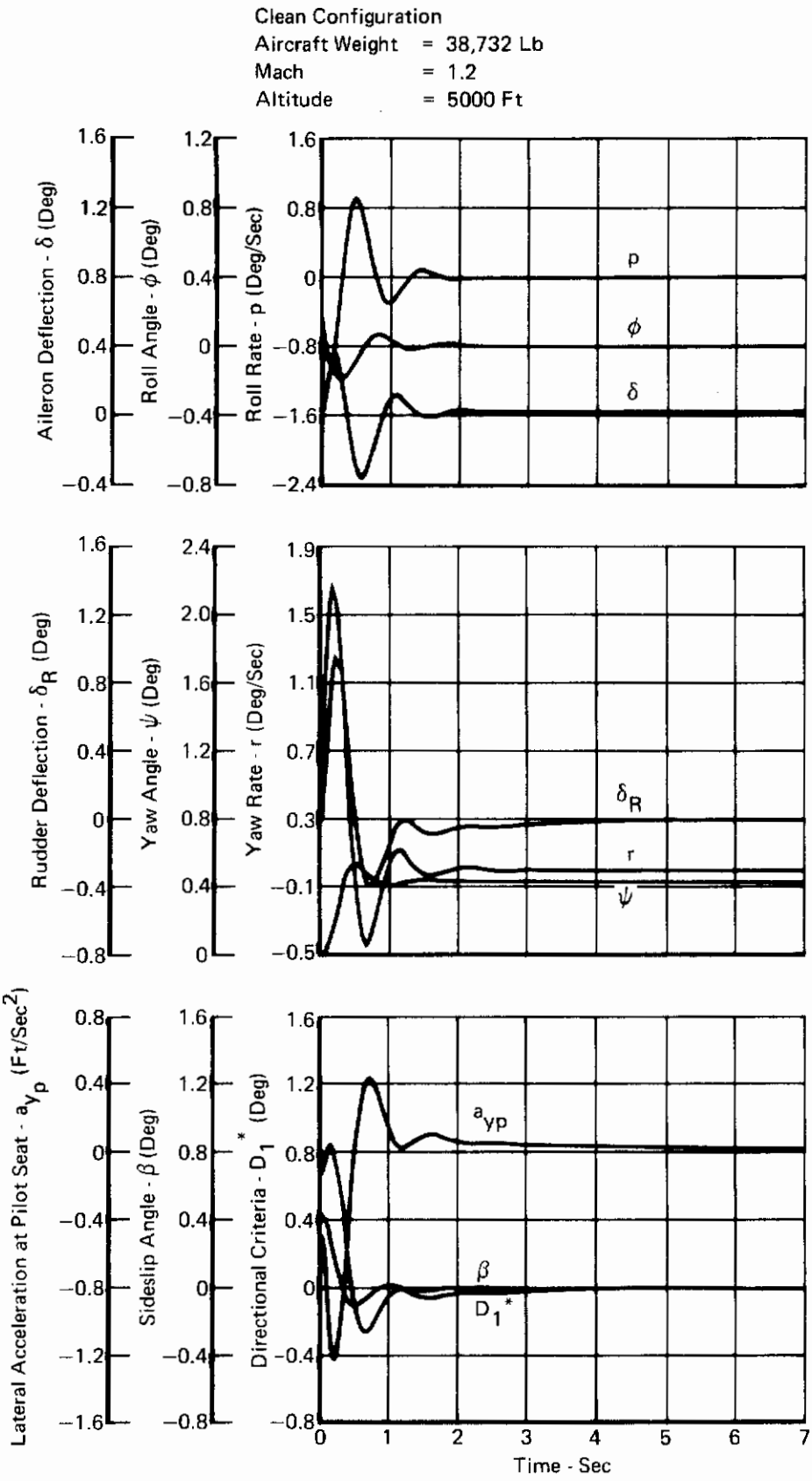

FIGURE 193
DYNAMIC RESPONSE TO A 10 FT/SEC SHARP EDGED WIND GUST

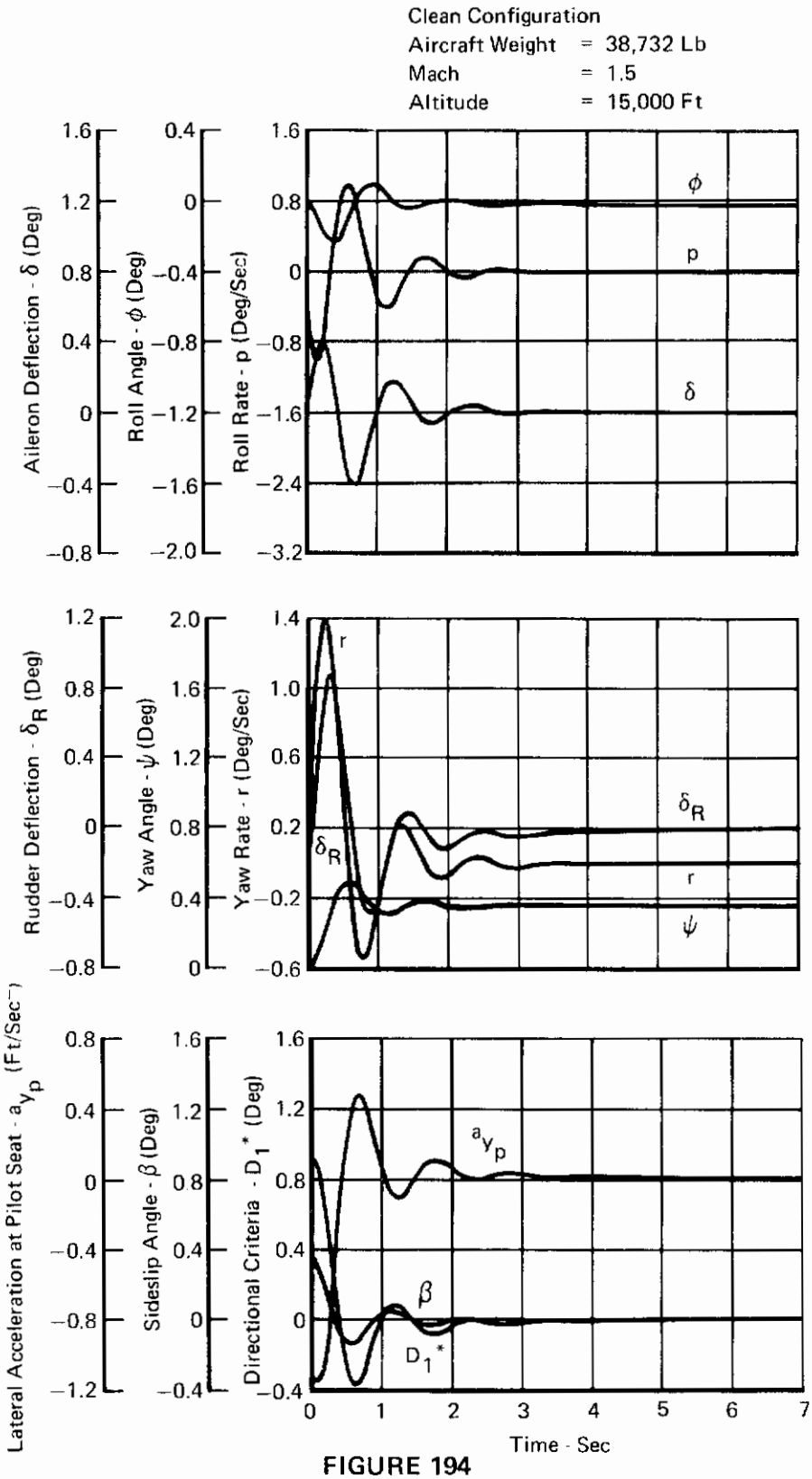

FIGURE 194

DYNAMIC RESPONSE TO A 10 FT/SEC SHARP EDGED WIND GUST

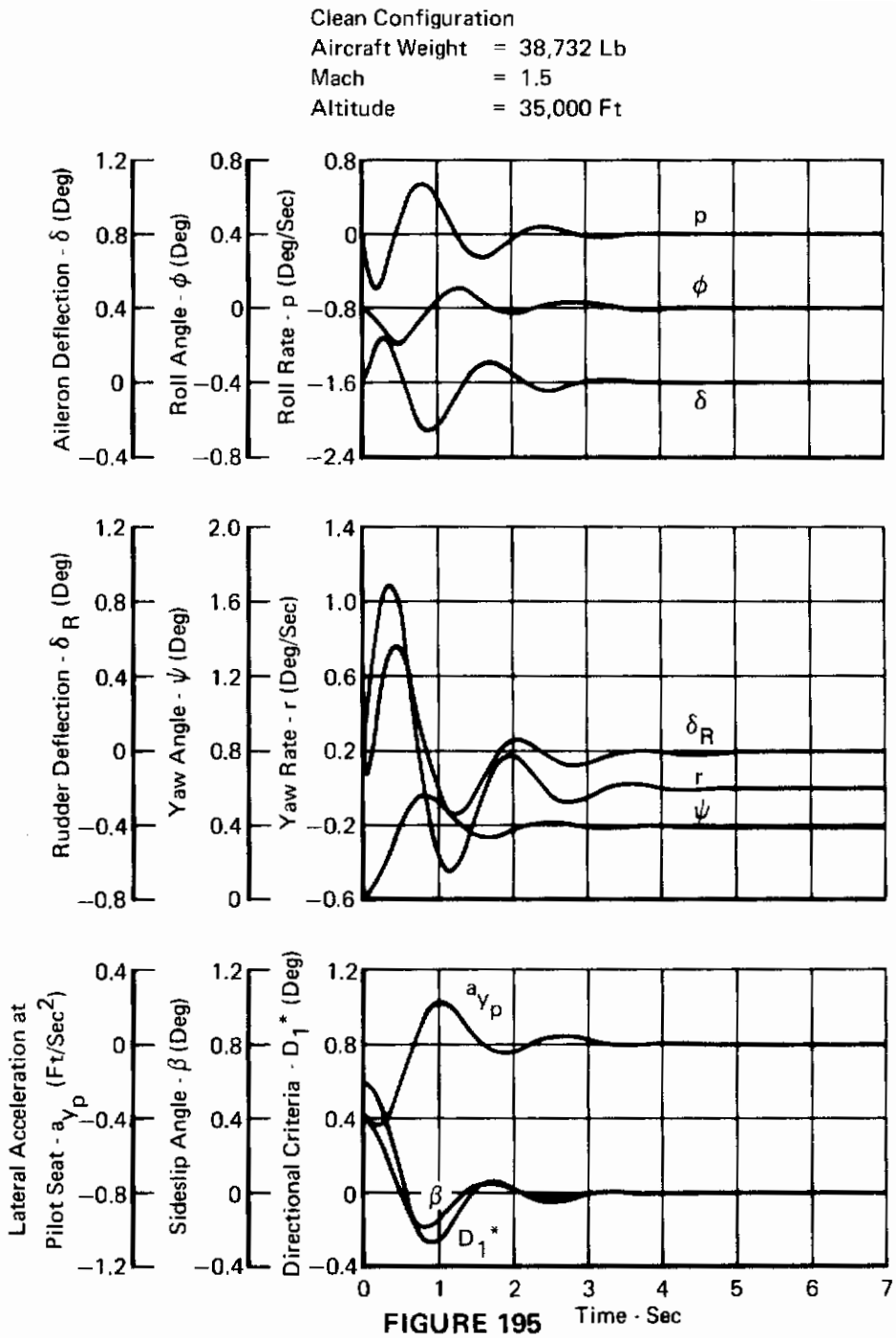

FIGURE 195

DYNAMIC RESPONSE TO A 10 FT/SEC SHARP EDGED WIND GUST

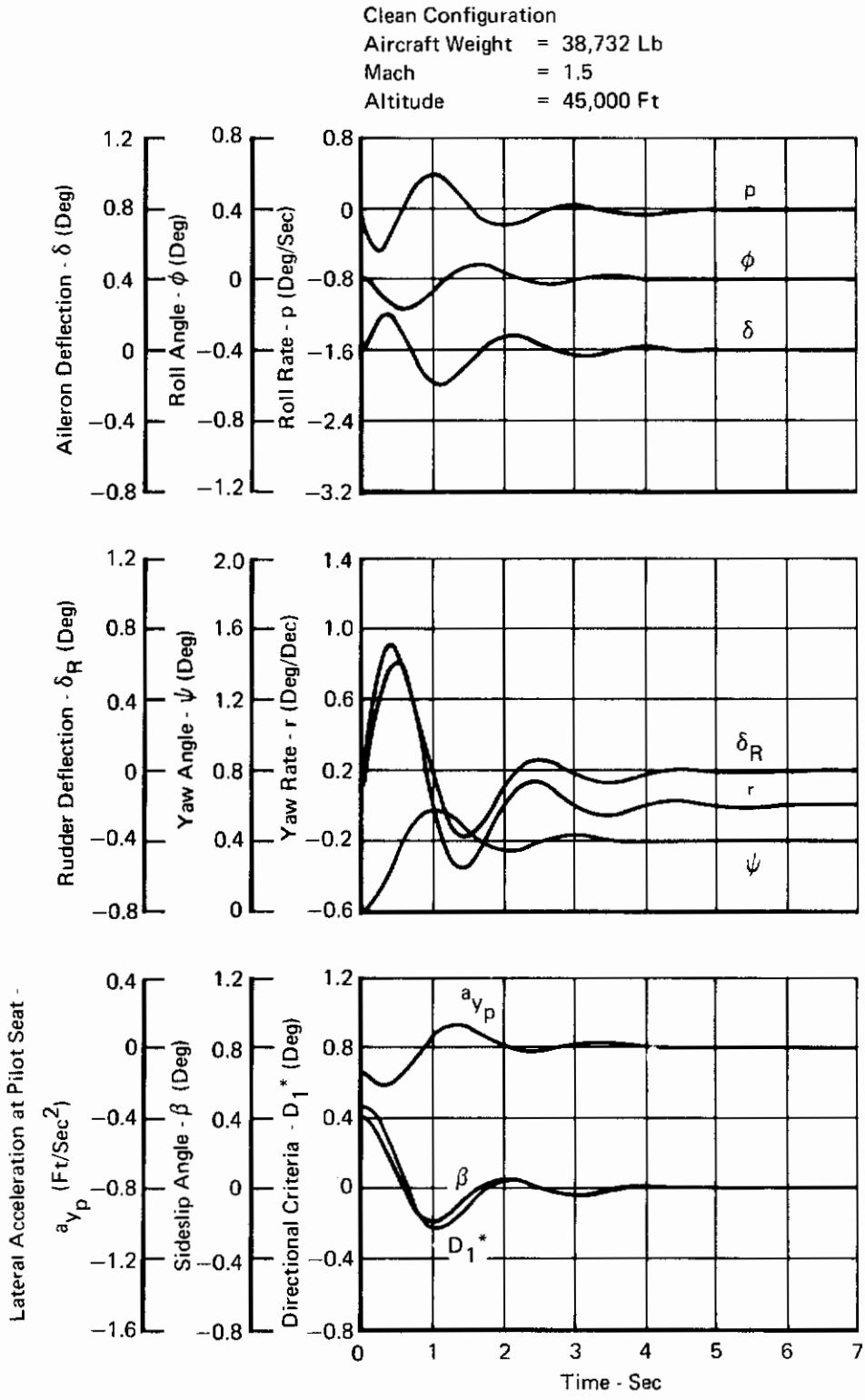

FIGURE 196
DYNAMIC RESPONSE TO A 10 FT/SEC SHARP EDGED WIND GUST

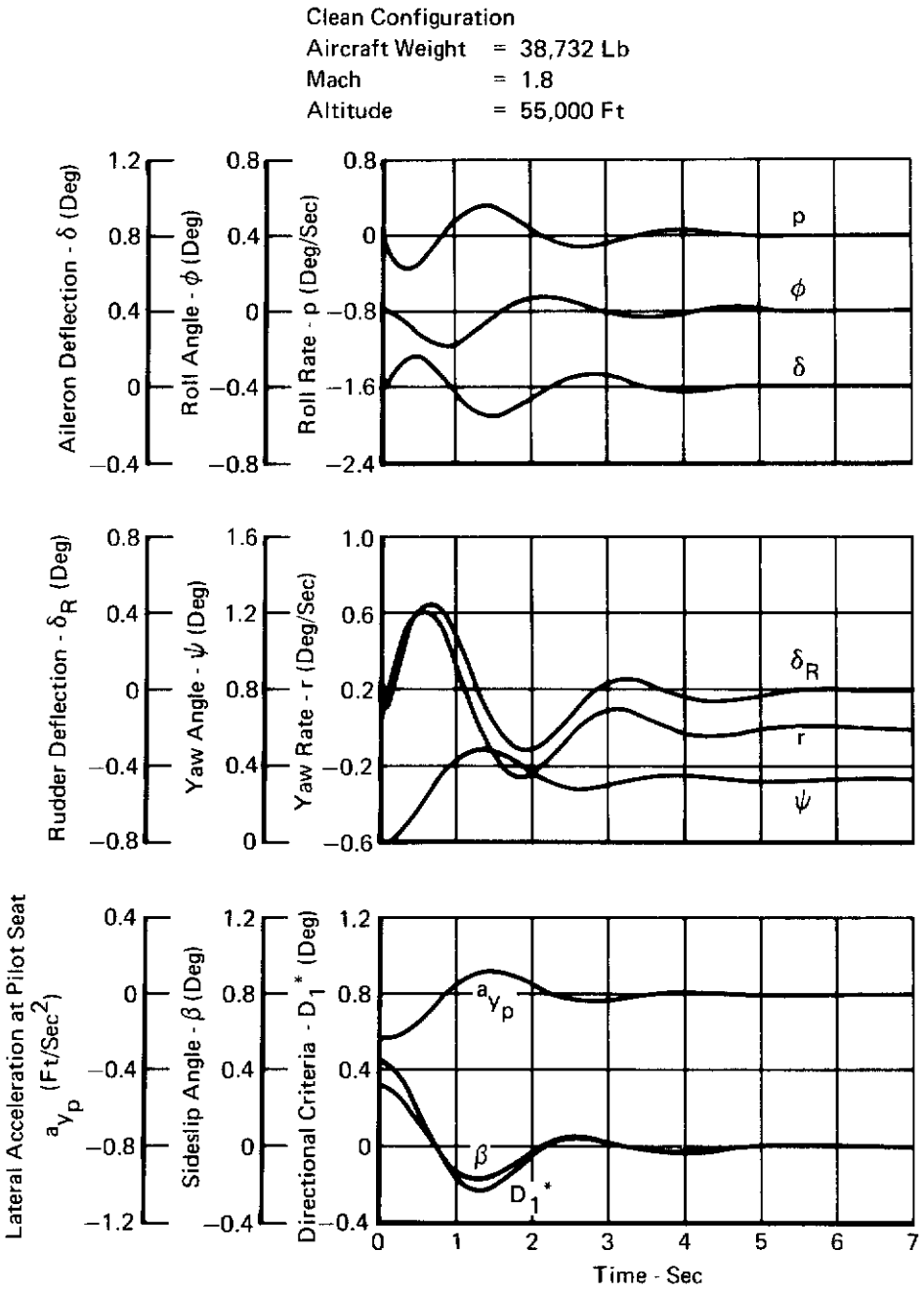

FIGURE 197

DYNAMIC RESPONSE TO A 10 FT/SEC SHARP EDGED WIND GUST

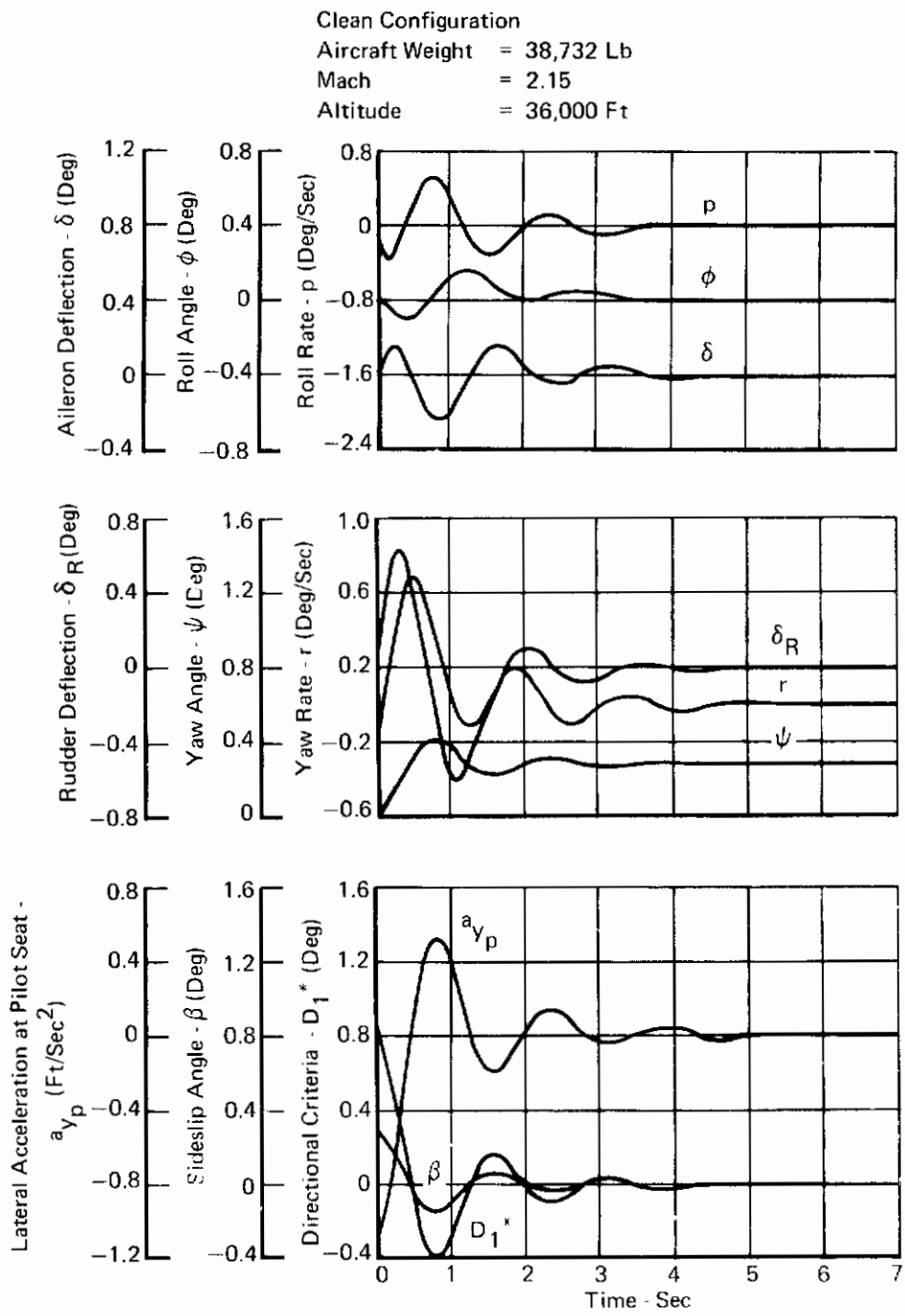

FIGURE 198
DYNAMIC RESPONSE TO A 10 FT/SEC SHARP EDGED WIND GUST

Landing Configuration
Aircraft Weight = 32,500 Lb
Mach = 0.2
Altitude = Sea Level

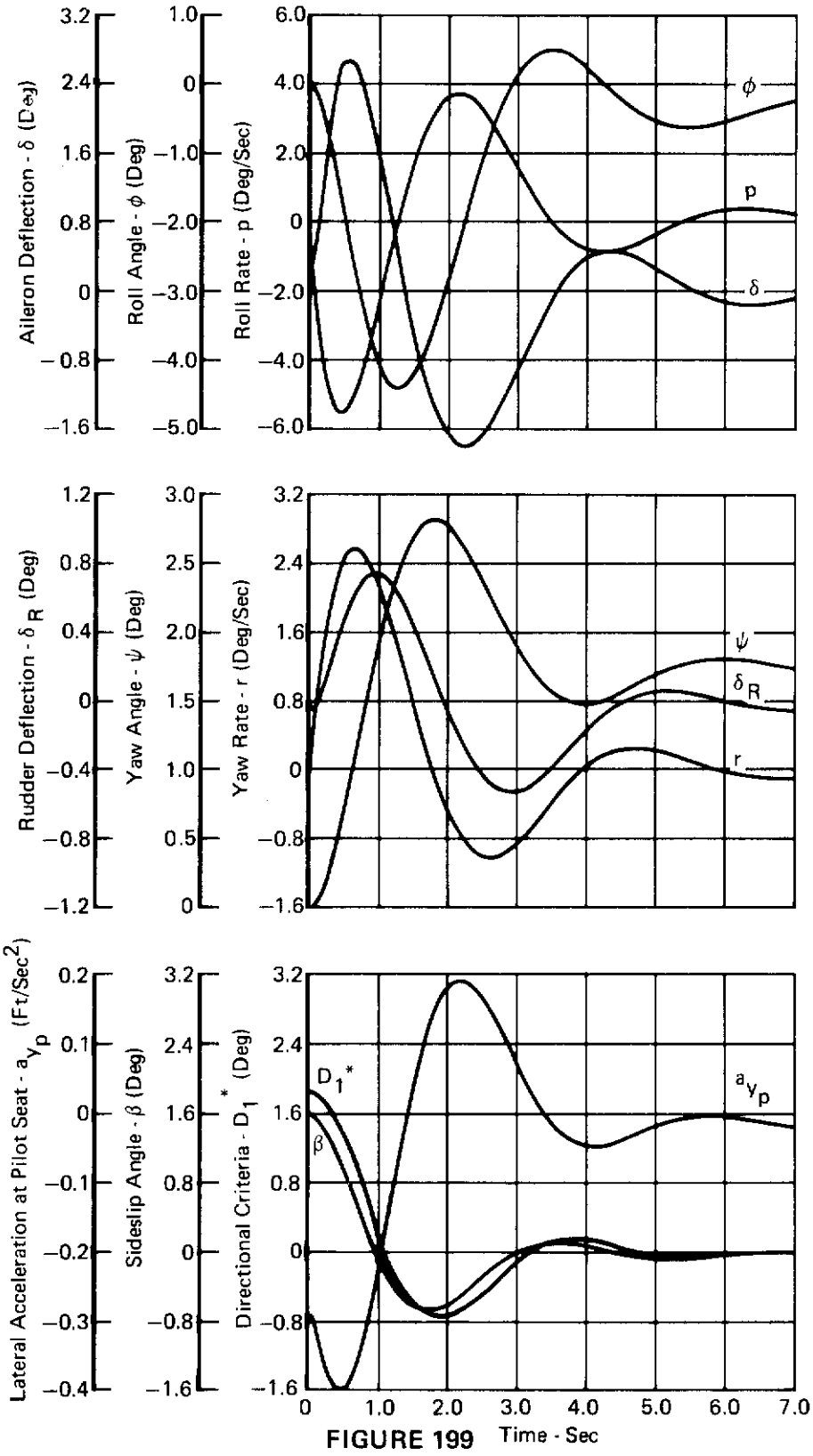

FIGURE 199
DYNAMIC RESPONSE TO A 10 FT/SEC SHARP EDGED WIND GUST

Landing Configuration
Aircraft Weight = 32,500 Lb
Mach = 0.3
Altitude = Sea Level

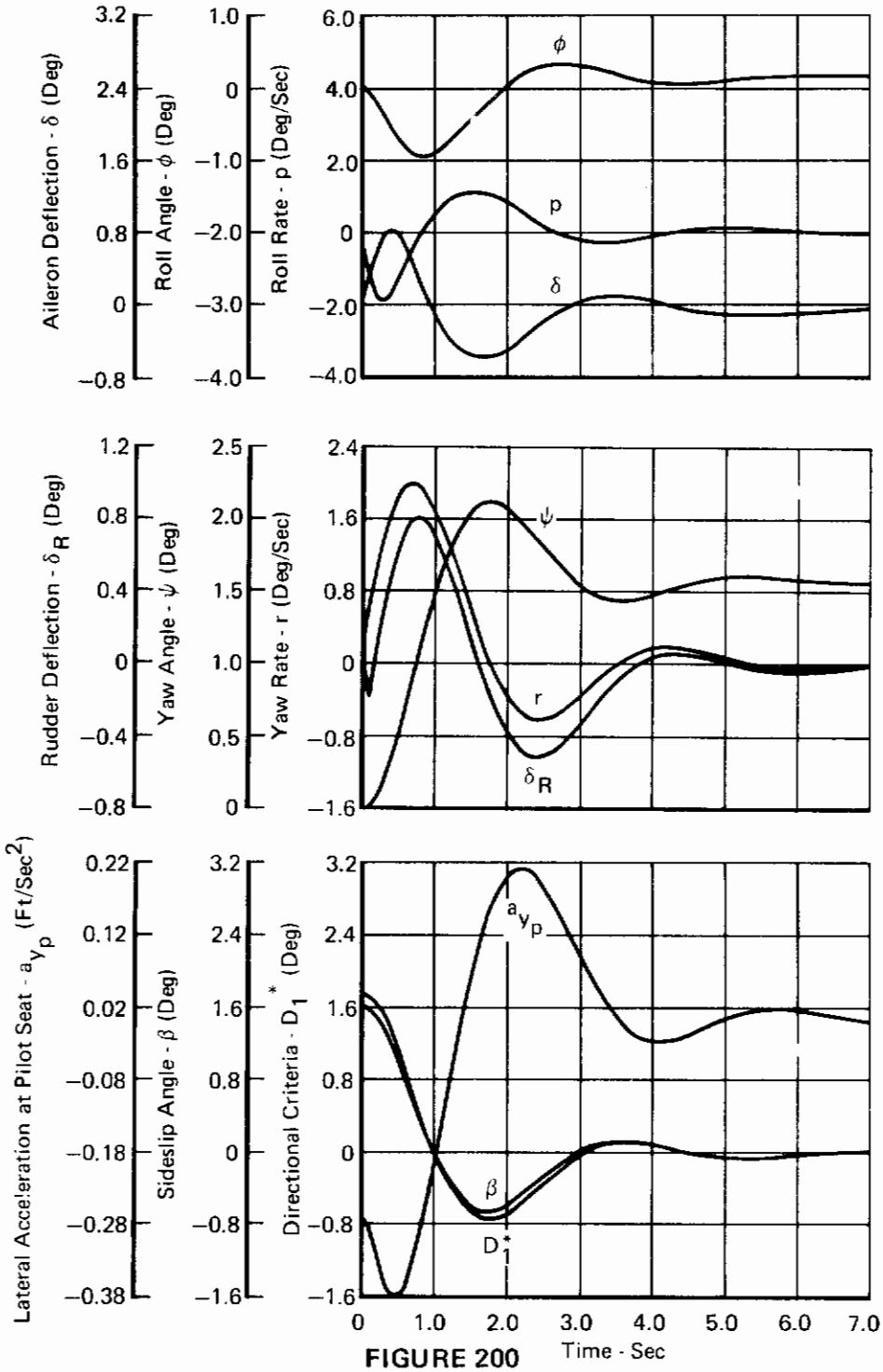

FIGURE 200
DYNAMIC RESPONSE TO A 10 FT/SEC SHARP EDGED WIND GUST

APPENDIX V

LATERAL-DIRECTIONAL STRUCTURAL MODE ANALYSIS

Three structural modes have been identified as factors to be considered in the design of the lateral-directional control system. The three modes are:

- the fuselage first torsion mode (η_4),
- the wing first asymmetric bending mode (η_5), and
- the fuselage first lateral bending mode (η_6).

The grounds for selecting these modes, the development of the equations describing them, and the computational methods employed in obtaining their equations are presented in AFFDL-TR-71-20, Section III. The resulting linearized set of six lateral-directional equations of motion are presented in Figure 201. Coefficients of the structural mode equations, for 12 flight conditions, are presented in Table XIV. The rigid equation coefficients are included in Appendix I.

This set of six equations includes no coupling from the structural dynamic modes into the rigid body equations. Coupling is therefore provided only through the control loops by means of the lateral-directional sensors. Equations representing the rigid and flexible body motions sensed by the rate gyros and lateral accelerometer are shown in Figure 201.

An initial analysis of the possible significance of the structural modes in the closed loop lateral-directional control system was obtained by analyzing each mode independently for its frequency, damping and sensitivity to control surface deflection at each of the 12 flight conditions. Upon reducing each structural equation to the characteristic equation of a single mode,

$$\ddot{\eta}_i = K_{\dot{\eta}_i}\,\dot{\eta}_i + K_{\eta_i}\,\eta_i$$

the frequency and damping of that mode at each flight condition are found as shown in Table XV. The maximum sensitivity of that mode to control surface deflection was then approximated by considering the peak amplitude of the mode's steady state response to a forced control surface oscillation at the mode's resonant frequency. Table XVI presents this sensitivity ratio for those modes included in the sensor math models.

Results of this initial analysis coupled with a review of the sensor math model equations revealed the following:

- the roll rate gyro is sensitive to all three modes directly,
- the yaw rate gyro and lateral accelerometer are sensitive mainly to the lateral bending mode,
- the η_4 mode has a frequency of 40 radians per second,

$$\dot{p} = L_p p + L_r r + L_\beta \beta + L_\delta \delta + L_{\delta_R} \delta_R$$

$$\dot{r} = N_p p + N_r r + N_\beta \beta + N_\delta \delta + N_{\delta_R} \delta_R$$

$$\dot{\beta} = Y_p p + Y_\phi \phi + Y_r r + Y_\beta \beta + Y_\delta \delta + Y_{\delta_R} \delta_R$$

$$\ddot{\eta}_4 = A_p p + A_r r + A_\beta \beta + A_{\dot{\eta}_4} \dot{\eta}_4 + A_{\eta_4} \eta_4 + A_{\dot{\eta}_5} \dot{\eta}_5 + A_{\eta_5} \eta_5 + A_{\dot{\eta}_6} \dot{\eta}_6 + A_{\eta_6} \eta_6 + A_{\dot{\delta}} \dot{\delta} + A_\delta \delta + A_{\dot{\delta}_R} \dot{\delta}_R + A_{\delta_R} \delta_R$$

$$\ddot{\eta}_5 = B_p p + B_r r + B_\beta \beta + B_{\dot{\eta}_4} \dot{\eta}_4 + B_{\eta_4} \eta_4 + B_{\dot{\eta}_5} \dot{\eta}_5 + B_{\eta_5} \eta_5 + B_{\dot{\eta}_6} \dot{\eta}_6 + B_{\eta_6} \eta_6 + B_{\dot{\delta}} \dot{\delta} + B_\delta \delta + B_{\dot{\delta}_R} \dot{\delta}_R + B_{\delta_R} \delta_R$$

$$\ddot{\eta}_6 = C_p p + C_r r + C_\beta \beta + C_{\dot{\eta}_4} \dot{\eta}_4 + C_{\eta_4} \eta_4 + C_{\dot{\eta}_5} \dot{\eta}_5 + C_{\eta_5} \eta_5 + C_{\dot{\eta}_6} \dot{\eta}_6 + C_{\eta_6} \eta_6 + C_{\dot{\delta}} \dot{\delta} + C_\delta \delta + C_{\dot{\delta}_R} \dot{\delta}_R + C_{\delta_R} \delta_R$$

Motion Detected by Lateral-Directional Sensors

$$p_G = p \cos \alpha_{p_G} - r \sin \alpha_{p_G} + \frac{\partial \phi_T}{\partial \eta_4} \dot{\eta}_4 + \frac{\partial \phi_T}{\partial \eta_5} \dot{\eta}_5 + \frac{\partial \phi_T}{\partial \eta_6} \dot{\eta}_6$$

$$r_G = p \sin \alpha_{r_G} + r \cos \alpha_{r_G} + \frac{\partial \Psi_T}{\partial \eta_6} \dot{\eta}_6$$

$$a_{y_s} = V (Y_p p + Y_r' r + Y_\beta \beta + Y_\delta \delta + Y_{\delta_R} \delta_R) - Z_o \dot{p} + X_o \dot{r} + \frac{\partial h_T}{\partial \eta_6} \ddot{\eta}_6$$

Where p_G ~ Angular velocity sensed by the roll rate gyro (rad/sec)

r_G ~ Angular velocity sensed by the yaw rate gyro (rad/sec)

a_{y_s} ~ Acceleration sensed by the lateral accelerometer (ft/sec^2)

X_o, Z_o ~ Projection of the position vector of the lateral accelerometer onto the "X" axis and "Z" axis respectively in the equation of motion axis system.

$Y_r' = Y_r + 1$

FIGURE 201

LINEARIZED LATERAL-DIRECTIONAL EQUATIONS OF MOTION INCLUDING FUSELAGE FIRST TORSION, WING FIRST ASYMMETRIC BENDING AND FUSELAGE FIRST LATERAL BENDING MODES

TABLE XIV
LATERAL-DIRECTIONAL STRUCTURAL MODE EQUATIONS COEFFICIENTS

Mach Number	0.5	0.5	0.84	0.9	0.9	0.9	1.2	1.5	1.5	1.5	1.8	2.15
Altitude (Ft)	5000	25,000	0	15,000	35,000	45,000	5000	15,000	35,000	45,000	55,000	36,000
Velocity (Ft/Sec)	548.76	508.19	937.75	951.96	875.95	871.62	1317.0	1586.6	1459.9	1452.7	1743.2	2081.3
Dynamic Pressure (Lb/Ft^2)	308.36	137.43	1045.1	677.1	282.33	174.58	177.48	1880.8	784.26	484.96	432.01	1538.4
$A_p \times 10^{-1}$	2.922	2.103	6.130	4.931	3.281	2.672	9.019	6.808	4.497	3.614	2.381	4.945
$A_r \times 10^{-1}$	2.665	1.594	5.140	4.137	2.550	1.883	7.489	9.379	5.973	4.629	4.044	5.864
$A_\beta \times 10^{-3}$	−0.4557	−0.2816	−1.433	−1.171	−0.6956	−0.5437	−3.277	−5.204	−3.091	−2.416	−2.437	−4.438
$A_{\dot{n}_4} \times 10^{+1}$	−8.688	−8.563	−9.040	−8.914	−8.701	−8.617	−9.377	−9.408	−9.020	−8.868	−8.757	−9.043
$A_{n_4} \times 10^{-3}$	−1.577	−1.571	−1.606	−1.592	−1.577	−1.573	−1.645	−1.634	−1.595	−1.584	−1.579	−1.604
$A_{\dot{n}_5} \times 10^{+1}$	−0.4244	−0.2832	−0.8360	−0.6732	−0.4347	−0.3408	−1.046	−1.055	−0.6808	−0.5347	−0.4426	−0.7606
$A_{n_5} \times 10^{-2}$	−0.2895	−0.1290	−1.100	−0.7139	−0.2977	−0.1841	−2.177	−2.119	−0.8835	−0.5463	−0.3874	−1.193
$A_{\dot{n}_6} \times 10^{+1}$	−1.359	−0.9070	−2.880	−2.313	−1.493	−1.171	−2.931	−2.165	−1.397	−1.097	−0.8586	−1.714
$A_{n_6} \times 10^{-2}$	−1.364	−0.6078	−5.680	−3.680	−1.534	−0.9490	−10.54	−7.053	−2.941	−1.819	−1.042	−3.675
$A_{\dot{\delta}}$	−2.619	−1.747	−4.730	−3.803	−2.456	−1.925	0.5746	−5.782	−3.730	−2.930	−2.726	−5.146
$A_\delta \times 10^{-3}$	−2.886	−1.286	−9.366	−6.068	−2.530	−1.565	−14.79	−9.796	−4.084	−2.526	−2.023	−7.166
$A_{\dot{\delta}_R}$	1.429	0.9537	2.490	2.009	1.297	1.017	2.949	2.931	1.891	1.485	1.351	2.421
$A_{\delta_R} \times 10^{-3}$	4.093	1.823	12.24	7.930	3.307	2.045	15.92	15.12	6.303	3.898	3.068	9.007
$B_p \times 10^{-1}$	3.636	2.606	7.620	6.121	4.068	3.307	13.46	10.32	6.801	5.454	3.631	7.407
$B_r \times 10^{-1}$	3.139	1.866	6.080	4.886	3.004	2.211	10.47	12.96	8.244	6.381	5.610	8.157
$B_\beta \times 10^{-3}$	−0.4660	−0.2880	−1.466	−1.198	−0.7114	−0.5560	−4.338	−6.890	−4.092	−3.198	−3.228	−5.876
$B_{\dot{n}_4} \times 10^{+1}$	−0.4913	−0.3278	−0.9850	−0.7925	−0.5117	−0.4012	−1.634	−1.635	−1.055	−0.8284	−0.6575	−1.090
$B_{n_4} \times 10^{-2}$	−0.1784	−0.0795	−0.7020	−0.4548	−0.1896	−0.1173	−1.597	−1.377	−0.5741	−0.3550	−0.2380	−0.7596
$B_{\dot{n}_5}$	−2.226	−2.197	−2.310	−2.279	−2.229	−2.210	−2.383	−2.374	−2.290	−2.257	−2.236	−2.309
$B_{n_5} \times 10^{-3}$	−4.577	−4.545	−4.740	−4.663	−4.579	−4.557	−5.027	−4.988	−4.715	−4.641	−4.603	−4.781
$B_{\dot{n}_6} \times 10^{+1}$	−3.428	−2.288	−7.080	−5.688	−3.673	−2.879	−9.066	−7.512	−4.846	−3.806	−2.983	−5.518
$B_{n_6} \times 10^{-2}$	−2.715	−1.210	−11.01	−7.128	−2.972	−1.838	−24.77	−18.74	−7.815	−4.832	−3.015	−10.08
$B_{\dot{\delta}}$	−0.7231	−0.4824	−1.344	−1.083	−0.6990	−0.5480	−2.036	−2.068	−1.334	−1.048	−0.9882	−1.863
$B_\delta \times 10^{-3}$	0.2134	0.0951	−0.3570	−0.2306	−0.0962	−0.05948	−2.602	−2.204	−0.9190	−0.5683	−0.4856	−1.742
$B_{\dot{\delta}_R}$	2.510	1.675	4.490	3.608	2.330	1.826	5.900	5.928	3.824	3.004	2.765	5.045
$B_{\delta_R} \times 10^{-3}$	5.320	2.370	15.62	10.12	4.219	2.610	23.00	21.10	8.799	5.441	4.472	13.18
$C_p \times 10^{-1}$	3.481	2.092	7.650	6.146	3.840	2.889	22.82	20.25	12.89	9.986	7.393	10.85
$C_r \times 10^{-1}$	−3.664	−2.645	−6.450	−5.186	−3.495	−2.888	−12.10	−15.16	−10.01	−8.037	−6.759	−12.34
$C_\beta \times 10^{-3}$	0.4379	0.2706	1.377	1.125	0.6684	0.5225	4.901	7.781	4.621	3.612	3.644	6.635
$C_{\dot{n}_4} \times 10^{+1}$	−0.2306	−0.1539	−0.4960	−0.3980	−0.2570	−0.2015	−0.9471	−0.5833	−0.3763	−0.2956	−0.1979	−0.4156
$C_{n_4} \times 10^{-2}$	−0.1722	−0.0767	−0.6770	−0.4387	−0.1829	−0.1131	−1.894	−1.633	−0.6809	−0.4210	−0.2825	−0.9009
$C_{\dot{n}_5} \times 10^{+1}$	−0.6642	−0.4432	−1.370	−1.100	−0.70995	−0.5566	−1.942	−1.585	−1.022	−0.8030	−0.6194	−1.144
$C_{n_5} \times 10^{-2}$	−0.4781	−0.2130	−1.920	−1.242	−0.5180	−0.3203	−4.716	−3.707	−1.546	−0.9557	−0.6099	−2.012
$C_{\dot{n}_6}$	−5.362	−5.117	−6.064	−5.783	−5.373	−5.212	−6.721	−6.654	−5.934	−5.654	−5.490	−6.163
$C_{n_6} \times 10^{-3}$	−6.530	−6.329	−7.559	−7.069	−6.544	−6.401	−10.61	−10.31	−7.895	−7.236	−6.912	−8.485
$C_{\dot{\delta}}$	−4.310	−2.876	−7.980	−6.410	−4.139	−3.245	−11.68	−11.71	−7.555	−5.934	−5.578	−10.54
$C_\delta \times 10^{-3}$	−0.00779	−0.003476	−4.940	−3.201	−1.335	−0.8256	−17.38	−13.77	−5.741	−3.550	−2.987	−10.68
$C_{\dot{\delta}_R}$	−2.993	−1.997	−5.410	−4.342	−2.803	−2.198	−7.389	−7.453	−4.808	−3.776	−3.491	−6.405
$C_{\delta_R} \times 10^{-3}$	−5.640	−2.513	−16.35	−10.59	−4.417	−2.732	−26.04	−23.42	−9.766	−6.039	−5.103	−15.04

TABLE XV
STRUCTURAL MODE FREQUENCIES AND DAMPING

Given the structural mode characteristic equation

$$\ddot{\eta}_i = K_{\dot{\eta}_i}\dot{\eta}_i + K_{\eta_i}\eta_i$$

$$\omega_{\eta_i} \approx \sqrt{-K_{\eta_i}} \qquad \zeta_{\eta_i} = \frac{-K_{\dot{\eta}_i}}{2\sqrt{-K_{\eta_i}}}$$

Flight Condition		Structural Mode					
		η_4		η_5		η_6	
Mach	Altitude (Ft)	ω_{η_4} Rad/Sec	ζ_{η_4}	ω_{η_5} Rad/Sec	ζ_{η_5}	ω_{η_6} Rad/Sec	ζ_{η_6}
0.5	5,000	39.71	0.0109	67.65	0.0165	80.81	0.0332
0.5	25,000	39.64	0.0108	67.42	0.0163	79.56	0.0322
0.84	SL	40.07	0.0113	68.85	0.0168	86.94	0.0349
0.9	15,000	39.90	0.0112	68.29	0.0167	84.08	0.0344
0.9	35,000	39.71	0.0110	67.69	0.0165	80.89	0.0332
0.9	45,000	39.66	0.0109	67.51	0.0164	80.01	0.0326
1.2	5,000	40.56	0.0116	70.90	0.0168	103.00	0.0326
1.5	15,000	40.42	0.0116	70.63	0.0168	101.54	0.0328
1.5	35,000	39.94	0.0113	68.67	0.0167	88.85	0.0334
1.5	45,000	39.80	0.0111	68.12	0.0166	85.06	0.0332
1.8	55,000	39.74	0.0110	67.85	0.0165	83.14	0.0330
2.15	36,000	40.05	0.0113	69.14	0.0167	92.11	0.0335

- the η_5 mode frequency varies from 67 radians per second at low $\bar{q}$ to 71 radians per second at high $\bar{q}$ flight conditions,
- the η_6 mode frequency varies from 79 radians per second at low $\bar{q}$ to 103 radians per second at high $\bar{q}$ flight conditions,
- the structural mode sensitivity to surface deflection increases with increasing $\bar{q}$,
- the η_4 mode will be the most significant mode in the lateral axis design due to both its low frequency and high sensitivity to aileron deflection, and,
- the η_6 mode will be the important mode consideration in the directional loop design.

TABLE XVI

STRUCTURAL MODE SENSITIVITY TO CONTROL SURFACE DEFLECTION AT THE MODE RESONANT FREQUENCIES

Given the single degree of freedom structural mode equation

$$\ddot{\eta}_i = K_{\dot{\eta}_i}\,\dot{\eta}_i + K_{\eta_i}\,\eta_i + K_{\delta_j}\,\delta_j$$

with a sinusoidal surface deflection

$$\delta_j = \delta_j \sin \omega_{\eta_i} t$$

where ω_{η_i} is the mode resonant frequency ($\sqrt{-K_{\eta_i}}$), the

a) mode steady state sensitivities are:

$$\eta_{i(t)} = \frac{K_{\delta_j}\,\delta_j}{(-K_{\dot{\eta}_i})\sqrt{-K_{\eta_i}}} \cos \omega_{\eta_i} t$$

$$\dot{\eta}_{i(t)} = \frac{-K_{\delta_j}\,\delta_j}{-K_{\dot{\eta}_i}} \sin \omega_{\eta_i} t$$

$$\ddot{\eta}_{i(t)} = \frac{-K_{\delta_j}\,\delta_j}{-K_{\dot{\eta}_i}} \sqrt{K_{\eta_i}} \cos \omega_{\eta_i} t$$

b) the peak sensitivity ratios are:

$$\frac{\eta_i}{\delta_j} = \frac{K_{\delta_i}}{(-K_{\dot{\eta}_i})\sqrt{-K_{\eta_i}}}$$

$$\frac{\dot{\eta}_i}{\delta_j} = \frac{K_{\delta_i}}{-K_{\dot{\eta}_i}}$$

$$\frac{\ddot{\eta}_i}{\delta_j} = \frac{K_{\delta_i}}{-K_{\dot{\eta}_i}} \sqrt{-K_{\eta_i}}$$

Flight Condition		Peak Sensitivity Ratio				
Mach	Altitude (Ft)	$\frac{\dot{\eta}_4}{\delta}$ (Rad Sec)$^{-1}$	$\frac{\dot{\eta}_5}{\delta}$ (Rad Sec)$^{-1}$	$\frac{\dot{\eta}_6}{\delta}$ (Rad Sec)$^{-1}$	$\frac{\dot{\eta}_6}{\delta_R}$ (Rad Sec)$^{-1}$	$\frac{\ddot{\eta}_6}{\delta_R}$ (Rad^{-1} Sec^{-2})
0.50	5,000	3,322	96	1.45	1,052	84,998
0.50	25,000	1,502	43	0.68	491	39,070
0.84	SL	10,360	155	814	2,696	234,418
0.90	15,000	6,807	101	535	1,831	153,965
0.90	35,000	2,908	43	248	822	66,502
0.90	45,000	1,816	27	158	524	41,937
1.20	5,000	15,773	1,092	2586	3,874	399,084
1.50	15,000	10,412	928	2069	3,520	357,382
1.50	35,000	4,528	401	967	1,646	146,233
1.50	45,000	2,848	252	628	1,068	90,857
1.80	55,000	2,310	217	544	930	77,278
2.15	36,000	7,924	754	1733	2,440	224,792

Minimization of the structural mode feedback through the control system can be achieved by proper sensor location and/or filtering networks. The effects of sensor location on structural mode pickup are presented in Figures 202 and 203. Employing the above data along with other practical considerations such as engine heat, fuel tank location, structural supports, etc., the selected lateral-directional sensor fuselage locations are:

- o roll rate gyro - F.S. 77
- o yaw rate gyro - F.S. 383
- o lateral accelerometer - F.S. 186

Initially the lateral accelerometer was located at F.S. 68. However, after review of the structural mode data it was relocated to its present position. At F.S. 186 the η_6 mode pickup is reduced by a factor of seven or greater from that present at F.S. 68.

The gain of the airframe structural mode response to control surface deflection is the product of the mode sensitivity ratio and the mode shape ordinate at the sensor location. These data are presented in Table XVII and show that:

- o The highest aileron induced structural mode gains are at flight condition 1.2 Mach at 5,000 feet and have values of 18.77 dB, -3.25 dB and 17.50 dB at the η_4, η_5 and η_6 mode resonant frequencies respectively,
- o The yaw rate airframe structural mode gains are all less than -12 dB, and
- o The airframe lateral acceleration gain in feet per second squared per radian at the lateral accelerometer location for the η_6 mode is greater than 35 dB at all flight conditions.

The criteria adpoted for the structural mode analysis required that the loop gain at all structural mode frequencies be -10 dB or less. The frequency responses of the lateral axis feedback loop including the 0.5 feedback gain are presented in Figure 204 and show an attenuation of -18 dB at 40 rad/sec and -27 dB at 103 rad/sec. Employing the above structural mode attenuation criteria, it is necessary to add a 10 dB 40 radian notch filter in the lateral loop for adequate loop attenuation of -10 dB at the structural modes of the 1.2 Mach at 5,000 feet flight condition. Figure 205 shows the gain and phase response of the 10 dB notch filter used in the lateral loop.

The yaw rate loop requires no structural filtering, due to the low airframe structural mode gain. The lateral acceleration loop structural mode attenuation requirements were found by forming a product of the airframe η_6 mode lateral acceleration gain, the lateral acceleration control loop gain at the η_6 mode frequency, and the rudder flexibility gain for that flight condition. Figure 206 presents the gain of the lateral acceleration loop dynamics. Table XVIII shows each of these gains along with the maximum lateral acceleration gain (K_{n_y}) allowed at each flight condition, if the loop is to meet the criteria of a -10 dB gain at the η_6 mode frequency. Maximum values of the K_{n_y} gain are shown for no structural filter and for a first order 40 rad/sec structural filter in the lateral acceleration loop. These data show that the

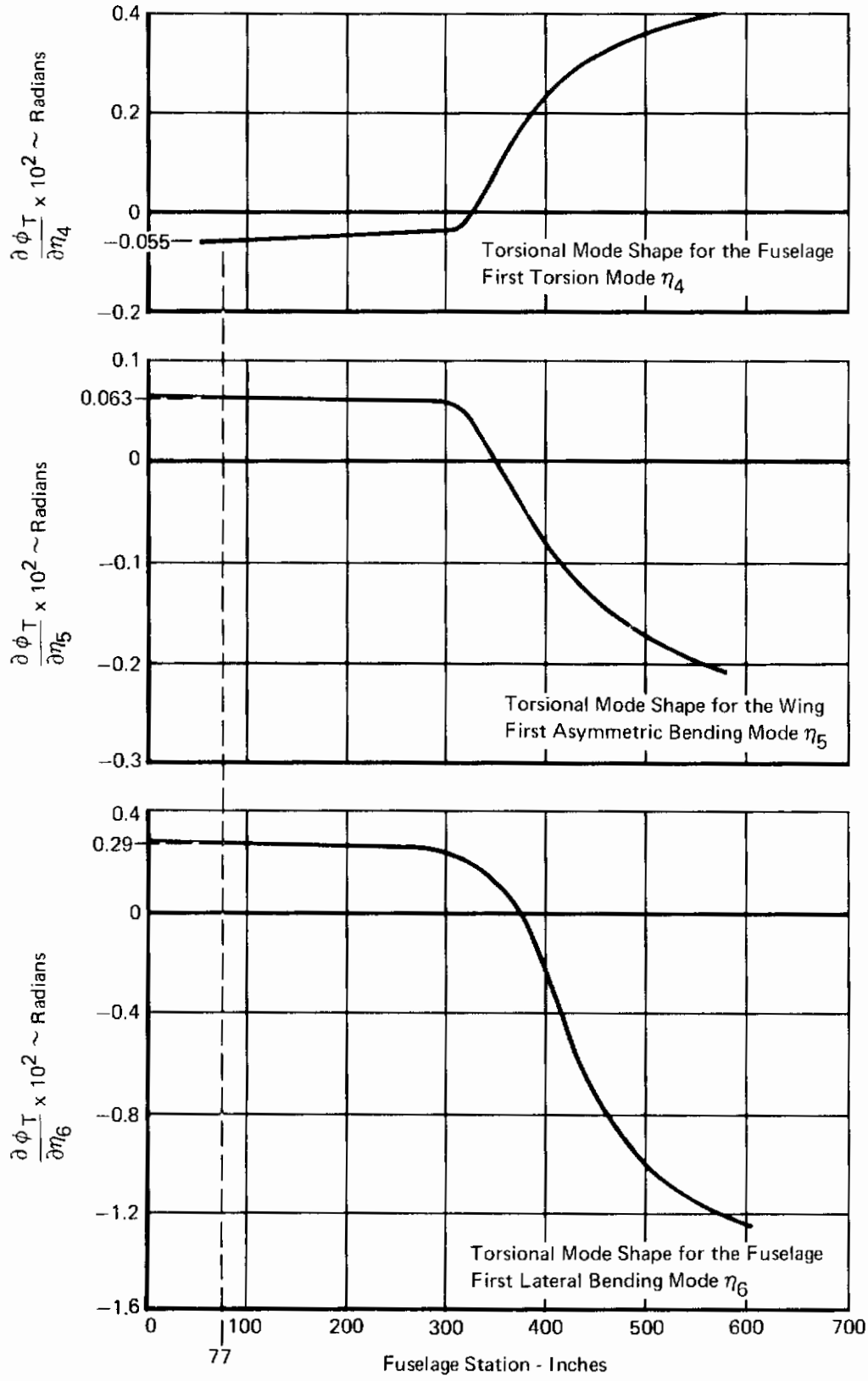

FIGURE 202
LATERAL-DIRECTIONAL STRUCTURAL MODE SHAPES

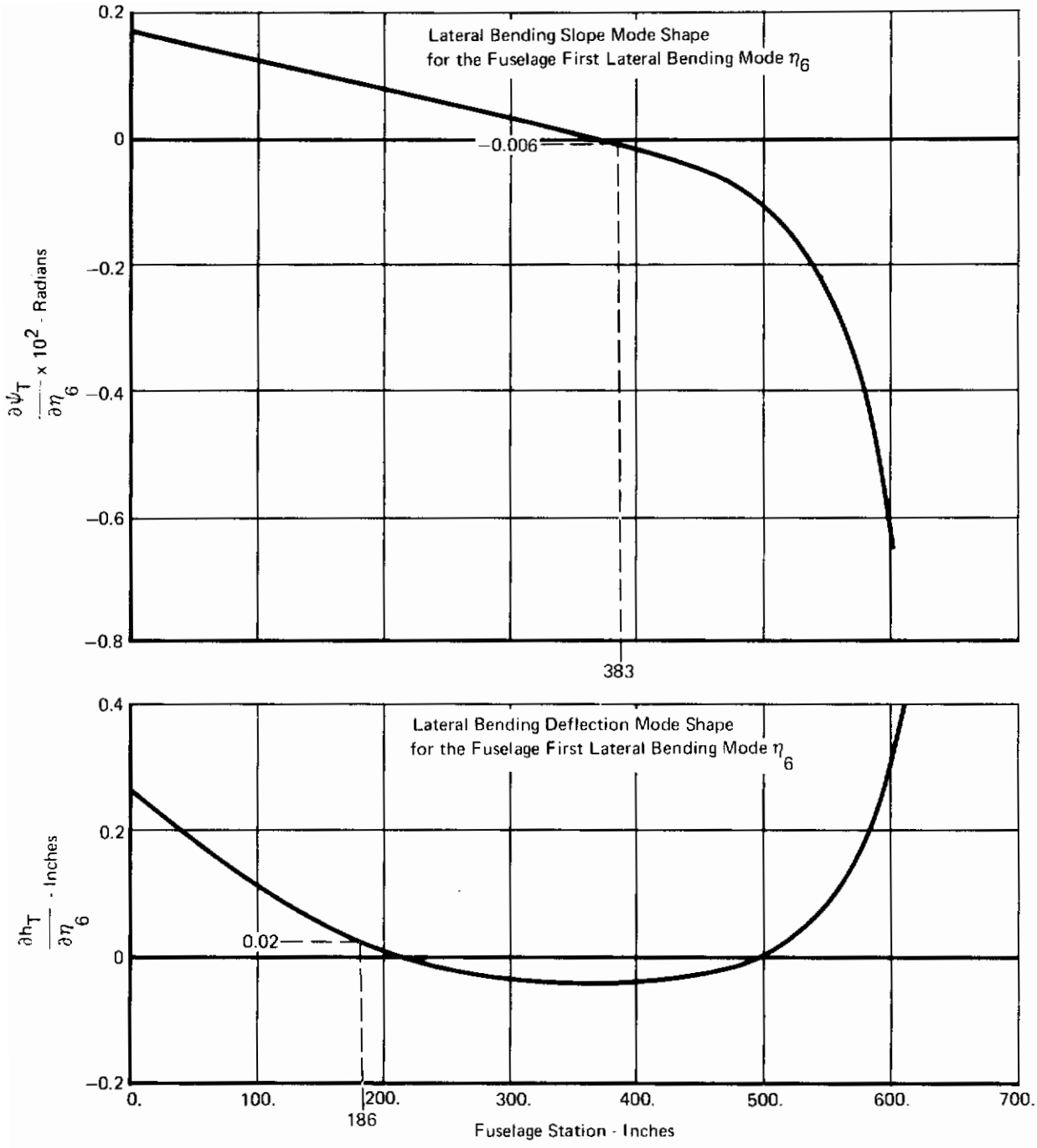

FIGURE 203

LATERAL-DIRECTIONAL STRUCTURAL MODE SHAPES

TABLE XVII

AIRFRAME STRUCTURAL MODE GAIN AT THE STRUCTURAL MODE RESONANT FREQUENCIES

Flight Condition		Roll Rate to Aileron Deflection						Yaw Rate to Rudder Deflection		Lateral Acceleration To Rudder Deflection	
Mach	Altitude (Ft)	$\omega_{\eta 4}$		$\omega_{\eta 5}$		$\omega_{\eta 6}$		$\omega_{\eta 6}$		$\omega_{\eta 6}$	
		Ratio*	dB	Ratio*	dB	Ratio*	dB	Ratio**	dB	Ratio***	dB
0.5	5,000	1.827	5.24	0.064	−24.38	0.004	−47.54	0.0631	−24.00	141.66	43.03
0.5	25,000	0.826	−1.66	0.0273	−31.28	0.002	−53.98	0.0295	−30.60	65.12	36.27
0.84	SL	5.698	15.12	0.0974	−20.23	2.363	7.47	0.1618	−15.82	390.70	51.84
0.9	15,000	3.744	11.47	0.0638	−23.90	1.605	4.11	0.1099	−19.18	256.61	48.19
0.9	35,000	1.599	4.08	0.0272	−31.31	0.721	−2.85	0.0493	−26.14	108.84	40.74
0.9	45,000	0.999	−0.01	0.0170	−35.39	0.459	−6.76	0.0315	−30.03	69.90	36.89
1.2	5,000	8.675	18.77	0.6879	−3.25	7.499	17.50	0.2325	−12.67	665.15	56.46
1.5	15,000	5.727	15.16	0.5849	−4.66	6.001	15.56	0.2112	−13.51	595.65	55.50
1.5	35,000	2.490	7.92	0.2528	−11.94	2.806	8.96	0.0988	−20.11	243.73	47.74
1.5	45,000	1.567	3.90	0.1586	−15.99	1.821	5.21	0.0641	−23.86	151.43	43.60
1.8	55,000	1.271	2.08	0.1368	−17.28	1.578	3.96	0.0558	−25.07	128.80	42.20
2.15	36,000	4.358	12.78	0.4753	− 6.46	5.026	14.02	0.1464	−16.69	374.66	51.47

*Ratio equals $\frac{\partial \phi_T}{\partial \eta_i} \cdot \frac{\dot{\eta}_i}{\delta}$ (Sec^{-1})

**Ratio equals $\frac{\partial \psi_T}{\partial \eta_6} \cdot \frac{\dot{\eta}_6}{\delta_R}$ (Sec^{-1})

***Ratio equals $\frac{\partial_{hT}}{\partial \eta_6} \cdot \frac{\ddot{\eta}_6}{\delta_R}$ $(Ft/Sec^2\ Rad)$

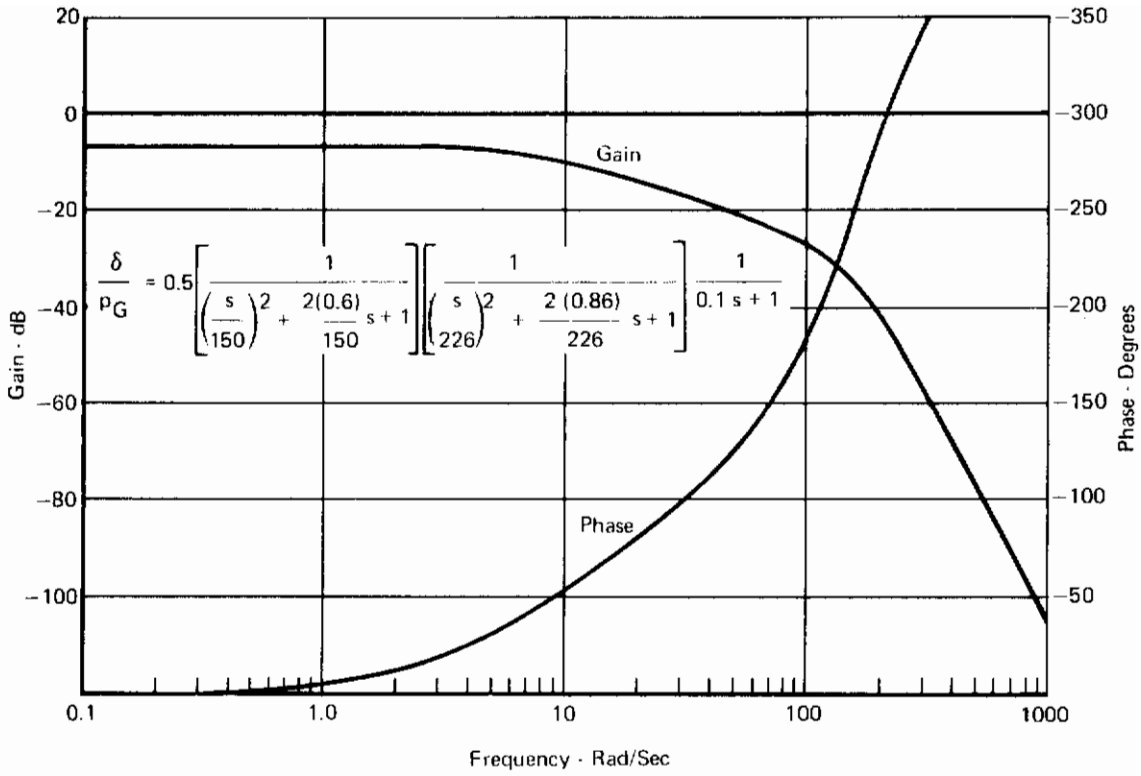

FIGURE 204
FREQUENCY RESPONSE OF THE ROLL RATE LOOP (δ/p_G)
WITHOUT STRUCTURAL FILTER

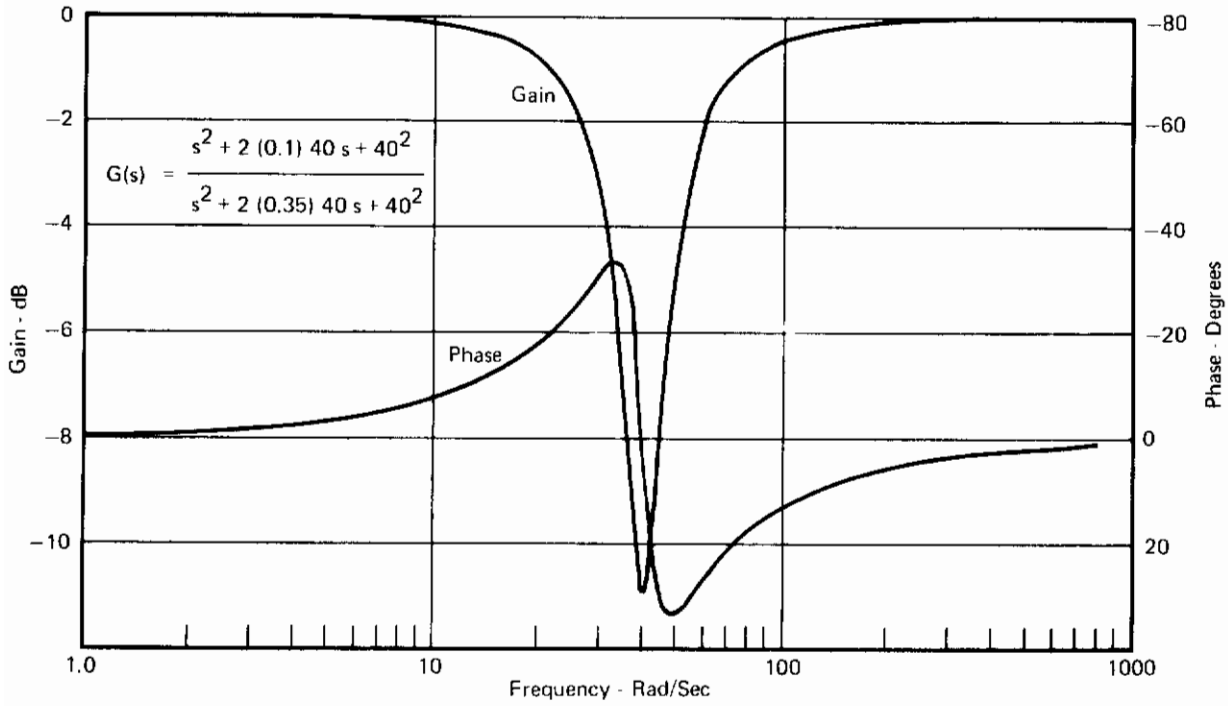

FIGURE 205
FREQUENCY RESPONSE OF ROLL LOOP STRUCTURAL FILTER

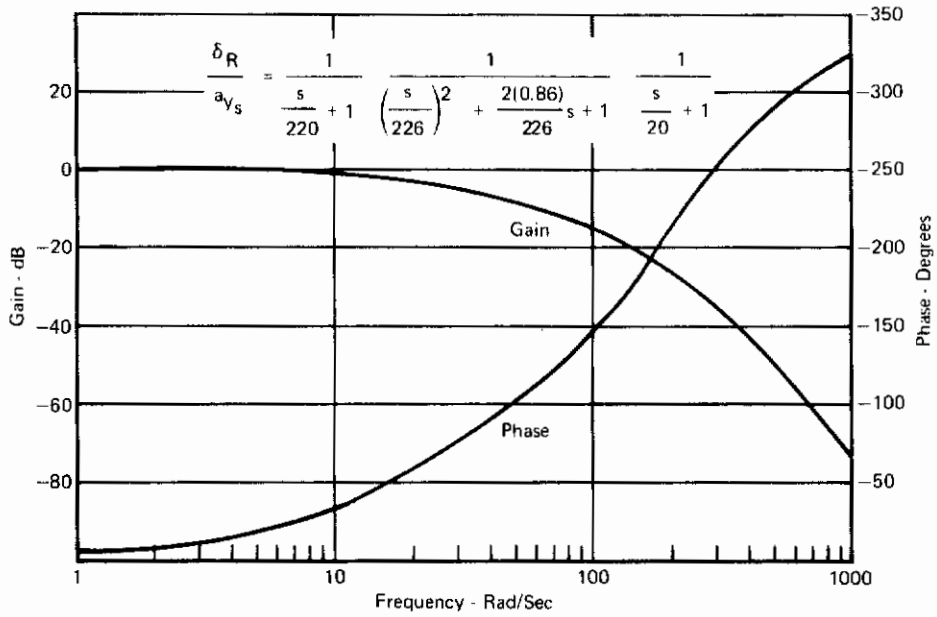

FIGURE 206
FREQUENCY RESPONSE OF THE LATERAL ACCELERATION LOOP δ_R/a_{y_s} WITH UNITY GAIN AND NO STRUCTURAL FILTER

TABLE XVIII
MAXIMUM LATERAL ACCELEROMETER GAIN

Flight Condition		ω_{n_6}	Gain at ω_{n_6}						
						Maximum Kny Gain****			
						No Filter		40 Radian Filter	
Mach	Altitude (Ft)	Rad/Sec	Airframe* (dB)	Control** Loop Dynamics (dB)	Rudder*** Flexibility K_f (dB)	(dB)	(Mag.)	(dB)	(Mag.)
0.5	5,000	80.8	43.0	−13.4	−1.3	−38.3	0.012	−31.25	0.027
0.5	25,000	79.6	36.3	−13.3	−0.6	−32.4	0.024	−25.45	0.053
0.84	SL	86.9	51.8	−14.1	−3.8	−43.9	0.006	−36.33	0.015
0.9	15,000	84.1	48.2	−13.8	−2.7	−41.7	0.008	−34.36	0.019
0.9	35,000	80.9	40.7	−13.4	−1.2	−36.1	0.015	−29.03	0.035
0.9	45,000	80.0	36.9	−13.4	−0.8	−32.7	0.023	25.71	0.051
1.2	5,000	103.0	56.5	−16.0	−11.3	−39.6	0.010	30.38	0.030
1.5	15,000	101.5	55.5	−15.9	−10.8	−39.2	0.011	30.08	0.031
1.5	35,000	88.9	47.7	−17.2	−6.2	−37.3	0.013	29.56	0.033
1.5	45,000	85.1	43.6	−14.0	−4.3	−35.3	0.017	27.88	0.040
1.8	55,000	83.1	42.2	−13.7	−3.1	−35.4	0.017	28.14	0.039
2.15	36,000	92.1	51.5	−14.6	−6.0	−40.9	0.009	32.91	0.022

* Data from Table XVII
** Data from Figure 206
*** Data from Table X
**** Maximum Kny gain for which the open lateral acceleration loop gain will be −10 dB or less at the n_6 mode resonant frequency

most critical flight condition is 0.84 Mach at sea level, which limits the maximum K_{n_y} gain to 0.015 radians per foot per second squared when the 40 radian structural filter is included in the lateral acceleration feedback loop. The SFCS employs a slightly lower gain of 0.014 radians per foot per second squared along with the 40 radian structural filter.

The results of the above analysis were compared with the frequency response data formed by using the six lateral-directional equations, sensor math models and control loop dynamics. Table XIX summarizes the final system gain margins, phase margins and structural mode attenuation as determined from these frequency responses. There is good correlation between the structural mode attenuation at the high $\bar{q}$ flight conditions as shown in Table XIX and the -10 dB or less predicted from the analysis. Figures 207 through 215 present unaugmented airframe frequency responses for three flight conditions. The structural mode amplitudes present compare favorably with those predicted in Table XVII. Figures 216 through 221 present open lateral loop and directional loop frequency responses with the SFCS. Data from these responses were used in forming Table XIX. Figures 222 through 233 time history responses show that the structural modes as defined will not interfere with the lateral-directional SFCS performance.

Figures 234 through 236 when compared with Figures 209, 212, and 215 show the increase in structural mode pickup by the lateral accelerometer when located at F.S. 68 as initially planned.

TABLE XIX

LATERAL-DIRECTIONAL GAIN AND PHASE MARGINS

Flight Condition Mach/Alt	Yaw Rate Gain (K_r)	Lateral Loop**							Directional Loop***						
		Phase Margin		Gain Margin		Gain (dB) at Flexible Modes			Phase Margin		Gain Margin		Gains (dB) at Flexible Modes		
		γ (Deg)	$\omega_\phi\left(\frac{\text{Rad}}{\text{Sec}}\right)$	a (dB)	$\omega_c\left(\frac{\text{Rad}}{\text{Sec}}\right)$	η_4	η_5	η_6	γ (Deg)	$\omega_\phi\left(\frac{\text{Rad}}{\text{Sec}}\right)$	a (dB)	$\omega_c\left(\frac{\text{Rad}}{\text{Sec}}\right)$	η_4	η_5	η_6
0.5/5K	1.5*	80.8	4.38	19.3	19.4	−24.5	−36.5	−34.1	90.1	4.5	26.0	49.5	−22.0	−42.3	−17.3
0.5/25K	0.75*	96.5	2.61	26.6	19.5	−32.0	−45.0	−39.0	116.2	1.85	37.5	54.5	−30.4	−53.0	−22.3
	1.5	98.0	2.55	25.6	18.4	−32.0	−45.0	−39.0	101.3	2.52	32.3	50.0	−28.3	−48.0	−22.9
	3.0	98.8	2.51	25.6	18.5	−32.0	−45.0	−39.0	89.1	4.0	26.7	45.3	−24.9	−37.0	−24.2
0.84/SL	0.75	63.3	6.9	15.4	20.5	−14.1	−27.0	−17.0	80.4	6.6	22.9	57.5	−15.4	−22.5	−13.4
	1.5*	61.1	7.3	15.4	20.5	−14.1	−25.4	−17.1	77.2	10.8	17.8	52.2	−13.4	−21.7	−14.0
	3.0	63.2	7.2	15.1	20.0	−14.2	−25.4	−17.2	53.7	17.8	12.4	47.0	−10.3	−19.9	−15.0
0.9/15K	1.5*	66.3	6.03	16.4	19.6	−17.6	−28.0	−20.2	82.3	7.9	20.1	52.5	−15.0	−26.2	−15.0
0.9/35K	1.5*	75.4	4.13	19.6	18.6	−25.7	−34.8	−26.8	89.7	4.25	27.2	51.5	−22.9	−41.8	−19.7
0.9/45K	0.75	82.5	2.96	23.1	18.0	−30.0	−38.0	−30.5	107.3	2.12	38.0	54.5	−30.5	−48.6	−22.2
1.2/5K	0.75*	85.5	4.57	21.7	20.0	−11.4	−22.2	− 9.1	102.4	6.2	37.0	53.4	−27.3	−24.7	−21.1
	1.5	87.9	4.42	21.4	19.6	−11.4	−22.2	− 9.1	82.7	6.9	30.8	49.2	−25.8	−25.0	−21.6
	3.0*	89.7	4.3	21.4	19.4	−11.4	−22.3	− 9.3	73.1	8.13	24.8	45.0	−22.8	−28.4	−22.7
1.5/15K	3.0*	100.5	3.25	22.8	19.3	−14.8	−24.8	−11.7	80.1	6.55	30.2	42.0	−30.0	−29.7	−22.1
1.5/35K	1.5*	82.7	3.55	21.0	19.0	−21.2	−30.0	−16.2	82.7	4.6	32.7	44.0	−31.1	−34.5	−20.3
1.5/45K	1.5*	87.3	3.0	22.2	18.4	−25.4	−32.0	−19.8	89.3	3.9	33.9	43.0	−32.8	−39.0	−21.3
1.8/55K	1.5*	95.0	2.0	24.9	18.0	−27.7	−33.0	−21.0	88.7	3.0	34.7	33.7	−38.5	−35.6	−20.7
2.15/36K	1.5*	99.6	2.48	24.0	18.3	−16.3	−26.0	−11.4	58.3	4.39	29.4	26.5	−43.9	−27.1	−17.9

η_4 First fuselage torsional mode - 40 Rad/Sec
η_5 Unsymmetric wing bending mode - 68 Rad/Sec
η_6 First lateral bending mode - 80 to 104 Rad/Sec

* Adaptive gain value
** Based on a frequency response of the open lateral loop with the directional loop closed
*** Based on a frequency response of the open directional loop with the lateral loop closed

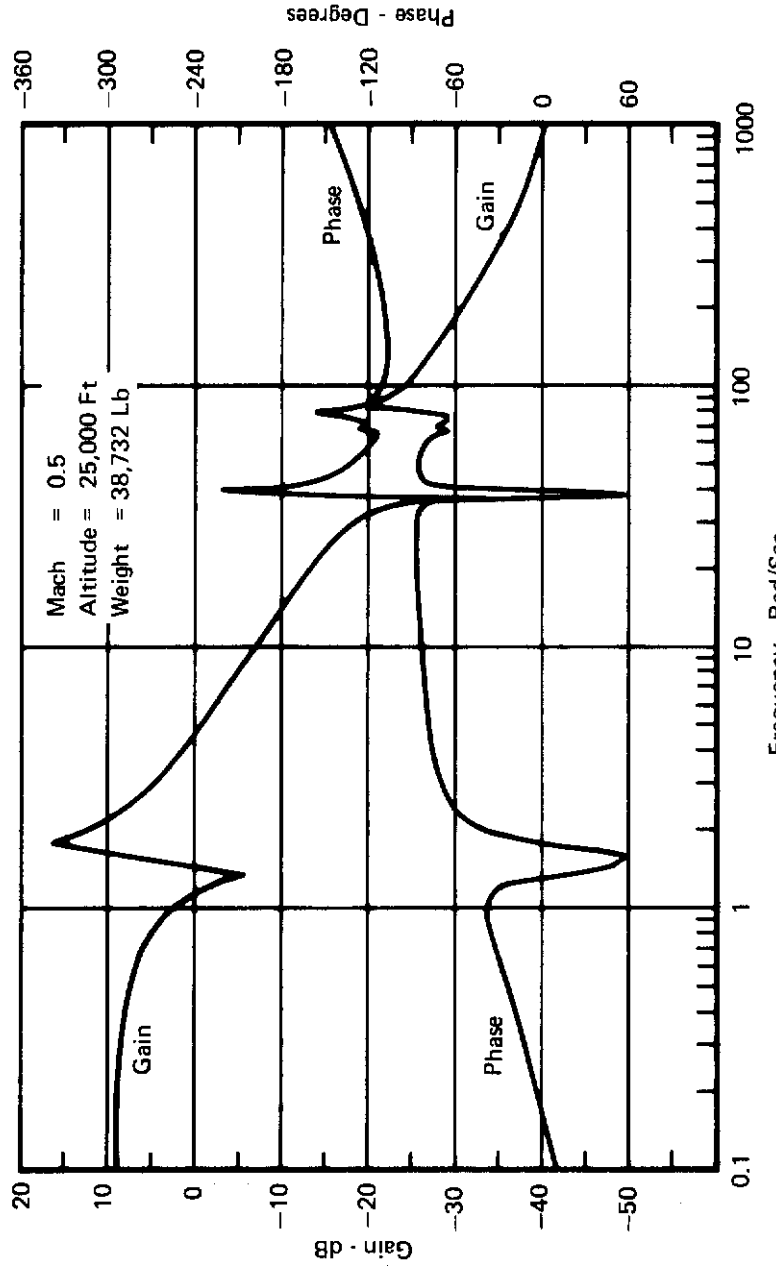

FIGURE 207
UNAUGMENTED AIRFRAME p/δ FREQUENCY RESPONSE SHOWING STRUCTURAL MODES

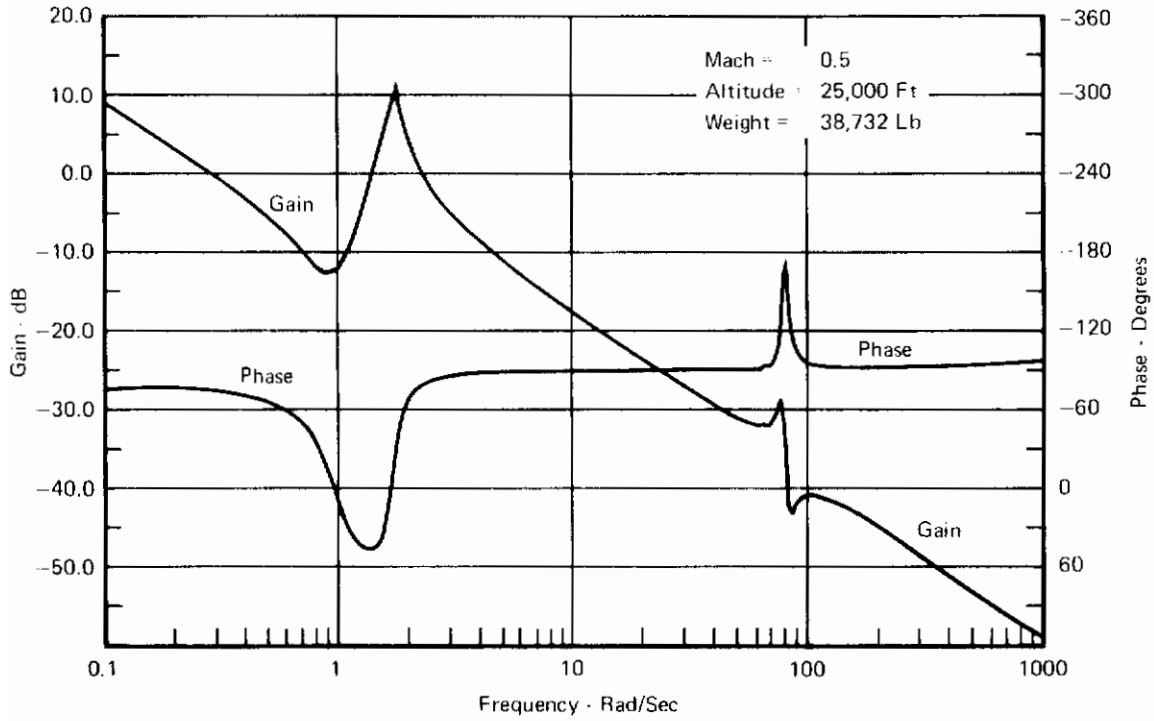

FIGURE 208

UNAUGMENTED AIRFRAME r/δ_R FREQUENCY RESPONSE SHOWING STRUCTURAL MODES

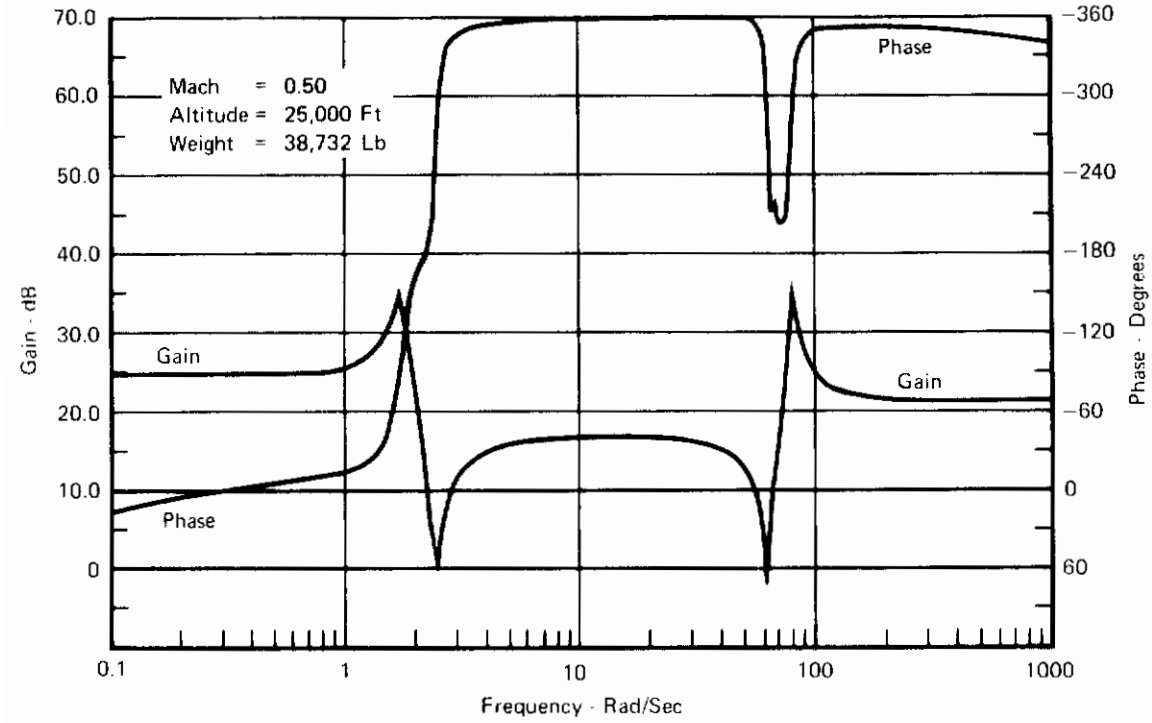

FIGURE 209

UNAUGMENTED AIRFRAME $a_{y_{s_{186}}}/\delta_R$ FREQUENCY RESPONSE SHOWING STRUCTURAL MODES

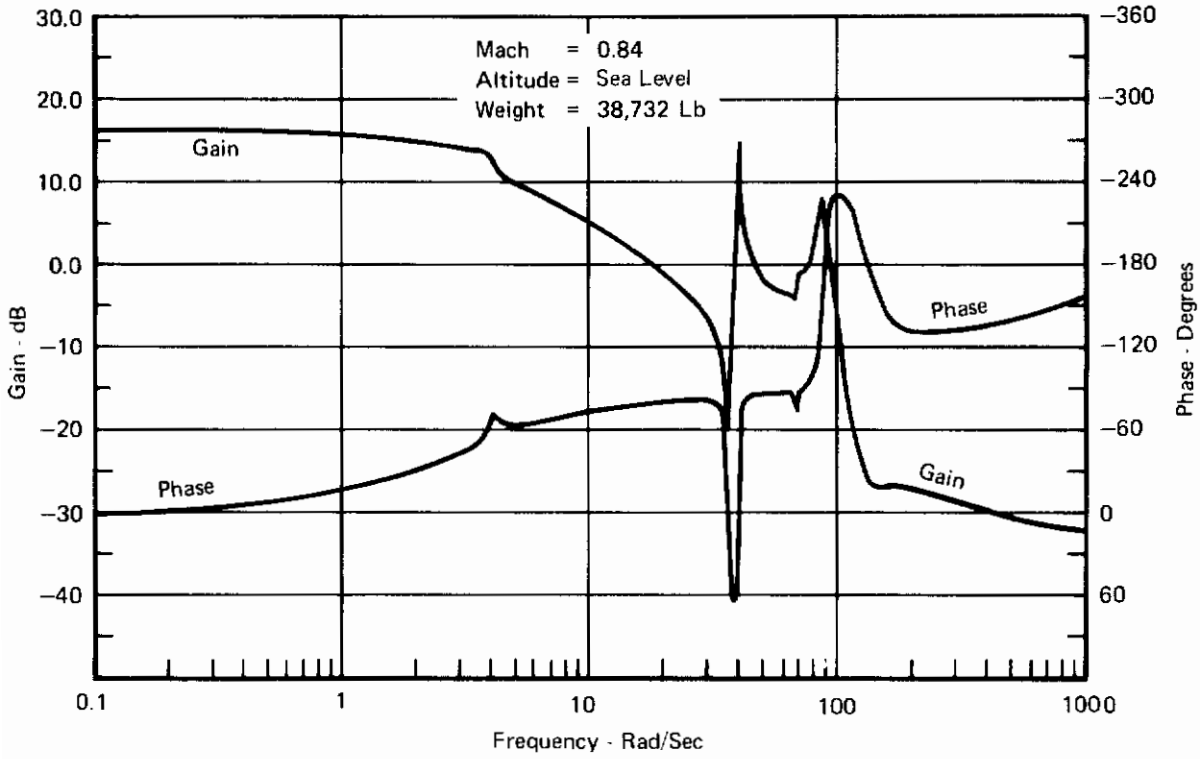

FIGURE 210

UNAUGMENTED AIRFRAME p/δ FREQUENCY RESPONSE SHOWING STRUCTURAL MODES

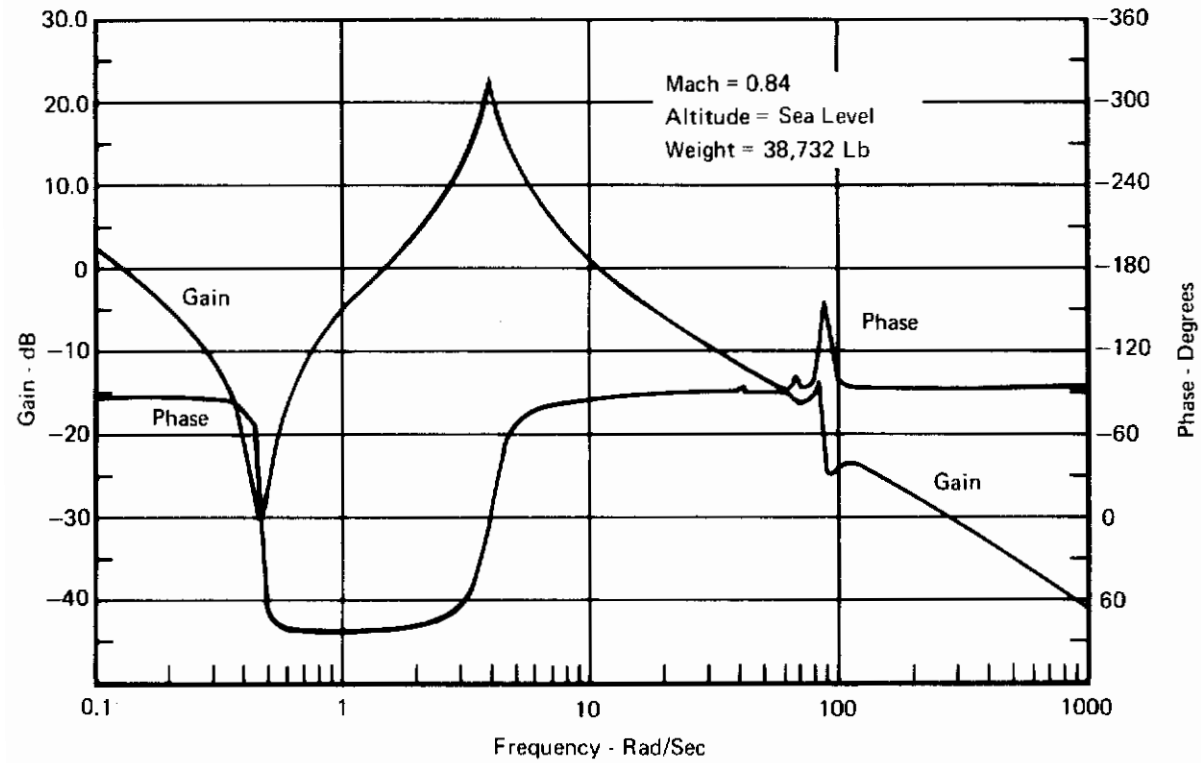

FIGURE 211

UNAUGMENTED AIRFRAME r/δ_R FREQUENCY RESPONSE SHOWING STRUCTURAL MODES

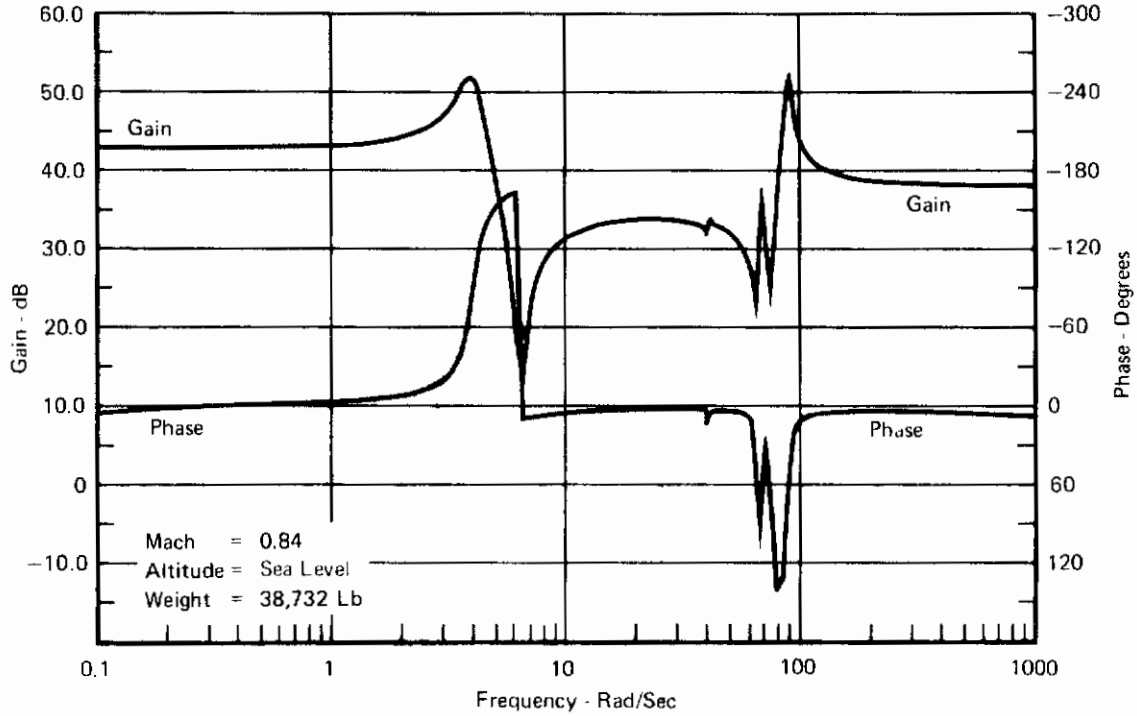

FIGURE 212

UNAUGMENTED AIRFRAME $a_{y_{s_{186}}}/\delta_R$ FREQUENCY RESPONSE SHOWING STRUCTURAL MODES

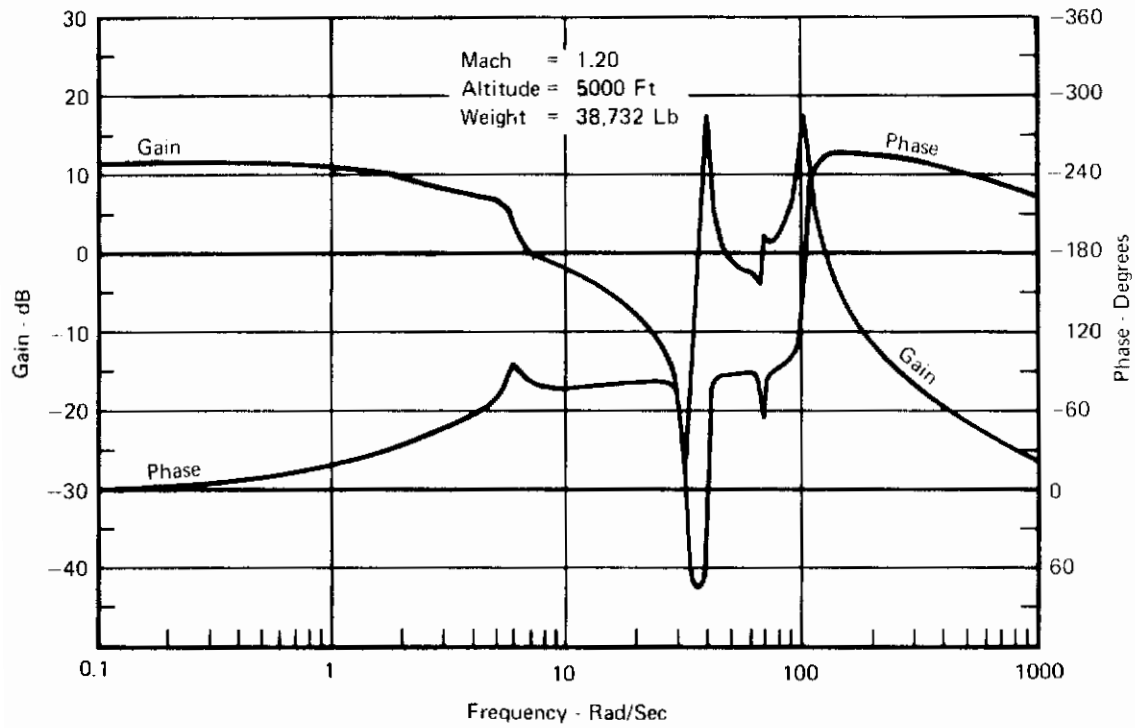

FIGURE 213

UNAUGMENTED AIRFRAME p/δ FREQUENCY RESPONSE SHOWING STRUCTURAL MODES

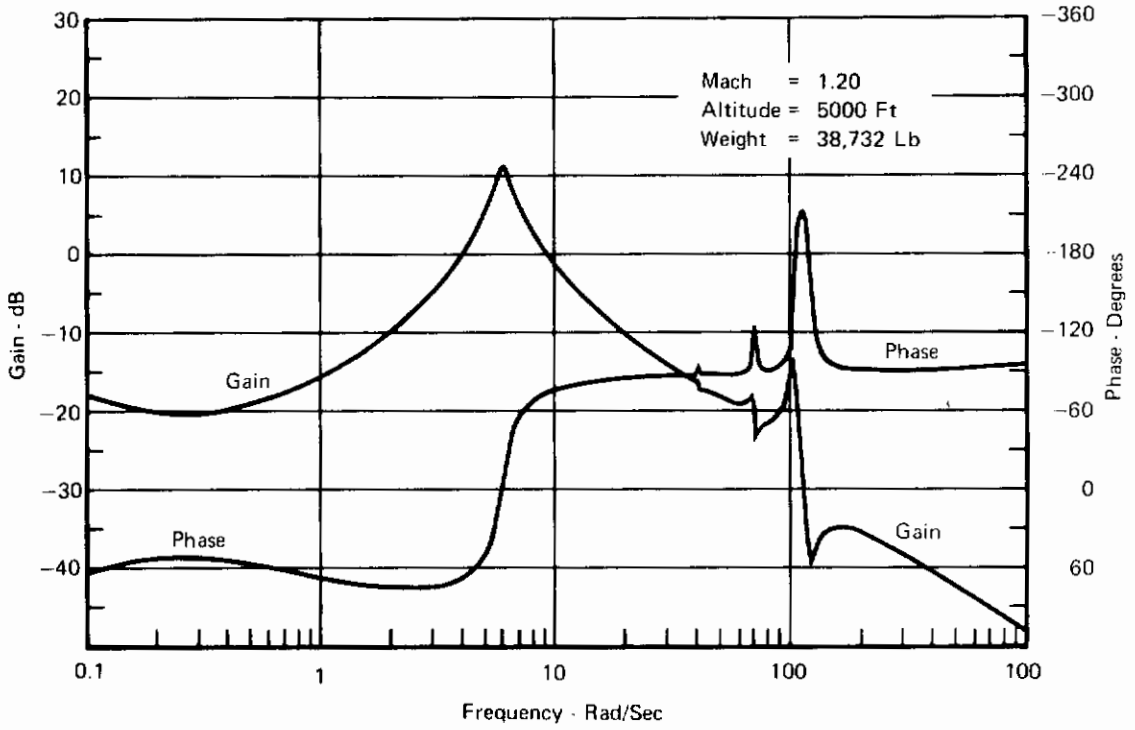

FIGURE 214
UNAUGMENTED AIRFRAME r/δ_R FREQUENCY RESPONSE SHOWING STRUCTURAL MODES

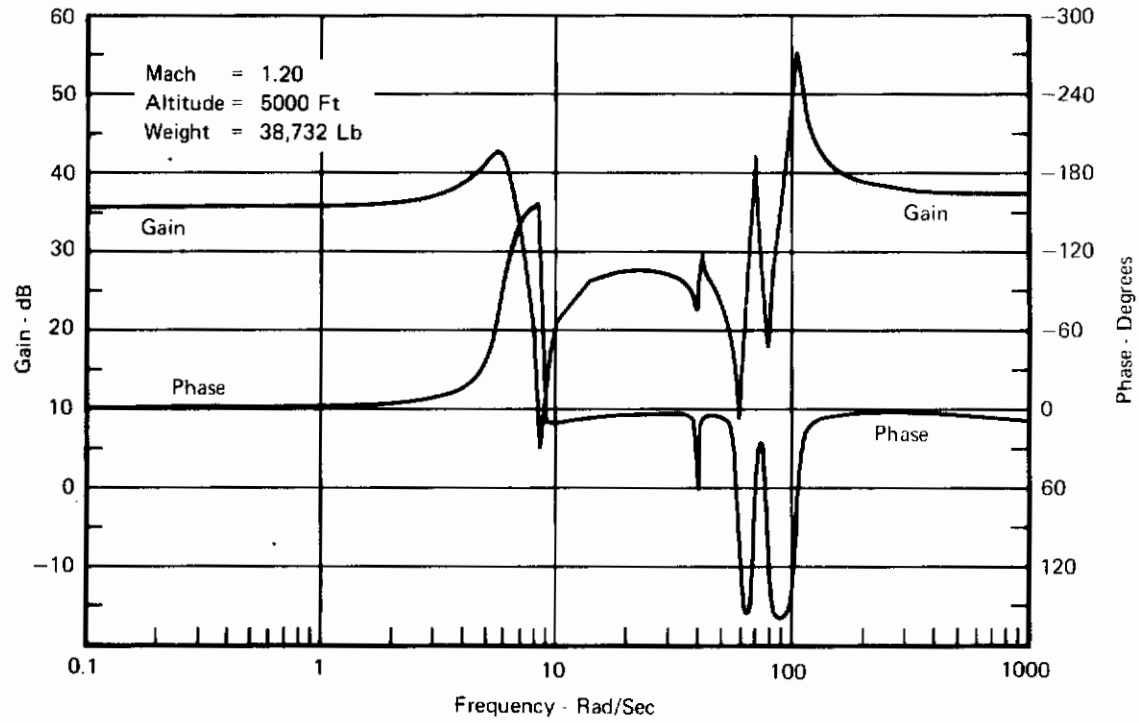

FIGURE 215
UNAUGMENTED AIRFRAME $a_{y_{s_{186}}}/\delta_R$ FREQUENCY RESPONSE SHOWING STRUCTURAL MODES

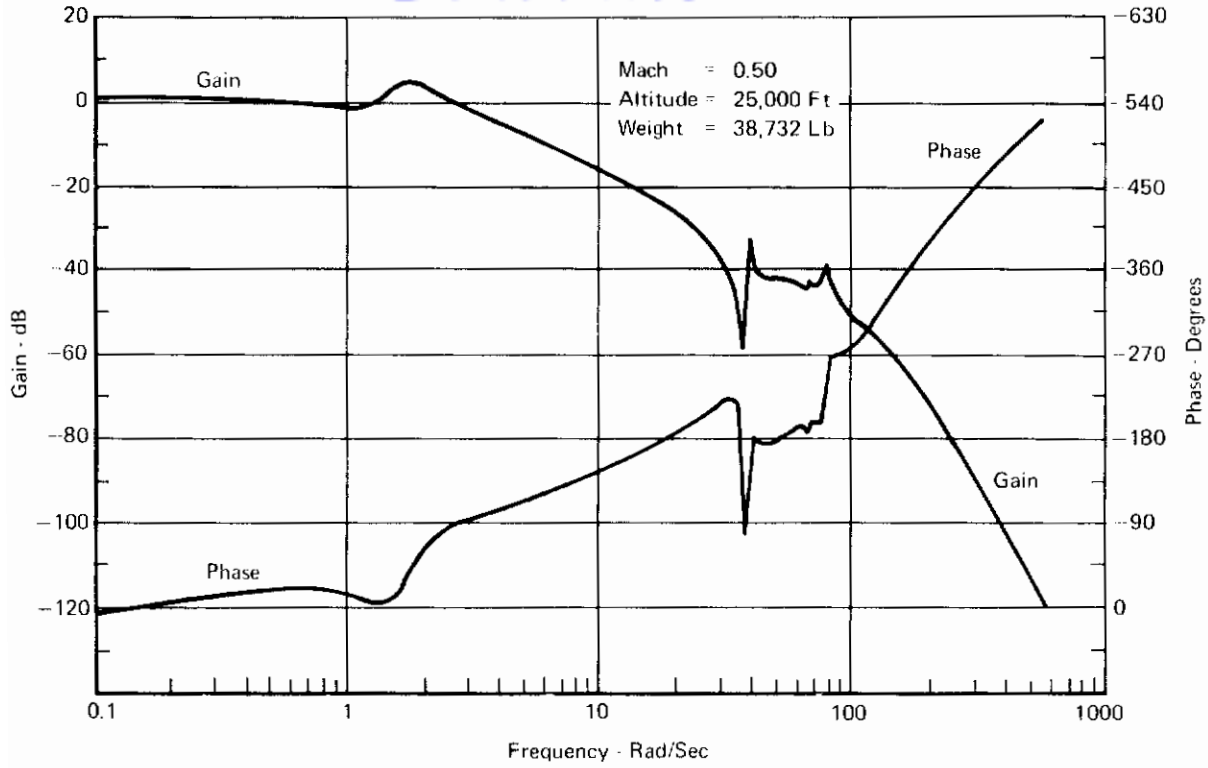

FIGURE 216

OPEN LATERAL LOOP FREQUENCY RESPONSE WITH DIRECTIONAL LOOP CLOSED (KR = 0.75)

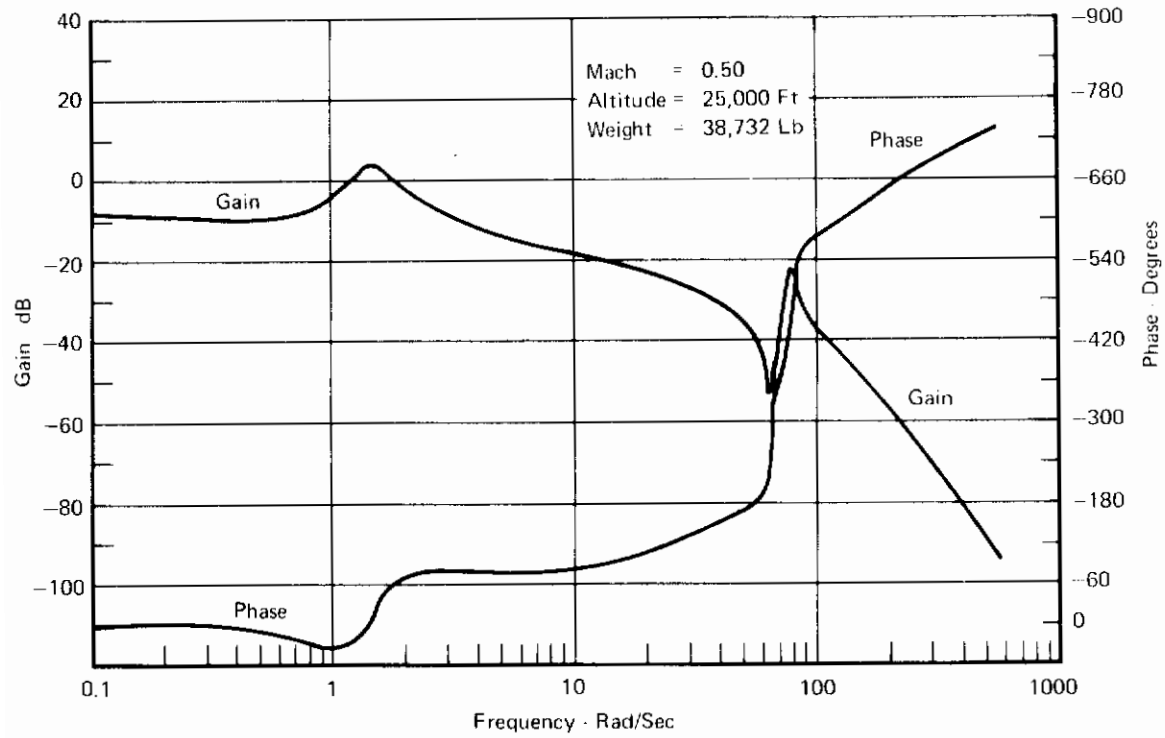

FIGURE 217

OPEN DIRECTIONAL LOOP FREQUENCY RESPONSE WITH LATERAL LOOP CLOSED (KR = 0.75)

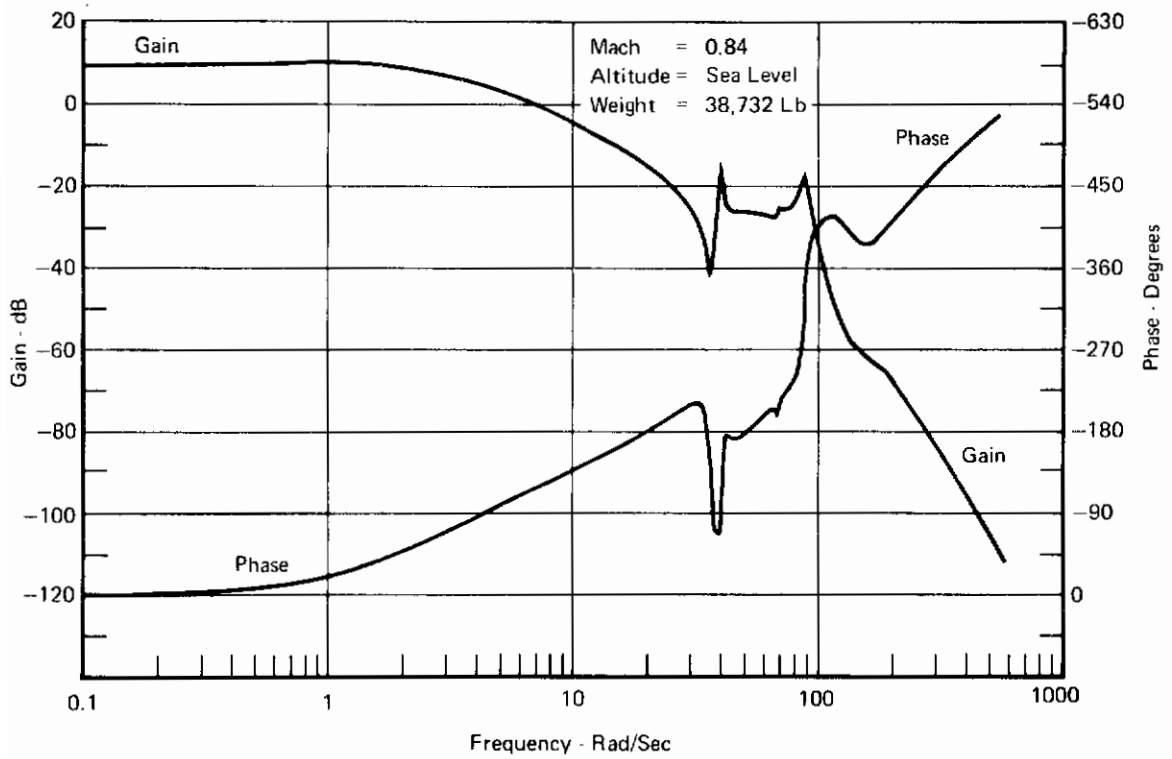

FIGURE 218
OPEN LATERAL LOOP FREQUENCY RESPONSE
WITH DIRECTIONAL LOOP CLOSED (KR = 1.50)

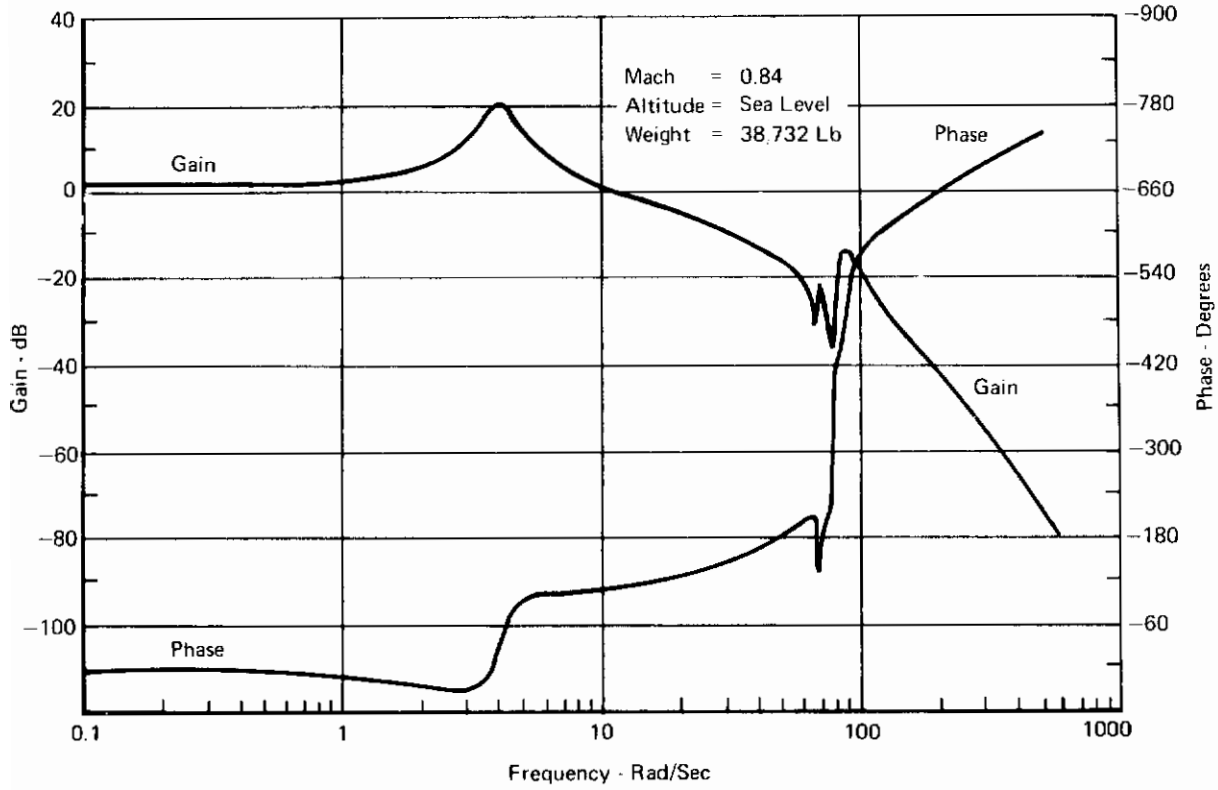

FIGURE 219
OPEN DIRECTIONAL LOOP FREQUENCY RESPONSE
WITH LATERAL LOOP CLOSED (KR = 1.50)

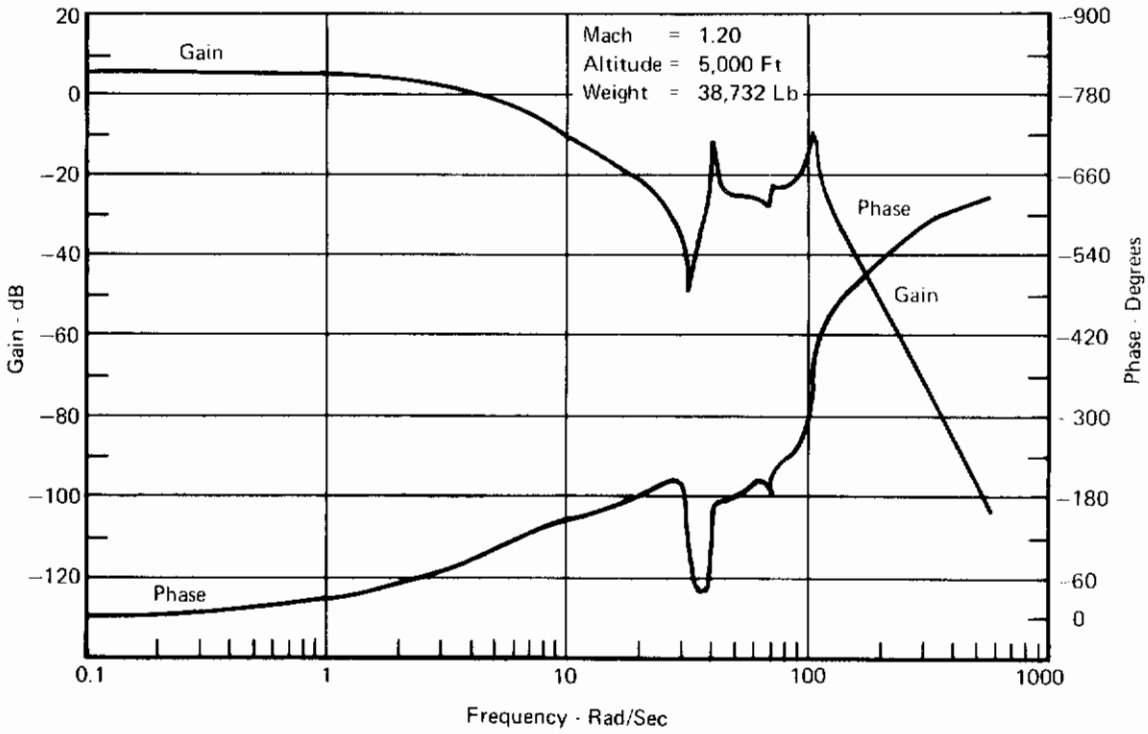

FIGURE 220
OPEN LATERAL LOOP FREQUENCY RESPONSE WITH DIRECTIONAL LOOP CLOSED (KR = 3.00)

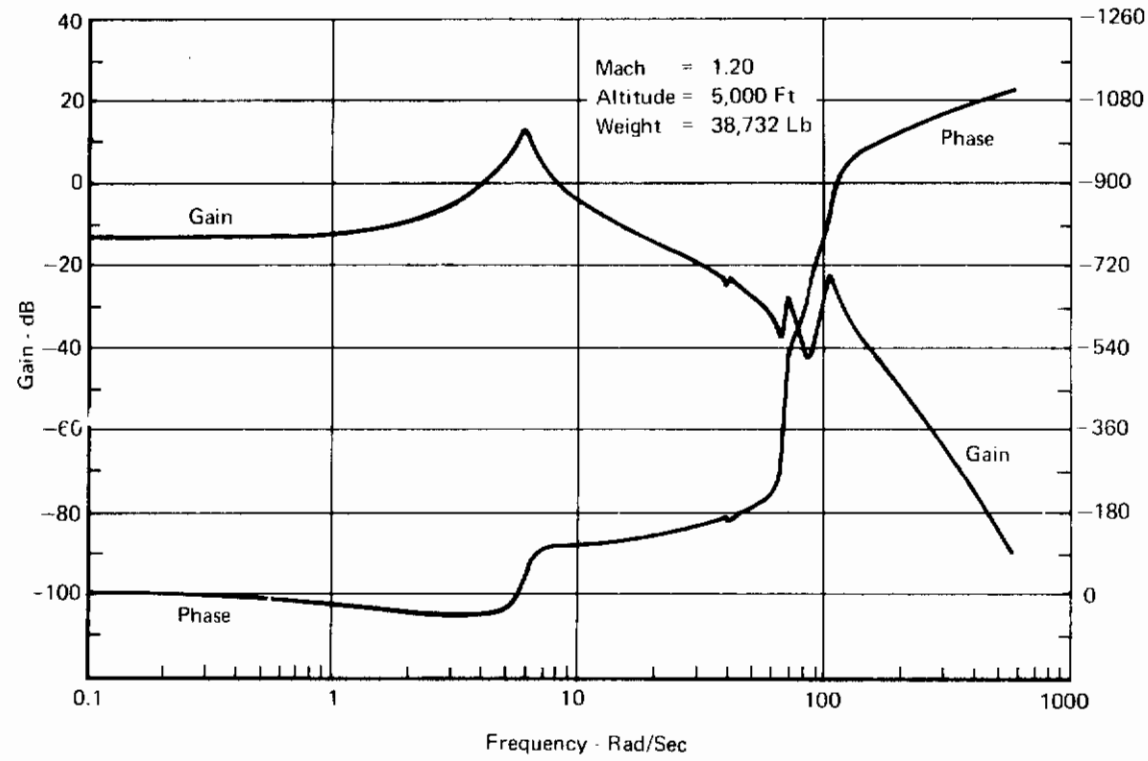

FIGURE 221
OPEN DIRECTIONAL LOOP FREQUENCY RESPONSE WITH LATERAL LOOP CLOSED (KR = 3.00)

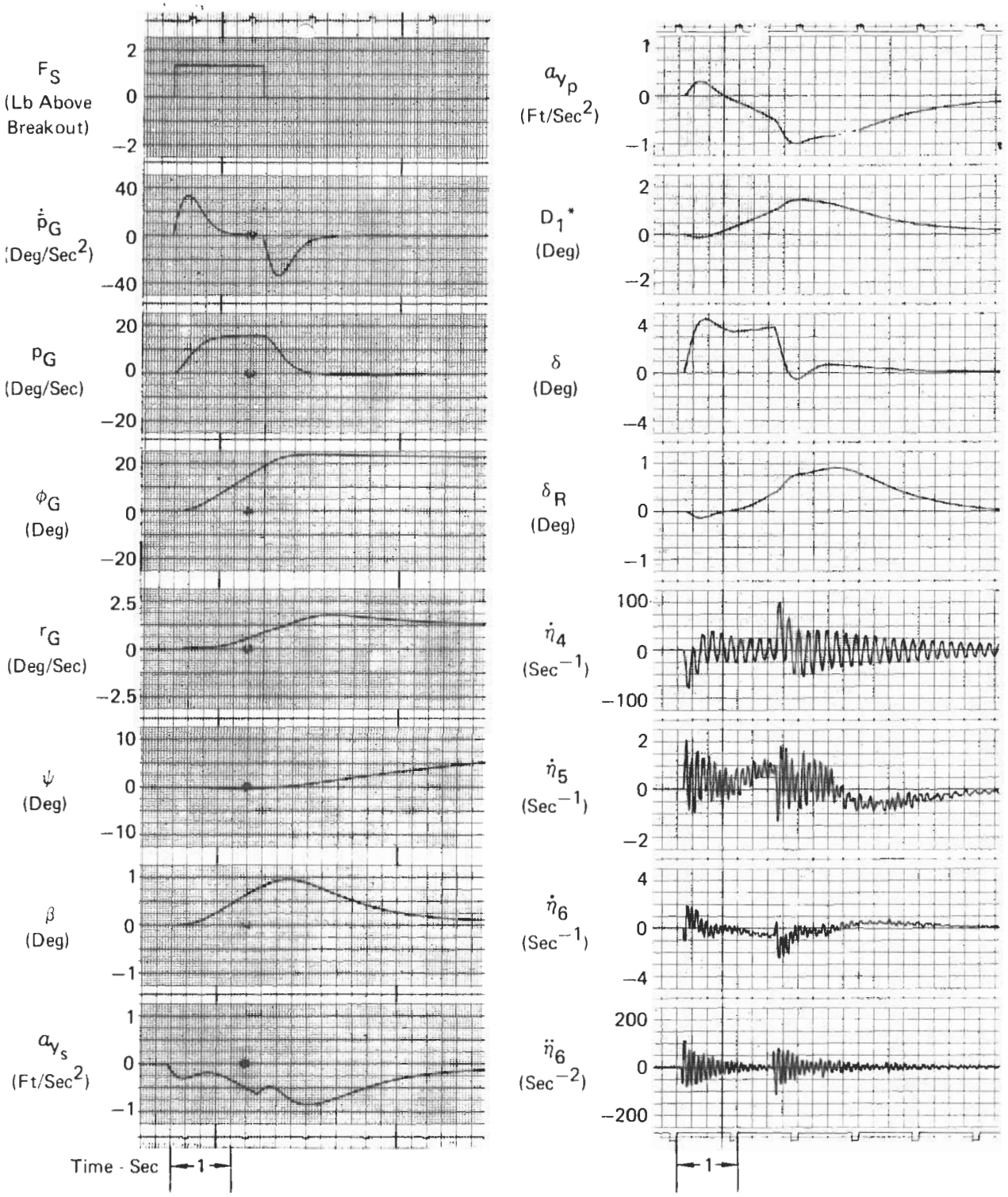

FIGURE 222

DYNAMIC RESPONSE TO LATERAL STICK FORCE

(Structural Dynamics Included)

(No Roll to Yaw Crossfeed)

Clean Configuration Weight 38,732 Lb Altitude 5000 Ft

Mach 0.5 KR 1.5

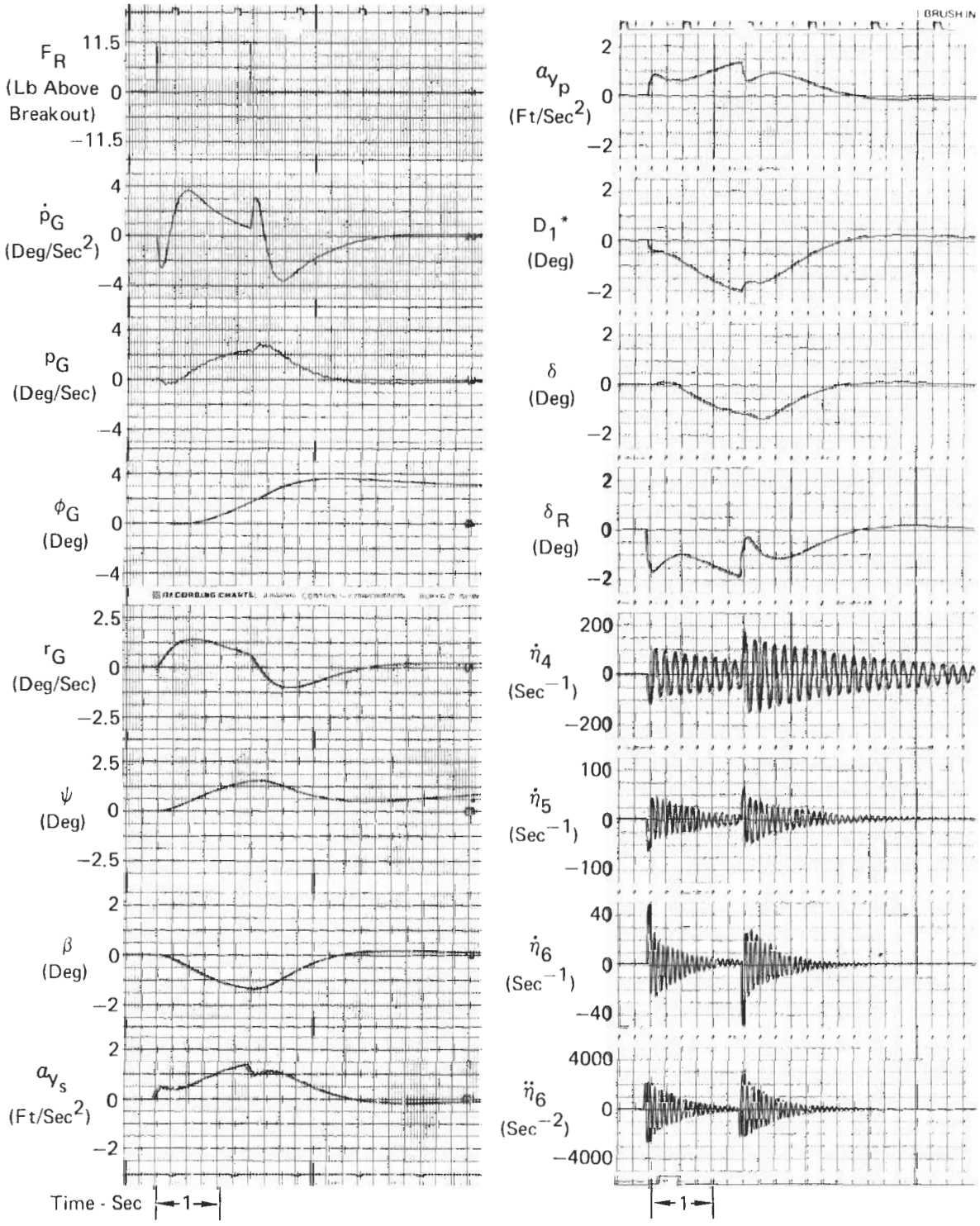

FIGURE 223
DYNAMIC RESPONSE TO RUDDER PEDAL FORCE
(Structural Dynamics Included)

Clean Configuration Weight 38,732 Lb Altitude 5000 Ft
Mach 0.5 KR 1.5

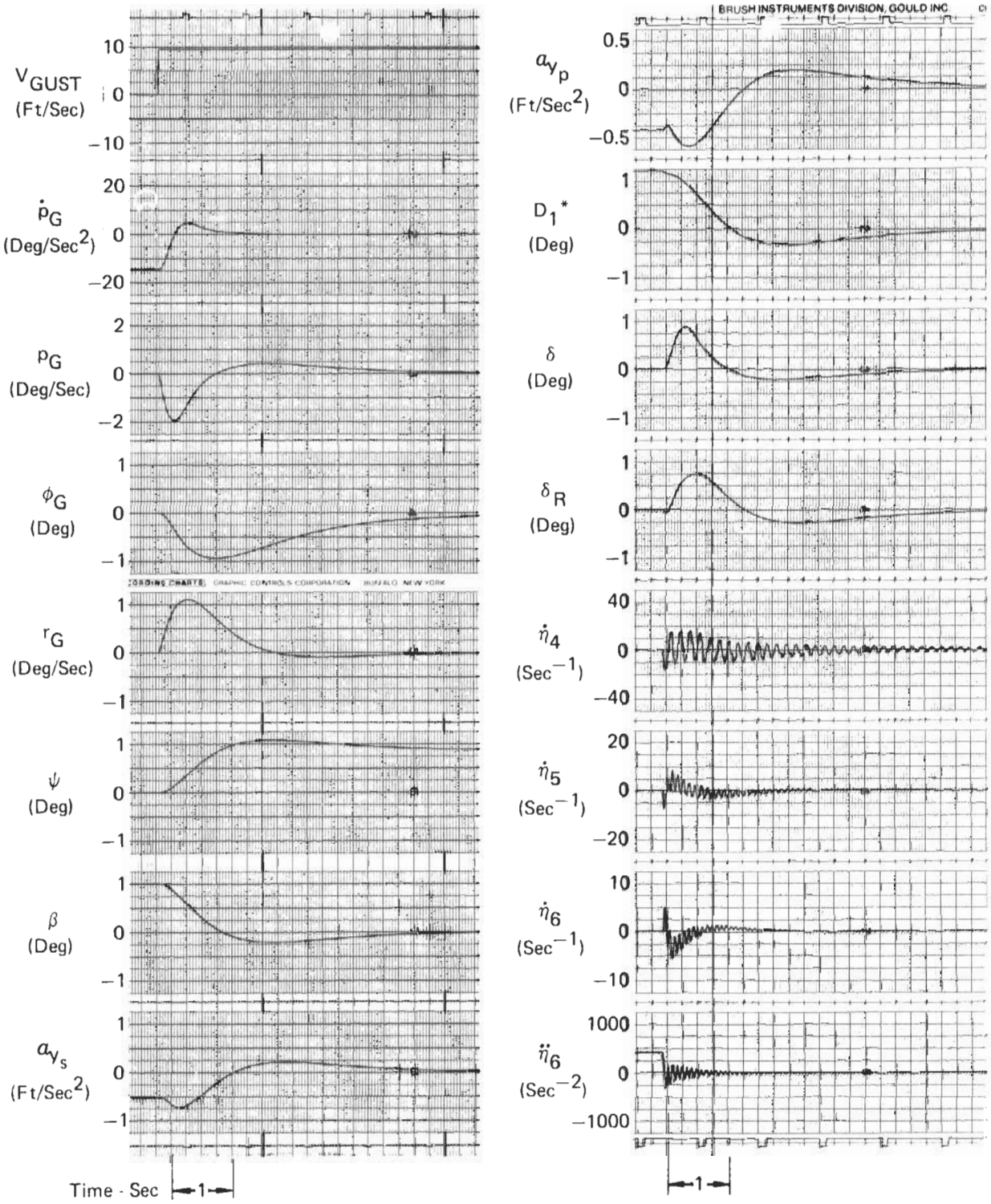

FIGURE 224

DYNAMIC RESPONSE TO SHARP EDGE GUST

(Structural Dynamics Included)

Clean Configuration Weight 38,732 Lb Altitude 5000 Ft

Mach 0.5 KR 1.5

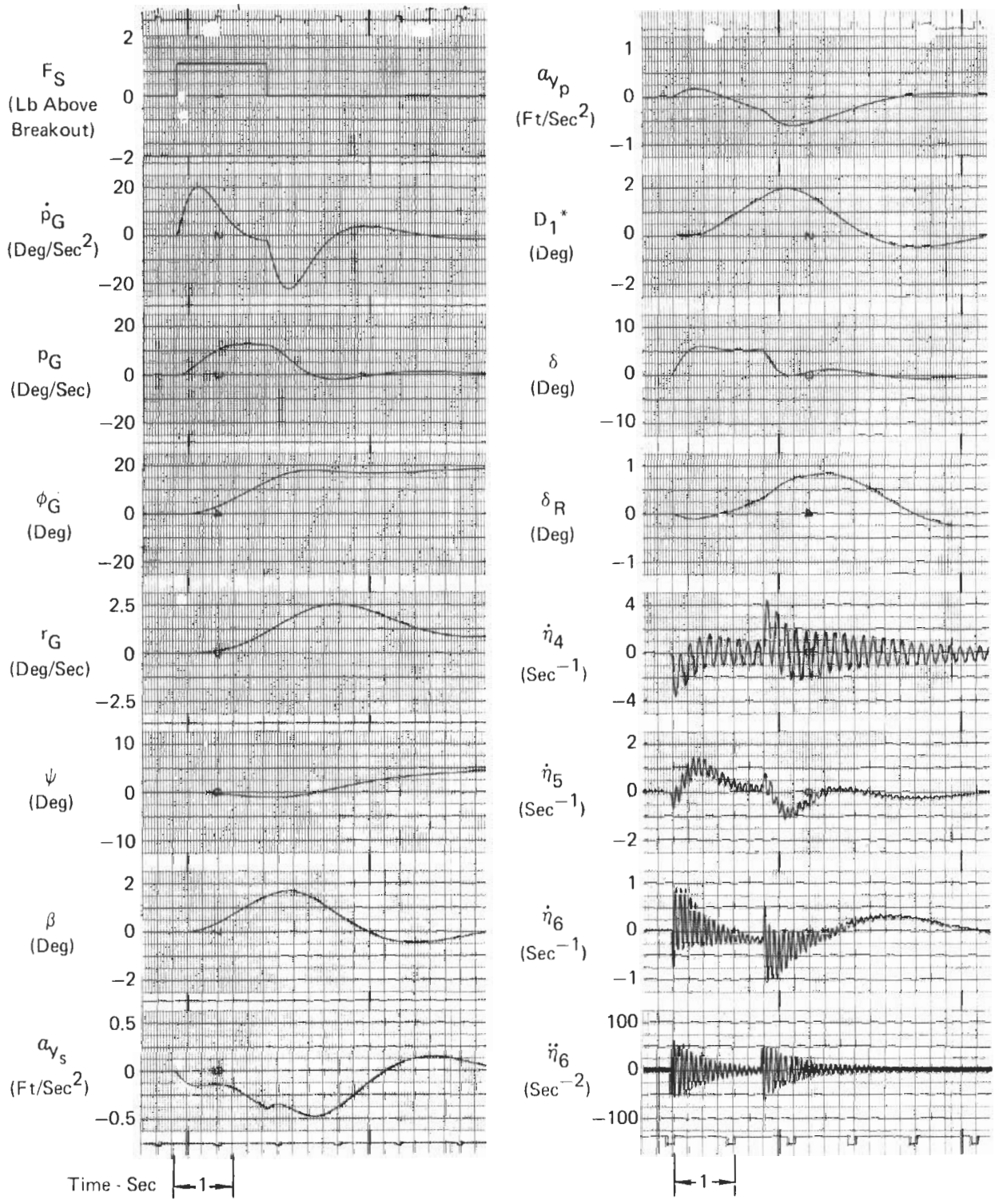

FIGURE 225
DYNAMIC RESPONSE TO LATERAL STICK FORCE
(Structural Dynamics Included)
(No Roll to Yaw Crossfeed)

Clean Configuration Weight 38,732 Lb Altitude 25,000 Ft
Mach 0.5 KR 0.75

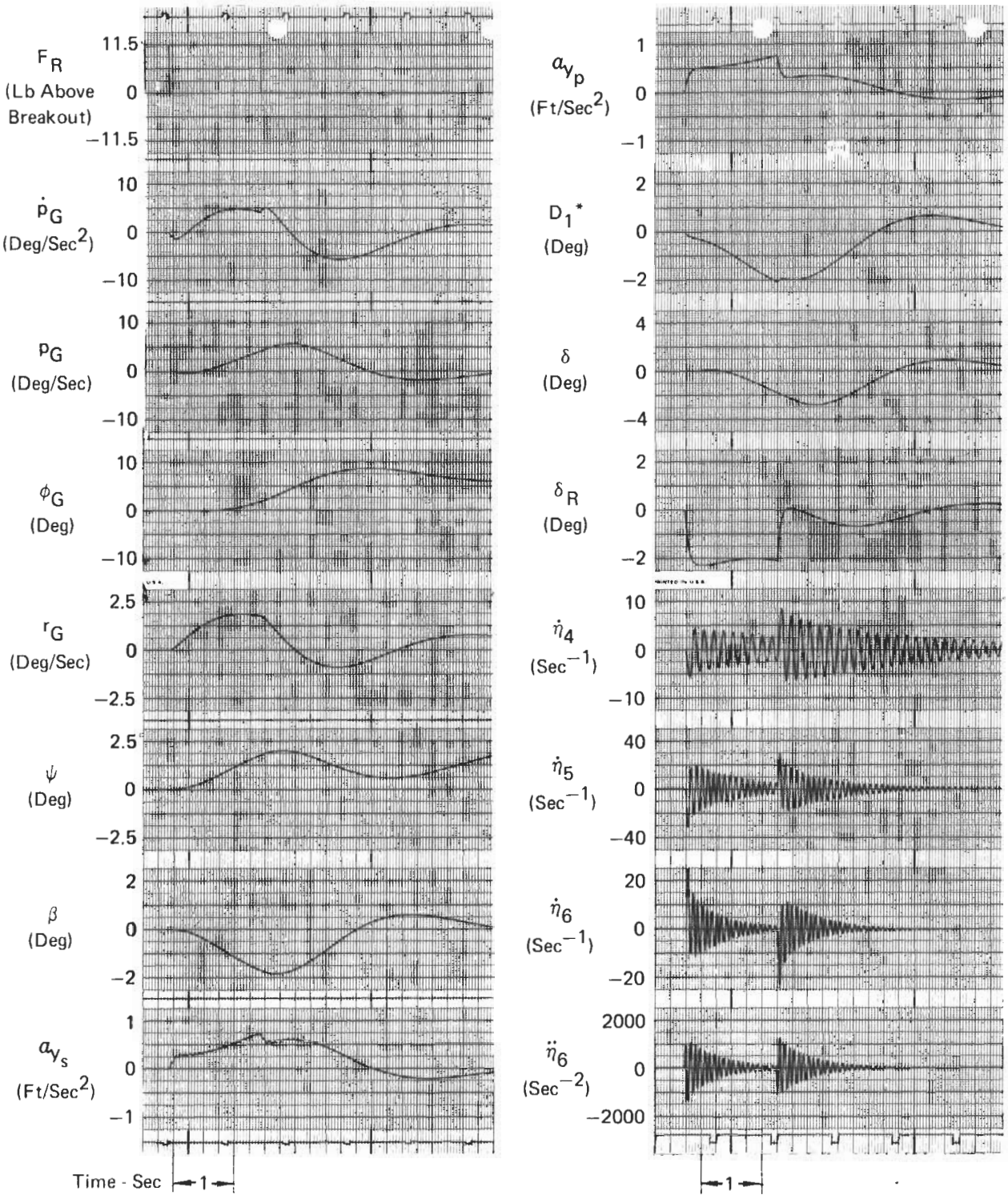

FIGURE 226
DYNAMIC RESPONSE TO RUDDER PEDAL FORCE
(Structural Dynamics Included)

Clean Configuration Weight 38,732 Lb Altitude 25,000 Ft
Mach 0.5 KR 0.75

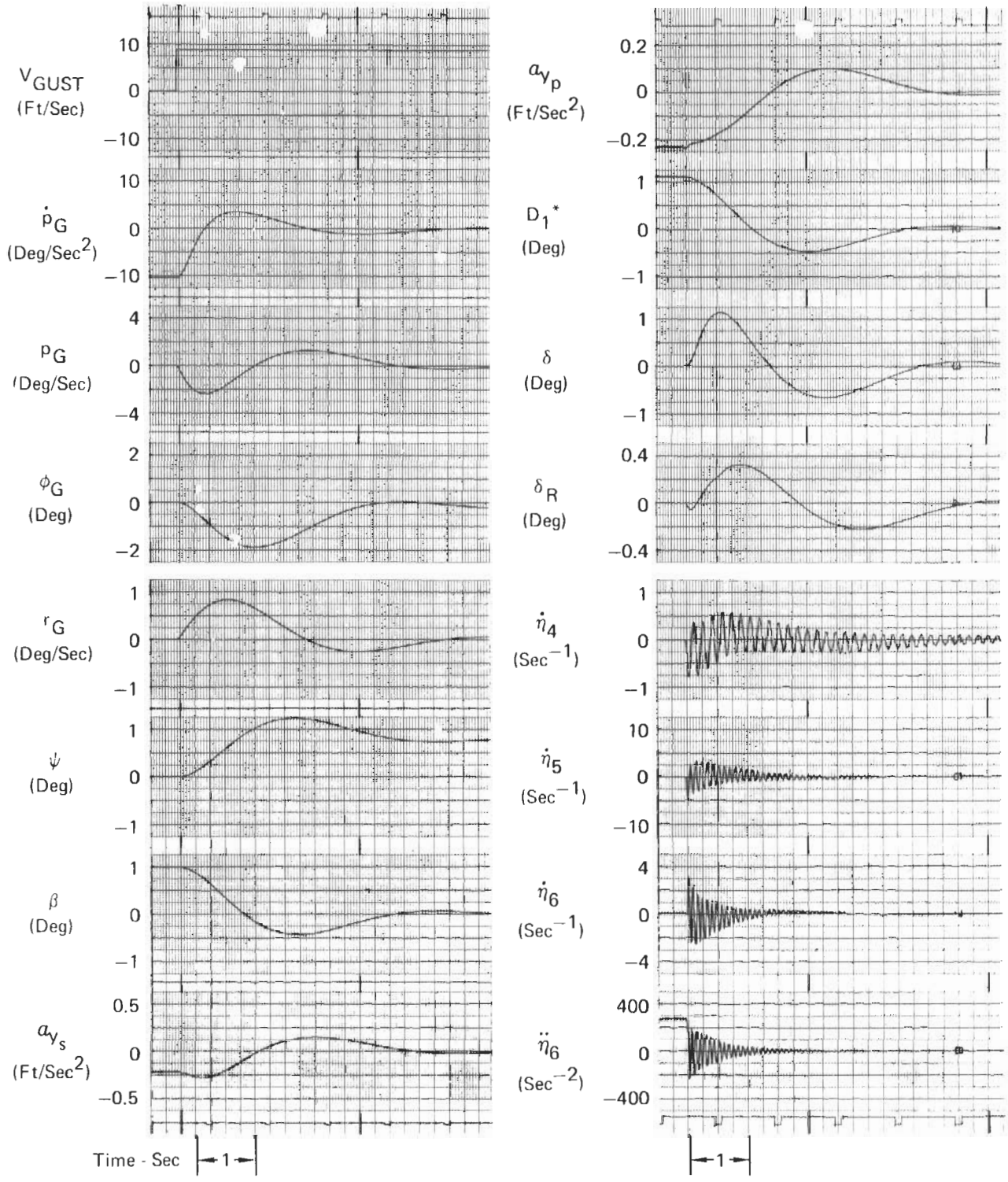

FIGURE 227
DYNAMIC RESPONSE TO SHARP EDGE GUST
(Structural Dynamics Included)

Clean Configuration Weight 38,732 Lb Altitude 25,000 Ft
Mach 0.5 KR 0.75

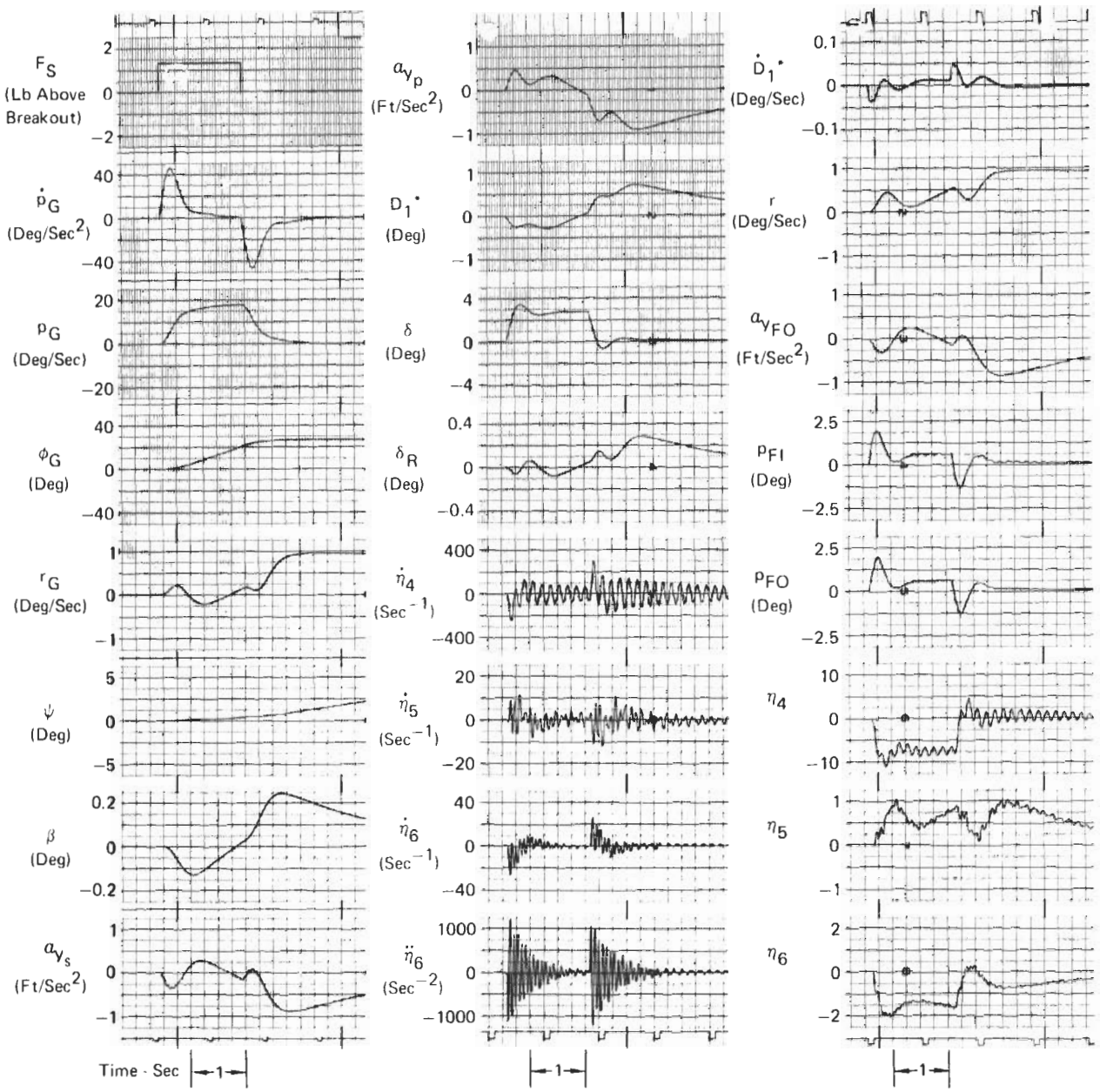

FIGURE 228
DYNAMIC RESPONSE TO LATERAL STICK FORCE
(Structural Dynamics Included)
(No Roll to Yaw Crossfeed)

Clean Configuration Weight 38,732 Lb Altitude Sea Level
Mach 0.84 KR 1.5

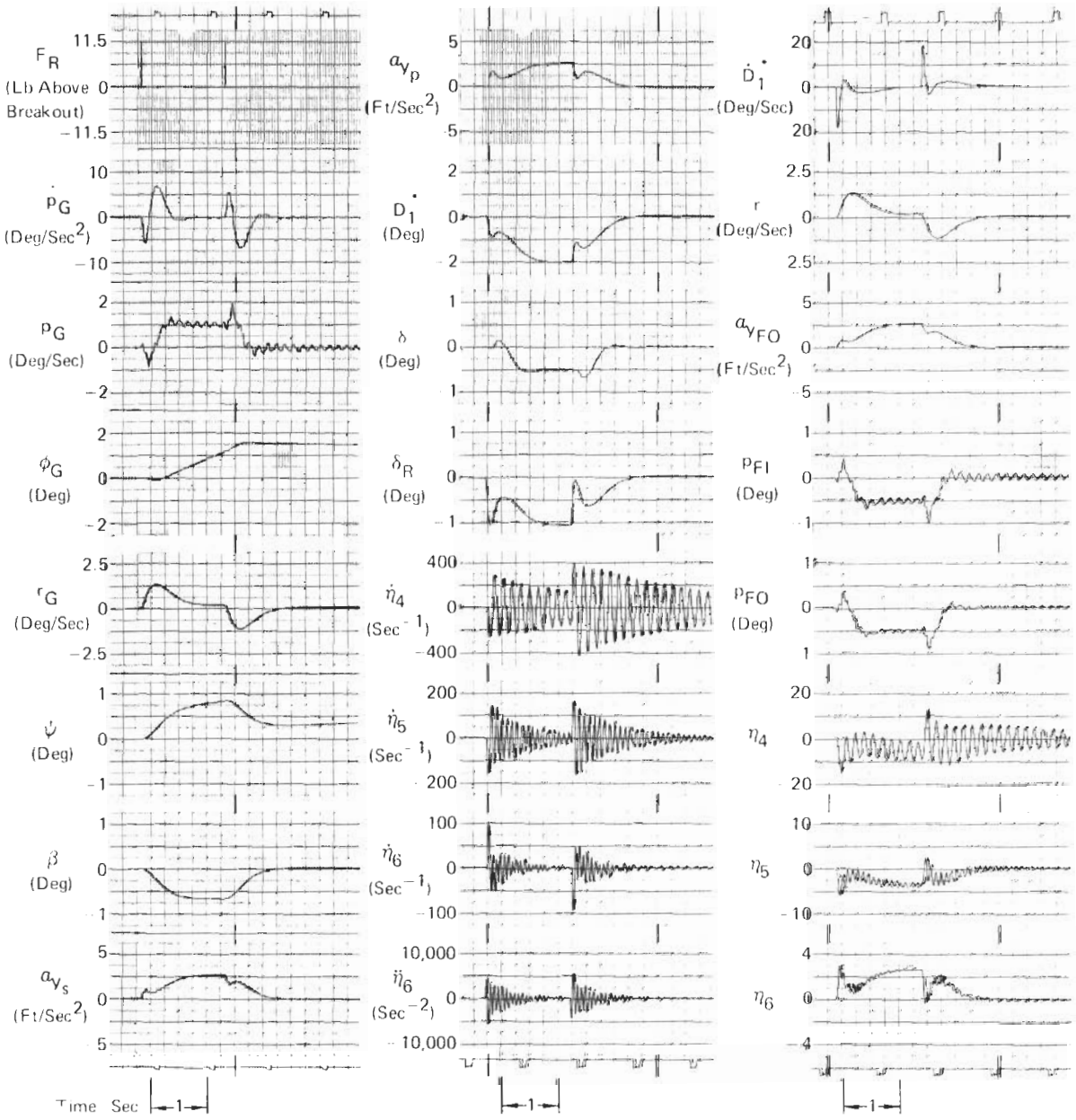

FIGURE 229

DYNAMIC RESPONSE TO RUDDER PEDAL FORCE

(Structural Dynamics Included)

Clean Configuration Weight 38,732 Lb Altitude Sea Level

Mach 0.84 KR 1.5

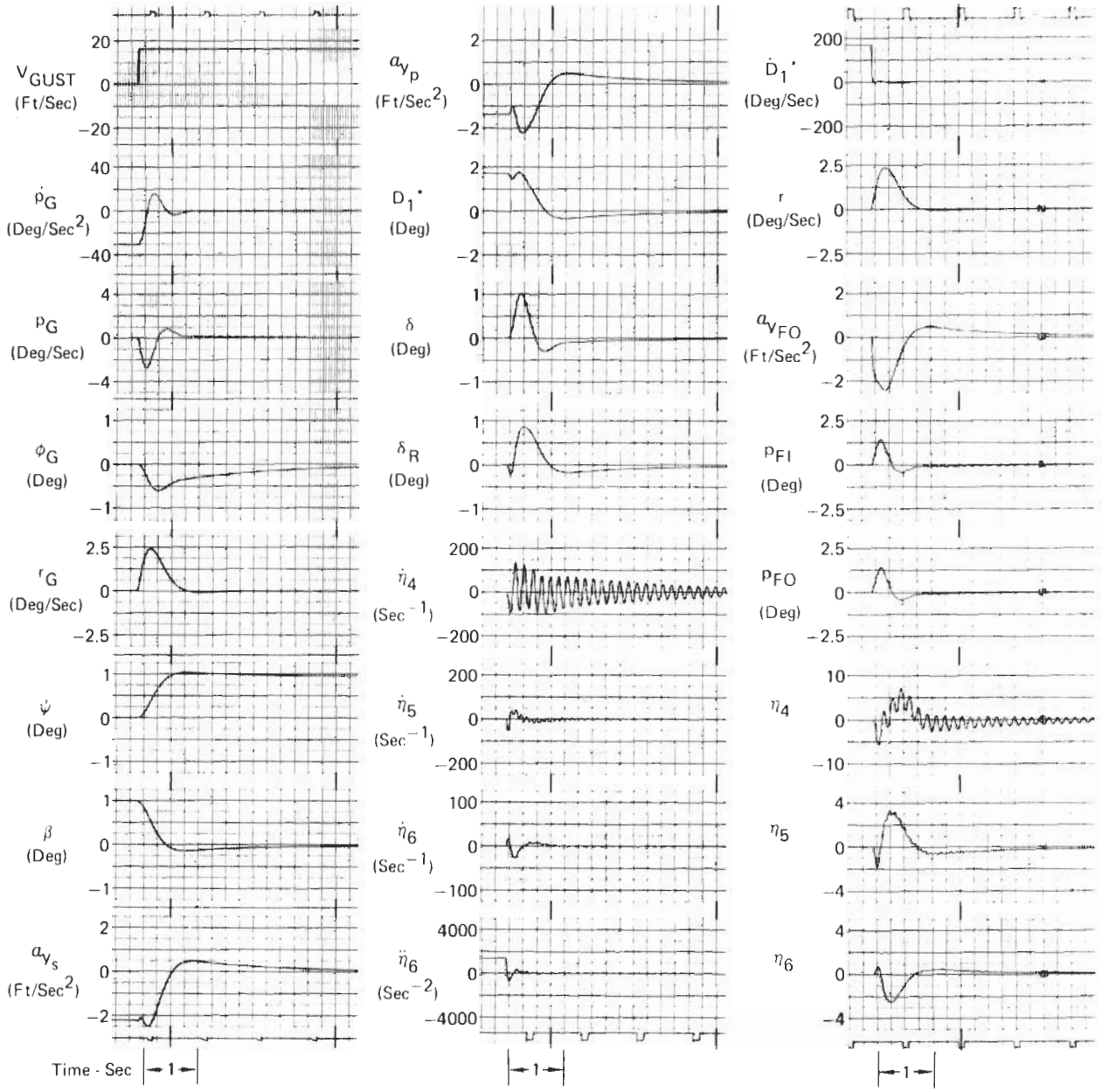

FIGURE 230

DYNAMIC RESPONSE TO SHARP EDGE GUST

(Structural Dynamics Included)

Clean Configuration Weight 38,732 Lb Altitude Sea Level

Mach 0.84 KR 1.5

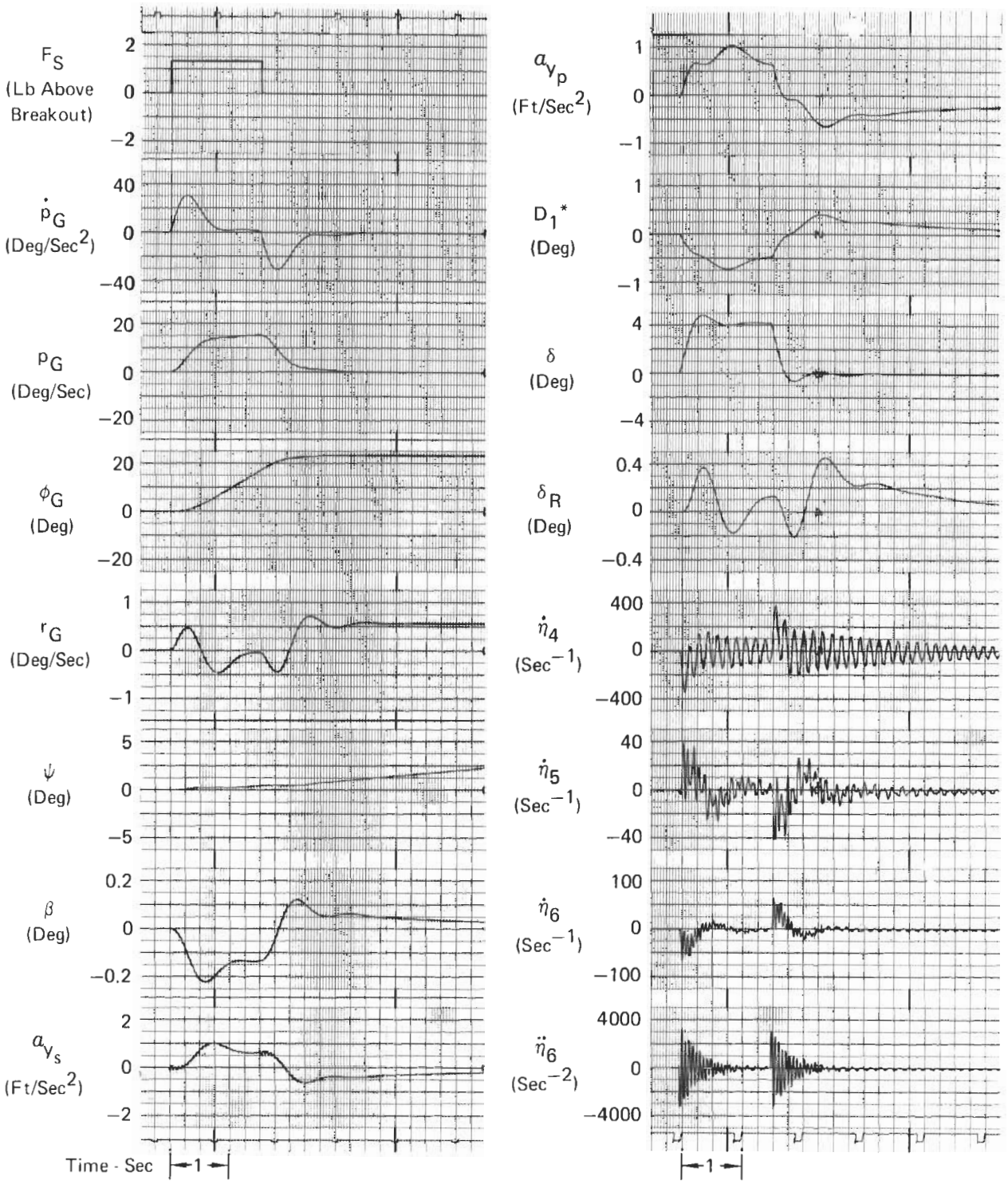

FIGURE 231
DYNAMIC RESPONSE TO LATERAL STICK FORCE
(Structural Dynamics Included)
(No Roll to Yaw Crossfeed)

Clean Configuration Weight 38,732 Lb Altitude 5000 Ft
Mach 1.2 KR 3.0

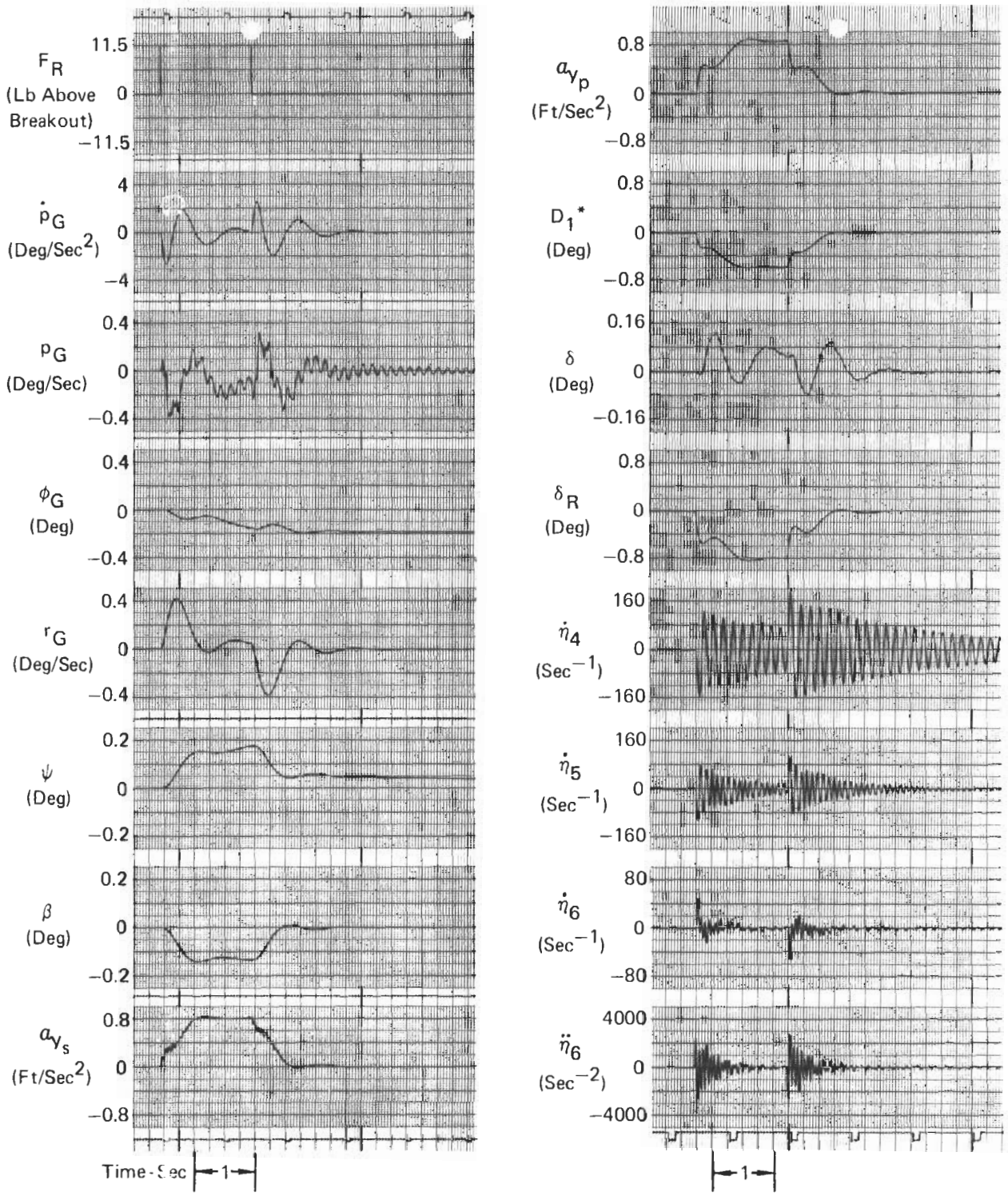

FIGURE 232

DYNAMIC RESPONSE TO RUDDER PEDAL FORCE

(Structural Dynamics Included)

Clean Configuration Weight 38,732 Lb Altitude 5000 Ft

Mach 1.2 KR 3.0

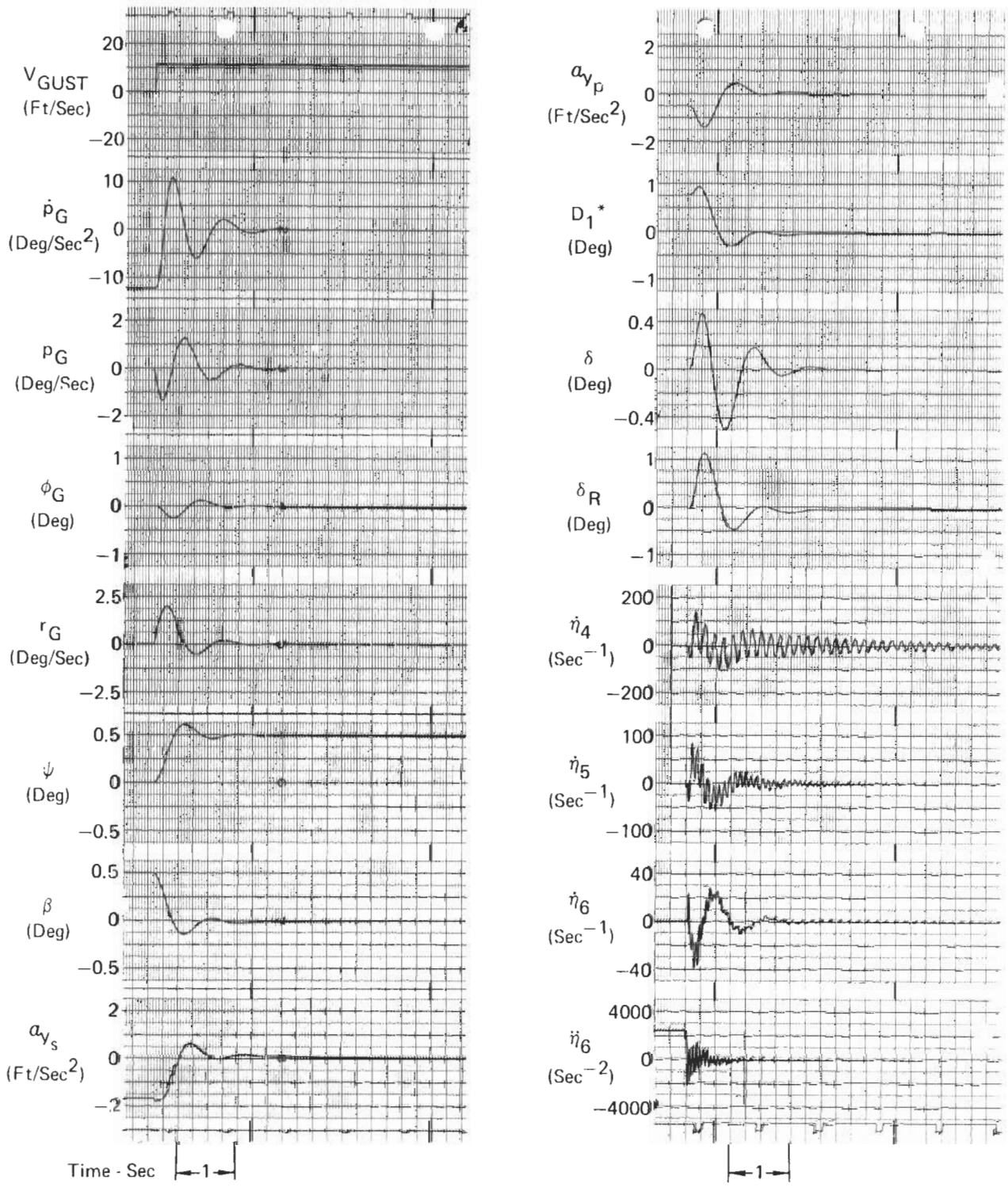

FIGURE 233
DYNAMIC RESPONSE TO SHARP EDGE GUST
(Structural Dynamics Included)

Clean Configuration Weight 38,732 Lb Altitude 5000 Ft
Mach 1.2 KR 3.0

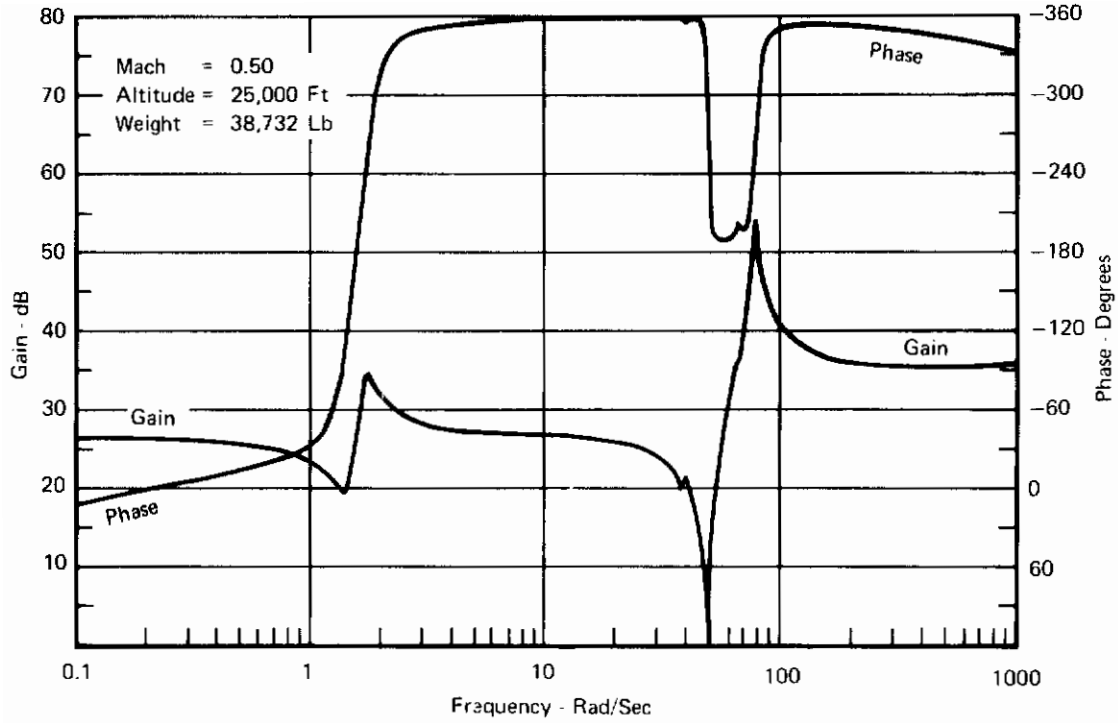

FIGURE 234

UNAUGMENTED AIRFRAME $a_{y_{s_{68}}}/\delta_R$ FREQUENCY RESPONSE

SHOWING STRUCTURAL MODES

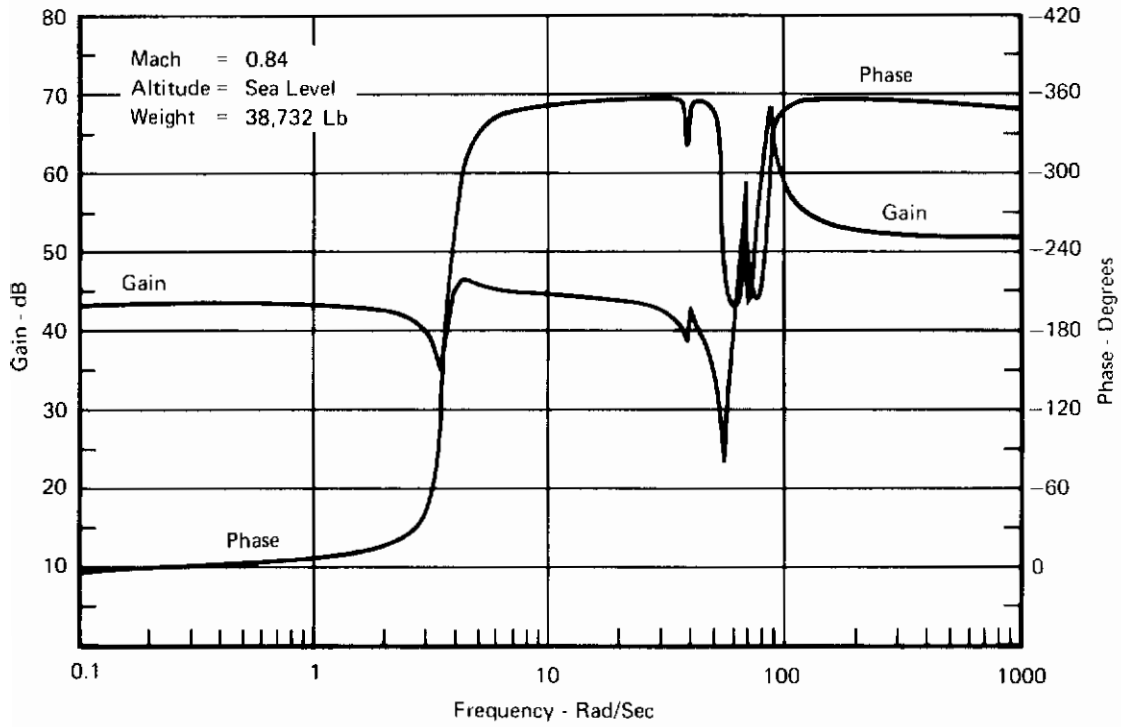

FIGURE 235

UNAUGMENTED AIRFRAME $a_{y_{s_{68}}}/\delta_R$ FREQUENCY RESPONSE

SHOWING STRUCTURAL MODES

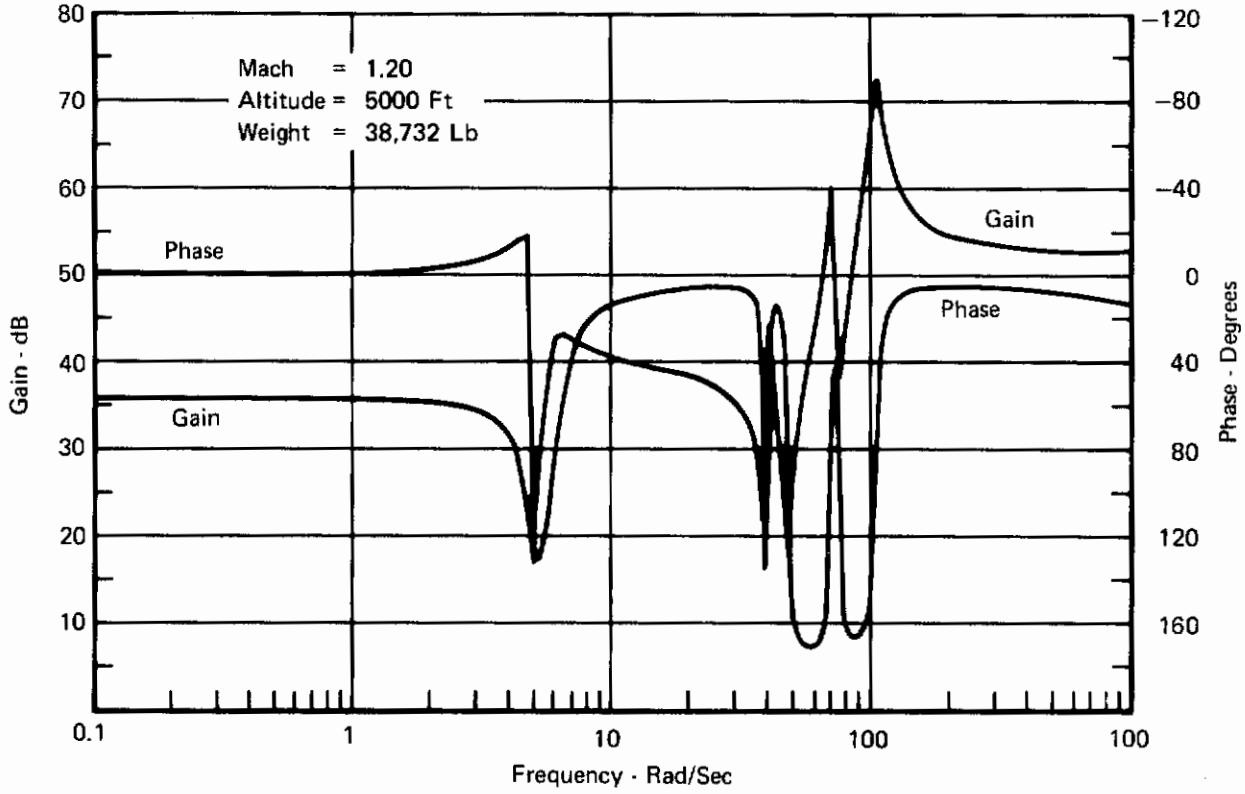

FIGURE 236

UNAUGMENTED AIRFRAME $a_{y_{s_{68}}}/\delta_R$ FREQUENCY RESPONSE SHOWING STRUCTURAL MODES

APPENDIX VI

SIMULATION HARDWARE

1. INTRODUCTION

Simulation hardware for the selected control system evaluation included a fixed base flight simulator crew station and the hybrid computing facility assembled by MCAUTO. Peripheral equipment generated an artificial horizon and special displays for air-to-air combat and landing approach tasks.

2. HYBRID COMPUTING FACILITY

The hybrid facility consisted of a Control Data Corporation 6600 digital computer, a PACE 231R analog computer and an Adage 784 digital-to-analog and analog-to-digital converter. Basic airframe equations of motion were programmed on the digital computer. Table look-up routines were utilized to obtain aerodynamic coefficients, thrust data, and other nonlinear effects. Control of logic switching and gain changing functions was performed using the digital computer. The analog computer served as an interface between the crew station and the digital program. Strip chart recorders, display facilities, and instrumentation for the crew station were driven from the analog computer. Analog-to-digital and digital-to-analog conversion was accomplished by the Adage 784 which also managed the logical discretes initiated in the crew station.

3. CREW STATION

The fixed base flight simulator crew station was equipped with conventional F-4E flight controls and panel instruments. The simulator also included a side stick controller and special SFCS panels.

a. Conventional Flight Controls

Conventional flight controls built into the crew station included the throttle, center stick control column, rudder pedals, and switches to extend landing gear, flaps, and speed brakes. In addition, switches were provided on the left console to disengage the pitch or yaw stability augmentation system (SAS).

(1) Throttles

The throttles were mounted in the left console of the crew station cockpit. A throttle angle of 20° to 120° could be selected. Mechanical stops also permitted discrete throttle settings of idle, military, or afterburner power to be applied. An electrical signal representing throttle position was converted to a digital parameter which represented the throttle

command to a twin-engine power plant delivering symmetrical thrust.

(2) Speed Brakes

A switch on the inboard throttle provided a capability to extend or retract the speed brakes in the aircraft simulation. The drag effects of the speed brakes were programmed in the six-degree-of-freedom equations of motion.

(3) Center Stick

Displacement and forces applied to the center column in the crew station generated command signals to the longitudinal or lateral channels of the digitally programmed flight control system. The modified longitudinal and lateral mechanical feel systems of the SFCS configuration were programmed on the digital computer to provide stick centering properties, force gradients, and stick dynamics to the simulator center stick. Command signals from the digital computer drove electrical torque motors which positioned the center stick in accordance with the mathematical models of the feel system. Mechanical trim inputs to the longitudinal channel were generated from a "coolie hat" trim switch on the center stick grip.

(4) Rudder Pedals

Rudder pedal displacement generated a command input to the directional channel of the flight control system. A mechanical linkage and springs provided feel system reaction forces and pedal return corresponding to the rudder feel system of the SFCS configuration.

(5) Flaps

Flap control was accomplished from the crew station by means of a switch located in the normal position under the left sill of the cockpit. Three switch positions commanded full flaps, half flap, or clean configuration. The flap position signal was applied to the digital program for use in selecting the proper aerodynamic data.

(6) Landing Gear

Landing gear extension or retraction was commanded using a switch located at the left edge of the main instrument panel. The gear position signal was applied to the digital program for use in selecting the proper gains.

b. Cockpit Instruments

Conventional cockpit instruments for the fixed base simulator crew station included: attitude director indicator (ADI), calibrated airspeed/Mach meter, angle-of-attack indicator, barometric altimeter, rate-of-climb indicator, normal accelerometer indicator, and engine tachometers. These instruments were continuously driven by the analog computer using the solutions to the equations of motion being solved by the digital computer as the simulation proceeded.

c. Miscellaneous Conventional Cockpit Hardware

Additional conventional hardware included a trigger on the center stick grip to control gun-firing in the simulated aircraft during air-to-air combat tasks, a gunsight consisting of a fixed centerline reticle, a speed brake warning light to indicate speed brake extension, and a microphone switch to allow communication by intercom.

d. Special SFCS Hardware

Several items of hardware were installed in the crew station specifically for the SFCS selected control system evaluation. A side stick controller was located on the right console of the crew station cockpit. Deflection of the side stick controller grip generated inputs to the flight control system's longitudinal and lateral channels in parallel to the center stick. A trigger switch on the side stick controller grip engaged the electrical back-up mode in all three axes. An emergency disconnect switch located on the center control column engaged the electrical back-up mode in the roll axis and the mechanical back-up mode in pitch and yaw axes.

e. SFCS Panels

Special panel hardware was installed specifically for the SFCS selected system evaluation. These panels included functional switches and display lights.

(1) Master Control and Display Panel

The master control and display panels consisted of switches and indicator lights used to select and indicate the SFCS modes. Three pushbutton switches with indicator lights selected and indicated the Normal or back-up mode in the pitch, roll, and yaw axes. Three solenoid-held toggle switches selected fixed gain or adaptive gain operation in the pitch, roll and yaw axes. A three-position switch for each axis provided high, medium, or low gain selection. The solenoid held ADAPTIVE/FIXED gain switches would not permit adaptive operation to be selected for an axis unless the gain-select switch was set for low gain in that axis.

(2) SFCS Trim Panel

The SFCS trim panel was located on the left console. It consisted of trim controls and an additional mode selection switch. The trim controls included three potentiometers for adjusting the electrical trim signals for the pitch, roll, and yaw channels. Also, a yaw vernier thumbwheel generated command inputs to the directional channel when an SFCS Normal or electrical back-up mode had been selected. Finally a two-position toggle switch permitted selection of Normal or TOL functions. The Normal mode provided neutral speed stability (NSS) except when the landing gear were extended. With the landing gear extended, selection of the Normal mode resulted in positive speed stability for take-off and landing.

(3) Phase IIA Panel

The Phase IIA panel consisted of the two solenoid-held switches for controlling the operation of the mechanical isolation mechanism (MIM). These switches permitted selection of the mechanical back-up or SFCS Normal modes in the pitch and yaw axes. Two switches for engaging pitch and yaw stability augmentation systems (SAS) during mechanical back-up operation were also located on this panel.

(4) DFG Input Panel

Functional switches were located on the left console of the crew station cockpit to command discrete function inputs to the pitch, roll, and yaw channels of the flight control system. These inputs are utilized to obtain discrete inputs for data correlation between simulation and flight test results.

4. PERIPHERAL EQUIPMENT

Peripheral equipment was utilized to provide visual displays required for several of the simulated tasks.

a. Display Generation Area

Visual displays were generated by equipment in the simulation area of the hybrid computer facility and transmitted to the crew station by closed circuit television.

(1) Artificial Horizon

An artificial horizon was generated for use during manoeuvering flight. The image depicted a cloud-covered earth with a distinct horizon. The motion of the image was correlated with the simulated aircraft's motion.

(2) Target Aircraft

An image of a target aircraft was utilized during air-to-air combat tasks. The image was generated in a model tunnel area where a gimballed aircraft model and a non-rotating television camera simulated the relative geometry of the two aircraft in combat. The television camera was driven along a track to simulate the range to the target aircraft. A subroutine to the main digital program generated the evasive maneuver of the target. The geometry and range were computed according to the relative motion between the simulated aircraft and the target in order to command the display.

(3) Terrain Map

Simulation of a landing approach involved use of a large-scale terrain model. The model measured 10 feet by 40 feet and was scaled 1000:1. This allowed translations of 10,000 feet laterally, 40,000 feet longitudinally, and 9600 feet vertically. The image of the landing strip as the simulated aircraft approached the runway was obtained from the motion of a television camera across the terrain map. The camera was driven in accordance with the attitude, position, and velocity of the aircraft.

b. Crew Station Area

The display equipment in the crew station area included a television reverse projection device and a large viewing screen. The visual displays were projected onto the viewing screen in front of the crew station cockpit. During air-to-air combat tasks the image of the target aircraft was superimposed on the image of the artificial horizon.

APPENDIX VII

SIMULATION SOFTWARE

1. INTRODUCTION

Software for the selected control system evaluation was mainly programmed for the digital computer, while an analog computer performed the master control functions and interfacing with the crew station.

2. ANALOG SOFTWARE

During this simulation the analog computer served as a buffer between the main digital program, cockpit instruments, strip chart recorders, and as a coordination device to generate the command voltages driving the display hardware. During studies of system response to failures, the failure inputs were generated from the analog computer. These failure insertions consisted of inputs up to ten percent of surface authority on a five second time constant. The failure waveform is shown in Figure 237.

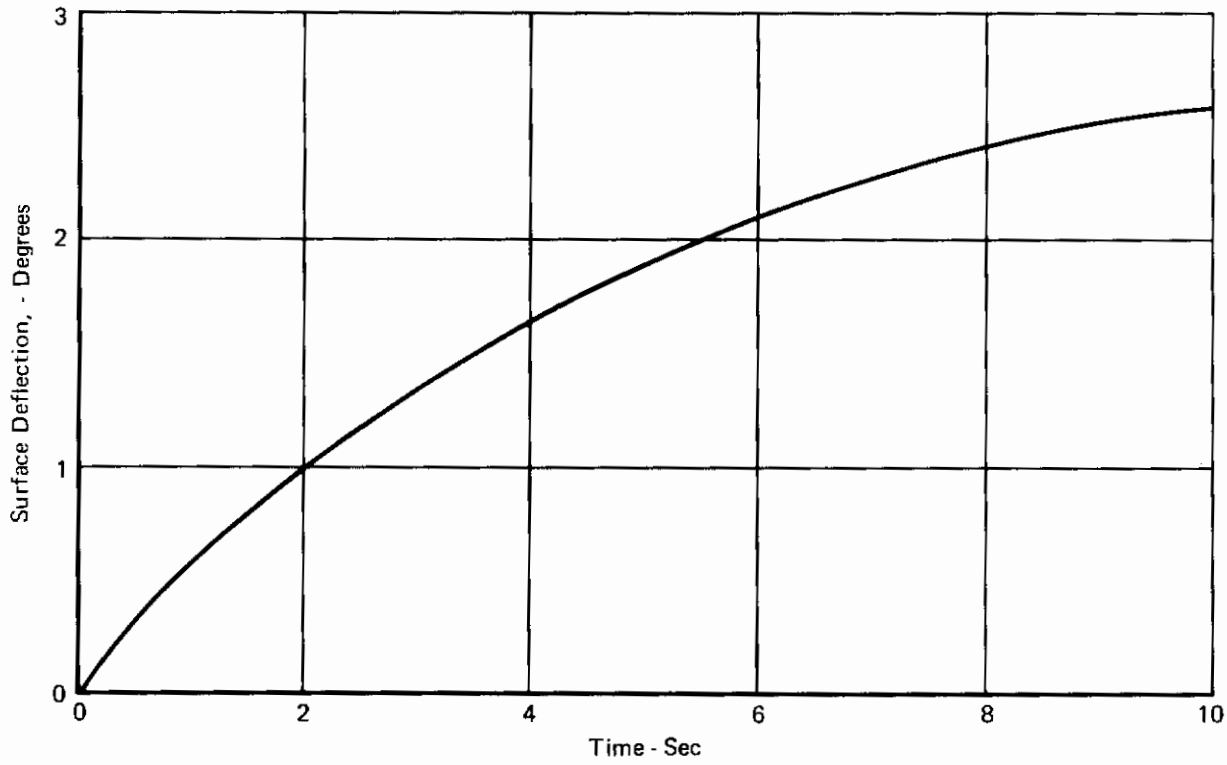

FIGURE 237
WAVEFORM OF FAILURE INSERTION

3. DIGITAL SOFTWARE

Digital programs were written in FORTRAN IV and submitted to a Control Data Corporation (CDC) 6600 Computer. The digital software included mechanization of: basic airframe characteristics, electronic flight control system components, secondary and surface actuators, switching logic, feel system components, and generation of command signals to peripheral equipment display generators. Nonlinear data and time-varying parameters were updated at 20 millisecond intervals.

a. Basic Airframe

The basic airframe mechanization was achieved using a set of non-linear differential equations in six-degrees-of-freedom representing the motion of a rigid aircraft subject to large angle perturbations. The three force equations and the moment equations were derived using a body axis coordinate system with the longitudinal axis aligned with the waterline. Additional equations described atmospheric properties, body acceleration, and Euler angular rates as well as velocity relative to an inertial reference frame. The set of equations describing motion of the simulated aircraft appears in Figure 238.

(1) Aerodynamic derivatives required by the equations of motion were obtained from tables of data as functions of Mach number, altitude, and angle of attack. Additional tables were used by the program to compute full flap or half flap aerodynamic coefficients or to simulate spin-stall aerodynamics. Flight during extension or retraction of flaps was simulated by programming transitions between full or half flap aerodynamics and the clean configuration.

(2) Propulsion data were obtained from similar tables as required by the equations of motion.

b. Flight Control System

The longitudinal and lateral-directional channels of the SFCS were programmed digitally. Block diagrams of these systems were presented in Sections III and IV.

c. Surface Actuators

The surface actuators were represented by mathematical models programmed for the digital computer. A block diagram of the surface actuator for the stabilator was presented in Section III.

d. SFCS Switching Logic

Switching logic pertaining to the SFCS modes was included in the digital software. Switching functions included the mechanical isolation mechanism (MIM), gain setting and changing operations, and the SFCS mode logic.

● Six Degree-of-Freedom Differential Equations

$$\dot{u} = vr - wq - g \sin\theta - \frac{\bar{q}S}{m} C_D + 0.9958 \frac{T}{m}$$

$$\dot{v} = wp - ur + g \sin\phi \cos\theta + \frac{\bar{q}S}{m} \left[\frac{b}{2V} \left(C_{y_p} p + C_{Y_r} r \right) + C_{y_\beta} \beta + C_{y_{\delta_a}} \delta a + C_{y_{\delta_{SP}}} \delta_{SP} + C_{y_{\delta_R}} \delta_R \right]$$

$$\dot{w} = uq - vp + g \cos\phi \cos\theta - \frac{\bar{q}S}{m} C_L - 0.0915 \frac{T}{m}$$

$$\dot{p} = \frac{1}{(I_X I_Z - I_{XZ}^2)} \left\{ I_{XZ} (I_X - I_Z) pq - (I_Z^2 + I_{XZ}^2 - I_Y I_Z) qr \right.$$

$$+ \bar{q}Sb I_Z \left[\frac{b}{2V} \left(C_{l_p} p + C_{l_r} r \right) + C_{l_\beta} \beta + C_{l_{\delta_a}} \delta_a + C_{l_{\delta_{SP}}} \delta_{SP} + C_{l_{\delta_R}} \delta_R \right]$$

$$\left. + \bar{q}Sb I_X \left[\frac{b}{2V} \left(C_{n_p} p + C_{n_r} r \right) + C_{n_\beta} \beta + C_{n_{\delta_a}} \delta_a + C_{n_{\delta_{SP}}} \delta_{SP} + C_{n_{\delta_R}} \delta_R \right] \right\}$$

$$\dot{q} = \frac{I_Z - I_X}{I_Y} pr + \frac{I_{XZ}}{I_Y} (r^2 - p^2) + \frac{\bar{q}S\bar{C}}{I_Y} \left[C_M + \frac{\bar{C}}{2V} \left(C_{m_{\dot{\alpha}}} \dot{\alpha} + C_{m_q} q \right) + C_{m_{\delta_S}} \delta_S \right]$$

$$+ \frac{T}{I_Y} \left[0.9958 \left(\frac{cg_{wl}}{12} - 2.7 \right) + 0.0915 \left(\frac{\% cg}{100} \bar{C} - 4.361 \right) \right]$$

$$\dot{r} = \frac{I_X - I_Y}{I_Z} pq + \frac{I_X}{I_Z} (\dot{p} - qr) + \frac{\bar{q}Sb}{I_Z} \left[\frac{b}{2V} \left(C_{n_p} p + C_{n_r} r \right) + C_{n_\beta} \beta + C_{n_{\delta_a}} \delta_a + C_{n_{\delta_{SP}}} \delta_{SP} + C_{n_{\delta_R}} \delta_R \right]$$

$$V = (u^2 + v^2 + w^2)^{1/2}$$

$$\alpha = \tan^{-1} \left(\frac{w}{u} \right)$$

$$\beta = \sin^{-1} \left(\frac{u}{V} \right)$$

● Atmospheric Property Equations

$$M = \frac{V}{1117.1 - 0.00412778h} \qquad h \leq 36{,}000 \text{ ft}$$

$$M = \frac{V}{968.5} \qquad h > 36{,}000 \text{ ft}$$

$$\rho = 2(0.034475 + 0.019213 \times 10^{-10} h^2 - 0.050381 \times 10^{-5} h)^2 \qquad h \leq 36{,}000 \text{ ft}$$

$$\rho = 2(0.039708 + 0.039227 \times 10^{-10} h^2 - 0.072121 \times 10^{-5} h)^2 \qquad h > 36{,}000 \text{ ft}$$

FIGURE 238
EQUATIONS OF MOTION

$$\bar{q} = \tfrac{1}{2}\rho V^2$$

$$V_{CAL} = 12.127\,\rho\,V \qquad M \leq 0.6$$

$$V_{CAL} = 60M - 36 + 12.127\,\rho\,V \qquad M > 0.6$$

- Acceleration Equations

$$a_{x_{cg}} = -\sin\theta - \frac{\bar{q}S}{mg} C_D + 0.9958\,\frac{T}{mg}$$

$$a_{Y_{cg}} = \frac{\bar{q}S}{mg}\left[\frac{b}{2V}\left(C_{y_p}p + C_{y_r}r\right) + C_{y_\beta}\beta + C_{y_{\delta_a}}\delta_a + C_{y_{\delta_{SP}}}\delta_{SP} + C_{y_{\delta_R}}\delta_R\right]$$

$$a_{Z_{cg}} = -\cos\phi\cos\theta + \frac{\bar{q}S}{mg} C_L + 0.0915\,\frac{T}{mg}$$

$$a_{Y_{acc}} = a_{Y_{cg}} + \frac{11.12}{g}\left(\dot{r} + pq\right) - \frac{0.65}{g}\left(\dot{p} - rq\right)$$

$$a_{Z_{acc}} = a_{Z_{cg}} + \frac{20.25}{g}\left(\dot{q} - pr\right)$$

$$a_{Y_p} = a_{Y_{cg}} + \frac{16.3}{g}\left(\dot{r} + pq\right)\cos\left(\alpha + 0.014\right) + \left(\dot{p} - rq\right)\sin\left(\alpha + 0.014\right)$$

$$a_{Z_p} = a_{Z_{cg}} + \frac{16.3}{g}\left(\dot{q} - pr\right)$$

$$N_{LF} = a_{z_p} + \cos\phi\cos\theta$$

- Euler Body Rate Equations

$$\dot{\psi} = \left(q\sin\phi + r\cos\phi\right)/\cos\theta$$

$$\dot{\theta} = q\cos\phi - r\sin\phi$$

$$\dot{\phi} = p + \dot{\psi}\sin\theta$$

- Inertial Frame Velocity Equations

$$\begin{bmatrix} V_N \\ V_E \\ \dot{h} \end{bmatrix} = \begin{bmatrix} \cos\theta\cos\psi & \sin\phi\sin\theta\cos\psi - \cos\phi\sin\psi & \cos\phi\sin\theta\cos\psi + \sin\phi\sin\psi \\ \cos\theta\sin\psi & \sin\phi\sin\theta\sin\psi + \cos\phi\cos\psi & \cos\phi\sin\theta\sin\psi - \sin\phi\cos\psi \\ \sin\theta & -\sin\phi\cos\theta & -\cos\phi\cos\theta \end{bmatrix} \begin{bmatrix} u \\ v \\ w \end{bmatrix}$$

FIGURE 238
EQUATIONS OF MOTION (CONTINUED)

(1) Operation of the MIM switches selected mechanical back-up or a Normal SFCS mode. MIM switches were available in the pitch and yaw axes. When a mechanical back-up mode was selected, stability augmentation systems (SAS) could be turned on for the pitch and yaw channels.

(2) Gain setting and changing operations involved the fixed gain and adaptive gain selection and the landing gear gain settings. In fixed gain operation, the simulator pilot manually selected High, Medium or Low gains. An adaptive gain changing operation could be selected when the gain select switch for that channel was set to Low. The pitch adaptive switch could not engage when the flight mode switch had been set to the TOL function. When adaptive gain operation was selected, the parameter identifier selected the proper gain levels for the flight control system. A block diagram of the parameter identifier and schedules of the adaptive and fixed gains are as previously shown. Simulated extension of the landing gear resulted in the selection of another set of gains.

(3) SFCS mode selection logic involved the NORMAL/BACK-UP pushbutton indicator lights, the emergency disconnect paddle switch on the center column or the sidestick trigger and the panel mounted NORMAL/TOL flight mode switch at the left console of the crew station. Selection of the Normal mode engaged the SFCS closed loop operation. Actuation of the emergency disconnect switch on the center stick engaged the mechanical back-up system in the pitch and yaw axes and the electrical back-up in the roll axis. The sidestick trigger engaged electrical back-up modes in all three axes. The flight mode switch selected the NORMAL or TOL functions. With electrical back-up selected or the landing gear extended, TOL became the normal function. In other conditions while neutral speed stability (NSS) was the normal function, the switch enabled the TOL function to be manually selected.

e. Trim

Electrical trim command signals for all three axes were generated at the trim control panel. Trim authority was originally established at +3° to -14° stabilator deflection in pitch, and 33 1/3% full surface travel in roll and yaw. The pitch, roll and yaw trim signals entered the flight control system at points identified on the respective block diagrams.

f. Feel System

The longitudinal feel system was mechanized as shown in the block diagram in Figure 239. Both the longitudinal and lateral feel systems functioned through torque motors which positioned the simulator stick.

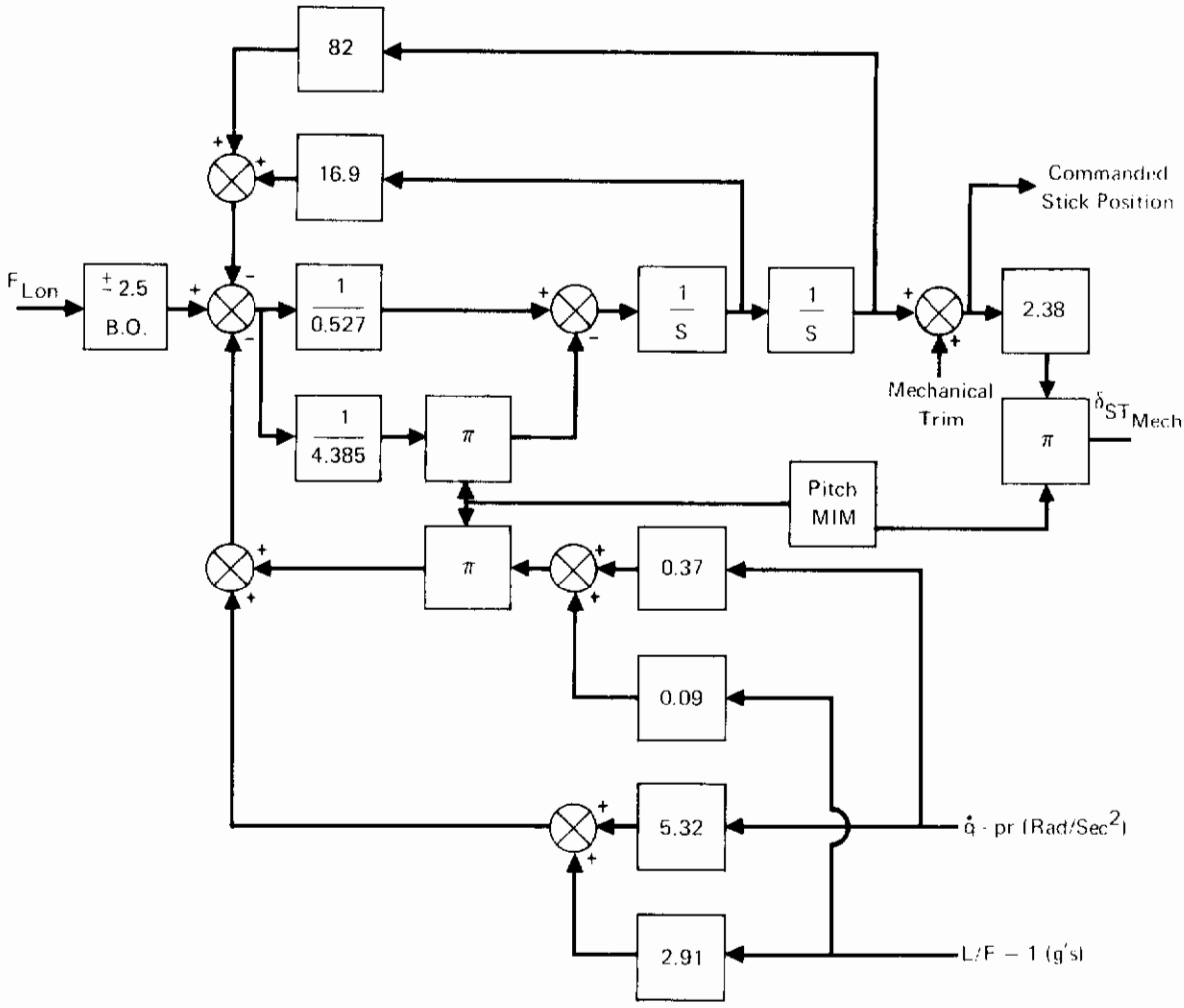

FIGURE 239
LONGITUDINAL MECHANICAL BACKUP

g. Stall Warning

A stall warning system was programmed as shown on the block diagram in Figure 240. Outputs of the stall warning system changed SFCS gains. A warning tone was delivered to the simulator pilot's headset during stall entry, simulating the normal F-4 audio tone generator.

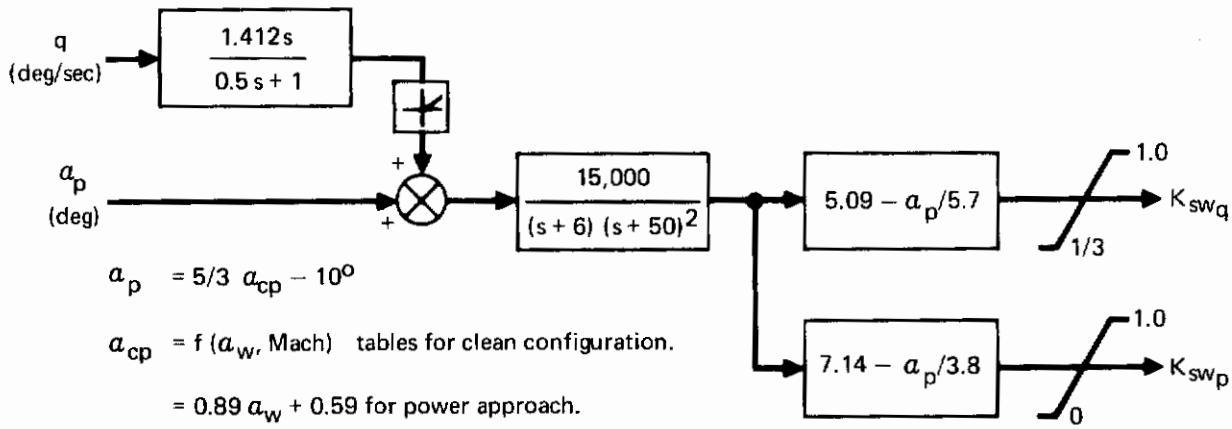

FIGURE 240

STALL WARNING BLOCK DIAGRAM

h. Display Command Generation

Digital software also provided display command signals required to simulate terrain following, air-to-air combat, and landing approach tasks. For the terrain following task, a digital program generated pitch and roll commands which were displayed to the pilot by needles on the attitude-director indicator. The needles were deflected upwards when climb was directed, down for dive, to the right when

a right turn was required and left for a left turn. The needles were nulled when the correct attitude or attitude rate had been achieved. Air-to-air combat simulation made use of a programmed evasive maneuver by the target requiring decreasing airspeed and altitude. The landing approach task also required digital software to represent the motion of the simulated aircraft as it approached the runway in order to coordinate the motion of the television camera with respect to the terrain map.

i. Discrete Function Inputs

Switches in the crew station cockpit commanded discrete function inputs to each axis of the flight control system. The input to the pitch axis corresponded to .5g of normal acceleration; the roll input represented 10°/sec roll rate; and the yaw axis channel input was equivalent to .25g of lateral acceleration.

j. Scoring

A scoring subroutine was established to evaluate performance during terrain following and air-to-air combat tasks. Samples taken during a scoring interval represented the time that angular errors fell within prescribed ranges. During the air-to-air combat task, total angular errors from the simulated aircraft's actual direction was computed for the pitch and roll axes. Cumulative distribution information was prepared from this data during each scoring run.

REFERENCES

1. Technical Report AFFDL-TR-70-135, "Survivable Flight Control System, Simplex Actuator Package", McDonnell Aircraft Company, November 1970.

2. Malcom, L.G. and Tobie, N.N., "New Short Period Handling Quality Criteria for Fighter Aircraft", The Boeing Company, Document No. D6-17841 T/N, October 1965.

3. T. Peter Neal, AIAA Paper No. 70-1002, "The Influence of Bobweights on Pilot Induced Oscillations", August 1970.

4. Chestnut, H. and Mayer, R.W., Servomechanisms and Regulating System Design, Vol. I, Wiley & Sons, Inc., New York, New York, 1951.

DOCUMENT CONTROL DATA - R & D

(Security classification of title, body of abstract and indexing annotation must be entered when the overall report is classified)

1. ORIGINATING ACTIVITY *(Corporate author)*
McDonnell Aircraft Company
McDonnell Douglas Corporation

2a. REPORT SECURITY CLASSIFICATION
Unclassified

2b. GROUP
N/A

3. REPORT TITLE
Survivable Flight Control System Interim Report No.1
Studies, Analyses and Approach
Supplement for Control Law Development Studies

4. DESCRIPTIVE NOTES *(Type of report and inclusive dates)*
Interim Report - July 1969 - May 1971

5. AUTHOR(S) *(First name, middle initial, last name)*
Robert L. Kisslinger
George J. Vetsch

6. REPORT DATE	7a. TOTAL NO. OF PAGES	7b. NO. OF REFS
May 1971	371	6

8a. CONTRACT OR GRANT NO.
F33615-69-C-1827, PZ05

b. PROJECT NO.
680J

c.

d.

9a. ORIGINATOR'S REPORT NUMBER(S)

9b. OTHER REPORT NO(S) *(Any other numbers that may be assigned this report)*
AFFDL-TR-71-20, Supplement 2

10. DISTRIBUTION STATEMENT
This document has been approved for public release. Its distribution is unlimited.

11. SUPPLEMENTARY NOTES

12. SPONSORING MILITARY ACTIVITY
Air Force Flight Dynamics Laboratory
Air Force Systems Command
Wright-Patterson Air Force Base, Ohio

13. ABSTRACT

The Survivable Flight Control System (SFCS) Program is an advanced development program of which the principal objective is the development and flight test demonstration of an SFCS utilizing Fly-By-Wire and Integrated Actuator Package techniques. The studies and analyses conducted to date have sufficiently defined the system requirements to provide a definition of an approach to the implementation of the SFCS. The results of these studies and the definition of the approach are presented in the basic report. The details of the Control Criteria, and Hydraulic Power and Actuation studies are presented in report supplements 1 and 3, respectively. The results of the Control Law Development studies are presented in this supplement 2.

As a result of previous fly-by-wire technology development programs, certain guidelines and requirements were specified early in the SFCS design. Those specifications which are relevent to the control law development study are as follows:

- Model following closed-loop control system, utilizing a blend of pitch rate and normal acceleration feedback for the pitch axis, roll rate feedback for the roll axis and a blend of yaw rate and lateral acceleration for the yaw axis.
- Selectable neutral speed stability with gear up
- Selectable fixed or adaptive gain operation

DD FORM 1 NOV 65 1473 (PAGE 1)

S/N 0101-807-6801

13. ABSTRACT (CONTINUED)

- o Direct electrical link to control surface for emergency operation
- o Center stick and sidestick fly-by-wire controllers
- o Roll to Yaw crossfeed
- o Structural mode compensation
- o Failure detection and isolation
- o Stall warning through increased stick force gradients
- o Quadruplex electronics, sensors, secondary actuators and a duplex integrated actuator package in order to provide a two-fail operate capability.
- o Mechanical back-up for Phase IIA (pitch and yaw axes only) and no mechanical back-up for Phases IIB and C.

Using the above guidelines, this study further defined the system concepts, requirements, and specific techniques to be utilized in the SFCS implementation. During the system synthesis, particular emphasis was placed on system stability, sensor location, gain schedules, appropriate filters, and component mechanization. Once the system math model was developed, both component and total system performance characteristics were investigated extensively. In addition to the comprehensive root locus and Bode analyses and small perturbation simulations, a six-degree-of-freedom, fixed base, nonlinear, large amplitude piloted simulation was conducted in order to evaluate the total system performance over the range of flight conditions and configurations available with the F-4 test aircraft.

The results of this study and simulation provided a basis for specifying the performance of the SFCS procured hardware. As a result of the design refinements which resulted from this work, the SFCS system will demonstrate superior stability and performance characteristics throughout the F-4 flight envelope.

14 KEY WORDS	LINK A		LINK B		LINK C	
	ROLE	WT	ROLE	WT	ROLE	WT
Adaptive Gains						
Control Law Development						
Aircraft Control System Analysis						
Flexibility Effects						
Fly-By-Wire						
F-4 Aircraft						
Lateral-Directional Control System						
Longitudinal Control System						
Manned Simulation						
Roll to Yaw Crossfeed						
Aircraft Stability						
Stall Warning						
Aircraft Structural Modes						